

**Ongoing Face Recognition
Vendor Test (FRVT)**
Part 1: Verification

Patrick Grother
Mei Ngan
Kayee Hanaoka
Joyce C. Yang
Austin Hom

*Information Access Division
Information Technology Laboratory*

This publication is available free of charge from:
<https://www.nist.gov/programs-projects/face-recognition-vendor-test-frvt-ongoing>

2021/12/16

ACKNOWLEDGMENTS

The authors are grateful for the long-standing support and collaboration of the the Department of Homeland Security's Science & Technology Directorate (S&T) and the Office of Biometric Identity Management (OBIM).

Additionally, the authors are grateful to staff in the NIST Biometrics Research Laboratory for infrastructure supporting rapid evaluation of algorithms.

DISCLAIMER

Specific hardware and software products identified in this report were used in order to perform the evaluations described in this document. In no case does identification of any commercial product, trade name, or vendor, imply recommendation or endorsement by the National Institute of Standards and Technology, nor does it imply that the products and equipment identified are necessarily the best available for the purpose.

INSTITUTIONAL REVIEW BOARD

The National Institute of Standards and Technology's Research Protections Office reviewed the protocol for this project and determined it is not human subjects research as defined in Department of Commerce Regulations, 15 CFR 27, also known as the Common Rule for the Protection of Human Subjects (45 CFR 46, Subpart A).

FRVT STATUS

This report is a draft NIST Interagency Report, and is open for comment. It is the thirty sixth edition of the report since the first was published in June 2017. Prior editions of this report are maintained on the FRVT [website](#), and may contain useful information about older algorithms and datasets no longer used in FRVT.

FRVT remains open: All [four tracks](#) of the FRVT are open to new algorithm submissions.

2021-12-16 changes since 2021-11-22:

- ▷ We have added results for first algorithms from five developers: Alfabetia, Cloudmatrix, Euronovate SA, FaceOnLive Inc, and Mobipin Technology.
- ▷ We have added results for new algorithms from ten returning developers: ACI Software, ITMO University, NEO Systems, Guangzhou Pixel Solutions, Panasonic R+D Center Singapore, Qnap Security, Scanovate, Tevian, Unissey, and Vietnam Posts and Telecommunications Group.
- ▷ We have retired results for eight algorithms per our policy to only list results for two algorithms per developer. Results for retired algorithms appear in prior versions of this report in the [archive](#).
- ▷ We have revamped Figure 19 showing performance on 20 pairs of open-source images. It now color-codes false negatives and positives against a default threshold value.

2021-11-22 changes since 2021-10-28:

- ▷ We have added results to the [website](#) for kiosk-collected images where the design and geometry configuration mean that many images have considerable downward pitch angle. In some images, the face is partially cropped. Some images have other background faces.
- ▷ We have stopped using child exploitation images in FRVT, as we lost access to the imagery. All results for that set have been removed from the [website](#), and will be removed from future PDF reports.
- ▷ We have added results for first algorithms from seven new developers: CUDO Communication, Daon, KuKe3D Technology, Mantra Softtech India, Maxvision Technology, Multi-Modality Intelligence, and Samsung-SDS.
- ▷ We have added results for new algorithms from seven returning developers: Acer Incorporated, Cloudwalk-Moontime Smart Technology, Gorilla Technology, ID3 Technology, Incode Technologies, NSENSE Corp., and SQIsoft.
- ▷ We have retired results for six algorithms per our policy to only list results for two algorithms per developer. Results for retired algorithms appear in prior versions of this report in the [archive](#).

2021-10-28 changes since 2021-09-08:

- ▷ We have substantially revised the algorithm-specific report cards that are linked from the [FRVT results page](#). (Example: [HTML](#)).
- ▷ We have added results for first algorithms from eight new developers: Beijing Mendaxia Technology, Beijing Hisign Technology, Biocube Matrics, Clearview AI, Reveal Media, Toppan ID Gate, Verigram, and Viettel High Technology.
- ▷ We have added results for new algorithms from thirty returning developers: 20Face, 3divi, Canon Inc Chunghwa Telecom, Corsight, Decatur Industries, Deepglint, Dermalog, FaceTag, Fiberhome Telecommunication Technologies, GeoVision, ICM Airport Technics, Imagus Technology, InsightFace AI, Kakao

Enterprise, Kookmin University, Line Corporation, N-Tech Lab, NotionTag Technologies, Realnetworks, Suprema ID, Taiwan-Certificate Authority, Toshiba, Tripleize, Trueface.ai, Veridas Digital Authentication, Visidon, VisionLabs, YooniK, and Yuan High-Tech Development.

- ▷ We have retired results for twenty algorithms per our policy to only list results for two algorithms per developer. Results for retired algorithms appear in prior versions of this report in the [archive](#).

2021-09-08 changes since 2021-08-02:

- ▷ We have added results for first algorithms from seven new developers: Griaule, SQISoft, Qnap Security, Techsign, Smart Engines, Verihubs, and Wuhan Tianyu Information Industry.
- ▷ We have added results for new algorithms from sixteen returning developers: ADVANCE.AI, AuthenMetric, CloudSmart Consulting, Code Everest Pvt, Cognitec Systems, Thales Gemalto Cogent, Intel Research Group, Omnidarde, Oz Forensics, Rank One Computing, Samsung S1 Corp, Securif AI, Tevian, TigerIT Americas, Universidade de Coimbra, and Vigilant Solutions
- ▷ We have retired results for eleven algorithms per our policy to only list results for two algorithms per developer. Results for retired algorithms appear in prior versions of this report in the [archive](#).

2021-08-02 changes since 2021-06-25:

- ▷ We have added results for first algorithms from eight new developers: Bee the Data, Closeli Inc, Coretech Knowledge Inc, Deepsense (France), ioNetworks Inc, Kakao Pay Corp, Seventh Sense Artificial Intelligence, and SK Telecom.
- ▷ We have added results for new algorithms from fifteen returning developers: Alchera Inc, Adera Global PTE, Aware, Bresee Technology, Cyberlink Corp, Expasoft LLC, Fujitsu Research and Development Center, Gorilla Technology, Idemia, Neurotechnology, NEO Systems, NHN Corp, Paravision, Panasonic R+D Center Singapore, and Shenzhen University-Macau University of Science and Technology.
- ▷ We have retired results for twelve algorithms per our policy to only list results for two algorithms per developer. Results for retired algorithms appear in prior versions of this report in the [archive](#).

2021-06-25 changes since 2021-05-21:

- ▷ We have added results for first algorithms from six new developers: Alice Biometrics, BOE Technology Group, Fincore, Neosecu, Sodec App, and Yuntu Data and Technology.
- ▷ We have added results for new algorithms from seven returning developers: Incode Technologies, HyperVerge, Mobbeel Solutions, Guangzhou Pixel Solutions, Remark Holdings, Sensetime, and Vietnam Posts and Telecommunications Group.
- ▷ We have retired results for four algorithms per our policy to only list results for two algorithms per developer. Results for retired algorithms appear in prior versions of this report in the [archive](#).

2021-05-21 changes since 2021-04-26:

- ▷ We have added results for first algorithms from five new developers: Ekin Smart City Technologies, Suprema ID, Tripleize, Taiwan-Certificate Authority, and Vision Intelligence Center of Meituan.
- ▷ We have added results for new algorithms from eight returning developers: ID3 Technology, Imagus Technology, Momentum Digital, N-Tech Lab, NSENSE, Shanghai Jiao Tong University, Vision-Box, and Yuan High-Tech Development

- ▷ We have retired results for seven algorithms per our policy to only list results for two algorithms per developer. Results for retired algorithms appear in prior versions of this report in the [archive](#).

2021-04-26 changes since 2021-04-16:

- ▷ We have added results for first algorithms from three new developers: Quantasoft, Rendip, and NEO Systems.
- ▷ We have added results for new algorithms from four returning developers: 3Divi, Realnetworks, Veridas Digital Authentication Solutions, and Universidade de Coimbra.
- ▷ We have retired results for three algorithms per our policy to only list results for two algorithms per developer. Results for retired algorithms appear in prior versions of this report in the [archive](#).

2021-04-16 changes since 2021-03-19:

- ▷ We have added results for first algorithms from six new developers: 20Face, Beijing DeepSense Technologies, BitCenter UK, Enface, FaceTag, InsightFace AI, Line Corporation, Lema Labs, Nanjing Kiwi Network Technology, Omnidarde, Regula Forensics, and Suprema.
- ▷ We have added results for new algorithms from ten returning developers: CloudSmart Consulting, Dermalog, GeoVision, Neurotechnology, Panasonic R+D Center Singapore, Samsung S1, Securif AI, Trueface.ai, Vigilant Solutions, and Visidon.
- ▷ We have retired results for ten algorithms per our policy to only list results for two algorithms per developer. Results for retired algorithms appear in prior versions of this report in the [archive](#).

2021-03-19 changes since 2021-03-05:

- ▷ We have added results for first algorithms from six new developers: Ajou University, AuthenMetric, Code Everest, Corsight, Papilon Savunma, and NHN Corp
- ▷ We have added results for new algorithms from seven returning developers: Alchera, Deepglint, Fiber-home Telecommunication Technologies, Kakao Enterprise, Kookmin University, Megvii/Face++, and NotionTag Technologies.
- ▷ We have updated many of the hyperlinked HTML report-cards to include seven figures on demographic dependence. Figures of this kind first appeared, and are documented in, the December 2019 document, [NIST Interagency Report 8280](#) on demographic differentials in face recognition. The figures quantify false negative dependence on demographics using “visa-border” comparisons, and false positive dependence using comparisons of “application” photos that uniformly of quality and similar to visa photos.

2021-03-05 changes since 2021-01-19:

- ▷ We have added results for first algorithms from three new developers: IVA Cognitive, Mobbeel, and MoreDian Technology.
- ▷ We have added results for new algorithms from returning developers: Ability Enterprise - Andro Video, ACI Software, Adera Global, AnyVision, BioID Technologies, China Electronics Import-Export, Cognitec Systems, Fujitsu Research and Development Center, Glory, Guangzhou Pixel Solutions, Hengrui AI Technology, Incode Technologies, Intel Research, iQIYI, Mobai, Oz Forensics, Paravision, VisionLabs, and Xforward AI Technology.

- ▷ We have added a new “resources” tab to the main [webpage](#). It includes sortable columns for data related to speed, model size, storage, and memory consumption.
- ▷ We have retired results for 13 algorithms per our policy to only list results for two algorithms per developer. Results for retired algorithms appear in prior versions of this report in the [archive](#).

2021-01-19 changes since 2020-12-18:

- ▷ This report adds results for first algorithms from four developers: Herta Security, Irex AI, Shenzhen University-Macau University of Science and Technology, and Vietnam Posts and Telecommunications Group. See Table 6 for more information.
- ▷ The report also includes results for thirteen developers who have previously submitted algorithms: Bresee Technology, Canon (previously Canon Information Technology (Beijing)), Cyberlink, CSA IntelliCloud Technology, Dahua Technology, ID3 Technology, Imagus Technology (Vixvizon), Moontime Smart Technology, N-Tech Lab, Thales Cogent, Veridas Digital Authentication Solutions, Vocord, and Yuan High-Tech Development.
- ▷ We have retired results for ten algorithms per our policy to only list results for two algorithms per developer. Results for retired algorithms appear in prior versions of this report in the [archive](#).

2020-12-18 changes since 2020-10-09:

- ▷ This report adds results for first algorithms from ten developers: BitCenter UK, CloudSmart Consulting, Cubox, Institute of Computing Technology, Naver Corp, Minivision, NSENSE Corp, Viettel Group, Visage Technologies, and Xiamen University. See Table 6 for more information.
- ▷ The report also includes results for eighteen developers who have previously submitted algorithms: ADVANCE.AI, Awidit Systems, Chosun University, Dermalog, GeoVision, ICM Airport Technics, Idemia, Institute of Information Technologies, Kakao Enterprise, Neurotechnology, Panasonic R+D Center Singapore, Rank One Computing, Sensetime Group, Shanghai Jiao Tong University, TigerIT Americas LLC, Vigilant Solutions, Winsense, and YooniK
- ▷ We have retired results for twelve algorithms per our policy to only list results for two algorithms per developer. Results for retired algorithms appear in prior versions of this report in the [archive](#).

Changes since September 18, 2020:

- ▷ This report adds results for first algorithms from five developers: Aigen, Cortica, Kookmin University, Securif AI and VinaI.
- ▷ The report also includes results for three developers who have previously submitted algorithms: Fujitsu Laboratories, Hengrui AI, and X-Forward AI.
- ▷ In the per-algorithm report-cards linked from tables and the main webpage, we have added a chart to showing reduction in error rates over the course of FRVT i.e. from 2017 onwards for all algorithms supplied by that developer. Similarly we have added a chart showing error rate reductions for our test of protective face mask verification.
- ▷ We plan to continue evaluating algorithms on various mask datasets. We hold that algorithms should be capable of detecting masks and verifying identity of all combinations of masked and unmasked faces. We have accordingly increased the amount of time allowed to extract those features from 1.0 to 1.5 seconds.

Changes since August 25, 2020:

- ▷ This report adds results for first algorithms from eight new developers. Akurat Satu Indonesia, Cybercore, Decatur Industries, Innef Labs, Satellite Innovation/Eocortex, Expasoft, and Mobai.
- ▷ The report includes results for seven developers who have previously submitted algorithms: 3Divi, BioID Technologies, Incode Technologies, Innovatrics, iSAP Solution, Synology, and Tevian.
- ▷ We have retired results for five algorithms per our policy to only list results for two algorithms per developer. Results for retired algorithms appear in prior versions of this report in the [archive](#).

Changes since July 27, 2020:

- ▷ We have introduced per-algorithm report sheets. These are HTML documents linked from the accuracy tables in this report (i.e. Table 24) and on the FRVT 1:1 [homepage](#). The sheets contain interactive graphics allowing, for example, mouseover exploration of FNMR(T) and FMR(T). Some of their content had previously appeared in this document.
- ▷ This report adds results for algorithms from six new developers. ACI Software, Bresee Technology, Fiberhome Telecommunication Technologies, Imageware Systems, Oz Forensics, and Pensees.
- ▷ The report includes results for thirteen developers who have previously submitted algorithms: Canon Information Technology (Beijing), Cyberlink, Dahua Technology, Gorilla Technology, ID3 Technology, Intel Research Group, iQIYI Inc, Momentum Digital, Netbridge Technology, Tech5 SA, Shenzhen AiMall Tech, Vigilant Solutions, and VisionLabs.
- ▷ We have retired results for nine algorithms per our policy to only list results for two algorithms per developer. Results for retired algorithms appear in prior versions of this report in the [archive](#).

Changes since May 18, 2020:

- ▷ The report is the first FRVT update since the pandemic closed it from March to June 2020.
- ▷ This report includes results for algorithms from nine new developers: GeoVision Inc, Su Zhou NaZhi-TianDi Intelligent Technology, YooniK, AYF Technology, PXL Vision AG, Yuan High-Tech Development, Beihang University-ERCACAT, ICM Airport Technics, and Staqu Technologies
- ▷ This report includes results for algorithms from 15 returning developers Acer Incorporated, Antheus Technologia, Chosun University, Chunghwa Telecom, Idemia, Moontime Smart Technology, Neurotechnology, Guangzhou Pixel Solutions, Panasonic R+D Center Singapore, Rank One Computing, Scanovate, Shanghai Universiy - Shanghai Film Academy, Synesis, Trueface.ai, and Veridas Digital Authentication Solutions
- ▷ We have retired results for ten algorithms per our policy to only list results for two algorithms per developer. Results for retired algorithms appear in prior versions of this report in the [archive](#).
- ▷ We separated timing and other resource consumption from the main participation table. The new Table 15 includes template generation durations for four kinds of images, not just mugshots.
- ▷ We have published a separate report, [NIST Interagency Report 8311](#) on accuracy of pre-pandemic algorithms on subjects wearing face masks. We plan to track improvements in accuracy on masked images going forward. In particular, we invite submission of algorithms that can detect whether a person is wearing a mask, extract features from the full face or the exposed periocular region, and do appropriate comparison. We do not intend to evaluate algorithms that assume 100% of images will be of masked individuals.

Changes since March 25, 2020:

- ▷ The report is a maintenance release - it does not add any new algorithms, and FRVT has been closed to new algorithms since mid March 2020.
- ▷ We modified the primary accuracy summary, Table 24, as follows:
 - ▷▷ For visa images, the column for FNMR at FMR = 0.0001 has been removed. The visa images are so highly controlled that the error rates for the most accurate algorithms are dominated by false rejection of very young children and by the presence of a few noisy greyscale images. For now, two visa columns remain: FNMR at $FMR = 10^{-6}$ and, for matched covariates, FNMR at $FMR = 10^{-4}$.
 - ▷▷ We have inserted a new column labelled "BORDER" giving accuracy for comparison of moderately poor webcam border-crossing photos that exhibit pose variations, poor compression, and low contrast due to strong background illumination. The accuracies are the worst from all cooperative image datasets used in FRVT.
- ▷ Accordingly, we updated the failure-to-template rates in Table 31.
- ▷ We withdrew a figure showing how false matches are concentrated in certain visa images used in cross-comparison, because it didn't attempt to include demographic information.

Changes since February 27, 2020:

- ▷ The report adds results algorithms from two new developers: Beijing Alleyes Technology, and the Chinese University of Hong Kong. Results for newly submitted algorithms from two other developers will appear in the next report.
- ▷ The report adds results for algorithms from thirteen returning developers: ASUSTek Computer, Aware, Cyberlink Corp, Gorilla Technology, Innovative Technology, Kakao Enterprise, Lomonosov Moscow State University, Panasonic R+D Center Singapore, Shenzhen AiMall Technology, Shenzhen Intellifusion Technologies, Synology, Tech5 SA, and Via Technologies.
- ▷ Per policy to only list results for two algorithms per developer, we have dropped results for algorithms from Aware, Cyberlink, Gorilla Technology, Kakao Enterprise, Lomonosov Moscow State University, Panasonic R+D Center Singapore, and Tech5 SA.

Changes since January 20, 2020:

- ▷ The report adds results for five new developers: Ability Enterprise (Andro Video), Chosun University, Fujitsu Research and Development Center, University of Coimbra, and Xforward AI Technology.
- ▷ The report adds results for algorithms from six returning developers: AlphaSSTG, Incode Technologies, Kneron, Shanghai Jiao Tong University, Vocord, and X-Laboratory.
- ▷ We have corrected template comparison timing numbers for algorithms submitted September 2019 to January 2020. The values reported previously were slower due to a software bug.
- ▷ We have dropped results for algorithms from Vocord and Incode per policy to only list results for two algorithms per developer.
- ▷ The [FRVT 1:1 homepage](#) has been updated with latest accuracy results.
- ▷ The [FRVT 1:N homepage](#) now includes an update to the September 2019 NIST Interagency Report 8271. The new report adds results for one-to-many search algorithms submitted to NIST from June 2019 to January 2020.

Changes since January 6, 2020:

- ▷ Section 2 has been updated to better describe the Visa and Border images. The caption for Table 24 has been updated to better relate the accuracy values to particular image comparisons.
- ▷ The report adds results for five new developers: Acer, Advance.AI, Expasoft, Netbridge Technology, and Videmo Intelligent Videoanalyse.
- ▷ The report adds results for algorithms from 7 returning developers: China Electronics Import-Export Corp, Intel Research Group, ITMO University, Neurotechnology, N-Tech Lab, Rokid, and VisionLabs.
- ▷ We have dropped results from this edition of the report per policy to only list results for two algorithms per developer: N-Tech Lab, Neurotechnology, ITMO, Visionlabs, and CEIEC.
- ▷ The [FRVT homepage](#) has been updated with latest accuracy results.

Changes since November 11, 2019:

- ▷ Table 15 has been updated to include runtime memory usage. This is the first time such a quantity has been reported. The value is the peak size of the resident set size logged during enrollment of single images.
- ▷ We have migrated summary results table to a new platform that supports sortable tables:
<https://pages.nist.gov/frvt/html/frvt11.html>
- ▷ The report adds results for four new developers: Antheus Technologia, BioID Technologies SA, Canon Information Tech. (Beijing), Samsung S1 (listed in the tables as S1), and Taiwan AI Labs.
- ▷ The report adds results for algorithms from 13 returning developers: Anke Investments, Chunghwa Telecom, Deepglint, Institute of Information Technologies, iQIYI, Kneron, Ping An Technology, Paravision, KanKan Ai, Rokid Corporation, Shanghai Universiy - Shanghai Film Academy, Veridas Digital Authentication Solutions, and Videonetics Technology.
- ▷ We have dropped results from this edition of the report per policy to only list results for two algorithms per developer: remarkai-000, veridas-001, sensetime-001, iit-000, anke-003, and everai-002. Results for these are available in prior editions of this report linked from the FRVT page.
- ▷ We issued [NIST Interagency Report 8280: FRVT Part 3: Demographics](#) on 2019-12-19. It includes results for many of the algorithms covered by this report.

Changes since October 16, 2019:

- ▷ The report adds results for ten new developers: Ai-Union Technology, ASUSTek Computer, DiDi ChuXing Technology, Innovative Technology, Luxand, MVision, Pyramid Cyber Security + Forensic, Scanovate, Shenzhen AiMall Tech, and TUPU Technology.
- ▷ The report adds results for 12 returning developers: CTBC Bank Glory Gorilla Technology Guangzhou Pixel Solutions Imagus Technology Incode Technologies Lomonosov Moscow State University Rank One Computing Samtech InfoNet Shanghai Ulucu Electronics Technology Synesis, and Winsense.
- ▷ We have dropped results from this edition of the report per policy to only list results for two algorithms per developer: glory-000, gorilla-002, incode-003, rankone-006, and synesis-004.
- ▷ Results for five recently submitted algorithms will appear in the next report.

Changes since September 11, 2019:

- ▷ The report adds results for five new participants: Awidit Systems (Awiros), Momenmtum Digital (Sertis), Trueface AI, Shanghai Jiao Tong University, and X-Laboratory.
- ▷ The reports adds results for five new algorithms from returning developers: Cyberlink, Hengrui AI Technology, Idemia, Panasonic R+D Singapore, and Tevian. This causes three algorithm, to be de-listed from the report per policy to list results for two algorithms per developer.

Changes since July 31 2019:

- ▷ The HTML table on the [FRVT 1:1 homepage](#) has been updated to include a column for cross-domain Visa-Border verification. Results for this new dataset appeared in the July 29 report under the name "CrossEV" - these are now renamed "Visa-Border".
- ▷ The [FRVT 1:1 homepage](#) lists algorithms according to lowest mean rank accuracy:

$$\begin{aligned} &\text{Rank(FNMR}_{\text{VISA}} \text{ at FMR = 0.000001}) + \\ &\text{Rank(FNMR}_{\text{VISA-BORDER}} \text{ at FMR = 0.000001}) + \\ &\text{Rank(FNMR}_{\text{MUGSHOT}} \text{ at FMR = 0.00001 after 14 years}) + \\ &\text{Rank(FNMR}_{\text{WILD}} \text{ at FMR = 0.00001}) \end{aligned}$$

This ordering rewards high accuracy across all datasets.
- ▷ The main results in Table 24 is now in landscape format to accomodate extra columns for the Visa-Border set, and mugshot comparisons after at least 12 years.
- ▷ The report adds results for nine new participants: Alpha SSTG, Intel Research, ULSee, Chungwa Telecon, iSAP Solution, Rokid, Shenzhen EI Networks, CSA Intellilcloud, Shenzhen Intellifusion Technologies.
- ▷ The reports adds results for six new algorithms from returning developers: Innovatrics, Dahua Technology, Tech5 SA, Intellivision, Nodeflux and Imperial College, London. One algorithm, from Imperial has been retired, per policy to list results for two algorithms per developer.
- ▷ The cross-country false match rate heatmaps have been replotted to reveal more structure by listing countries by region instead of alphabetically.
- ▷ The next version of this report will be posted around October 18, 2019.

Changes since July 3 2019:

- ▷ The HTML table on the [FRVT 1:1 homepage](#) has been updated to list the 20 most accurate developers rather than algorithms, choosing the most accurate algorithm from each developer based on visa and mugshot results. Also, the algorithms are ordered in terms of lowest mean rank across mugshot, visa and wild datasets, rewarding broad accuracy over a good result on one particular dataset.
- ▷ This report includes results for a new dataset - see the column labelled "visa-border" in Table 5. It compares a new set of high quality visa-like portraits with a set webcam border-crossing photos that exhibit moderately poor pose variations and background illumination. The two new sets are described in sections 2.2 and 2.3. The comparisons are "cross-domain" in that the algorithm must compare "visa" and "wild" images. Results for other algorithms will be added in future reports as they become available.
- ▷ This report adds results for algorithms from 9 developers submitted in early July 2019. These are from 3DiVi, Camvi, EverAI-Paravision, Facesoft, Farbar (F8), Institute of Information Technologies, Shanghai U. Film Academy, Via Technologies, and Ulucu Electronics Tech. Six of these are new participants.
- ▷ Several other algorithms have been submitted and are being evaluated. Results will be released in the next report, scheduled for September 5. That report will include results for new datasets.

- ▷ Older algorithms from Everai, Camvi and 3DiVi, have been retired, per the policy to list only two algorithms per developer.

Changes since June 2019:

- ▷ This report adds results for algorithms from 18 developers submitted in early June 2019. These are from CTBC Bank, Deep Glint, Thales Cogent, Ever AI Paravision, Gorilla Technology, Imagus, Incode, Kneron, N-Tech Lab, Neurotechnology, Notiontag Technologies, Star Hybrid, Videonetics, Vigilant Solutions, Winsense, Anke Investments, CEIEC, and DSK. Nine of these are new participants.
- ▷ Several other algorithms have been submitted and are being evaluated. Results will be released in the next report, scheduled for August 1.
- ▷ Older algorithms from Everai, Thales Cogent, Gorilla Technology, Incode, Neurotechnology, N-Tech Lab and Vigilant Solutions have been retired, per the policy to list only two algorithms per developer.

Changes since April 2019:

- ▷ This report adds results for nine algorithms from nine developers submitted in early June 2019. These are from Tencent Deepsea, Hengrui, Kedacom, Moontime, Guangzhou Pixel, Rank One Computing, Synesis, Sensetime and Vocord.
- ▷ Another 23 algorithms have been submitted and are being evaluated. Results will be released in the next report, scheduled for July 3.
- ▷ Older algorithms for Rank One, Synesis, and Vocord have been retired, per the policy to list only two algorithms per developer.

Changes since February 2019:

- ▷ This report adds results for 49 algorithms from 42 developers submitted in early March 2019.
- ▷ This report omits results for algorithms that we retired. We retired for three reasons: 1. The developer submitted a new algorithm, and we only list two. 2. The algorithm needs a GPU, and we no longer allow GPU-based algorithms. 3. Inoperable algorithms.
- ▷ Previous results for retired algorithms are available in older editions of this report linked [here](#).
- ▷ The mugshot database used from February 2017 to January 2019 has been replaced with an extract of the mugshot database documented in NIST Interagency Report 8238, November 2018. The new mugshot set is described in section [2.4](#) and is adopted because:
 - ▷▷ It has much better identity label integrity, so that false non-match rates are substantially lower than those reported in FRVT 1:1 reports to date - see Figure [76](#).
 - ▷▷ It includes images collected over a 17 year period such that ageing can be much better characterized - - see Figure [273](#).
- ▷ Using the new mugshot database, Figure [273](#) shows accuracy for four demographic groups identified in the biographic metadata that accompanies the data: black females, black males, white females and white males.
- ▷ The report adds Figure [19](#) with results for the twenty human-difficult pairs used in the May 2018 paper *Face recognition accuracy of forensic examiners, superrecognizers, and face recognition algorithms* by Phillips et al. [\[1\]](#).
- ▷ The report uses an update to the wild image database that corrects some ground truth labels.
- ▷ Some results for the child exploitation database are not complete. They are typically updated less frequently than for other image sets.

Contents

ACKNOWLEDGMENTS	1
DISCLAIMER	1
INSTITUTIONAL REVIEW BOARD	1
1 METRICS	44
1.1 CORE ACCURACY	44
2 DATASETS	45
2.1 VISA IMAGES	45
2.2 APPLICATION IMAGES	45
2.3 BORDER CROSSING IMAGES	45
2.4 MUGSHOT IMAGES	46
2.5 WILD IMAGES	46
3 RESULTS	46
3.1 TEST GOALS	46
3.2 TEST DESIGN	47
3.3 FAILURE TO ENROLL	50
3.4 RECOGNITION ACCURACY	57
3.5 GENUINE DISTRIBUTION STABILITY	274
3.5.1 EFFECT OF BIRTH PLACE ON THE GENUINE DISTRIBUTION	274
3.5.2 EFFECT OF AGEING	306
3.5.3 EFFECT OF AGE ON GENUINE SUBJECTS	330
3.6 IMPOSTOR DISTRIBUTION STABILITY	364
3.6.1 EFFECT OF BIRTH PLACE ON THE IMPOSTOR DISTRIBUTION	364
3.6.2 EFFECT OF AGE ON IMPOSTORS	368

List of Tables

1 PARTICIPANT INFORMATION	18
2 PARTICIPANT INFORMATION	19
3 PARTICIPANT INFORMATION	20
4 PARTICIPANT INFORMATION	21
5 PARTICIPANT INFORMATION	22
6 PARTICIPANT INFORMATION	23
7 ALGORITHM SUMMARY	24
8 ALGORITHM SUMMARY	25
9 ALGORITHM SUMMARY	26
10 ALGORITHM SUMMARY	27
11 ALGORITHM SUMMARY	28
12 ALGORITHM SUMMARY	29
13 ALGORITHM SUMMARY	30
14 ALGORITHM SUMMARY	31
15 ALGORITHM SUMMARY	32
16 FALSE NON-MATCH RATE	33
17 FALSE NON-MATCH RATE	34
18 FALSE NON-MATCH RATE	35
19 FALSE NON-MATCH RATE	36
20 FALSE NON-MATCH RATE	37
21 FALSE NON-MATCH RATE	38

22	FALSE NON-MATCH RATE	39
23	FALSE NON-MATCH RATE	40
24	FALSE NON-MATCH RATE	41
25	FAILURE TO ENROL RATES	50
26	FAILURE TO ENROL RATES	51
27	FAILURE TO ENROL RATES	52
28	FAILURE TO ENROL RATES	53
29	FAILURE TO ENROL RATES	54
30	FAILURE TO ENROL RATES	55
31	FAILURE TO ENROL RATES	56

List of Figures

1	PERFORMANCE SUMMARY: FNMR VS. TEMPLATE SIZE TRADEOFF	42
2	PERFORMANCE SUMMARY: FNMR VS. TEMPLATE TIME TRADEOFF	43
3	EXAMPLE IMAGES	47
(A)	VISA	47
(B)	MUGSHOT	47
(C)	WILD	47
(D)	BORDER	47
4	PERFORMANCE ON 20 HUMAN-DIFFICULT PAIRS	58
5	PERFORMANCE ON 20 HUMAN-DIFFICULT PAIRS	59
6	PERFORMANCE ON 20 HUMAN-DIFFICULT PAIRS	60
7	PERFORMANCE ON 20 HUMAN-DIFFICULT PAIRS	61
8	PERFORMANCE ON 20 HUMAN-DIFFICULT PAIRS	62
9	PERFORMANCE ON 20 HUMAN-DIFFICULT PAIRS	63
10	PERFORMANCE ON 20 HUMAN-DIFFICULT PAIRS	64
11	PERFORMANCE ON 20 HUMAN-DIFFICULT PAIRS	65
12	PERFORMANCE ON 20 HUMAN-DIFFICULT PAIRS	66
13	PERFORMANCE ON 20 HUMAN-DIFFICULT PAIRS	67
14	PERFORMANCE ON 20 HUMAN-DIFFICULT PAIRS	68
15	PERFORMANCE ON 20 HUMAN-DIFFICULT PAIRS	69
16	PERFORMANCE ON 20 HUMAN-DIFFICULT PAIRS	70
17	PERFORMANCE ON 20 HUMAN-DIFFICULT PAIRS	71
18	PERFORMANCE ON 20 HUMAN-DIFFICULT PAIRS	72
19	PERFORMANCE ON 20 HUMAN-DIFFICULT PAIRS	73
20	ERROR TRADEOFF CHARACTERISTIC: VISA IMAGES	74
21	ERROR TRADEOFF CHARACTERISTIC: VISA IMAGES	75
22	ERROR TRADEOFF CHARACTERISTIC: VISA IMAGES	76
23	ERROR TRADEOFF CHARACTERISTIC: VISA IMAGES	77
24	ERROR TRADEOFF CHARACTERISTIC: VISA IMAGES	78
25	ERROR TRADEOFF CHARACTERISTIC: VISA IMAGES	79
26	ERROR TRADEOFF CHARACTERISTIC: VISA IMAGES	80
27	ERROR TRADEOFF CHARACTERISTIC: VISA IMAGES	81
28	ERROR TRADEOFF CHARACTERISTIC: VISA IMAGES	82
29	ERROR TRADEOFF CHARACTERISTIC: VISA IMAGES	83
30	ERROR TRADEOFF CHARACTERISTIC: VISA IMAGES	84
31	ERROR TRADEOFF CHARACTERISTIC: VISA IMAGES	85
32	ERROR TRADEOFF CHARACTERISTIC: VISA IMAGES	86
33	ERROR TRADEOFF CHARACTERISTIC: VISA IMAGES	87
34	ERROR TRADEOFF CHARACTERISTIC: VISA IMAGES	88
35	ERROR TRADEOFF CHARACTERISTIC: VISA IMAGES	89
36	ERROR TRADEOFF CHARACTERISTIC: VISA IMAGES	90
37	ERROR TRADEOFF CHARACTERISTIC: VISA IMAGES	91
38	ERROR TRADEOFF CHARACTERISTIC: VISA IMAGES	92

39	ERROR TRADEOFF CHARACTERISTIC: VISA IMAGES	93
40	ERROR TRADEOFF CHARACTERISTIC: VISA IMAGES	94
41	ERROR TRADEOFF CHARACTERISTIC: VISA IMAGES	95
42	ERROR TRADEOFF CHARACTERISTIC: VISA IMAGES	96
43	ERROR TRADEOFF CHARACTERISTIC: VISA IMAGES	97
44	ERROR TRADEOFF CHARACTERISTIC: VISA IMAGES	98
45	ERROR TRADEOFF CHARACTERISTIC: VISA IMAGES	99
46	ERROR TRADEOFF CHARACTERISTIC: VISA IMAGES	100
47	ERROR TRADEOFF CHARACTERISTIC: VISA IMAGES	101
48	ERROR TRADEOFF CHARACTERISTIC: VISA IMAGES	102
49	ERROR TRADEOFF CHARACTERISTIC: VISA IMAGES	103
50	ERROR TRADEOFF CHARACTERISTIC: VISA IMAGES	104
51	ERROR TRADEOFF CHARACTERISTIC: VISA IMAGES	105
52	ERROR TRADEOFF CHARACTERISTIC: VISA IMAGES	106
53	ERROR TRADEOFF CHARACTERISTIC: VISA IMAGES	107
54	ERROR TRADEOFF CHARACTERISTIC: VISA IMAGES	108
55	ERROR TRADEOFF CHARACTERISTIC: VISA IMAGES	109
56	ERROR TRADEOFF CHARACTERISTIC: VISA IMAGES	110
57	ERROR TRADEOFF CHARACTERISTIC: VISA IMAGES	111
58	ERROR TRADEOFF CHARACTERISTIC: MUGSHOT IMAGES	112
59	ERROR TRADEOFF CHARACTERISTIC: MUGSHOT IMAGES	113
60	ERROR TRADEOFF CHARACTERISTIC: MUGSHOT IMAGES	114
61	ERROR TRADEOFF CHARACTERISTIC: MUGSHOT IMAGES	115
62	ERROR TRADEOFF CHARACTERISTIC: MUGSHOT IMAGES	116
63	ERROR TRADEOFF CHARACTERISTIC: MUGSHOT IMAGES	117
64	ERROR TRADEOFF CHARACTERISTIC: MUGSHOT IMAGES	118
65	ERROR TRADEOFF CHARACTERISTIC: MUGSHOT IMAGES	119
66	ERROR TRADEOFF CHARACTERISTIC: MUGSHOT IMAGES	120
67	ERROR TRADEOFF CHARACTERISTIC: MUGSHOT IMAGES	121
68	ERROR TRADEOFF CHARACTERISTIC: MUGSHOT IMAGES	122
69	ERROR TRADEOFF CHARACTERISTIC: MUGSHOT IMAGES	123
70	ERROR TRADEOFF CHARACTERISTIC: MUGSHOT IMAGES	124
71	ERROR TRADEOFF CHARACTERISTIC: MUGSHOT IMAGES	125
72	ERROR TRADEOFF CHARACTERISTIC: MUGSHOT IMAGES	126
73	ERROR TRADEOFF CHARACTERISTIC: MUGSHOT IMAGES	127
74	ERROR TRADEOFF CHARACTERISTIC: MUGSHOT IMAGES	128
75	ERROR TRADEOFF CHARACTERISTIC: MUGSHOT IMAGES	129
76	ERROR TRADEOFF CHARACTERISTIC: MUGSHOT IMAGES	130
77	ERROR TRADEOFF CHARACTERISTIC: WILD IMAGES	131
78	ERROR TRADEOFF CHARACTERISTIC: WILD IMAGES	132
79	ERROR TRADEOFF CHARACTERISTIC: WILD IMAGES	133
80	ERROR TRADEOFF CHARACTERISTIC: WILD IMAGES	134
81	ERROR TRADEOFF CHARACTERISTIC: WILD IMAGES	135
82	ERROR TRADEOFF CHARACTERISTIC: WILD IMAGES	136
83	ERROR TRADEOFF CHARACTERISTIC: WILD IMAGES	137
84	ERROR TRADEOFF CHARACTERISTIC: WILD IMAGES	138
85	ERROR TRADEOFF CHARACTERISTIC: WILD IMAGES	139
86	ERROR TRADEOFF CHARACTERISTIC: WILD IMAGES	140
87	ERROR TRADEOFF CHARACTERISTIC: WILD IMAGES	141
88	ERROR TRADEOFF CHARACTERISTIC: WILD IMAGES	142
89	ERROR TRADEOFF CHARACTERISTIC: WILD IMAGES	143
90	ERROR TRADEOFF CHARACTERISTIC: WILD IMAGES	144
91	ERROR TRADEOFF CHARACTERISTIC: WILD IMAGES	145
92	ERROR TRADEOFF CHARACTERISTIC: WILD IMAGES	146
93	FALSE MATCH RATES WITHIN AND ACROSS DEMOGRAPHIC GROUPS	147
94	FALSE MATCH RATES WITHIN AND ACROSS DEMOGRAPHIC GROUPS	148
95	FALSE MATCH RATES WITHIN AND ACROSS DEMOGRAPHIC GROUPS	149

96	FALSE MATCH RATES WITHIN AND ACROSS DEMOGRAPHIC GROUPS	150
97	FALSE MATCH RATES WITHIN AND ACROSS DEMOGRAPHIC GROUPS	151
98	FALSE MATCH RATES WITHIN AND ACROSS DEMOGRAPHIC GROUPS	152
99	FALSE MATCH RATES WITHIN AND ACROSS DEMOGRAPHIC GROUPS	153
100	FALSE MATCH RATES WITHIN AND ACROSS DEMOGRAPHIC GROUPS	154
101	FALSE MATCH RATES WITHIN AND ACROSS DEMOGRAPHIC GROUPS	155
102	FALSE MATCH RATES WITHIN AND ACROSS DEMOGRAPHIC GROUPS	156
103	FALSE MATCH RATES WITHIN AND ACROSS DEMOGRAPHIC GROUPS	157
104	FALSE MATCH RATES WITHIN AND ACROSS DEMOGRAPHIC GROUPS	158
105	FALSE MATCH RATES WITHIN AND ACROSS DEMOGRAPHIC GROUPS	159
106	FALSE MATCH RATES WITHIN AND ACROSS DEMOGRAPHIC GROUPS	160
107	FALSE MATCH RATES WITHIN AND ACROSS DEMOGRAPHIC GROUPS	161
108	FALSE MATCH RATES WITHIN AND ACROSS DEMOGRAPHIC GROUPS	162
109	FALSE MATCH RATES WITHIN AND ACROSS DEMOGRAPHIC GROUPS	163
110	FALSE MATCH RATES WITHIN AND ACROSS DEMOGRAPHIC GROUPS	164
111	FALSE MATCH RATES WITHIN AND ACROSS DEMOGRAPHIC GROUPS	165
112	SEX AND RACE EFFECTS: MUGSHOT IMAGES	166
113	SEX AND RACE EFFECTS: MUGSHOT IMAGES	167
114	SEX AND RACE EFFECTS: MUGSHOT IMAGES	168
115	SEX AND RACE EFFECTS: MUGSHOT IMAGES	169
116	SEX AND RACE EFFECTS: MUGSHOT IMAGES	170
117	SEX AND RACE EFFECTS: MUGSHOT IMAGES	171
118	SEX AND RACE EFFECTS: MUGSHOT IMAGES	172
119	SEX AND RACE EFFECTS: MUGSHOT IMAGES	173
120	SEX AND RACE EFFECTS: MUGSHOT IMAGES	174
121	SEX AND RACE EFFECTS: MUGSHOT IMAGES	175
122	SEX AND RACE EFFECTS: MUGSHOT IMAGES	176
123	SEX AND RACE EFFECTS: MUGSHOT IMAGES	177
124	SEX AND RACE EFFECTS: MUGSHOT IMAGES	178
125	SEX AND RACE EFFECTS: MUGSHOT IMAGES	179
126	SEX AND RACE EFFECTS: MUGSHOT IMAGES	180
127	SEX AND RACE EFFECTS: MUGSHOT IMAGES	181
128	SEX AND RACE EFFECTS: MUGSHOT IMAGES	182
129	SEX AND RACE EFFECTS: MUGSHOT IMAGES	183
130	SEX AND RACE EFFECTS: MUGSHOT IMAGES	184
131	SEX EFFECTS: VISA IMAGES	185
132	SEX EFFECTS: VISA IMAGES	186
133	SEX EFFECTS: VISA IMAGES	187
134	SEX EFFECTS: VISA IMAGES	188
135	SEX EFFECTS: VISA IMAGES	189
136	SEX EFFECTS: VISA IMAGES	190
137	SEX EFFECTS: VISA IMAGES	191
138	SEX EFFECTS: VISA IMAGES	192
139	SEX EFFECTS: VISA IMAGES	193
140	SEX EFFECTS: VISA IMAGES	194
141	SEX EFFECTS: VISA IMAGES	195
142	SEX EFFECTS: VISA IMAGES	196
143	SEX EFFECTS: VISA IMAGES	197
144	SEX EFFECTS: VISA IMAGES	198
145	SEX EFFECTS: VISA IMAGES	199
146	SEX EFFECTS: VISA IMAGES	200
147	SEX EFFECTS: VISA IMAGES	201
148	SEX EFFECTS: VISA IMAGES	202
149	SEX EFFECTS: VISA IMAGES	203
150	SEX EFFECTS: VISA IMAGES	204
151	SEX EFFECTS: VISA IMAGES	205
152	SEX EFFECTS: VISA IMAGES	206

153 SEX EFFECTS: VISA IMAGES	207
154 SEX EFFECTS: VISA IMAGES	208
155 SEX EFFECTS: VISA IMAGES	209
156 SEX EFFECTS: VISA IMAGES	210
157 SEX EFFECTS: VISA IMAGES	211
158 SEX EFFECTS: VISA IMAGES	212
159 SEX EFFECTS: VISA IMAGES	213
160 SEX EFFECTS: VISA IMAGES	214
161 SEX EFFECTS: VISA IMAGES	215
162 SEX EFFECTS: VISA IMAGES	216
163 FALSE MATCH RATE CALIBRATION: MUGSHOT IMAGES	217
164 FALSE MATCH RATE CALIBRATION: MUGSHOT IMAGES	218
165 FALSE MATCH RATE CALIBRATION: MUGSHOT IMAGES	219
166 FALSE MATCH RATE CALIBRATION: MUGSHOT IMAGES	220
167 FALSE MATCH RATE CALIBRATION: MUGSHOT IMAGES	221
168 FALSE MATCH RATE CALIBRATION: MUGSHOT IMAGES	222
169 FALSE MATCH RATE CALIBRATION: MUGSHOT IMAGES	223
170 FALSE MATCH RATE CALIBRATION: MUGSHOT IMAGES	224
171 FALSE MATCH RATE CALIBRATION: MUGSHOT IMAGES	225
172 FALSE MATCH RATE CALIBRATION: MUGSHOT IMAGES	226
173 FALSE MATCH RATE CALIBRATION: MUGSHOT IMAGES	227
174 FALSE MATCH RATE CALIBRATION: MUGSHOT IMAGES	228
175 FALSE MATCH RATE CALIBRATION: MUGSHOT IMAGES	229
176 FALSE MATCH RATE CALIBRATION: MUGSHOT IMAGES	230
177 FALSE MATCH RATE CALIBRATION: MUGSHOT IMAGES	231
178 FALSE MATCH RATE CALIBRATION: MUGSHOT IMAGES	232
179 FALSE MATCH RATE CALIBRATION: MUGSHOT IMAGES	233
180 FALSE MATCH RATE CALIBRATION: MUGSHOT IMAGES	234
181 FALSE MATCH RATE CALIBRATION: MUGSHOT IMAGES	235
182 FALSE MATCH RATE CALIBRATION: VISA IMAGES	236
183 FALSE MATCH RATE CALIBRATION: VISA IMAGES	237
184 FALSE MATCH RATE CALIBRATION: VISA IMAGES	238
185 FALSE MATCH RATE CALIBRATION: VISA IMAGES	239
186 FALSE MATCH RATE CALIBRATION: VISA IMAGES	240
187 FALSE MATCH RATE CALIBRATION: VISA IMAGES	241
188 FALSE MATCH RATE CALIBRATION: VISA IMAGES	242
189 FALSE MATCH RATE CALIBRATION: VISA IMAGES	243
190 FALSE MATCH RATE CALIBRATION: VISA IMAGES	244
191 FALSE MATCH RATE CALIBRATION: VISA IMAGES	245
192 FALSE MATCH RATE CALIBRATION: VISA IMAGES	246
193 FALSE MATCH RATE CALIBRATION: VISA IMAGES	247
194 FALSE MATCH RATE CALIBRATION: VISA IMAGES	248
195 FALSE MATCH RATE CALIBRATION: VISA IMAGES	249
196 FALSE MATCH RATE CALIBRATION: VISA IMAGES	250
197 FALSE MATCH RATE CALIBRATION: VISA IMAGES	251
198 FALSE MATCH RATE CALIBRATION: VISA IMAGES	252
199 FALSE MATCH RATE CALIBRATION: VISA IMAGES	253
200 FALSE MATCH RATE CALIBRATION: VISA IMAGES	254
201 FALSE MATCH RATE CALIBRATION: VISA IMAGES	255
202 FALSE MATCH RATE CALIBRATION: VISA IMAGES	256
203 FALSE MATCH RATE CALIBRATION: VISA IMAGES	257
204 FALSE MATCH RATE CALIBRATION: VISA IMAGES	258
205 FALSE MATCH RATE CALIBRATION: VISA IMAGES	259
206 FALSE MATCH RATE CALIBRATION: VISA IMAGES	260
207 FALSE MATCH RATE CALIBRATION: VISA IMAGES	261
208 FALSE MATCH RATE CALIBRATION: VISA IMAGES	262
209 FALSE MATCH RATE CALIBRATION: VISA IMAGES	263

210	FALSE MATCH RATE CALIBRATION: VISA IMAGES	264
211	FALSE MATCH RATE CALIBRATION: VISA IMAGES	265
212	FALSE MATCH RATE CALIBRATION: VISA IMAGES	266
213	FALSE MATCH RATE CALIBRATION: VISA IMAGES	267
214	FALSE MATCH RATE CALIBRATION: VISA IMAGES	268
215	FALSE MATCH RATE CALIBRATION: VISA IMAGES	269
216	FALSE MATCH RATE CALIBRATION: VISA IMAGES	270
217	FALSE MATCH RATE CALIBRATION: VISA IMAGES	271
218	FALSE MATCH RATE CALIBRATION: VISA IMAGES	272
219	FALSE MATCH RATE CALIBRATION: VISA IMAGES	273
220	EFFECT OF COUNTRY OF BIRTH ON FNMR	275
221	EFFECT OF COUNTRY OF BIRTH ON FNMR	276
222	EFFECT OF COUNTRY OF BIRTH ON FNMR	277
223	EFFECT OF COUNTRY OF BIRTH ON FNMR	278
224	EFFECT OF COUNTRY OF BIRTH ON FNMR	279
225	EFFECT OF COUNTRY OF BIRTH ON FNMR	280
226	EFFECT OF COUNTRY OF BIRTH ON FNMR	281
227	EFFECT OF COUNTRY OF BIRTH ON FNMR	282
228	EFFECT OF COUNTRY OF BIRTH ON FNMR	283
229	EFFECT OF COUNTRY OF BIRTH ON FNMR	284
230	EFFECT OF COUNTRY OF BIRTH ON FNMR	285
231	EFFECT OF COUNTRY OF BIRTH ON FNMR	286
232	EFFECT OF COUNTRY OF BIRTH ON FNMR	287
233	EFFECT OF COUNTRY OF BIRTH ON FNMR	288
234	EFFECT OF COUNTRY OF BIRTH ON FNMR	289
235	EFFECT OF COUNTRY OF BIRTH ON FNMR	290
236	EFFECT OF COUNTRY OF BIRTH ON FNMR	291
237	EFFECT OF COUNTRY OF BIRTH ON FNMR	292
238	EFFECT OF COUNTRY OF BIRTH ON FNMR	293
239	EFFECT OF COUNTRY OF BIRTH ON FNMR	294
240	EFFECT OF COUNTRY OF BIRTH ON FNMR	295
241	EFFECT OF COUNTRY OF BIRTH ON FNMR	296
242	EFFECT OF COUNTRY OF BIRTH ON FNMR	297
243	EFFECT OF COUNTRY OF BIRTH ON FNMR	298
244	EFFECT OF COUNTRY OF BIRTH ON FNMR	299
245	EFFECT OF COUNTRY OF BIRTH ON FNMR	300
246	EFFECT OF COUNTRY OF BIRTH ON FNMR	301
247	EFFECT OF COUNTRY OF BIRTH ON FNMR	302
248	EFFECT OF COUNTRY OF BIRTH ON FNMR	303
249	EFFECT OF COUNTRY OF BIRTH ON FNMR	304
250	EFFECT OF COUNTRY OF BIRTH ON FNMR	305
251	ERROR TRADEOFF CHARACTERISTIC: MUGSHOT IMAGES	307
252	ERROR TRADEOFF CHARACTERISTIC: MUGSHOT IMAGES	308
253	ERROR TRADEOFF CHARACTERISTIC: MUGSHOT IMAGES	309
254	ERROR TRADEOFF CHARACTERISTIC: MUGSHOT IMAGES	310
255	ERROR TRADEOFF CHARACTERISTIC: MUGSHOT IMAGES	311
256	ERROR TRADEOFF CHARACTERISTIC: MUGSHOT IMAGES	312
257	ERROR TRADEOFF CHARACTERISTIC: MUGSHOT IMAGES	313
258	ERROR TRADEOFF CHARACTERISTIC: MUGSHOT IMAGES	314
259	ERROR TRADEOFF CHARACTERISTIC: MUGSHOT IMAGES	315
260	ERROR TRADEOFF CHARACTERISTIC: MUGSHOT IMAGES	316
261	ERROR TRADEOFF CHARACTERISTIC: MUGSHOT IMAGES	317
262	ERROR TRADEOFF CHARACTERISTIC: MUGSHOT IMAGES	318
263	ERROR TRADEOFF CHARACTERISTIC: MUGSHOT IMAGES	319
264	ERROR TRADEOFF CHARACTERISTIC: MUGSHOT IMAGES	320
265	ERROR TRADEOFF CHARACTERISTIC: MUGSHOT IMAGES	321
266	ERROR TRADEOFF CHARACTERISTIC: MUGSHOT IMAGES	322

267	ERROR TRADEOFF CHARACTERISTIC: MUGSHOT IMAGES	323
268	ERROR TRADEOFF CHARACTERISTIC: MUGSHOT IMAGES	324
269	ERROR TRADEOFF CHARACTERISTIC: MUGSHOT IMAGES	325
270	ERROR TRADEOFF CHARACTERISTIC: MUGSHOT IMAGES	326
271	ERROR TRADEOFF CHARACTERISTIC: MUGSHOT IMAGES	327
272	ERROR TRADEOFF CHARACTERISTIC: MUGSHOT IMAGES	328
273	ERROR TRADEOFF CHARACTERISTIC: MUGSHOT IMAGES	329
274	EFFECT OF SUBJECT AGE ON FNMR	331
275	EFFECT OF SUBJECT AGE ON FNMR	332
276	EFFECT OF SUBJECT AGE ON FNMR	333
277	EFFECT OF SUBJECT AGE ON FNMR	334
278	EFFECT OF SUBJECT AGE ON FNMR	335
279	EFFECT OF SUBJECT AGE ON FNMR	336
280	EFFECT OF SUBJECT AGE ON FNMR	337
281	EFFECT OF SUBJECT AGE ON FNMR	338
282	EFFECT OF SUBJECT AGE ON FNMR	339
283	EFFECT OF SUBJECT AGE ON FNMR	340
284	EFFECT OF SUBJECT AGE ON FNMR	341
285	EFFECT OF SUBJECT AGE ON FNMR	342
286	EFFECT OF SUBJECT AGE ON FNMR	343
287	EFFECT OF SUBJECT AGE ON FNMR	344
288	EFFECT OF SUBJECT AGE ON FNMR	345
289	EFFECT OF SUBJECT AGE ON FNMR	346
290	EFFECT OF SUBJECT AGE ON FNMR	347
291	EFFECT OF SUBJECT AGE ON FNMR	348
292	EFFECT OF SUBJECT AGE ON FNMR	349
293	EFFECT OF SUBJECT AGE ON FNMR	350
294	EFFECT OF SUBJECT AGE ON FNMR	351
295	EFFECT OF SUBJECT AGE ON FNMR	352
296	EFFECT OF SUBJECT AGE ON FNMR	353
297	EFFECT OF SUBJECT AGE ON FNMR	354
298	EFFECT OF SUBJECT AGE ON FNMR	355
299	EFFECT OF SUBJECT AGE ON FNMR	356
300	EFFECT OF SUBJECT AGE ON FNMR	357
301	EFFECT OF SUBJECT AGE ON FNMR	358
302	EFFECT OF SUBJECT AGE ON FNMR	359
303	EFFECT OF SUBJECT AGE ON FNMR	360
304	EFFECT OF SUBJECT AGE ON FNMR	361
305	EFFECT OF SUBJECT AGE ON FNMR	362
306	WORST CASE REGIONAL EFFECT FNMR	365
307	IMPOSTOR DISTRIBUTION SHIFTS FOR SELECT COUNTRY PAIRS	367

	Location	Developer Name	Short Name	Seq. Num.	Validation Date
1	NL	20Face	20face-000	000	2021-04-12
2	NL	20Face	20face-001	001	2021-09-29
3	US	3Divi	3divi-006	006	2021-04-14
4	US	3Divi	3divi-007	007	2021-09-27
5	TH	ACI Software	acisw-003	003	2020-08-03
6	TH	ACI Software	acisw-007	007	2021-11-15
7	SG	ADVANCE.AI	advance-002	002	2019-12-19
8	SG	ADVANCE.AI	advance-003	003	2021-08-05
9	TW	ASUSTek Computer Inc	asusaics-000	000	2019-10-24
10	TW	ASUSTek Computer Inc	asusaics-001	001	2020-02-25
11	CN	AYF Technology	ayftech-001	001	2020-07-06
12	TW	Ability Enterprise - Andro Video	androvideo-000	000	2021-01-25
13	TW	Acer Incorporated	acer-001	001	2020-06-30
14	TW	Acer Incorporated	acer-002	002	2021-11-10
15	SG	Adera Global PTE	adera-002	002	2021-02-16
16	SG	Adera Global PTE	adera-003	003	2021-07-12
17	TH	Ai First	aifirst-001	001	2019-11-21
18	TW	AiUnion Technology	aiunionface-000	000	2019-10-22
19	TH	Aigen	aigen-001	001	2020-10-06
20	TH	Aigen	aigen-002	002	2021-03-15
21	KR	Ajou University	ajou-001	001	2021-03-08
22	ID	Akurat Satu Indonesia	ptakuratsatu-000	000	2020-09-11
23	KR	Alchera Inc	alchera-002	002	2021-03-05
24	KR	Alchera Inc	alchera-003	003	2021-07-13
25	ID	Alfabeta	alfabeta-001	001	2021-12-02
26	ES	Alice Biometrics	alice-000	000	2021-06-15
27	RU	Alivia / Innovation Sys	isystems-001	001	2018-06-12
28	RU	Alivia / Innovation Sys	isystems-002	002	2018-10-18
29	IN	AllGoVision	allgovision-000	000	2019-03-01
30	CN	AlphaSSTG	alphaface-001	001	2019-09-03
31	CN	AlphaSSTG	alphaface-002	002	2020-02-20
32	GB	Amplified Group	amplifiedgroup-001	001	2019-03-01
33	CN	Anke Investments	anke-004	004	2019-06-27
34	CN	Anke Investments	anke-005	005	2019-11-21
35	BR	Antheus Technologia	antheus-000	000	2019-12-05
36	BR	Antheus Technologia	antheus-001	001	2020-06-25
37	GB	AnyVision	anyvision-004	004	2018-06-15
38	GB	AnyVision	anyvision-005	005	2021-02-03
39	CN	AuthenMetric	authenmetric-002	002	2021-03-10
40	CN	AuthenMetric	authenmetric-003	003	2021-08-09
41	US	Aware	aware-005	005	2020-02-27
42	US	Aware	aware-006	006	2021-07-03
43	IN	Awidit Systems	awiros-001	001	2019-09-23
44	IN	Awidit Systems	awiros-002	002	2020-10-28
45	JP	Ayonix	ayonix-000	000	2017-06-22
46	CN	BOE Technology Group	boetech-001	001	2021-06-22
47	ES	Bee the Data	beethedata-000	000	2021-07-26
48	CN	Beihang University-ERCACAT	ercacat-001	001	2020-07-06
49	CN	Beijing Alleyes Technology	alleyes-000	000	2020-03-09
50	CN	Beijing DeepSense Technologies	deepsense-000	000	2021-03-19
51	CN	Beijing Hisign Technology	hisign-001	001	2021-09-24
52	CN	Beijing Mendaxia Technology	mendaxiatech-000	000	2021-09-15
53	CN	Beijing Vion Technology Inc	vion-000	000	2018-10-19
54	CH	BioID Technologies SA	biodtechswiss-001	001	2020-08-28
55	CH	BioID Technologies SA	biodtechswiss-002	002	2021-02-17
56	IN	Biocube Matrics	biocube-001	001	2021-09-08
57	UK	BitCenter UK	farfaces-001	001	2021-04-09
58	CN	Bitmain	bm-001	001	2018-10-17
59	CN	Bresee Technology	bresee-001	001	2020-12-30
60	CN	Bresee Technology	bresee-002	002	2021-06-30
61	CN	CSA IntelliCloud Technology	intelllicloudai-001	001	2019-08-13
62	CN	CSA IntelliCloud Technology	intelllicloudai-002	002	2020-12-17
63	TW	CTBC Bank	ctcbcbank-000	000	2019-06-28
64	TW	CTBC Bank	ctcbcbank-001	001	2019-10-28
65	KR	CUDO Communication	cudocommunication-001	001	2021-10-20
66	US	Camvi Technologies	camvi-002	002	2018-10-19
67	US	Camvi Technologies	camvi-004	004	2019-07-12
68	CN	Canon Inc	canon-002	002	2020-12-29
69	JP	Canon Inc	canon-003	003	2021-09-15
70	CN	China Electronics Import-Export Corp	ceiec-003	003	2020-01-06

Table 1: Summary of participant information included in this report.

	Location	Developer Name	Short Name	Seq. Num.	Validation Date
71	CN	China Electronics Import-Export Corp	ceiec-004	004	2021-01-18
72	CN	China University of Petroleum	upc-001	001	2019-06-05
73	CN	Chinese University of Hong Kong	cuhkee-001	001	2020-03-18
74	KR	Chosun University	chosun-001	001	2020-07-01
75	KR	Chosun University	chosun-002	002	2020-11-25
76	TW	Chunghwa Telecom	chtface-003	003	2020-06-24
77	TW	Chunghwa Telecom	chtface-004	004	2021-10-08
78	US	Clearview AI Inc	clearviewai-000	000	2021-09-22
79	CN	Closeli Inc	closeli-001	001	2021-07-15
80	US	CloudSmart Consulting LLC	csc-002	002	2021-03-24
81	US	CloudSmart Consulting LLC	csc-003	003	2021-08-26
82	TW	Cloudmatrix	cloudmatrix-000	000	2021-10-22
83	CN	Cloudwalk - Hengrui AI Technology	cloudwalk-hr-003	003	2020-09-25
84	CN	Cloudwalk - Hengrui AI Technology	cloudwalk-hr-004	004	2021-02-10
85	CN	Cloudwalk - Hengrui AI Technology	cloudwalk-mt-004	004	2021-11-09
86	CN	Cloudwalk - Moontime Smart Technology	cloudwalk-mt-003	003	2020-12-22
87	IN	Code Everest Pvt	facex-001	001	2021-03-08
88	IN	Code Everest Pvt	facex-002	002	2021-08-24
89	DE	Cognitec Systems GmbH	cognitec-002	002	2021-02-24
90	DE	Cognitec Systems GmbH	cognitec-003	003	2021-07-30
91	TW	Coretech Knowledge Inc	coretech-000	000	2021-07-12
92	IL	Corsight	corsight-001	001	2021-03-11
93	IL	Corsight	corsight-002	002	2021-09-01
94	IL	Cortica	cor-001	001	2020-09-24
95	KR	Cubox	cubox-001	001	2020-12-07
96	KR	Cubox	cubox-002	002	2021-08-24
97	JP	Cybercore	cybercore-000	000	2020-08-26
98	US	Cyberextruder	cyberextruder-001	001	2017-08-02
99	US	Cyberextruder	cyberextruder-002	002	2018-01-30
100	TW	Cyberlink Corp	cyberlink-006	006	2021-01-08
101	TW	Cyberlink Corp	cyberlink-007	007	2021-07-16
102	CN	DSK	dsk-000	000	2019-06-28
103	CN	Dahua Technology	dahua-005	005	2020-08-13
104	CN	Dahua Technology	dahua-006	006	2020-12-30
105	IE	Daon	daon-000	000	2021-11-03
106	US	Decatur Industries Inc	decatur-000	000	2020-08-18
107	US	Decatur Industries Inc	decatur-001	001	2021-09-27
108	CN	Deepglint	deepglint-003	003	2021-03-03
109	CN	Deepglint	deepglint-004	004	2021-09-17
110	FR	Deepsense	dps-000	000	2021-07-16
111	DE	Dermalog	dermalog-008	008	2021-03-25
112	DE	Dermalog	dermalog-009	009	2021-10-06
113	CN	DiDi ChuXing Technology	didiglobalface-001	001	2019-10-23
114	GB	Digital Barriers	digitalbarriers-002	002	2019-03-01
115	TR	Ekin Smart City Technologies	ekin-002	002	2021-05-04
116	RU	Enface	enface-000	000	2021-04-09
117	CH	Euronovate SA	euronovate-001	001	2021-11-15
118	RU	Expasoft LLC	expasoft-001	001	2020-09-03
119	RU	Expasoft LLC	expasoft-002	002	2021-07-26
120	DE	FaceOnLive Inc	faceonlive-001	001	2021-11-23
121	GB	FaceSoft	facesoft-000	000	2019-07-10
122	KR	FaceTag Co	facetag-000	000	2021-03-22
123	KR	FaceTag Co	facetag-001	001	2021-08-17
124	TW	FarBar Inc	f8-001	001	2019-07-11
125	UK	Fincore Ltd	fincore-000	000	2021-06-07
126	CN	Fujitsu Research and Development Center	fujitsulab-002	002	2021-02-24
127	CN	Fujitsu Research and Development Center	fujitsulab-003	003	2021-07-12
128	US	Gemalto Cogent	cogent-005	005	2020-12-29
129	US	Gemalto Cogent	cogent-006	006	2021-07-28
130	TW	GeoVision Inc	geo-002	002	2021-04-01
131	TW	GeoVision Inc	geo-003	003	2021-09-15
132	JP	Glory	glory-002	002	2019-11-12
133	JP	Glory	glory-003	003	2021-01-15
134	TW	Gorilla Technology	gorilla-007	007	2021-06-28
135	TW	Gorilla Technology	gorilla-008	008	2021-11-08
136	US	Griaule	griaule-000	000	2021-08-20
137	CN	Guangzhou Pixel Solutions	pixelall-006	006	2021-06-17
138	CN	Guangzhou Pixel Solutions	pixelall-007	007	2021-12-01
139	ES	Herta Security	hertasecurity-000	000	2021-01-05
140	CN	Hikvision Research Institute	hik-001	001	2019-03-01

Table 2: Summary of participant information included in this report.

	Location	Developer Name	Short Name	Seq. Num.	Validation Date
141	IN	HyperVerge Inc	hyperverge-001	001	2020-12-13
142	IN	HyperVerge Inc	hyperverge-002	002	2021-05-27
143	AU	ICM Airport Technics	icm-002	002	2020-11-13
144	AU	ICM Airport Technics	icm-003	003	2021-09-06
145	FR	ID3 Technology	id3-006	006	2020-12-17
146	FR	ID3 Technology	id3-008	008	2021-11-10
147	RU	ITMO University	itmo-007	007	2020-01-06
148	RU	ITMO University	itmo-008	008	2021-11-19
149	RU	IVA Cognitive	ivacognitive-001	001	2021-01-29
150	FR	Idemia	idemia-007	007	2020-12-04
151	FR	Idemia	idemia-008	008	2021-07-07
152	US	Imageware Systems	iws-000	000	2020-08-12
153	AU	Imagus Technology Pty	imagus-002	002	2020-12-31
154	AU	Imagus Technology Pty	imagus-004	004	2021-09-20
155	GB	Imperial College London	imperial-000	000	2019-03-01
156	GB	Imperial College London	imperial-002	002	2019-08-28
157	US	Incode Technologies Inc	incode-009	009	2021-06-22
158	US	Incode Technologies Inc	incode-010	010	2021-10-22
159	IN	Innef Labs	innefulabs-000	000	2020-09-04
160	GB	Innovative Technology	innovativetechnologyltd-001	001	2019-10-22
161	GB	Innovative Technology	innovativetechnologyltd-002	002	2020-02-26
162	SK	Innovatrics	innovatrics-006	006	2019-08-13
163	SK	Innovatrics	innovatrics-007	007	2020-08-19
164	CN	InsightFace AI	insightface-000	000	2021-03-17
165	CN	InsightFace AI	insightface-001	001	2021-09-27
166	CN	Institute of Computing Technology	icthtc-000	000	2020-11-29
167	RU	Institute of Information Technologies	iit-002	002	2019-12-04
168	RU	Institute of Information Technologies	iit-003	003	2020-12-01
169	IS	Intel Research Group	intelresearch-003	003	2021-01-18
170	IS	Intel Research Group	intelresearch-004	004	2021-08-24
171	US	Intellivision	intellivision-001	001	2017-10-10
172	US	Intellivision	intellivision-002	002	2019-08-23
173	US	IrexAI	irex-000	000	2020-12-17
174	IL	Is It You	isityou-000	000	2017-06-26
175	KR	Kakao Enterprise	kakao-005	005	2021-03-09
176	KR	Kakao Enterprise	kakao-006	006	2021-10-13
177	KR	Kakao Pay Corp	kakaopay-001	001	2021-07-06
178	SG	Kedacom International Pte	kedacom-000	000	2019-06-03
179	US	Kneron Inc	kneron-003	003	2019-07-01
180	US	Kneron Inc	kneron-005	005	2020-02-21
181	KR	Kookmin University	kookmin-002	002	2021-03-05
182	KR	Kookmin University	kookmin-003	003	2021-10-07
183	CN	KuKe3D Technology	kuke3d-001	001	2021-10-28
184	IN	Lema Labs	lemalabs-001	001	2021-04-13
185	JP	Line Corporation	line-000	000	2021-03-31
186	JP	Line Corporation	line-001	001	2021-09-26
187	RU	Lomonosov Moscow State University	intsysmsu-001	001	2019-10-22
188	RU	Lomonosov Moscow State University	intsysmsu-002	002	2020-03-12
189	IN	Lookman Electroplast Industries	lookman-002	002	2018-06-13
190	IN	Lookman Electroplast Industries	lookman-004	004	2019-06-03
191	US	Luxand Inc	luxand-000	000	2019-11-07
192	RU	MVision	mvision-001	001	2019-11-12
193	IN	Mantra Softech India	mantra-000	000	2021-10-28
194	CN	Maxvision Technology	maxvision-000	000	2021-10-27
195	CN	Megvii/Face++	megvii-003	003	2021-03-08
196	GB	MicroFocus	microfocus-001	001	2018-06-13
197	GB	MicroFocus	microfocus-002	002	2018-10-17
198	CN	Minivision	minivision-000	000	2020-10-28
199	NO	Mobai	mobai-000	000	2020-08-26
200	NO	Mobai	mobai-001	001	2021-02-17
201	ES	Mobbel Solutions	mobbl-000	000	2021-01-28
202	ES	Mobbel Solutions	mobbl-001	001	2021-06-16
203	KR	Mobipin Technology	mobilpin-000	000	2021-11-23
204	TH	Momentum Digital	sertis-000	000	2019-10-07
205	TH	Momentum Digital	sertis-002	002	2021-05-13
206	CN	MoreDian Technology	moreedian-000	000	2021-02-24
207	CN	Multi-Modality Intelligence	multimodality-000	000	2021-10-19
208	RU	N-Tech Lab	ntechlab-010	010	2021-04-30
209	RU	N-Tech Lab	ntechlab-011	011	2021-09-13
210	CA	NEO Systems	neosystems-002	002	2021-07-03

Table 3: Summary of participant information included in this report.

	Location	Developer Name	Short Name	Seq. Num.	Validation Date
211	CA	NEO Systems	neosystems-003	003	2021-11-11
212	KR	NHN Corp	nhn-001	001	2021-03-15
213	KR	NHN Corp	nhn-002	002	2021-07-15
214	KR	NSENSE Corp	nsensecorp-002	002	2021-05-06
215	KR	NSENSE Corp	nsensecorp-003	003	2021-10-29
216	CN	Nanjing Kiwi Network Technology	kiwitech-000	000	2021-03-19
217	KR	Naver Corp	clova-000	000	2020-10-21
218	KR	Neosecu Co	openface-001	001	2021-06-15
219	TW	Netbridge Technology Incoporation	netbridgetech-001	001	2020-01-08
220	TW	Netbridge Technology Incoporation	netbridgetech-002	002	2020-08-11
221	LT	Neurotechnology	neurotechnology-011	011	2021-03-26
222	LT	Neurotechnology	neurotechnology-012	012	2021-07-26
223	ID	Nodeflux	nodeflux-002	002	2019-08-13
224	IN	NotionTag Technologies Private Limited	notiontag-001	001	2021-03-04
225	IN	NotionTag Technologies Private Limited	notiontag-002	002	2021-09-17
226	US	Omnigarde Ltd	omnigarde-000	000	2021-04-05
227	US	Omnigarde Ltd	omnigarde-001	001	2021-08-23
228	RU	Oz Forensics LLC	oz-002	002	2021-01-18
229	RU	Oz Forensics LLC	oz-003	003	2021-08-09
230	CH	PXL Vision AG	pxl-001	001	2020-06-30
231	SG	Panasonic R+D Center Singapore	psl-008	008	2021-07-21
232	SG	Panasonic R+D Center Singapore	psl-009	009	2021-12-08
233	TR	Papilon Savunma	papsav1923-001	001	2021-03-10
234	US	Paravision (EverAI)	paravision-004	004	2019-12-11
235	US	Paravision (EverAI)	paravision-008	008	2021-06-30
236	SG	Pensees Pte	pensees-001	001	2020-08-17
237	IN	Pyramid Cyber Security + Forensic (P)	pyramid-000	000	2019-11-04
238	TW	Qnap Security	qnap-000	000	2021-08-09
239	TW	Qnap Security	qnap-001	001	2021-12-09
240	CZ	Quantasoft	quantasoft-003	003	2021-04-19
241	US	Rank One Computing	rankone-010	010	2020-11-05
242	US	Rank One Computing	rankone-011	011	2021-08-27
243	US	Realnetworks Inc	realnetworks-004	004	2021-04-15
244	US	Realnetworks Inc	realnetworks-005	005	2021-09-27
245	US	Regula Forensics	regula-000	000	2021-04-13
246	CN	Remark Holdings	remarkai-001	001	2019-03-01
247	CN	Remark Holdings	remarkai-003	003	2021-06-22
248	SG	Rendip	rendip-000	000	2021-04-19
249	UK	Reveal Media Ltd	revealmedia-005	005	2021-09-24
250	CN	Rokid Corporation	rokid-000	000	2019-08-01
251	CN	Rokid Corporation	rokid-001	001	2019-12-13
252	KR	SK Telecom	sktelecom-000	000	2021-07-09
253	KR	SQISoft	sqisoft-001	001	2021-07-27
254	KR	SQISoft	sqisoft-002	002	2021-11-03
255	DE	Saffe	saffe-001	001	2018-10-19
256	DE	Saffe	saffe-002	002	2019-03-01
257	KR	Samsung S1 Corp	s1-002	002	2021-03-24
258	KR	Samsung S1 Corp	s1-003	003	2021-08-24
259	KR	Samsung-SDS	samsungsds-000	000	2021-10-28
260	IN	Samtech InfoNet Limited	samtech-001	001	2019-10-15
261	RU	Satellite Innovation/Eocortex	eocortex-000	000	2020-08-26
262	IL	Scanovate	scanovate-002	002	2020-06-26
263	IL	Scanovate	scanovate-003	003	2021-11-15
264	RO	Securif AI	securifai-001	001	2020-10-06
265	RO	Securif AI	securifai-003	003	2021-08-03
266	CN	Sensetime Group	sensetime-004	004	2020-11-20
267	CN	Sensetime Group	sensetime-005	005	2021-05-24
268	SG	Seventh Sense Artificial Intelligence	seventhsense-000	000	2021-06-29
269	US	Shaman Software	shaman-000	000	2017-12-05
270	US	Shaman Software	shaman-001	001	2018-01-13
271	CN	Shanghai Jiao Tong University	sjtu-003	003	2020-11-02
272	CN	Shanghai Jiao Tong University	sjtu-004	004	2021-05-13
273	CN	Shanghai Ulucu Electronics Technology	uluface-002	002	2019-07-10
274	CN	Shanghai Ulucu Electronics Technology	uluface-003	003	2019-11-12
275	CN	Shanghai University - Shanghai Film Academy	shu-002	002	2019-12-10
276	CN	Shanghai University - Shanghai Film Academy	shu-003	003	2020-06-24
277	CN	Shanghai Yitu Technology	yitu-003	003	2019-03-01
278	CN	Shenzhen AiMall Tech	aimall-002	002	2020-03-12
279	CN	Shenzhen AiMall Tech	aimall-003	003	2020-08-12
280	CN	Shenzhen EI Networks	einetworks-000	000	2019-08-13

Table 4: Summary of participant information included in this report.

	Location	Developer Name	Short Name	Seq. Num.	Validation Date
281	CN	Shenzhen Inst Adv Integrated Tech CAS	siat-002	002	2018-06-13
282	CN	Shenzhen Inst Adv Integrated Tech CAS	siat-004	004	2019-03-01
283	CN	Shenzhen Intellifusion Technologies	intellifusion-001	001	2019-08-22
284	CN	Shenzhen Intellifusion Technologies	intellifusion-002	002	2020-03-18
285	CN	Shenzhen University-Macau University of Science and Technology	sztu-000	000	2020-12-17
286	CN	Shenzhen University-Macau University of Science and Technology	sztu-001	001	2021-07-13
287	RU	Smart Engines	smartengines-000	000	2021-08-25
288	DE	Smilart	smilart-002	002	2018-02-06
289	DE	Smilart	smilart-003	003	2018-06-18
290	TR	Sodec App Inc	sodec-000	000	2021-06-02
291	IN	Staqu Technologies	st aqu-000	000	2020-07-15
292	CN	Star Hybrid Limited	starhybrid-001	001	2019-06-19
293	CN	Su Zhou NaZhiTianDi intelligent technology	nazhai-000	000	2020-06-25
294	KR	Suprema	suprema-000	000	2021-03-31
295	KR	Suprema ID Inc	suprema-001	001	2021-09-23
296	KR	Suprema ID Inc	supremaid-001	001	2021-05-04
297	RU	Synesis	synesis-006	006	2019-10-10
298	RU	Synesis	synesis-007	007	2020-06-24
299	TW	Synology Inc	synology-000	000	2019-10-23
300	TW	Synology Inc	synology-002	002	2020-08-20
301	CN	TUPU Technology	tuputech-000	000	2019-10-11
302	TW	Taiwan AI Labs	ailabs-001	001	2019-12-18
303	TW	Taiwan-Certificate Authority Incorporation	twface-000	000	2021-05-14
304	TW	Taiwan-Certificate Authority Incorporation	twface-001	001	2021-09-14
305	CH	Tech5 SA	tech5-004	004	2020-03-09
306	CH	Tech5 SA	tech5-005	005	2020-07-24
307	TR	Techsign	techsign-000	000	2021-08-25
308	CN	Tencent Deepsea Lab	deepsea-001	001	2019-06-03
309	RU	Tevian	tevian-007	007	2021-08-06
310	RU	Tevian	tevian-008	008	2021-12-06
311	US	TigerIT Americas LLC	tiger-003	003	2018-10-16
312	US	TigerIT Americas LLC	tiger-005	005	2021-07-29
313	RU	Tinkoff Bank	tinkoff-001	001	2021-05-13
314	CN	TongYi Transportation Technology	tongyi-005	005	2019-06-12
315	TW	Toppan ID Gate	toppanidgate-000	000	2021-09-28
316	JP	Toshiba	toshiba-003	003	2019-03-01
317	JP	Toshiba	toshiba-004	004	2021-09-27
318	JP	Tripleize	aize-001	001	2021-04-23
319	JP	Tripleize	aize-002	002	2021-10-08
320	US	Trueface.ai	trueface-002	002	2021-03-29
321	US	Trueface.ai	trueface-003	003	2021-09-30
322	CN	ULSee Inc	ulsee-001	001	2019-07-31
323	FR	Unissey	unissey-001	001	2021-11-29
324	PT	Universidade de Coimbra	visteam-001	001	2021-03-16
325	PT	Universidade de Coimbra	visteam-002	002	2021-08-20
326	US	VCognition	vcog-002	002	2017-06-12
327	ES	Veridas Digital Authentication Solutions S.L.	veridas-006	006	2021-04-15
328	ES	Veridas Digital Authentication Solutions S.L.	veridas-007	007	2021-09-02
329	KZ	Verigram	verigram-000	000	2021-09-06
330	TW	Via Technologies Inc	via-000	000	2019-07-08
331	TW	Via Technologies Inc	via-001	001	2020-01-08
332	DE	Videmo Intelligent Videoanalyse	videmo-000	000	2019-12-19
333	IN	Videonetics Technology Pvt	videonetics-001	001	2019-06-19
334	IN	Videonetics Technology Pvt	videonetics-002	002	2019-11-21
335	VN	Vietnam Posts and Telecommunications Group	vnpt-002	002	2021-06-08
336	VN	Vietnam Posts and Telecommunications Group	vnpt-003	003	2021-12-01
337	VN	Viettel Group	vts-000	000	2020-11-04
338	VN	Viettel High Technology	viettelhightech-000	000	2021-08-04
339	US	Vigilant Solutions	vigilantsolutions-010	010	2021-04-07
340	US	Vigilant Solutions	vigilantsolutions-011	011	2021-08-07
341	VN	VinAI Research VietNam	vinai-000	000	2020-09-24
342	SE	Visage Technologies	visage-000	000	2020-12-09
343	FI	Visidon	vd-002	002	2021-04-12
344	FI	Visidon	vd-003	003	2021-10-12
345	CN	Vision Intelligence Center of Meituan	meituan-000	000	2021-05-14
346	PT	Vision-Box	visionbox-001	001	2019-03-01
347	PT	Vision-Box	visionbox-002	002	2021-04-29
348	RU	VisionLabs	visionlabs-010	010	2021-01-25
349	RU	VisionLabs	visionlabs-011	011	2021-10-13
350	RU	Vocord	vocord-008	008	2020-01-31

Table 5: Summary of participant information included in this report.

	Location	Developer Name	Short Name	Seq. Num.	Validation Date
351	RU	Vocord	vocord-009	009	2020-12-28
352	CN	Winsense	winsense-001	001	2019-10-16
353	CN	Winsense	winsense-002	002	2020-11-20
354	CN	Wuhan Tianyu Information Industry	wuhantianyu-001	001	2021-08-05
355	CN	Xforward AI Technology	xforwardai-001	001	2020-09-25
356	CN	Xforward AI Technology	xforwardai-002	002	2021-02-10
357	CN	Xiamen Meiya Pico Information	meiya-001	001	2019-03-01
358	CN	Xiamen University	xm-000	000	2020-10-19
359	PT	YooniK	yoonik-001	001	2020-10-26
360	PT	YooniK	yoonik-002	002	2021-09-06
361	TW	Yuan High-Tech Development	yuan-002	002	2021-05-17
362	TW	Yuan High-Tech Development	yuan-003	003	2021-09-17
363	CN	Yuntu Data and Technology	ytu-000	000	2021-06-16
364	CN	Zhuhai Yisheng Electronics Technology	yisheng-004	004	2018-06-12
365	CN	iQIYI Inc	iqface-000	000	2019-06-04
366	CN	iQIYI Inc	iqface-003	003	2021-02-23
367	TW	iSAP Solution Corporation	isap-001	001	2019-08-07
368	TW	iSAP Solution Corporation	isap-002	002	2020-09-01
369	TW	ioNetworks Inc	ionetworks-000	000	2021-07-20

Table 6: Summary of participant information included in this report.

NAME	ALGORITHM	CONFIG	LIBRARY	TEMPLATE							COMPARISON ⁴			
								GENERATION TIME (ms) ⁴				TIME (ns) ⁵		
				(KB) ¹	(KB) ²	(MB) ³	SIZE (B)	MUGSHOT	480x720	960x1440	1600x2400	3000x4500	GENUINE	IMPOSTOR
45	awiros-001	15871971	87480	1388	24512 ± 0	997 ± 6	698 ± 4	6138 ± 6	14225 ± 7	53556 ± 8	1201079 ± 44	1191050 ± 45		
46	awiros-002	295953108	203723	103562	222048 ± 0	103479 ± 0	88500 ± 0	80534 ± 0	85618 ± 0	147946 ± 1	1881966 ± 31	1881957 ± 25		
47	ayftech-001	200113346	43580	143731	33512 ± 0	78408 ± 23	77476 ± 52	163814 ± 108	3081827 ± 384	3105412 ± 1029	53615 ± 16	100885 ± 44		
48	ayonix-000	59909936	5252	569	671036 ± 0	218 ± 2	-	-	-	-	56621 ± 23	57620 ± 26		
49	beethedata-000	233318297	1087592	101555	2342048 ± 0	97465 ± 0	76467 ± 0	61468 ± 0	46467 ± 0	30467 ± 0	1962121 ± 34	1962110 ± 38		
50	biocube-001	25631585	6192987	68458	3394096 ± 0	47282 ± 22	34292 ± 24	78521 ± 57	106684 ± 59	2121282 ± 68	33221787 ± 96	33221812 ± 109		
51	bioditechswiss-001	1207059515	120811	261455	36512 ± 0	286966 ± 4	3011270 ± 270	2921294 ± 96	2861409 ± 157	2661793 ± 79	2192610 ± 25	2202624 ± 32		
52	bioditechswiss-002	762660868	114842	197993	26512 ± 0	26917 ± 2	229930 ± 2	212952 ± 2	187947 ± 3	1721058 ± 11	2002177 ± 29	2012170 ± 31		
53	bm-001	294640228	38076	22148	164 ± 0	90444 ± 88	-	-	-	-	1841887 ± 31	1831877 ± 26		
54	boetech-001	267649084	88710	2491384	2262048 ± 0	40271 ± 1	27268 ± 1	19273 ± 0	18286 ± 1	16318 ± 1	35868519 ± 1921	35867648 ± 822		
55	bresee-001	294790077	23227	2231214	1962048 ± 0	3361223 ± 3	2891216 ± 1	3011331 ± 1	2501227 ± 1	2271360 ± 1	34637240 ± 655	34737167 ± 584		
56	bresee-002	321154814	30902	3011956	1952048 ± 0	206743 ± 4	2751143 ± 2	2611146 ± 2	2321148 ± 2	1971176 ± 2	1721778 ± 22	1711775 ± 23		
57	camvi-002	241949538	225285	144737	611024 ± 0	185677 ± 7	160726 ± 36	177869 ± 28	2261129 ± 43	2942785 ± 113	52612 ± 26	51603 ± 20		
58	camvi-004	287471548	615819	181919	2072048 ± 0	210759 ± 10	201861 ± 17	221986 ± 34	2591279 ± 51	2962891 ± 158	102948 ± 40	103963 ± 31		
59	canon-002	457207046	130232	175891	3294096 ± 0	3511308 ± 2	3081315 ± 1	2991326 ± 2	2731345 ± 1	2431452 ± 1	2896211 ± 25	2886194 ± 25		
60	canon-003	2612070631	101378	3625472	3666180 ± 0	3441263 ± 3	2991263 ± 1	2851283 ± 1	2691320 ± 1	2481482 ± 2	2684783 ± 17	2654780 ± 19		
61	ceiec-003	266620201	88707	62430	2422048 ± 0	231817 ± 4	212883 ± 57	187897 ± 60	170899 ± 72	145944 ± 72	2042256 ± 38	2042241 ± 54		
62	ceiec-004	269799940	67011	55408	872048 ± 0	2961024 ± 1	2491027 ± 1	2321027 ± 1	2051030 ± 1	1691055 ± 1	1811844 ± 26	1801836 ± 20		
63	chosun-001	783990750	707	79491	942048 ± 0	218783 ± 2	190826 ± 4	3251662 ± 13	3303679 ± 67	32711694 ± 243	110998 ± 25	1181035 ± 11		
64	chosun-002	239617968	31875	65450	2032048 ± 0	34248 ± 3	28273 ± 3	3201495 ± 14	3327920 ± 90	32980302 ± 1349	57623 ± 17	64634 ± 13		
65	chtface-003	371869498	369529	2201178	1942048 ± 0	150594 ± 16	159720 ± 33	2401050 ± 41	3111884 ± 90	3125606 ± 334	1952110 ± 37	2032219 ± 65		
66	chtface-004	419487869	311027	2641487	2152048 ± 0	57332 ± 0	38323 ± 1	25329 ± 1	20335 ± 1	21377 ± 1	1671727 ± 17	1661720 ± 16		
67	clearviewai-000	350711038	211852	3292750	1242048 ± 0	3621402 ± 1	3191403 ± 1	3121412 ± 1	2891420 ± 1	2381418 ± 1	1571592 ± 37	1561561 ± 37		
68	closeli-001	430430427	9851	148773	3404096 ± 0	243839 ± 1	196843 ± 1	172841 ± 1	153845 ± 1	129865 ± 1	2745404 ± 17	2745400 ± 25		
69	cloudmatrix-000	317378456	542141	140727	2172048 ± 0	209754 ± 10	168750 ± 2	152754 ± 4	135764 ± 1	111793 ± 2	35349192 ± 206	35349275 ± 176		
70	cloudwalk-hr-003	392949139	144263	196984	2882057 ± 0	153606 ± 0	115588 ± 0	97594 ± 0	84612 ± 1	-	2966982 ± 80	2956972 ± 84		
71	cloudwalk-hr-004	514986414	520169	2511394	2522049 ± 0	255873 ± 1	209877 ± 1	182876 ± 1	162879 ± 1	136902 ± 3	31011652 ± 127	30911608 ± 123		
72	cloudwalk-mt-003	502133796	494959	2411342	2512049 ± 0	270923 ± 1	223918 ± 1	202926 ± 1	177925 ± 1	143936 ± 1	30911620 ± 179	31111661 ± 128		
73	cloudwalk-mt-004	1417833104	512628	3615426	2052048 ± 0	271923 ± 2	224919 ± 1	195918 ± 0	176919 ± 0	140927 ± 1	31111744 ± 170	31011631 ± 126		
74	clova-000	203182777	6824	70464	1812048 ± 0	89437 ± 0	62431 ± 0	47435 ± 0	40452 ± 2	38508 ± 7	1741794 ± 16	1771795 ± 19		
75	cogent-005	1921839276	75276	3312806	3012523 ± 0	3341221 ± 2	2931236 ± 1	2871289 ± 2	2881420 ± 4	2541602 ± 5	33824854 ± 69	33824858 ± 71		
76	cogent-006	1104043825	58108	2681547	701062 ± 0	214768 ± 0	178789 ± 1	167831 ± 2	179930 ± 1	152971 ± 1	1761802 ± 17	1781797 ± 23		
77	cognitec-002	403546749	62354	117624	2542052 ± 0	26192 ± 6	19219 ± 6	17233 ± 8	15241 ± 6	15314 ± 10	2413250 ± 41	2413241 ± 48		
78	cognitec-003	482773320	62502	159817	2682052 ± 0	69366 ± 9	54403 ± 9	37408 ± 9	33424 ± 9	39509 ± 13	2463417 ± 51	2493433 ± 53		
79	cor-001	1223627342	11240	2291249	2902060 ± 0	197699 ± 3	203863 ± 76	176865 ± 80	158872 ± 89	148952 ± 39	369270145 ± 2259	369282686 ± 11788		
80	coretech-000	190897979	43964	52393	17512 ± 0	152602 ± 15	137659 ± 12	2581139 ± 24	2331149 ± 25	1931165 ± 23	20333 ± 14	20321 ± 13		
81	corsight-001	1472269967	31525	3072040	2922064 ± 0	3481291 ± 3	3021285 ± 1	2901293 ± 1	2621303 ± 2	2281379 ± 3	368249340 ± 1713	368248929 ± 1909		
82	corsight-002	1510319809	32093	3082061	2952080 ± 0	3471290 ± 1	3031287 ± 1	2881290 ± 1	2641307 ± 2	2321388 ± 4	33924953 ± 637	33724263 ± 578		
83	csc-002	0	519768	2471376	47544 ± 0	101473 ± 0	85494 ± 0	64481 ± 1	53490 ± 1	42514 ± 5	24367 ± 11	25371 ± 10		
84	csc-003	0	400435	2771609	46544 ± 0	111499 ± 0	89500 ± 1	71502 ± 0	57508 ± 1	46535 ± 4	26393 ± 8	28397 ± 7		
85	ctcbank-000	263381717	599238	105570	1522048 ± 0	134568 ± 43	121606 ± 38	131690 ± 53	116711 ± 50	121831 ± 51	2513551 ± 87	2674805 ± 209		
86	ctcbank-001	282123885	599238	112603	992048 ± 0	172652 ± 35	177781 ± 30	181875 ± 43	169898 ± 51	1631030 ± 47	2573926 ± 45	2573924 ± 56		
87	cubox-001	378498689	75427	119649	1412048 ± 0	264907 ± 1	220902 ± 1	190903 ± 0	174917 ± 0	141931 ± 0	1431379 ± 37	1481417 ± 38		
88	cubox-002	555268218	90975	3021964	2102048 ± 0	268921 ± 1	225921 ± 1	199922 ± 1	181933 ± 1	1591003 ± 1	1902008 ± 72	1901969 ± 57		

Notes

- 1 The configuration size does not capture static data included in libraries.
- 2 The library size is the combined total of all files provided in the submission lib folder. These libraries e.g. OpenCV may or may not be installed on any end user's platform natively and would not need to be installed with the algorithm. Some developers put neural network models in their libraries.
- 3 The memory usage is the peak resident set size reported by the ps system call during template generation.
- 4 The median template creation times are measured on Intel® Xeon® CPU E5-2630 v4 @ 2.20GHz processors.
- 5 The comparison durations, in nanoseconds, are estimated using std::chrono::high_resolution_clock which on the machine in (2) counts 1ns clock ticks. Precision is somewhat worse than that however. The ± value is the median absolute deviation times 1.48 for Normal consistency.

Table 8: Summary of algorithms and properties included in this report. The red superscripts give ranking for the quantity in that column.

ALGORITHM			CONFIG	LIBRARY	TEMPLATE						COMPARISON ⁴		
NAME		DATA	DATA	MEMORY	SIZE	GENERATION TIME (ms) ⁴						TIME (ns) ⁵	
	(KB) ¹	(KB) ²	(MB) ³	(B)	MUGSHOT	480x720	960x1440	1600x2400	3000x4500	GENUINE	IMPOSTOR		
89	cudocommunication-001	394504775	341277	208 1077	91 2048 ± 0	272 925 ± 1	226 923 ± 1	203 928 ± 1	180 932 ± 0	150 964 ± 1	213 2534 ± 20	215 2537 ± 20	
90	cuhkee-001	806762318	74917	321 2515	262 2052 ± 0	288 977 ± 31	-	-	-	-	222 2719 ± 60	223 2783 ± 56	
91	cybercore-000	88073082	55441	33 200	31 512 ± 0	176 655 ± 3	147 689 ± 71	120 649 ± 6	95 648 ± 8	81 680 ± 6	318 14800 ± 75	320 15757 ± 782	
92	cyberextruder-001	124120800	13629	27 178	2 256 ± 0	263 893 ± 25	-	-	-	-	121 1083 ± 16	123 1079 ± 19	
93	cyberextruder-002	172963574	13924	32 194	247 2048 ± 0	122 532 ± 6	-	-	-	-	178 1803 ± 14	173 1779 ± 22	
94	cyberlink-006	349866738	102456	252 1400	368 6212 ± 0	191 690 ± 1	152 702 ± 0	138 703 ± 0	117 712 ± 0	102 741 ± 0	13 270 ± 13	16 271 ± 13	
95	cyberlink-007	389168020	102446	285 1743	367 6212 ± 0	200 725 ± 1	163 732 ± 1	146 734 ± 1	124 736 ± 1	110 767 ± 1	17 304 ± 19	18 304 ± 16	
96	dahua-005	1624985571	169478	367 7360	325 4096 ± 0	365 1418 ± 34	-	-	-	-	103 957 ± 23	105 969 ± 19	
97	dahua-006	851600617	119261	359 5068	153 2048 ± 0	361 1398 ± 2	318 1397 ± 1	311 1404 ± 1	284 1402 ± 1	235 1402 ± 1	11 249 ± 13	14 250 ± 11	
98	daon-000	287464249	2307	306 2013	293 2065 ± 0	131 562 ± 3	117 581 ± 5	156 791 ± 9	150 838 ± 15	170 1055 ± 32	321 16052 ± 88	321 16041 ± 85	
99	decatur-000	358907752	171271	178 907	346 4100 ± 0	297 1024 ± 2	-	-	-	-	308 11439 ± 80	308 11418 ± 112	
100	decatur-001	351095179	253734	265 1507	267 2052 ± 0	312 1103 ± 2	260 1064 ± 2	244 1063 ± 2	214 1067 ± 2	177 1084 ± 2	51 610 ± 19	50 602 ± 8	
101	deepglint-003	858178673	262081	315 2374	365 6144 ± 0	323 1159 ± 1	276 1145 ± 1	262 1148 ± 1	231 1148 ± 1	192 1163 ± 1	323 17227 ± 41	323 17210 ± 51	
102	deepglint-004	1099143717	261571	340 3084	231 2048 ± 0	370 1470 ± 1	327 1474 ± 1	319 1485 ± 1	294 1474 ± 1	249 1492 ± 2	283 5961 ± 34	284 5955 ± 29	
103	deepsea-001	151037339	336250	50 358	56 1024 ± 0	166 630 ± 7	169 752 ± 37	149 746 ± 30	121 727 ± 32	118 820 ± 32	147 1401 ± 37	150 1467 ± 50	
104	deepsense-000	365684327	936618	368 7618	243 2048 ± 0	181 664 ± 3	135 645 ± 1	121 660 ± 2	108 687 ± 2	116 808 ± 3	31 480 ± 22	33 459 ± 34	
105	dermalog-008	0	937895	358 4989	20 512 ± 0	75 404 ± 2	55 410 ± 3	44 424 ± 5	35 430 ± 5	33 477 ± 5	29 468 ± 31	22 328 ± 13	
106	dermalog-009	0	319363	123 664	23 512 ± 0	61 349 ± 0	44 351 ± 0	27 352 ± 0	23 357 ± 0	22 389 ± 0	32 487 ± 34	27 385 ± 29	
107	didiglobalface-001	266086235	70680	91 527	156 2048 ± 0	155 612 ± 1	132 633 ± 3	115 634 ± 3	97 650 ± 15	79 666 ± 4	105 973 ± 20	107 988 ± 20	
108	digitalbarriers-002	84994577	598577	297 1930	283 2056 ± 0	29 209 ± 11	22 250 ± 19	38 411 ± 37	141 808 ± 72	275 2236 ± 123	315 13409 ± 228	316 13267 ± 206	
109	dps-000	607	2211812	203 1058	342 4096 ± 0	249 868 ± 2	217 893 ± 6	315 1445 ± 9	327 2910 ± 38	323 9345 ± 17	152 1473 ± 37	152 1479 ± 37	
110	dsk-000	12254510	782905	36 252	30 512 ± 0	52 304 ± 47	37 317 ± 33	225 1001 ± 96	326 2660 ± 170	325 10451 ± 832	300 7152 ± 115	298 7134 ± 111	
111	einetworks-000	381551539	219883	173 880	271 2056 ± 0	170 645 ± 3	-	-	-	-	270 4876 ± 66	270 5156 ± 77	
112	ekin-002	52668576	278	19 139	304 3072 ± 0	330 1186 ± 13	285 1180 ± 12	268 1181 ± 11	244 1191 ± 11	201 1207 ± 8	261 4294 ± 80	278 5569 ± 112	
113	enface-000	378468370	153781	122 662	53 1024 ± 0	130 555 ± 4	106 558 ± 4	124 669 ± 6	194 987 ± 15	281 2349 ± 54	298 7059 ± 62	296 6980 ± 65	
114	eocortex-000	262080175	59432	35 224	106 2048 ± 0	53 305 ± 22	43 341 ± 25	51 440 ± 47	45 464 ± 45	41 513 ± 44	100 923 ± 11	101 918 ± 11	
115	ercatc-001	831102356	58012	332 2816	266 2052 ± 0	306 1052 ± 3	-	-	-	-	214 2551 ± 62	212 2501 ± 81	
116	euronovate-001	0	1774966	238 1308	72 1177 ± 0	302 1034 ± 2	278 1165 ± 3	264 1160 ± 3	237 1177 ± 3	196 1172 ± 2	362 81294 ± 591	362 81631 ± 931	
117	expasoft-001	39994987	983064	20 142	90 2048 ± 0	6 70 ± 0	374 ± 0	377 ± 0	73 ± 0	374 ± 0	160 1660 ± 35	160 1676 ± 48	
118	expasoft-002	39691196	59825	24 168	115 2048 ± 0	434 ± 0	234 ± 0	234 ± 0	134 ± 0	134 ± 0	305 8870 ± 78	305 8838 ± 77	
119	f8-001	279529297	19668	233 1276	89 2048 ± 0	236 822 ± 39	-	-	-	-	320 15262 ± 139	319 15277 ± 212	
120	faceonlive-001	0	71529	47 302	287 2056 ± 0	22 179 ± 0	11 179 ± 0	13 190 ± 0	11 217 ± 0	18 343 ± 1	117 1064 ± 37	117 1033 ± 35	
121	facesoft-000	379002927	10612	152 796	183 2048 ± 0	184 675 ± 18	140 669 ± 3	129 686 ± 3	103 675 ± 5	84 687 ± 2	203 2239 ± 28	205 2277 ± 96	
122	facetag-000	1261907727	4022	192 965	51 684 ± 0	62 355 ± 17	49 369 ± 8	223 989 ± 33	323 2408 ± 91	321 7930 ± 316	359 72003 ± 625	360 71912 ± 612	
123	facetag-001	1288445598	4022	240 1329	348 4100 ± 0	292 991 ± 3	241 995 ± 3	229 1018 ± 3	218 1069 ± 5	213 1284 ± 8	242 3323 ± 28	242 3287 ± 34	
124	facex-001	312396751	930372	338 2931	134 2048 ± 0	82 422 ± 4	64 434 ± 4	77 520 ± 7	125 737 ± 13	258 1670 ± 27	182 1871 ± 23	181 1846 ± 29	
125	facex-002	312396751	928334	341 3095	163 2048 ± 0	83 426 ± 5	61 429 ± 4	75 516 ± 8	122 730 ± 12	263 1738 ± 36	58 631 ± 25	55 614 ± 19	
126	farfaces-001	354810878	44581	37 261	32 512 ± 0	326 1179 ± 1	283 1180 ± 1	267 1180 ± 0	240 1185 ± 1	202 1209 ± 2	98 855 ± 25	97 860 ± 31	
127	fiberhome-nanjing-003	361365058	1482309	166 845	244 2048 ± 0	317 1136 ± 7	272 1134 ± 4	257 1132 ± 3	229 1139 ± 3	188 1154 ± 5	123 1097 ± 38	125 1083 ± 42	
128	fiberhome-nanjing-004	454429945	1482313	200 1048	311 4096 ± 0	354 1321 ± 5	307 1304 ± 3	295 1307 ± 2	266 1308 ± 3	223 1326 ± 5	140 1276 ± 40	140 1265 ± 38	
129	fincore-000	262774045	19409	95 535	233 2048 ± 0	115 508 ± 3	90 505 ± 0	72 508 ± 1	59 513 ± 2	47 535 ± 1	170 1765 ± 31	169 1763 ± 22	
130	fujitsulab-002	0	1088887	278 1613	353 4104 ± 0	339 1237 ± 2	290 1222 ± 2	277 1236 ± 1	253 1251 ± 2	225 1327 ± 2	224 2836 ± 25	224 2809 ± 44	
131	fujitsulab-003	678158225	318209	366 6907	351 4104 ± 0	282 951 ± 20	232 941 ± 19	211 952 ± 19	192 971 ± 20	167 1045 ± 21	225 2855 ± 16	226 2849 ± 19	
132	geo-002	378781240	98667	198 1018	119 2048 ± 0	222 791 ± 1	180 793 ± 0	157 794 ± 0	138 795 ± 1	113 803 ± 1	245 3407 ± 45	247 3422 ± 65	

Notes

- 1 The configuration size does not capture static data included in libraries.
- 2 The library size is the combined total of all files provided in the submission lib folder. These libraries e.g. OpenCV may or may not be installed on any end user's platform natively and would not need to be installed with the algorithm. Some developers put neural network models in their libraries.
- 3 The memory usage is the peak resident set size reported by the ps system call during template generation.
- 4 The median template creation times are measured on Intel® Xeon® CPU E5-2630 v4 @ 2.20GHz processors.
- 5 The comparison durations, in nanoseconds, are estimated using std::chrono::high_resolution_clock which on the machine in (2) counts 1ns clock ticks. Precision is somewhat worse than that however. The ± value is the median absolute deviation times 1.48 for Normal consistency.

ALGORITHM			CONFIG	LIBRARY	TEMPLATE						COMPARISON ⁴	
NAME		DATA	DATA	MEMORY	SIZE	GENERATION TIME (ms) ⁴				TIME (ns) ⁵		
		(KB) ¹	(KB) ²	(MB) ³	(B)	MUGSHOT	480x720	960x1440	1600x2400	3000x4500	GENUINE	IMPOSTOR
221	mvision-001	232962922	149531	139723	16512 ± 0	192691 ± 21	153702 ± 19	135697 ± 24	115708 ± 29	88710 ± 27	1281123 ± 40	1321154 ± 38
222	nazhiai-000	560624381	16141	3252716	1322048 ± 0	188683 ± 3	146687 ± 2	169835 ± 27	152840 ± 31	125834 ± 34	2022230 ± 34	1992133 ± 81
223	neosystems-002	613827997	349942	2261222	982048 ± 0	3161135 ± 2	3321855 ± 3	3302258 ± 5	3192238 ± 3	2762247 ± 3	32818752 ± 167	32818610 ± 213
224	neosystems-003	613828829	349942	2241215	1592048 ± 0	3191143 ± 2	3311836 ± 7	3312260 ± 3	3212273 ± 6	2772273 ± 3	32819130 ± 223	32819167 ± 186
225	netbridgetech-001	136302786	205875	85508	3384096 ± 0	785 ± 1	483 ± 0	484 ± 0	492 ± 0	4113 ± 4	3069280 ± 74	3069446 ± 512
226	netbridgetech-002	263871604	49931	46299	1702048 ± 0	242838 ± 6	195838 ± 2	171839 ± 1	151839 ± 3	127859 ± 3	2272893 ± 65	2333050 ± 123
227	neurotechnology-011	372877031	51141	2621462	39514 ± 0	223798 ± 1	182802 ± 1	164827 ± 3	159873 ± 2	1731059 ± 15	2114 ± 11	2114 ± 8
228	neurotechnology-012	151378192	51395	157814	4256 ± 0	72384 ± 0	50387 ± 0	36404 ± 1	38435 ± 1	58583 ± 7	3119 ± 7	3116 ± 7
229	nhn-001	344464916	817674	121662	3124096 ± 0	3001027 ± 3	2511029 ± 1	2331029 ± 1	2101044 ± 1	1801090 ± 1	35556650 ± 260	35656639 ± 210
230	nhn-002	372194536	817674	125667	3164096 ± 0	3181141 ± 3	2731138 ± 2	2591141 ± 2	2341151 ± 6	1991203 ± 2	35456608 ± 579	35556549 ± 606
231	nodeflux-002	793260136	690213	71466	1212048 ± 0	199708 ± 4	155709 ± 4	142716 ± 5	120716 ± 7	98736 ± 3	2493475 ± 62	2463408 ± 143
232	notiontag-001	94979467	427967	104566	50584 ± 0	273929 ± 35	2641092 ± 39	3333709 ± 81	33310233 ± 180	-	34843636 ± 286	34843724 ± 330
233	notiontag-002	278515288	967207	3342840	3002120 ± 0	92453 ± 2	69453 ± 3	53453 ± 3	41458 ± 2	31471 ± 3	33120278 ± 194	33120195 ± 186
234	nsensecorp-002	191919991	122407	100554	1922048 ± 0	58333 ± 0	40333 ± 0	26337 ± 0	21338 ± 0	19351 ± 0	35145965 ± 213	35145988 ± 158
235	nsensecorp-003	204692907	117041	137710	1692048 ± 0	177661 ± 0	138664 ± 0	123662 ± 1	101659 ± 1	75659 ± 0	34944658 ± 51	35044654 ± 72
236	ntechlab-010	715357382	217167	3392991	761280 ± 0	3251177 ± 2	2841180 ± 2	2751197 ± 2	2491224 ± 1	2241326 ± 3	27405 ± 13	29416 ± 31
237	ntechlab-011	805820346	209458	3656867	731280 ± 0	3211148 ± 2	2741142 ± 1	2631159 ± 1	2411185 ± 1	2141290 ± 3	4179 ± 11	5173 ± 11
238	omnigarde-000	270395030	32882	90523	621024 ± 0	278944 ± 0	214887 ± 0	186888 ± 1	168892 ± 0	139902 ± 0	2202671 ± 35	2192620 ± 29
239	omnigarde-001	205336408	32882	69464	350512 ± 0	279941 ± 0	217883 ± 1	182886 ± 1	167891 ± 1	133898 ± 0	1481405 ± 31	1451379 ± 26
240	openface-001	0	40111	14100	1652048 ± 0	17148 ± 1	10154 ± 0	30365 ± 3	30409 ± 9	64616 ± 31	49608 ± 14	52604 ± 13
241	oz-002	733207161	170261	3453561	2942065 ± 0	3081064 ± 3	2791171 ± 3	3322953 ± 6	3317352 ± 13	32826658 ± 29	365131108 ± 1408	365126758 ± 913
242	oz-003	495766974	519652	37011949	2692053 ± 0	3571375 ± 12	3171388 ± 3	3271773 ± 16	3432039 ± 6	3023209 ± 5	36173905 ± 456	36173892 ± 444
243	papsav1923-001	285911345	52652	73473	1302048 ± 0	164626 ± 1	130628 ± 1	112630 ± 1	96648 ± 2	103744 ± 3	79725 ± 25	82731 ± 28
244	paravision-004	570030501	145440	2711572	3244096 ± 0	238289 ± 2	19834 ± 6	168332 ± 2	147833 ± 4	122833 ± 2	82737 ± 31	80718 ± 38
245	paravision-008	555203492	204400	2591448	3284096 ± 0	196699 ± 0	151700 ± 0	137701 ± 0	113702 ± 1	87702 ± 0	21337 ± 17	23330 ± 13
246	pensees-001	1658297650	408932	2961922	3708200 ± 0	3141108 ± 3	3231448 ± 17	3141439 ± 10	2931464 ± 5	2521546 ± 9	2383151 ± 34	2373143 ± 25
247	pixellass-006	0	746305	185934	3022560 ± 0	2981024 ± 3	2501028 ± 2	2351033 ± 1	2061032 ± 1	1681054 ± 2	84754 ± 14	81722 ± 10
248	pixellass-007	0	444912	2431349	1862048 ± 0	2991026 ± 4	2541038 ± 2	2491089 ± 2	2191087 ± 2	1831124 ± 2	76708 ± 14	76701 ± 19
249	psl-008	977255943	524525	3493807	3083144 ± 0	3641412 ± 4	3211415 ± 3	3131416 ± 2	2871418 ± 2	2391418 ± 2	12259 ± 22	15252 ± 22
250	psl-009	420891941	411504	3605369	3564168 ± 0	3591382 ± 2	3151381 ± 1	3081383 ± 1	2801383 ± 2	2301385 ± 1	18316 ± 14	17289 ± 14
251	ptakuratsatu-000	29	585434	2421347	44538 ± 0	256875 ± 3	204863 ± 48	204928 ± 9	190958 ± 17	1761066 ± 26	2825900 ± 103	2815687 ± 167
252	pxl-001	112759507	78231	23168	19512 ± 0	11101 ± 5	7104 ± 5	11189 ± 12	29408 ± 27	2461470 ± 144	2785598 ± 45	2795590 ± 68
253	pyramid-000	381551539	219883	154804	2822056 ± 0	137583 ± 2	-	-	-	-	2997147 ± 59	3017586 ± 425
254	qnap-000	191213193	15598	40272	1822048 ± 0	201726 ± 9	71457 ± 1	54458 ± 0	44464 ± 1	34482 ± 2	66660 ± 25	68654 ± 29
255	qnap-001	200919086	13399	43286	932048 ± 0	157614 ± 1	127615 ± 1	111627 ± 1	89623 ± 1	68634 ± 2	64649 ± 11	66648 ± 14
256	quantssoft-003	379410922	211354	2041058	2162048 ± 0	167632 ± 2	133634 ± 0	114632 ± 0	91631 ± 1	70634 ± 0	8201 ± 7	8203 ± 8
257	rankone-010	441	138435	1283	8261 ± 0	27193 ± 1	-	-	-	-	14282 ± 13	13234 ± 16
258	rankone-011	437	179209	21146	7261 ± 0	132567 ± 1	102557 ± 1	91567 ± 1	73586 ± 1	82682 ± 3	15283 ± 14	11220 ± 19
259	realnetworks-004	176471448	913988	3182467	2742056 ± 0	56330 ± 4	41333 ± 3	33402 ± 7	72585 ± 15	2361402 ± 51	1321210 ± 29	1361202 ± 17
260	realnetworks-005	176387363	56755	132697	2752056 ± 0	30211 ± 4	17205 ± 3	20290 ± 6	60515 ± 17	2171312 ± 78	1331213 ± 17	1371207 ± 16
261	regula-000	268743079	29384	115610	2062048 ± 0	3311187 ± 1	2711126 ± 1	2561129 ± 0	2271132 ± 1	1901159 ± 1	35491 ± 16	36500 ± 22
262	remarkai-001	247662347	868314	141730	2652052 ± 0	240831 ± 6	198849 ± 18	2411055 ± 25	2451198 ± 34	2511519 ± 38	1371229 ± 20	94805 ± 56
263	remarkai-003	287249016	58559	3523896	3504100 ± 0	291986 ± 1	240993 ± 1	224992 ± 1	199999 ± 3	1611019 ± 2	92787 ± 20	91793 ± 22
264	rendip-000	0	437653	126682	2042048 ± 0	96464 ± 2	72458 ± 0	62473 ± 0	50483 ± 1	54556 ± 4	40576 ± 13	42573 ± 11

Notes

- 1 The configuration size does not capture static data included in libraries.
- 2 The library size is the combined total of all files provided in the submission lib folder. These libraries e.g. OpenCV may or may not be installed on any end user's platform natively and would not need to be installed with the algorithm. Some developers put neural network models in their libraries.
- 3 The memory usage is the peak resident set size reported by the ps system call during template generation.
- 4 The median template creation times are measured on Intel® Xeon® CPU E5-2630 v4 @ 2.20GHz processors.
- 5 The comparison durations, in nanoseconds, are estimated using std::chrono::high_resolution_clock which on the machine in (2) counts 1ns clock ticks. Precision is somewhat worse than that however. The ± value is the median absolute deviation times 1.48 for Normal consistency.

Table 12: Summary of algorithms and properties included in this report. The red superscripts give ranking for the quantity in that column.

	ALGORITHM	CONFIG	LIBRARY	TEMPLATE								COMPARISON ⁴							
				NAME	DATA	DATA	MEMORY	SIZE	GENERATION TIME (ms) ⁴				TIME (ns) ⁵						
									(KB) ¹	(KB) ²	(MB) ³	(B)	MUGSHOT	480x720	960x1440	1600x2400	3000x4500	GENUINE	IMPOSTOR
353	visteam-001	190915457	30878	⁵⁶ visteam-001	³²² 4096 ± 0	²⁵⁰ 869 ± 7	²⁰⁶ 872 ± 6	²⁵³ 1121 ± 15	³⁰⁴ 1719 ± 38	³⁰⁶ 4375 ± 157	²⁹⁷ 7054 ± 108	²⁹⁷ 7025 ± 109							
354	visteam-002	190915457	30888	⁹⁸ visteam-002	³¹⁸ 4096 ± 0	²³⁸ 829 ± 5	¹⁹³ 832 ± 6	¹⁷⁰ 839 ± 7	¹⁵⁶ 853 ± 6	¹⁶⁰ 1013 ± 14	²⁹⁵ 6952 ± 118	²⁹⁴ 6970 ± 120							
355	vnpt-002	278169517	3203296	⁷⁸ vnpt-002	²¹⁸ 2048 ± 0	²⁰⁴ 739 ± 2	¹⁶² 731 ± 2	¹⁴⁸ 740 ± 1	¹²⁷ 742 ± 2	¹⁰⁸ 763 ± 2	⁸⁸ 766 ± 13	⁸⁸ 762 ± 13							
356	vnpt-003	378835561	297799	¹³⁸ vnpt-003	³³² 4096 ± 0	³⁵² 1315 ± 4	³⁰⁹ 1315 ± 4	²⁹⁷ 1318 ± 2	²⁷⁵ 1350 ± 3	²⁴¹ 1428 ± 3	³⁰¹ 7397 ± 31	³⁰⁰ 7384 ± 29							
357	vocord-008	618359916	345047	²⁷⁰ vocord-008	¹⁵⁵⁹ 3032	³⁰³ 2688 ± 0	²⁸³ 962 ± 2	²³⁸ 976 ± 2	²⁴³ 1061 ± 3	²⁵¹ 1236 ± 23	²⁶⁷ 1851 ± 9	²³¹ 3015 ± 50	²²⁹ 2988 ± 62						
358	vocord-009	1413255249	201560	³⁵⁶ vocord-009	⁴¹⁶² 832	³¹⁸ 1920 ± 0	³⁷¹ 1472 ± 2	³²⁶ 1472 ± 1	³²² 1549 ± 1	³⁰² 1667 ± 2	²⁷³ 2064 ± 2	¹⁹³ 2052 ± 50	¹⁹⁵ 2056 ± 39						
359	vts-000	262747358	169760	²⁸¹ vts-000	⁹⁵ 2048 ± 0	¹⁰⁸ 486 ± 1	⁸⁰ 481 ± 0	⁶⁵ 484 ± 0	⁵¹ 485 ± 1	⁴³ 517 ± 0	³⁶⁴ 124209 ± 352	³⁶⁴ 123652 ± 358							
360	winsense-001	270774312	32035	¹⁸³ winsense-001	⁹²² 1280 ± 0	²¹³ 766 ± 7	²⁵⁹ 1058 ± 47	²²⁰ 983 ± 97	²¹² 1053 ± 119	²¹⁹ 1320 ± 84	¹⁵⁸ 1631 ± 28	¹⁸⁹ 1964 ± 171							
361	winsense-002	288132712	25780	²⁸⁶ winsense-002	¹⁷⁸¹ 1582	²⁰⁴⁸ 2048 ± 0	¹¹⁰ 494 ± 2	⁸⁷ 498 ± 1	⁷⁶ 519 ± 1	⁶³ 537 ± 1	⁶⁹ 634 ± 1	¹⁶² 1683 ± 8	¹⁶¹ 1685 ± 7						
362	wuhantianyu-001	476280956	66457	¹⁷¹ wuhantianyu-001	⁸⁶⁶ 1032	²⁰⁴⁸ 2048 ± 0	¹⁶⁹ 642 ± 1	¹³⁴ 642 ± 1	¹¹⁹ 644 ± 0	⁹⁸ 652 ± 0	⁸⁶ 697 ± 0	³⁰⁷ 9502 ± 151	³⁰⁷ 9920 ± 253						
363	x-laboratory-000	532501437	197310	²⁶⁶ x-laboratory-000	¹⁵²⁴ 2782	²⁰⁵⁶ 2056 ± 0	²²⁵ 808 ± 7	²¹⁸ 897 ± 113	¹⁹² 907 ± 103	¹⁶⁴ 886 ± 103	⁸⁰ 673 ± 39	⁸⁰ 725 ± 19	⁸⁵ 749 ± 34						
364	x-laboratory-001	640144084	398792	²⁹³ x-laboratory-001	¹⁸⁴⁴ 2862	²⁰⁵⁶ 2056 ± 0	¹⁴³ 586 ± 2	¹²⁰ 596 ± 5	¹⁰³ 603 ± 6	⁸⁷ 620 ± 7	¹¹² 793 ± 14	⁹⁴ 813 ± 28	⁹⁸ 872 ± 32						
365	xforwardai-001	348262545	51163	³¹¹ xforwardai-001	²¹⁷³ 240	²⁰⁴⁸ 2048 ± 0	³²⁸ 1180 ± 2	²⁸⁶ 1182 ± 1	²⁷³ 1194 ± 1	²⁴² 1186 ± 2	²⁰⁰ 1203 ± 1	⁹¹ 779 ± 17	⁹² 797 ± 13						
366	xforwardai-002	724700382	51163	³⁰⁴ xforwardai-002	¹⁹⁸⁹ 3342	⁴⁰⁹⁶ 4096 ± 0	²⁷⁷ 944 ± 1	²³³ 942 ± 1	²⁰⁸ 943 ± 4	¹⁸² 935 ± 1	¹⁵¹ 967 ± 1	¹⁴⁹ 1406 ± 8	¹⁴⁷ 1405 ± 13						
367	xm-000	591914905	148920	¹²⁸ xm-000	⁶⁸⁸ 2592	²⁰⁵² 2052 ± 0	²⁵⁷ 878 ± 2	²¹⁰ 882 ± 1	²²² 988 ± 2	²⁵⁴ 1258 ± 3	²⁸⁵ 2434 ± 7	¹⁵⁹ 1634 ± 17	¹⁵⁸ 1632 ± 20						
368	yisheng-004	498023846	38653	²³⁴ yisheng-004	¹²⁷⁹ 3092	³⁷⁰⁴ 3704 ± 0	⁷⁰ 378 ± 12	-	-	-	-	⁷¹ 693 ± 137	³⁸ 526 ± 34						
369	yitu-003	1562336990	138919	³⁴⁸ yitu-003	³⁷³⁷ 2972	²⁰⁸² 2082 ± 0	²⁴⁸ 860 ± 0	-	-	-	-	³²⁴ 18305 ± 71	³²⁴ 18286 ± 62						
370	yoonik-001	354948637	265353	³¹² yoоник-001	²¹⁹² 140	²⁰⁴⁸ 2048 ± 0	³³⁵ 1223 ± 3	²⁹⁵ 1238 ± 1	²⁷⁸ 1238 ± 1	²⁵² 1240 ± 1	²⁰⁶ 1240 ± 1	⁷⁴ 706 ± 29	⁷⁵ 690 ± 26						
371	yoonik-002	464609963	265415	³³⁰ yoоник-002	²⁷⁵⁵ 1612	²⁰⁴⁸ 2048 ± 0	³²⁰ 1145 ± 4	²⁷⁰ 1123 ± 2	²⁵⁵ 1124 ± 2	²²⁵ 1125 ± 2	¹⁸⁵ 1126 ± 3	⁸⁷ 761 ± 32	⁸⁴ 736 ± 32						
372	ytu-000	1512817409	44032	³²⁰ ytu-000	²⁴⁸⁴ 1622	²⁰⁴⁸ 2048 ± 0	¹¹⁹ 530 ± 0	⁹⁶ 533 ± 0	¹¹⁷ 640 ± 0	¹⁵⁷ 861 ± 2	²⁶⁹ 1949 ± 8	³⁴⁴ 31797 ± 131	³⁴⁵ 31794 ± 133						
373	yuan-002	379363758	165662	³³³ yuan-002	²⁸³⁸ 1122	²⁰⁴⁸ 2048 ± 0	³⁶⁶ 1420 ± 3	³²² 1429 ± 4	³²¹ 1511 ± 4	³⁰³ 1695 ± 4	²⁸⁴ 2408 ± 5	²⁰⁶ 2297 ± 23	²⁰⁷ 2310 ± 31						
374	yuan-003	379309572	147783	³³⁷ yuan-003	²⁸⁸⁵ 1352	²⁰⁴⁸ 2048 ± 0	³⁶³ 1405 ± 2	³²⁰ 1413 ± 3	³¹⁶ 1446 ± 3	²⁹⁶ 1547 ± 5	²⁶⁸ 1878 ± 5	²⁰⁷ 2320 ± 32	²⁰⁶ 2287 ± 34						

Notes

- 1 The configuration size does not capture static data included in libraries.
- 2 The library size is the combined total of all files provided in the submission lib folder. These libraries e.g. OpenCV may or may not be installed on any end user's platform natively and would not need to be installed with the algorithm. Some developers put neural network models in their libraries.
- 3 The memory usage is the peak resident set size reported by the ps system call during template generation.
- 4 The median template creation times are measured on Intel® Xeon® CPU E5-2630 v4 @ 2.20GHz processors.
- 5 The comparison durations, in nanoseconds, are estimated using std::chrono::high_resolution_clock which on the machine in (2) counts 1ns clock ticks. Precision is somewhat worse than that however. The ± value is the median absolute deviation times 1.48 for Normal consistency.

Table 15: Summary of algorithms and properties included in this report. The red superscripts give ranking for the quantity in that column.

		FALSE NON-MATCH RATE (FNMR)																	
	Algorithm	CONSTRAINED, COOPERATIVE												LESS CONSTRAINED, NON-COOP.					
	Name	VISAMC	VISA	MUGSHOT	MUGSHOT12+YRS	VISABORDER	BORDER	BORDER	WILD	CHILDEXP									
	FMR	0.0001	1E-06	1E-05	1E-05	1E-06	1E-06	1E-06	0.0001	0.01									
1	20face-000	0.1268	318	0.1828	315	0.1748	323	0.2768	322	0.1765	311	0.1864	260	0.0927	288	0.0405	225	-	
2	20face-001	0.0521	301	0.0732	300	0.1414	318	0.2549	320	0.0769	295	0.1354	256	0.0419	257	0.0295	130	-	
3	3divi-006	0.0064	131	0.0094	129	0.0047	106	0.0066	109	0.0091	112	0.0191	132	0.0113	116	0.0289	112	-	
4	3divi-007	0.0024	26	0.0038	30	0.0028	26	0.0034	27	0.0046	38	0.0101	54	0.0082	64	0.0300	141	-	
5	acer-001	0.0294	283	0.0504	288	0.0240	281	0.0463	281	0.0436	277	0.0622	228	0.0360	250	0.0307	153	-	
6	acer-002	0.0169	254	0.0262	255	0.0103	211	0.0167	221	0.0182	214	0.0281	175	0.0159	170	0.0297	135	-	
7	acisw-003	0.9682	373	0.9971	372	0.7892	361	0.8738	360	0.8752	354	0.8275	321	0.6698	343	0.4470	345	-	
8	acisw-007	0.4276	348	0.5493	351	0.8425	362	0.9185	361	0.8424	349	0.9976	342	0.9930	357	0.4963	349	-	
9	adera-002	0.0052	94	0.0071	90	0.0047	104	0.0064	105	0.0087	104	0.0159	103	0.0136	143	0.0990	285	-	
10	adera-003	0.0043	74	0.0059	72	0.0036	65	0.0043	51	0.0076	86	0.0151	92	0.0128	135	0.0989	284	-	
11	advance-002	0.0089	175	0.0137	178	0.0073	168	0.0115	173	0.0400	271	0.0722	234	0.0593	273	0.0498	248	-	
12	advance-003	0.0060	123	0.0087	116	0.0052	119	0.0067	110	0.0389	270	0.4914	290	0.1291	297	0.0508	250	-	
13	aifirst-001	0.0119	215	0.0170	210	0.0084	189	0.0127	185	0.0131	171	0.0212	141	0.0138	146	0.0432	233	0.4301	9
14	aigen-001	0.0124	222	0.0219	232	0.0143	249	0.0217	244	0.0236	240	0.8960	324	0.3255	319	0.0681	269	-	
15	aigen-002	0.0192	266	0.0343	271	0.0256	282	0.0402	276	0.0389	269	0.9196	327	0.3876	325	0.1096	292	-	
16	ailabs-001	0.0158	248	0.0276	261	0.0192	268	0.0317	268	0.0352	264	0.0608	225	0.0434	261	0.0338	192	-	
17	aimall-002	0.0119	217	0.0167	208	0.0224	276	0.0411	277	0.0233	237	0.0373	203	0.0235	225	0.0327	181	-	
18	aimall-003	0.0033	47	0.0041	37	0.0033	55	0.0035	32	0.0056	59	0.0109	60	0.0087	75	0.0312	163	-	
19	aiunionface-000	0.0104	201	0.0154	197	0.0082	186	0.0122	176	0.0141	181	0.0243	157	0.0169	179	0.0306	150	-	
20	aize-001	0.0223	274	0.0344	272	0.0199	269	0.0313	266	0.0367	265	0.0522	219	0.0359	249	0.0446	238	-	
21	aize-002	0.0210	272	0.0327	267	0.0280	285	0.0489	284	0.0504	282	0.0692	231	0.0434	260	0.0854	279	-	
22	ajou-001	0.0093	185	0.0147	190	0.0071	165	0.0126	180	0.0173	211	0.0274	170	0.0186	195	0.0348	198	-	
23	alchera-002	0.0107	204	0.0157	200	0.0104	215	0.0229	247	0.0144	186	0.0246	158	0.0198	207	0.0328	183	-	
24	alchera-003	0.0044	75	0.0055	66	0.0031	41	0.0039	41	0.0042	27	0.0077	24	0.0065	26	0.0339	194	-	
25	alfabeta-001	0.4867	358	0.5831	354	0.6855	351	0.8156	353	0.8253	348	0.7765	316	0.6416	342	0.3427	338	-	
26	alice-000	0.0119	218	0.0192	220	0.0106	217	0.0170	222	0.0167	204	0.0265	167	0.0150	162	0.0288	104	-	
27	alleyes-000	0.0058	114	0.0090	122	0.0055	129	0.0087	148	0.0068	81	0.0105	58	0.0076	49	0.0282	67	-	
28	allgovision-000	0.0346	290	0.0527	291	0.0232	277	0.0339	269	0.0372	268	0.0620	227	0.0443	262	0.0607	264	-	
29	alphaface-001	0.0065	133	0.0097	136	0.0039	77	0.0063	104	0.0083	99	-	-	-	0.0280	54	-		
30	alphaface-002	0.0052	97	0.0075	100	0.0030	32	0.0044	54	1.0000	363	0.0115	68	0.0084	70	0.0279	46	-	
31	amplifiedgroup-001	0.5034	360	0.5848	355	0.6973	354	0.8316	354	0.7807	344	0.7724	314	0.6354	339	0.4250	342	-	
32	androvideo-000	0.0243	277	0.0438	284	0.0239	279	0.0365	274	0.0483	281	0.1870	261	0.0635	275	0.1163	295	-	
33	anke-004	0.0080	165	0.0154	198	0.0073	167	0.0112	171	0.0102	140	0.0178	122	0.0118	123	0.0288	106	0.3577	4
34	anke-005	0.0070	142	0.0109	156	0.0059	140	0.0094	154	0.0105	143	0.0142	81	0.0102	96	0.0289	110	0.3337	3
35	antheus-000	0.2564	332	0.3776	335	0.7240	356	0.8699	357	0.8899	355	0.9872	333	0.9483	351	0.7668	356	0.9233	47
36	antheus-001	0.1311	319	0.2306	321	0.5113	340	0.6797	340	0.8748	353	0.9908	336	0.9649	355	0.7586	355	-	
37	anyvision-004	0.0267	281	0.0385	279	0.0258	283	0.0487	283	0.0234	239	0.0301	180	0.0191	200	0.0470	242	0.4633	10
38	anyvision-005	0.0023	24	0.0037	28	0.0027	25	0.0035	31	0.0049	43	0.0084	33	0.0069	36	0.0285	83	-	
39	asusaics-000	0.0125	226	0.0209	226	0.0085	190	0.0134	193	0.0143	184	0.7189	308	0.0285	240	0.0295	129	-	
40	asusaics-001	0.0125	224	0.0210	227	0.0085	192	0.0134	194	0.0143	185	0.7437	311	0.0289	241	0.0295	128	-	
41	authenmetric-002	0.0092	183	0.0134	177	0.0095	208	0.0177	225	0.0192	223	0.0463	211	0.0236	226	0.0306	152	-	
42	authenmetric-003	0.0036	55	0.0053	62	0.0039	81	0.0051	73	0.0095	128	0.9930	337	0.5932	337	0.0290	115	-	
43	aware-005	0.0457	298	0.0643	295	0.0603	305	0.1094	306	0.0613	288	0.1075	251	0.0491	264	0.0314	165	-	
44	aware-006	0.0487	299	0.0819	304	0.0529	301	0.1090	305	0.1011	304	0.1058	247	0.0502	266	0.0317	169	-	

Table 16: FNMR is the proportion of mated comparisons below a threshold set to achieve the FMR given in the header on the fourth row. FMR is the proportion of impostor comparisons at or above that threshold. The light grey values give rank over all algorithms in that column. The pink columns use only same-sex impostors; others are selected regardless of demographics. The exception, in the green column, uses “matched-covariates” i.e. impostors of the same sex, age group, and country of birth. The second pink column includes effects of extended ageing. Missing entries for border, visa, mugshot and wild images generally mean the algorithm did not run to completion. For child exploitation, missing entries arise because NIST executes those runs only infrequently. The VISA columns compare images described in section 2.1. The MUGSHOT columns compare images described in section 2.4. The VISA-BORDER column compare images described in section 2.2 with those of section 2.3. The BORDER column compares images described in section 2.3. The WILD columns compare images described in section 2.5. The CHILD-EXPLOITATION columns compare images described in section ??.

		FALSE NON-MATCH RATE (FNMR)													
	Algorithm	CONSTRAINED, COOPERATIVE								LESS CONSTRAINED, NON-COOP.					
	Name	VISAMC	VISA	MUGSHOT	MUGSHOT12+YRS	VISABORDER	BORDER	BORDER	WILD	CHILDEXP					
	FMR	0.0001	1E-06	1E-05	1E-05	1E-06	1E-06	1E-06	0.0001	0.01					
45	awiros-001	0.4044	345	0.4622	343	0.5530	342	0.6518	339	0.2008	315	0.1994	265	0.1386	300
46	awiros-002	0.1990	326	0.2561	324	0.3319	332	0.4411	331	0.3821	328	0.9938	338	0.2634	313
47	ayftech-001	0.0946	314	0.1941	316	0.2438	328	0.3625	326	0.1558	309	0.1589	257	0.0936	289
48	ayonix-000	0.4351	351	0.4872	344	0.6150	348	0.7510	347	0.6557	337	0.6361	301	0.4981	331
49	beethedata-000	0.0127	227	0.0195	221	0.0092	202	0.0157	213	0.0171	208	0.0306	182	0.0204	209
50	biocube-001	0.5596	363	0.6834	361	0.7700	360	0.8712	358	0.8446	350	0.9661	330	0.7922	346
51	bioidtechswiss-001	0.0054	104	0.0072	91	0.0069	160	0.0124	179	0.0060	65	0.0094	43	0.0065	29
52	bioidtechswiss-002	0.0049	84	0.0067	85	0.0064	150	0.0116	174	0.0067	79	0.0117	69	0.0086	73
53	bm-001	0.7431	368	0.9494	369	0.9586	364	0.9843	363	0.9049	356	0.9021	326	0.8395	349
54	boetech-001	0.0662	308	0.0802	303	0.0493	298	0.0791	298	0.0682	292	0.1074	250	0.0758	283
55	bresee-001	0.0085	173	0.0143	185	0.0086	196	0.0153	211	0.0108	148	0.0168	112	0.0115	120
56	bresee-002	0.0079	163	0.0101	147	0.0065	153	0.0079	131	0.0129	167	0.0263	165	0.0224	221
57	camvi-002	0.0125	225	0.0221	233	0.0089	200	0.0145	203	0.0142	182	0.2650	275	0.0166	178
58	camvi-004	0.0171	258	0.0316	266	0.0042	90	0.0049	69	0.0097	134	0.6636	303	0.0141	150
59	canon-002	0.0034	52	0.0050	55	0.0026	19	0.0033	26	0.0043	29	0.0182	125	0.0065	28
60	canon-003	0.0041	71	0.0059	70	0.0030	31	0.0040	43	0.0040	21	0.0073	17	0.0059	17
61	ceiec-003	0.0071	150	0.0107	154	0.0061	144	0.0079	133	0.0160	196	0.0316	185	0.0260	234
62	ceiec-004	0.0038	63	0.0051	56	0.0045	103	0.0053	76	0.0062	72	0.3939	284	0.0104	103
63	chosun-001	0.0525	302	0.0936	306	0.0742	309	0.1263	309	0.0978	303	1.0000	358	0.9354	350
64	chosun-002	0.0390	293	0.0646	296	0.0339	292	0.0576	292	0.0455	279	0.6904	305	0.1746	306
65	chtface-003	0.0091	179	0.0146	188	0.0083	188	0.0128	187	0.0132	172	0.0220	148	0.0149	160
66	chtface-004	0.0046	78	0.0062	79	0.0052	118	0.0080	135	0.0088	110	0.0152	93	0.0106	106
67	clearviewai-000	0.0010	4	0.0019	7	0.0024	6	0.0028	13	0.0030	5	0.0058	6	0.0050	5
68	closeli-001	0.0136	230	0.0163	203	0.0039	79	0.0054	79	0.0072	83	1.0000	353	0.0094	87
69	cloudmatrix-000	0.0192	267	0.0340	270	0.0133	243	0.0220	245	0.9837	358	1.0000	355	0.0281	238
70	cloudwalk-hr-003	0.0026	33	0.0041	39	0.0040	85	0.0058	88	0.0060	70	0.9992	345	0.0094	85
71	cloudwalk-hr-004	0.0009	1	0.0018	5	0.0034	57	0.0028	17	0.0052	50	0.9992	346	0.0093	84
72	cloudwalk-mt-003	0.0013	8	0.0022	8	0.0026	16	0.0027	10	0.0039	17	0.0076	19	0.0067	31
73	cloudwalk-mt-004	0.0009	3	0.0013	1	0.0024	8	0.0021	1	0.0028	3	0.0054	3	0.0050	6
74	clova-000	0.0099	195	0.0150	192	0.0094	206	0.0147	206	0.0136	174	0.0213	143	0.0152	166
75	cogent-005	0.0060	121	0.0112	161	0.0064	152	0.0070	114	0.0095	127	0.0184	128	0.0135	140
76	cogent-006	0.0046	79	0.0059	73	0.0036	62	0.0047	60	0.0058	63	0.0113	65	0.0091	80
77	cognitec-002	0.0066	135	0.0101	148	0.0079	177	0.0108	168	0.0181	213	0.0317	186	0.0237	227
78	cognitec-003	0.0038	61	0.0052	58	0.0054	128	0.0057	86	0.0225	234	0.0416	209	0.0388	253
79	cor-001	0.0075	156	0.0113	163	0.0055	132	0.0084	142	0.0091	114	0.0148	87	0.0092	83
80	coretech-000	0.7699	370	1.0000	373	1.0000	373	-	1.0000	371	1.0000	368	1.0000	375	1.0000
81	corsight-001	0.0040	66	0.0057	69	0.0033	54	0.0047	59	0.0045	32	0.0095	46	0.0063	24
82	corsight-002	0.0053	98	0.0068	87	0.0030	36	0.0041	45	0.0039	19	0.0079	26	0.0054	11
83	csc-002	0.0099	196	0.0132	175	0.0077	172	0.0142	200	0.0126	165	0.0195	134	0.0146	156
84	csc-003	0.0053	99	0.0065	82	0.0037	70	0.0047	62	0.0074	84	0.0124	75	0.0112	115
85	ctbcbank-000	0.0168	253	0.0250	249	0.0146	252	0.0224	246	0.0211	231	0.8964	325	0.3779	324
86	ctbcbank-001	0.0155	246	0.0235	242	0.0148	257	0.0243	252	0.0207	228	0.9279	328	0.3469	321
87	cubox-001	0.0064	132	0.0080	108	0.0037	69	0.0055	81	0.0060	66	0.0111	62	0.0077	50
88	cubox-002	0.0034	51	0.0041	38	0.0025	13	0.0025	8	0.0033	8	0.0064	10	0.0058	16

Table 17: FNMR is the proportion of mated comparisons below a threshold set to achieve the FMR given in the header on the fourth row. FMR is the proportion of impostor comparisons at or above that threshold. The light grey values give rank over all algorithms in that column. The pink columns use only same-sex impostors; others are selected regardless of demographics. The exception, in the green column, uses “matched-covariates” i.e. impostors of the same sex, age group, and country of birth. The second pink column includes effects of extended ageing. Missing entries for border, visa, mugshot and wild images generally mean the algorithm did not run to completion. For child exploitation, missing entries arise because NIST executes those runs only infrequently. The VISA columns compare images described in section 2.1. The MUGSHOT columns compare images described in section 2.4. The VISA-BORDER column compare images described in section 2.2 with those of section 2.3. The BORDER column compares images described in section 2.3. The WILD columns compare images described in section 2.5. The CHILD-EXPLOITATION columns compare images described in section ??.

FNMR(T)
FMR(T)
"False non-match rate"
"False match rate"

		FALSE NON-MATCH RATE (FNMR)																	
	Algorithm	CONSTRAINED, COOPERATIVE								LESS CONSTRAINED, NON-COOP.									
	Name	VISAMC	VISA	MUGSHOT	MUGSHOT12+YRS	VISABORDER	BORDER	BORDER	WILD	CHILDEXP									
	FMR	0.0001	1E-06	1E-05	1E-05	1E-06	1E-06	1E-05	0.0001	0.01									
89	cudocommunication-001	0.4777	356	1.0000	375	0.4373	336	0.5360	333	1.0000	366	1.0000	362	1.0000	369	1.0000	375	-	
90	cuhk01-001	0.0036	58	0.0045	47	0.0031	45	0.0046	57	0.0051	49	0.0095	47	0.0079	55	0.1492	304	-	
91	cybercore-000	0.0728	310	0.1110	309	0.1521	320	0.2375	317	0.1874	314	0.1907	262	0.1178	295	0.1191	298	-	
92	cyberextruder-001	0.1972	324	0.2547	323	0.4686	339	0.6387	338	0.3807	327	0.3806	282	0.2582	310	0.1747	310	0.7804	40
93	cyberextruder-002	0.0811	312	0.1336	311	0.1465	319	0.2266	316	0.2086	318	1.0000	371	1.0000	370	0.1000	287	0.6105	22
94	cyberlink-006	0.0042	72	0.0054	64	0.0043	92	0.0049	67	0.0052	54	0.0097	50	0.0077	51	0.0278	34	-	
95	cyberlink-007	0.0032	45	0.0053	61	0.0041	88	0.0043	49	0.0052	53	0.0243	156	0.0084	71	0.0280	51	-	
96	dahua-005	0.0031	43	0.0046	48	0.0035	61	0.0049	70	0.0046	35	0.0076	20	0.0062	23	0.0277	32	-	
97	dahua-006	0.0027	34	0.0039	33	0.0031	43	0.0039	42	0.0039	18	0.0067	14	0.0058	15	0.0280	48	-	
98	daon-000	0.0095	191	0.0117	165	0.0068	157	0.0077	128	0.0092	119	0.0174	118	0.0137	145	0.0331	185	-	
99	decatur-000	0.0714	309	0.1115	310	0.0608	306	0.1106	307	0.0866	298	1.0000	356	0.0714	280	0.0658	267	-	
100	decatur-001	0.0424	295	0.0711	298	0.0237	278	0.0458	280	0.0447	278	1.0000	351	0.9969	359	0.0280	53	-	
101	deepglint-003	0.0027	36	0.0038	31	0.0030	35	0.0032	25	0.0043	28	0.0082	31	0.0076	48	0.0279	40	-	
102	deepglint-004	0.0025	29	0.0034	25	0.0039	80	0.0061	101	0.0050	47	0.0091	39	0.0082	63	0.0285	89	-	
103	deepsea-001	0.0136	231	0.0215	229	0.0142	248	0.0214	243	0.0163	200	0.0250	160	0.0192	201	0.0347	197	0.5606	18
104	deepline-000	0.0145	237	0.0265	257	0.0113	231	0.0196	236	0.0151	189	0.0215	145	0.0129	136	0.0290	114	-	
105	dermalog-008	0.0096	193	0.0166	207	0.0086	194	0.0133	192	0.0165	202	0.0586	223	0.0226	222	0.0277	31	-	
106	dermalog-009	0.0067	137	0.0094	128	0.0051	117	0.0069	112	0.0116	158	0.0312	183	0.0177	186	0.0270	3	-	
107	didiglobalface-001	0.0055	107	0.0092	125	0.0030	33	0.0045	55	0.0088	107	0.0119	72	0.0085	72	0.0282	66	0.4270	7
108	digitalbarriers-002	0.3360	341	0.3690	333	0.0877	311	0.1557	310	0.0971	302	0.0951	243	0.0497	265	0.0436	235	-	
109	dps-000	0.0115	210	0.0176	214	0.0149	259	0.0185	231	0.0173	210	0.0275	172	0.0180	189	0.1067	290	-	
110	dsk-000	0.1526	321	0.2169	319	0.3787	333	0.5426	335	0.3115	321	0.3089	278	0.1994	307	0.2201	320	0.7313	33
111	einetworks-000	0.0099	197	0.0180	216	0.0088	199	0.0140	198	0.0130	169	0.0225	151	0.0147	158	0.0293	124	-	
112	ekin-002	0.1168	316	0.2042	317	0.1530	321	0.2524	319	0.1777	313	0.2773	276	0.1347	299	0.4801	348	-	
113	enface-000	0.0028	38	0.0049	52	0.0043	95	0.0072	116	0.0058	64	0.0150	90	0.0090	79	0.0290	119	-	
114	eocortex-000	0.3485	342	0.6943	362	0.1122	314	0.1574	311	0.2155	320	0.2257	271	0.1606	305	0.2546	330	-	
115	ercacat-001	0.0036	57	0.0044	45	0.0033	52	0.0047	63	0.0106	145	0.0202	138	0.0184	192	0.0258	1	-	
116	euronav-001	0.2786	333	0.3608	332	0.4489	338	0.6105	337	0.5010	331	0.5392	294	0.3769	323	0.4333	343	-	
117	expasoft-001	0.0328	289	0.0488	286	0.0211	273	0.0342	271	0.0629	291	0.6483	302	0.2816	315	0.0552	259	-	
118	expasoft-002	0.0170	255	0.0274	259	0.0787	310	0.0768	297	0.1629	310	0.9996	347	0.9631	354	0.0337	190	-	
119	f8-001	0.0249	278	0.0336	268	0.0178	265	0.0232	248	0.0303	257	0.0615	226	0.0408	256	0.0475	244	0.5272	15
120	faceonline-001	0.0269	282	0.0359	275	0.0387	295	0.0721	296	0.0246	248	0.0349	196	0.0220	216	0.0548	257	-	
121	facesoft-000	0.0085	172	0.0112	160	0.0064	151	0.0107	167	0.0091	113	0.0171	115	0.0107	107	0.0275	18	0.4992	12
122	facetag-000	0.2836	334	0.4081	339	0.2933	330	0.4303	329	0.3448	323	0.6312	300	0.3530	322	0.2087	319	-	
123	facetag-001	0.2920	336	0.4538	341	0.3220	331	0.4371	330	1.0000	376	1.0000	375	0.3254	318	0.3072	336	-	
124	facex-001	1.0000	375	1.0000	374	1.0000	368	-	1.0000	369	1.0000	366	1.0000	364	1.0000	366	-		
125	facex-002	0.0803	311	0.1404	312	0.1283	316	0.1979	314	0.1440	308	0.1952	264	0.1299	298	0.2377	323	-	
126	farfaces-001	0.4890	359	0.5860	356	0.5650	343	0.7268	344	0.8015	346	0.7511	312	0.5892	336	0.1976	317	-	
127	fiberhome-nanjing-003	0.0090	176	0.0139	182	0.0082	185	0.0144	201	0.0110	152	0.0174	116	0.0107	108	0.0272	8	-	
128	fiberhome-nanjing-004	0.0037	60	0.0056	68	0.0031	40	0.0043	50	0.0043	30	0.0083	32	0.0061	21	0.0272	7	-	
129	fincore-000	0.0309	286	0.0502	287	0.0281	286	0.0510	286	0.0521	284	0.0815	237	0.0522	267	0.0681	270	-	
130	fujitsulab-002	0.0091	181	0.0124	169	0.0105	216	0.0156	212	0.0169	207	0.0345	194	0.0146	157	0.0282	63	-	
131	fujitsulab-003	0.0045	77	0.0065	83	0.0057	137	0.0083	140	0.0080	93	0.0154	98	0.0101	93	0.0280	47	-	
132	geo-002	0.0171	257	0.0187	219	0.0035	60	0.0051	75	0.0064	74	0.0117	70	0.0083	68	0.0302	145	-	

Table 18: FNMR is the proportion of mated comparisons below a threshold set to achieve the FMR given in the header on the fourth row. FMR is the proportion of impostor comparisons at or above that threshold. The light grey values give rank over all algorithms in that column. The pink columns use only same-sex impostors; others are selected regardless of demographics. The exception, in the green column, uses “matched-covariates” i.e. impostors of the same sex, age group, and country of birth. The second pink column includes effects of extended ageing. Missing entries for border, visa, mugshot and wild images generally mean the algorithm did not run to completion. For child exploitation, missing entries arise because NIST executes those runs only infrequently. The VISA columns compare images described in section 2.1. The MUGSHOT columns compare images described in section 2.4. The VISA-BORDER column compare images described in section 2.2 with those of section 2.3. The BORDER column compares images described in section 2.3. The WILD columns compare images described in section 2.5. The CHILD-EXPLOITATION columns compare images described in section ??.

		FALSE NON-MATCH RATE (FNMR)																	
	Algorithm	CONSTRAINED, COOPERATIVE								LESS CONSTRAINED, NON-COOP.									
	Name	VISAMC	VISA	MUGSHOT	MUGSHOT12+YRS	VISABORDER	BORDER	BORDER	WILD	CHILDEXP									
	FMR	0.0001	1E-06	1E-05	1E-05	1E-06	1E-06	1E-05	0.0001	0.01									
133	geo-003	0.0180	261	0.0313	265	0.0239	280	0.0552	287	0.0319	262	0.0487	215	0.0222	219	0.0308	160	-	
134	glory-002	0.0241	276	0.0311	264	0.0116	235	0.0151	210	0.0157	193	0.0264	166	0.0188	198	0.1265	299	-	
135	glory-003	0.0076	159	0.0125	172	0.0077	174	0.0103	164	0.0130	168	0.0205	139	0.0143	153	0.0763	273	-	
136	gorilla-007	0.0074	154	0.0111	159	0.0065	154	0.0126	181	0.0100	138	0.0151	91	0.0102	95	0.0278	35	-	
137	gorilla-008	0.0058	116	0.0091	123	0.0049	110	0.0079	132	0.0079	92	0.0126	77	0.0091	81	0.0278	38	-	
138	griaule-000	0.0071	147	0.0099	139	0.0050	113	0.0072	115	0.0160	194	0.0304	181	0.0267	236	0.0338	191	-	
139	hertasecurity-000	0.0630	306	0.0780	302	0.0503	300	0.0898	300	0.0738	293	0.0693	233	0.0420	258	0.0575	262	-	
140	hik-001	0.0096	192	0.0125	171	0.0093	205	0.0164	219	0.0108	149	0.0937	241	0.0127	133	0.0271	5	-	
141	hisign-001	0.0036	54	0.0050	54	0.0034	56	0.0046	56	0.0079	91	0.0153	97	0.0133	138	0.0286	96	-	
142	hyperverge-001	1.0000	376	1.0000	376	1.0000	376	-	1.0000	364	1.0000	360	1.0000	367	1.0000	374	-		
143	hyperverge-002	0.0050	86	0.0066	84	0.0035	59	0.0051	72	0.0062	71	0.0107	59	0.0074	45	0.0276	27	-	
144	icm-002	0.0143	235	0.0249	248	0.0144	250	0.0256	253	0.0236	242	0.0386	205	0.0263	235	0.0339	193	-	
145	icm-003	0.0138	232	0.0222	235	0.0149	258	0.0282	261	0.0227	235	0.0384	204	0.0257	232	0.0333	187	-	
146	icthtc-000	0.0260	280	0.0396	280	0.0207	272	0.0339	270	0.0291	254	0.0474	213	0.0346	247	0.0459	241	-	
147	id3-006	0.0072	152	0.0103	149	0.0049	111	0.0074	122	0.0095	126	0.0165	110	0.0119	126	0.9938	364	-	
148	id3-008	0.0039	64	0.0055	67	0.0032	48	0.0042	46	0.0081	97	0.0155	99	0.0134	139	0.8856	360	-	
149	idemia-007	0.0024	27	0.0039	34	0.0032	50	0.0038	39	0.0046	37	0.0092	41	0.0070	39	0.0288	108	-	
150	idemia-008	0.0023	25	0.0032	21	0.0023	4	0.0028	12	0.0034	11	0.0067	13	0.0056	13	0.0290	117	-	
151	iit-002	0.0111	208	0.0177	215	0.0085	191	0.0140	197	0.0193	224	0.0332	191	0.0260	233	0.1373	301	-	
152	iit-003	0.0082	170	0.0151	195	0.0053	121	0.0084	143	0.0122	163	0.0199	136	0.0137	144	0.0407	226	-	
153	imagus-002	0.0062	125	0.0086	114	0.0053	123	0.0075	123	0.0121	161	0.0207	140	0.0161	172	0.0735	272	-	
154	imagus-004	0.0063	127	0.0094	132	0.0055	131	0.0081	137	0.0098	135	0.0157	102	0.0111	112	0.0283	74	-	
155	imperial-000	0.0067	138	0.0108	155	0.0080	181	0.0134	195	0.0087	105	0.0581	221	0.0102	97	0.0281	58	-	
156	imperial-002	0.0058	115	0.0081	111	0.0055	130	0.0085	145	0.0083	100	0.0157	101	0.0103	98	0.0273	12	0.5151	13
157	incode-009	0.0044	76	0.0067	86	0.0034	58	0.0051	71	0.0049	44	0.0091	38	0.0067	32	0.0296	133	-	
158	incode-010	0.0041	69	0.0063	81	0.0028	27	0.0043	48	0.0047	41	0.0077	23	0.0061	20	0.0296	134	-	
159	innefulabs-000	0.0122	219	0.0199	222	0.0112	229	0.0197	237	0.0222	233	0.0372	202	0.0271	237	0.0348	200	-	
160	innovativetechnologyltd-001	0.0578	304	0.0938	307	0.0501	299	0.0981	301	0.0592	287	0.0779	236	0.0422	259	0.0449	240	-	
161	innovativetechnologyltd-002	0.0451	297	0.0716	299	0.0541	302	0.1009	303	0.0506	283	0.0682	229	0.0371	251	0.0804	278	-	
162	innovatrics-006	0.0058	113	0.0089	121	0.0061	145	0.0096	158	0.0096	131	0.0165	111	0.0103	99	0.0281	56	0.3056	2
163	innovatrics-007	0.0040	68	0.0054	65	0.0057	136	0.0078	129	0.0079	90	0.0123	73	0.0088	76	0.0282	68	-	
164	insightface-000	0.0018	18	0.0027	17	0.0029	28	0.0030	24	0.0038	16	0.0077	22	0.0068	34	0.0276	26	-	
165	insightface-001	0.0009	2	0.0014	2	0.0027	22	0.0024	4	0.0035	13	0.0070	15	0.0065	27	0.0279	42	-	
166	intellicloudai-001	0.0142	234	0.0234	240	0.0092	204	0.0145	202	0.0162	198	0.0371	201	0.0171	181	0.0409	227	-	
167	intellicloudai-002	0.0059	119	0.0085	113	0.0060	142	0.0069	113	0.0108	147	0.2477	274	0.0171	180	0.0303	146	-	
168	intellifusion-001	0.0072	151	0.0094	131	0.0056	135	0.0085	146	0.0111	154	0.0212	142	0.0143	152	0.0289	109	0.5454	16
169	intellifusion-002	0.0059	118	0.0077	102	0.0040	84	0.0074	121	0.0085	103	0.5352	293	0.0104	104	0.0305	149	-	
170	intellivision-001	0.1335	320	0.2205	320	0.1090	312	0.1670	312	0.1385	306	0.1676	258	0.1170	294	0.2445	325	0.7766	39
171	intellivision-002	0.1000	315	0.1775	314	0.0610	307	0.1009	302	0.0805	297	0.1074	249	0.0682	276	0.0768	274	-	
172	intelresearch-003	0.0046	81	0.0062	77	0.0038	74	0.0060	95	0.0088	109	0.0168	113	0.0136	141	0.0304	148	-	
173	intelresearch-004	0.0025	28	0.0035	26	0.0032	47	0.0038	37	0.0049	45	0.0094	42	0.0072	40	0.0290	118	-	
174	intsyssmsu-001	0.9543	372	0.9888	371	0.9923	365	-	0.9977	359	0.9955	339	0.9892	356	0.7871	357	-		
175	intsyssmsu-002	0.0130	228	0.0254	251	0.0137	246	0.0267	259	0.0160	195	0.0267	169	0.0145	155	0.0289	113	-	
176	ionetworks-000	0.0060	124	0.0087	117	0.0044	96	0.0058	90	0.0080	96	0.0144	85	0.0112	113	0.0319	171	-	

Table 19: FNMR is the proportion of mated comparisons below a threshold set to achieve the FMR given in the header on the fourth row. FMR is the proportion of impostor comparisons at or above that threshold. The light grey values give rank over all algorithms in that column. The pink columns use only same-sex impostors; others are selected regardless of demographics. The exception, in the green column, uses “matched-covariates” i.e. impostors of the same sex, age group, and country of birth. The second pink column includes effects of extended ageing. Missing entries for border, visa, mugshot and wild images generally mean the algorithm did not run to completion. For child exploitation, missing entries arise because NIST executes those runs only infrequently. The VISA columns compare images described in section 2.1. The MUGSHOT columns compare images described in section 2.4. The VISA-BORDER column compare images described in section 2.2 with those of section 2.3. The BORDER column compares images described in section 2.3. The WILD columns compare images described in section 2.5. The CHILD-EXPLOITATION columns compare images described in section ??.

Algorithm	FALSE NON-MATCH RATE (FNMR)																	
	CONSTRAINED, COOPERATIVE										LESS CONSTRAINED, NON-COOP.							
	Name	VisAMC	VISA	MUGSHOT	MUGSHOT12+YRS	VISABORDER	BORDER	BORDER	WILD	CHILDEXP								
	FMR	0.0001	1E-06	1E-05	1E-05	1E-06	1E-06	1E-06	0.0001	0.01								
177 iqface-000	0.0091	180	0.0143	183	0.0075	171	0.0110	169	0.0171	209	0.2234	269	0.0359	248	0.0381	217	0.6490	24
178 iqface-003	0.0058	112	0.0079	106	0.0051	116	0.0058	91	0.0104	142	0.0200	137	0.0193	202	0.0402	223	-	
179 irex-000	0.0052	95	0.0099	140	0.0056	134	0.0083	141	0.0137	177	0.0163	109	0.0078	53	0.0285	85	-	
180 isap-001	0.5092	361	0.6588	359	0.6899	353	0.7978	350	0.7200	340	0.7253	309	0.5373	333	0.1931	315	-	
181 isap-002	0.0114	209	0.0186	218	0.0087	197	0.0151	209	0.0156	192	0.5134	292	0.0333	243	0.0354	208	-	
182 isityou-000	0.5682	364	0.7033	363	1.0000	375	-	1.0000	365	1.0000	361	1.0000	368	1.0000	373	1.0000	69	
183 isystems-001	0.0149	243	0.0245	246	0.0138	247	0.0210	241	0.0209	230	0.0332	190	0.0223	220	0.0524	254	0.5152	14
184 isystems-002	0.0118	213	0.0182	217	0.0111	226	0.0162	217	0.0166	203	0.0284	176	0.0195	204	0.0516	251	0.4876	11
185 itmo-007	0.0080	166	0.0125	170	0.0107	218	0.0185	229	0.0167	205	0.0222	150	0.0144	154	0.0300	140	-	
186 itmo-008	0.0090	178	0.0150	194	0.0058	139	0.0059	94	0.0187	219	0.0355	197	0.0339	244	0.1498	305	-	
187 ivacognitive-001	0.0189	264	0.0351	273	0.0123	238	0.0235	249	0.0198	226	0.0274	171	0.0155	167	0.0296	132	-	
188 iws-000	0.4824	357	0.5801	353	0.6859	352	0.8155	352	0.8251	347	0.7756	315	0.6400	341	0.3251	337	-	
189 kakao-005	0.0040	65	0.0059	71	0.0036	68	0.0057	85	0.0085	102	0.0239	154	0.0125	131	0.0280	52	-	
190 kakao-006	0.0016	14	0.0029	19	0.0024	5	0.0028	18	0.0035	12	0.0065	12	0.0057	14	0.0335	188	-	
191 kakaopay-001	0.0152	245	0.0252	250	0.0145	251	0.0270	260	0.0232	236	0.0344	193	0.0194	203	0.0416	230	-	
192 kedacom-000	0.0055	105	0.0081	110	0.0111	228	0.0120	175	0.0415	273	0.0966	245	0.0686	277	0.2511	328	0.7650	37
193 kiwitech-000	0.0076	158	0.0105	151	0.0081	183	0.0128	188	0.0096	129	0.0163	108	0.0101	94	0.0279	45	-	
194 kneron-003	0.0542	303	0.0902	305	0.0346	293	0.0562	290	0.0919	300	0.1251	254	0.0973	290	0.3053	335	0.6962	29
195 kneron-005	0.0157	247	0.0259	253	0.0126	241	0.0212	242	0.0406	272	0.0693	232	0.0542	269	0.0471	243	-	
196 kookmin-002	0.0054	102	0.0077	101	0.0043	93	0.0065	106	0.0123	164	0.7591	313	0.0198	206	0.0285	86	-	
197 kookmin-003	0.0043	73	0.0060	75	0.0036	67	0.0053	78	0.0111	155	0.9831	332	0.0185	194	0.0286	93	-	
198 kuke3d-001	0.0058	111	0.0104	150	0.0083	187	0.0093	153	0.0270	251	0.9901	335	0.8341	348	0.0404	224	-	
199 lemalabs-001	0.0111	207	0.0175	212	0.0088	198	0.0142	199	0.0143	183	0.0228	152	0.0140	148	0.0281	55	-	
200 line-000	0.0172	259	0.0236	243	0.0109	222	0.0194	234	0.0183	215	0.0291	177	0.0204	210	0.0298	136	-	
201 line-001	0.0025	30	0.0040	35	0.0026	21	0.0034	30	0.0045	34	0.4127	286	0.0080	59	0.0283	73	-	
202 lookman-002	0.0297	284	0.0547	292	0.0339	291	0.0562	289	0.0614	289	0.0960	244	0.0790	284	0.2640	332	-	
203 lookman-004	0.0074	155	0.0099	141	0.0124	240	0.0149	207	0.0430	276	0.0866	239	0.0694	278	0.2516	329	0.7664	38
204 luxand-000	0.2056	327	0.2814	326	0.4053	335	0.5365	334	0.3497	324	0.3743	281	0.2605	311	0.2222	322	-	
205 mantra-000	0.0037	59	0.0052	59	0.0054	126	0.0056	83	0.0097	133	0.0181	124	0.0151	163	0.0350	204	-	
206 maxvision-000	0.0078	162	0.0106	153	0.0110	224	0.0147	205	0.0368	267	1.0000	365	0.1545	303	0.0445	237	-	
207 megvii-003	0.0064	130	0.0094	127	0.0136	245	0.0260	255	0.0050	46	0.0080	27	0.0059	19	0.0288	99	-	
208 meituan-000	0.0197	268	0.0424	283	0.0078	175	0.0074	120	0.0103	141	0.0193	133	0.0164	175	0.1063	289	-	
209 meiya-001	0.0171	256	0.0275	260	0.0159	263	0.0261	257	0.0311	259	0.2250	270	0.0245	230	0.0363	213	-	
210 mendaxiatech-000	0.0027	35	0.0036	27	0.0029	29	0.0036	34	0.0031	6	0.0057	5	0.0051	8	0.0275	19	-	
211 microfocus-001	0.4482	353	0.5524	352	0.7256	357	0.8416	355	0.7301	341	0.6926	306	0.5180	332	0.2567	331	0.6890	28
212 microfocus-002	0.3605	343	0.5057	346	0.5783	345	0.7223	343	0.5909	332	0.5963	299	0.4160	328	0.1582	307	0.6517	25
213 minivision-000	0.0033	48	0.0048	51	0.0038	75	0.0049	66	0.0055	58	0.0094	45	0.0079	57	0.0273	9	-	
214 mobai-000	0.0360	292	0.0439	285	0.0372	294	0.0700	294	0.0367	266	0.0939	242	0.0795	285	0.2640	333	-	
215 mobai-001	0.0199	271	0.0219	231	0.0047	105	0.0061	98	0.0093	124	0.0174	117	0.0138	147	0.1045	288	-	
216 mobbl-000	0.2938	337	0.3861	336	0.5391	341	0.6888	341	0.6545	336	0.8027	317	0.6207	338	0.5471	351	-	
217 mobbl-001	0.3208	338	0.4375	340	0.5680	344	0.7193	342	0.6282	334	0.5783	297	0.3984	326	0.1866	313	-	
218 mobipintech-000	0.0090	177	0.0149	191	0.0039	83	0.0057	84	0.0115	157	0.0465	212	0.0182	191	0.0315	167	-	
219 moreedian-000	0.3874	344	0.4912	345	0.9988	366	-	0.9990	360	0.9999	349	0.9998	361	0.4788	347	-		
220 multimodality-000	0.0034	50	0.0047	50	0.0036	66	0.0044	53	0.0077	87	0.9976	343	0.4456	329	0.0287	97	-	

Table 20: FNMR is the proportion of mated comparisons below a threshold set to achieve the FMR given in the header on the fourth row. FMR is the proportion of impostor comparisons at or above that threshold. The light grey values give rank over all algorithms in that column. The pink columns use only same-sex impostors; others are selected regardless of demographics. The exception, in the green column, uses “matched-covariates” i.e. impostors of the same sex, age group, and country of birth. The second pink column includes effects of extended ageing. Missing entries for border, visa, mugshot and wild images generally mean the algorithm did not run to completion. For child exploitation, missing entries arise because NIST executes those runs only infrequently. The VISA columns compare images described in section 2.1. The MUGSHOT columns compare images described in section 2.4. The VISA-BORDER column compare images described in section 2.2 with those of section 2.3. The BORDER column compares images described in section 2.3. The WILD columns compare images described in section 2.5. The CHILD-EXPLOITATION columns compare images described in section ??.

Algorithm	FALSE NON-MATCH RATE (FNMR)																	
	CONSTRAINED, COOPERATIVE																	
	Name	VisAMC	VISA	MUGSHOT	MUGSHOT12+YRS	VisABORDER	BORDER	BORDER	WILD	CHILDEXP								
FMR	0.0001	1E-06	1E-05	1E-05	1E-06	1E-06	1E-05	0.0001	0.01									
221	mvision-001	0.0191	265	0.0233	238	0.0204	271	0.0356	272	0.0198	227	0.0337	192	0.0242	229	0.0431	232	-
222	nazhai-000	0.0040	67	0.0059	74	0.0036	63	0.0048	65	0.0057	60	0.0125	76	0.0083	67	0.0275	20	-
223	neosystems-002	0.2905	335	0.4077	338	0.2028	326	0.3252	324	0.4088	329	0.5519	295	0.3331	320	0.4500	346	-
224	neosystems-003	0.2429	329	0.3349	329	0.1844	324	0.2999	323	0.5942	333	0.3936	283	0.2292	308	0.1404	302	-
225	netbridgeTech-001	0.4749	355	0.6599	360	0.4438	337	0.5676	336	0.4491	330	1.0000	352	0.9541	352	0.1098	293	-
226	netbridgeTech-002	0.0101	199	0.0166	205	0.0077	173	0.0127	184	0.0133	173	0.8215	319	0.0523	268	0.0351	206	-
227	neurotechnology-011	0.0050	87	0.0087	115	0.0061	146	0.0097	160	0.0077	89	0.0404	208	0.0092	82	0.0293	126	-
228	neurotechnology-012	0.0051	93	0.0070	89	0.0038	72	0.0056	82	0.0066	78	0.0112	64	0.0075	46	0.0279	44	-
229	rhn-001	0.0066	136	0.0098	137	0.0053	122	0.0079	134	0.0093	120	0.0156	100	0.0109	110	0.0308	159	-
230	rhn-002	0.0068	141	0.0096	135	0.0057	138	0.0087	149	0.0136	176	0.0253	162	0.0186	197	0.0302	144	-
231	nodeflux-002	0.0186	263	0.0340	269	0.0261	284	0.0451	279	0.0548	285	1.0000	357	1.0000	363	0.0299	138	-
232	notiontag-001	0.6846	366	0.8006	366	0.3955	334	0.5247	332	0.8669	352	0.8313	322	0.6362	340	0.2221	321	-
233	notiontag-002	0.0066	134	0.0089	119	0.0045	102	0.0061	99	0.0077	88	0.0137	80	0.0104	101	0.0299	137	-
234	nsensecorp-002	0.4277	349	0.5375	349	0.6734	350	0.7924	349	0.7194	339	0.6937	307	0.5617	334	0.5530	352	-
235	nsensecorp-003	0.0251	279	0.0295	263	0.0212	274	0.0305	264	0.0131	170	0.2139	268	0.0141	151	0.0872	281	-
236	ntechlab-010	0.0013	9	0.0017	3	0.0024	12	0.0029	22	0.0031	7	0.0058	7	0.0050	7	0.0292	121	-
237	ntechlab-011	0.0012	6	0.0019	6	0.0024	10	0.0028	20	0.0029	4	0.0055	4	0.0047	3	0.0288	105	-
238	omnigarde-000	0.0633	307	0.1002	308	0.1109	313	0.2042	315	0.1288	305	0.5113	291	0.1227	296	0.0357	210	-
239	omnigarde-001	0.0168	252	0.0260	254	0.0203	270	0.0402	275	0.0243	245	0.0327	188	0.0177	184	0.0288	101	-
240	openface-001	0.1804	323	0.2921	327	0.2878	329	0.3906	328	0.2054	317	0.2338	273	0.1549	304	0.2445	326	-
241	oz-002	0.0071	148	0.0099	144	0.0099	209	0.0100	162	0.0139	179	0.0502	216	0.0202	208	0.5084	350	-
242	oz-003	0.0095	190	0.0143	184	0.0054	127	0.0077	127	0.0096	130	0.0175	120	0.0118	124	0.0288	107	-
243	papsav1923-001	0.0078	161	0.0130	174	0.0068	158	0.0105	166	0.0119	159	0.0221	149	0.0136	142	0.0293	123	-
244	paravision-004	0.0030	41	0.0046	49	0.0030	34	0.0036	33	0.0091	116	0.0188	131	0.0173	182	0.0288	103	0.2467
245	paravision-008	0.0018	17	0.0025	13	0.0024	7	0.0025	7	0.0036	14	0.0070	16	0.0063	25	0.0279	41	-
246	pensees-001	0.0087	174	0.0133	176	0.0071	163	0.0122	178	0.0145	187	0.0252	161	0.0195	205	0.0283	71	-
247	pixelall-006	0.0032	46	0.0042	41	0.0032	46	0.0039	40	0.0063	73	0.9960	340	0.0723	281	0.0283	70	-
248	pixelall-007	0.0036	56	0.0049	53	0.0039	78	0.0044	52	0.0068	80	0.9873	334	0.0217	215	0.0285	90	-
249	psl-008	0.0026	31	0.0040	36	0.0024	9	0.0028	19	0.0041	23	0.0077	21	0.0055	12	0.0280	49	-
250	psl-009	0.0161	250	0.0294	262	0.0023	3	0.0025	5	0.0036	15	0.0065	11	0.0048	4	0.0482	247	-
251	ptakuratsatu-000	0.0060	120	0.0089	120	0.0070	161	0.0104	165	0.0096	132	0.0152	95	0.0100	91	0.0284	78	-
252	pxl-001	0.0488	300	0.0752	301	0.0586	304	0.1087	304	0.0946	301	0.1065	248	0.0625	274	0.1088	291	-
253	pyramid-000	0.0136	229	0.0233	239	0.0117	236	0.0192	233	0.0185	218	0.0322	187	0.0206	212	0.0304	147	-
254	qnap-000	0.0149	242	0.0228	236	0.0155	261	0.0267	258	0.0238	244	0.8329	323	0.0396	255	0.0324	176	-
255	qnap-001	0.0148	239	0.0215	230	0.0103	212	0.0162	216	0.0183	217	0.0301	179	0.0186	196	0.0360	212	-
256	quantasoft-003	0.0081	169	0.0113	164	0.0056	133	0.0076	125	0.0091	115	0.0161	105	0.0107	109	0.0414	229	-
257	rankone-010	0.0079	164	0.0112	162	0.0061	143	0.0081	138	0.0088	108	0.0149	88	0.0117	122	0.0320	174	-
258	rankone-011	0.0049	85	0.0075	99	0.0038	71	0.0048	64	0.0060	69	0.0143	84	0.0080	60	0.0359	211	-
259	realnetworks-004	0.0075	157	0.0101	146	0.0066	155	0.0097	161	0.0108	151	0.0187	130	0.0131	137	0.0285	91	-
260	realnetworks-005	0.0070	143	0.0093	126	0.0063	149	0.0089	151	0.0092	118	0.0161	106	0.0104	102	0.0289	111	-
261	regula-000	0.0184	262	0.0376	278	0.0103	213	0.0185	228	0.0120	160	0.9983	344	0.0231	223	0.0273	11	-
262	remarkai-001	0.0144	236	0.0256	252	0.0102	210	0.0159	214	0.0162	199	0.0582	222	0.0185	193	0.0308	157	-
263	remarkai-003	0.0047	82	0.0063	80	0.0033	53	0.0049	68	0.0054	55	0.0100	53	0.0072	41	0.0275	22	-
264	rendip-000	0.0055	106	0.0077	103	0.0048	108	0.0060	96	0.0080	94	0.0142	83	0.0110	111	0.0433	234	-

Table 21: FNMR is the proportion of mated comparisons below a threshold set to achieve the FMR given in the header on the fourth row. FMR is the proportion of impostor comparisons at or above that threshold. The light grey values give rank over all algorithms in that column. The pink columns use only same-sex impostors; others are selected regardless of demographics. The exception, in the green column, uses “matched-covariates” i.e. impostors of the same sex, age group, and country of birth. The second pink column includes effects of extended ageing. Missing entries for border, visa, mugshot and wild images generally mean the algorithm did not run to completion. For child exploitation, missing entries arise because NIST executes those runs only infrequently. The VISA columns compare images described in section 2.1. The MUGSHOT columns compare images described in section 2.4. The VISA-BORDER column compare images described in section 2.2 with those of section 2.3. The BORDER column compares images described in section 2.3. The WILD columns compare images described in section 2.5. The CHILD-EXPLOITATION columns compare images described in section ??.

		FALSE NON-MATCH RATE (FNMR)																	
	Algorithm	CONSTRAINED, COOPERATIVE								LESS CONSTRAINED, NON-COOP.									
	Name	VISAMC	VISA	MUGSHOT	MUGSHOT12+YRS	VISABORDER	BORDER	BORDER	WILD	CHILDEXP									
	FMR	0.0001	1E-06	1E-05	1E-05	1E-06	1E-06	1E-05	0.0001	0.01									
265	revealmedia-005	0.0050	90	0.0074	98	0.0050	114	0.0068	111	0.0075	85	0.0124	74	0.0104	105	0.3960	341	-	
266	rokid-000	0.0093	186	0.0145	187	0.0073	169	0.0102	163	0.0164	201	0.0280	174	0.0214	214	0.0857	280	-	
267	rokid-001	0.0105	203	0.0162	202	0.0094	207	0.0163	218	0.0181	212	0.0276	173	0.0165	177	0.0325	179	-	
268	s1-002	0.0095	189	0.0144	186	0.0112	230	0.0196	235	0.0234	238	0.0371	200	0.0282	239	0.1167	296	-	
269	s1-003	0.0051	92	0.0073	94	0.0044	97	0.0063	103	0.0052	52	0.0096	49	0.0070	37	0.1321	300	-	
270	saffe-001	0.4339	350	0.5261	347	0.7539	359	0.8736	359	0.7977	345	0.9810	331	0.7435	345	0.3887	340	0.8973	45
271	saffe-002	0.0119	216	0.0206	223	0.0107	221	0.0177	224	0.0244	246	0.9998	348	0.2785	314	0.0308	156	-	
272	samsungsds-000	0.0046	80	0.0069	88	0.0132	242	0.0081	136	0.0099	136	0.0179	123	0.0162	173	0.1874	314	-	
273	samtech-001	0.0197	269	0.0365	276	0.0146	255	0.0241	251	0.0238	243	0.0394	206	0.0251	231	0.0337	189	-	
274	scanovate-002	0.0175	260	0.0355	274	0.0146	253	0.0286	262	0.0269	250	0.0301	178	0.0178	187	0.0301	143	-	
275	scanovate-003	0.0054	101	0.0080	109	0.0054	124	0.0072	118	0.0312	260	0.0599	224	0.0568	271	0.0283	69	-	
276	securifai-001	0.4538	354	0.6142	357	0.5844	346	0.7428	345	0.7051	338	0.9961	341	0.9558	353	0.1963	316	-	
277	securifai-003	0.4086	346	0.7577	365	0.7233	355	0.8070	351	0.7787	343	1.0000	359	0.9988	360	0.8326	359	-	
278	sensetime-004	0.0026	32	0.0038	29	0.0022	2	0.0023	3	0.0042	25	0.0082	30	0.0078	52	0.0293	122	-	
279	sensetime-005	0.0019	19	0.0029	18	0.0022	1	0.0021	2	0.0023	1	0.0044	1	0.0039	1	0.0273	10	-	
280	sertis-000	0.0118	214	0.0208	225	0.0080	179	0.0127	183	0.0110	153	0.0176	121	0.0114	118	0.0285	88	-	
281	sertis-002	0.0049	83	0.0061	76	0.0039	82	0.0061	102	0.0055	57	0.0099	52	0.0070	38	0.0281	57	-	
282	seventhsense-000	0.0067	140	0.0099	143	0.0045	100	0.0065	107	0.0093	121	0.0169	114	0.0124	130	0.0275	21	-	
283	shaman-000	0.9297	371	0.9774	370	0.9990	367	-		0.9999	361	1.0000	354	0.9999	362	0.9575	362	0.9618	49
284	shaman-001	0.3346	340	0.4616	342	0.2368	327	0.3723	327	0.3574	325	0.3527	280	0.2304	309	0.1498	306	0.8990	46
285	shu-002	-		0.0079	107	0.0146	254	0.0308	265	1.0000	362	0.0183	126	0.0115	119	0.0284	79	-	
286	shu-003	0.0028	37	0.0041	40	0.0050	112	0.0088	150	0.0081	98	0.0133	79	0.0094	86	0.0283	75	-	
287	siat-002	0.0091	182	0.0126	173	0.0109	223	0.0190	232	0.0276	253	0.0516	218	0.0464	263	0.0520	253	0.4277	8
288	siat-004	0.0067	139	0.0099	142	0.0152	260	-		0.0275	252	0.4823	289	0.4823	330	1.0000	365	-	
289	sjtu-003	0.0017	16	0.0033	23	0.0030	37	0.0037	35	0.0058	61	0.0104	55	0.0081	62	0.0284	82	-	
290	sjtu-004	0.0014	10	0.0025	12	0.0027	23	0.0028	21	0.0046	36	0.0086	35	0.0073	42	0.0272	6	-	
291	sktelecom-000	0.0038	62	0.0054	63	0.0031	38	0.0051	74	0.0042	24	0.3418	279	0.0061	22	0.0293	125	-	
292	smartengines-000	0.6240	365	0.7562	364	0.9552	363	0.9784	362	0.9515	357	0.9288	329	0.8200	347	0.8037	358	-	
293	smilart-002	0.2440	330	0.3532	331	-		-		0.3785	326	0.4145	287	0.2611	312	-	0.6999	30	
294	smilart-003	0.6944	367	0.8836	367	0.0695	308	0.1193	308	0.0894	299	0.1221	253	0.0737	282	0.1190	297	-	
295	sodec-000	0.0033	49	0.0044	46	0.0040	86	0.0053	77	0.0054	56	0.0096	48	0.0080	58	0.0274	14	-	
296	sqisoft-001	0.1220	317	0.2088	318	0.1978	325	0.3386	325	0.2111	319	0.2798	277	0.1474	302	0.0519	252	-	
297	sqisoft-002	0.0082	171	0.0124	167	0.0051	115	0.0086	147	0.0102	139	0.0183	127	0.0122	128	0.0287	98	-	
298	stagu-000	0.0139	233	0.0208	224	0.0104	214	0.0145	204	0.0156	191	0.8063	318	0.1408	301	0.0332	186	-	
299	starhybrid-001	0.0108	205	0.0138	179	0.0081	182	0.0113	172	0.0152	190	0.0265	168	0.0189	199	0.0350	205	0.5584	17
300	suprema-000	0.0064	129	0.0092	124	0.0081	184	0.0096	159	0.0139	180	0.0254	164	0.0220	217	0.1131	294	-	
301	suprema-001	0.0041	70	0.0053	60	0.0038	76	0.0047	61	0.0060	68	0.0111	61	0.0095	88	0.0382	218	-	
302	supremaid-001	0.0053	100	0.0073	97	0.0045	101	0.0066	108	0.0099	137	0.0186	129	0.0148	159	0.0352	207	-	
303	synesis-006	0.0070	144	0.0096	133	0.0107	219	0.0166	220	-		0.0128	78	0.0089	77	0.0292	120	-	
304	synesis-007	0.0050	88	0.0073	95	0.0062	148	0.0076	124	-		0.0105	56	0.0080	61	0.0288	100	-	
305	synology-000	0.0149	240	0.0238	244	0.0148	256	0.0261	256	0.0221	232	0.0331	189	0.0209	213	0.0330	184	-	
306	synology-002	0.0104	202	0.0153	196	0.0107	220	0.0184	227	0.0189	221	0.2032	266	0.0180	188	0.0312	162	-	
307	sztu-000	0.0092	184	0.0139	181	0.0091	201	0.0201	239	0.0136	175	0.0685	230	0.0118	125	0.0270	2	-	
308	sztu-001	0.0031	42	0.0043	44	0.0025	14	0.0028	16	0.0051	48	0.0113	66	0.0089	78	0.0275	17	-	

Table 22: FNMR is the proportion of mated comparisons below a threshold set to achieve the FMR given in the header on the fourth row. FMR is the proportion of impostor comparisons at or above that threshold. The light grey values give rank over all algorithms in that column. The pink columns use only same-sex impostors; others are selected regardless of demographics. The exception, in the green column, uses “matched-covariates” i.e. impostors of the same sex, age group, and country of birth. The second pink column includes effects of extended ageing. Missing entries for border, visa, mugshot and wild images generally mean the algorithm did not run to completion. For child exploitation, missing entries arise because NIST executes those runs only infrequently. The VISA columns compare images described in section 2.1. The MUGSHOT columns compare images described in section 2.4. The VISA-BORDER column compare images described in section 2.2 with those of section 2.3. The BORDER column compares images described in section 2.3. The WILD columns compare images described in section 2.5. The CHILD-EXPLOITATION columns compare images described in section ??.

Algorithm	FALSE NON-MATCH RATE (FNMR)										LESS CONSTRAINED, NON-COOP.							
	CONSTRAINED, COOPERATIVE																	
	Name	VISAMC	VISA	MUGSHOT	MUGSHOT12+YRS	VISABORDER	BORDER	BORDER	WILD	CHILDEXP								
FMR	0.0001	1E-06	1E-05	1E-05	1E-06	1E-06	1E-06	1E-05	0.0001	0.01								
309 tech5-004	0.0123	220	0.0234	241	0.0086	195	0.0162	215	0.0065	77	0.0112	63	0.0082	65	0.0281	60	-	
310 tech5-005	0.0054	103	0.0072	92	0.0069	159	0.0122	177	0.0060	67	0.0094	44	0.0066	30	0.0349	202	-	
311 techsign-000	0.0325	288	0.0511	289	0.0435	297	0.0710	295	0.0746	294	0.1104	252	0.0841	286	0.0639	266	-	
312 tevian-007	0.0019	20	0.0027	16	0.0032	49	0.0041	44	0.0045	31	0.0086	34	0.0078	54	0.0310	161	-	
313 tevian-008	0.0012	7	0.0017	4	0.0033	51	0.0042	47	0.0042	26	0.0081	28	0.0068	35	0.0290	116	-	
314 tiger-003	0.0313	287	0.0602	294	0.0188	267	0.0359	273	0.0344	263	-	-	-	0.0482	246	0.5610	19	
315 tiger-005	0.0624	305	0.2450	322	0.0292	289	0.0556	288	0.0430	275	1.0000	350	0.9964	358	0.0278	37	-	
316 tinkoff-001	0.0145	238	0.0244	245	0.0318	290	0.0636	293	0.0236	241	1.0000	363	0.0339	245	0.0563	261	-	
317 tongyi-005	0.0073	153	0.0146	189	0.0187	266	0.0421	278	0.0161	197	0.0215	144	0.0149	161	0.0399	221	0.6195	23
318 toppanidgate-000	0.0021	21	0.0033	22	0.0026	17	0.0028	14	0.0039	20	0.0075	18	0.0068	33	0.0376	216	-	
319 toshiba-003	0.0125	223	0.0214	228	0.0085	193	0.0131	191	-	-	0.0241	155	0.0151	165	0.0282	61	-	
320 toshiba-004	0.0030	40	0.0042	42	0.0025	15	0.0027	11	0.0034	10	0.0063	9	0.0053	10	0.0278	36	-	
321 trueface-002	0.0060	122	0.0096	134	0.0048	107	0.0061	100	0.0112	156	0.0198	135	0.0155	168	0.0793	277	-	
322 trueface-003	0.0070	146	0.0094	130	0.0053	120	0.0081	139	0.0122	162	0.0217	147	0.0159	171	0.0785	276	-	
323 tutuptech-000	0.3218	339	0.3696	334	-	-	-	-	0.3237	322	0.4304	288	0.2973	317	0.9415	361	-	
324 twface-000	0.0051	91	0.0072	93	0.0041	89	0.0058	87	0.0071	82	0.0153	96	0.0100	90	0.0276	25	-	
325 twface-001	0.0036	53	0.0051	57	0.0031	44	0.0038	36	0.0049	42	0.0091	40	0.0075	47	0.0277	29	-	
326 ulsee-001	0.0151	244	0.0246	247	0.0113	232	0.0185	230	0.0187	220	0.6766	304	0.0181	190	0.0316	168	-	
327 ultinous-000	0.2343	328	0.3484	330	-	-	-	-	-	-	-	-	-	0.9447	48	-		
328 ultinous-001	0.2485	331	0.4003	337	-	-	-	-	-	-	-	-	-	0.6847	27	-		
329 uluface-002	0.0081	167	0.0123	166	0.0071	162	0.0095	157	0.0107	146	1.0000	369	0.0140	149	0.0444	236	0.6729	26
330 uluface-003	0.0100	198	0.0150	193	0.0079	176	0.0128	186	-	-	-	-	-	0.0635	265	-		
331 unissey-001	0.0095	188	0.0160	201	0.0134	244	0.0150	208	0.0147	188	0.0253	163	0.0163	174	0.0946	283	-	
332 upc-001	0.0234	275	0.0519	290	0.0291	288	0.0490	285	0.0294	255	0.2316	272	0.0389	254	0.0314	166	0.4224	6
333 vcog-002	0.7522	369	0.9033	368	-	-	-	-	-	-	-	-	-	0.7523	35	-		
334 vd-002	0.0429	296	0.0704	297	0.0569	303	0.0844	299	0.0801	296	0.0937	240	0.0577	272	0.0556	260	-	
335 vd-003	0.0199	270	0.0222	234	0.0115	234	0.0130	190	0.0138	178	0.0239	153	0.0177	185	0.0389	219	-	
336 veridas-006	0.0098	194	0.0167	209	0.0079	178	0.0127	182	0.0127	166	0.0217	146	0.0151	164	0.0286	95	-	
337 veridas-007	0.0063	128	0.0083	112	0.0044	98	0.0058	89	0.0080	95	0.0152	94	0.0120	127	0.0284	80	-	
338 verigram-000	0.0032	44	0.0043	43	0.0031	39	0.0034	28	0.0093	123	0.0175	119	0.0164	176	0.0276	24	-	
339 verihubs-inteligensia-000	0.0070	145	0.0098	138	0.0048	109	0.0076	126	0.0092	117	0.0160	104	0.0117	121	0.0283	72	-	
340 via-000	0.0216	273	0.0365	277	0.0177	264	0.0287	263	0.0296	256	0.0572	220	0.0290	242	0.0349	201	0.7638	36
341 via-001	0.0149	241	0.0229	237	0.0114	233	0.0177	226	0.0183	216	0.4056	285	0.0176	183	0.0373	215	-	
342 videmo-000	0.0298	285	0.0423	281	0.0155	262	0.0260	254	0.0246	247	0.0397	207	0.0239	228	0.0541	256	-	
343 videonetis-001	0.5483	362	0.6446	358	0.7517	358	0.8607	356	0.8664	351	0.8255	320	0.6956	344	0.2986	334	0.7297	32
344 videonetis-002	0.4274	347	0.5329	348	0.6081	347	0.7438	346	0.7775	342	0.7297	310	0.5756	335	0.1976	318	0.7435	34
345 viettelheightech-000	0.0117	212	0.0166	206	0.0110	225	0.0198	238	0.0167	206	0.0249	159	0.0158	169	0.0409	228	-	
346 vigilantsolutions-010	0.0109	206	0.0164	204	0.0074	170	0.0095	156	0.0209	229	0.0365	199	0.0233	224	0.0277	30	-	
347 vigilantsolutions-011	0.0124	221	0.0176	213	0.0073	166	0.0095	155	0.0196	225	0.0360	198	0.0221	218	0.0274	13	-	
348 vinai-000	0.0081	168	0.0124	168	0.0045	99	0.0072	117	0.0089	111	0.1814	259	0.0112	114	0.0274	15	-	
349 vion-000	0.0419	294	0.0590	293	0.0422	296	0.0478	282	0.0581	286	0.0968	246	0.0847	287	0.2479	327	0.8765	42
350 visage-000	0.0933	313	0.1441	313	0.1316	317	0.2416	318	0.1395	307	0.1920	263	0.1001	291	0.0500	249	-	
351 visionbox-001	0.0159	249	0.0270	258	0.0111	227	0.0173	223	0.0190	222	0.0315	184	0.0205	211	0.0389	220	-	
352 visionbox-002	0.0058	110	0.0079	104	0.0060	141	0.0074	119	0.0084	101	0.0149	89	0.0113	117	0.0447	239	-	

Table 23: FNMR is the proportion of mated comparisons below a threshold set to achieve the FMR given in the header on the fourth row. FMR is the proportion of impostor comparisons at or above that threshold. The light grey values give rank over all algorithms in that column. The pink columns use only same-sex impostors; others are selected regardless of demographics. The exception, in the green column, uses “matched-covariates” i.e. impostors of the same sex, age group, and country of birth. The second pink column includes effects of extended ageing. Missing entries for border, visa, mugshot and wild images generally mean the algorithm did not run to completion. For child exploitation, missing entries arise because NIST executes those runs only infrequently. The VISA columns compare images described in section 2.1. The MUGSHOT columns compare images described in section 2.4. The VISA-BORDER column compare images described in section 2.2 with those of section 2.3. The BORDER column compares images described in section 2.3. The WILD columns compare images described in section 2.5. The CHILD-EXPLOITATION columns compare images described in section ??.

	Algorithm	FALSE NON-MATCH RATE (FNMR)											
		CONSTRAINED, COOPERATIVE								LESS CONSTRAINED, NON-COOP.			
		Name	VISAMC	VISA	MUGSHOT	MUGSHOT12+YRS	VISABORDER	BORDER	BORDER	WILD	CHILDEXP		
	FMR	0.0001	1E-06	1E-05	1E-05	1E-05	1E-06	1E-06	1E-05	0.0001	0.01		
353	visionlabs-010	0.0017	15	0.0024	11	0.0026	18	0.0030	23	0.0033	9	0.0061	8
354	visionlabs-011	0.0012	5	0.0022	9	0.0024	11	0.0026	9	0.0028	2	0.0053	2
355	visteam-001	0.4417	352	0.5385	350	0.6410	349	0.7788	348	0.6386	335	0.5904	298
356	visteam-002	0.1564	322	0.2789	325	0.1581	322	0.2567	321	0.1776	312	0.2090	267
357	vnpt-002	0.0351	291	0.0424	282	0.0220	275	0.0316	267	0.0471	280	0.0817	238
358	vnpt-003	0.0117	211	0.0138	180	0.0040	87	0.0058	92	0.0087	106	0.0161	107
359	vocord-008	0.0029	39	0.0038	32	0.0042	91	0.0055	80	0.0045	33	0.0086	36
360	vocord-009	0.0022	23	0.0029	20	0.0036	64	0.0046	58	0.0052	51	0.0098	51
361	vts-000	0.0103	200	0.0174	211	0.0080	180	0.0129	189	0.0250	249	0.0450	210
362	winsense-001	0.0062	126	0.0099	145	0.0092	203	0.0210	240	0.0093	122	0.0144	86
363	winsense-002	0.0050	89	0.0073	96	0.0038	73	0.0059	93	0.0064	75	0.0118	71
364	wuhantianyu-001	0.0163	251	0.0262	256	0.0281	287	0.0569	291	0.0316	261	0.0486	214
365	x-laboratory-000	0.0071	149	0.0106	152	0.0123	239	0.0138	196	0.0419	274	0.5629	296
366	x-laboratory-001	0.0059	117	0.0110	157	0.0054	125	0.0078	130	0.0094	125	0.0142	82
367	xforwardai-001	0.0021	22	0.0034	24	0.0027	24	0.0028	15	0.0046	39	0.0088	37
368	xforwardai-002	0.0016	13	0.0023	10	0.0026	20	0.0025	6	0.0040	22	0.0081	29
369	xm-000	0.0015	11	0.0026	15	0.0031	42	0.0038	38	0.0058	62	0.0105	57
370	yisheng-004	0.1988	325	0.3329	328	0.1147	315	0.1849	313	0.2044	316	-	-
371	yitu-003	0.0015	12	0.0026	14	0.0066	156	0.0085	144	0.0064	76	0.0114	67
372	yoonik-001	0.0057	108	0.0079	105	0.0043	94	0.0061	97	0.0307	258	0.0762	235
373	yoonik-002	0.0052	96	0.0062	78	0.0029	30	0.0034	29	0.0615	290	0.1279	255
374	ytu-000	0.0057	109	0.0087	118	0.0121	237	0.0238	250	0.0047	40	0.0078	25
375	yuan-002	0.0094	187	0.0154	199	0.0071	164	0.0110	170	0.0108	150	0.0348	195
376	yuan-003	0.0078	160	0.0111	158	0.0062	147	0.0091	152	0.0106	144	0.0511	217

Table 24: FNMR is the proportion of mated comparisons below a threshold set to achieve the FMR given in the header on the fourth row. FMR is the proportion of impostor comparisons at or above that threshold. The light grey values give rank over all algorithms in that column. The pink columns use only same-sex impostors; others are selected regardless of demographics. The exception, in the green column, uses “matched-covariates” i.e. impostors of the same sex, age group, and country of birth. The second pink column includes effects of extended ageing. Missing entries for border, visa, mugshot and wild images generally mean the algorithm did not run to completion. For child exploitation, missing entries arise because NIST executes those runs only infrequently. The VISA columns compare images described in section 2.1. The MUGSHOT columns compare images described in section 2.4. The VISA-BORDER column compare images described in section 2.2 with those of section 2.3. The BORDER column compares images described in section 2.3. The WILD columns compare images described in section 2.5. The CHILD-EXPLOITATION columns compare images described in section ??.

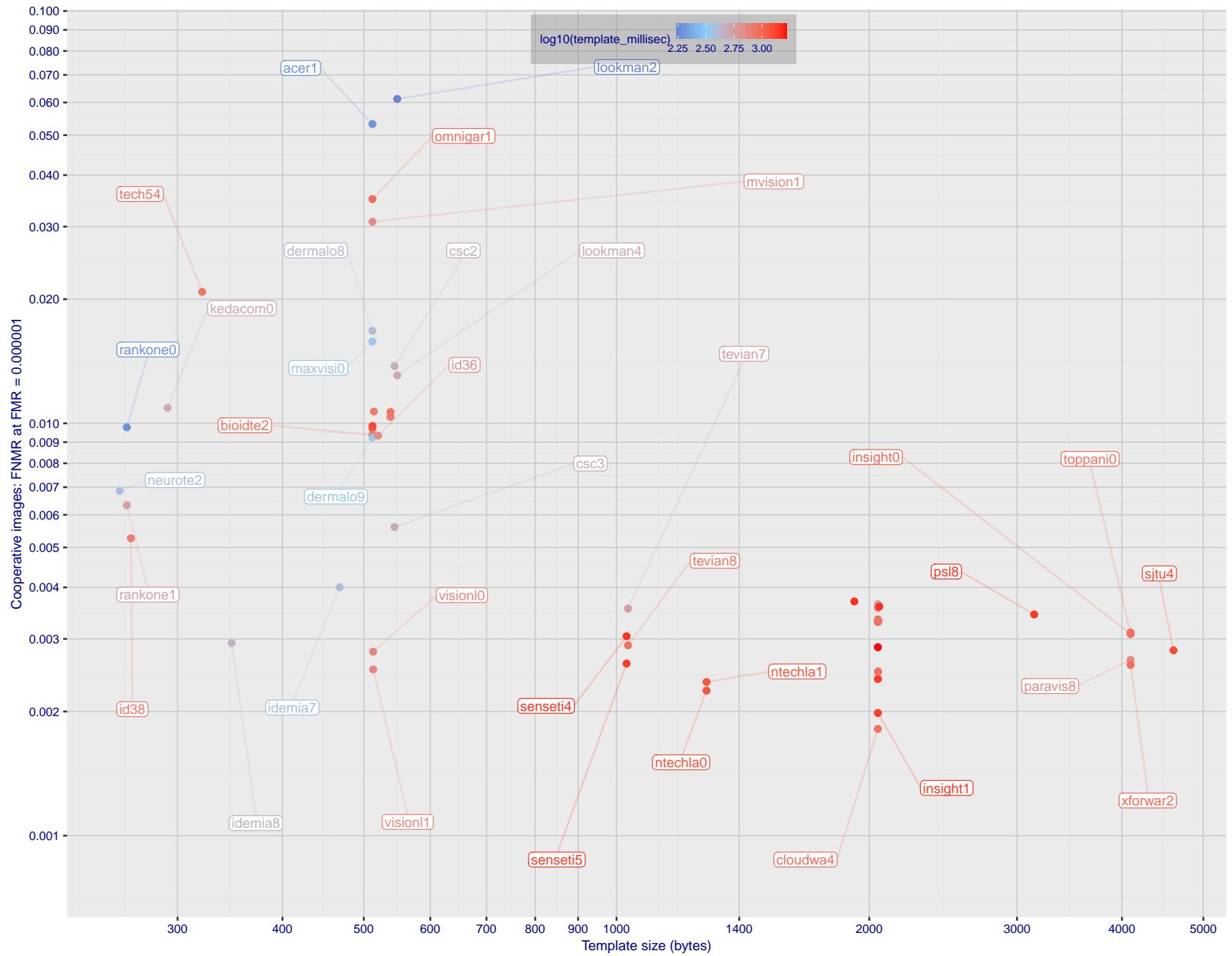


Figure 1: The points show false non-match rates (FNMR) versus the size of the encoded template. FNMR is the geometric mean of FNMR values for visa and mugshot images (from Figs. 57 and 76) at the false match rate (FMR) given in the y-axis label. The color of the points encodes template generation time - which spans at least one order of magnitude. Durations are measured on a single core of a c. 2016 Intel Xeon CPU E5-2630 v4 running at 2.20GHz. Algorithms with poor FNMR are omitted.

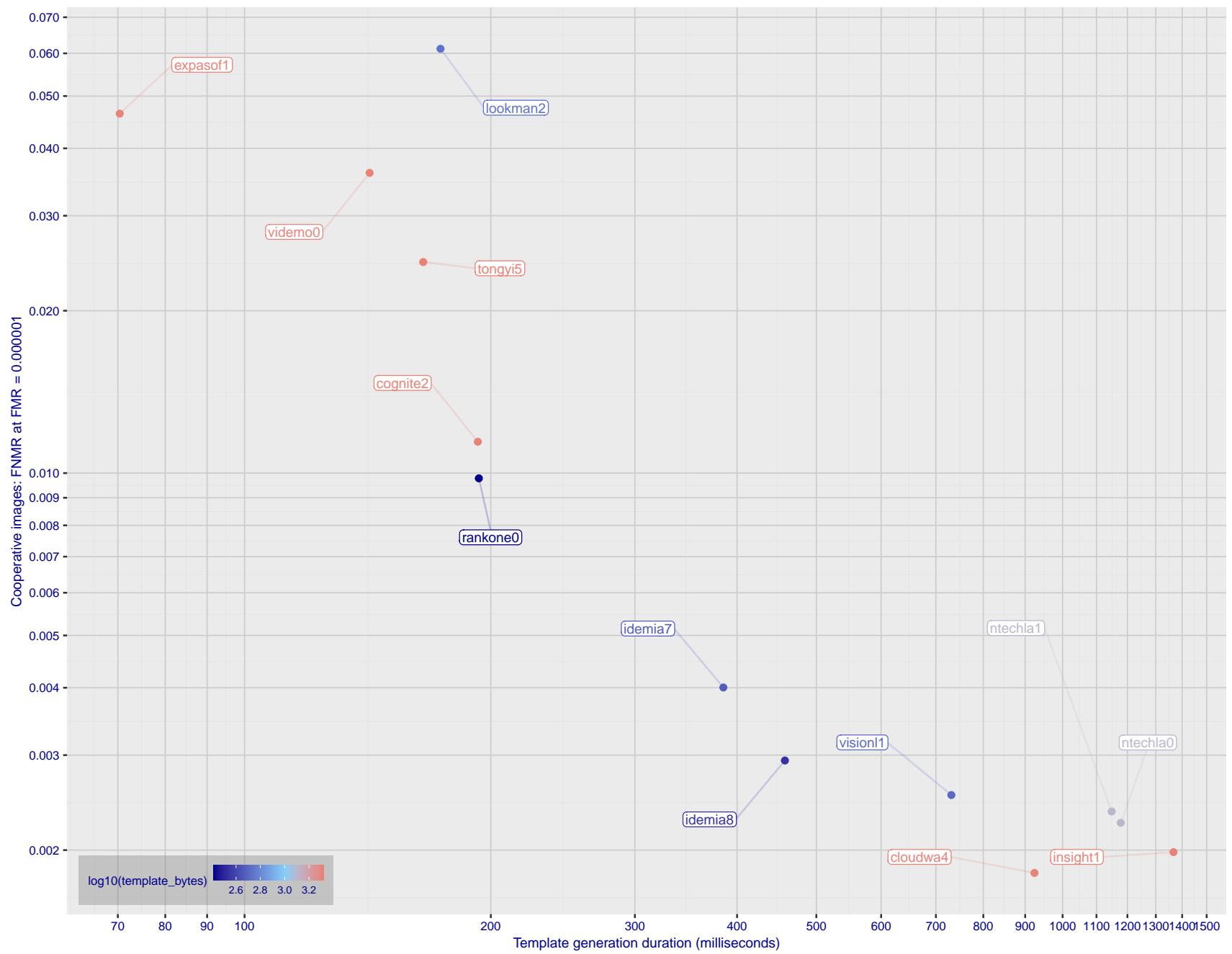


Figure 2: The points show false non-match rates (FNMR) versus the duration of the template generation operation. FNMR is the geometric mean of FNMR values for visa and mugshot images (from Figs. 57 and 76) at a false match rate (FMR) given in the y-axis label. Template generation time is a median estimated over 640 x 480 pixel portraits. It is measured on a single core of a c. 2016 Intel Xeon CPU E5-2630 v4 running at 2.20GHz. The color of the points encodes template size - which span two orders of magnitude. Algorithms with poor FNMR are omitted.

1 Metrics

1.1 Core accuracy

Given a vector of N genuine scores, u , the false non-match rate (FNMR) is computed as the proportion below some threshold, T:

$$\text{FNMR}(T) = 1 - \frac{1}{N} \sum_{i=1}^N H(u_i - T) \quad (1)$$

where $H(x)$ is the unit step function, and $H(0)$ taken to be 1.

Similarly, given a vector of N impostor scores, v , the false match rate (FMR) is computed as the proportion above T:

$$\text{FMR}(T) = \frac{1}{N} \sum_{i=1}^N H(v_i - T) \quad (2)$$

The threshold, T, can take on any value. We typically generate a set of thresholds from quantiles of the observed impostor scores, v , as follows. Given some interesting false match rate range, $[\text{FMR}_L, \text{FMR}_U]$, we form a vector of K thresholds corresponding to FMR measurements evenly spaced on a logarithmic scale

$$T_k = Q_v(1 - \text{FMR}_k) \quad (3)$$

where Q is the quantile function, and FMR_k comes from

$$\log_{10} \text{FMR}_k = \log_{10} \text{FMR}_L + \frac{k}{K} [\log_{10} \text{FMR}_U - \log_{10} \text{FMR}_L] \quad (4)$$

Error tradeoff characteristics are plots of FNMR(T) vs. FMR(T). These are plotted with $\text{FMR}_U \rightarrow 1$ and FMR_L as low as is sustained by the number of impostor comparisons, N. This is somewhat higher than the “rule of three” limit $3/N$ because samples are not independent, due to re-use of images.

2 Datasets

2.1 Visa images

- ▷ The number of images is on the order of 10^5 .
- ▷ The number of subjects is on the order of 10^5 .
- ▷ The number of subjects with two images is on the order of 10^4 .
- ▷ The images have geometry in reasonable conformance with the ISO/IEC 19794-5 Full Frontal image type. Pose is generally excellent.
- ▷ The images are of size 252x300 pixels. The mean interocular distance (IOD) is 69 pixels.
- ▷ The images are of subjects from greater than 100 countries, with significant imbalance due to visa issuance patterns.
- ▷ The images are of subjects of all ages, including children, again with imbalance due to visa issuance demand.
- ▷ Many of the images are live capture. A substantial number of the images are photographs of paper photographs.
- ▷ When these images are input to the algorithm, they are labelled as being of type "ISO" - see Table 4 of the FRVT API.

2.2 Application images

- ▷ The number of images is on the order of 10^6 .
- ▷ The number of subjects is on the order of 10^6 .
- ▷ The number of subjects with two images is on the order of 10^6 .
- ▷ The images have geometry in good conformance with the ISO/IEC 19794-5 Full Frontal image type. Pose is generally excellent.
- ▷ The images are of size 300x300 pixels. The mean interocular distance (IOD) is 61 pixels.
- ▷ The images are of subjects from greater than 100 countries, with significant imbalance due to population and immigration patterns.
- ▷ The images are of subjects of adults with imbalance due to population and immigration patterns and demand.
- ▷ All of the images are live capture.
- ▷ When these images are input to the algorithm, they are labelled as being of type "ISO" - see Table 4 of the FRVT API.

2.3 Border crossing images

- ▷ The number of images is on the order of 10^6 .
- ▷ The number of subjects is on the order of 10^6 .
- ▷ The number of subjects with two images is on the order of 10^6 .
- ▷ The images are taken with a camera oriented by an attendant toward a cooperating subject. This is done under time constraints so there are roll, pitch and yaw angle variations. Also background illumination is sometimes strong, so the face is under-exposed. There is some perspective distortion due to close range images. Some faces are partially cropped.
- ▷ The images are of subjects from greater than 100 countries, with significant imbalance due to population and immigration patterns.
- ▷ The images are of subjects of adults with imbalance due to population and immigration patterns and demand.

- ▷ The images have mean IOD of 38 pixels.
- ▷ The images are all live capture.
- ▷ When these images are input to the algorithm, they are labelled as being of type "WILD" - see Table 4 of the FRVT API.

2.4 Mugshot images

- ▷ The number of images is on the order of 10^6 .
- ▷ The number of subjects is on the order of 10^6 .
- ▷ The number of subjects with two images is on the order of 10^6 .
- ▷ The images have geometry in reasonable conformance with the ISO/IEC 19794-5 Full Frontal image type.
- ▷ The images are of variable sizes. The median IOD is 105 pixels. The mean IOD is 113 pixels. The 1-st, 5-th, 10-th, 25-th, 75-th, 90-th and 99-th percentiles are 34, 58, 70, 87, 121, 161 and 297 pixels.
- ▷ The images are of subjects from the United States.
- ▷ The images are of adults.
- ▷ The images are all live capture.
- ▷ When these images are input to the algorithm, they are labelled as being of type "mugshot" - see Table 4 of the FRVT API.

2.5 Wild images

- ▷ The number of images is on the order of 10^5 .
- ▷ The number of subjects is on the order of 10^3 .
- ▷ The number of subjects with two images on the order of 10^3 .
- ▷ The images include many photojournalism-style images. Images are given to the algorithm using a variable but generally tight crop of the head. Resolution varies very widely. The images are very unconstrained, with wide yaw and pitch pose variation. Faces can be occluded, including hair and hands.
- ▷ The images are of adults.
- ▷ All of the images are live capture, none are scanned.
- ▷ When these images are input to the algorithm, they are labelled as being of type "WILD" - see Table 4 of the FRVT API.

3 Results

3.1 Test goals

- ▷ To state absolute accuracy for different kinds of images, including those with and without subject cooperation.
- ▷ To state comparative accuracy, across algorithms.

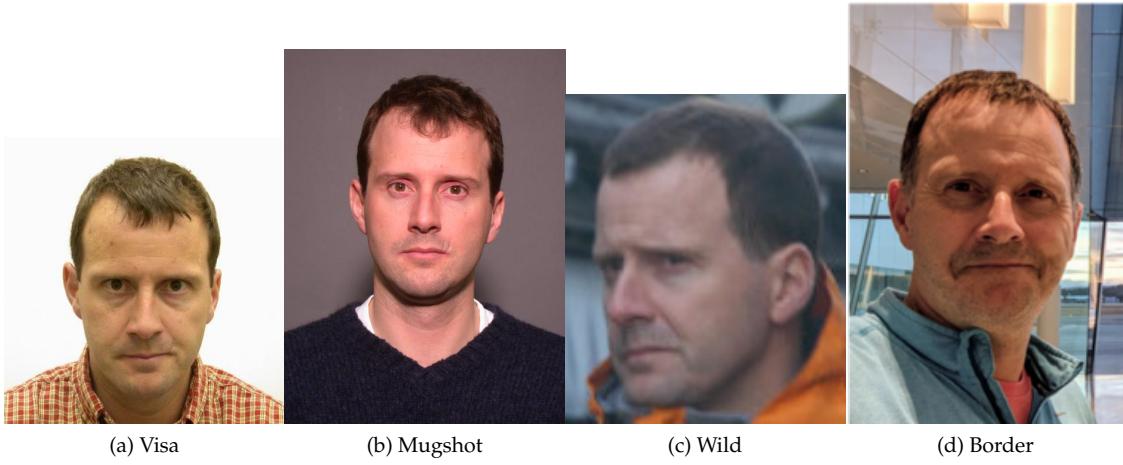


Figure 3: The figure gives simulated samples of image types used in this report.

3.2 Test design

Method: For visa images:

- ▷ The comparisons are of visa photos against visa photos.
- ▷ The number of genuine comparisons is on the order of 10^4 .
- ▷ The number of impostor comparisons is on the order of 10^{10} .
- ▷ The comparisons are fully zero-effort, meaning impostors are paired without attention to sex, age or other covariates. However, later analysis is conducted on subsets.
- ▷ The number of persons is on the order of 10^5 .
- ▷ The number of images used to make 1 template is 1.
- ▷ The number of templates used to make each comparison score is two corresponding to simple one-to-one verification.

Method: For mugshot images:

- ▷ The comparisons are of mugshot photos against mugshot photos.
- ▷ The number of genuine comparisons is on the order of 10^6 .
- ▷ The number of impostor comparisons is on the order of 10^8 .
- ▷ The impostors are paired by sex, but not by age or other covariates.
- ▷ The number of persons is on the order of 10^6 .
- ▷ The number of images used to make 1 template is 1.
- ▷ The number of templates used to make each comparison score is two corresponding to simple one-to-one verification.

Method: For visa-border comparisons:

- ▷ The comparisons are of visa-like frontals against border crossing webcam photos.
- ▷ The number of genuine comparisons is on the order of 10^6 .
- ▷ The number of impostor comparisons is on the order of 10^8 .

- ▷ The impostors are paired by sex, but not by age or other covariates.
- ▷ The number of persons is on the order of 10^6 .
- ▷ The number of images used to make 1 template is 1.
- ▷ The number of templates used to make each comparison score is two corresponding to simple one-to-one verification.

Method: For border-border comparisons:

- ▷ The comparisons are of border crossing webcam photos.
- ▷ The number of genuine comparisons is on the order of 10^6 .
- ▷ The number of impostor comparisons is on the order of 10^8 .
- ▷ The impostors are paired by sex, but not by age or other covariates.
- ▷ The number of persons is on the order of 10^6 .
- ▷ The number of images used to make 1 template is 1.
- ▷ The number of templates used to make each comparison score is two corresponding to simple one-to-one verification.

Method: For wild images:

- ▷ The comparisons are of wild photos against wild photos.
- ▷ The number of genuine comparisons is on the order of 10^6 .
- ▷ The number of impostor comparisons is on the order of 10^7 .
- ▷ The comparisons are fully zero-effort, meaning impostors are paired without attention to sex, age or other covariates.
- ▷ The number of persons is on the order of 10^4 .
- ▷ The number of images used to make 1 template is 1.
- ▷ The number of templates used to make each comparison score is two corresponding to simple one-to-one verification.

Method: For child exploitation images:

- ▷ The comparisons are of unconstrained child exploitation photos against others of the same type.
- ▷ The number of genuine comparisons is on the order of 10^4 .
- ▷ The number of impostor comparisons is on the order of 10^7 .
- ▷ The comparisons are fully zero-effort, meaning impostors are paired without attention to sex, age or other covariates.
- ▷ The number of persons is on the order of 10^3 .
- ▷ The number of images used to make 1 template is 1.
- ▷ The number of templates used to make each comparison score is two corresponding to simple one-to-one verification.
- ▷ We produce two performance statements. First, is a DET as used for visa and mugshot images. The second is a cumulative match characteristic (CMC) summarizing a simulated one-to-many search process. This is done as follows.
 - We regard M enrollment templates as items in a gallery.

- These M templates come from $M > N$ individuals, because multiple images of a subject are present in the gallery under separate identifiers.
- We regard the verification templates as search templates.
- For each search we compute the rank of the highest scoring mate.
- This process should properly be conducted with a 1:N algorithm, such as those tested in NIST IR 8009. We use the 1:1 algorithms in a simulated 1:N mode here to a) better reflect what a child exploitation analyst does, and b) to show algorithm efficacy is better than that revealed in the verification DETs.

3.3 Failure to enroll

	Algorithm Name	Failure to Enrol Rate ¹						
		APPLICATION	BORDER	CHILD-EXPLOIT	MUGSHOT	VISA	WILD	
	Name	SEC. 2.2	SEC. 2.3	SEC. ??	SEC. 2.4	SEC. 2.1	SEC. 2.5	
1	20face-000	0.0000	190	0.0008	189	- 188	0.0000	113 0.0004 203 0.0004 160
2	20face-001	0.0000	209	0.0008	190	- 266	0.0000	116 0.0004 204 0.0004 156
3	3divi-006	0.0000	244	0.0007	167	- 319	0.0001	199 0.0002 117 0.0005 198
4	3divi-007	0.0000	158	0.0007	165	- 126	0.0001	198 0.0002 115 0.0005 199
5	acer-001	0.0000	174	0.0011	230	- 94	0.0001	177 0.0004 221 0.0004 169
6	acer-002	0.0000	306	0.0008	184	- 96	0.0003	262 0.0004 222 0.0011 245
7	acisw-003	0.0000	19	0.0000	12	- 97	0.0000	35 0.0000 13 0.0001 106
8	acisw-007	0.0000	35	0.0000	21	- 93	0.0000	24 0.0000 19 0.0000 63
9	adera-002	0.0000	292	0.0034	301	- 286	0.0003	270 0.0005 309 0.0505 340
10	adera-003	0.0000	291	0.0034	300	- 141	0.0003	269 0.0005 306 0.0505 341
11	advance-002	0.0000	237	0.0013	251	- 335	0.0000	163 0.0004 227 0.0009 236
12	advance-003	0.0000	284	0.0012	240	- 315	0.0001	216 0.0004 261 0.0011 241
13	aifirst-001	0.0000	84	0.0000	50	0.0000	14	0.0000 95 0.0000 53 0.0000 85
14	aigen-001	0.0000	104	0.0000	64	- 217	0.0000	83 0.0000 73 0.0000 21
15	aigen-002	0.0000	37	0.0000	23	- 56	0.0000	22 0.0000 29 0.0000 68
16	ailabs-001	0.0000	223	0.0090	340	- 367	0.0007	317 0.0005 282 0.0016 258
17	aimall-002	0.0000	298	0.0043	313	- 348	0.0012	331 0.0005 301 0.0005 209
18	aimall-003	0.0000	268	0.0012	244	- 163	0.0004	284 0.0005 275 0.0004 181
19	aiunionface-000	0.0000	143	0.0000	87	- 327	0.0000	54 0.0000 93 0.0000 89
20	aize-001	0.0001	331	0.0040	308	- 169	0.0026	351 0.0022 354 0.0058 288
21	aize-002	0.0000	133	0.0014	255	- 343	0.0005	304 0.0004 205 0.0071 295
22	ajou-001	0.0000	224	0.0020	277	- 366	0.0001	201 0.0004 267 0.0045 282
23	alchera-002	0.0000	196	0.0008	194	- 174	0.0001	222 0.0004 175 0.0003 147
24	alchera-003	0.0001	342	0.0013	249	- 172	0.0002	248 0.0004 229 0.0036 275
25	alfabeta-001	0.0005	351	0.0650	367	- 322	0.0024	346 0.0018 350 0.1071 358
26	alice-000	0.0000	96	0.0006	144	- 251	0.0000	128 0.0004 177 0.0004 180
27	alleyes-000	0.0000	194	0.0010	215	- 162	0.0002	229 0.0004 240 0.0004 187
28	allgovision-000	0.0007	355	0.0062	331	- 356	0.0026	350 0.0052 367 0.0131 310
29	alphaface-001	0.0000	195	0.0012	235	- 171	0.0000	164 0.0004 239 0.0004 167
30	alphaface-002	0.0000	218	0.0012	236	- 250	0.0000	167 0.0004 241 0.0004 162
31	amplifiedgroup-001	0.0114	368	0.1023	371	- 208	0.0189	370 0.0279 375 0.1390 367
32	androvideo-000	0.0000	155	0.0000	95	- 314	0.0000	47 0.0000 96 0.0002 110
33	anke-004	0.0000	241	0.0011	227	0.0944	31	0.0001 206 0.0004 251 0.0006 220
34	anke-005	0.0000	221	0.0012	238	0.1228	33	0.0001 220 0.0004 257 0.0007 223
35	antheus-000	0.0000	75	0.0000	44	0.0000	15	0.0000 101 0.0000 49 0.0242 324
36	antheus-001	0.0000	98	0.0000	59	- 213	0.0000	86 0.0000 76 0.0242 325
37	anyvision-004	0.0000	279	0.0017	267	0.1660	36	0.0001 219 0.0004 211 0.0080 298
38	anyvision-005	0.0000	165	0.0013	246	- 109	0.0000	142 0.0004 174 0.0004 183
39	asusaics-000	0.0000	156	0.0000	96	- 320	0.0000	46 0.0000 94 0.0000 39
40	asusaics-001	0.0000	87	0.0000	51	- 267	0.0000	94 0.0000 51 0.0000 3
41	authenmetric-002	0.0000	7	0.0000	5	- 132	0.0000	41 0.0000 3 0.0000 49
42	authenmetric-003	0.0000	51	0.0000	31	- 210	0.0000	14 0.0000 30 0.0000 71
43	aware-005	0.0000	252	0.0020	275	- 72	0.0001	228 0.0004 245 0.0011 239
44	aware-006	0.0000	236	0.0009	202	- 337	0.0000	144 0.0004 218 0.0006 217
45	awirovs-001	0.0039	360	0.0369	362	- 53	0.0386	371 0.0872 376 0.3415 371
46	awirovs-002	0.0000	308	0.0038	306	- 54	0.0007	316 0.0012 342 0.0208 320
47	ayftech-001	0.0002	344	0.0046	319	- 311	0.0043	360 0.0011 333 0.0091 303
48	ayonix-000	0.0053	363	0.0341	359	0.0000	6	0.0113 367 0.0137 372 0.1194 362
49	beethedata-000	0.0005	350	0.0042	312	- 299	0.0002	236 0.0010 327 0.0006 213
50	biocube-001	0.0006	353	0.0391	363	- 268	0.0015	336 0.0020 353 0.0253 329
51	biodtechswiss-001	0.0000	210	0.0007	161	- 273	0.0000	134 0.0004 234 0.0025 271
52	biodtechswiss-002	0.0000	243	0.0007	164	- 316	0.0000	137 0.0004 231 0.0005 210
53	bm-001	0.0000	15	0.0000	10	0.0000	2	0.0000 104 0.0000 15 0.0000 56
54	boetech-001	0.0087	366	0.0272	352	- 219	0.0032	357 0.0160 373 0.0946 355
55	bressee-001	0.0000	172	0.0010	220	- 92	0.0002	234 0.0003 145 0.0003 119
56	bressee-002	0.0000	289	0.0020	278	- 252	0.0008	318 0.0004 194 0.0031 274
57	camvi-002	0.0000	73	0.0000	43	0.0000	7	0.0000 1 0.0000 42 0.0000 83
58	camvi-004	0.0000	27	0.0000	103	0.0000	3	0.0000 30 0.0000 11 0.0000 54

Table 25: FTE is the proportion of failed template generation attempts. Failures can occur because the software throws an exception, or because the software electively refuses to process the input image. This would typically occur if a face is not detected. FTE is measured as the number of function calls that give EITHER a non-zero error code OR that give a “small” template. This is defined as one whose size is less than 0.3 times the median template size for that algorithm. This second rule is needed because some algorithms incorrectly fail to return a non-zero error code when template generation fails.

¹The effects of FTE are included in the accuracy results of this report by regarding any template comparison involving a failed template to produce a low similarity score. Thus higher FTE results in higher FNMR and lower FMR.

	Algorithm	Failure to Enrol Rate ¹						
		APPLICATION	BORDER	CHILD-EXPLOIT	MUGSHOT	VISA	WILD	
Name	SEC. 2.2	SEC. 2.3	SEC. ??	SEC. 2.4	SEC. 2.1	SEC. 2.5		
59 canon-002	0.0000	83	0.0000	49	-	261	0.0000	96
60 canon-003	0.0000	164	0.0008	179	-	110	0.0000	161
61 cieiec-003	0.0000	100	0.0013	252	-	215	0.0001	183
62 cieiec-004	0.0000	126	0.0008	188	-	363	0.0000	140
63 chosun-001	0.0000	123	0.0000	76	-	359	0.0000	67
64 chosun-002	0.0000	40	0.0000	24	-	62	0.0000	21
65 chtface-003	0.0000	286	0.0018	270	-	201	0.0001	188
66 chtface-004	0.0000	140	0.0017	264	-	321	0.0000	152
67 clearviewwai-000	0.0000	197	0.0003	123	-	176	0.0000	154
68 closeli-001	0.0000	24	0.0000	15	-	118	0.0000	32
69 cloudmatrix-000	0.0000	253	0.0012	241	-	209	0.0001	179
70 cloudwalk-hr-003	0.0000	160	0.0008	191	-	137	0.0001	187
71 cloudwalk-hr-004	0.0000	171	0.0011	234	-	84	0.0004	286
72 cloudwalk-mt-003	0.0000	163	0.0007	156	-	102	0.0002	242
73 cloudwalk-mt-004	0.0000	204	0.0009	195	-	291	0.0002	250
74 clova-000	0.0000	300	0.0022	280	-	79	0.0006	311
75 cogent-005	0.0000	95	0.0000	57	-	247	0.0000	88
76 cogent-006	0.0000	93	0.0000	54	-	241	0.0000	90
77 cognitec-002	0.0001	326	0.0069	333	-	269	0.0003	279
78 cognitec-003	0.0001	327	0.0194	348	-	313	0.0003	276
79 cor-001	0.0000	206	0.0006	148	-	258	0.0002	257
80 coretech-000	0.0000	147	0.0000	89	-	303	0.0000	50
81 corsight-001	0.0000	238	0.0006	153	-	300	0.0001	224
82 corsight-002	0.0000	183	0.0005	142	-	71	0.0001	207
83 csc-002	0.0015	358	0.0033	297	-	256	0.0006	313
84 csc-003	0.0015	357	0.0033	296	-	85	0.0006	312
85 ctcbank-000	0.0001	329	0.0051	324	0.3285	43	0.0011	329
86 ctcbank-001	0.0000	309	0.0036	305	-	152	0.0005	299
87 cubox-001	0.0000	99	0.0000	60	-	216	0.0000	84
88 cubox-002	0.0000	262	0.0006	151	-	341	0.0002	256
89 cudocommunication-001	0.0000	115	0.0000	72	-	233	0.0000	73
90 cuhkee-001	0.0000	189	0.0011	233	-	183	0.0000	114
91 cybercore-000	0.0000	161	0.0073	336	-	138	0.0001	196
92 cyberextruder-001	0.0029	359	0.0293	353	0.5338	49	0.0024	344
93 cyberextruder-002	0.0013	356	0.0840	370	0.2672	42	0.0027	352
94 cyberlink-006	0.0000	81	0.0005	136	-	255	0.0000	112
95 cyberlink-007	0.0000	122	0.0003	117	-	362	0.0000	110
96 dahua-005	0.0000	151	0.0000	101	-	304	0.0000	143
97 dahua-006	0.0000	39	0.0000	100	-	59	0.0000	157
98 daon-000	0.0000	313	0.0028	289	-	108	0.0014	335
99 decatur-000	0.0000	264	0.0020	274	-	326	0.0004	292
100 decatur-001	0.0000	198	0.0009	207	-	279	0.0001	193
101 deepglint-003	0.0000	207	0.0004	132	-	265	0.0002	249
102 deepglint-004	0.0000	162	0.0005	137	-	144	0.0002	253
103 deepsea-001	0.0000	138	0.0000	86	0.0000	19	0.0000	57
104 deepsense-000	0.0000	31	0.0006	154	-	81	0.0000	124
105 dermalog-008	0.0000	305	0.0031	294	-	340	0.0006	308
106 dermalog-009	0.0000	302	0.0031	293	-	161	0.0006	306
107 didiglobalface-001	0.0000	231	0.0012	237	0.2175	38	0.0000	166
108 digitalbarriers-002	0.0001	334	0.0045	316	-	260	0.0028	354
109 dps-000	0.0000	107	0.0000	66	-	229	0.0000	78
110 dsk-000	0.0000	30	0.0000	17	0.0000	1	0.0000	28
111 einetworks-000	0.0000	310	0.0017	266	-	253	0.0002	246
112 ekin-002	0.0000	3	0.0000	102	-	125	0.0000	109
113 enfase-000	0.0000	146	0.0012	243	-	336	0.0000	149
114 eocortex-000	0.0095	367	0.0602	366	-	131	0.0094	366
115 ercacat-001	0.0000	14	0.0005	138	-	145	0.0000	148
116 euronovate-001	0.0255	373	0.0102	342	-	281	0.0021	341

Table 26: FTE is the proportion of failed template generation attempts. Failures can occur because the software throws an exception, or because the software electively refuses to process the input image. This would typically occur if a face is not detected. FTE is measured as the number of function calls that give EITHER a non-zero error code OR that give a “small” template. This is defined as one whose size is less than 0.3 times the median template size for that algorithm. This second rule is needed because some algorithms incorrectly fail to return a non-zero error code when template generation fails.

¹ The effects of FTE are included in the accuracy results of this report by regarding any template comparison involving a failed template to produce a low similarity score. Thus higher FTE results in higher FNMR and lower FMR.

	Algorithm	Failure to Enrol Rate ¹											
		APPLICATION	BORDER	CHILD-EXPLOIT	MUGSHOT	VISA	WILD	SEC. 2.2	SEC. 2.3	SEC. ??	SEC. 2.4	SEC. 2.1	SEC. 2.5
117	expasoft-001	0.0000	64	0.0000	39	-	175	0.0000	4	0.0000	39	0.0000	80
118	expasoft-002	0.0000	36	0.0000	22	-	52	0.0000	23	0.0000	28	0.0000	67
119	f8-001	0.0003	347	0.0059	330	0.2026	37	0.0035	358	0.0030	365	0.0087	301
120	faceonlive-001	0.0000	319	0.0029	292	-	310	0.0013	333	0.0011	332	0.0160	315
121	facesoft-000	0.0000	9	0.0000	6	0.0000	4	0.0000	39	0.0000	5	0.0000	51
122	facetag-000	0.0000	61	0.0000	37	-	160	0.0000	7	0.0000	41	0.0000	81
123	facetag-001	0.0000	32	0.0000	19	-	87	0.0000	26	0.0000	21	0.0000	61
124	facex-001	0.0001	341	0.0360	361	-	288	0.0047	363	0.0027	360	0.1109	360
125	facex-002	0.0001	340	0.0360	360	-	61	0.0047	362	0.0027	359	0.1109	359
126	farfaces-001	0.0000	307	0.0007	163	-	296	0.0003	273	0.0003	138	0.0006	221
127	fiberhome-nanjing-003	0.0000	119	0.0004	131	-	357	0.0000	68	0.0003	128	0.0001	93
128	fiberhome-nanjing-004	0.0000	60	0.0004	130	-	198	0.0000	8	0.0003	126	0.0001	96
129	fincore-000	0.0000	226	0.0008	193	-	369	0.0001	173	0.0004	237	0.0006	215
130	fujitsulab-002	0.0000	55	0.0009	200	-	184	0.0001	215	0.0003	127	0.0003	127
131	fujitsulab-003	0.0000	86	0.0008	182	-	262	0.0001	205	0.0001	110	0.0003	121
132	geo-002	0.0000	178	0.0015	257	-	55	0.0001	169	0.0004	256	0.0017	259
133	geo-003	0.0000	193	0.0010	214	-	192	0.0000	117	0.0004	253	0.0013	254
134	glory-002	0.0003	345	0.0045	315	-	312	0.0015	337	0.0011	337	0.0557	344
135	glory-003	0.0000	269	0.0027	286	-	167	0.0004	285	0.0005	280	0.0244	326
136	gorilla-007	0.0000	180	0.0009	211	-	66	0.0001	191	0.0004	228	0.0004	172
137	gorilla-008	0.0000	182	0.0009	212	-	74	0.0001	190	0.0004	232	0.0004	171
138	griaule-000	0.0000	316	0.0026	284	-	342	0.0004	294	0.0010	326	0.0023	268
139	hertasecurity-000	0.0133	370	0.0077	338	-	236	0.0025	349	0.0243	374	0.0171	317
140	hik-001	0.0000	124	0.0000	106	-	360	0.0000	66	0.0000	83	0.0000	29
141	hisign-001	0.0000	57	0.0000	34	-	187	0.0000	10	0.0000	34	0.0000	78
142	hyperverge-001	0.0000	323	0.0072	334	-	82	0.0015	339	0.0014	345	0.0042	279
143	hyperverge-002	0.0000	67	0.0008	181	-	148	0.0002	258	0.0004	190	0.0004	191
144	icm-002	0.0000	120	0.0001	109	-	353	0.0000	69	0.0000	104	0.0000	88
145	icm-003	0.0000	46	0.0001	108	-	200	0.0000	18	0.0000	103	0.0000	90
146	icttc-000	0.0001	339	0.0047	322	-	113	0.0028	355	0.0029	362	0.0086	300
147	id3-006	0.0000	267	0.0009	210	-	212	0.0004	288	0.0005	297	0.0008	233
148	id3-008	0.0000	12	0.0006	152	-	140	0.0001	223	0.0004	163	0.0003	123
149	idemia-007	0.0000	85	0.0004	134	-	264	0.0000	120	0.0003	151	0.0003	131
150	idemia-008	0.0000	23	0.0004	133	-	115	0.0000	119	0.0003	150	0.0003	133
151	iit-002	0.0000	314	0.0021	279	-	154	0.0009	326	0.0005	308	0.0443	339
152	iit-003	0.0000	199	0.0008	192	-	278	0.0000	141	0.0004	169	0.0069	293
153	imagus-002	0.0000	274	0.0018	268	-	374	0.0000	150	0.0004	226	0.0296	330
154	imagus-004	0.0000	128	0.0000	78	-	368	0.0000	64	0.0000	80	0.0000	31
155	imperial-000	0.0000	42	0.0000	26	-	63	0.0000	20	0.0000	25	0.0000	66
156	imperial-002	0.0000	129	0.0000	79	0.0000	20	0.0000	63	0.0000	78	0.0000	24
157	incode-009	0.0000	263	0.0009	204	-	323	0.0002	240	0.0004	186	0.0007	228
158	incode-010	0.0000	251	0.0009	203	-	95	0.0002	238	0.0004	183	0.0007	229
159	innefuleabs-000	0.0000	230	0.0024	281	-	339	0.0003	272	0.0005	294	0.0004	175
160	innovativetechnologyltd-001	0.0001	338	0.0050	323	-	292	0.0024	348	0.0025	357	0.0055	287
161	innovativetechnologyltd-002	0.0000	276	0.0046	318	-	351	0.0057	365	0.0005	296	0.0247	328
162	innovatrics-006	0.0000	203	0.0009	209	0.0350	24	0.0000	146	0.0004	168	0.0003	151
163	innovatrics-007	0.0000	233	0.0007	172	-	349	0.0001	171	0.0003	139	0.0003	135
164	insightface-000	0.0000	34	0.0000	20	-	91	0.0000	25	0.0000	18	0.0000	62
165	insightface-001	0.0000	108	0.0000	67	-	228	0.0000	79	0.0000	70	0.0000	15
166	intellicloudai-001	0.0000	76	0.0000	45	-	282	0.0000	100	0.0000	48	0.0001	99
167	intellicloudai-002	0.0000	38	0.0008	185	-	60	0.0000	139	0.0004	164	0.0012	248
168	intellifusion-001	0.0000	175	0.0005	140	0.0949	32	0.0001	186	0.0003	153	0.0005	205
169	intellifusion-002	0.0000	145	0.0000	104	-	332	0.0000	107	0.0000	90	0.0001	100
170	intellivision-001	0.0042	361	0.0296	354	0.5495	50	0.0048	364	0.0042	366	0.1358	365
171	intellivision-002	0.0000	324	0.0046	317	-	196	0.0012	330	0.0005	311	0.0146	312
172	intelresearch-003	0.0000	212	0.0006	146	-	238	0.0000	130	0.0004	181	0.0003	152
173	intelresearch-004	0.0000	176	0.0006	147	-	58	0.0000	127	0.0004	180	0.0003	142
174	intsysmsu-001	0.0000	110	0.0010	219	-	226	0.0001	202	0.0004	216	0.0004	184

Table 27: FTE is the proportion of failed template generation attempts. Failures can occur because the software throws an exception, or because the software electively refuses to process the input image. This would typically occur if a face is not detected. FTE is measured as the number of function calls that give EITHER a non-zero error code OR that give a “small” template. This is defined as one whose size is less than 0.3 times the median template size for that algorithm. This second rule is needed because some algorithms incorrectly fail to return a non-zero error code when template generation fails.

¹The effects of FTE are included in the accuracy results of this report by regarding any template comparison involving a failed template to produce a low similarity score. Thus higher FTE results in higher FNMR and lower FMR.

Name	Algorithm	Failure to Enrol Rate ¹							
		APPLICATION		BORDER		CHILD-EXPLOIT		MUGSHOT	
		SEC. 2.2	SEC. 2.3	SEC. ??	SEC. 2.4	SEC. 2.1	SEC. 2.5	VISA	WILD
175	intsysmsu-002	0.0000	1	0.0010	217	-	128	0.0001	200
176	ionetworks-000	0.0000	28	0.0016	262	-	77	0.0004	282
177	iqface-000	0.0000	134	0.0000	83	0.0000	18	0.0000	59
178	iqface-003	0.0000	311	0.0076	337	-	103	0.0006	307
179	irex-000	0.0000	280	0.0009	208	-	191	0.0000	155
180	isap-001	0.0000	69	0.0000	41	-	146	0.0000	3
181	isap-002	0.0000	54	0.0000	33	-	185	0.0000	12
182	isityou-000	0.0068	365	0.0316	357	0.4714	46	0.0023	343
183	isystems-001	0.0000	318	0.0035	303	0.1421	35	0.0010	328
184	isystems-002	0.0000	317	0.0035	302	0.1421	34	0.0010	327
185	itmo-007	0.0000	152	0.0009	199	-	306	0.0003	280
186	itmo-008	0.0000	71	0.0135	346	-	149	0.0024	347
187	ivacognitive-001	0.0000	248	0.0011	229	-	116	0.0001	180
188	iws-000	0.0005	352	0.0650	368	-	331	0.0024	345
189	kakao-005	0.0000	8	0.0000	98	-	135	0.0000	38
190	kakao-006	0.0000	261	0.0009	205	-	376	0.0000	122
191	kakaopay-001	0.0000	245	0.0013	250	-	142	0.0001	182
192	kedacom-000	0.0000	132	0.0000	82	0.0000	17	0.0000	60
193	kiwitech-000	0.0000	201	0.0009	196	-	284	0.0004	291
194	kneron-003	0.0239	371	0.0306	355	0.4883	48	0.0044	361
195	kneron-005	0.0000	320	0.0226	349	-	111	0.0006	305
196	kookmin-002	0.0000	130	0.0000	80	-	372	0.0000	62
197	kookmin-003	0.0000	117	0.0000	74	-	232	0.0000	71
198	kuke3d-001	0.0000	116	0.0000	71	-	235	0.0000	74
199	lemalabs-001	0.0000	142	0.0005	141	-	330	0.0002	243
200	line-000	0.0000	82	0.0000	48	-	259	0.0000	97
201	line-001	0.0000	149	0.0000	90	-	301	0.0000	51
202	lookman-002	0.0000	25	0.0000	16	-	120	0.0000	31
203	lookman-004	0.0000	131	0.0000	81	0.0000	21	0.0000	61
204	luxand-000	0.0000	153	0.0000	92	-	309	0.0000	48
205	mantra-000	0.0001	328	0.0041	311	-	117	0.0003	271
206	maxvision-000	0.0000	33	0.0000	99	-	86	0.0000	27
207	megvii-003	0.0000	202	0.0010	224	-	283	0.0002	255
208	meituan-000	0.0000	26	0.0001	111	-	124	0.0000	118
209	meiya-001	0.0000	315	0.0028	290	-	249	0.0004	293
210	mendaxiatech-000	0.0000	192	0.0010	213	-	195	0.0002	252
211	microfocus-001	0.0001	335	0.0053	326	0.0791	29	0.0008	321
212	microfocus-002	0.0001	337	0.0053	327	0.0791	30	0.0008	320
213	minivision-000	0.0000	63	0.0000	38	-	168	0.0000	6
214	mobai-000	0.0000	288	0.0114	344	-	271	0.0003	275
215	mobai-001	0.0000	259	0.0040	307	-	218	0.0001	208
216	mobbl-000	0.0116	369	0.0720	369	-	199	0.0119	368
217	mobbl-001	0.0000	312	0.0052	325	-	159	0.0002	232
218	mobipintech-000	0.0000	50	0.0000	30	-	207	0.0000	15
219	moreidian-000	0.0000	227	0.0009	197	-	371	0.0004	290
220	multimodality-000	0.0000	2	0.0000	1	-	127	0.0000	44
221	mvision-001	0.0000	121	0.0000	75	-	354	0.0000	70
222	nazhiai-000	0.0000	88	0.0000	52	-	275	0.0000	93
223	neosystems-002	0.0000	49	0.0000	29	-	203	0.0000	16
224	neosystems-003	0.0000	80	0.0000	47	-	294	0.0000	98
225	netbridge-tech-001	0.0000	125	0.0000	77	-	361	0.0000	65
226	netbridge-tech-002	0.0000	29	0.0000	18	-	75	0.0000	29
227	neurotechnology-011	0.0000	260	0.0013	245	-	370	0.0002	233
228	neurotechnology-012	0.0000	303	0.0010	226	-	166	0.0001	218
229	nhn-001	0.0000	167	0.0019	271	-	122	0.0001	192
230	nhn-002	0.0000	91	0.0004	135	-	243	0.0000	138
231	nodeflux-002	0.0000	170	0.0261	351	-	83	0.0008	319
232	notiontag-001	0.0000	13	0.0000	8	-	143	0.0027	353

Table 28: FTE is the proportion of failed template generation attempts. Failures can occur because the software throws an exception, or because the software electively refuses to process the input image. This would typically occur if a face is not detected. FTE is measured as the number of function calls that give EITHER a non-zero error code OR that give a “small” template. This is defined as one whose size is less than 0.3 times the median template size for that algorithm. This second rule is needed because some algorithms incorrectly fail to return a non-zero error code when template generation fails.

¹ The effects of FTE are included in the accuracy results of this report by regarding any template comparison involving a failed template to produce a low similarity score. Thus higher FTE results in higher FNMR and lower FMR.

	Algorithm Name	Failure to Enrol Rate ¹						
		APPLICATION	BORDER	CHILD-EXPLOIT	MUGSHOT	VISA	WILD	
	Name	SEC. 2.2	SEC. 2.3	SEC. ??	SEC. 2.4	SEC. 2.1	SEC. 2.5	
233	notiontag-002	0.0000	78	0.0000	46	-	289	0.0000
234	nsensecorp-002	0.0000	219	0.0009	198	-	224	0.0003
235	nsensecorp-003	0.0000	45	0.0000	107	-	73	0.0000
236	ntechlab-010	0.0000	208	0.0005	139	-	270	0.0001
237	ntechlab-011	0.0000	68	0.0003	119	-	147	0.0000
238	omnigarde-000	0.0000	232	0.0008	178	-	345	0.0000
239	omnigarde-001	0.0000	181	0.0008	177	-	69	0.0000
240	openface-001	0.0000	293	0.0104	343	-	119	0.0004
241	oz-002	0.0000	139	0.0003	120	-	352	0.0000
242	oz-003	0.0000	114	0.0002	113	-	230	0.0000
243	papsav1923-001	0.0000	186	0.0007	166	-	182	0.0001
244	paravision-004	0.0000	282	0.0007	175	0.0570	26	0.0002
245	paravision-008	0.0000	74	0.0010	216	-	158	0.0001
246	pensee-001	0.0000	214	0.0000	56	-	244	0.0000
247	pixelall-006	0.0000	148	0.0000	91	-	302	0.0000
248	pixelall-007	0.0000	97	0.0000	58	-	254	0.0000
249	psl-008	0.0000	166	0.0003	121	-	123	0.0000
250	psl-009	0.0000	159	0.0004	129	-	134	0.0000
251	ptakuratsatu-000	0.0000	240	0.0007	173	-	298	0.0001
252	pxl-001	0.0000	325	0.0044	314	-	317	0.0005
253	pyramid-000	0.0001	333	0.0041	310	-	355	0.0005
254	qnap-000	0.0000	43	0.0007	174	-	64	0.0002
255	qnap-001	0.0000	228	0.0000	105	-	373	0.0000
256	quantasoft-003	0.0000	290	0.0015	259	-	358	0.0005
257	rankone-010	0.0000	109	0.0000	68	-	227	0.0000
258	rankone-011	0.0000	102	0.0000	62	-	220	0.0000
259	realnetworks-004	0.0000	239	0.0003	118	-	297	0.0000
260	realnetworks-005	0.0000	173	0.0002	116	-	90	0.0000
261	regula-000	0.0000	17	0.0000	11	-	99	0.0000
262	remarkai-001	0.0000	48	0.0000	28	-	205	0.0000
263	remarkai-003	0.0000	235	0.0007	162	-	334	0.0000
264	rendip-000	0.0000	275	0.0016	261	-	338	0.0002
265	revealmedia-005	0.0000	281	0.0007	169	-	156	0.0009
266	rokid-000	0.0000	59	0.0072	335	-	197	0.0001
267	rokid-001	0.0000	141	0.0013	248	-	324	0.0000
268	s1-002	0.0000	256	0.0089	339	-	157	0.0001
269	s1-003	0.0000	47	0.0002	115	-	202	0.0007
270	saffe-001	0.0000	11	0.0000	7	0.0000	5	0.0000
271	saffe-002	0.0000	157	0.0000	97	-	318	0.0000
272	samsungsds-000	0.0000	272	0.0055	329	-	274	0.0038
273	samtech-001	0.0001	332	0.0032	295	-	170	0.0004
274	scanovate-002	0.0000	249	0.0018	269	-	78	0.0000
275	scanovate-003	0.0000	254	0.0233	350	-	194	0.0006
276	securifai-001	0.0000	41	0.0000	25	-	65	0.0000
277	securifai-003	0.0000	70	0.0000	42	-	150	0.0000
278	sensetime-004	0.0000	211	0.0011	232	-	272	0.0000
279	sensetime-005	0.0000	53	0.0004	128	-	186	0.0000
280	sertis-000	0.0000	66	0.0007	168	-	178	0.0000
281	sertis-002	0.0000	150	0.0007	159	-	305	0.0000
282	seventhsense-000	0.0000	188	0.0006	155	-	179	0.0001
283	shaman-000	0.0000	113	0.0000	70	0.0000	11	0.0000
284	shaman-001	0.0000	118	0.0000	73	0.0000	13	0.0000
285	shu-002	0.0000	247	0.0010	221	-	106	0.0005
286	shu-003	0.0000	105	0.0007	157	-	223	0.0001
287	siat-002	0.0000	215	0.0012	242	0.0616	27	0.0000
288	siat-004	0.0000	168	0.0011	231	-	121	0.0000
289	sjtu-003	0.0000	20	0.0005	143	-	104	0.0000
290	sjtu-004	0.0000	58	0.0000	36	-	193	0.0000

Table 29: FTE is the proportion of failed template generation attempts. Failures can occur because the software throws an exception, or because the software electively refuses to process the input image. This would typically occur if a face is not detected. FTE is measured as the number of function calls that give EITHER a non-zero error code OR that give a “small” template. This is defined as one whose size is less than 0.3 times the median template size for that algorithm. This second rule is needed because some algorithms incorrectly fail to return a non-zero error code when template generation fails.

¹ The effects of FTE are included in the accuracy results of this report by regarding any template comparison involving a failed template to produce a low similarity score. Thus higher FTE results in higher FNMR and lower FMR.

	Algorithm	Failure to Enrol Rate ¹						
		APPLICATION	BORDER	CHILD-EXPLOIT	MUGSHOT	VISA	WILD	
Name	SEC. 2.2	SEC. 2.3	SEC. ??	SEC. 2.4	SEC. 2.1	SEC. 2.5		
291	sktelecom-000	0.0000	205	0.0008	187	-	295	0.0000
292	smartengines-000	0.0066	364	0.0150	347	-	136	0.0022
293	smilart-002	0.0000	321	0.0036	304	0.2422	41	-
294	smilart-003	0.0003	346	0.0100	341	-	276	0.0014
295	sodec-000	0.0000	135	0.0000	84	-	344	0.0000
296	sqisoft-001	0.0000	77	0.0003	125	-	285	0.0000
297	sqisoft-002	0.0000	90	0.0003	124	-	237	0.0000
298	stachu-000	0.0000	137	0.0000	85	-	350	0.0000
299	starhybrid-001	0.0001	336	0.0033	299	0.2340	40	0.0009
300	suprema-000	0.0000	258	0.0017	265	-	257	0.0002
301	suprema-001	0.0000	273	0.0027	285	-	214	0.0003
302	supremaid-001	0.0000	220	0.0020	276	-	221	0.0001
303	synesis-006	0.0000	94	0.0003	126	-	245	0.0000
304	synesis-007	0.0000	225	0.0013	247	-	365	0.0002
305	synology-000	0.0000	89	0.0000	53	-	239	0.0000
306	synology-002	0.0000	56	0.0000	35	-	189	0.0000
307	sztu-000	0.0000	52	0.0000	32	-	181	0.0000
308	sztu-001	0.0000	6	0.0000	4	-	133	0.0000
309	tech5-004	0.0000	229	0.0008	180	-	375	0.0003
310	tech5-005	0.0000	222	0.0007	176	-	234	0.0000
311	techsign-000	0.0007	354	0.0334	358	-	114	0.0020
312	tevian-007	0.0000	179	0.0015	260	-	67	0.0002
313	tevian-008	0.0000	216	0.0006	145	-	246	0.0000
314	tiger-003	0.0000	169	-	373	0.0619	28	0.0001
315	tiger-005	0.0000	191	0.0009	206	-	190	0.0001
316	tinkoff-001	0.0000	257	0.0008	186	-	287	0.0001
317	tongyi-005	0.0000	65	0.0000	40	0.0000	8	0.0000
318	toppanidgate-000	0.0000	177	0.0008	183	-	57	0.0004
319	toshiba-003	0.0000	10	0.0001	110	-	139	0.0001
320	toshiba-004	0.0000	16	0.0000	9	-	100	0.0000
321	trueface-002	0.0000	265	0.0046	321	-	333	0.0003
322	trueface-003	0.0000	255	0.0046	320	-	177	0.0003
323	tuputech-000	0.0003	348	0.0116	345	-	328	-
324	twface-000	0.0000	154	0.0000	93	-	308	0.0000
325	twface-001	0.0000	106	0.0000	65	-	222	0.0000
326	ulsee-001	0.0000	44	0.0000	27	-	70	0.0000
327	ultinous-000	-	376	-	376	0.0007	23	-
328	ultinous-001	-	375	-	375	0.0007	22	-
329	uluface-002	0.0000	101	0.0000	61	0.0000	9	0.0000
330	uluface-003	0.0000	127	0.0001	112	-	364	0.0002
331	unissey-001	0.0000	5	0.0000	3	-	129	0.0000
332	upc-001	0.0000	299	0.0003	122	0.0450	25	0.0003
333	vcog-002	-	374	-	372	0.2209	39	-
334	vd-002	0.0000	92	0.0000	55	-	240	0.0000
335	vd-003	0.0001	330	0.0041	309	-	277	0.0030
336	veridas-006	0.0000	296	0.0026	282	-	151	0.0001
337	veridas-007	0.0000	297	0.0026	283	-	347	0.0001
338	verigram-000	0.0000	271	0.0068	332	-	290	0.0003
339	verihubs-inteligensia-000	0.0000	187	0.0029	291	-	180	0.0001
340	via-000	0.0000	112	0.0000	69	0.0000	12	0.0000
341	via-001	0.0000	4	0.0000	2	-	130	0.0000
342	videomo-000	0.0000	250	0.0019	272	-	89	0.0003
343	videonetics-001	0.0004	349	0.0309	356	0.4799	47	0.0015
344	videonetics-002	0.0000	266	0.0459	365	0.4598	45	0.0006
345	viettelhightech-000	0.0000	304	0.0019	273	-	155	0.0007
346	vigilantsolutions-010	0.0000	287	0.0028	288	-	263	0.0001
347	vigilantsolutions-011	0.0000	285	0.0028	287	-	68	0.0001
348	vinai-000	0.0000	22	0.0000	14	-	107	0.0000

Table 30: FTE is the proportion of failed template generation attempts. Failures can occur because the software throws an exception, or because the software electively refuses to process the input image. This would typically occur if a face is not detected. FTE is measured as the number of function calls that give EITHER a non-zero error code OR that give a “small” template. This is defined as one whose size is less than 0.3 times the median template size for that algorithm. This second rule is needed because some algorithms incorrectly fail to return a non-zero error code when template generation fails.

¹The effects of FTE are included in the accuracy results of this report by regarding any template comparison involving a failed template to produce a low similarity score. Thus higher FTE results in higher FNMR and lower FMR.

	Algorithm	Failure to Enrol Rate ¹											
		Name	APPLICATION		BORDER		CHILD-EXPLOIT		MUGSHOT		VISA		
			SEC. 2.2	SEC. 2.3	SEC. ??	SEC. 2.4	SEC. 2.1	SEC. 2.5	SEC. 2.2	SEC. 2.3	SEC. ??	SEC. 2.4	
349	vion-000	0.0050	362	0.0392	364	0.6388	51	0.0130	369	0.0078	370	0.1389	366
350	visage-000	0.0000	301	0.0054	328	-	88	0.0009	322	0.0006	314	0.0064	291
351	visionbox-001	0.0000	322	0.0033	298	-	173	0.0005	303	0.0011	336	0.0028	272
352	visionbox-002	0.0000	79	0.0017	263	-	293	0.0000	145	0.0004	269	0.0046	283
353	visionlabs-010	0.0000	283	0.0009	201	-	231	0.0001	221	0.0004	215	0.0006	219
354	visionlabs-011	0.0000	72	0.0006	150	-	153	0.0001	185	0.0004	176	0.0004	161
355	visteam-001	0.0000	277	0.0014	253	-	112	0.0002	239	0.0004	219	0.0011	244
356	visteam-002	0.0000	278	0.0014	254	-	80	0.0002	235	0.0004	223	0.0011	243
357	vnpt-002	0.0000	242	0.0002	114	-	307	0.0003	277	0.0003	125	0.0001	103
358	vnpt-003	0.0000	62	0.0004	127	-	164	0.0002	230	0.0004	161	0.0001	105
359	vocord-008	0.0000	184	0.0015	258	-	206	0.0003	278	0.0001	108	0.0007	225
360	vocord-009	0.0000	185	0.0006	149	-	204	0.0001	226	0.0003	121	0.0003	126
361	vts-000	0.0000	270	0.0011	228	-	165	0.0001	227	0.0004	264	0.0013	250
362	winsense-001	0.0000	103	0.0000	63	0.0000	10	0.0000	81	0.0000	74	0.0000	22
363	winsense-002	0.0000	144	0.0000	88	-	325	0.0000	53	0.0000	92	0.0000	37
364	wuhantianyu-001	0.0000	18	0.0007	160	-	98	0.0001	172	0.0004	208	0.0002	115
365	x-laboratory-000	0.0247	372	0.0000	94	0.0000	16	0.0005	302	0.0002	114	0.0000	38
366	x-laboratory-001	0.0000	200	0.0012	239	-	280	0.0001	214	0.0004	254	0.0007	222
367	xforwardai-001	0.0000	234	0.0007	171	-	329	0.0003	267	0.0004	250	0.0004	159
368	xforwardai-002	0.0000	213	0.0007	170	-	242	0.0003	268	0.0004	248	0.0004	157
369	xm-000	0.0000	136	0.0007	158	-	346	0.0001	175	0.0003	136	0.0004	195
370	yisheng-004	0.0002	343	-	374	0.4279	44	0.0013	332	0.0006	316	0.0321	331
371	yitu-003	0.0000	21	0.0000	13	-	105	0.0009	323	0.0000	17	0.0000	58
372	yoonik-001	0.0000	111	0.0014	256	-	225	0.0001	225	0.0004	249	0.0017	261
373	yoonik-002	0.0000	246	0.0010	218	-	101	0.0003	260	0.0006	312	0.0005	203
374	ytu-000	0.0000	217	0.0010	225	-	248	0.0002	254	0.0004	247	0.0011	247
375	yuan-002	0.0000	295	0.0010	223	-	211	0.0005	300	0.0005	292	0.0005	208
376	yuan-003	0.0000	294	0.0010	222	-	76	0.0005	301	0.0005	291	0.0005	207

Table 31: FTE is the proportion of failed template generation attempts. Failures can occur because the software throws an exception, or because the software electively refuses to process the input image. This would typically occur if a face is not detected. FTE is measured as the number of function calls that give EITHER a non-zero error code OR that give a “small” template. This is defined as one whose size is less than 0.3 times the median template size for that algorithm. This second rule is needed because some algorithms incorrectly fail to return a non-zero error code when template generation fails.

¹ The effects of FTE are included in the accuracy results of this report by regarding any template comparison involving a failed template to produce a low similarity score. Thus higher FTE results in higher FNMR and lower FMR.

3.4 Recognition accuracy

Core algorithm accuracy is stated via:

▷ **Cooperative subjects**

- The summary table of Figure 24;
- The visa image DETs of Figure 57;
- The mugshot DETs of Figure 76;
- The mugshot ageing profiles of Figure 273;
- The human-difficult pairs of Figure 19

▷ **Non-cooperative subjects**

- The photojournalism DET of Figure 92

Figure 219 shows dependence of false match rate on algorithm score threshold. This allows a deployer to set a threshold to target a particular false match rate appropriate to the security objectives of the application.

Figure 181 likewise shows FMR(T) but for mugshots, and specially four subsets of the population.

Note that in both the mugshot and visa sets false match rates vary with the ethnicity, age, and sex, of the enrollee and impostor. For example figure 111 summarizes FMR for impostors paired from four groups black females, black males, white females, white males.

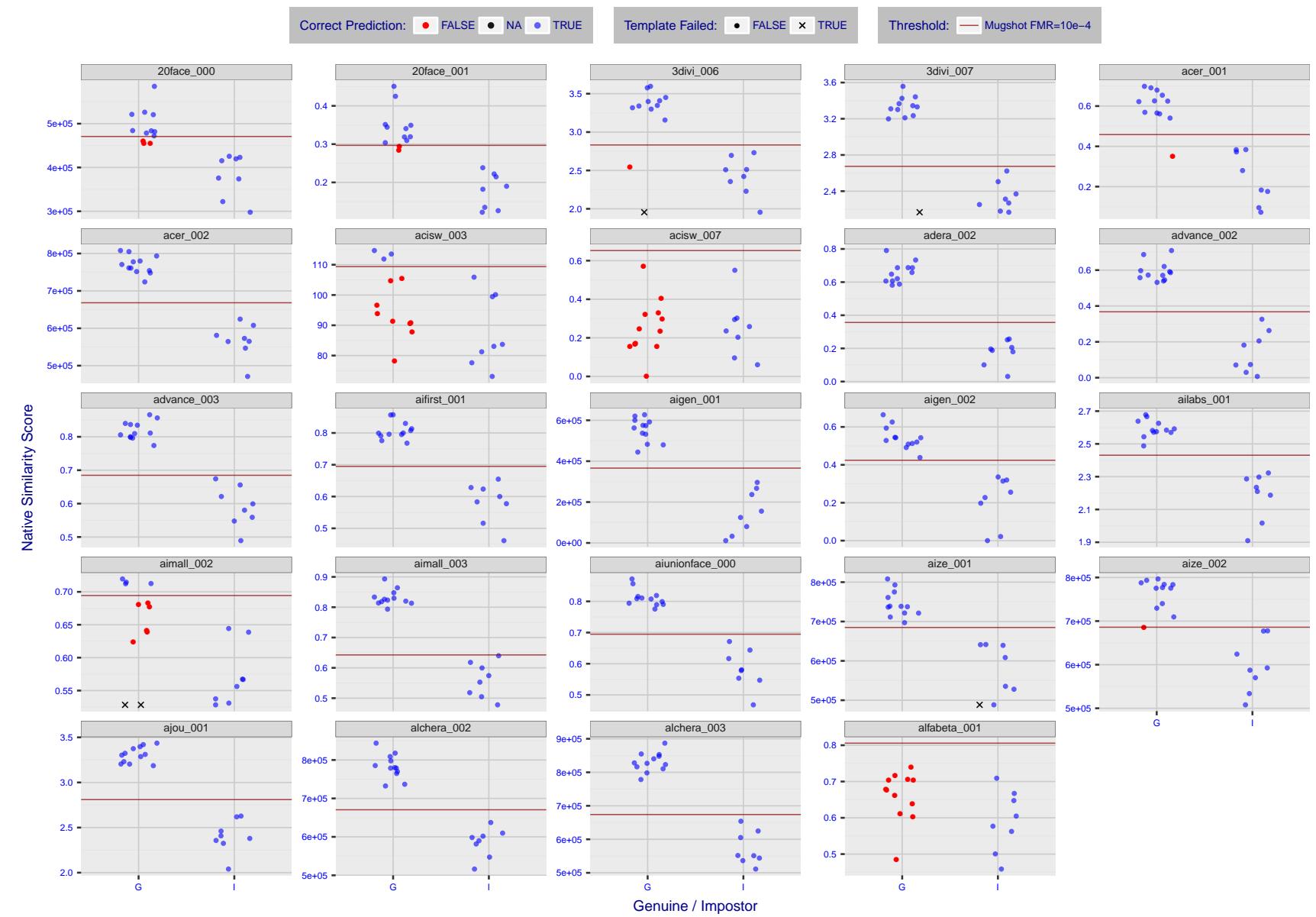


Figure 4: The figure shows algorithms' similarity scores for 12 genuine and 8 impostor image pairs used in the May 2018 paper Face recognition accuracy of forensic examiners, superrecognizers, and face recognition algorithms (Phillips et al. [1]). The threshold (red horizontal line) is a value calibrated to give $FMR = 0.0001$ on mugshot images. Points above the threshold correspond to pairs predicted to be genuine, and points below the threshold correspond to pairs predicted to be impostors. The figure shows whether the predicted class (genuine or impostor) matches the real class. Blue denotes a correct prediction, and red denotes incorrect. An X represents face detection failure in either of the images in the pair. Note that the sample size ($n=20$) is small, and the figure may change substantially if larger or different sets are used. The images can be downloaded from the [Supplemental Information](#) page provided with that publication.

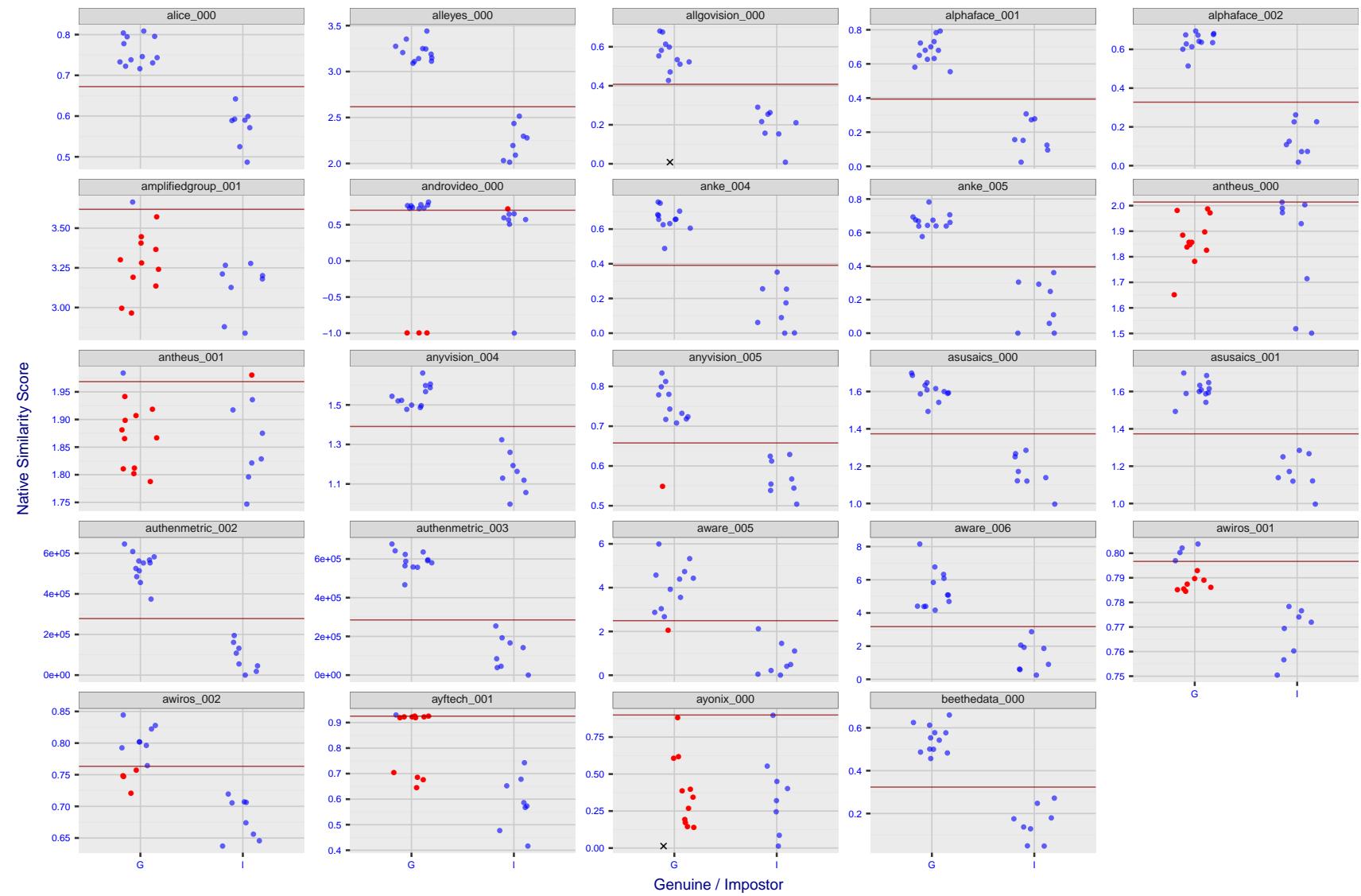


Figure 5: The figure shows algorithms' similarity scores for 12 genuine and 8 impostor image pairs used in the May 2018 paper Face recognition accuracy of forensic examiners, superrecognizers, and face recognition algorithms (Phillips et al. [1]). The threshold (red horizontal line) is a value calibrated to give $FMR = 0.0001$ on mugshot images. Points above the threshold correspond to pairs predicted to be genuine, and points below the threshold correspond to pairs predicted to be impostors. The figure shows whether the predicted class (genuine or impostor) matches the real class. Blue denotes a correct prediction, and red denotes incorrect. An X represents face detection failure in either of the images in the pair. Note that the sample size ($n=20$) is small, and the figure may change substantially if larger or different sets are used. The images can be downloaded from the [Supplemental Information](#) page provided with that publication.

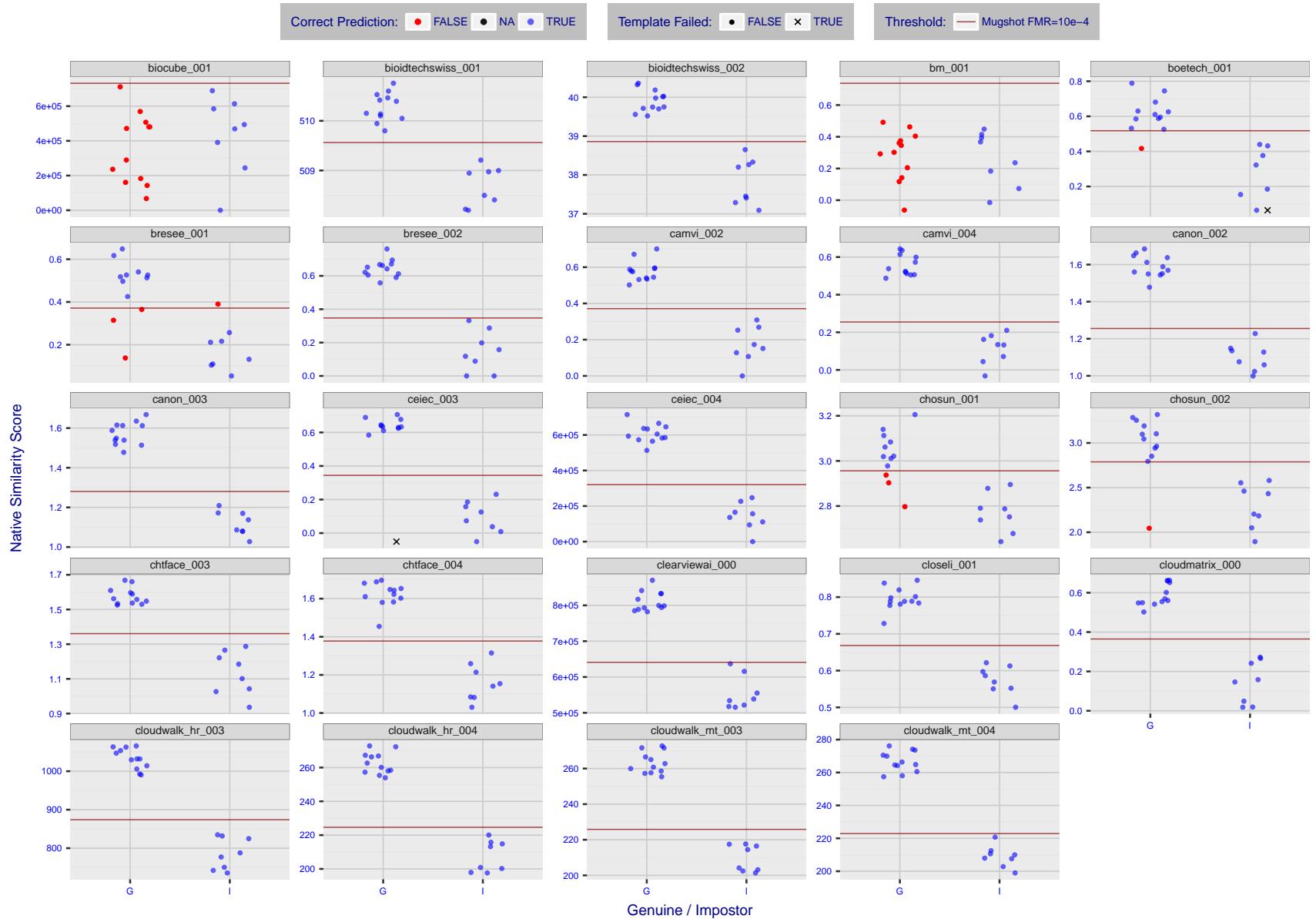


Figure 6: The figure shows algorithms' similarity scores for 12 genuine and 8 impostor image pairs used in the May 2018 paper Face recognition accuracy of forensic examiners, superrecognizers, and face recognition algorithms (Phillips et al. [1]). The threshold (red horizontal line) is a value calibrated to give $FMR = 0.0001$ on mugshot images. Points above the threshold correspond to pairs predicted to be genuine, and points below the threshold correspond to pairs predicted to be impostors. The figure shows whether the predicted class (genuine or impostor) matches the real class. Blue denotes a correct prediction, and red denotes incorrect. An X represents face detection failure in either of the images in the pair. Note that the sample size ($n=20$) is small, and the figure may change substantially if larger or different sets are used. The images can be downloaded from the [Supplemental Information](#) page provided with that publication.

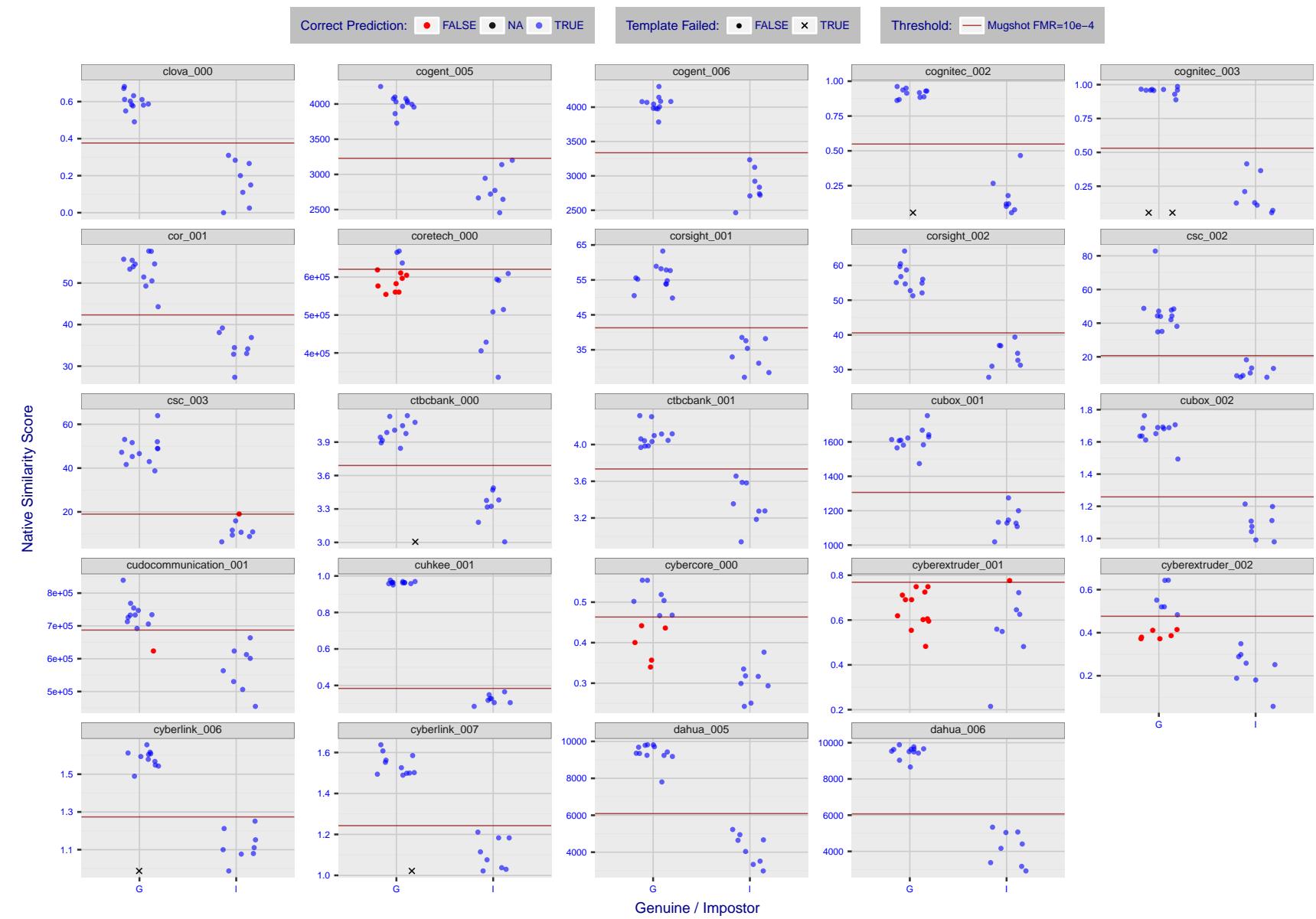


Figure 7: The figure shows algorithms' similarity scores for 12 genuine and 8 impostor image pairs used in the May 2018 paper Face recognition accuracy of forensic examiners, superrecognizers, and face recognition algorithms (Phillips et al. [1]). The threshold (red horizontal line) is a value calibrated to give $FMR = 0.0001$ on mugshot images. Points above the threshold correspond to pairs predicted to be genuine, and points below the threshold correspond to pairs predicted to be impostors. The figure shows whether the predicted class (genuine or impostor) matches the real class. Blue denotes a correct prediction, and red denotes incorrect. An X represents face detection failure in either of the images in the pair. Note that the sample size ($n=20$) is small, and the figure may change substantially if larger or different sets are used. The images can be downloaded from the [Supplemental Information](#) page provided with that publication.

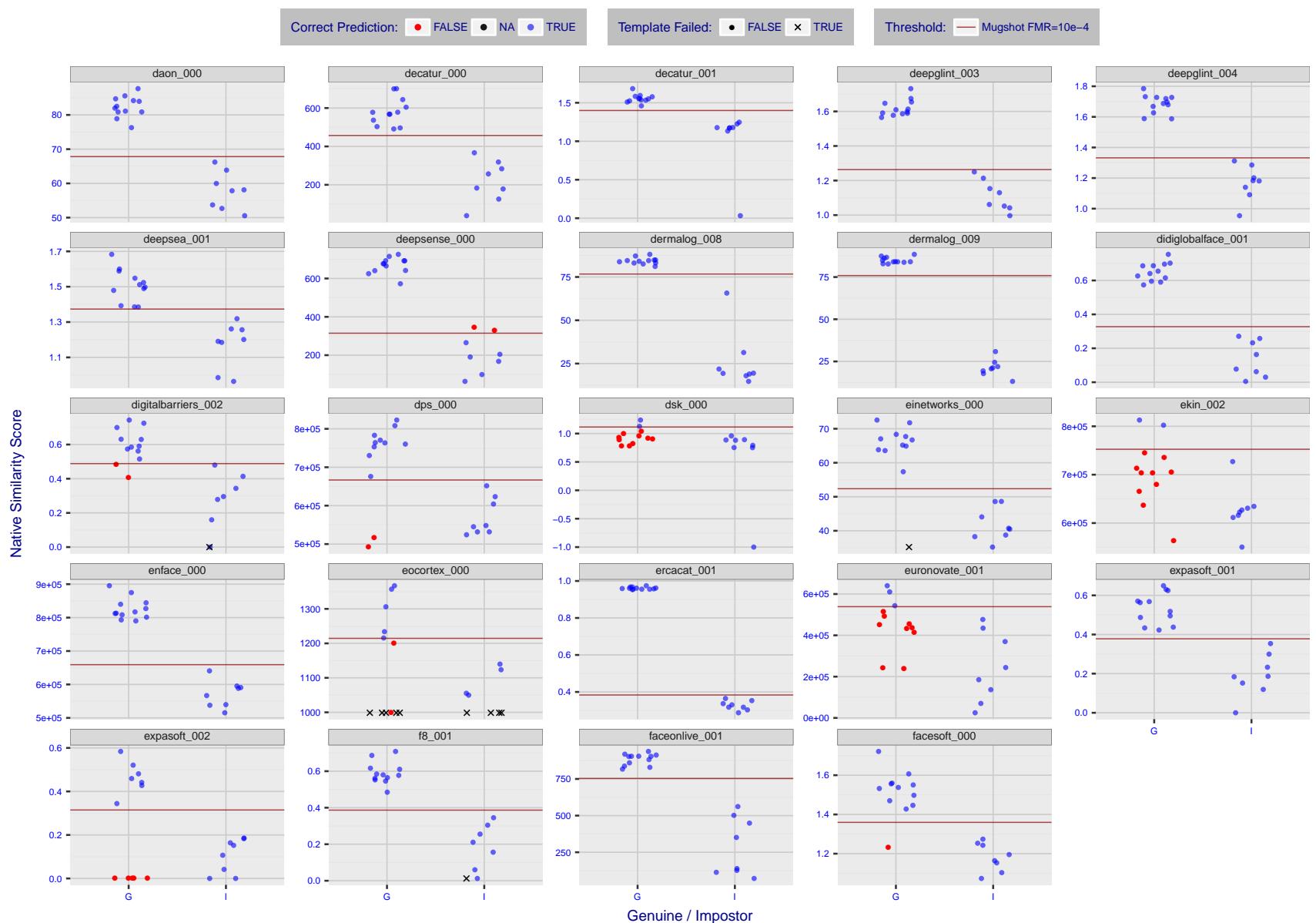


Figure 8: The figure shows algorithms' similarity scores for 12 genuine and 8 impostor image pairs used in the May 2018 paper Face recognition accuracy of forensic examiners, superrecognizers, and face recognition algorithms (Phillips et al. [1]). The threshold (red horizontal line) is a value calibrated to give $FMR = 0.0001$ on mugshot images. Points above the threshold correspond to pairs predicted to be genuine, and points below the threshold correspond to pairs predicted to be impostors. The figure shows whether the predicted class (genuine or impostor) matches the real class. Blue denotes a correct prediction, and red denotes incorrect. An X represents face detection failure in either of the images in the pair. Note that the sample size ($n=20$) is small, and the figure may change substantially if larger or different sets are used. The images can be downloaded from the [Supplemental Information](#) page provided with that publication.

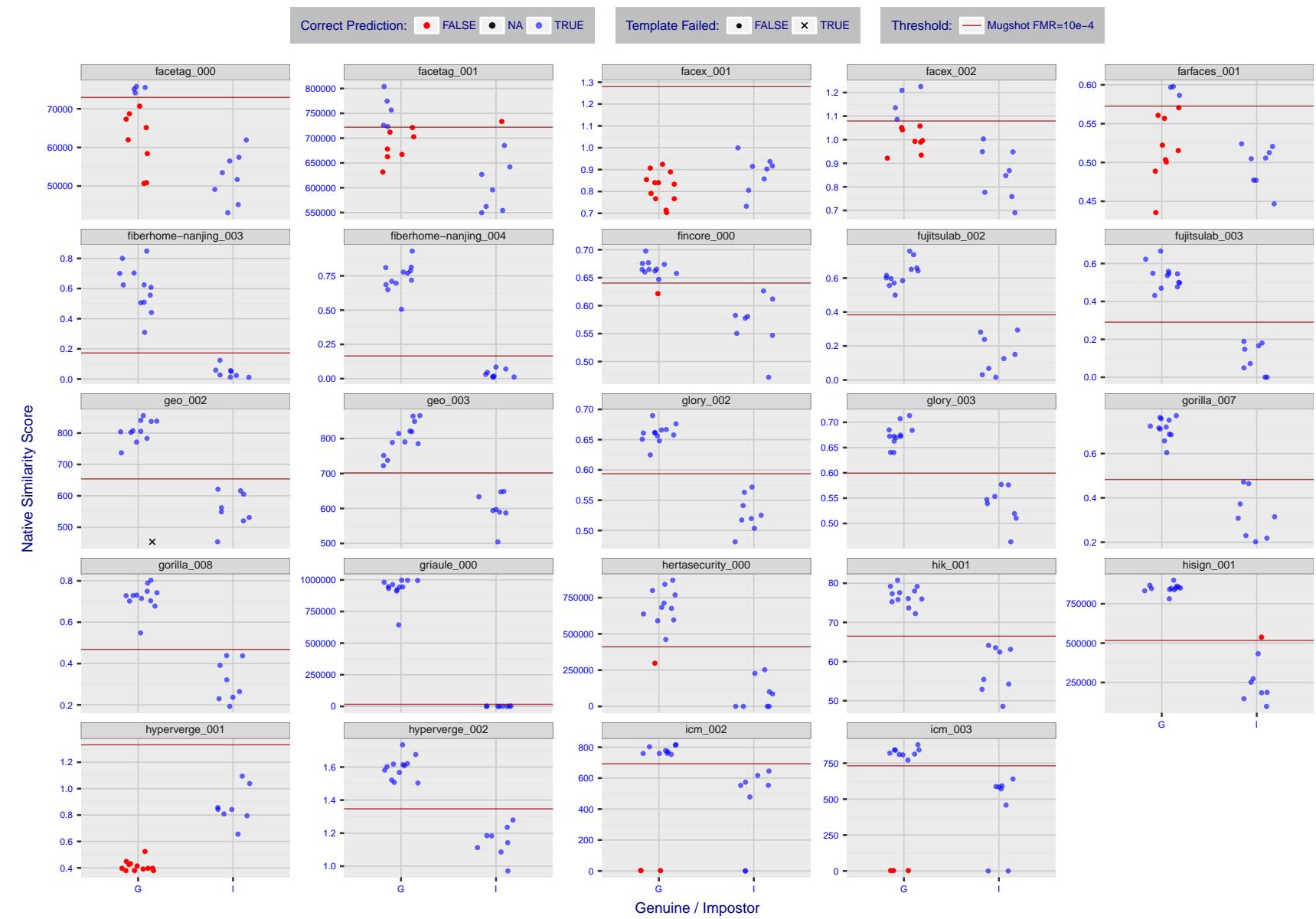


Figure 9: The figure shows algorithms' similarity scores for 12 genuine and 8 impostor image pairs used in the May 2018 paper Face recognition accuracy of forensic examiners, superrecognizers, and face recognition algorithms (Phillips et al. [1]). The threshold (red horizontal line) is a value calibrated to give $FMR = 0.0001$ on mugshot images. Points above the threshold correspond to pairs predicted to be genuine, and points below the threshold correspond to pairs predicted to be impostors. The figure shows whether the predicted class (genuine or impostor) matches the real class. Blue denotes a correct prediction, and red denotes incorrect. An X represents face detection failure in either of the images in the pair. Note that the sample size ($n=20$) is small, and the figure may change substantially if larger or different sets are used. The images can be downloaded from the [Supplemental Information](#) page provided with that publication.

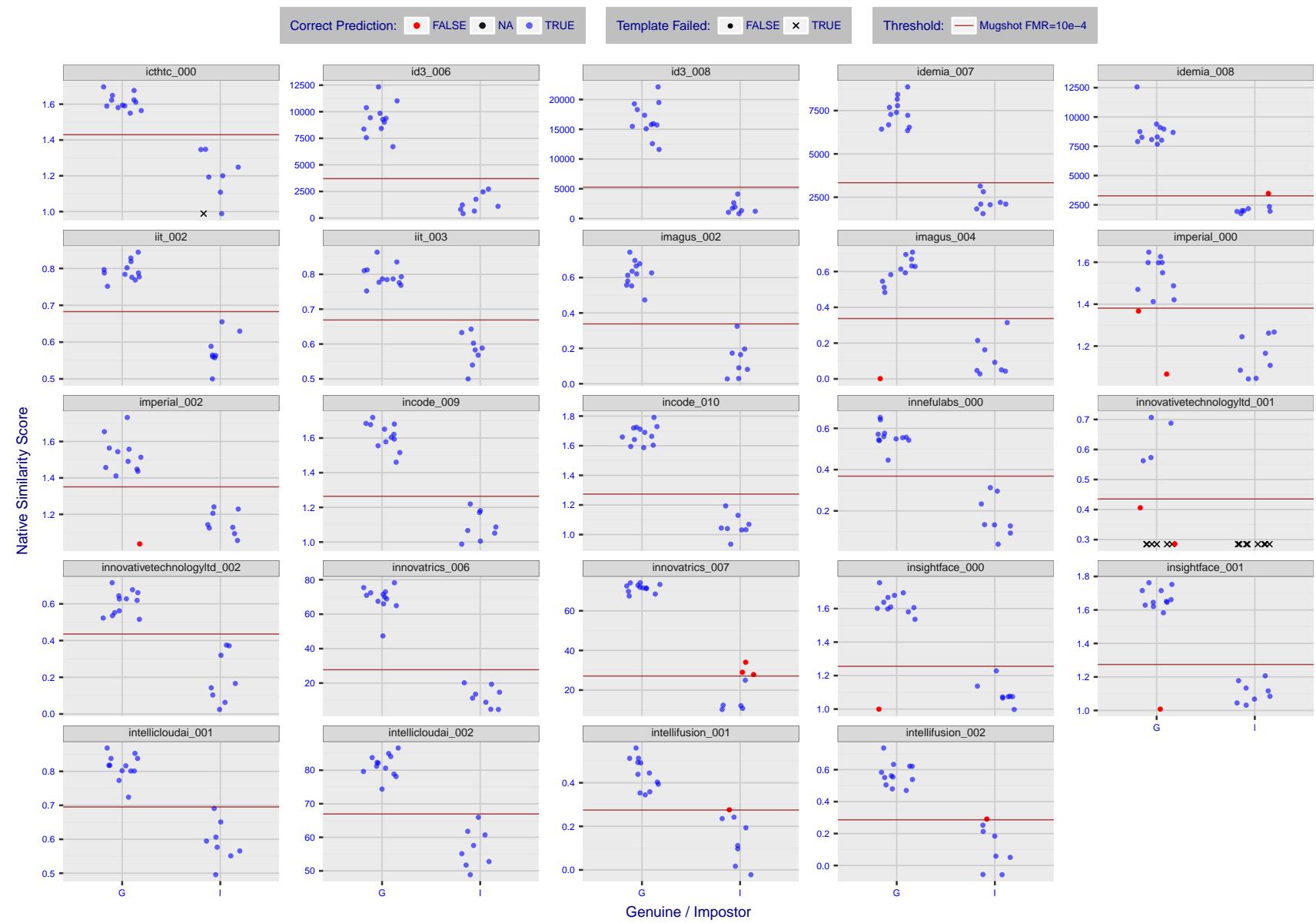


Figure 10: The figure shows algorithms' similarity scores for 12 genuine and 8 impostor image pairs used in the May 2018 paper [Face recognition accuracy of forensic examiners, superrecognizers, and face recognition algorithms](#) (Phillips et al. [1]). The threshold (red horizontal line) is a value calibrated to give $FMR = 0.0001$ on mugshot images. Points above the threshold correspond to pairs predicted to be genuine, and points below the threshold correspond to pairs predicted to be impostors. The figure shows whether the predicted class (genuine or impostor) matches the real class. Blue denotes a correct prediction, and red denotes incorrect. An X represents face detection failure in either of the images in the pair. Note that the sample size ($n=20$) is small, and the figure may change substantially if larger or different sets are used. The images can be downloaded from the [Supplemental Information](#) page provided with that publication.

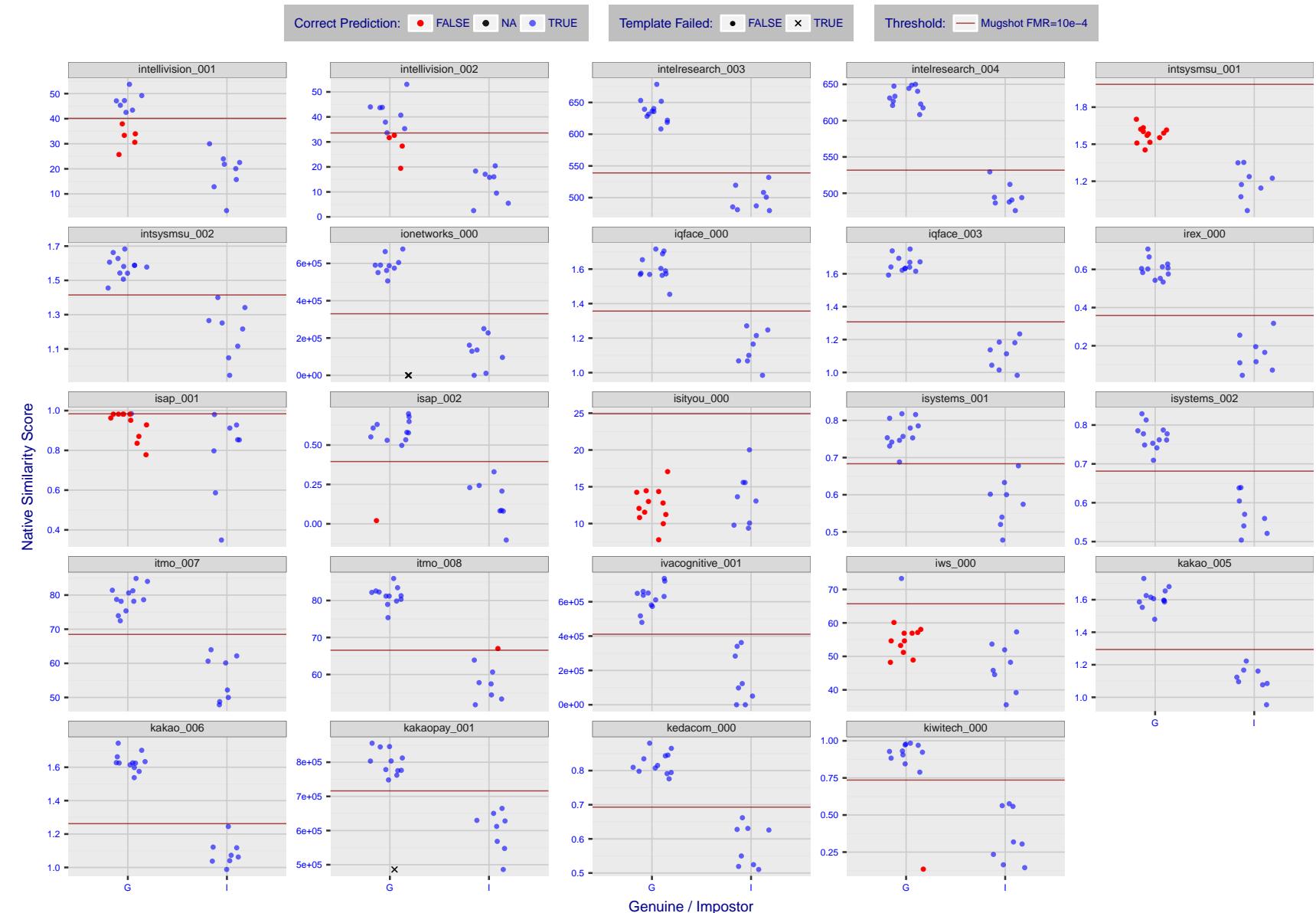


Figure 11: The figure shows algorithms' similarity scores for 12 genuine and 8 impostor image pairs used in the May 2018 paper [Face recognition accuracy of forensic examiners, superrecognizers, and face recognition algorithms](#) (Phillips et al. [1]). The threshold (red horizontal line) is a value calibrated to give $FMR = 0.0001$ on mugshot images. Points above the threshold correspond to pairs predicted to be genuine, and points below the threshold correspond to pairs predicted to be impostors. The figure shows whether the predicted class (genuine or impostor) matches the real class. Blue denotes a correct prediction, and red denotes incorrect. An X represents face detection failure in either of the images in the pair. Note that the sample size ($n=20$) is small, and the figure may change substantially if larger or different sets are used. The images can be downloaded from the [Supplemental Information](#) page provided with that publication.

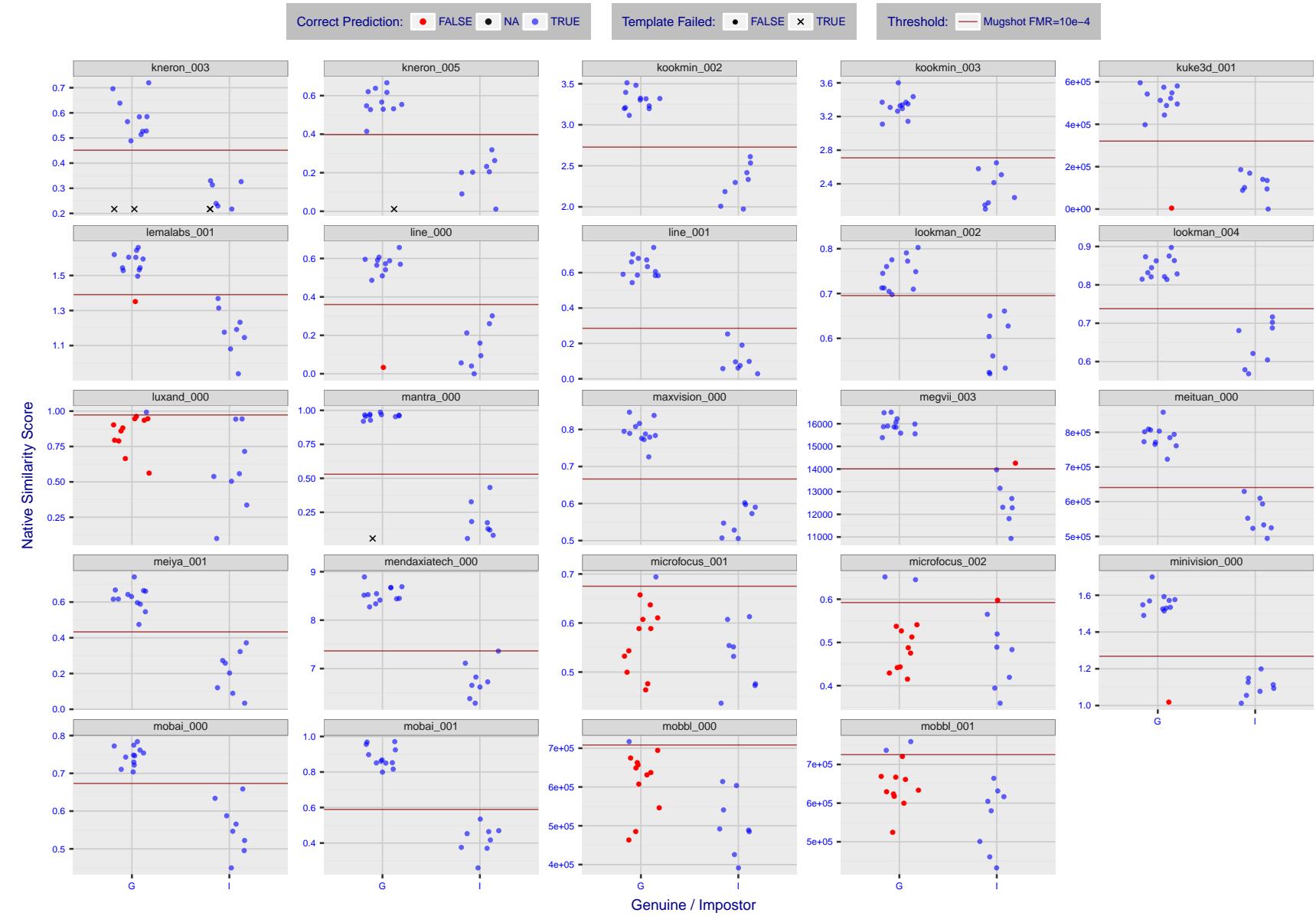


Figure 12: The figure shows algorithms' similarity scores for 12 genuine and 8 impostor image pairs used in the May 2018 paper [Face recognition accuracy of forensic examiners, superrecognizers, and face recognition algorithms](#) (Phillips et al. [1]). The threshold (red horizontal line) is a value calibrated to give $FMR = 0.0001$ on mugshot images. Points above the threshold correspond to pairs predicted to be genuine, and points below the threshold correspond to pairs predicted to be impostors. The figure shows whether the predicted class (genuine or impostor) matches the real class. Blue denotes a correct prediction, and red denotes incorrect. An X represents face detection failure in either of the images in the pair. Note that the sample size ($n=20$) is small, and the figure may change substantially if larger or different sets are used. The images can be downloaded from the [Supplemental Information](#) page provided with that publication.

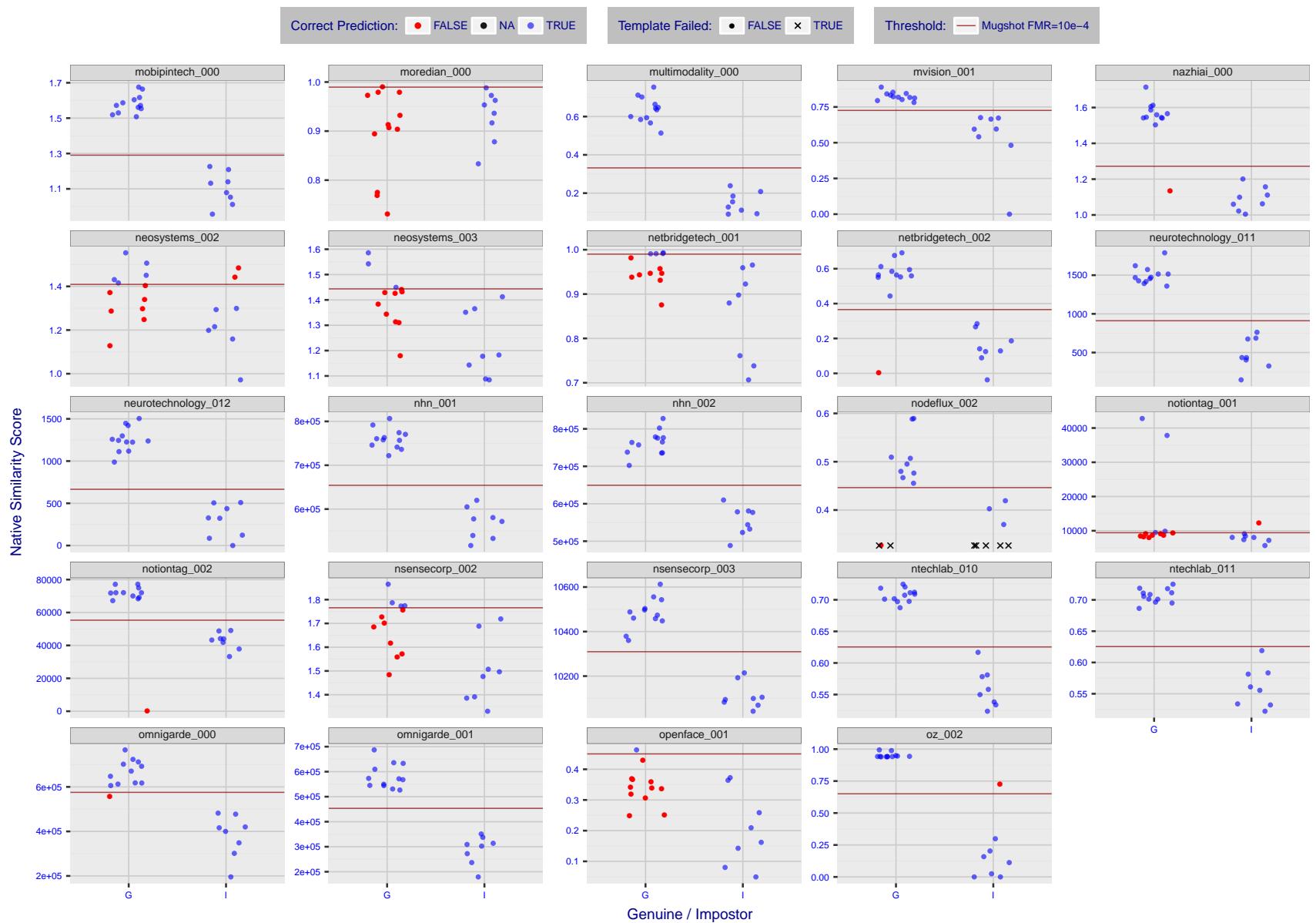


Figure 13: The figure shows algorithms' similarity scores for 12 genuine and 8 impostor image pairs used in the May 2018 paper Face recognition accuracy of forensic examiners, superrecognizers, and face recognition algorithms (Phillips et al. [1]). The threshold (red horizontal line) is a value calibrated to give $FMR = 0.0001$ on mugshot images. Points above the threshold correspond to pairs predicted to be genuine, and points below the threshold correspond to pairs predicted to be impostors. The figure shows whether the predicted class (genuine or impostor) matches the real class. Blue denotes a correct prediction, and red denotes incorrect. An X represents face detection failure in either of the images in the pair. Note that the sample size ($n=20$) is small, and the figure may change substantially if larger or different sets are used. The images can be downloaded from the [Supplemental Information](#) page provided with that publication.

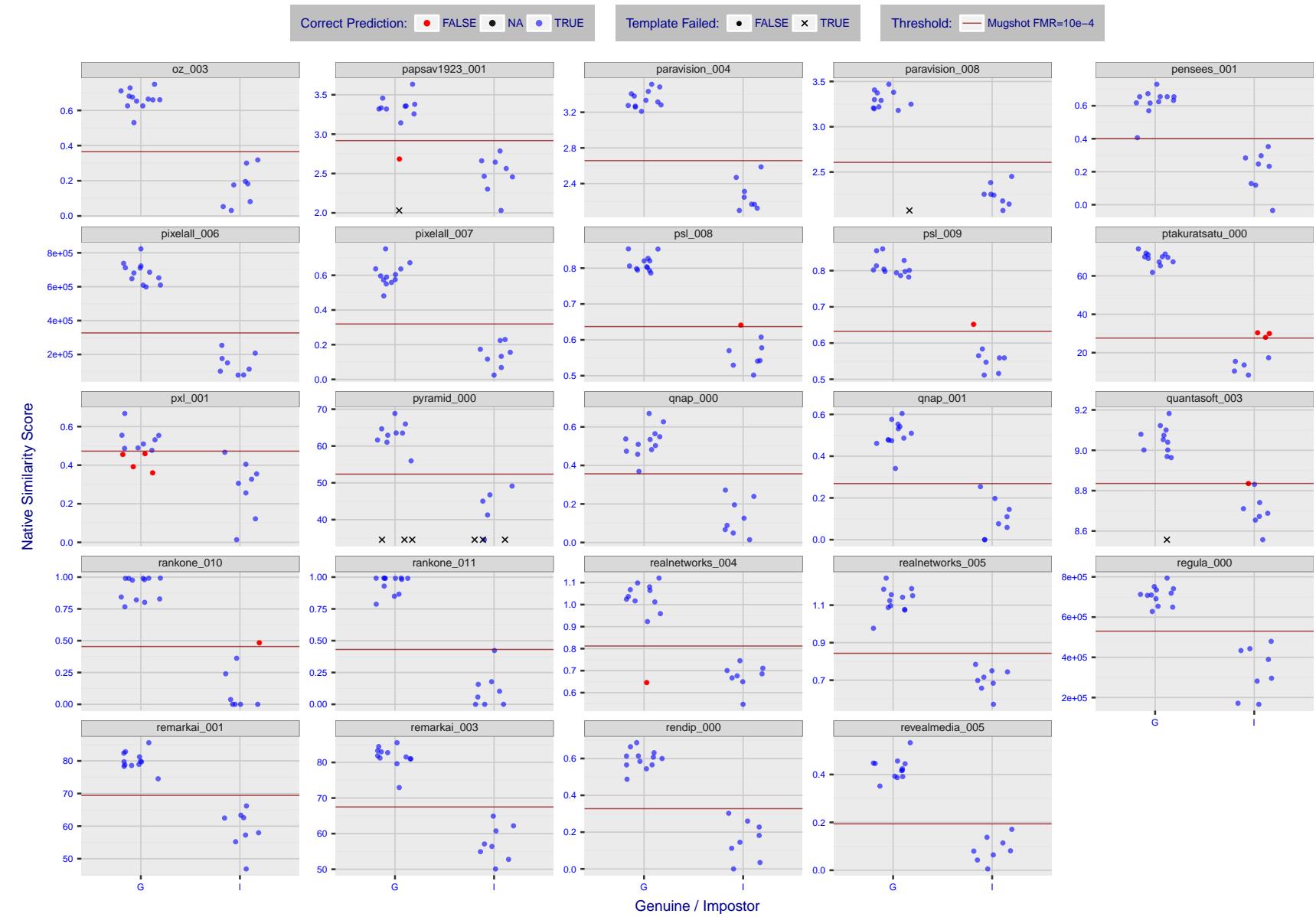


Figure 14: The figure shows algorithms' similarity scores for 12 genuine and 8 impostor image pairs used in the May 2018 paper [Face recognition accuracy of forensic examiners, superrecognizers, and face recognition algorithms](#) (Phillips et al. [1]). The threshold (red horizontal line) is a value calibrated to give $FMR = 0.0001$ on mugshot images. Points above the threshold correspond to pairs predicted to be genuine, and points below the threshold correspond to pairs predicted to be impostors. The figure shows whether the predicted class (genuine or impostor) matches the real class. Blue denotes a correct prediction, and red denotes incorrect. An X represents face detection failure in either of the images in the pair. Note that the sample size ($n=20$) is small, and the figure may change substantially if larger or different sets are used. The images can be downloaded from the [Supplemental Information](#) page provided with that publication.

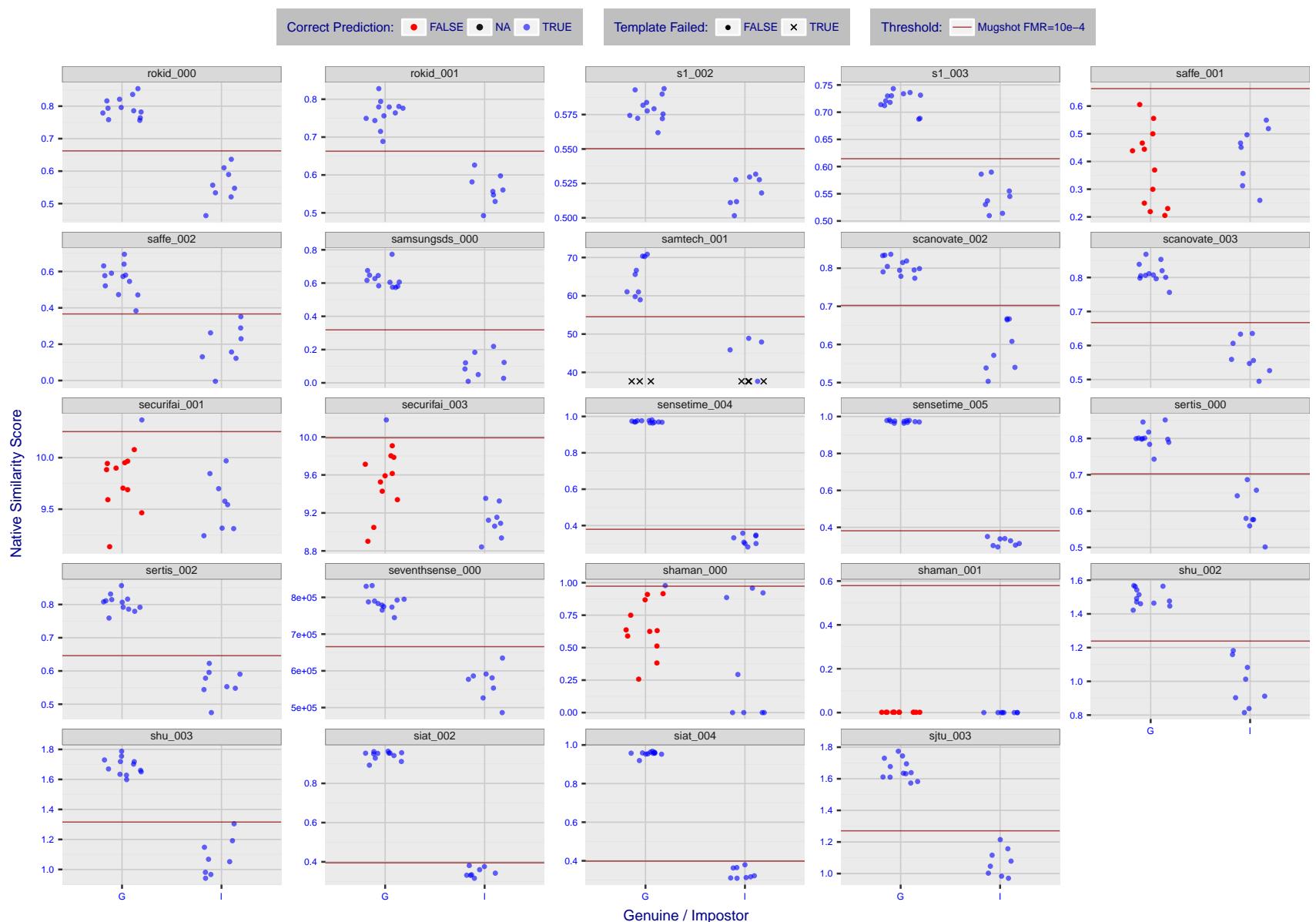


Figure 15: The figure shows algorithms' similarity scores for 12 genuine and 8 impostor image pairs used in the May 2018 paper Face recognition accuracy of forensic examiners, superrecognizers, and face recognition algorithms (Phillips et al. [1]). The threshold (red horizontal line) is a value calibrated to give $FMR = 0.0001$ on mugshot images. Points above the threshold correspond to pairs predicted to be genuine, and points below the threshold correspond to pairs predicted to be impostors. The figure shows whether the predicted class (genuine or impostor) matches the real class. Blue denotes a correct prediction, and red denotes incorrect. An X represents face detection failure in either of the images in the pair. Note that the sample size ($n=20$) is small, and the figure may change substantially if larger or different sets are used. The images can be downloaded from the [Supplemental Information](#) page provided with that publication.

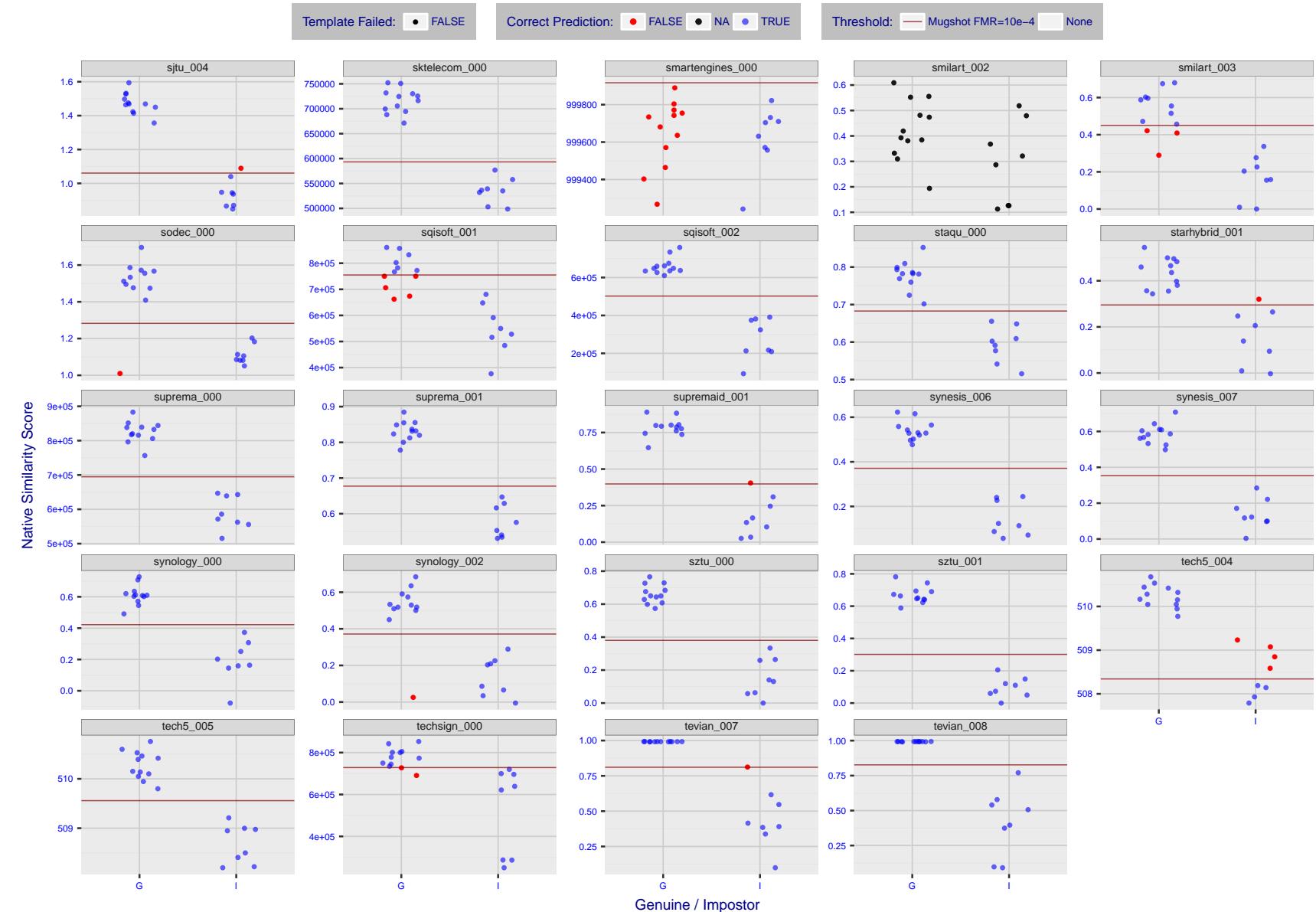


Figure 16: The figure shows algorithms' similarity scores for 12 genuine and 8 impostor image pairs used in the May 2018 paper [Face recognition accuracy of forensic examiners, superrecognizers, and face recognition algorithms](#) (Phillips et al. [1]). The threshold (red horizontal line) is a value calibrated to give $FMR = 0.0001$ on mugshot images. Points above the threshold correspond to pairs predicted to be genuine, and points below the threshold correspond to pairs predicted to be impostors. The figure shows whether the predicted class (genuine or impostor) matches the real class. Blue denotes a correct prediction, and red denotes incorrect. An X represents face detection failure in either of the images in the pair. Note that the sample size ($n=20$) is small, and the figure may change substantially if larger or different sets are used. The images can be downloaded from the [Supplemental Information](#) page provided with that publication.

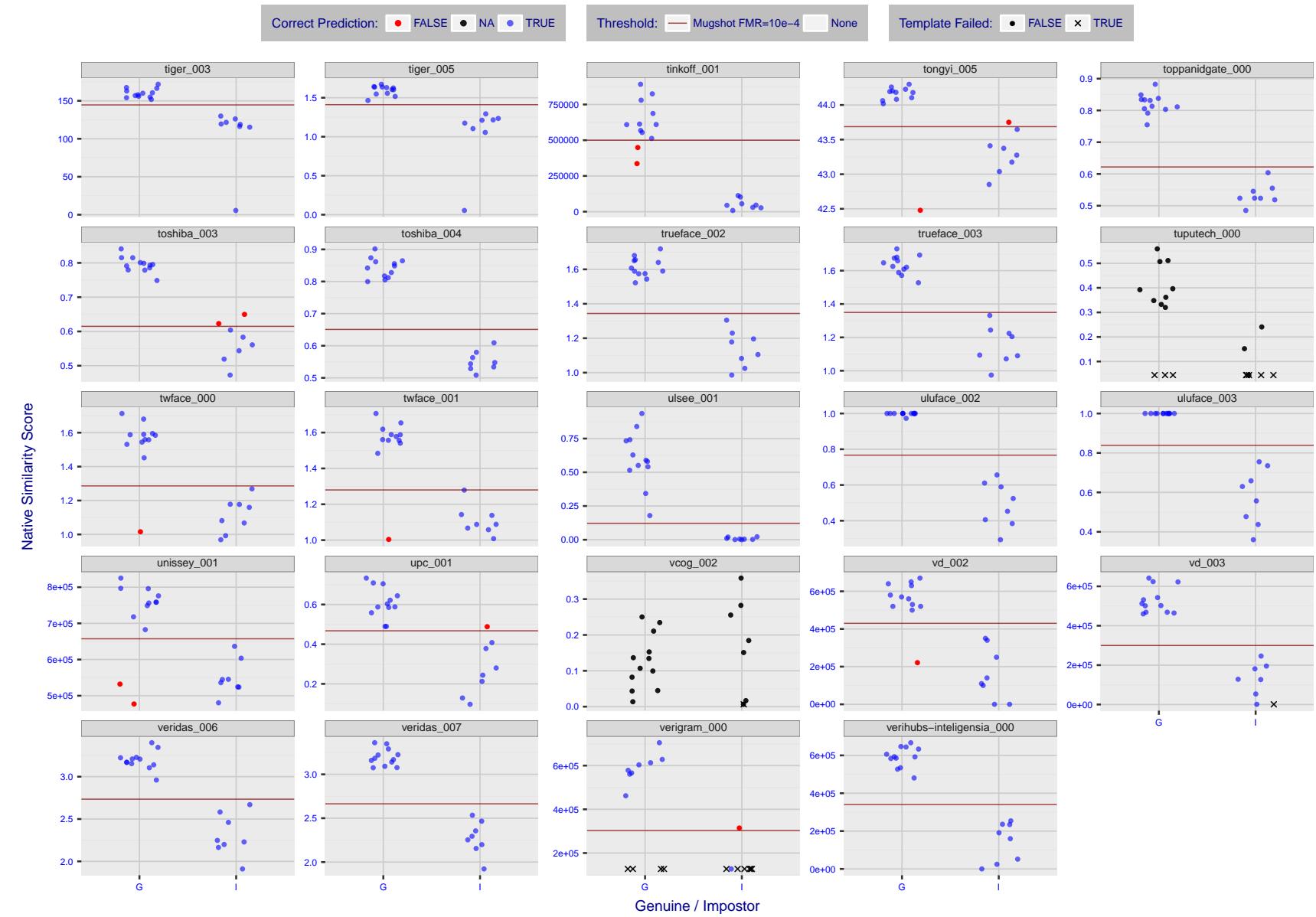


Figure 17: The figure shows algorithms' similarity scores for 12 genuine and 8 impostor image pairs used in the May 2018 paper [Face recognition accuracy of forensic examiners, superrecognizers, and face recognition algorithms](#) (Phillips et al. [1]). The threshold (red horizontal line) is a value calibrated to give $FMR = 0.0001$ on mugshot images. Points above the threshold correspond to pairs predicted to be genuine, and points below the threshold correspond to pairs predicted to be impostors. The figure shows whether the predicted class (genuine or impostor) matches the real class. Blue denotes a correct prediction, and red denotes incorrect. An X represents face detection failure in either of the images in the pair. Note that the sample size ($n=20$) is small, and the figure may change substantially if larger or different sets are used. The images can be downloaded from the [Supplemental Information](#) page provided with that publication.

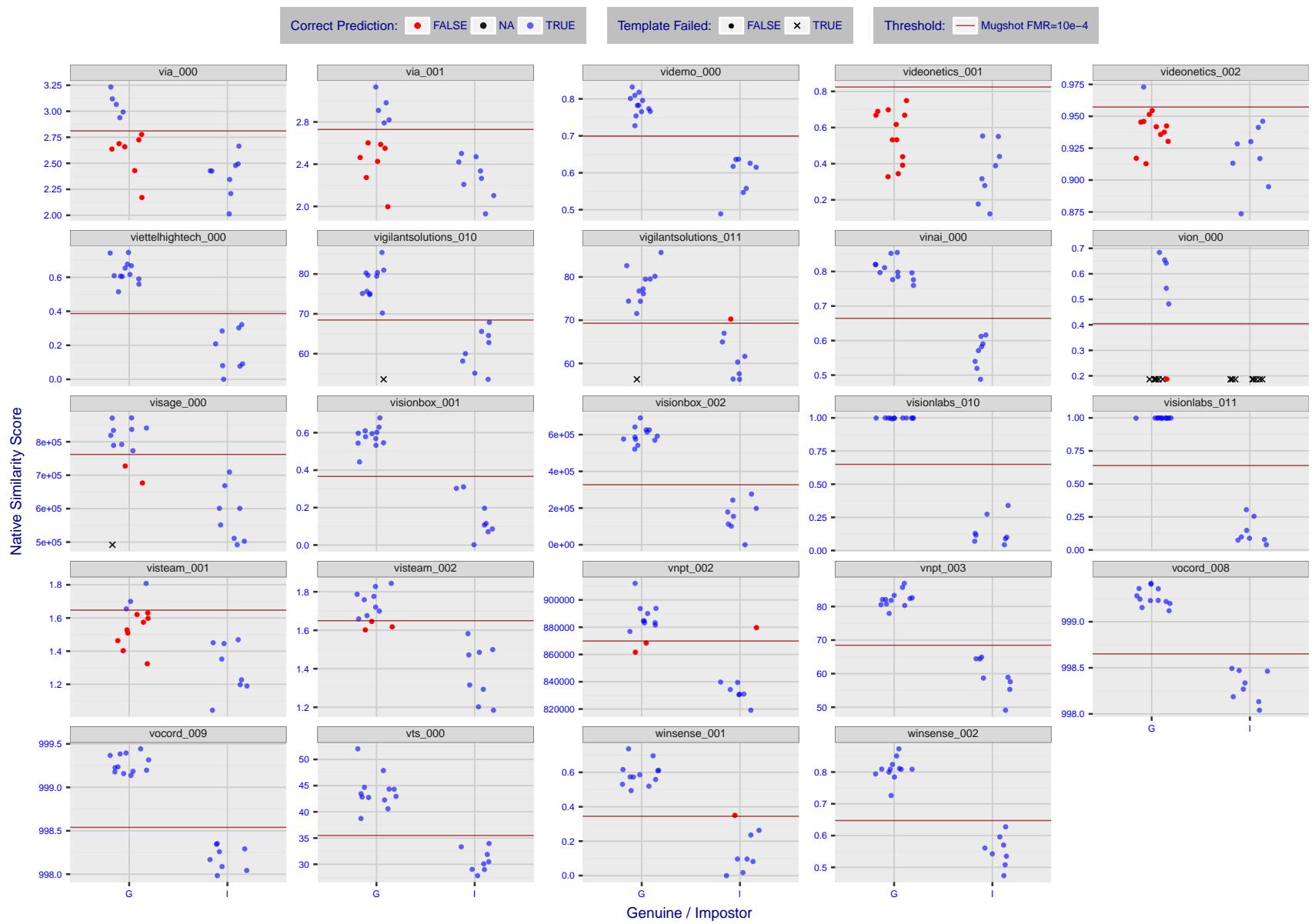


Figure 18: The figure shows algorithms' similarity scores for 12 genuine and 8 impostor image pairs used in the May 2018 paper [Face recognition accuracy of forensic examiners, superrecognizers, and face recognition algorithms](#) (Phillips et al. [1]). The threshold (red horizontal line) is a value calibrated to give $FMR = 0.0001$ on mugshot images. Points above the threshold correspond to pairs predicted to be genuine, and points below the threshold correspond to pairs predicted to be impostors. The figure shows whether the predicted class (genuine or impostor) matches the real class. Blue denotes a correct prediction, and red denotes incorrect. An X represents face detection failure in either of the images in the pair. Note that the sample size ($n=20$) is small, and the figure may change substantially if larger or different sets are used. The images can be downloaded from the [Supplemental Information](#) page provided with that publication.

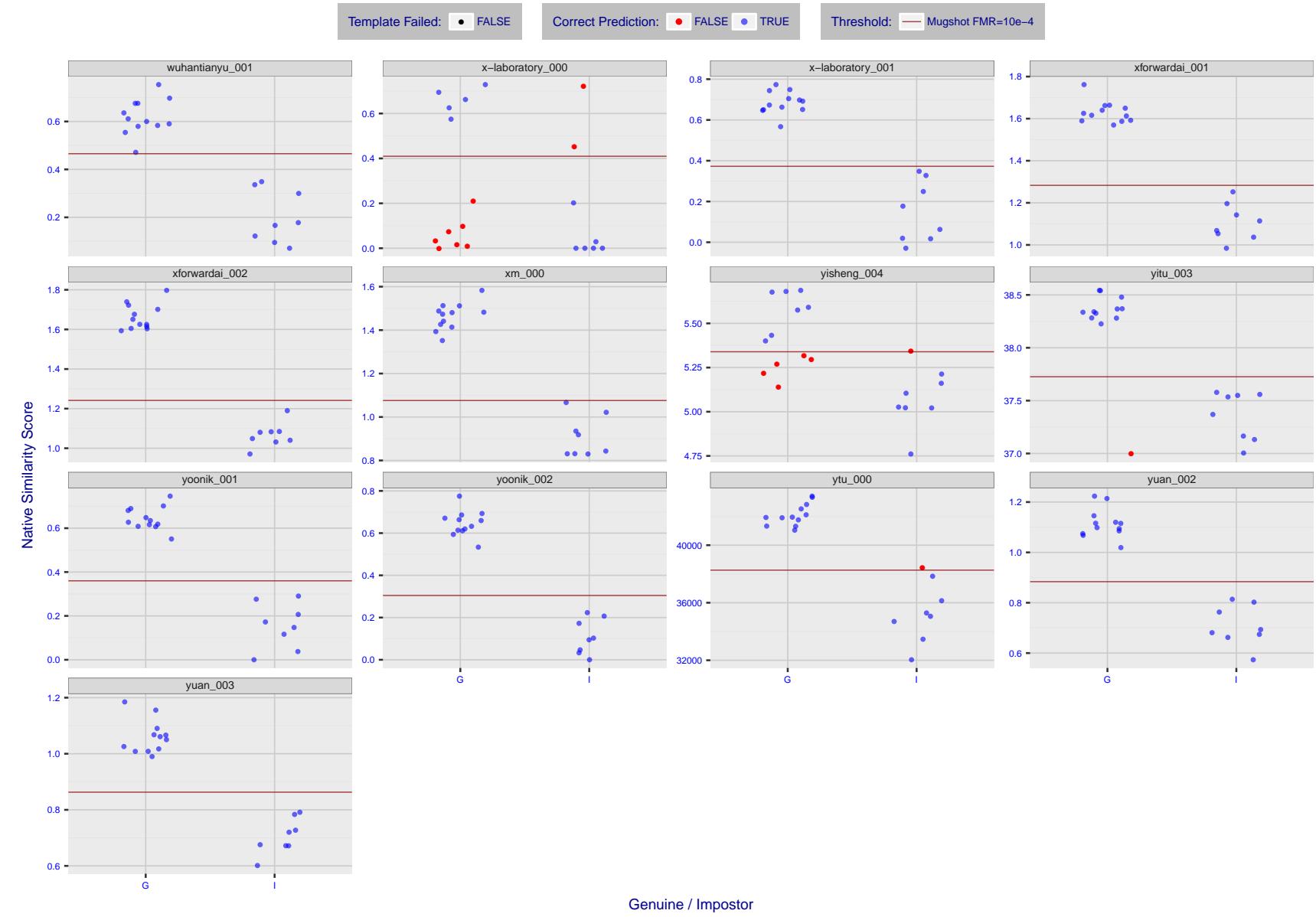


Figure 19: The figure shows algorithms' similarity scores for 12 genuine and 8 impostor image pairs used in the May 2018 paper [Face recognition accuracy of forensic examiners, superrecognizers, and face recognition algorithms](#) (Phillips et al. [1]). The threshold (red horizontal line) is a value calibrated to give $FMR = 0.0001$ on mugshot images. Points above the threshold correspond to pairs predicted to be genuine, and points below the threshold correspond to pairs predicted to be impostors. The figure shows whether the predicted class (genuine or impostor) matches the real class. Blue denotes a correct prediction, and red denotes incorrect. An X represents face detection failure in either of the images in the pair. Note that the sample size ($n=20$) is small, and the figure may change substantially if larger or different sets are used. The images can be downloaded from the [Supplemental Information](#) page provided with that publication.

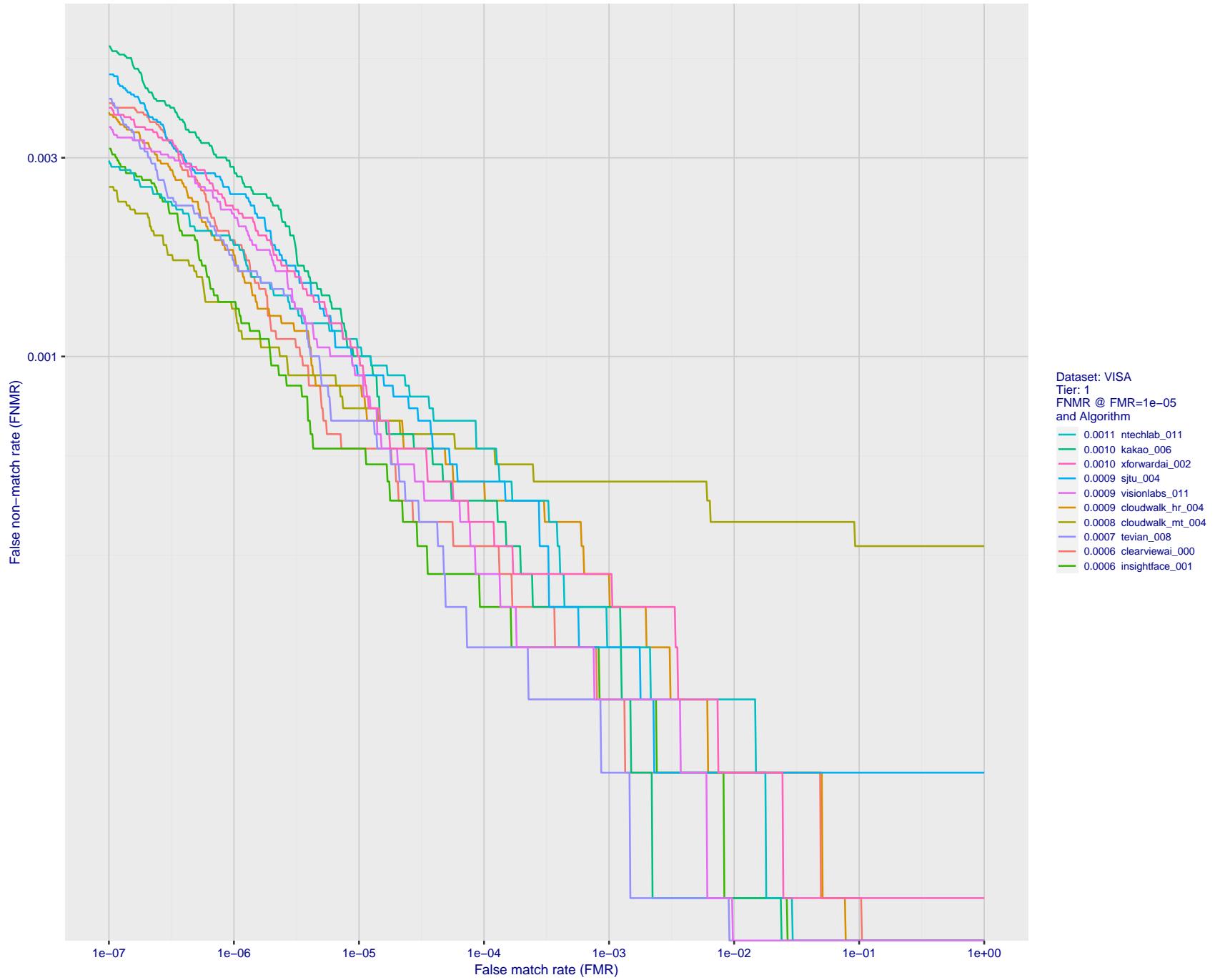


Figure 20: For the visa images, detection error tradeoff (DET) characteristics showing false non-match rate vs. false match rate plotted parametrically on threshold, T . The scales are logarithmic in order to show many decades of FMR.

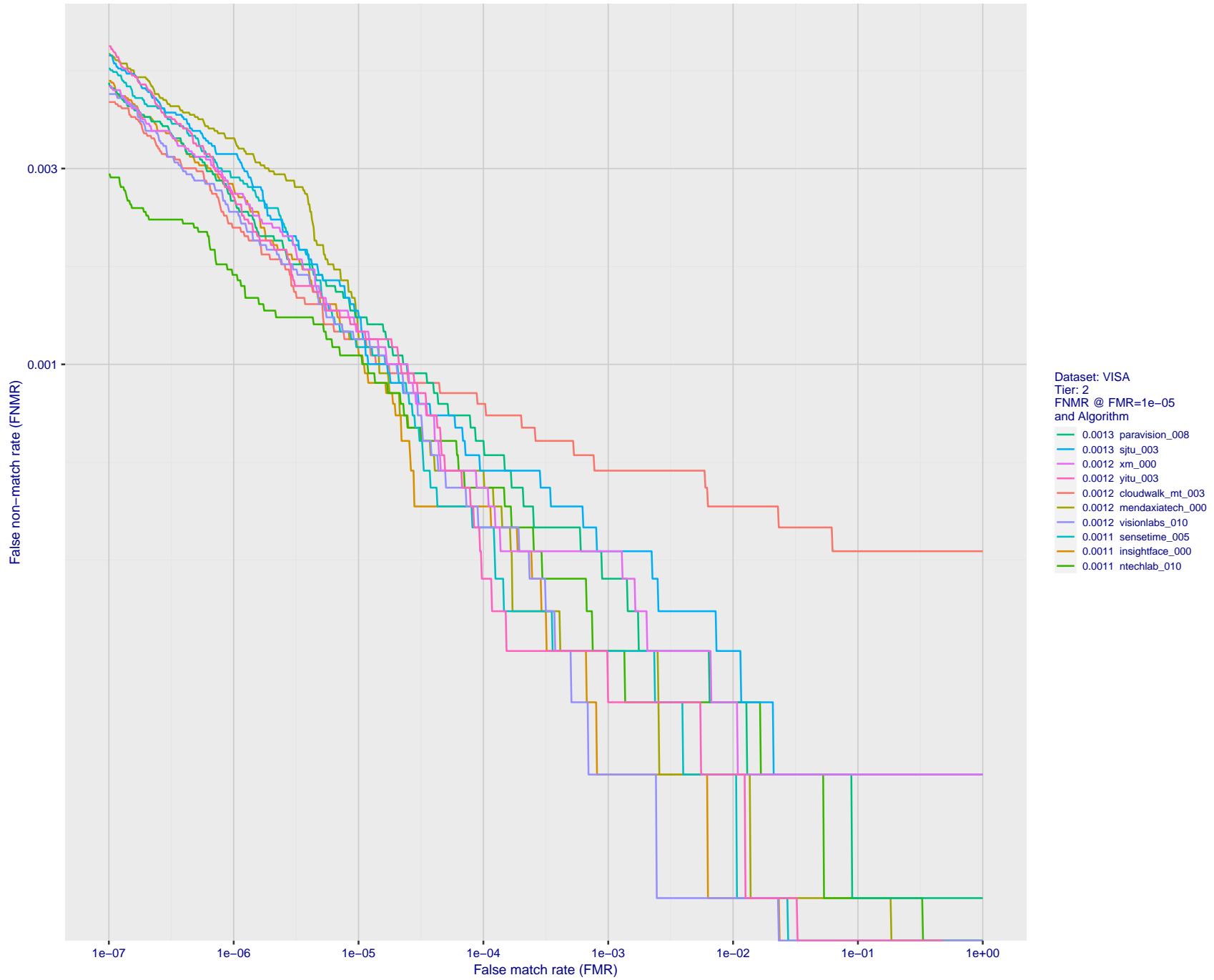


Figure 21: For the visa images, detection error tradeoff (DET) characteristics showing false non-match rate vs. false match rate plotted parametrically on threshold, T . The scales are logarithmic in order to show many decades of FMR.

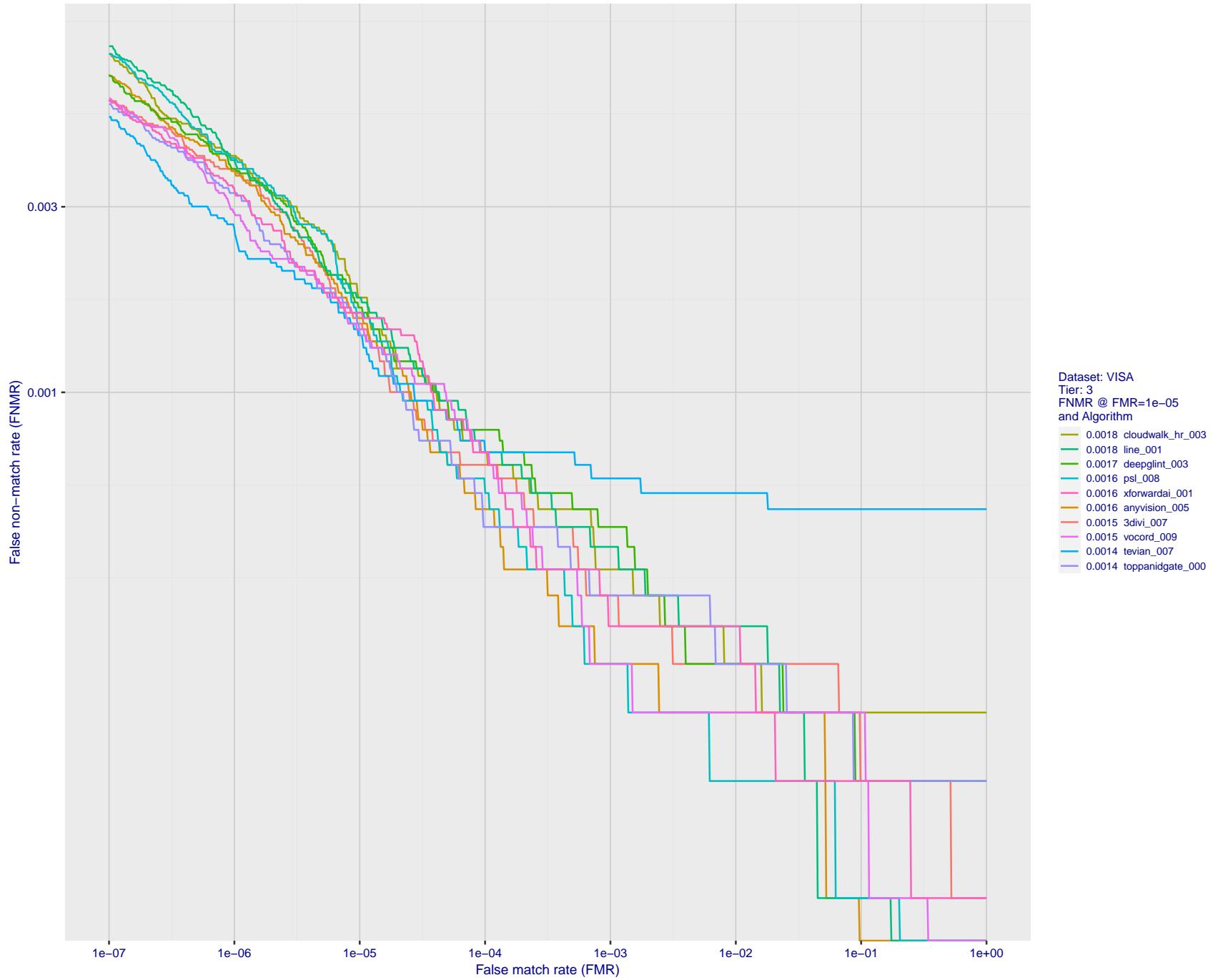


Figure 22: For the visa images, detection error tradeoff (DET) characteristics showing false non-match rate vs. false match rate plotted parametrically on threshold, T . The scales are logarithmic in order to show many decades of FMR.

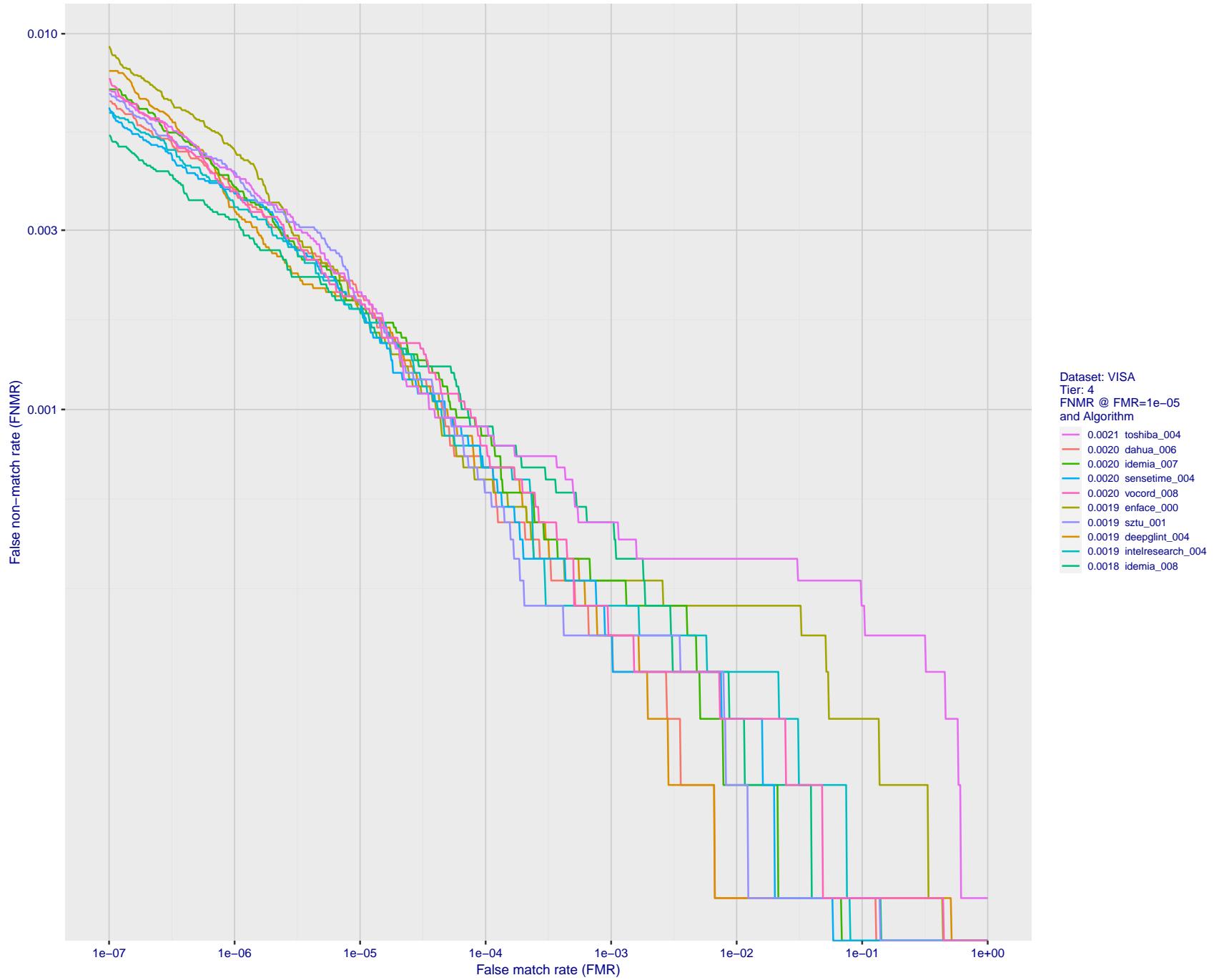


Figure 23: For the visa images, detection error tradeoff (DET) characteristics showing false non-match rate vs. false match rate plotted parametrically on threshold, T . The scales are logarithmic in order to show many decades of FMR.

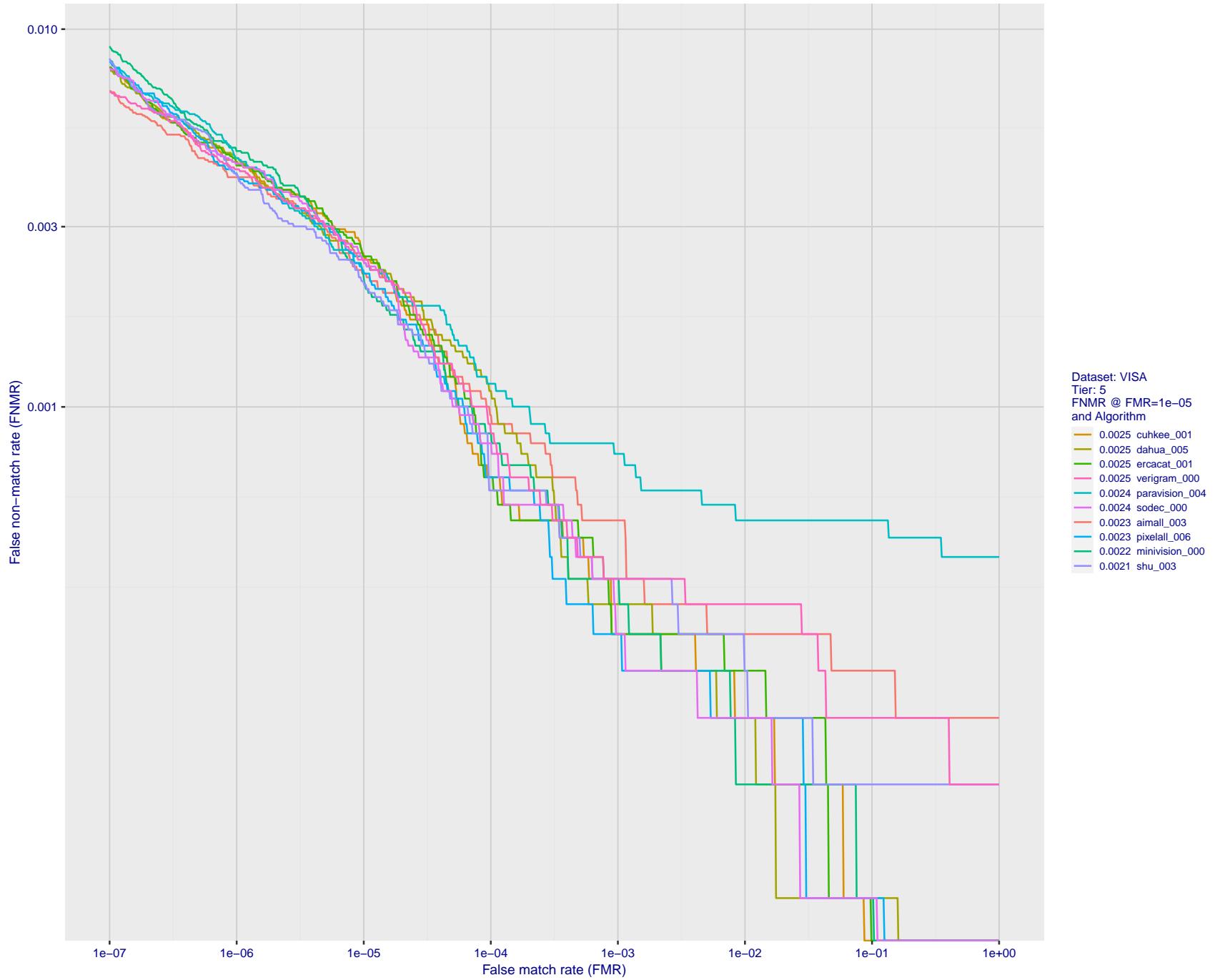


Figure 24: For the visa images, detection error tradeoff (DET) characteristics showing false non-match rate vs. false match rate plotted parametrically on threshold, T . The scales are logarithmic in order to show many decades of FMR.

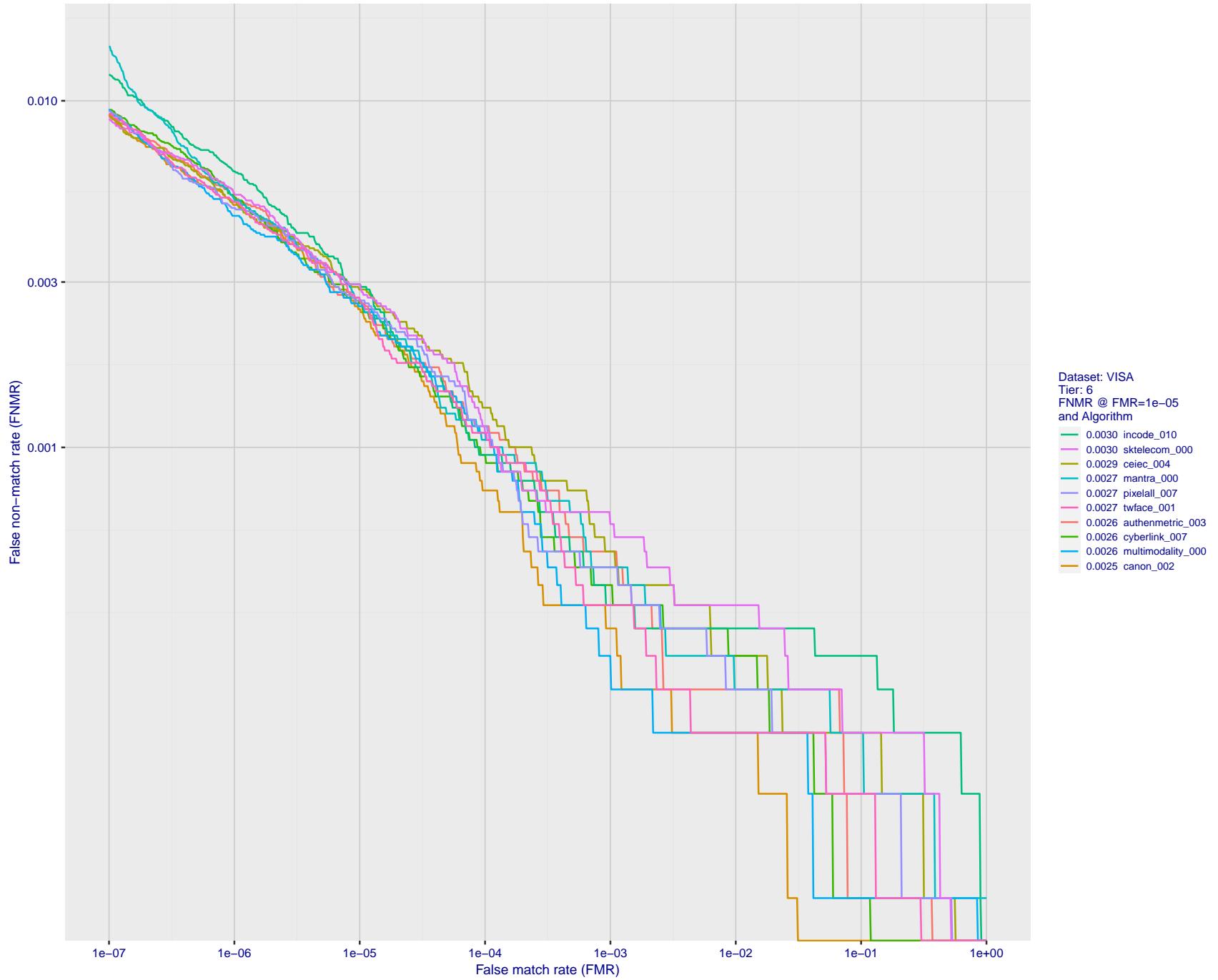


Figure 25: For the visa images, detection error tradeoff (DET) characteristics showing false non-match rate vs. false match rate plotted parametrically on threshold, T . The scales are logarithmic in order to show many decades of FMR.

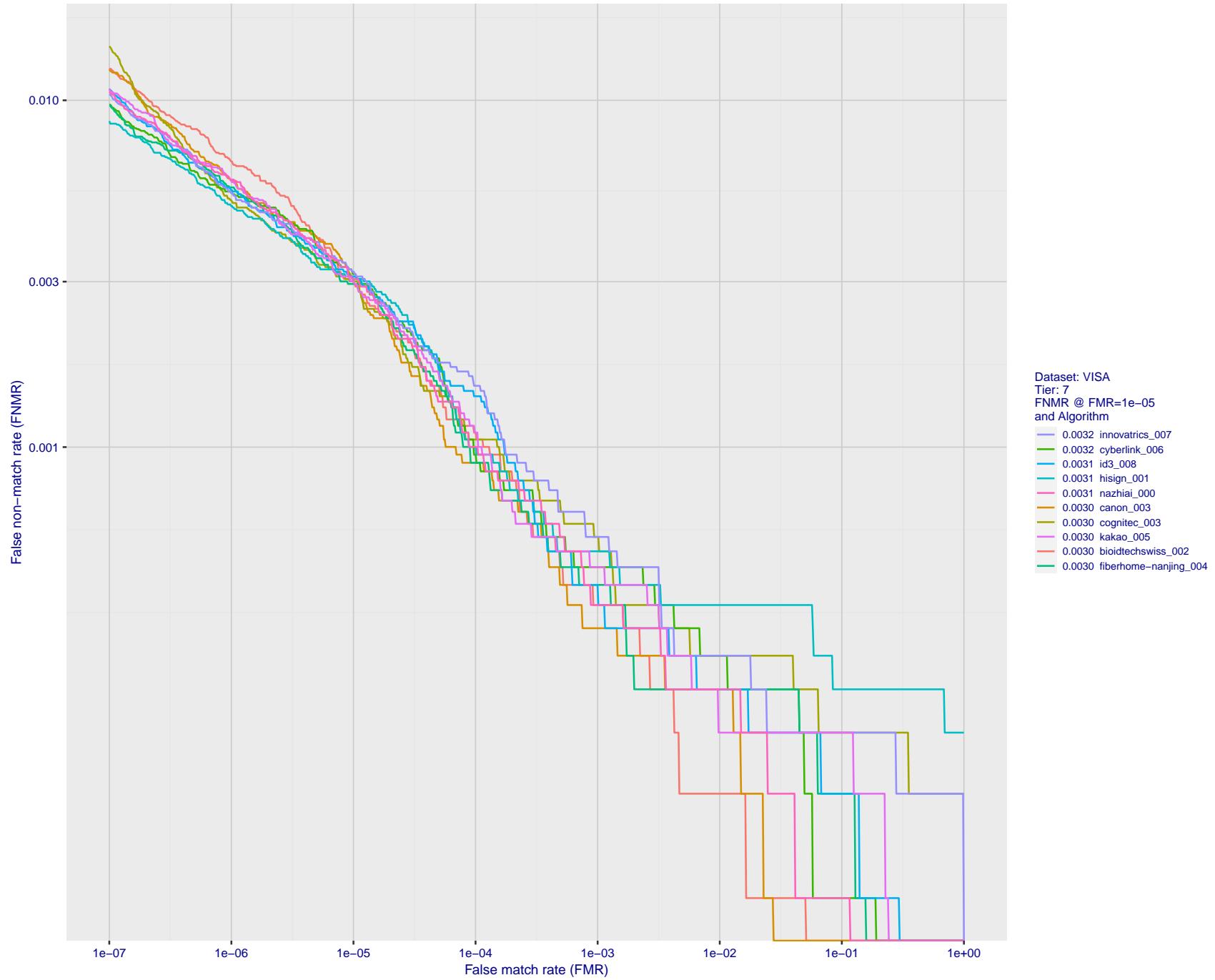


Figure 26: For the visa images, detection error tradeoff (DET) characteristics showing false non-match rate vs. false match rate plotted parametrically on threshold, T . The scales are logarithmic in order to show many decades of FMR.

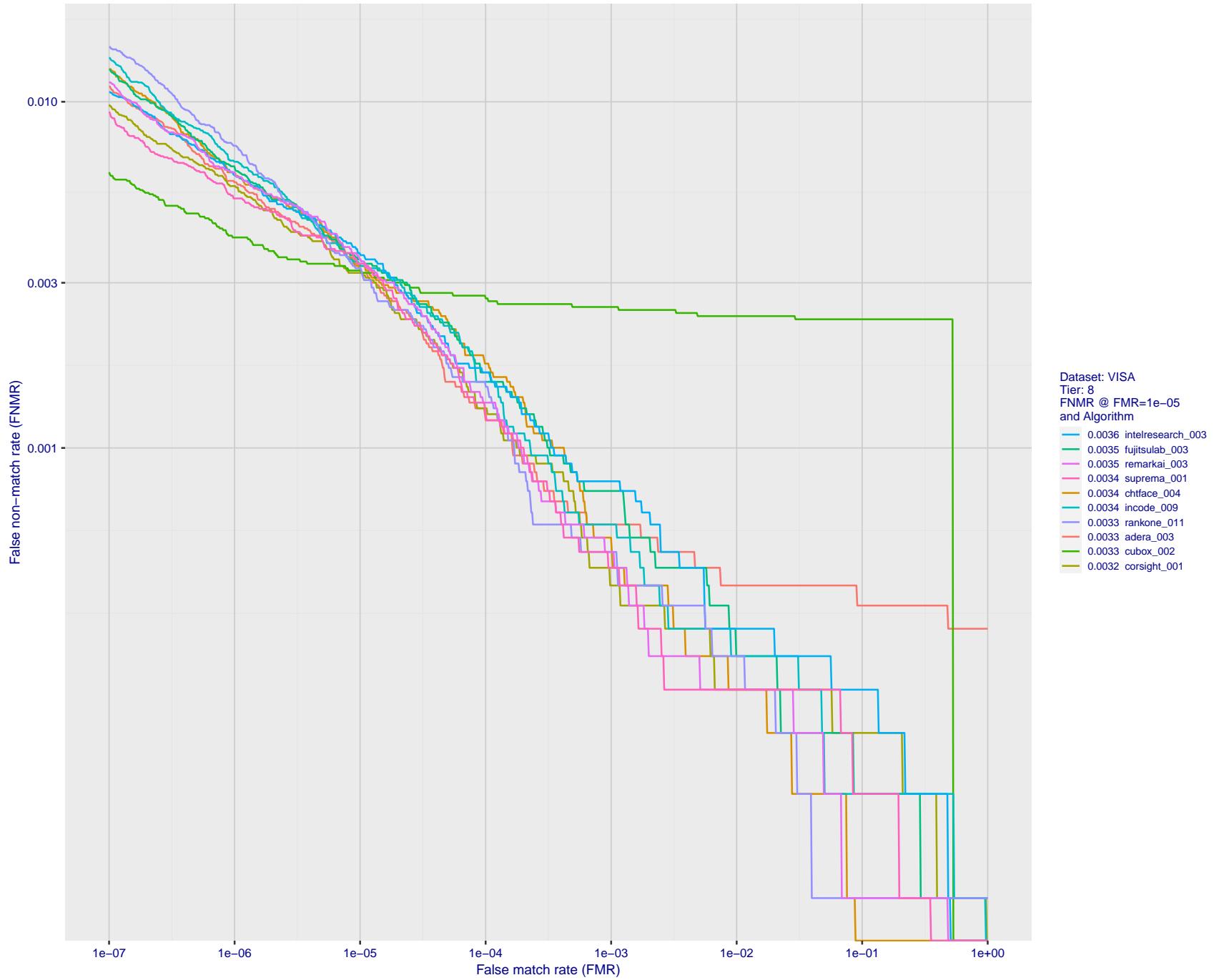


Figure 27: For the visa images, detection error tradeoff (DET) characteristics showing false non-match rate vs. false match rate plotted parametrically on threshold, T . The scales are logarithmic in order to show many decades of FMR.

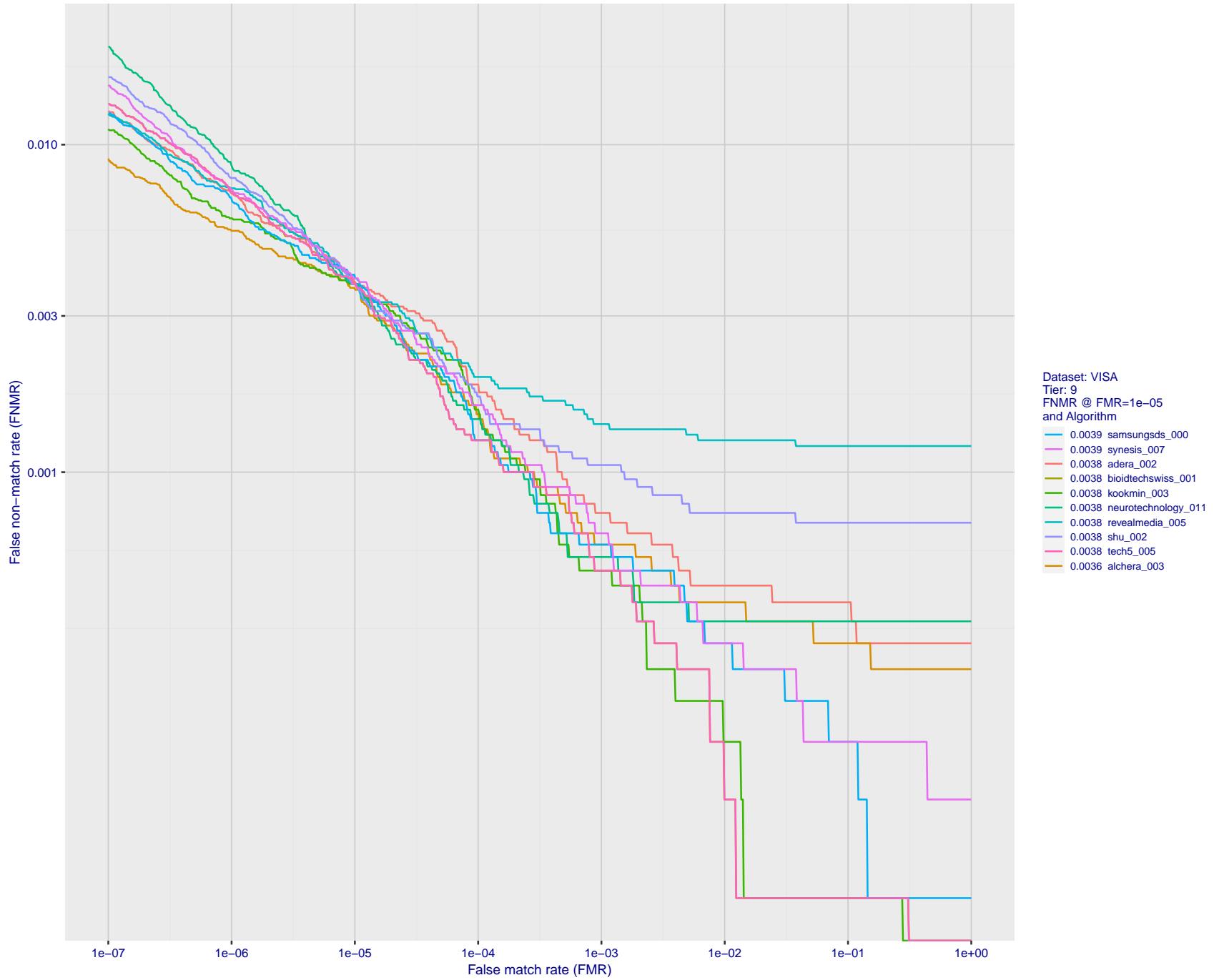


Figure 28: For the visa images, detection error tradeoff (DET) characteristics showing false non-match rate vs. false match rate plotted parametrically on threshold, T . The scales are logarithmic in order to show many decades of FMR.

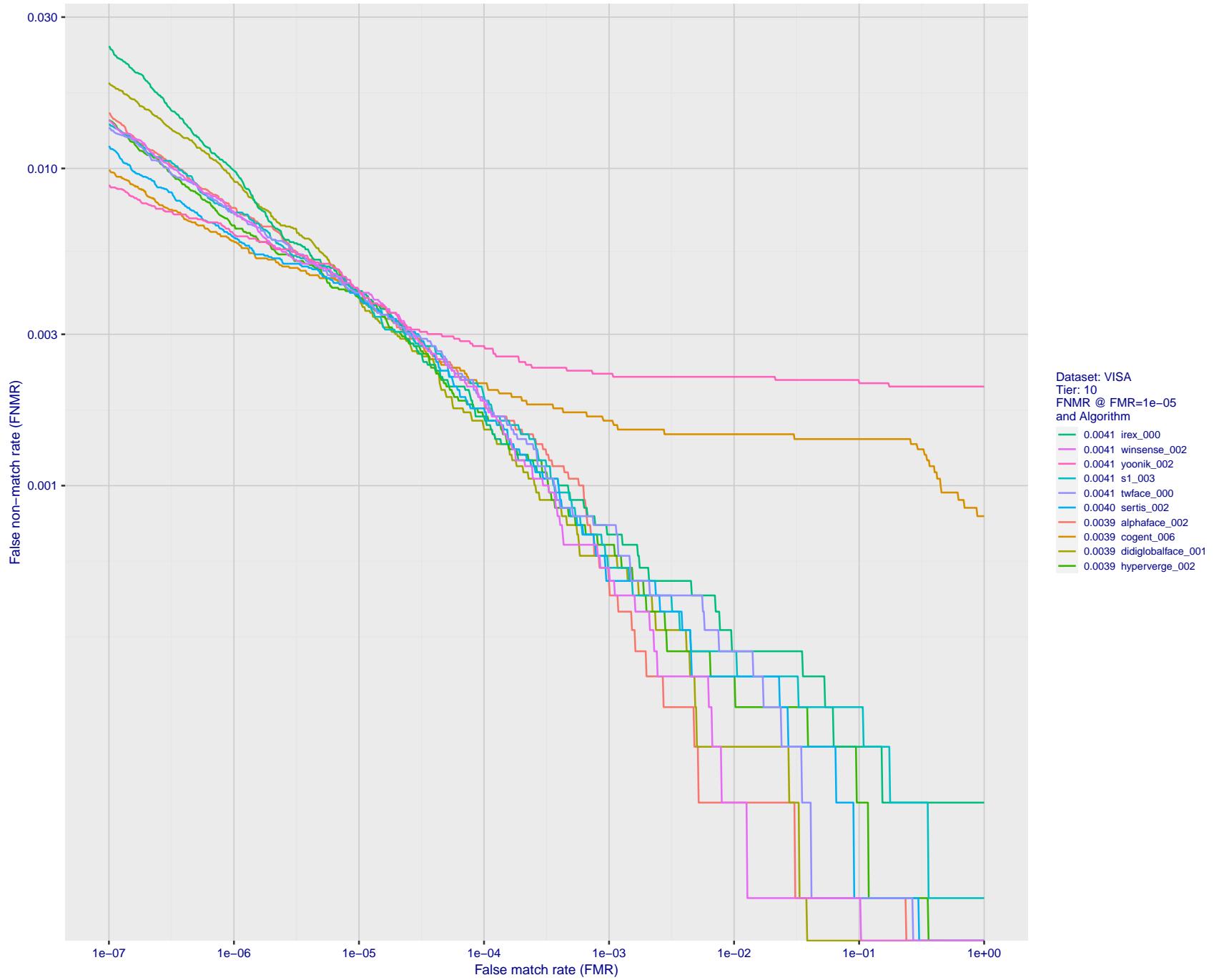


Figure 29: For the visa images, detection error tradeoff (DET) characteristics showing false non-match rate vs. false match rate plotted parametrically on threshold, T . The scales are logarithmic in order to show many decades of FMR.

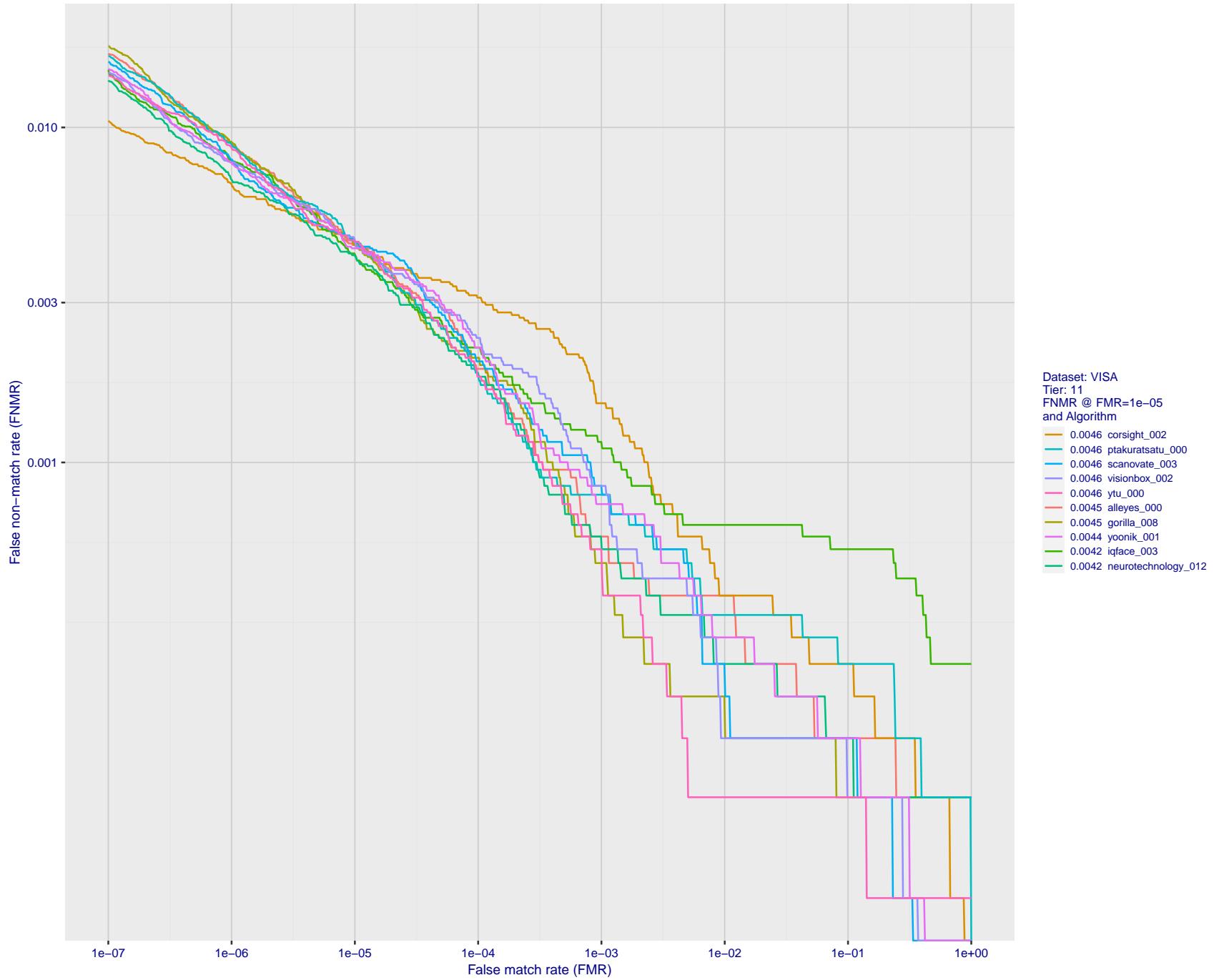


Figure 30: For the visa images, detection error tradeoff (DET) characteristics showing false non-match rate vs. false match rate plotted parametrically on threshold, T . The scales are logarithmic in order to show many decades of FMR.

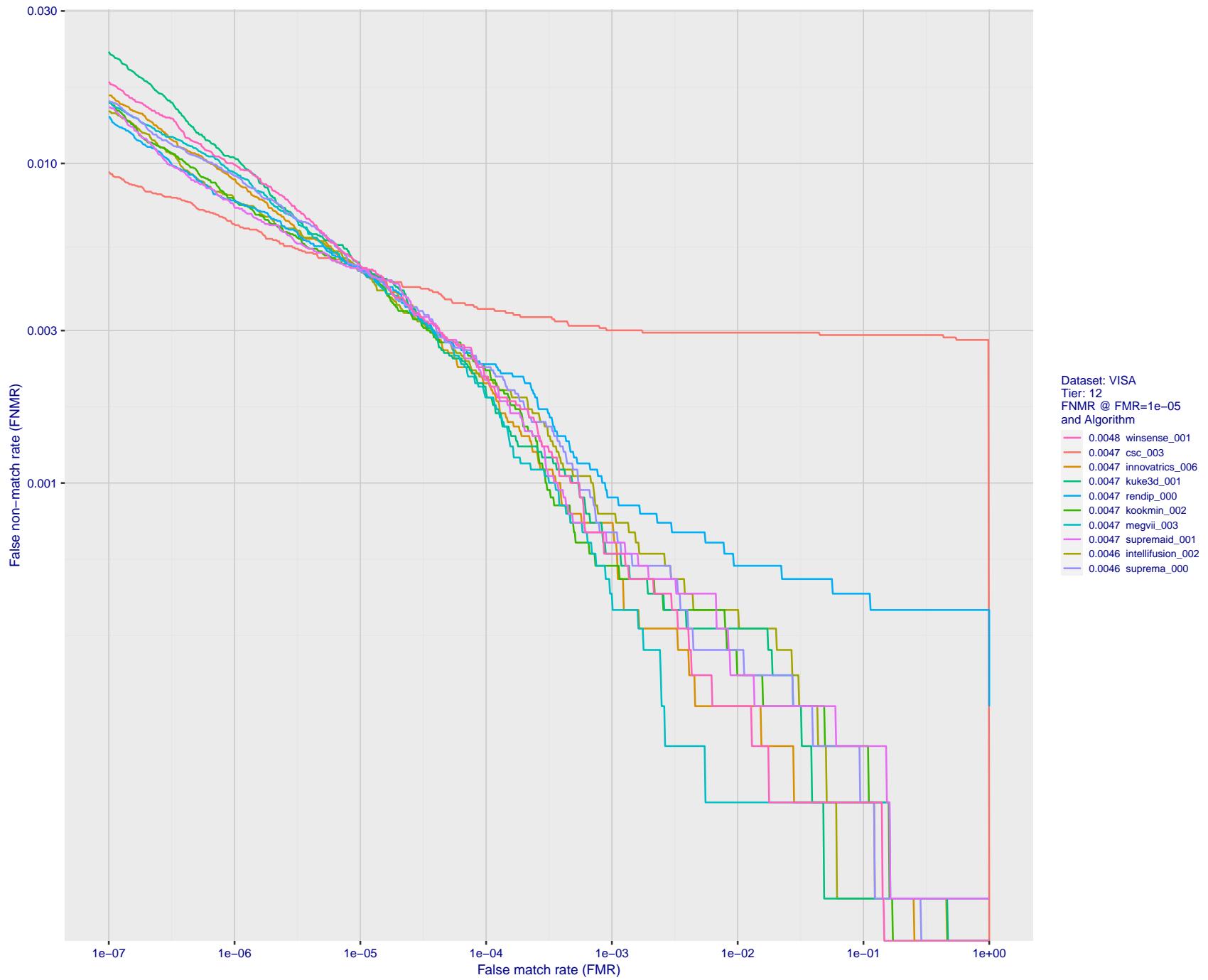


Figure 31: For the visa images, detection error tradeoff (DET) characteristics showing false non-match rate vs. false match rate plotted parametrically on threshold, T . The scales are logarithmic in order to show many decades of FMR.

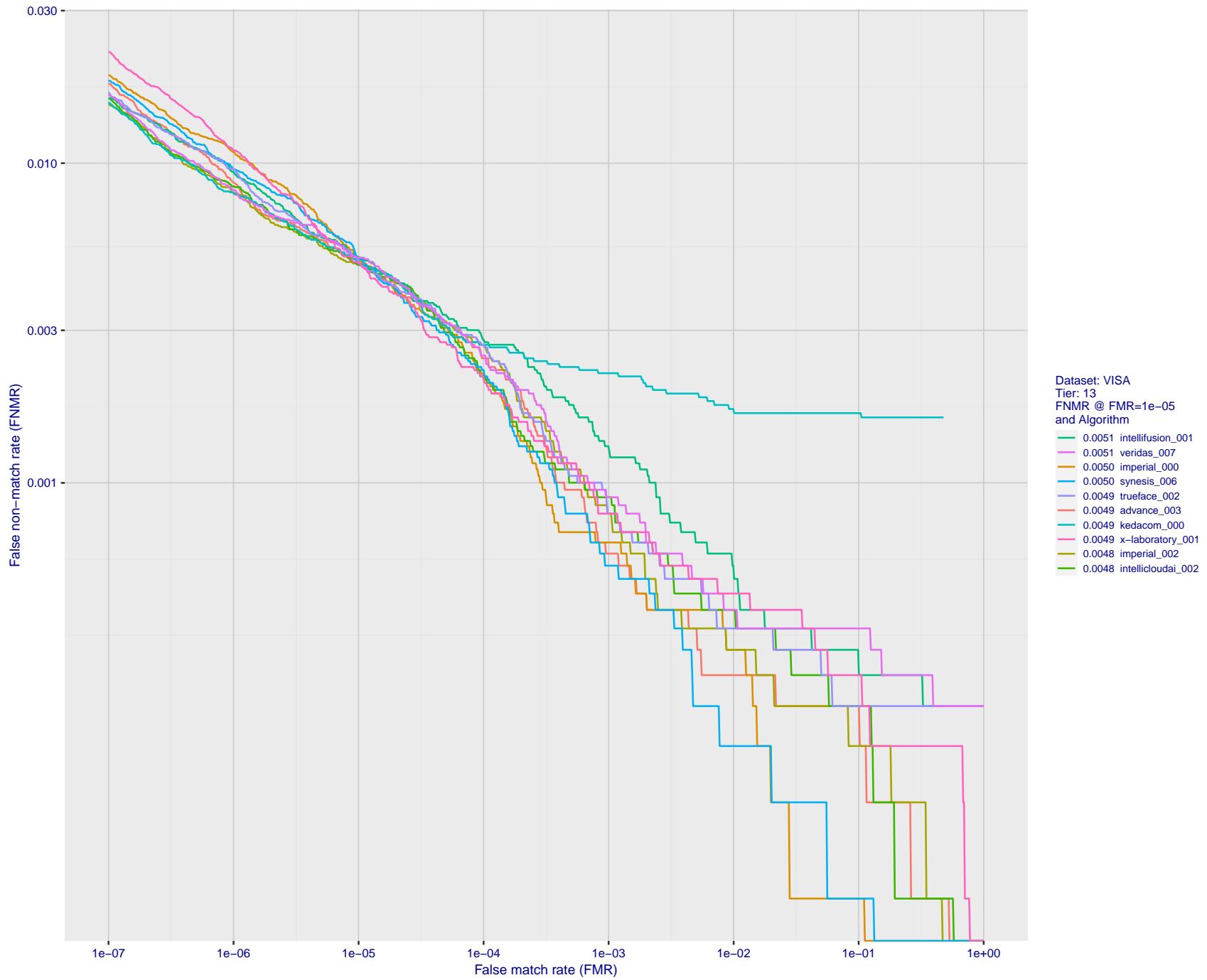


Figure 32: For the visa images, detection error tradeoff (DET) characteristics showing false non-match rate vs. false match rate plotted parametrically on threshold, T . The scales are logarithmic in order to show many decades of FMR.

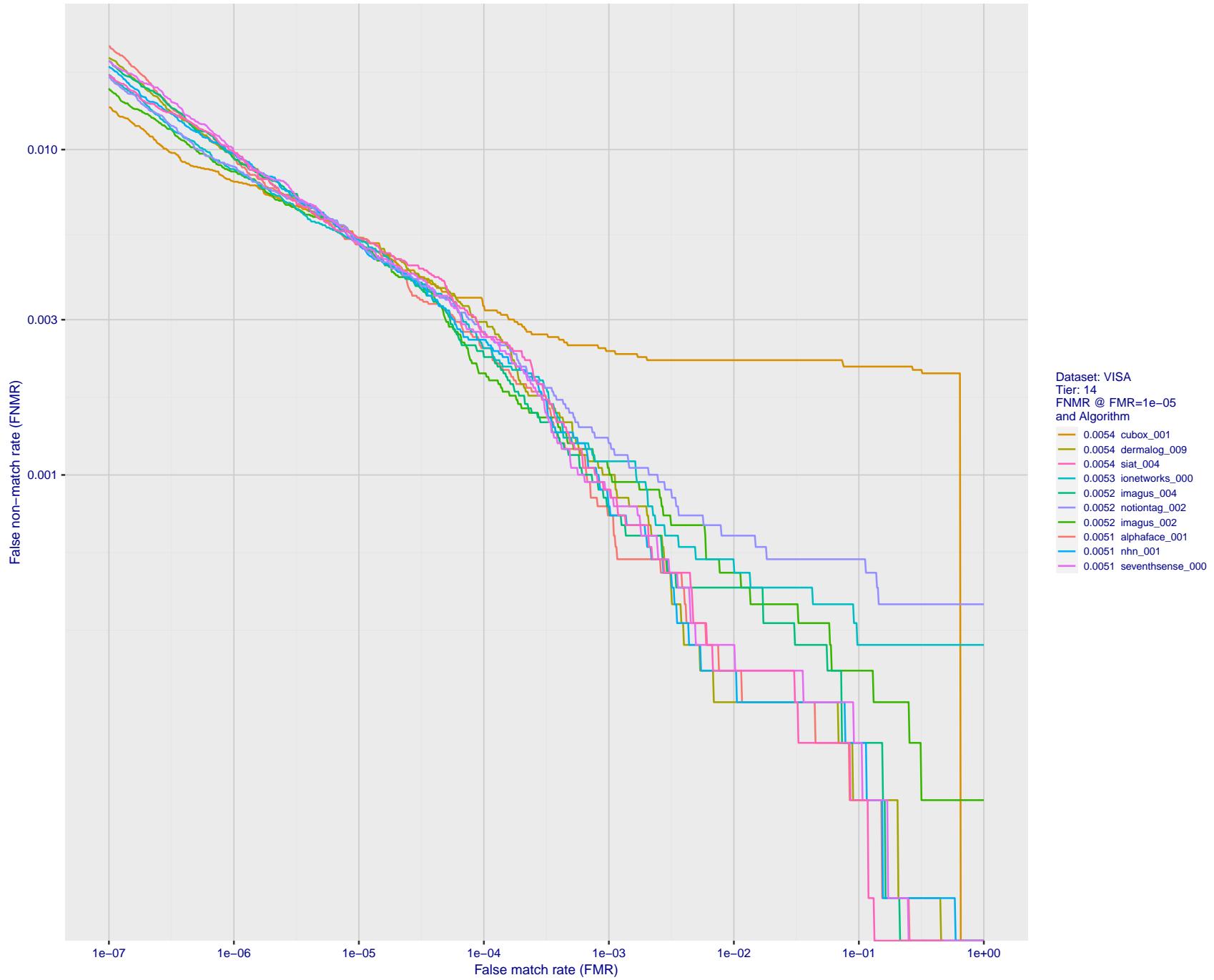


Figure 33: For the visa images, detection error tradeoff (DET) characteristics showing false non-match rate vs. false match rate plotted parametrically on threshold, T . The scales are logarithmic in order to show many decades of FMR.

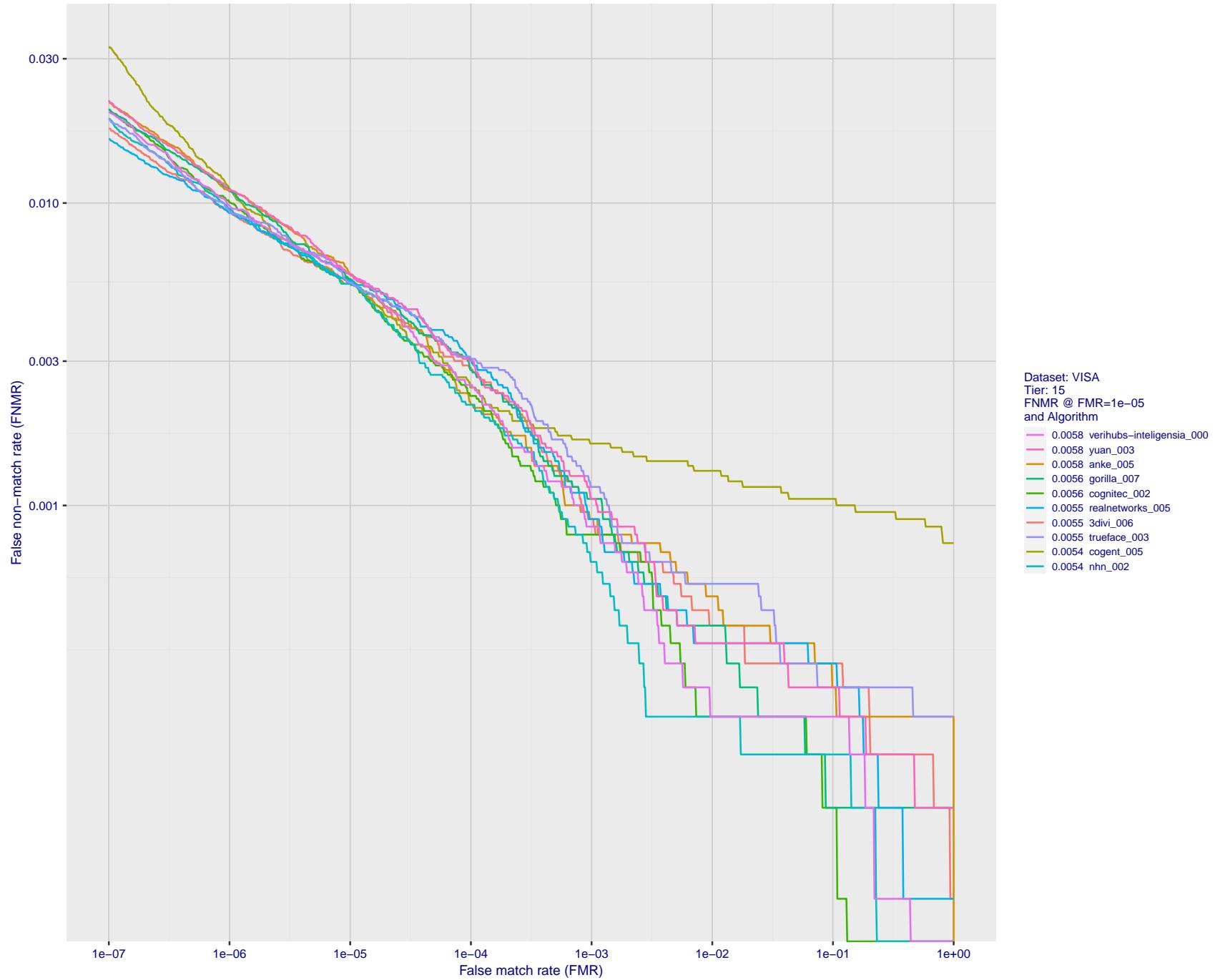


Figure 34: For the visa images, detection error tradeoff (DET) characteristics showing false non-match rate vs. false match rate plotted parametrically on threshold, T . The scales are logarithmic in order to show many decades of FMR.

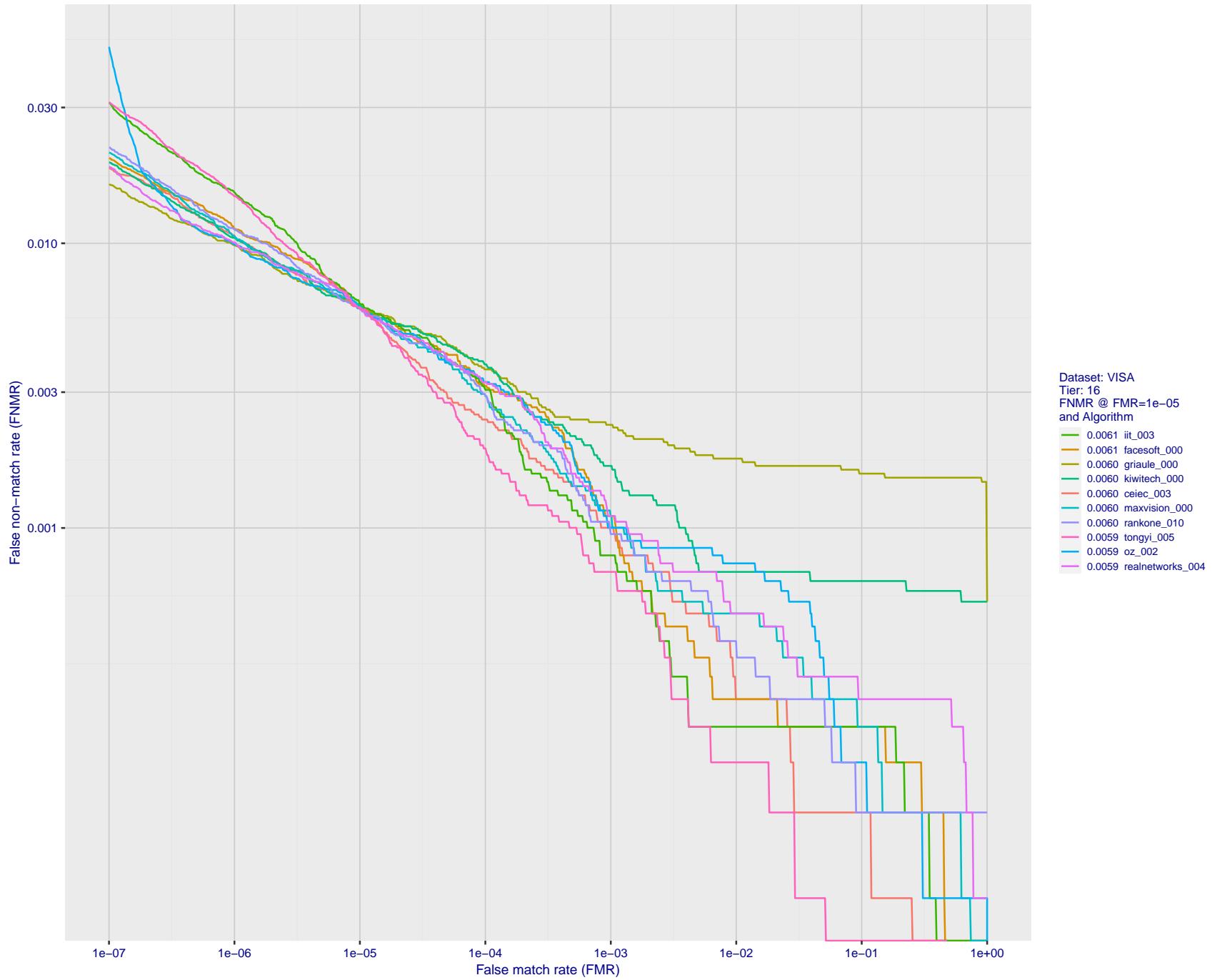


Figure 35: For the visa images, detection error tradeoff (DET) characteristics showing false non-match rate vs. false match rate plotted parametrically on threshold, T . The scales are logarithmic in order to show many decades of FMR.

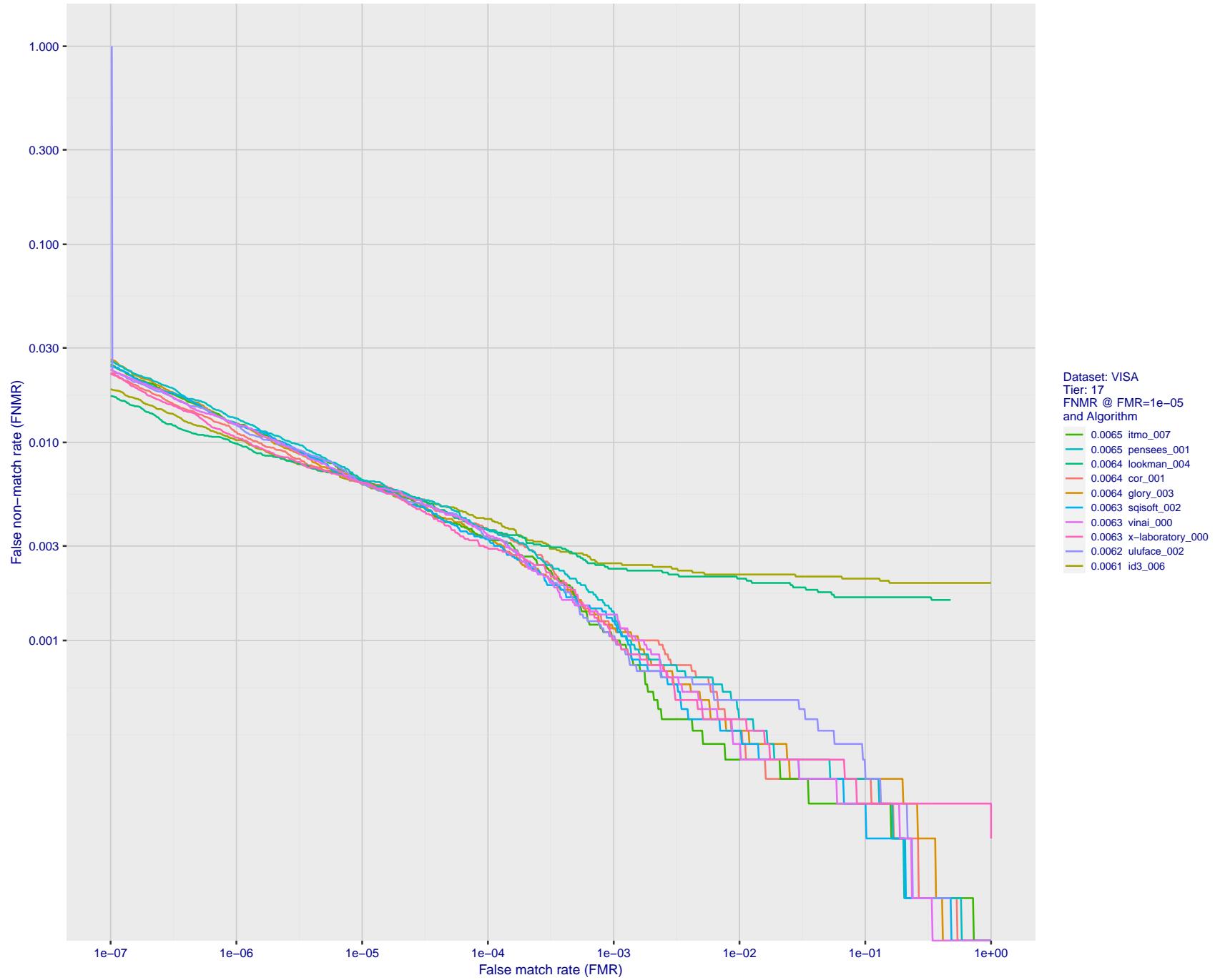


Figure 36: For the visa images, detection error tradeoff (DET) characteristics showing false non-match rate vs. false match rate plotted parametrically on threshold, T . The scales are logarithmic in order to show many decades of FMR.

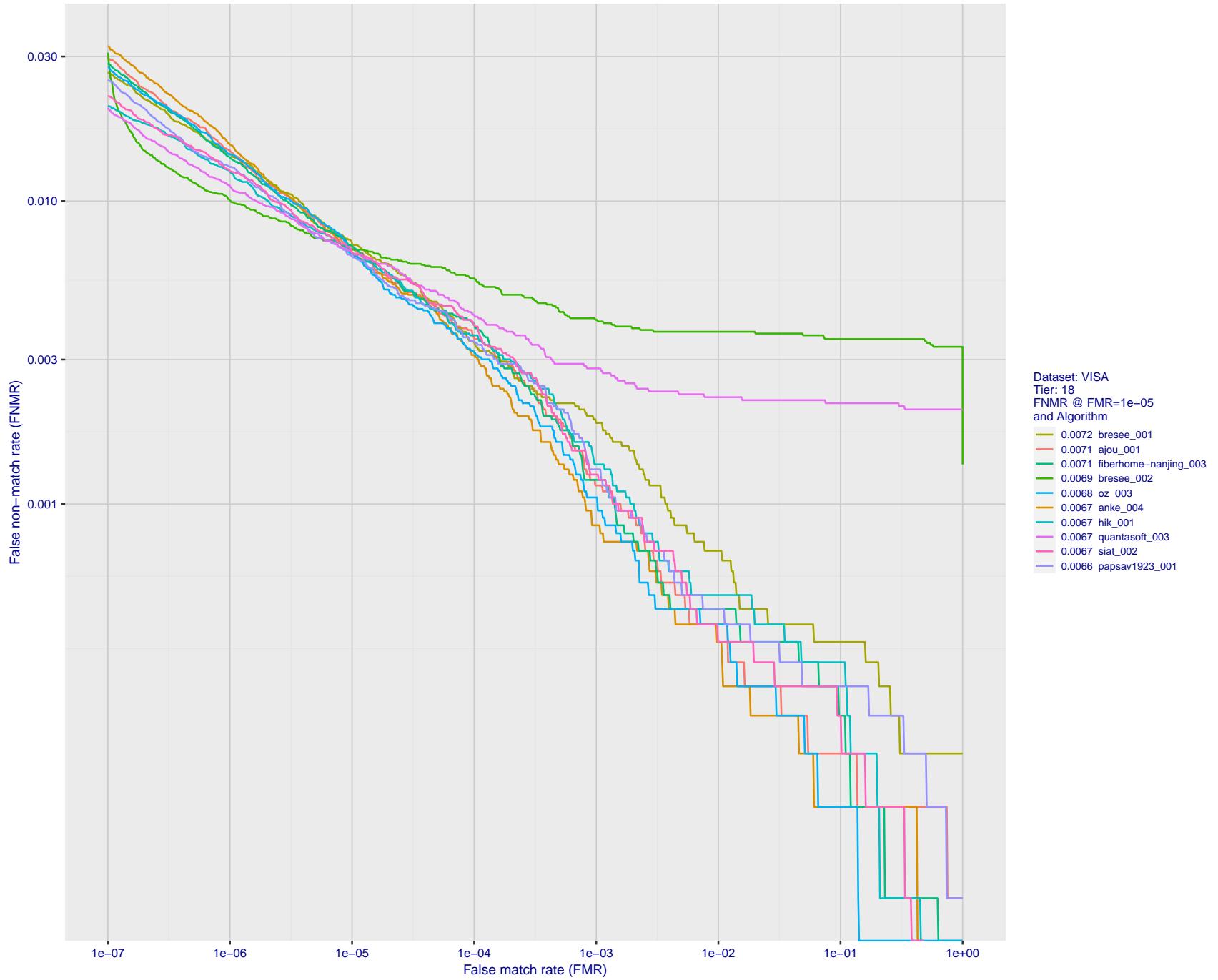


Figure 37: For the visa images, detection error tradeoff (DET) characteristics showing false non-match rate vs. false match rate plotted parametrically on threshold, T . The scales are logarithmic in order to show many decades of FMR.

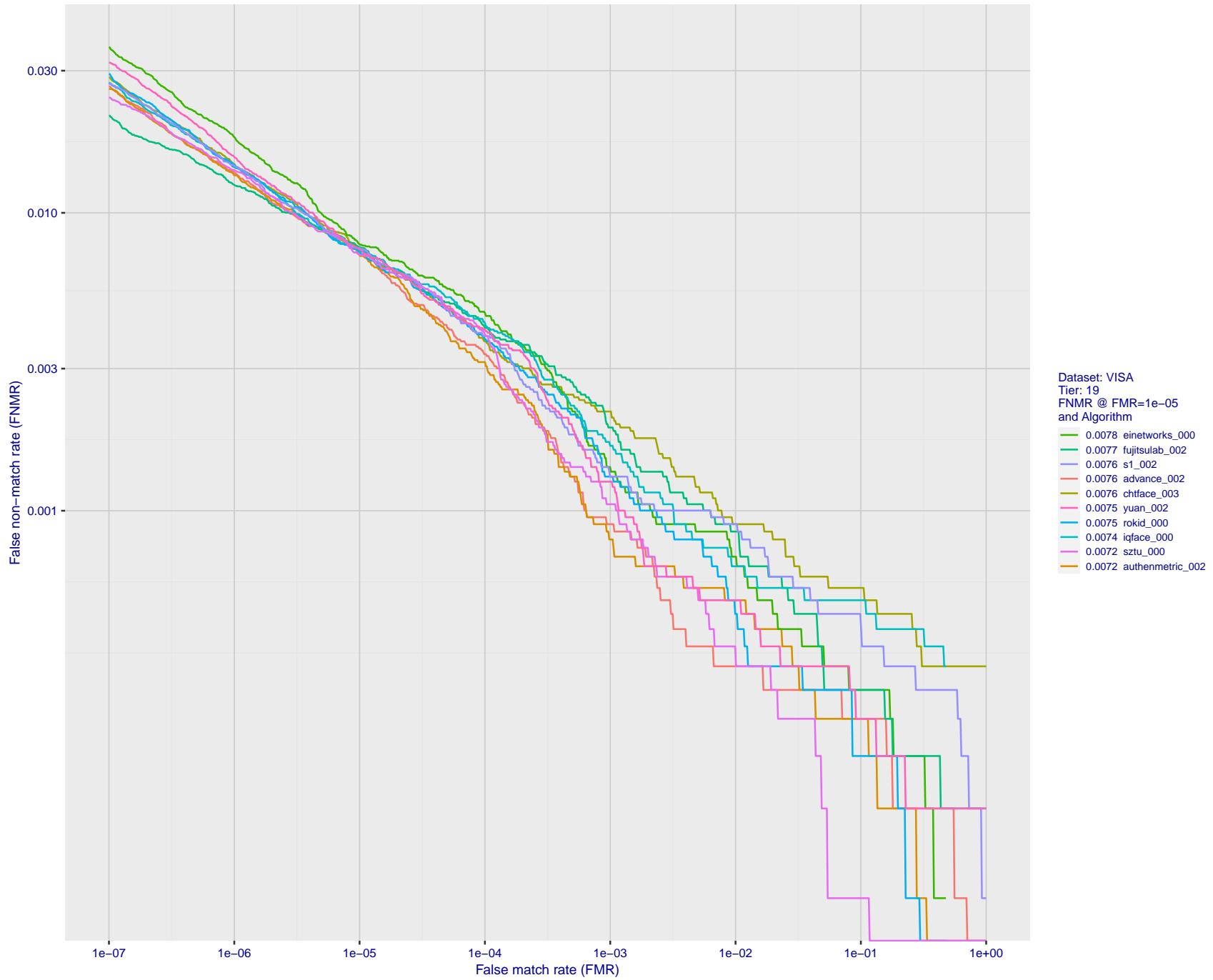


Figure 38: For the visa images, detection error tradeoff (DET) characteristics showing false non-match rate vs. false match rate plotted parametrically on threshold, T . The scales are logarithmic in order to show many decades of FMR.

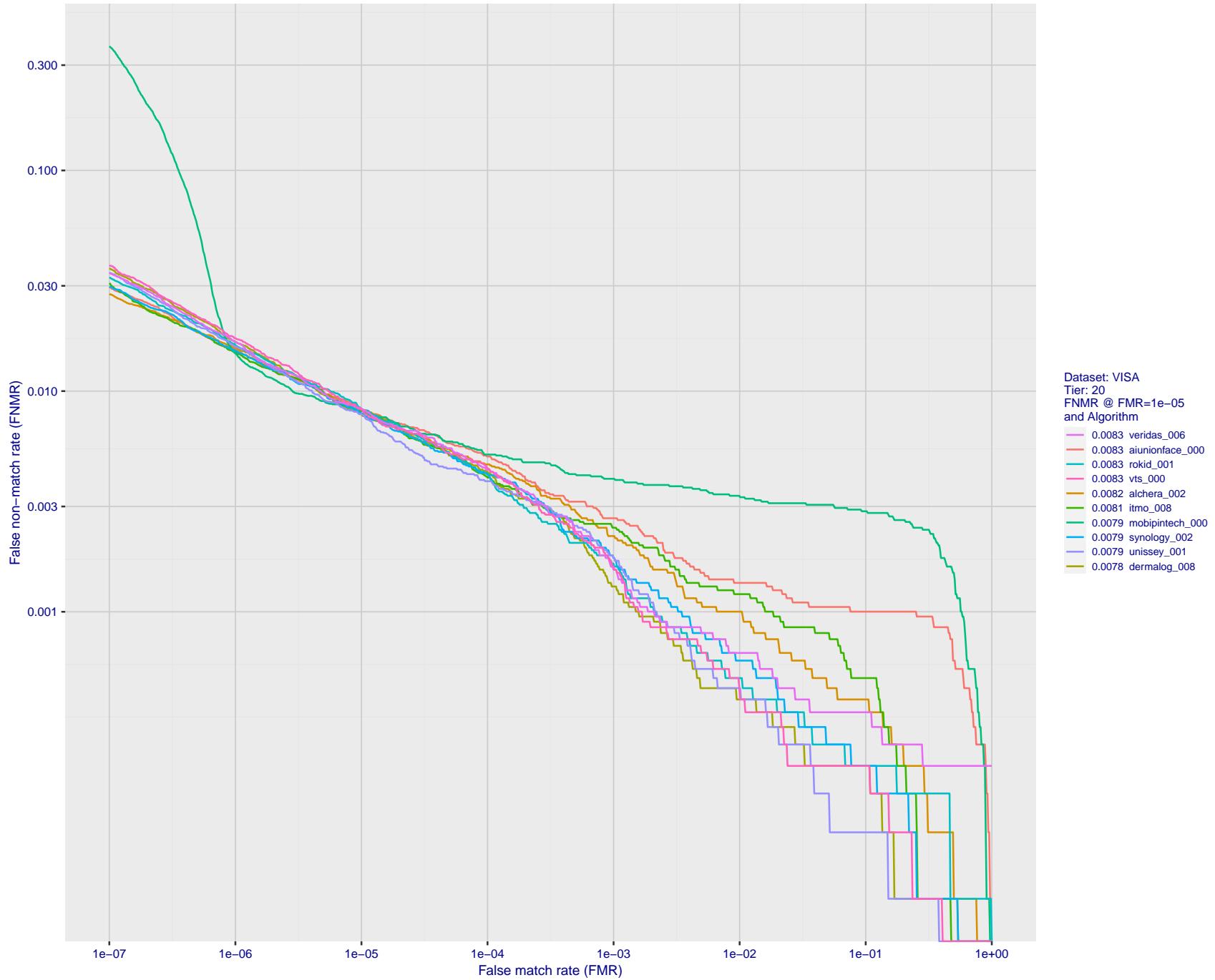


Figure 39: For the visa images, detection error tradeoff (DET) characteristics showing false non-match rate vs. false match rate plotted parametrically on threshold, T . The scales are logarithmic in order to show many decades of FMR.

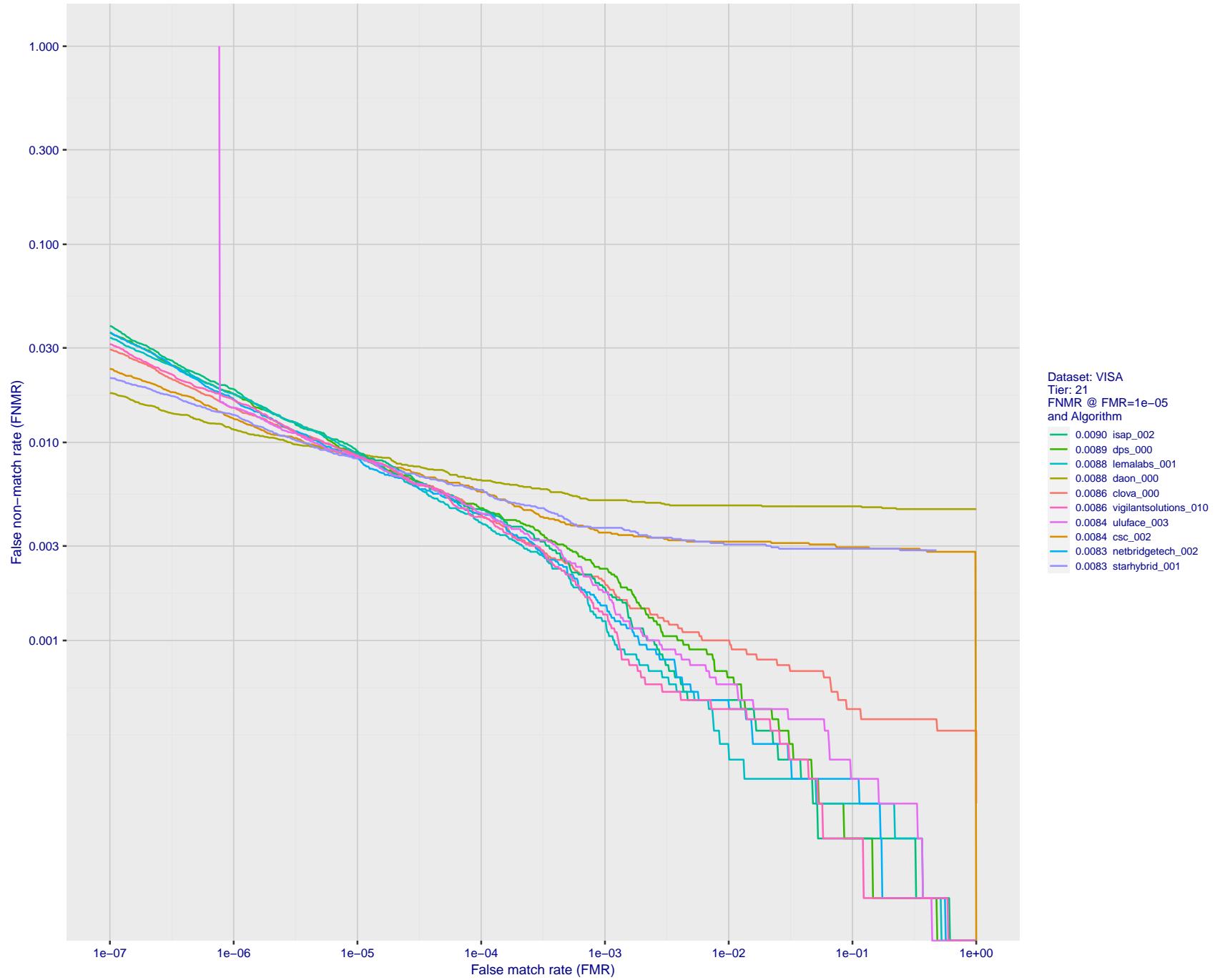


Figure 40: For the visa images, detection error tradeoff (DET) characteristics showing false non-match rate vs. false match rate plotted parametrically on threshold, T . The scales are logarithmic in order to show many decades of FMR.

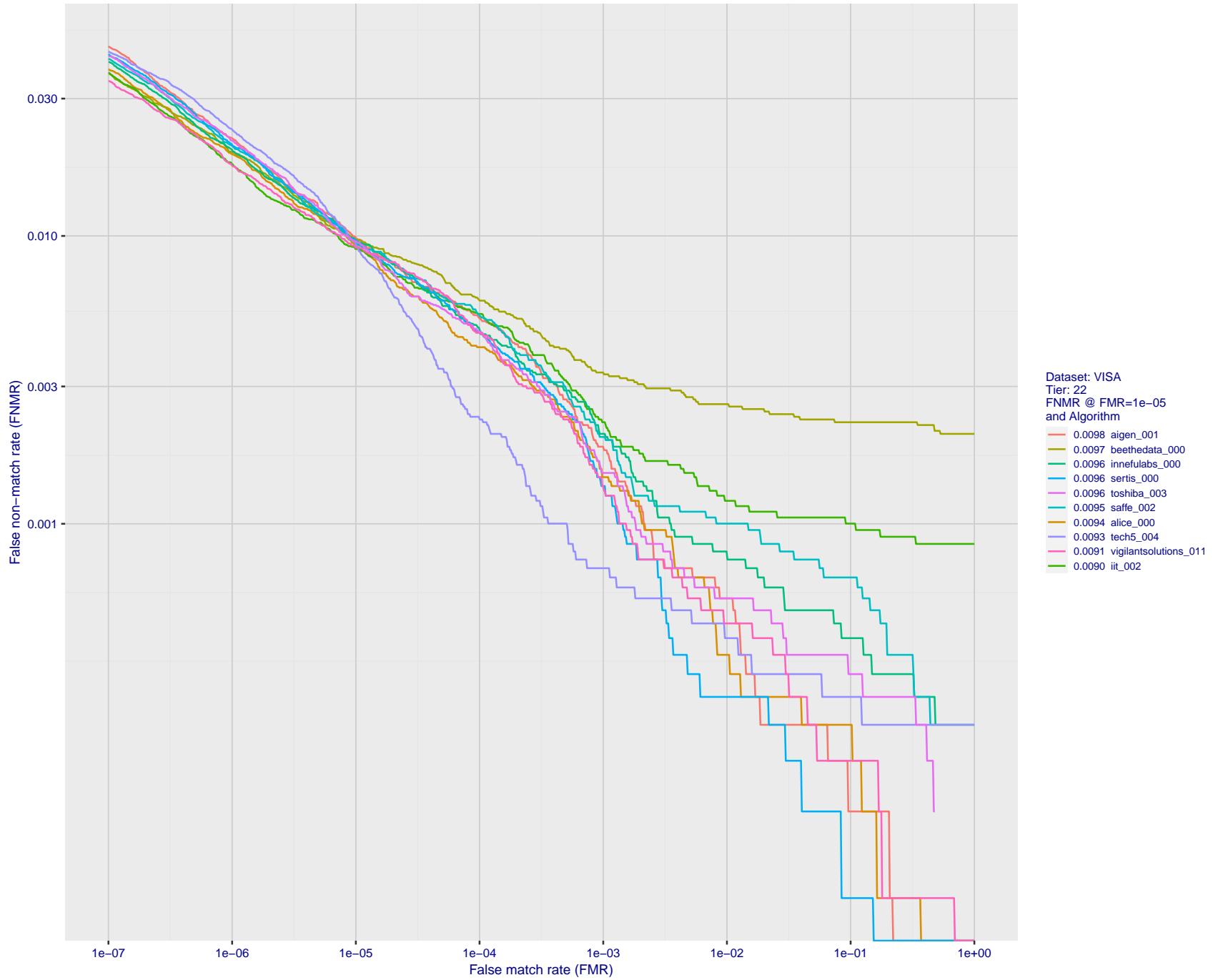


Figure 41: For the visa images, detection error tradeoff (DET) characteristics showing false non-match rate vs. false match rate plotted parametrically on threshold, T . The scales are logarithmic in order to show many decades of FMR.

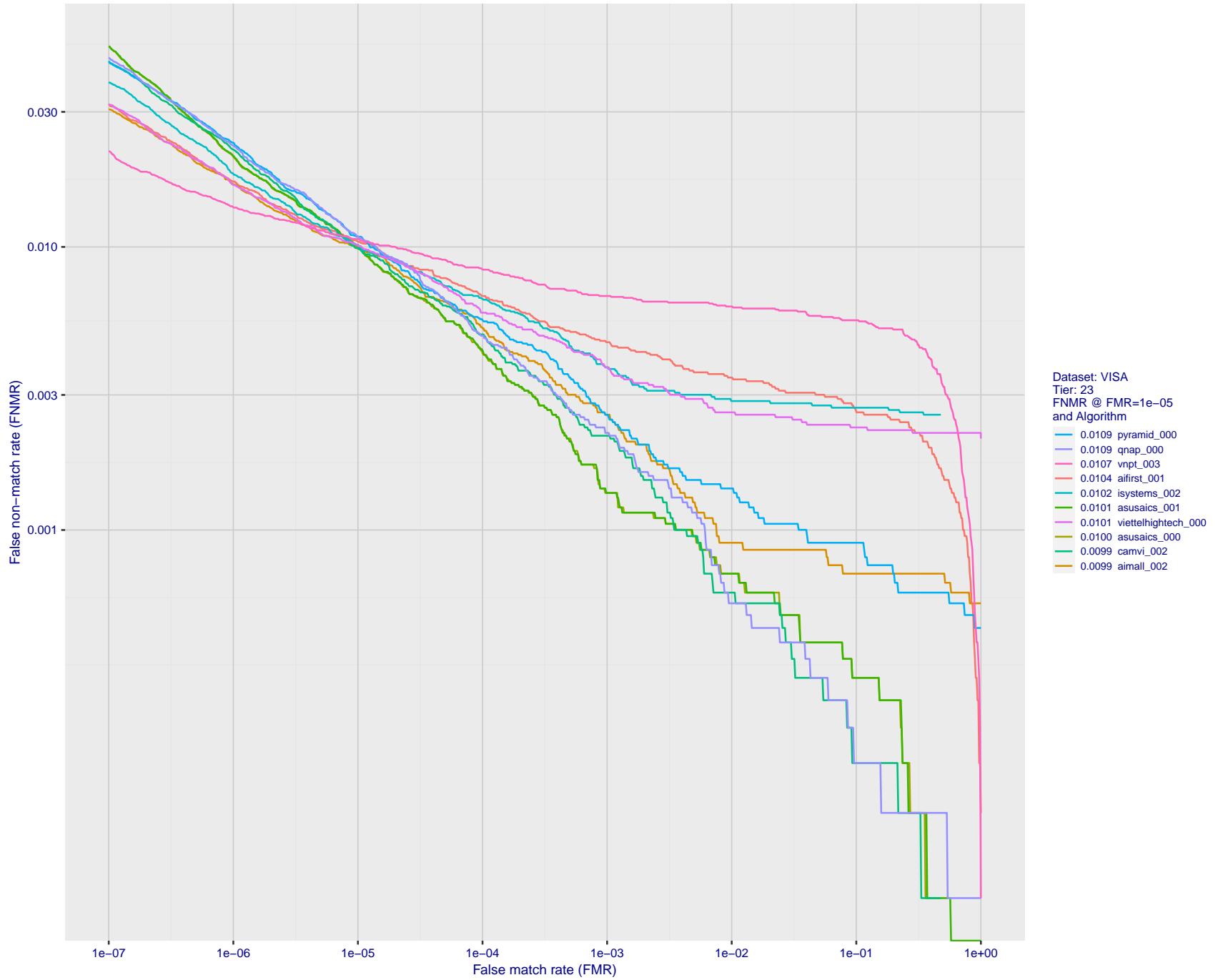


Figure 42: For the visa images, detection error tradeoff (DET) characteristics showing false non-match rate vs. false match rate plotted parametrically on threshold, T . The scales are logarithmic in order to show many decades of FMR.

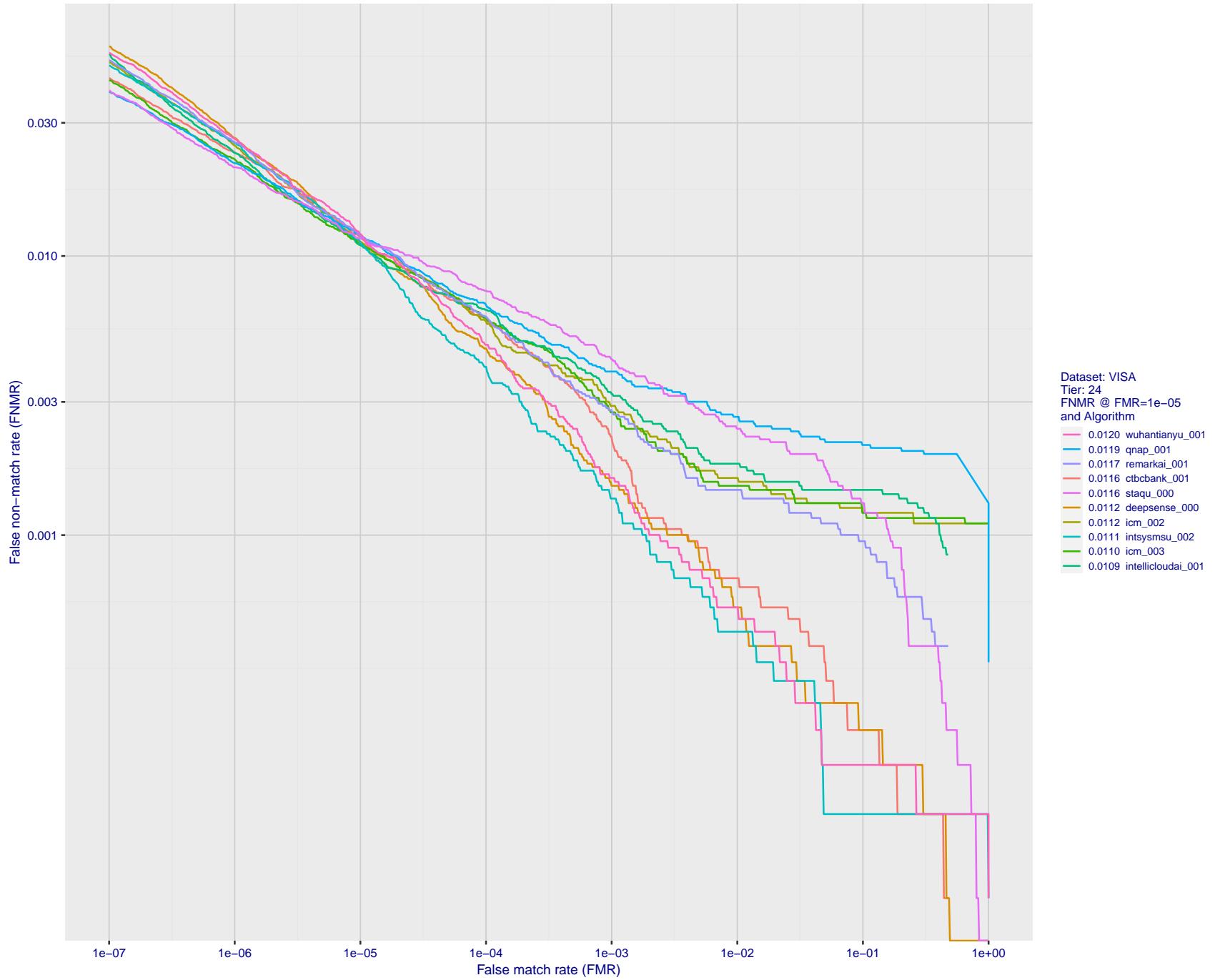


Figure 43: For the visa images, detection error tradeoff (DET) characteristics showing false non-match rate vs. false match rate plotted parametrically on threshold, T . The scales are logarithmic in order to show many decades of FMR.

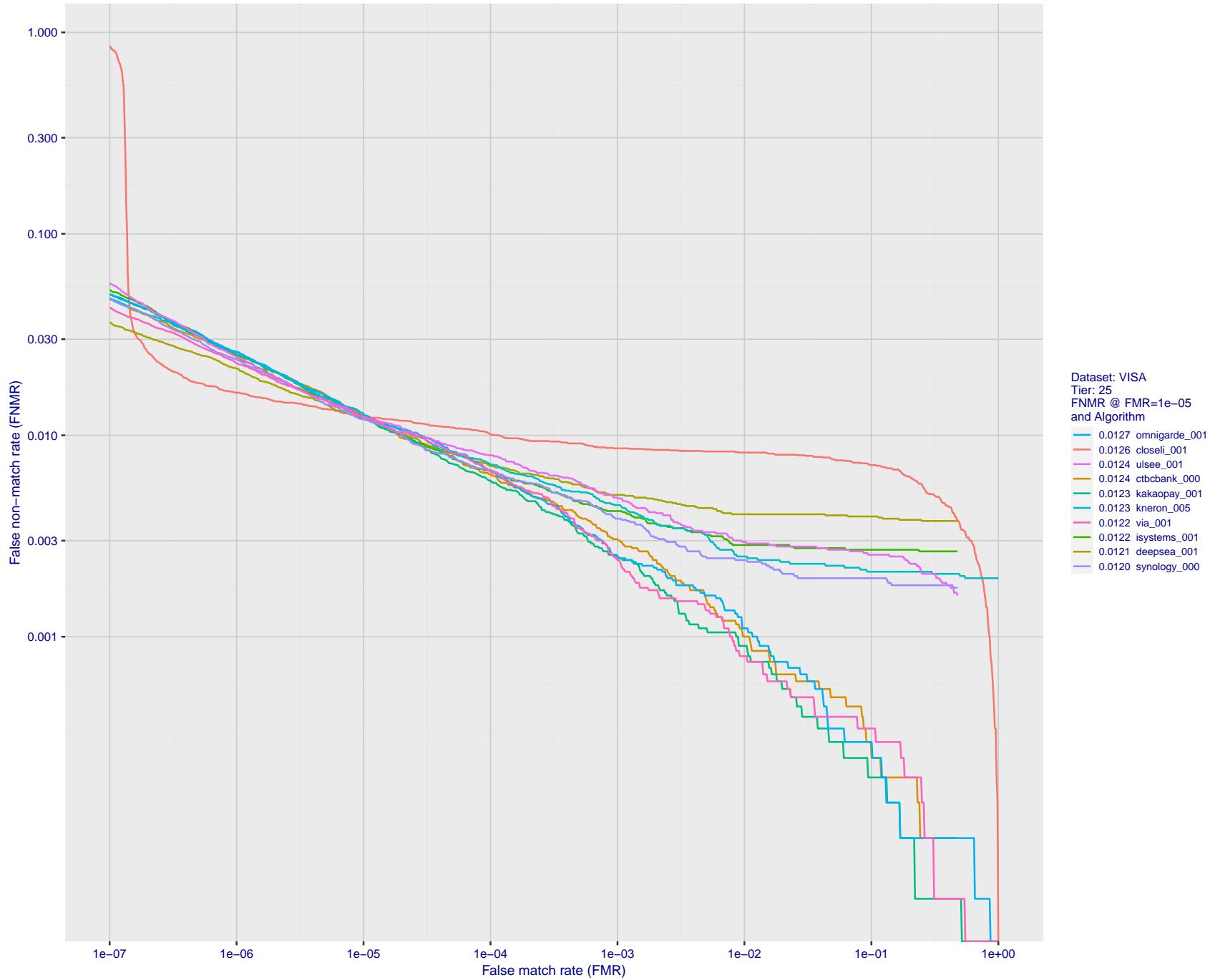


Figure 44: For the visa images, detection error tradeoff (DET) characteristics showing false non-match rate vs. false match rate plotted parametrically on threshold, T . The scales are logarithmic in order to show many decades of FMR.

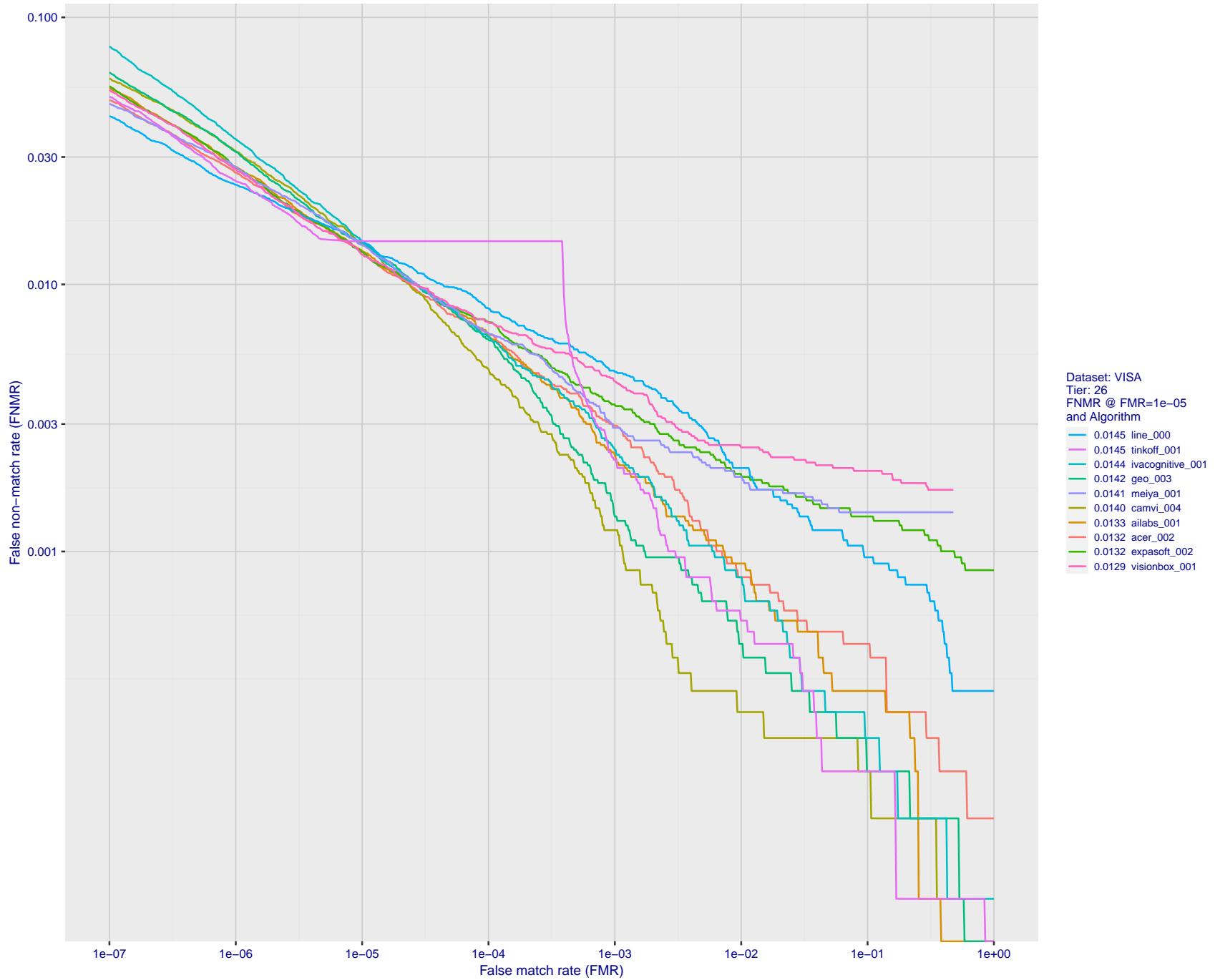


Figure 45: For the visa images, detection error tradeoff (DET) characteristics showing false non-match rate vs. false match rate plotted parametrically on threshold, T . The scales are logarithmic in order to show many decades of FMR.

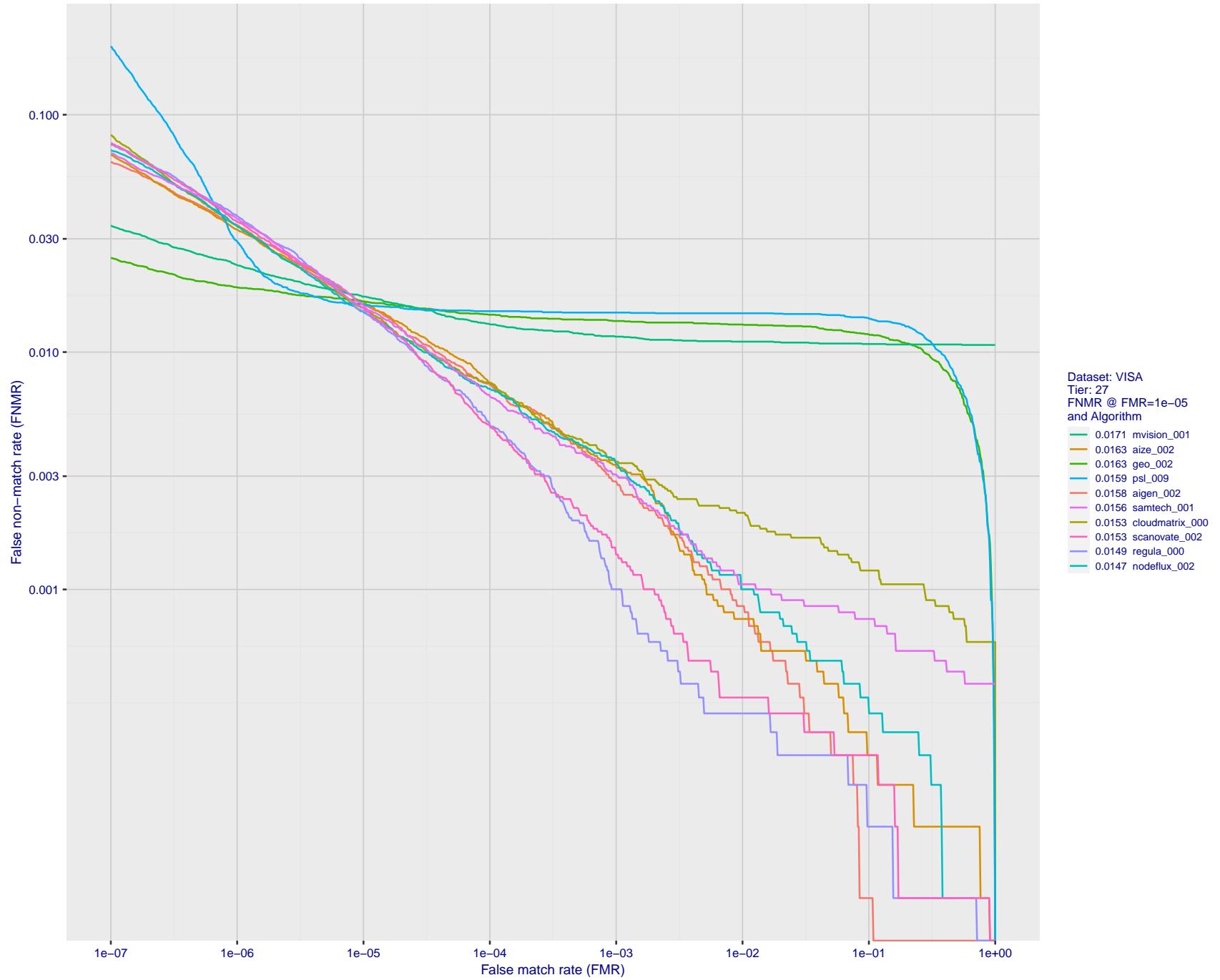


Figure 46: For the visa images, detection error tradeoff (DET) characteristics showing false non-match rate vs. false match rate plotted parametrically on threshold, T . The scales are logarithmic in order to show many decades of FMR.

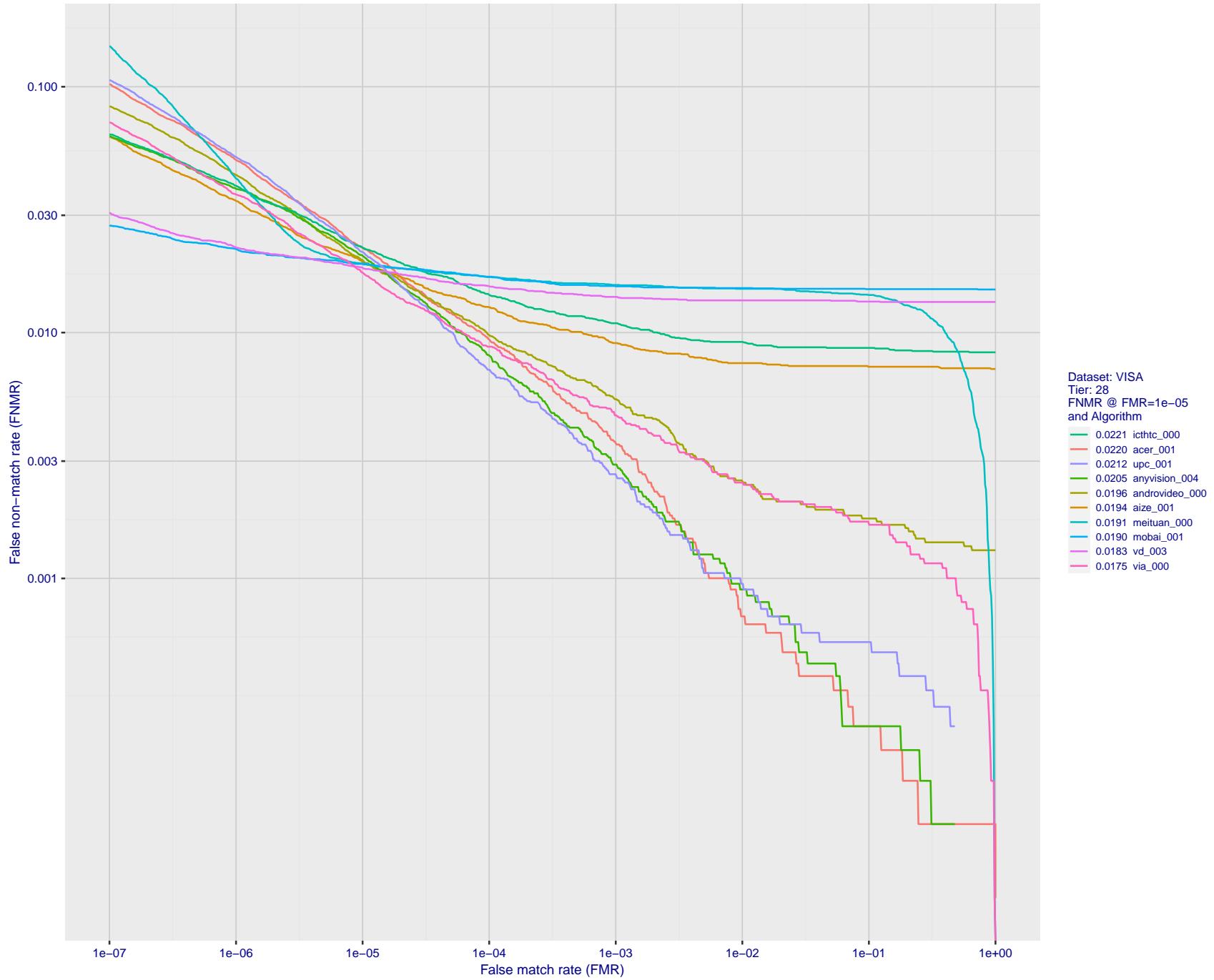


Figure 47: For the visa images, detection error tradeoff (DET) characteristics showing false non-match rate vs. false match rate plotted parametrically on threshold, T . The scales are logarithmic in order to show many decades of FMR.

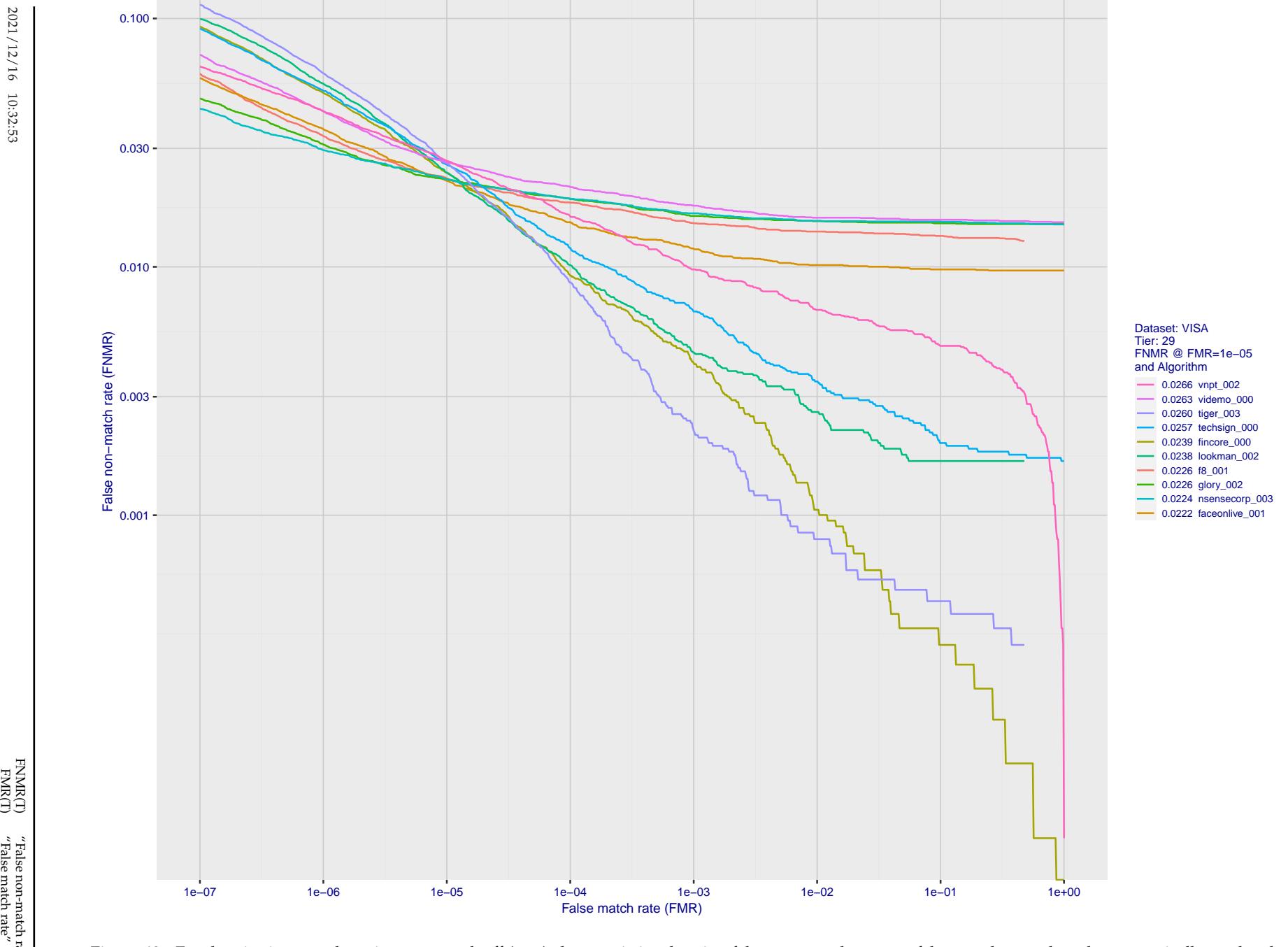


Figure 48: For the visa images, detection error tradeoff (DET) characteristics showing false non-match rate vs. false match rate plotted parametrically on threshold, T . The scales are logarithmic in order to show many decades of FMR.

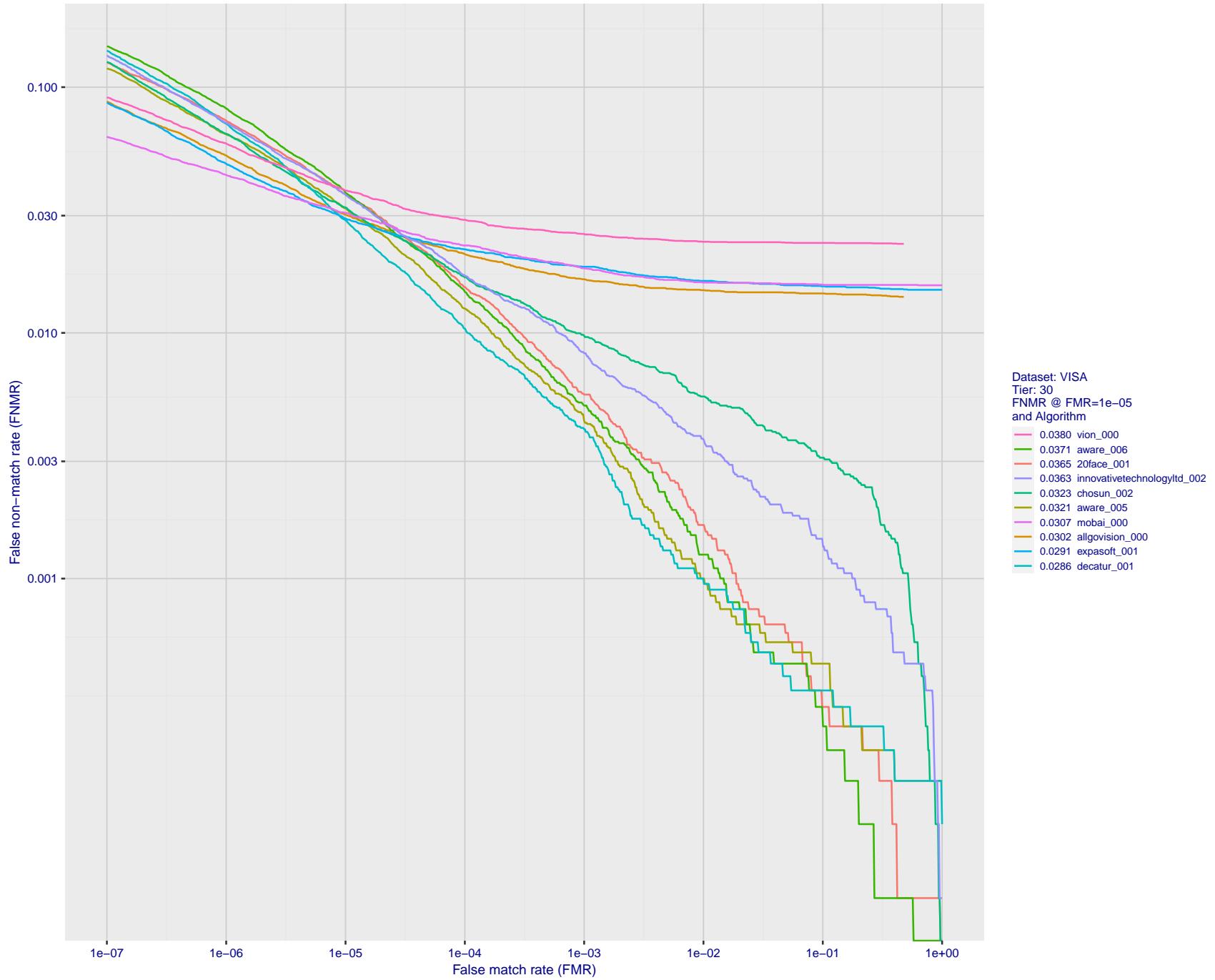


Figure 49: For the visa images, detection error tradeoff (DET) characteristics showing false non-match rate vs. false match rate plotted parametrically on threshold, T . The scales are logarithmic in order to show many decades of FMR.

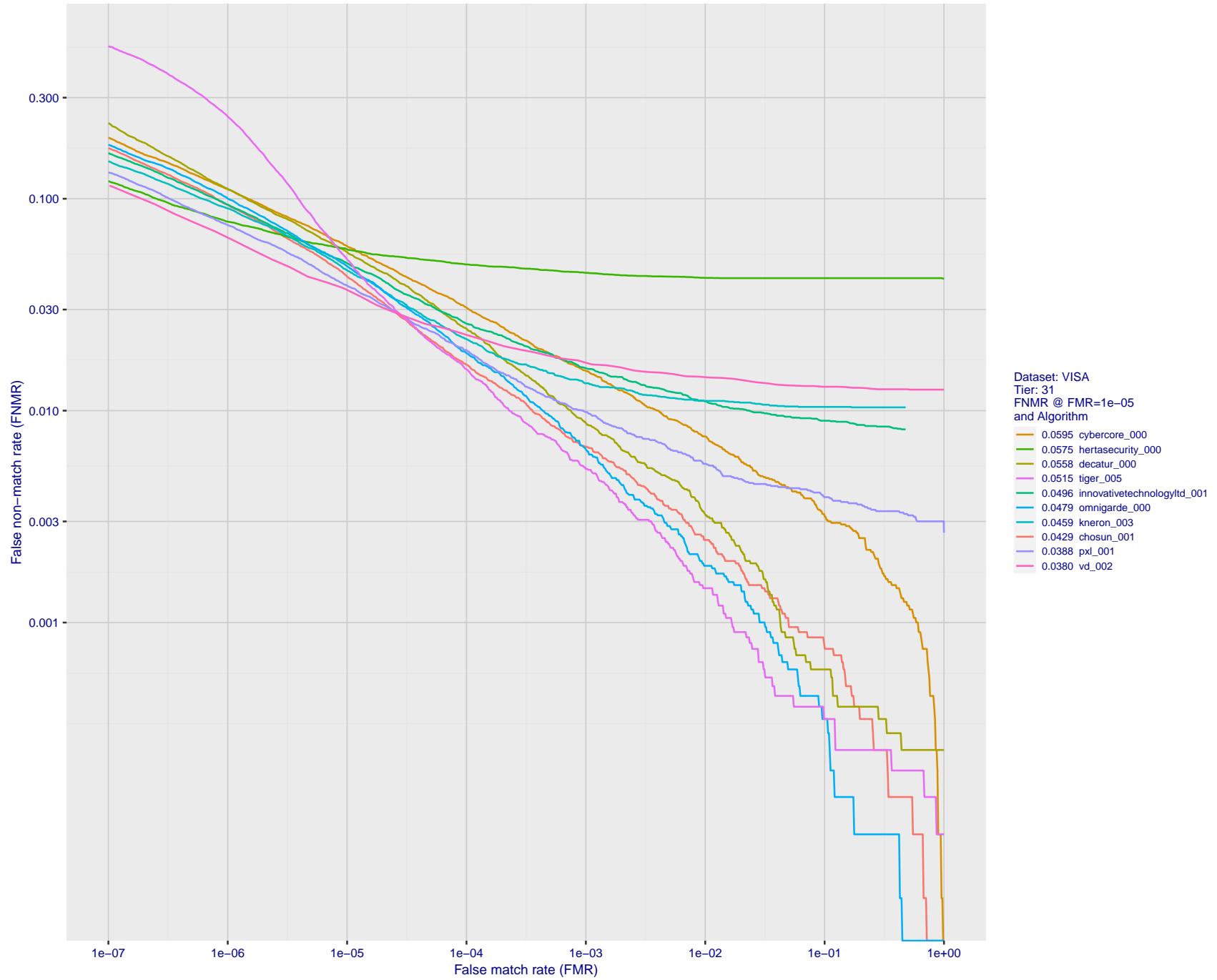


Figure 50: For the visa images, detection error tradeoff (DET) characteristics showing false non-match rate vs. false match rate plotted parametrically on threshold, T . The scales are logarithmic in order to show many decades of FMR.

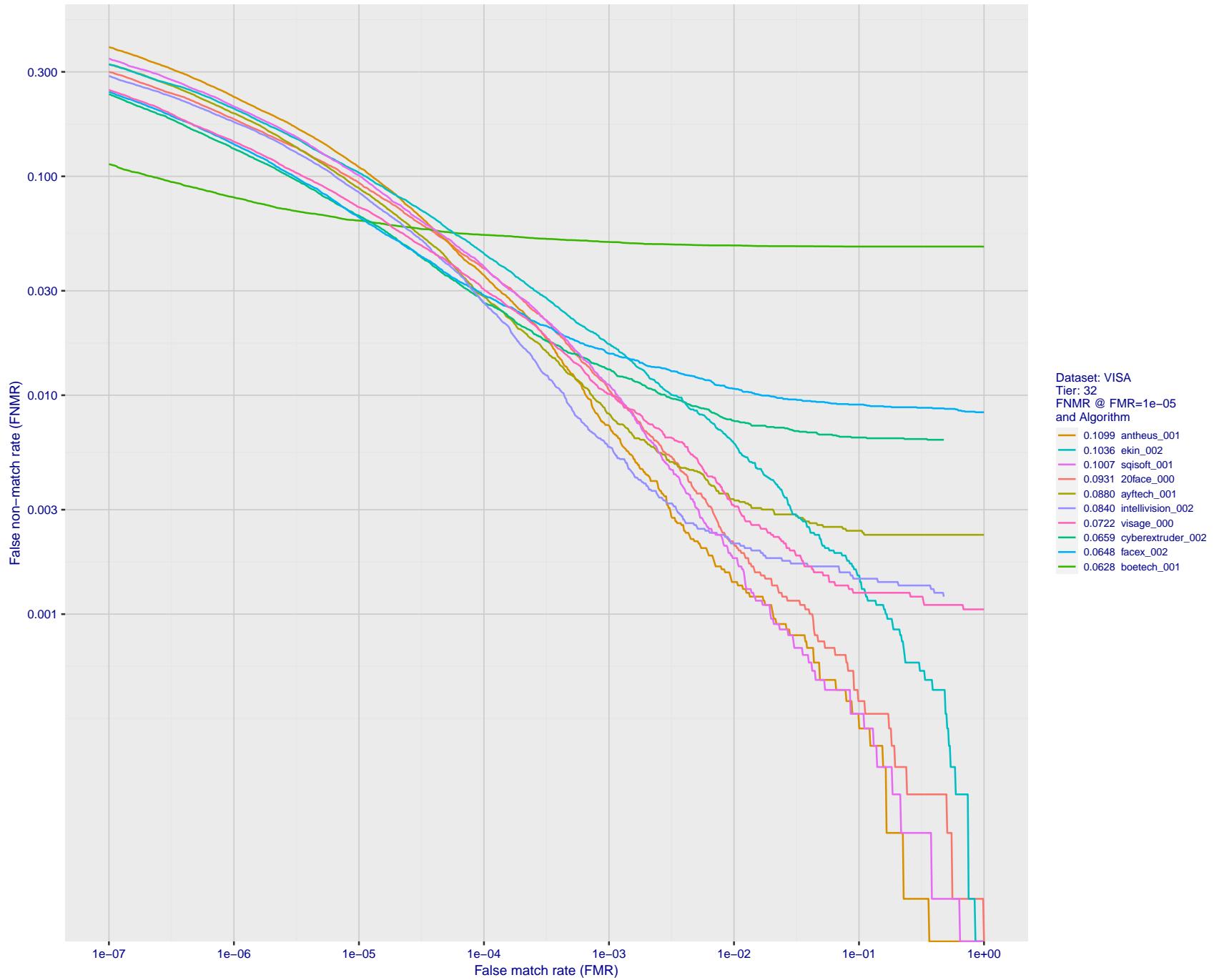


Figure 51: For the visa images, detection error tradeoff (DET) characteristics showing false non-match rate vs. false match rate plotted parametrically on threshold, T . The scales are logarithmic in order to show many decades of FMR.

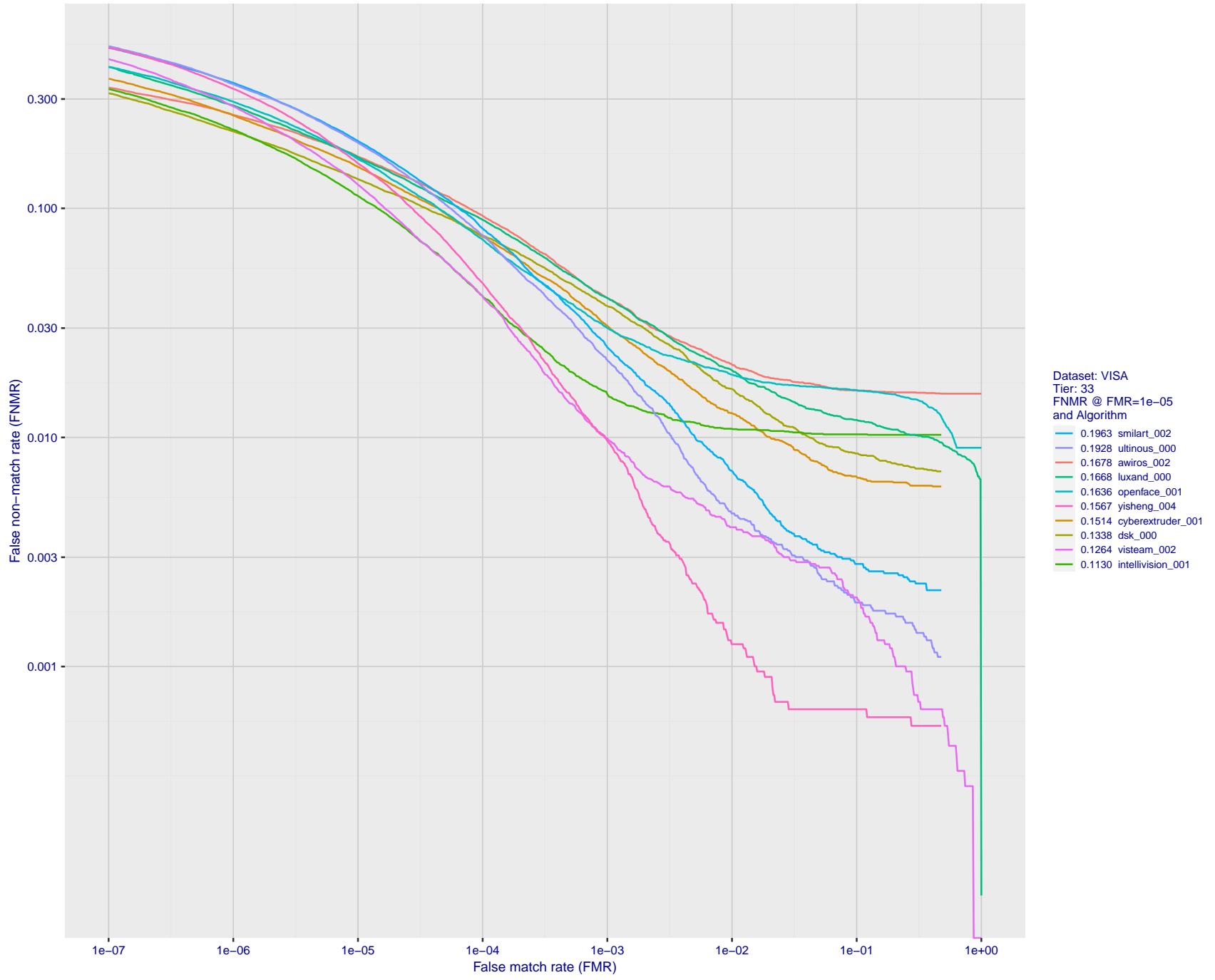


Figure 52: For the visa images, detection error tradeoff (DET) characteristics showing false non-match rate vs. false match rate plotted parametrically on threshold, T . The scales are logarithmic in order to show many decades of FMR.

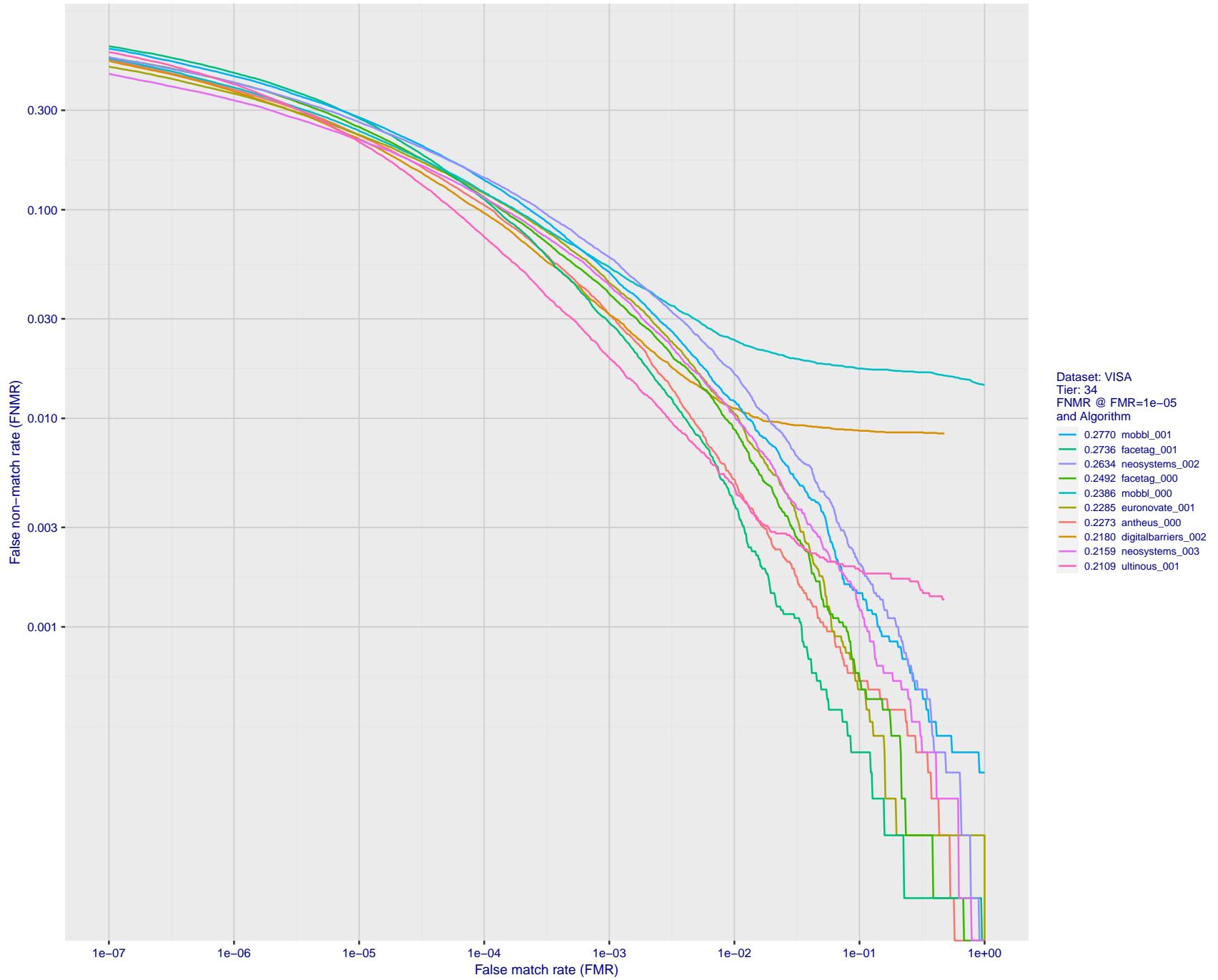


Figure 53: For the visa images, detection error tradeoff (DET) characteristics showing false non-match rate vs. false match rate plotted parametrically on threshold, T . The scales are logarithmic in order to show many decades of FMR.

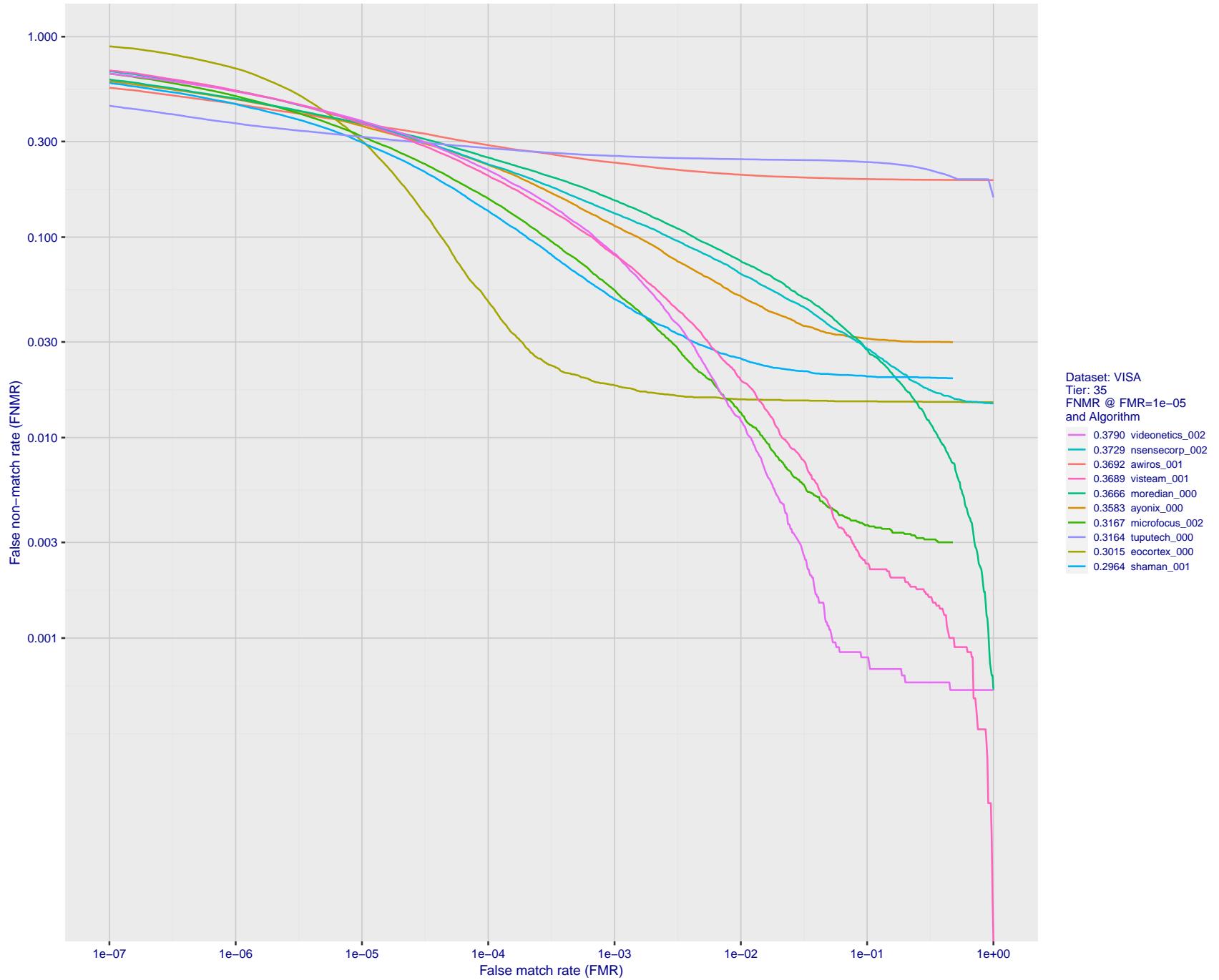


Figure 54: For the visa images, detection error tradeoff (DET) characteristics showing false non-match rate vs. false match rate plotted parametrically on threshold, T . The scales are logarithmic in order to show many decades of FMR.

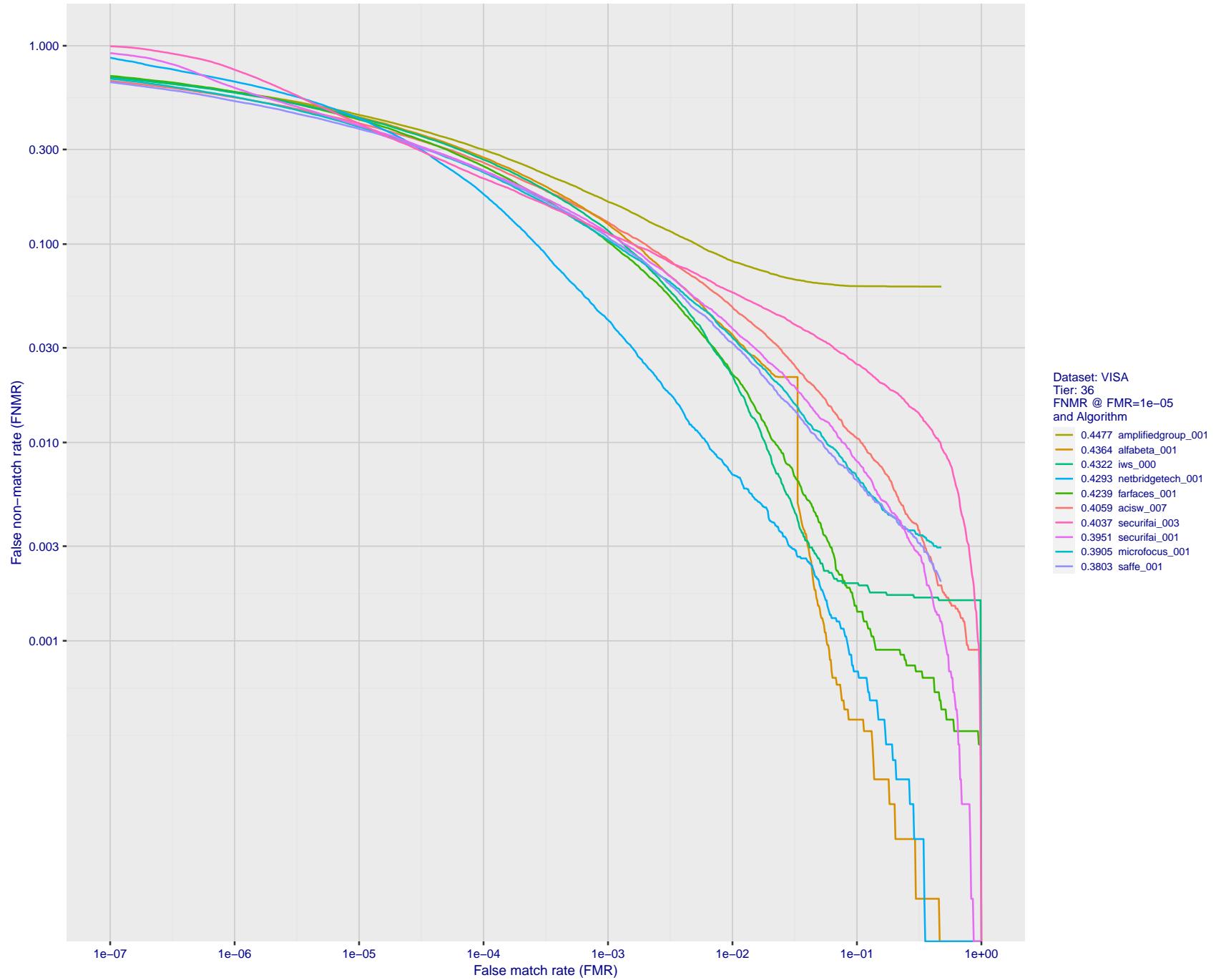


Figure 55: For the visa images, detection error tradeoff (DET) characteristics showing false non-match rate vs. false match rate plotted parametrically on threshold, T . The scales are logarithmic in order to show many decades of FMR.

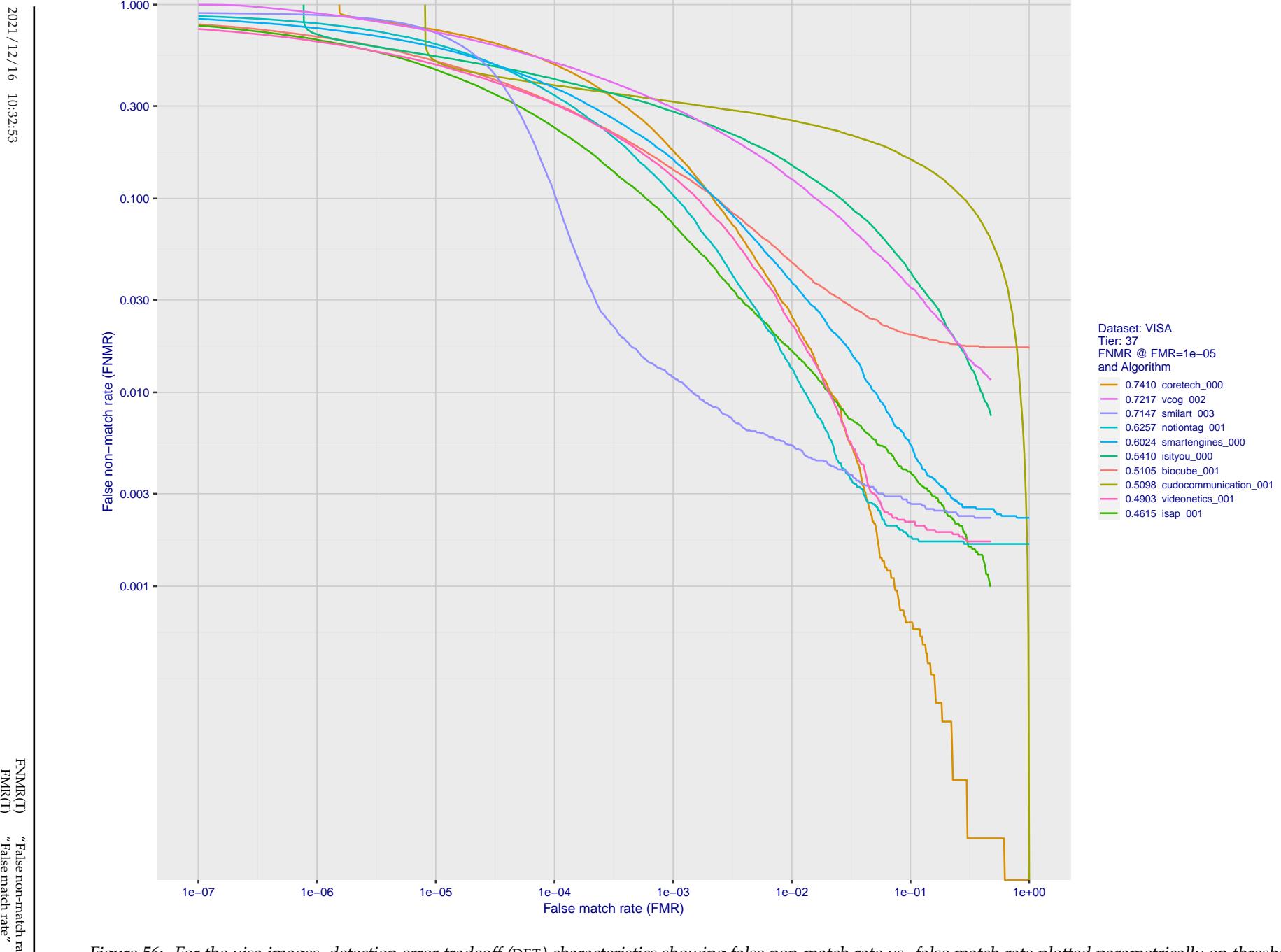


Figure 56: For the visa images, detection error tradeoff (DET) characteristics showing false non-match rate vs. false match rate plotted parametrically on threshold, T . The scales are logarithmic in order to show many decades of FMR.

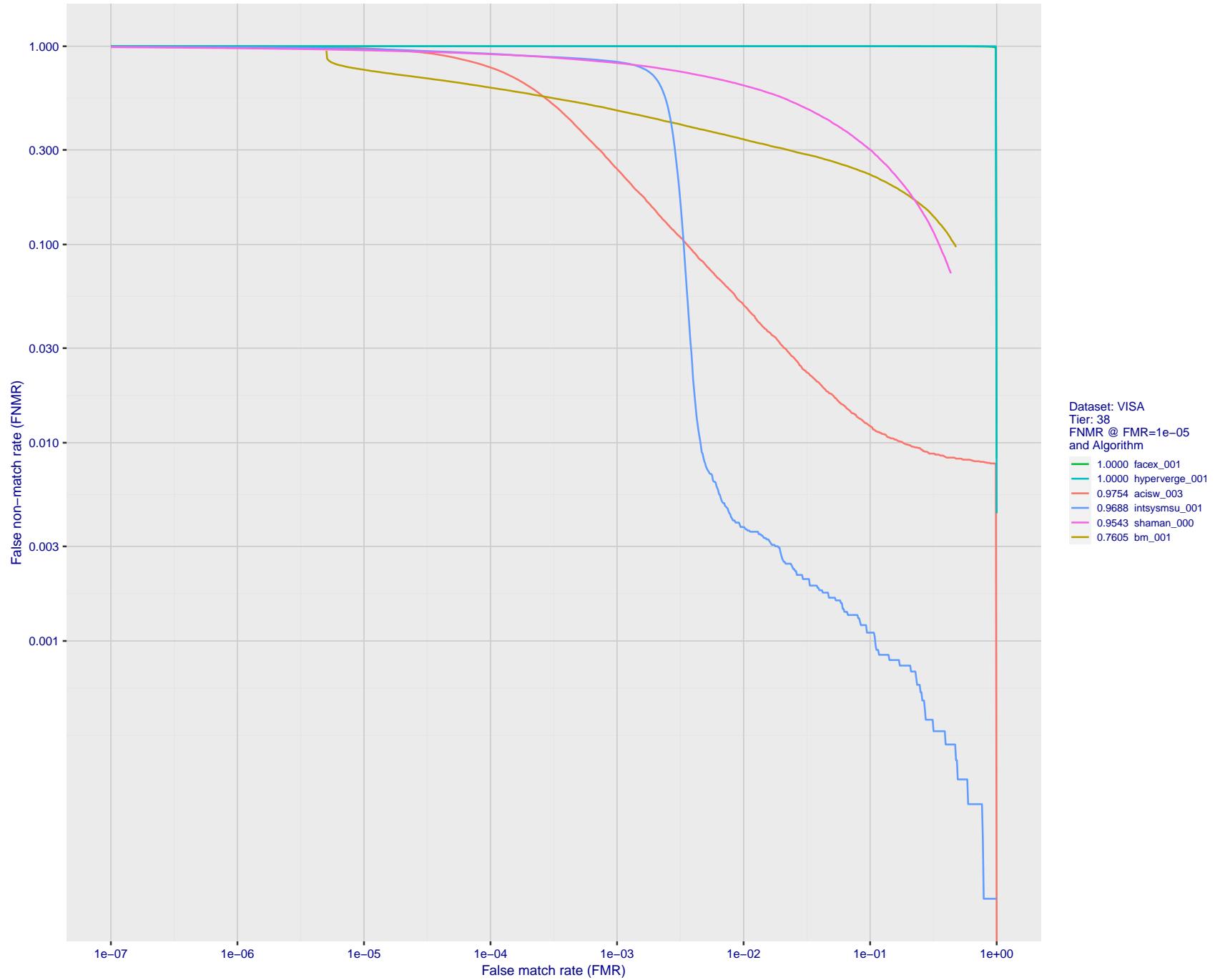


Figure 57: For the visa images, detection error tradeoff (DET) characteristics showing false non-match rate vs. false match rate plotted parametrically on threshold, T . The scales are logarithmic in order to show many decades of FMR.

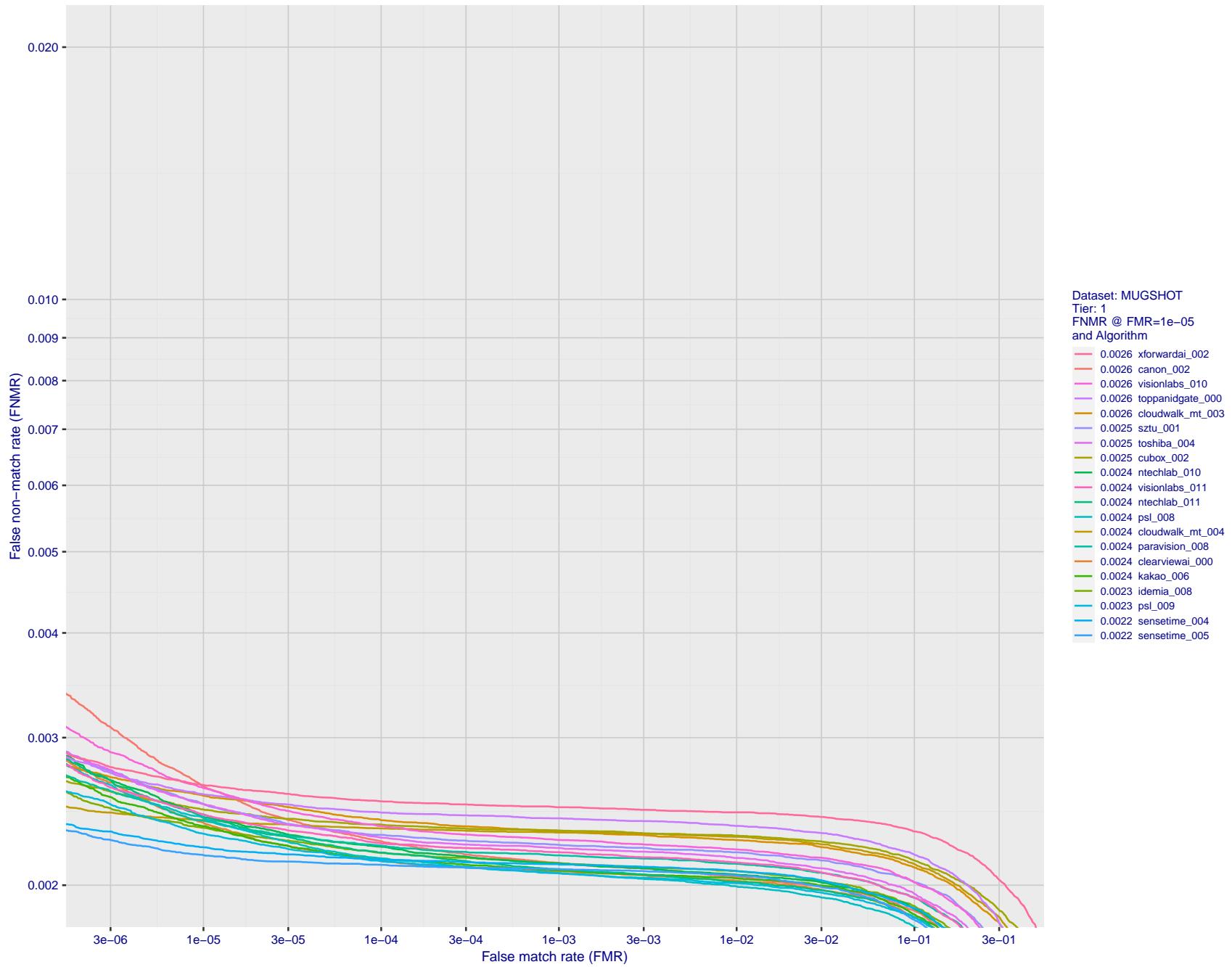


Figure 58: For the mugshot images, detection error tradeoff (DET) characteristics showing false non-match rate vs. false match rate plotted parametrically on threshold, T . The scales are logarithmic in order to show decades of FMR.

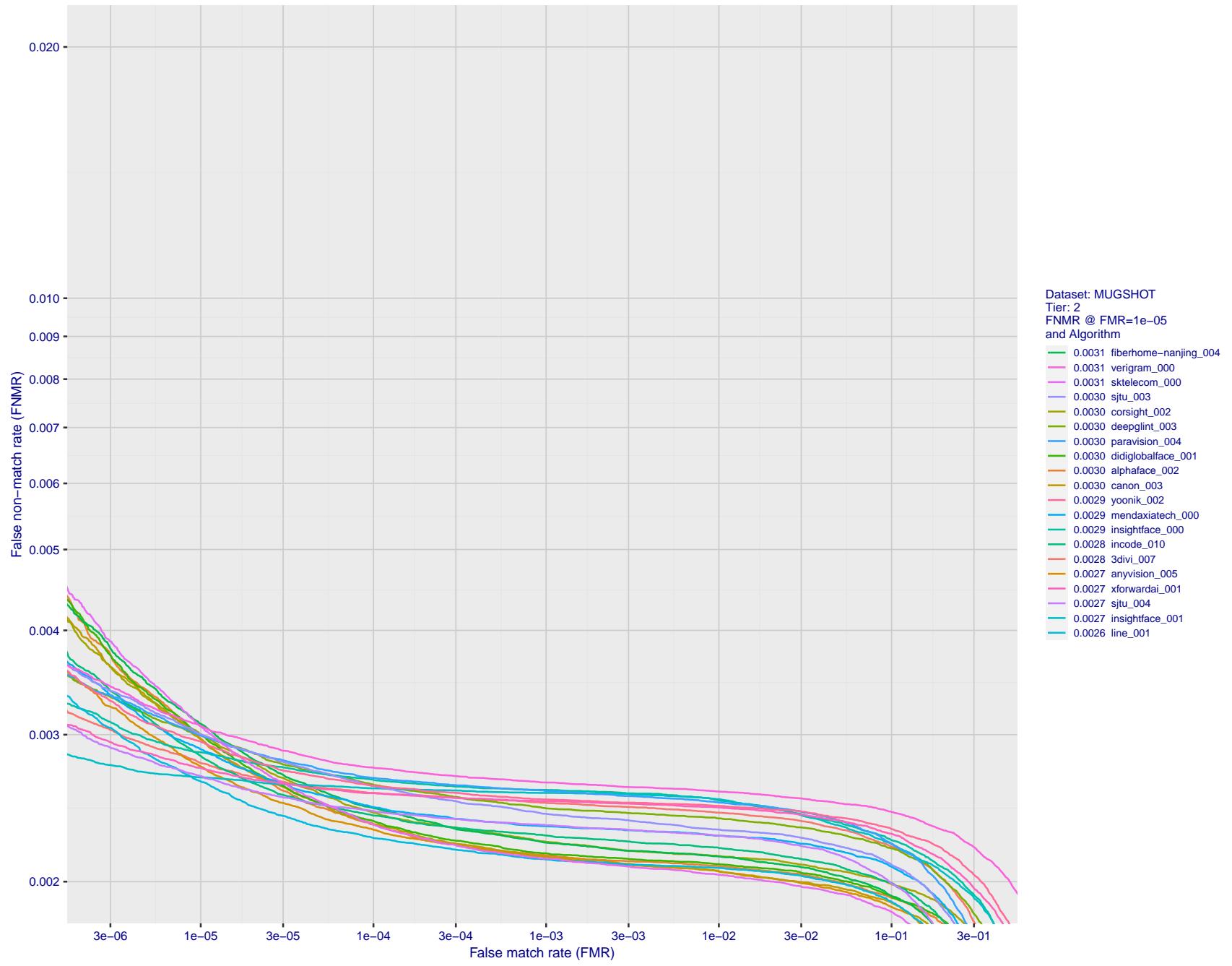


Figure 59: For the mugshot images, detection error tradeoff (DET) characteristics showing false non-match rate vs. false match rate plotted parametrically on threshold, T . The scales are logarithmic in order to show decades of FMR.

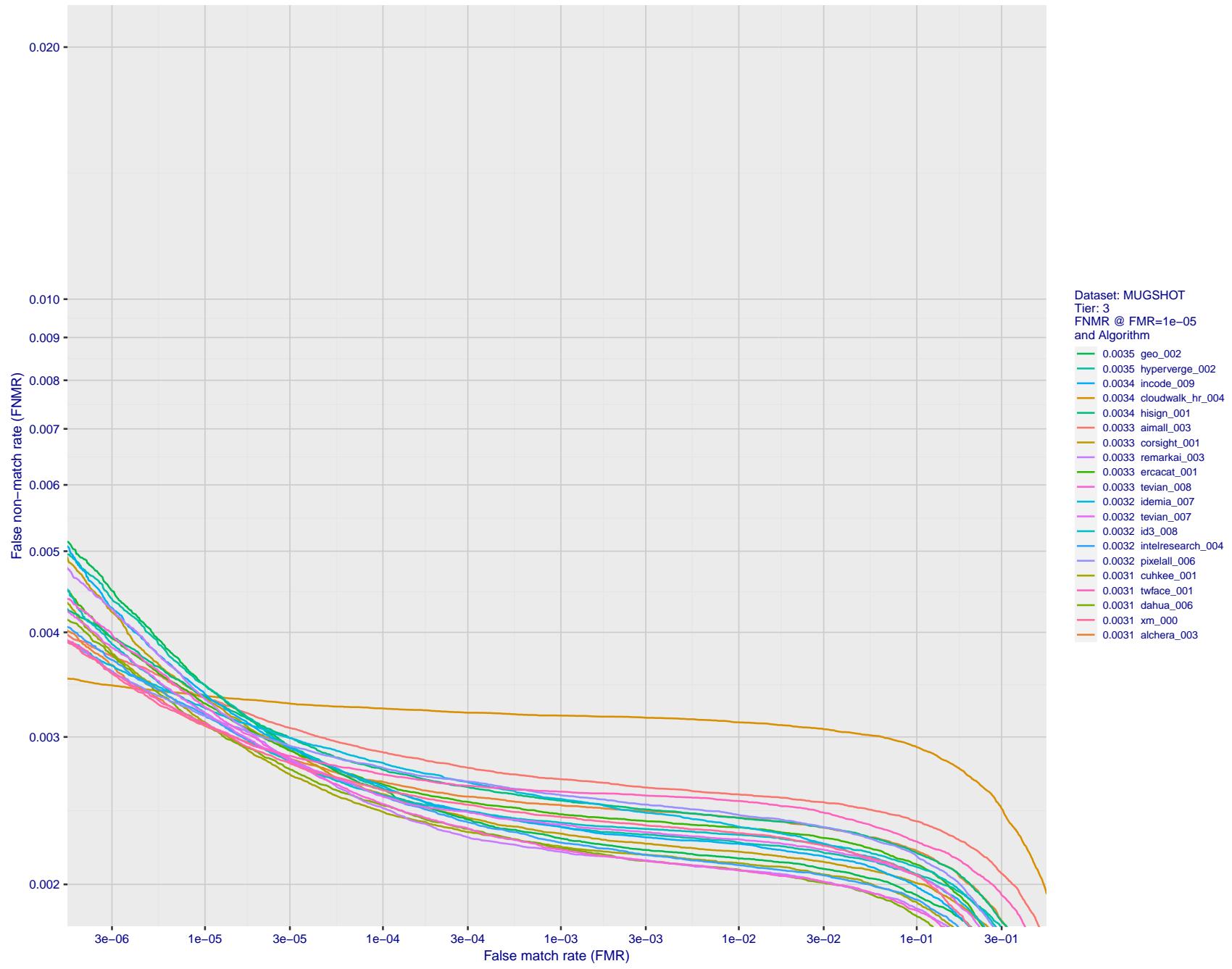


Figure 60: For the mugshot images, detection error tradeoff (DET) characteristics showing false non-match rate vs. false match rate plotted parametrically on threshold, T . The scales are logarithmic in order to show decades of FMR.

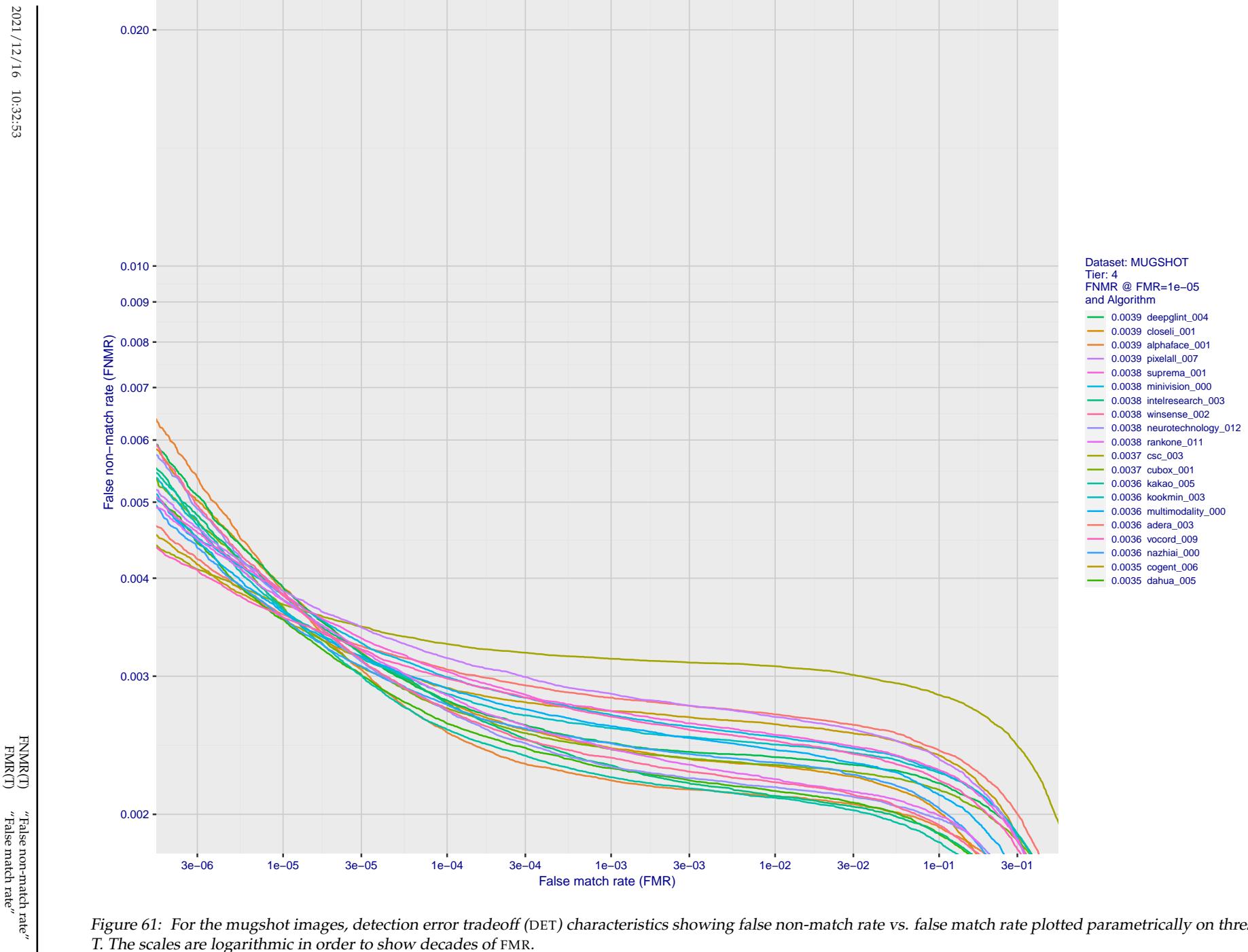


Figure 61: For the mugshot images, detection error tradeoff (DET) characteristics showing false non-match rate vs. false match rate plotted parametrically on threshold, T . The scales are logarithmic in order to show decades of FMR.

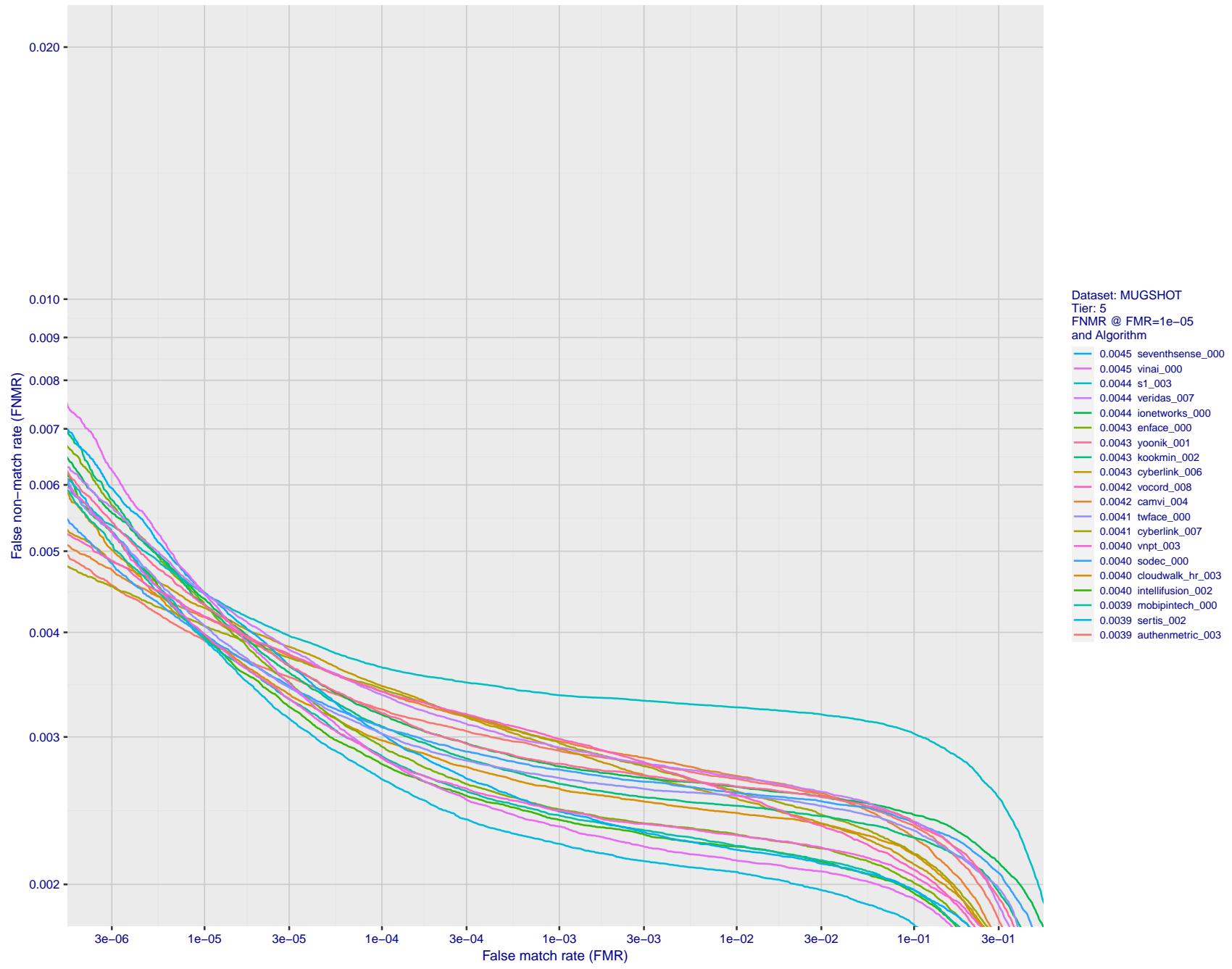


Figure 62: For the mugshot images, detection error tradeoff (DET) characteristics showing false non-match rate vs. false match rate plotted parametrically on threshold, T . The scales are logarithmic in order to show decades of FMR.

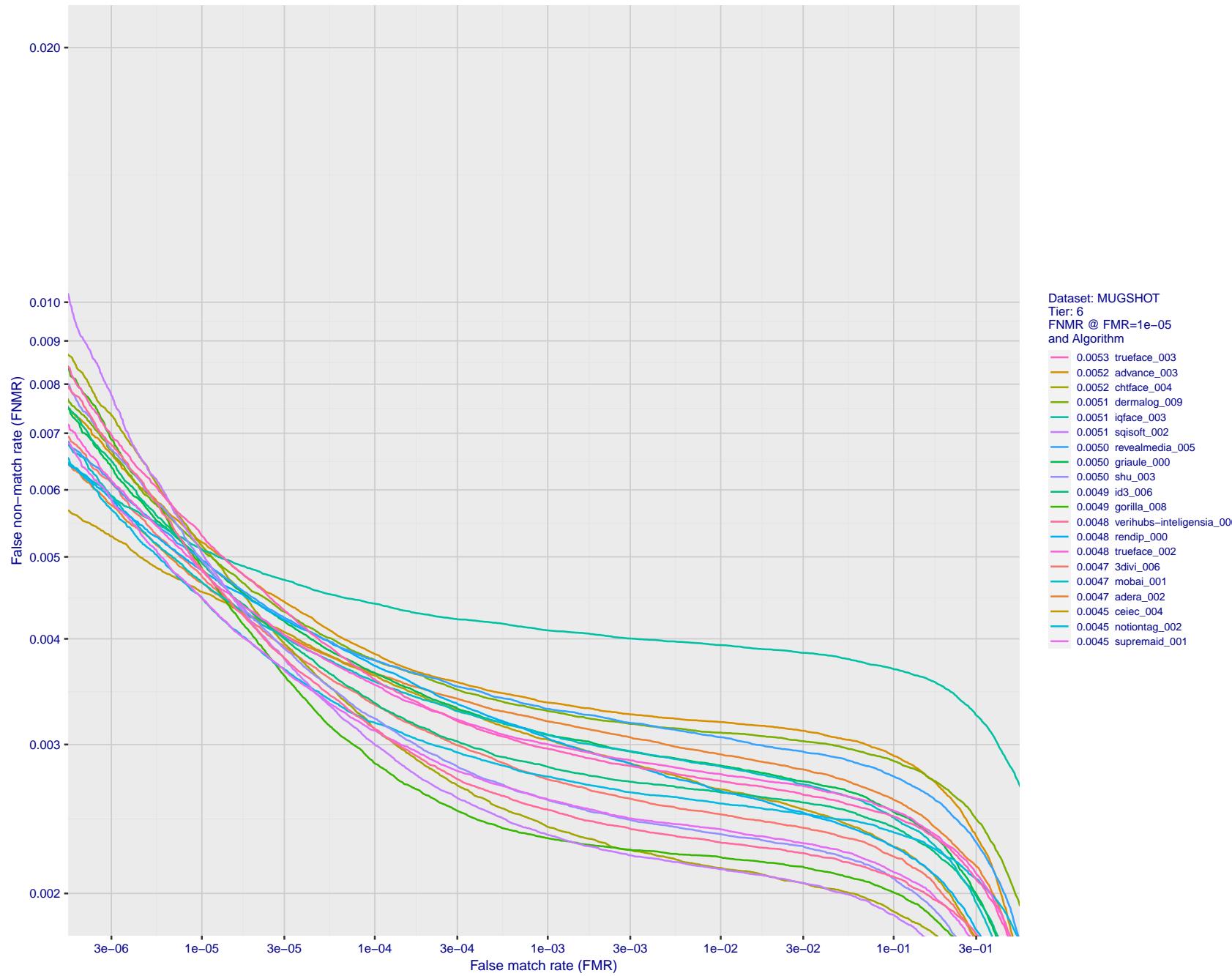


Figure 63: For the mugshot images, detection error tradeoff (DET) characteristics showing false non-match rate vs. false match rate plotted parametrically on threshold, T . The scales are logarithmic in order to show decades of FMR.

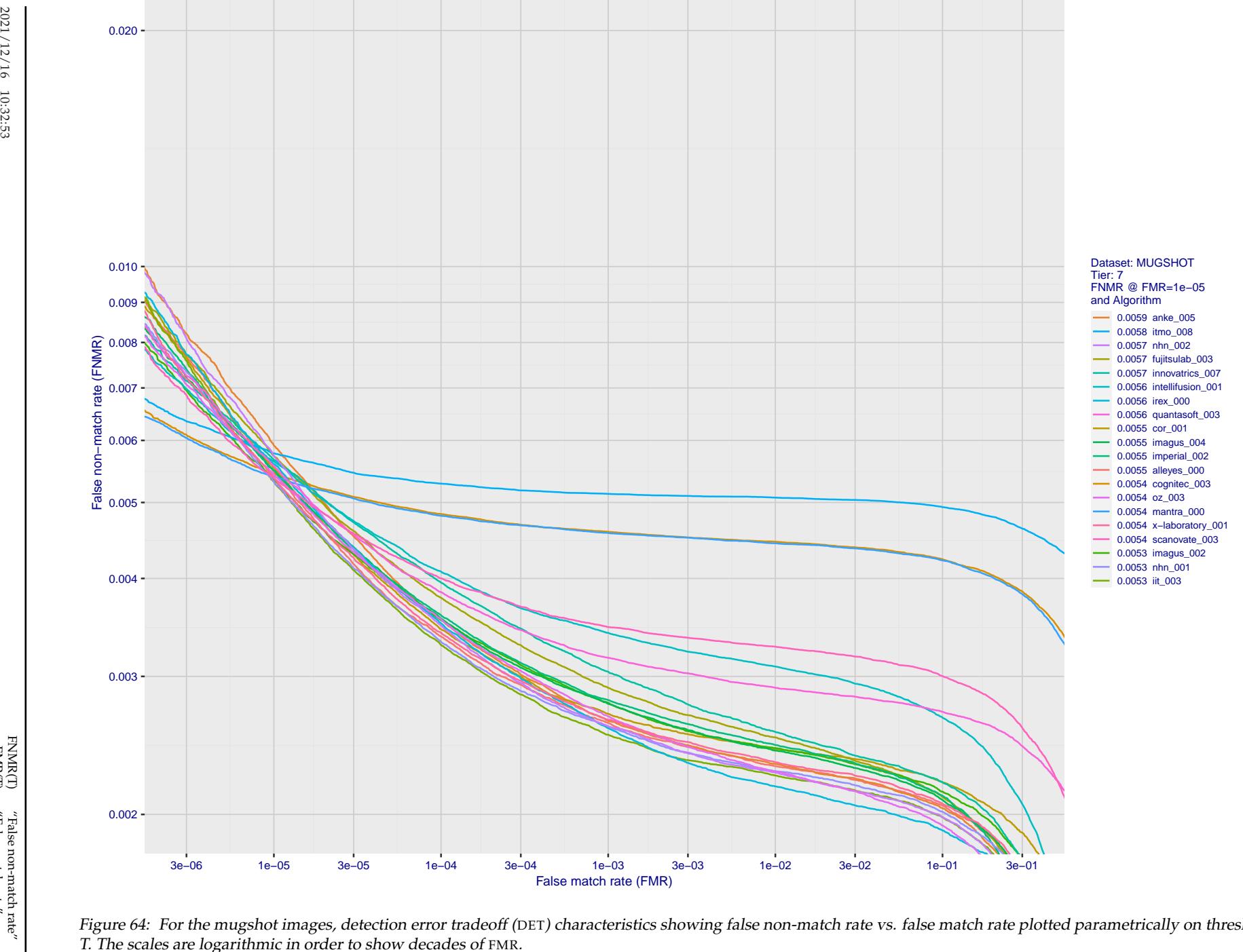


Figure 64: For the mugshot images, detection error tradeoff (DET) characteristics showing false non-match rate vs. false match rate plotted parametrically on threshold, T . The scales are logarithmic in order to show decades of FMR.

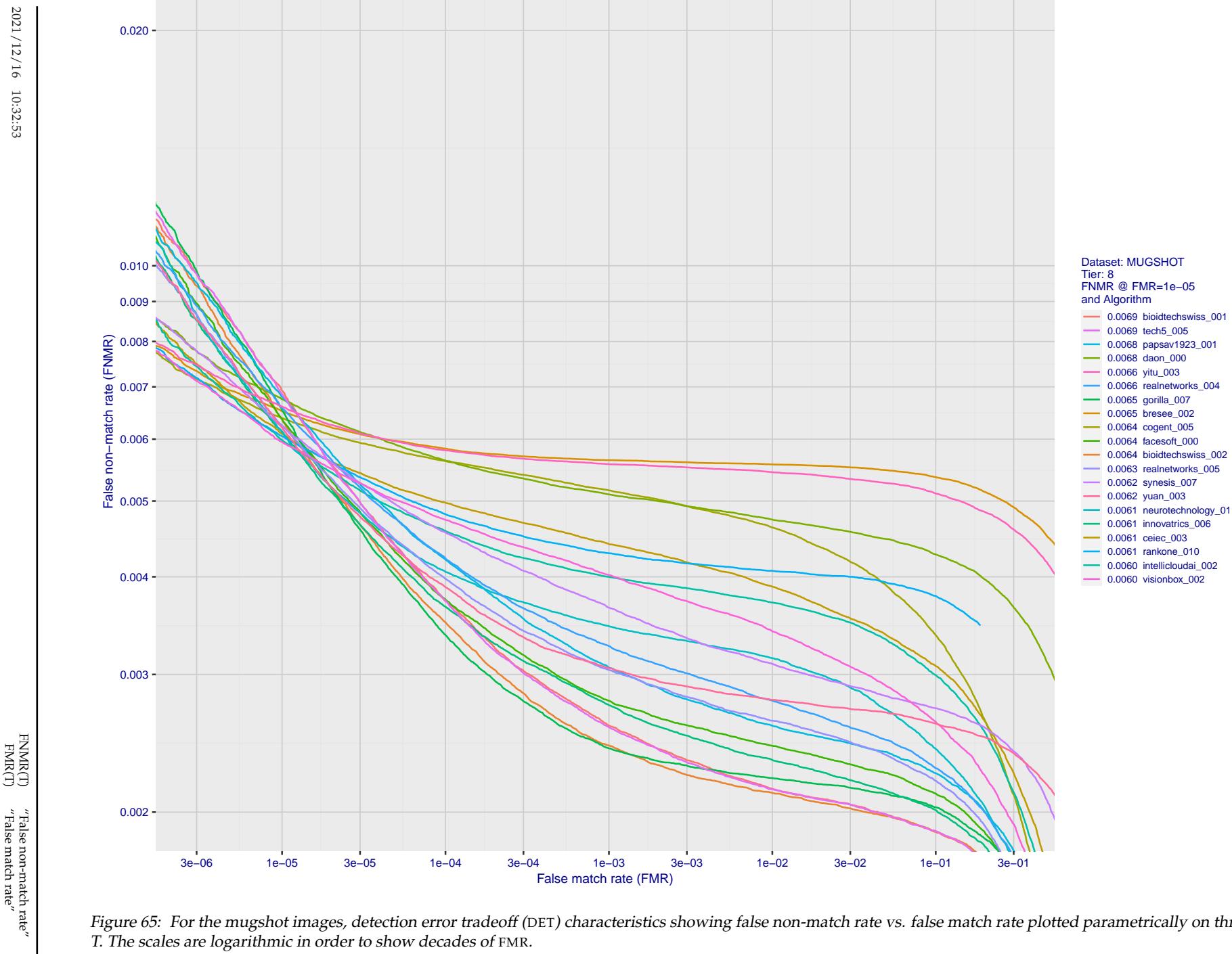
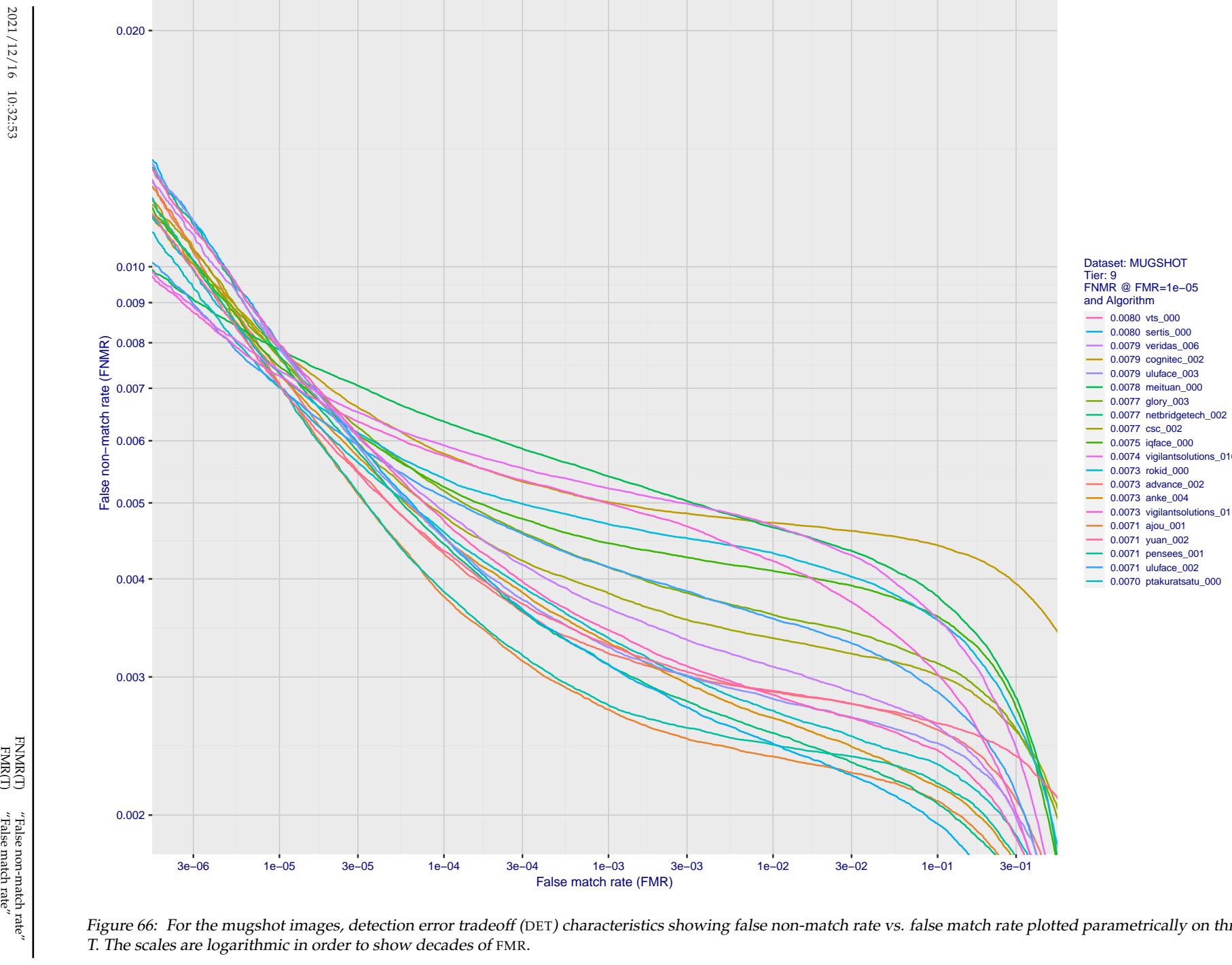


Figure 65: For the mugshot images, detection error tradeoff (DET) characteristics showing false non-match rate vs. false match rate plotted parametrically on threshold, T . The scales are logarithmic in order to show decades of FMR.



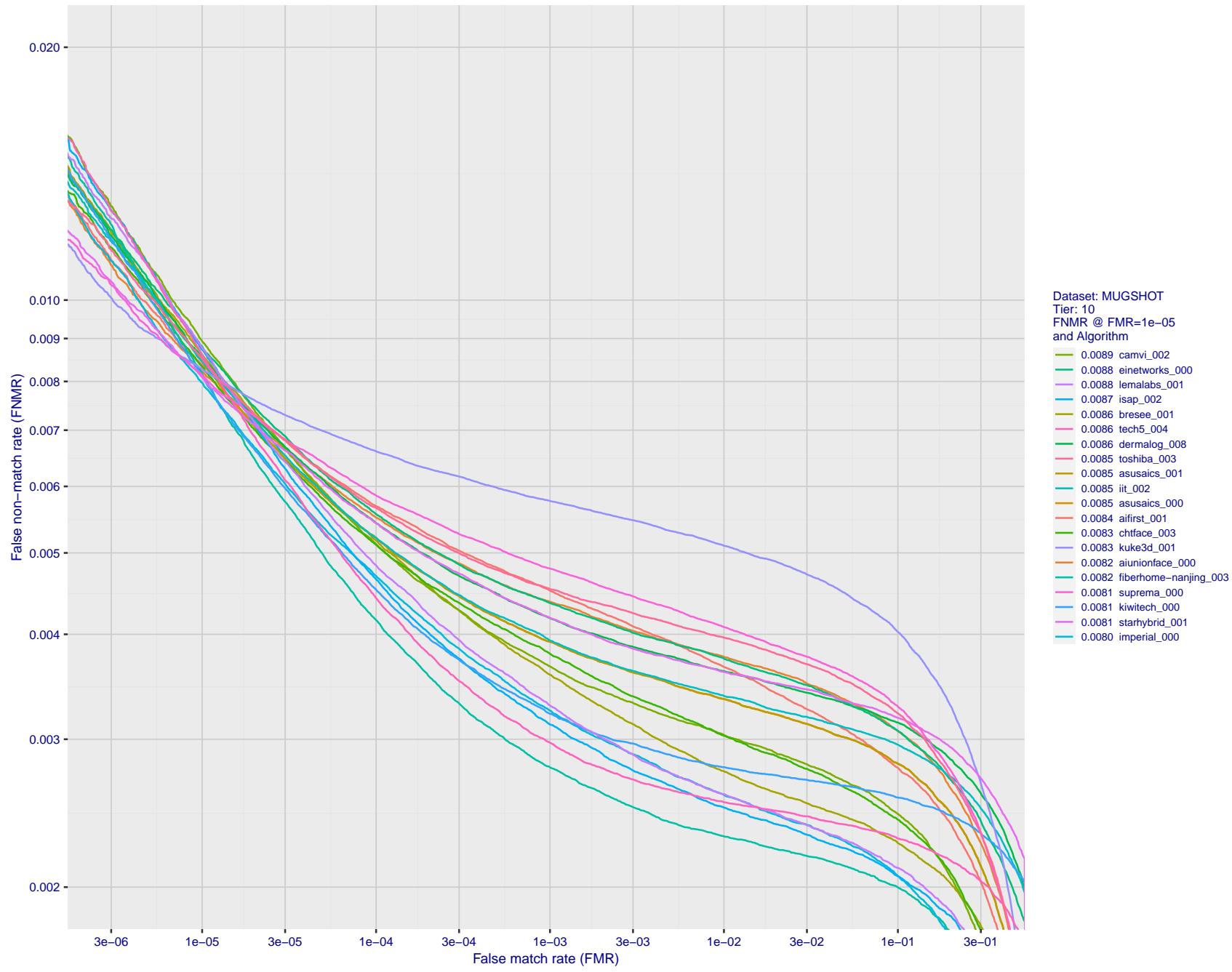
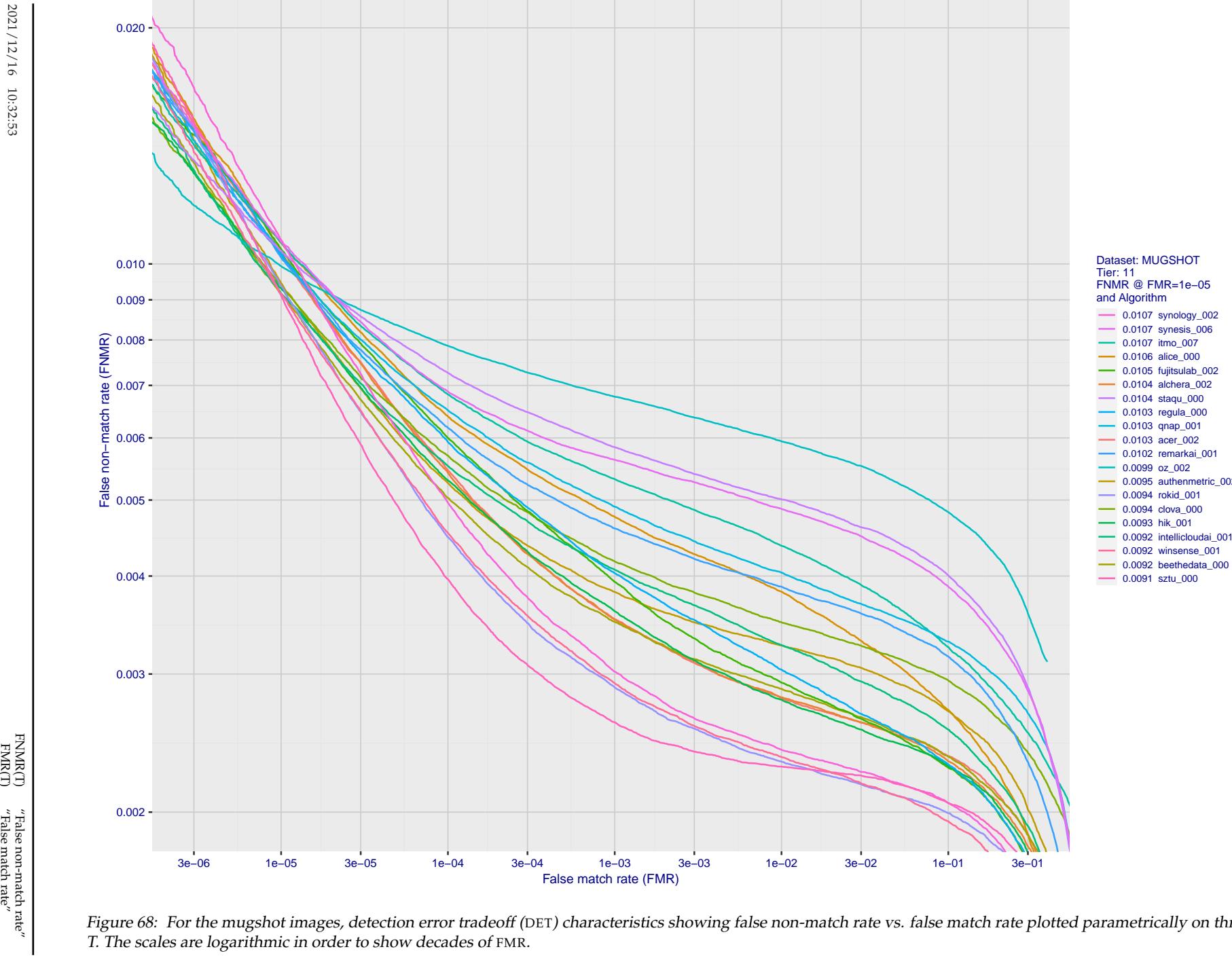


Figure 67: For the mugshot images, detection error tradeoff (DET) characteristics showing false non-match rate vs. false match rate plotted parametrically on threshold, T . The scales are logarithmic in order to show decades of FMR.



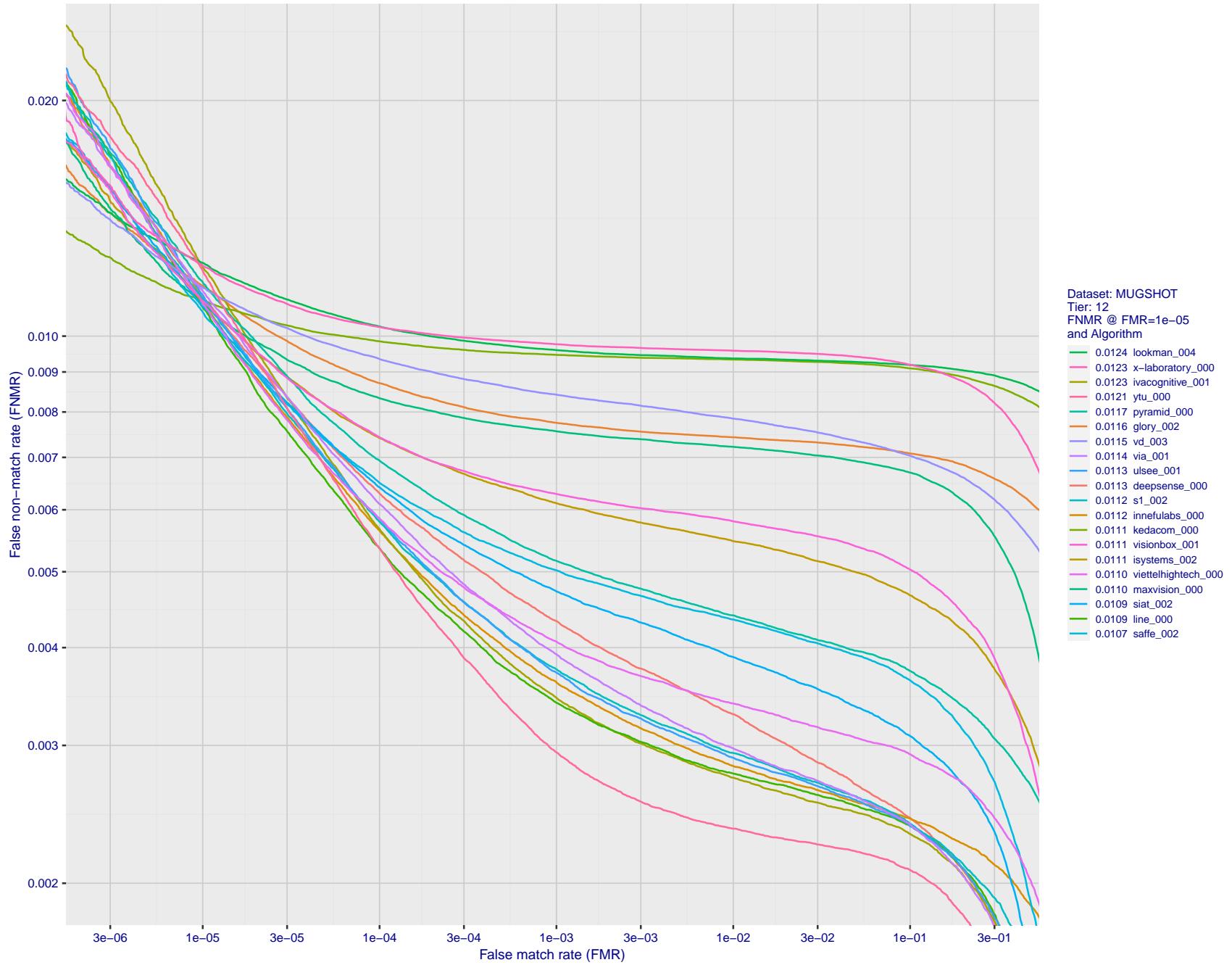


Figure 69: For the mugshot images, detection error tradeoff (DET) characteristics showing false non-match rate vs. false match rate plotted parametrically on threshold, T . The scales are logarithmic in order to show decades of FMR.

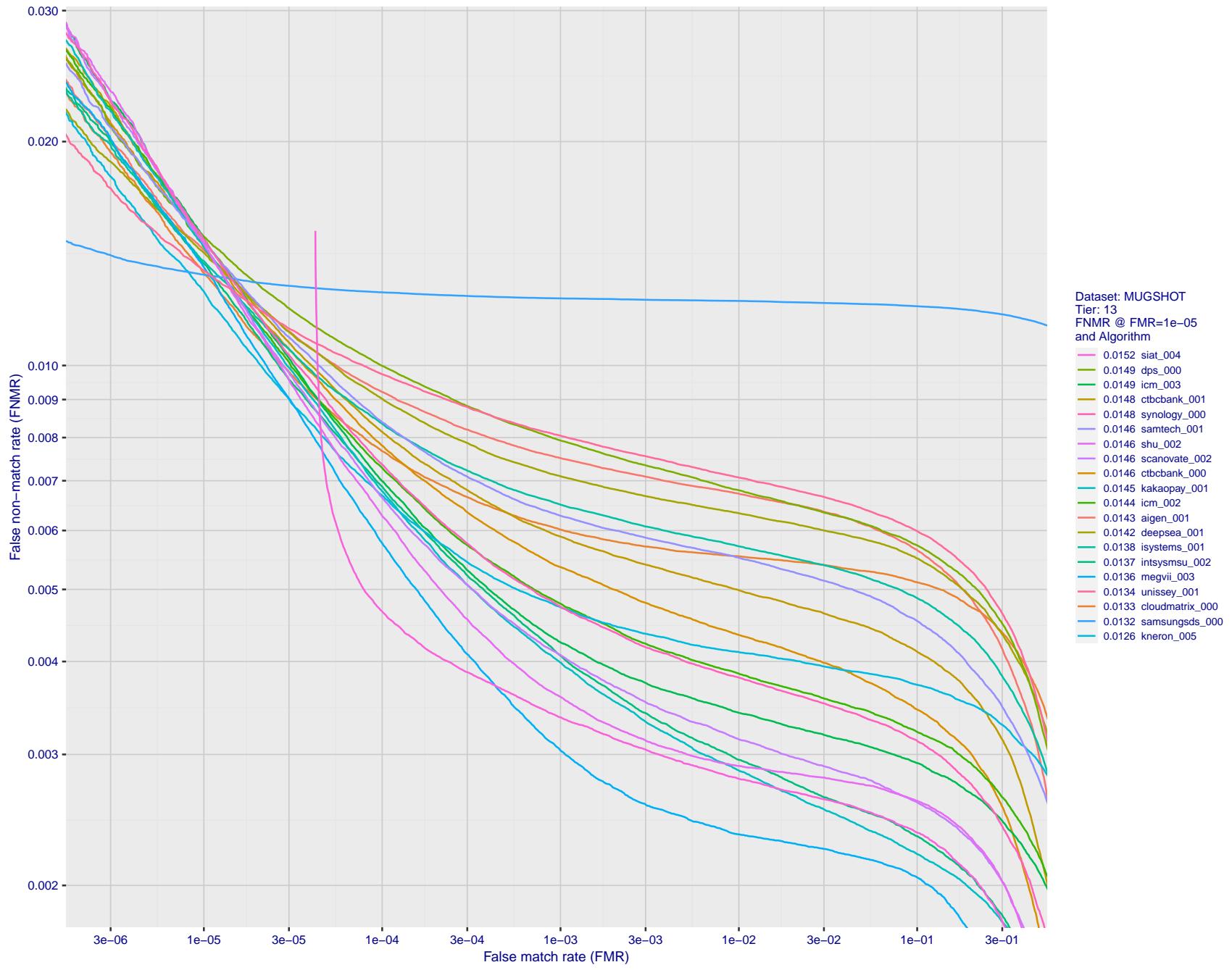


Figure 70: For the mugshot images, detection error tradeoff (DET) characteristics showing false non-match rate vs. false match rate plotted parametrically on threshold, T . The scales are logarithmic in order to show decades of FMR.

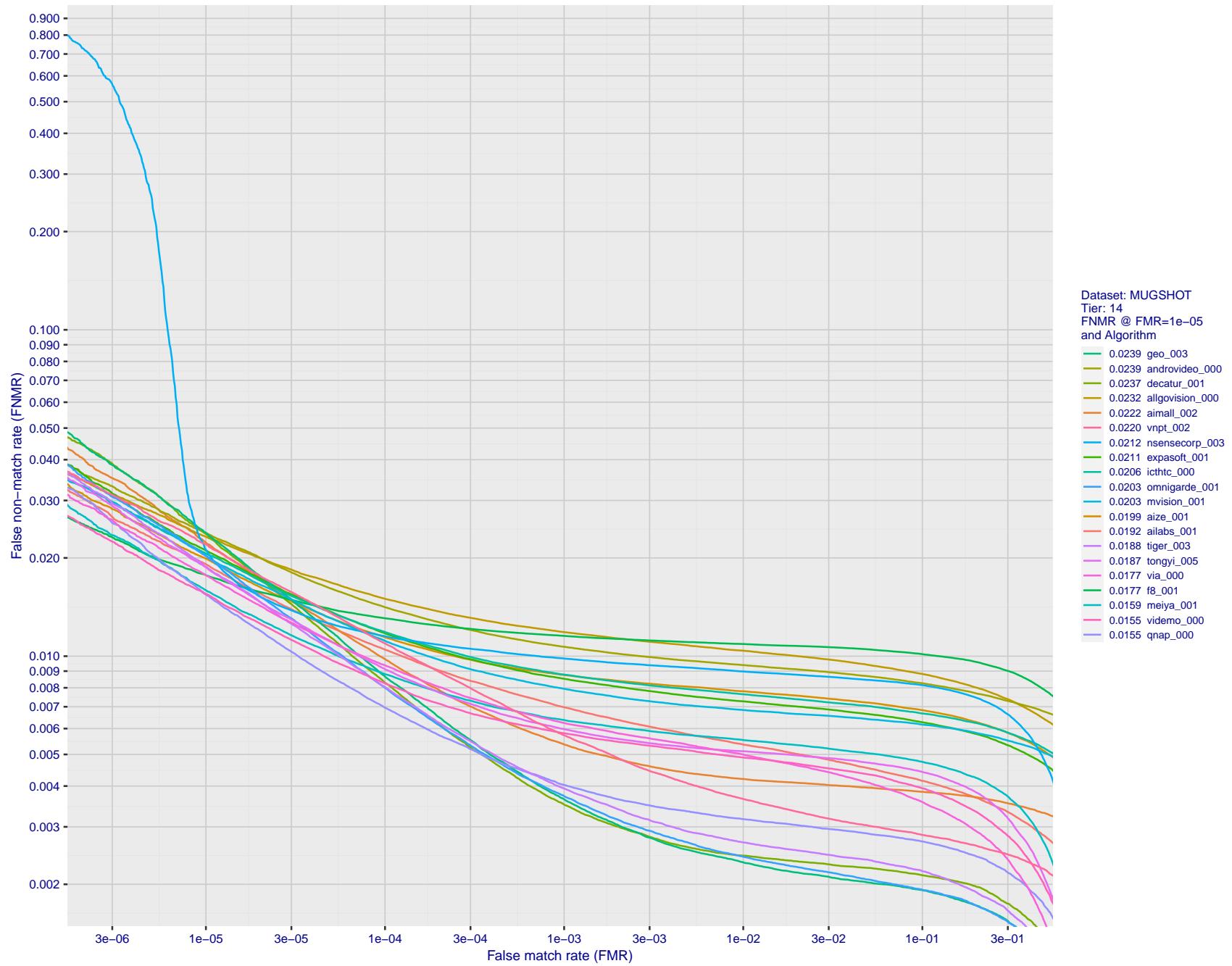


Figure 71: For the mugshot images, detection error tradeoff (DET) characteristics showing false non-match rate vs. false match rate plotted parametrically on threshold, T . The scales are logarithmic in order to show decades of FMR.

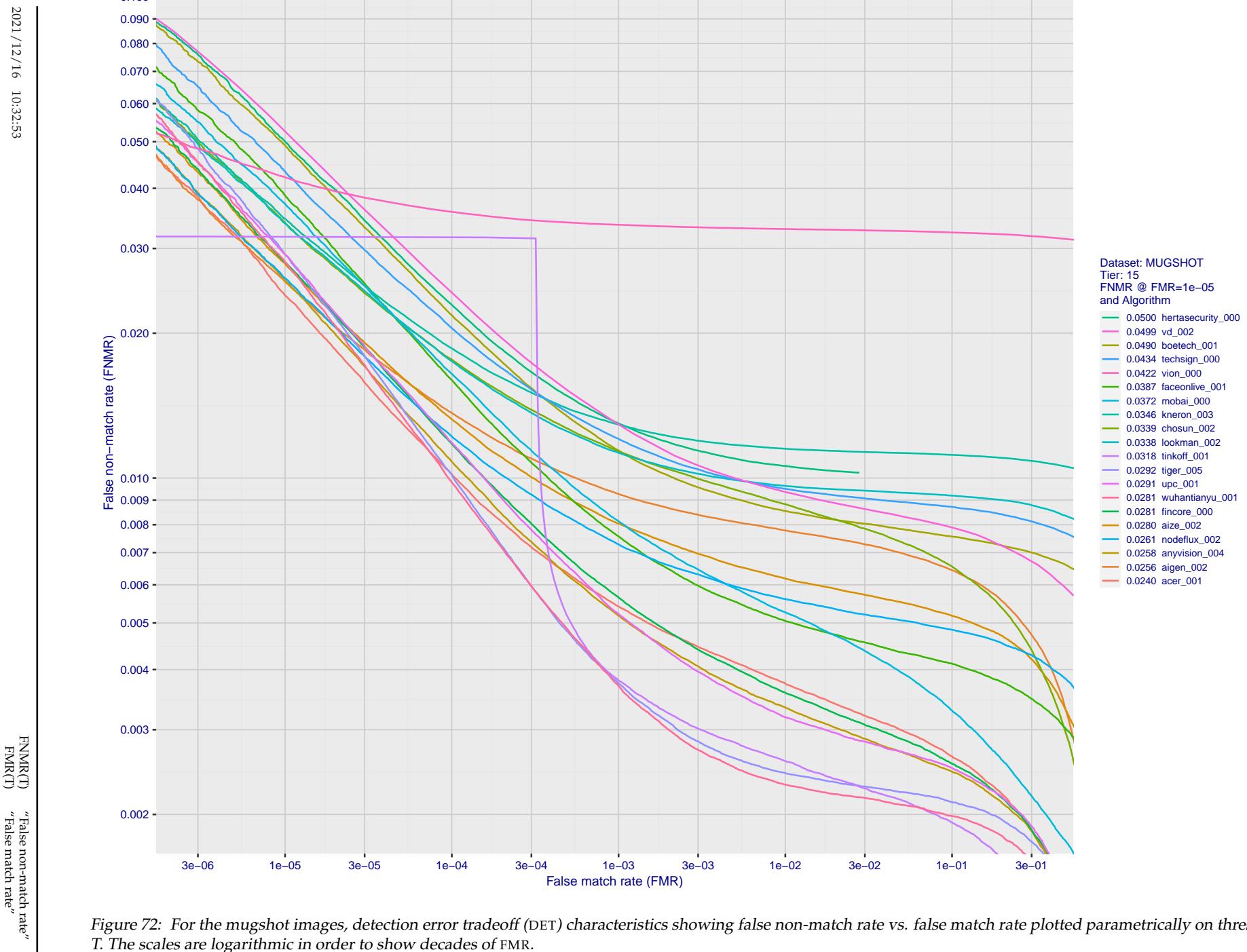


Figure 72: For the mugshot images, detection error tradeoff (DET) characteristics showing false non-match rate vs. false match rate plotted parametrically on threshold, T. The scales are logarithmic in order to show decades of FMR.

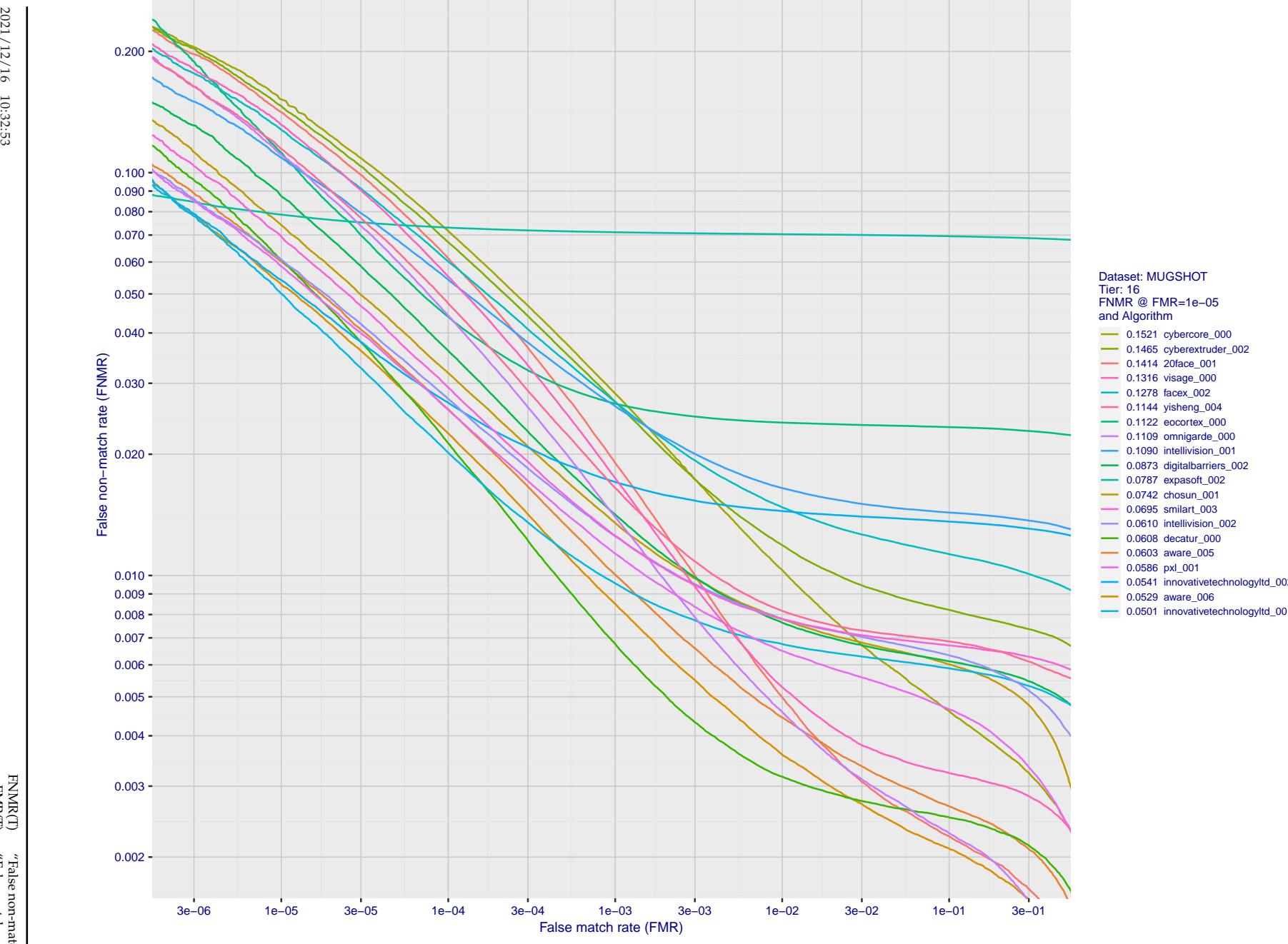


Figure 73: For the mugshot images, detection error tradeoff (DET) characteristics showing false non-match rate vs. false match rate plotted parametrically on threshold, T . The scales are logarithmic in order to show decades of FMR.

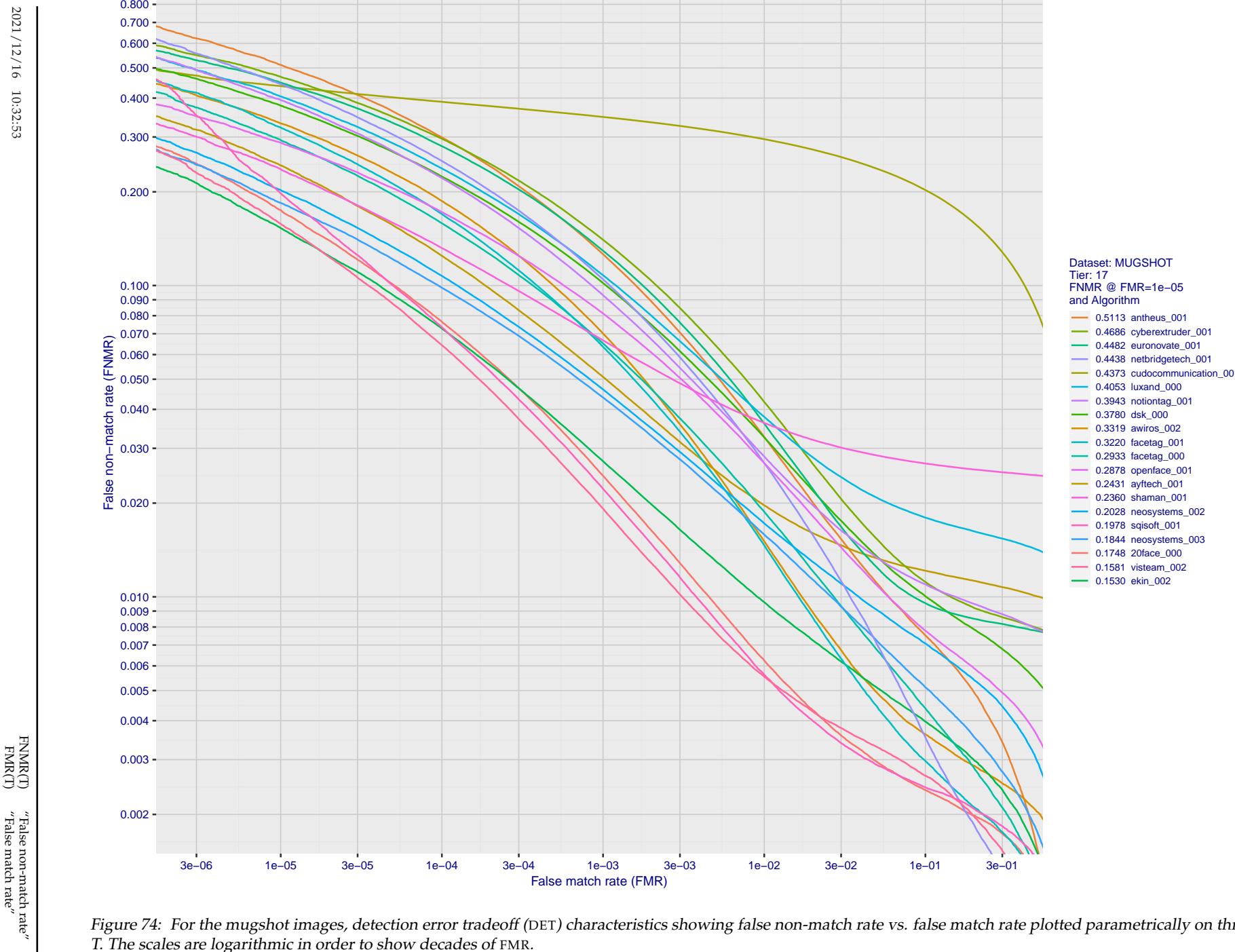


Figure 74: For the mugshot images, detection error tradeoff (DET) characteristics showing false non-match rate vs. false match rate plotted parametrically on threshold, T . The scales are logarithmic in order to show decades of FMR.

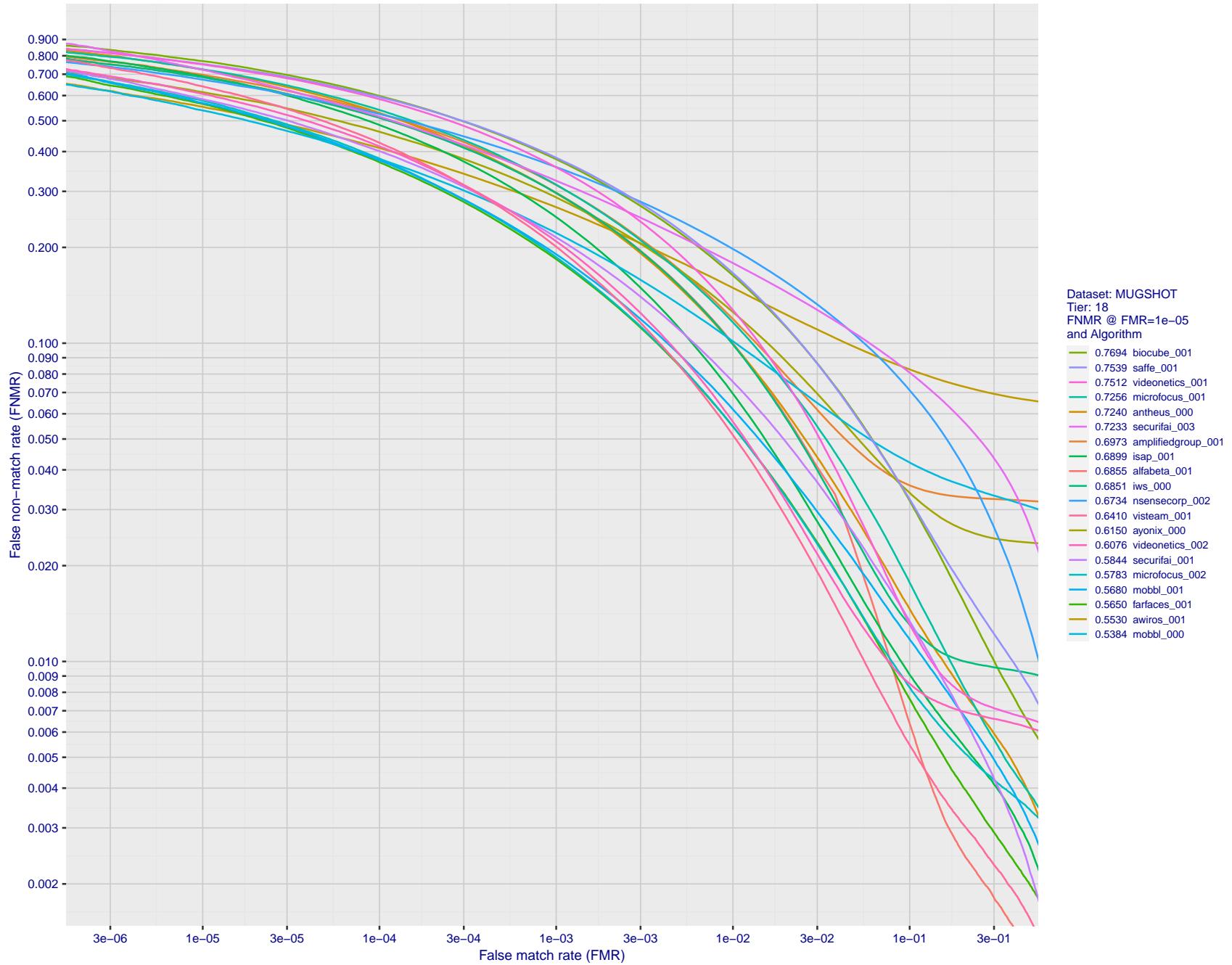


Figure 75: For the mugshot images, detection error tradeoff (DET) characteristics showing false non-match rate vs. false match rate plotted parametrically on threshold, T . The scales are logarithmic in order to show decades of FMR.

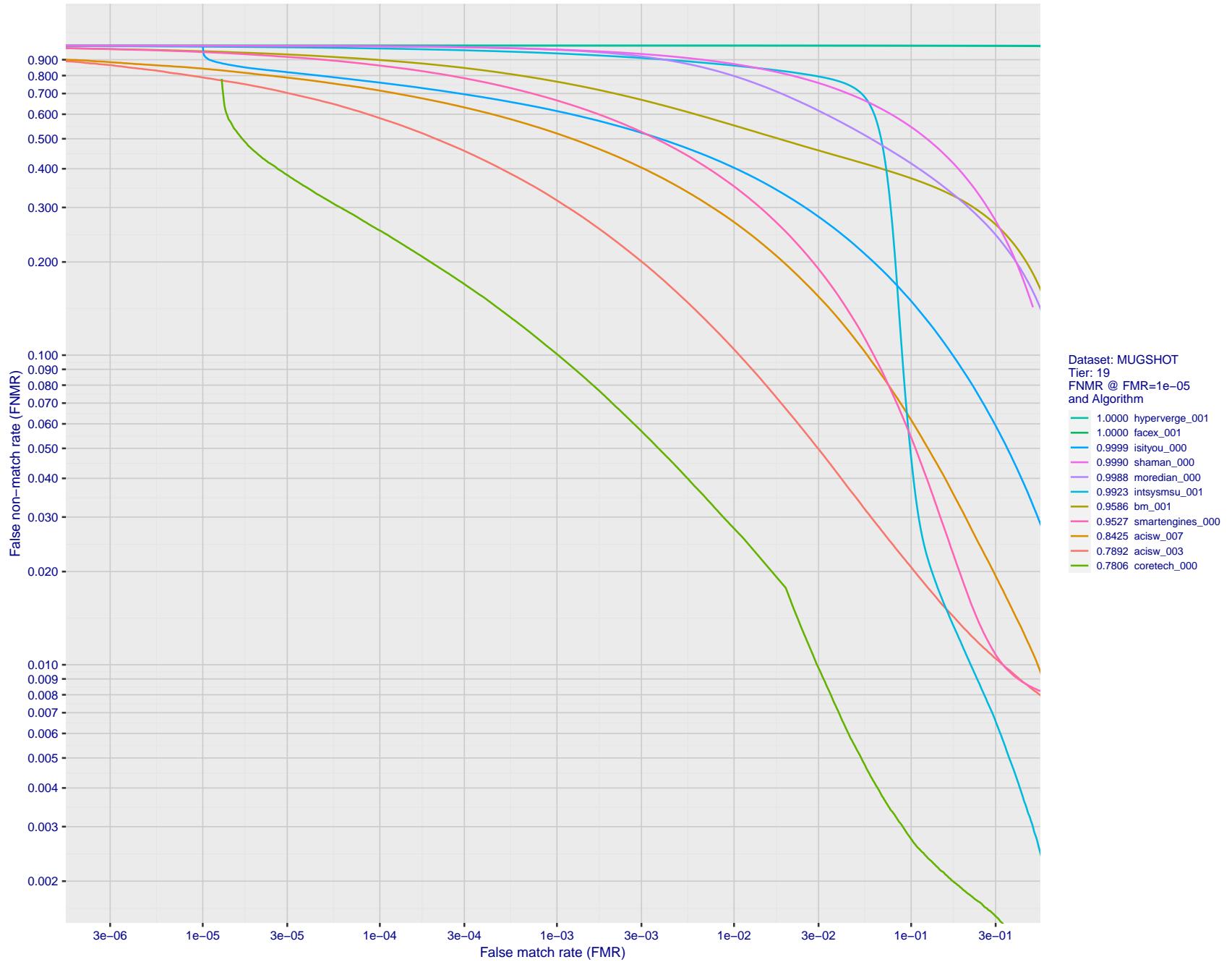


Figure 76: For the mugshot images, detection error tradeoff (DET) characteristics showing false non-match rate vs. false match rate plotted parametrically on threshold, T . The scales are logarithmic in order to show decades of FMR.

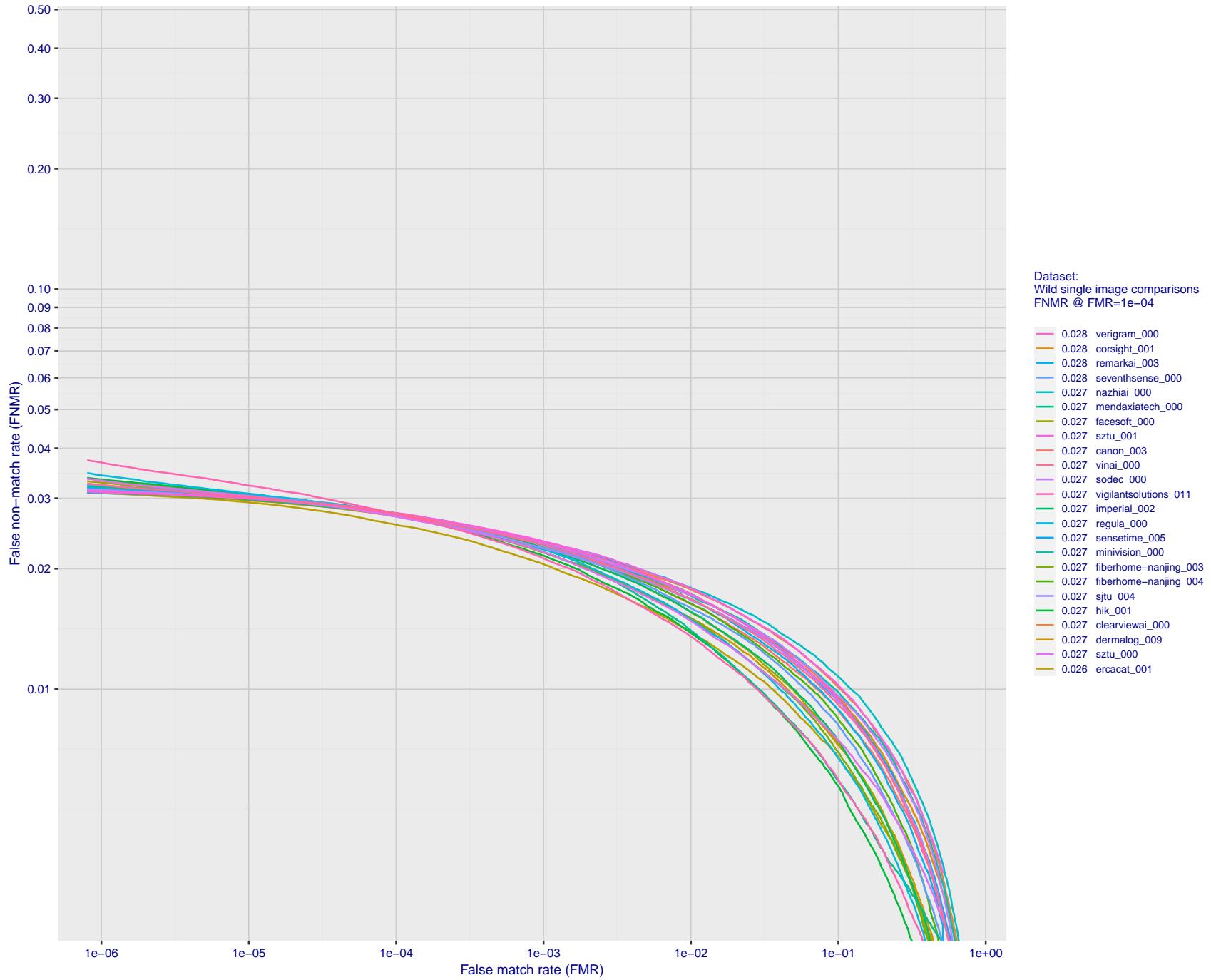


Figure 77: For the 2018 wild image comparisons, detection error tradeoff (DET) characteristics showing false non-match rate vs. false match rate plotted parametrically on threshold, T . The scales are logarithmic in order to show several decades of FMR.

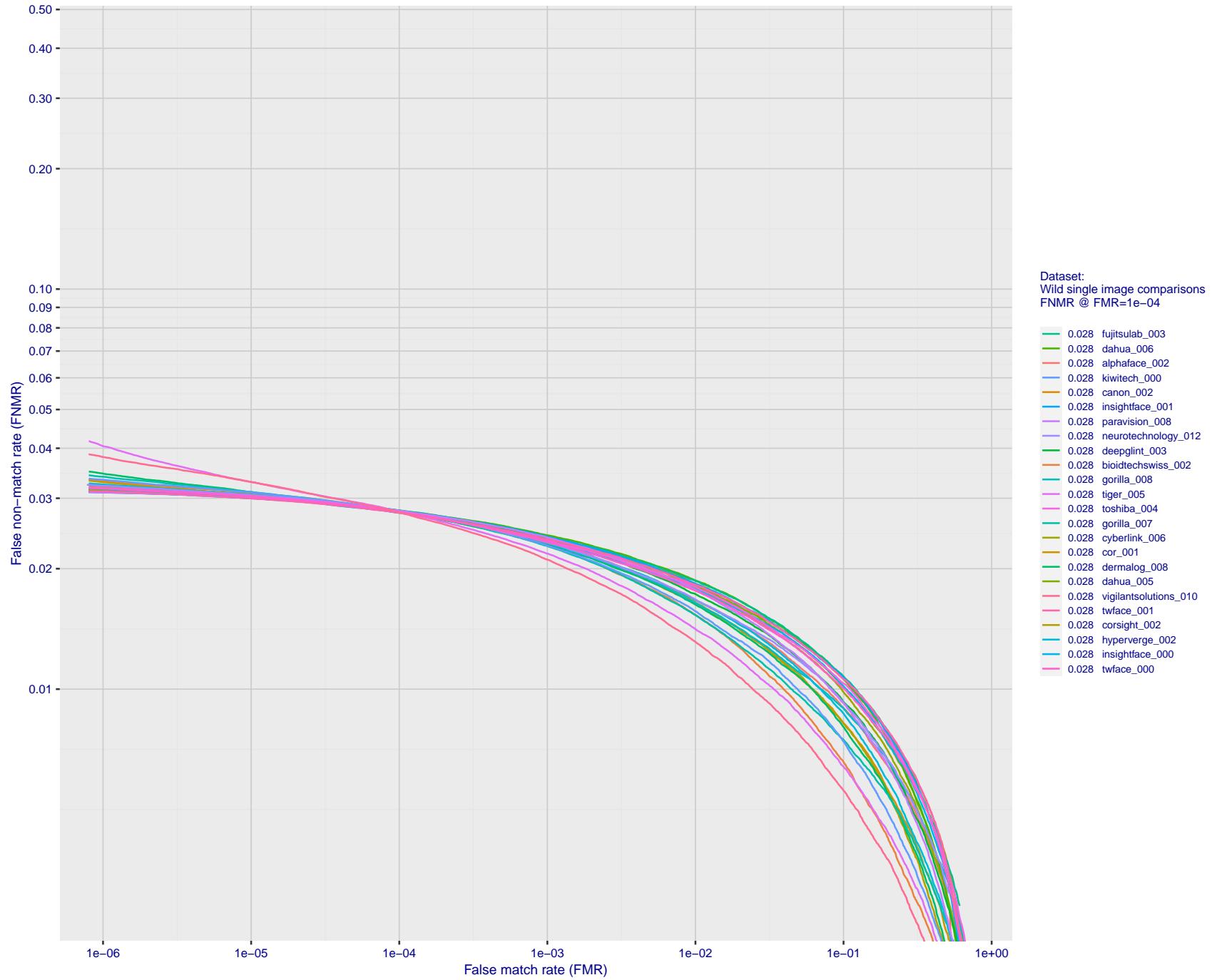


Figure 78: For the 2018 wild image comparisons, detection error tradeoff (DET) characteristics showing false non-match rate vs. false match rate plotted parametrically on threshold, T . The scales are logarithmic in order to show several decades of FMR.

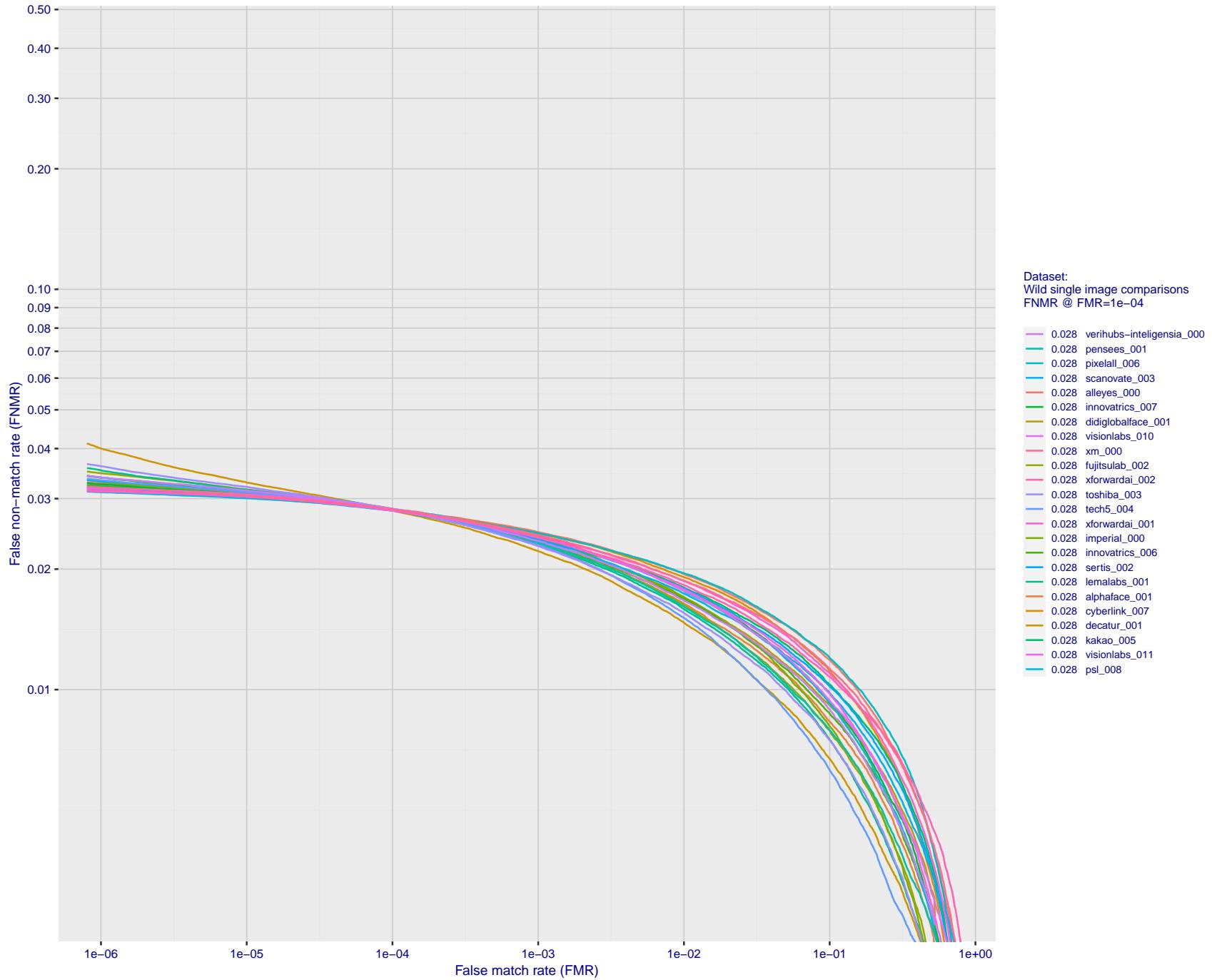


Figure 79: For the 2018 wild image comparisons, detection error tradeoff (DET) characteristics showing false non-match rate vs. false match rate plotted parametrically on threshold, T . The scales are logarithmic in order to show several decades of FMR.

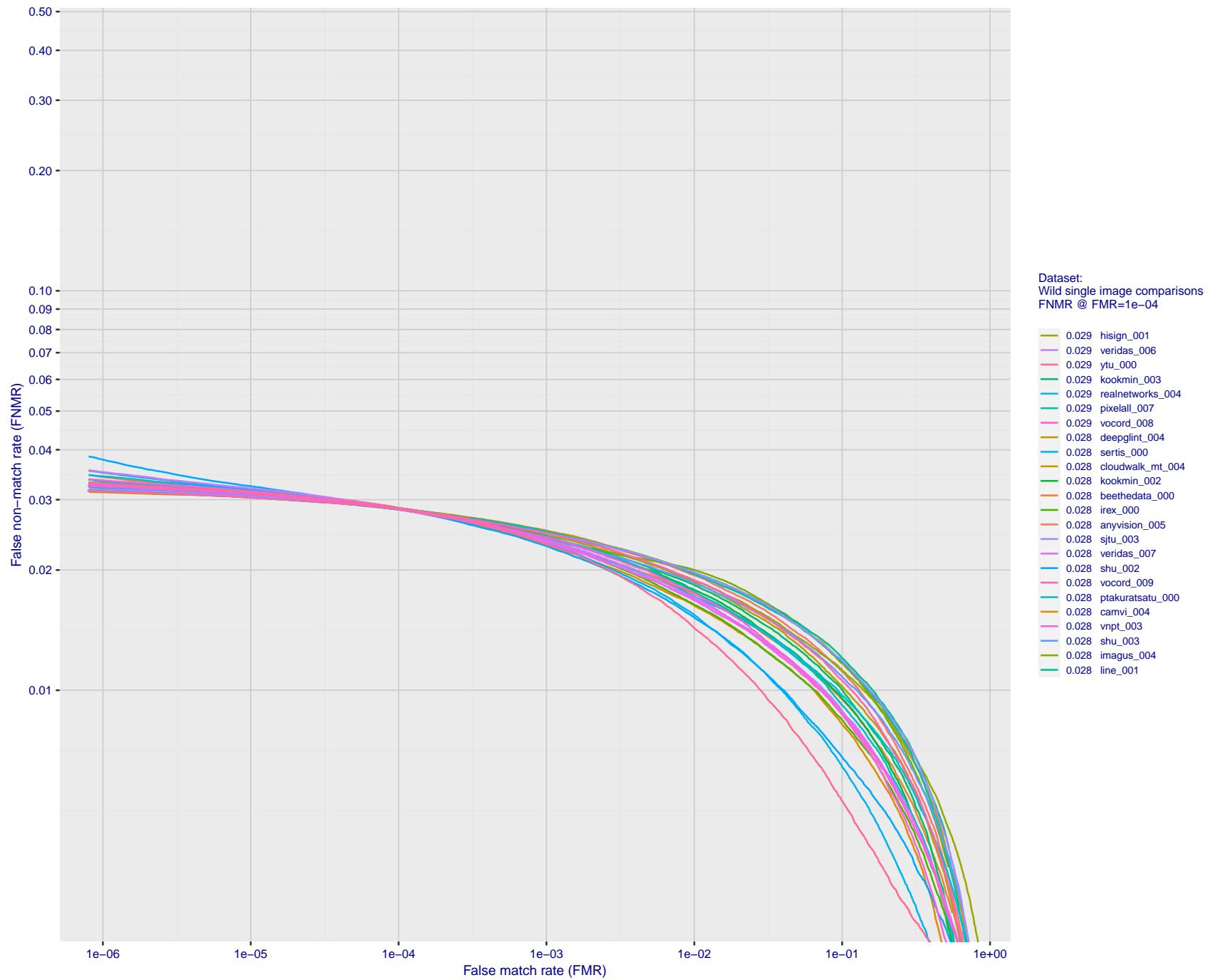


Figure 80: For the 2018 wild image comparisons, detection error tradeoff (DET) characteristics showing false non-match rate vs. false match rate plotted parametrically on threshold, T . The scales are logarithmic in order to show several decades of FMR.

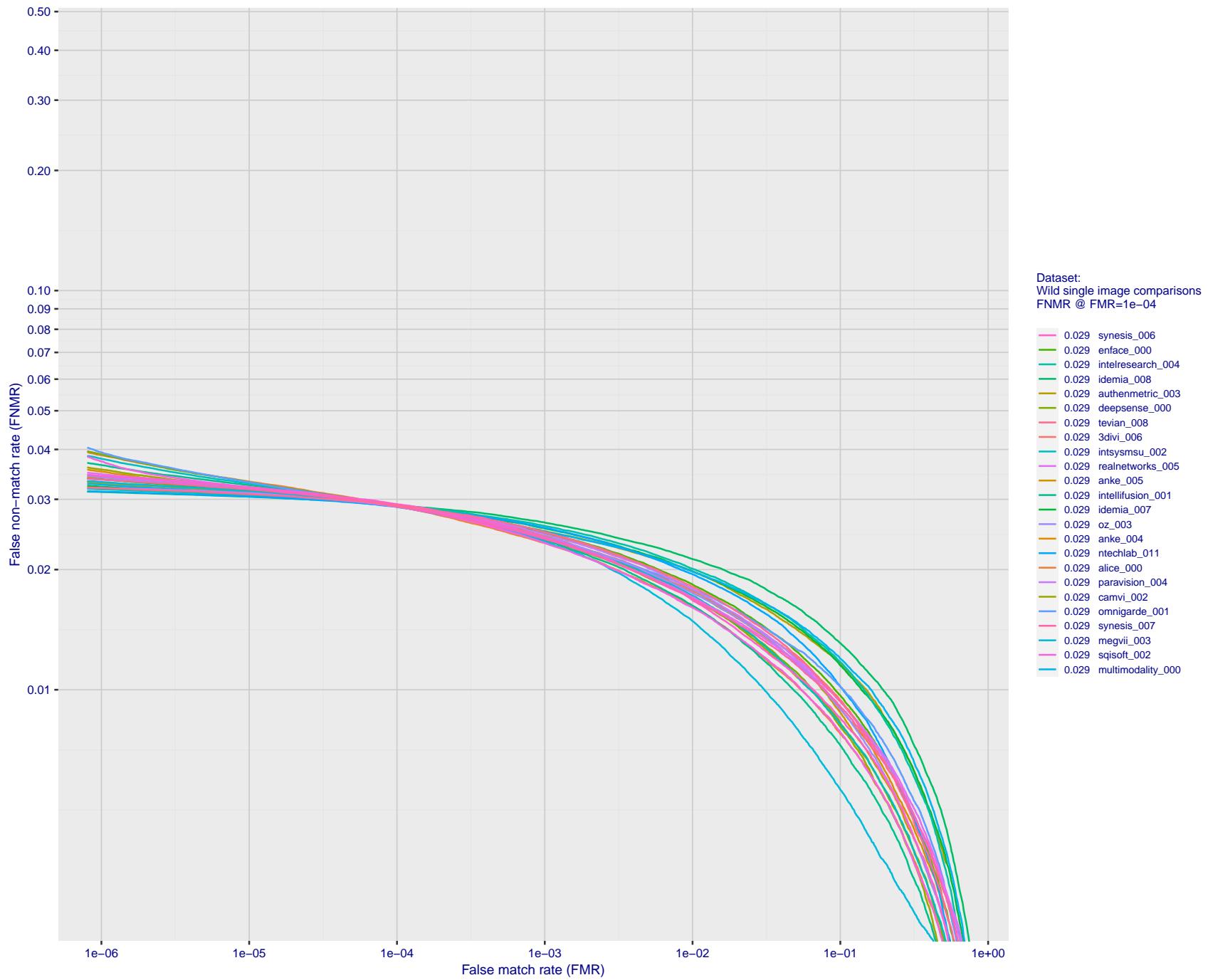


Figure 81: For the 2018 wild image comparisons, detection error tradeoff (DET) characteristics showing false non-match rate vs. false match rate plotted parametrically on threshold, T . The scales are logarithmic in order to show several decades of FMR.

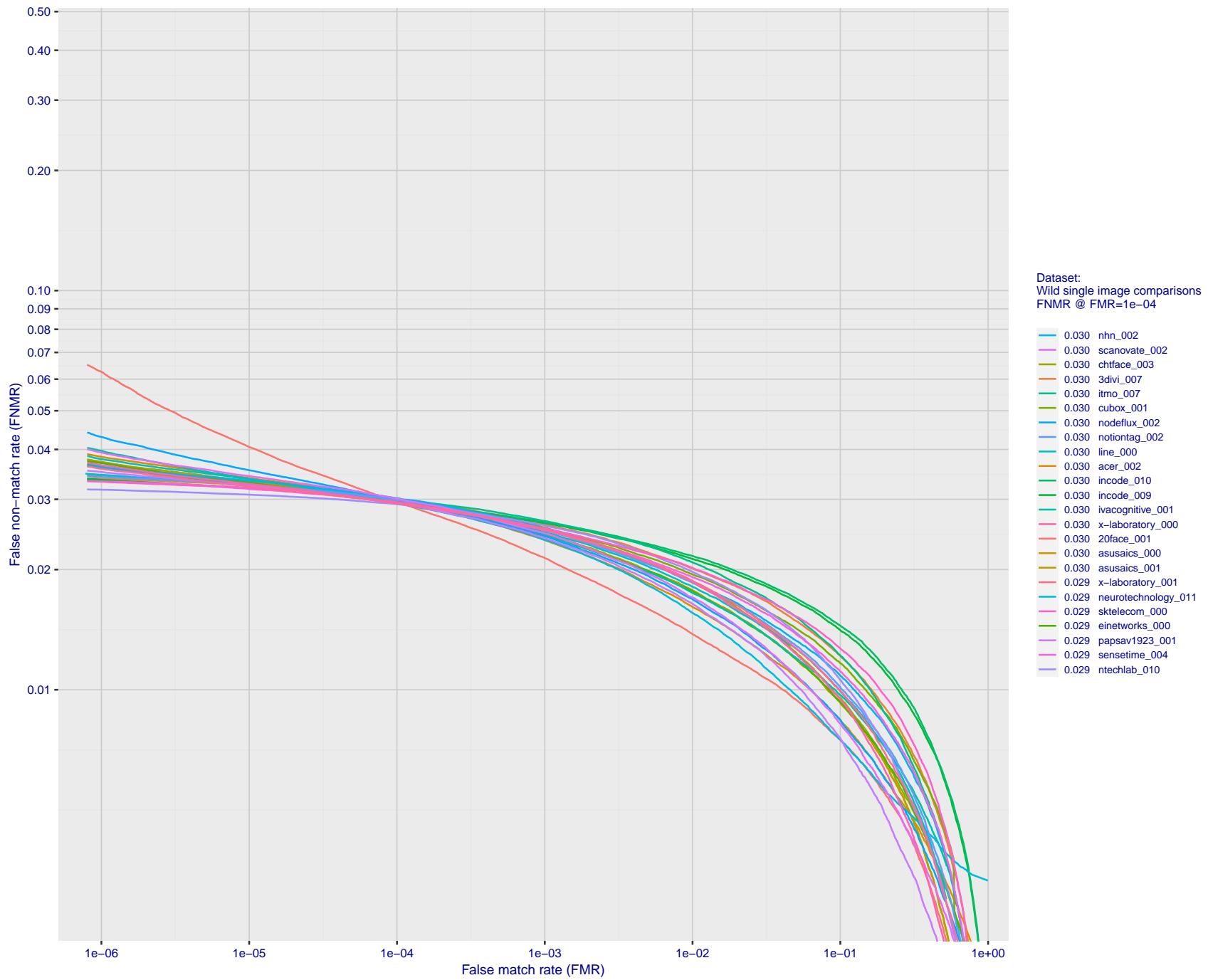


Figure 82: For the 2018 wild image comparisons, detection error tradeoff (DET) characteristics showing false non-match rate vs. false match rate plotted parametrically on threshold, T. The scales are logarithmic in order to show several decades of FMR.

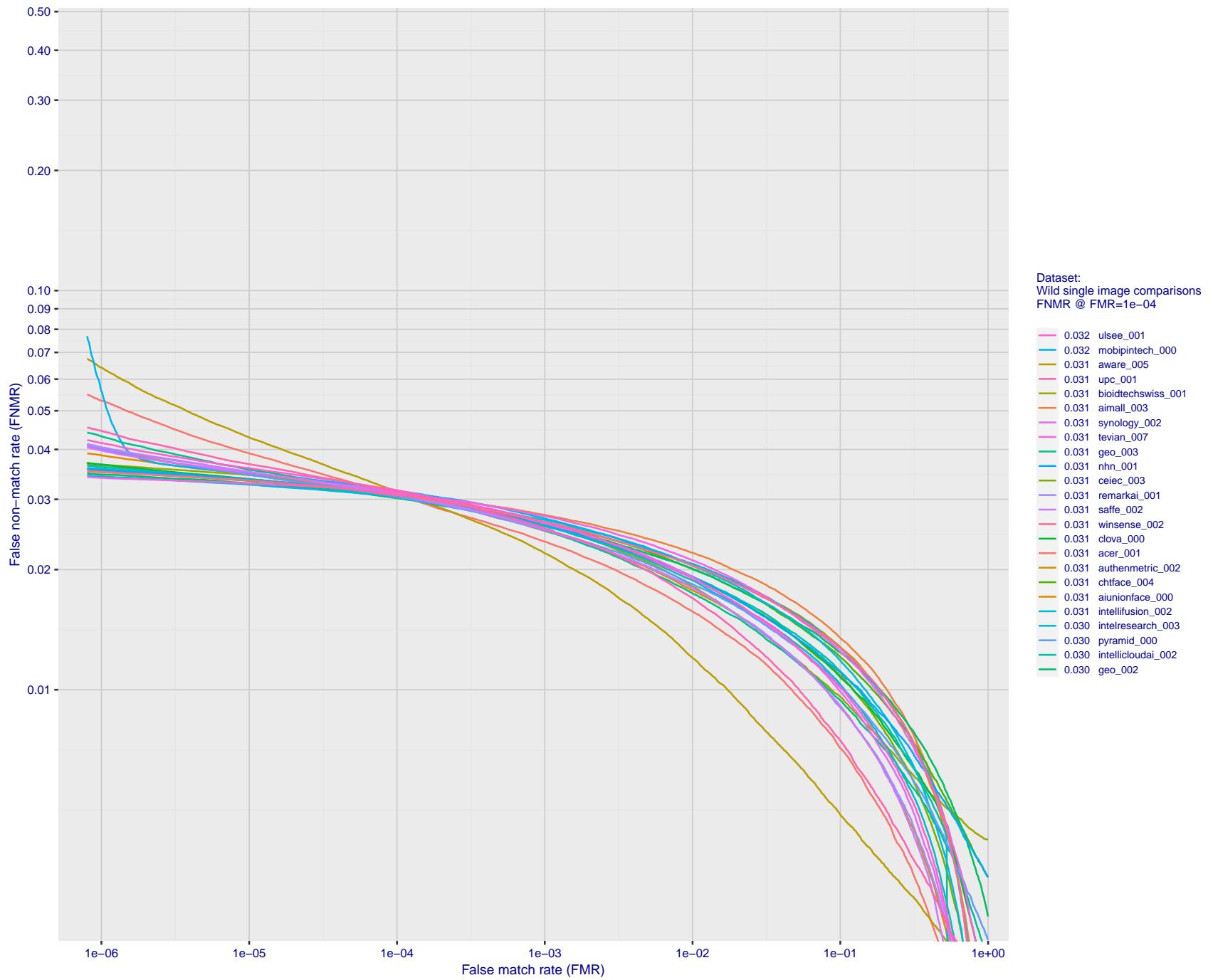


Figure 83: For the 2018 wild image comparisons, detection error tradeoff (DET) characteristics showing false non-match rate vs. false match rate plotted parametrically on threshold, T . The scales are logarithmic in order to show several decades of FMR.

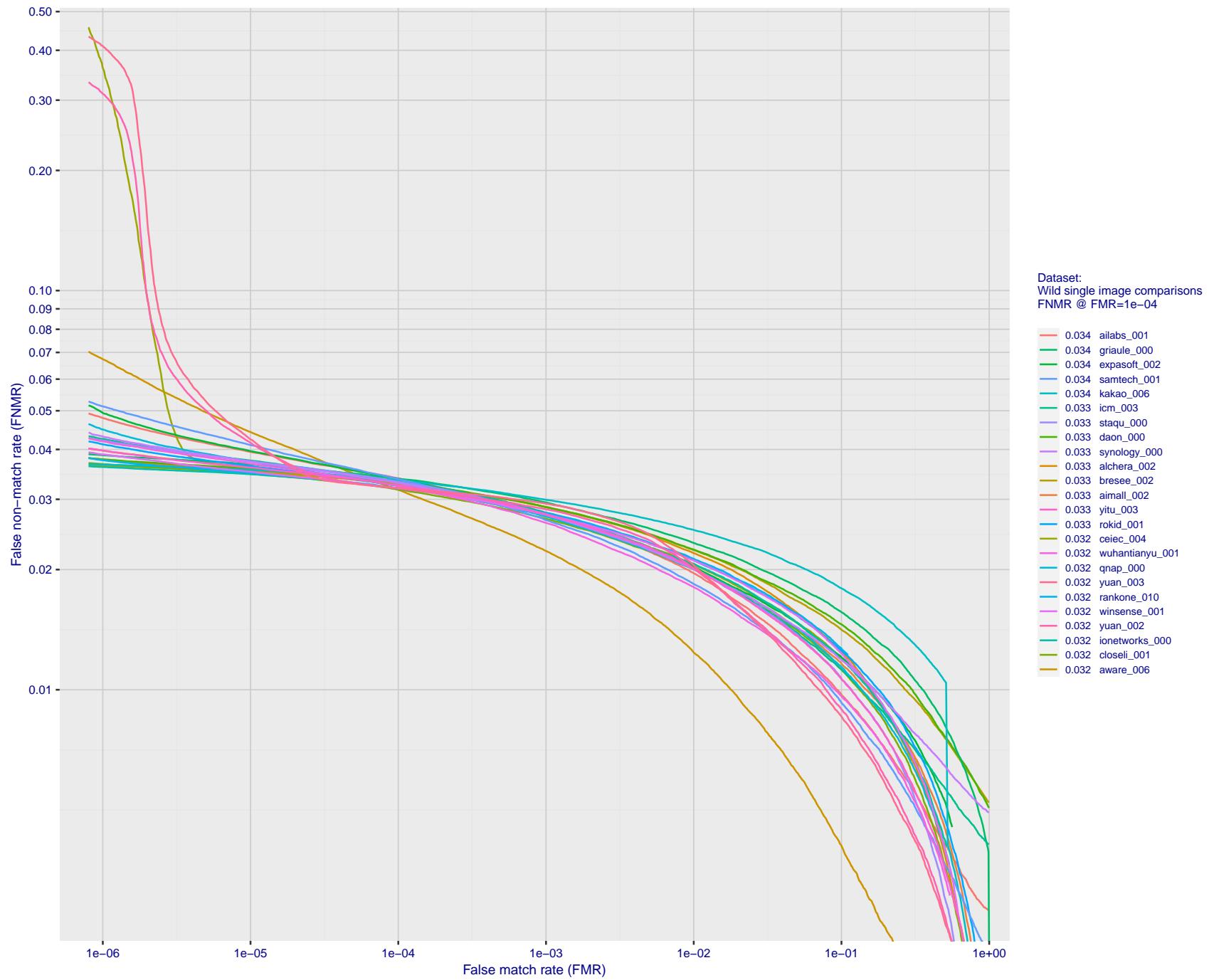


Figure 84: For the 2018 wild image comparisons, detection error tradeoff (DET) characteristics showing false non-match rate vs. false match rate plotted parametrically on threshold, T. The scales are logarithmic in order to show several decades of FMR.

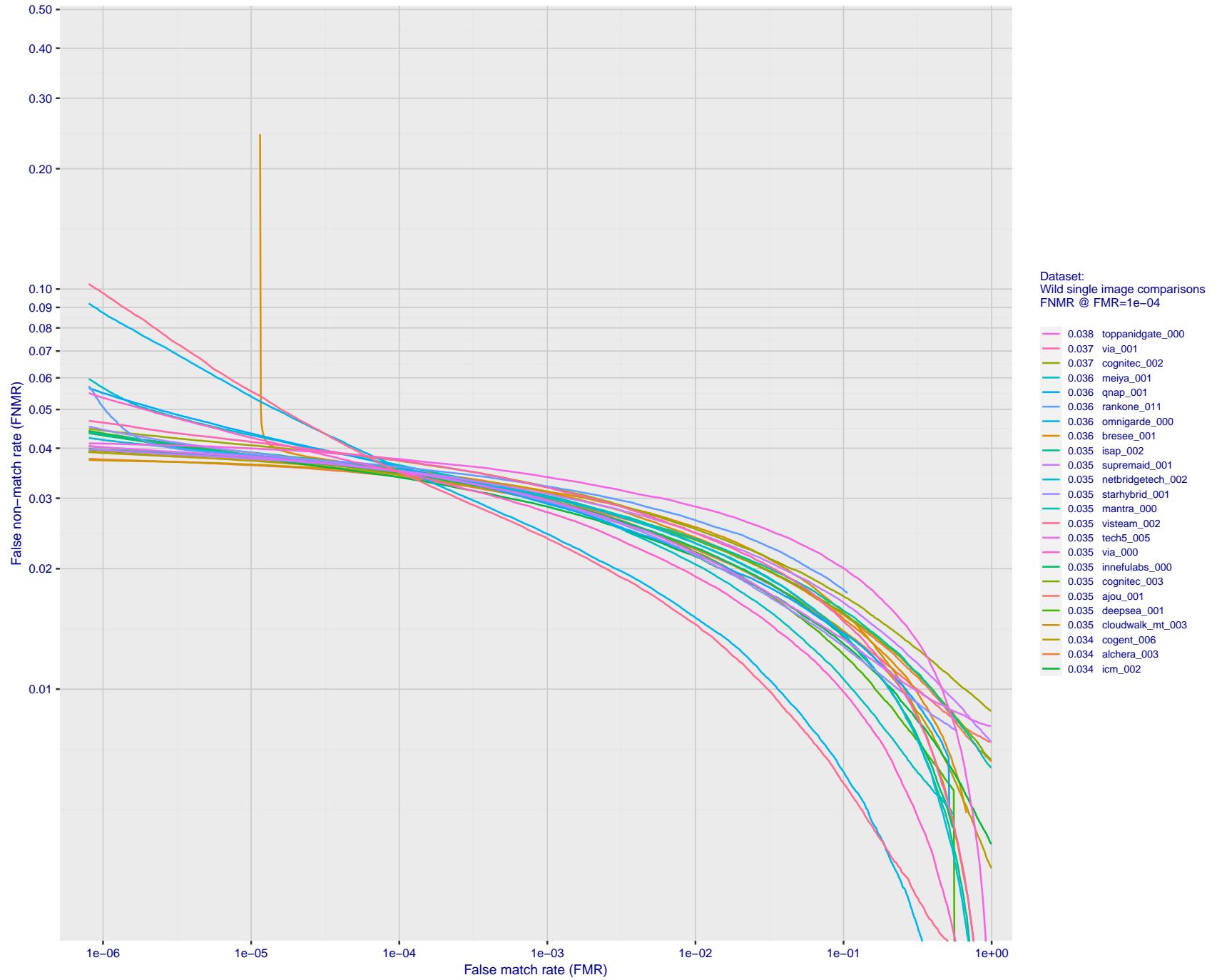


Figure 85: For the 2018 wild image comparisons, detection error tradeoff (DET) characteristics showing false non-match rate vs. false match rate plotted parametrically on threshold, T. The scales are logarithmic in order to show several decades of FMR.

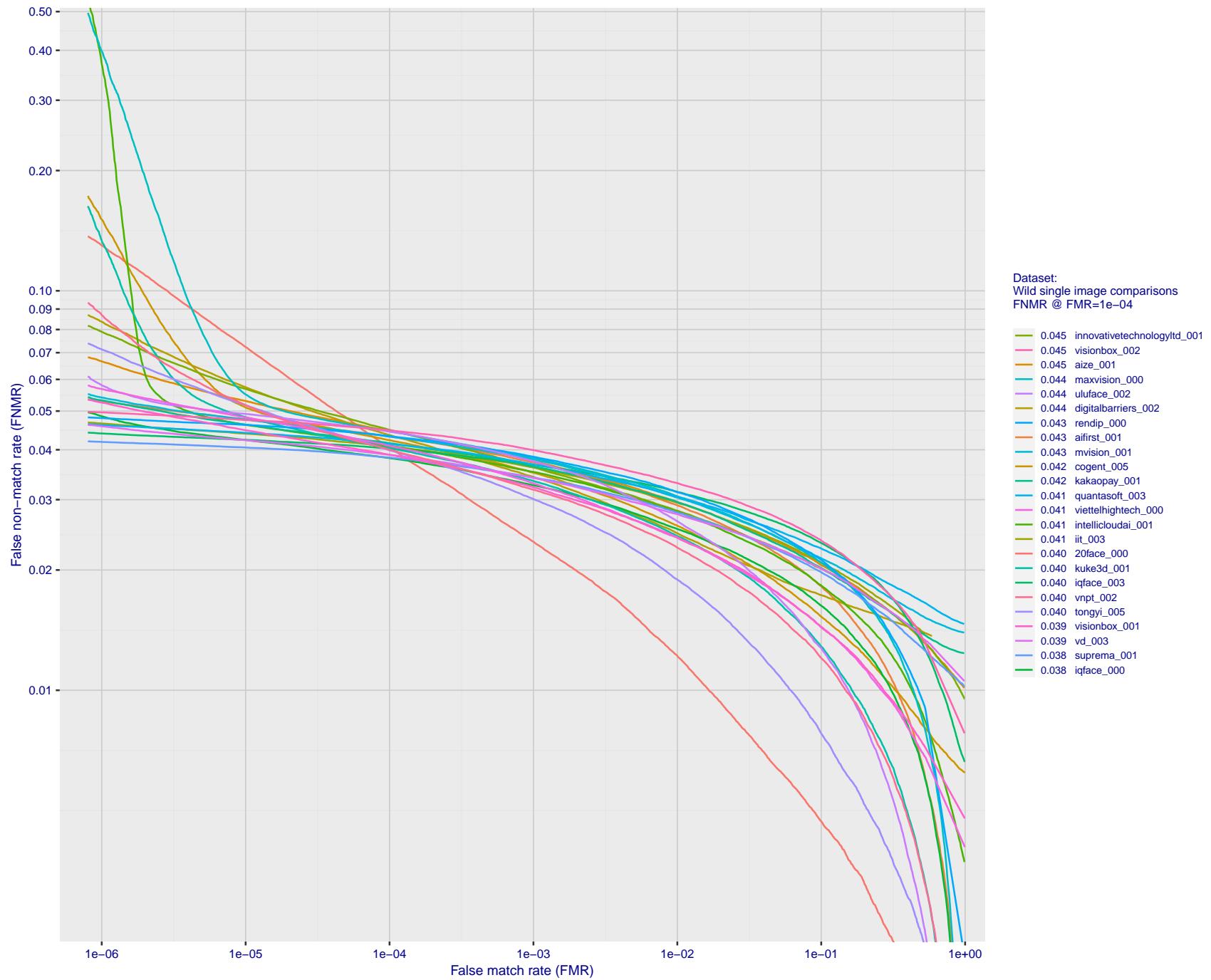


Figure 86: For the 2018 wild image comparisons, detection error tradeoff (DET) characteristics showing false non-match rate vs. false match rate plotted parametrically on threshold, T . The scales are logarithmic in order to show several decades of FMR.

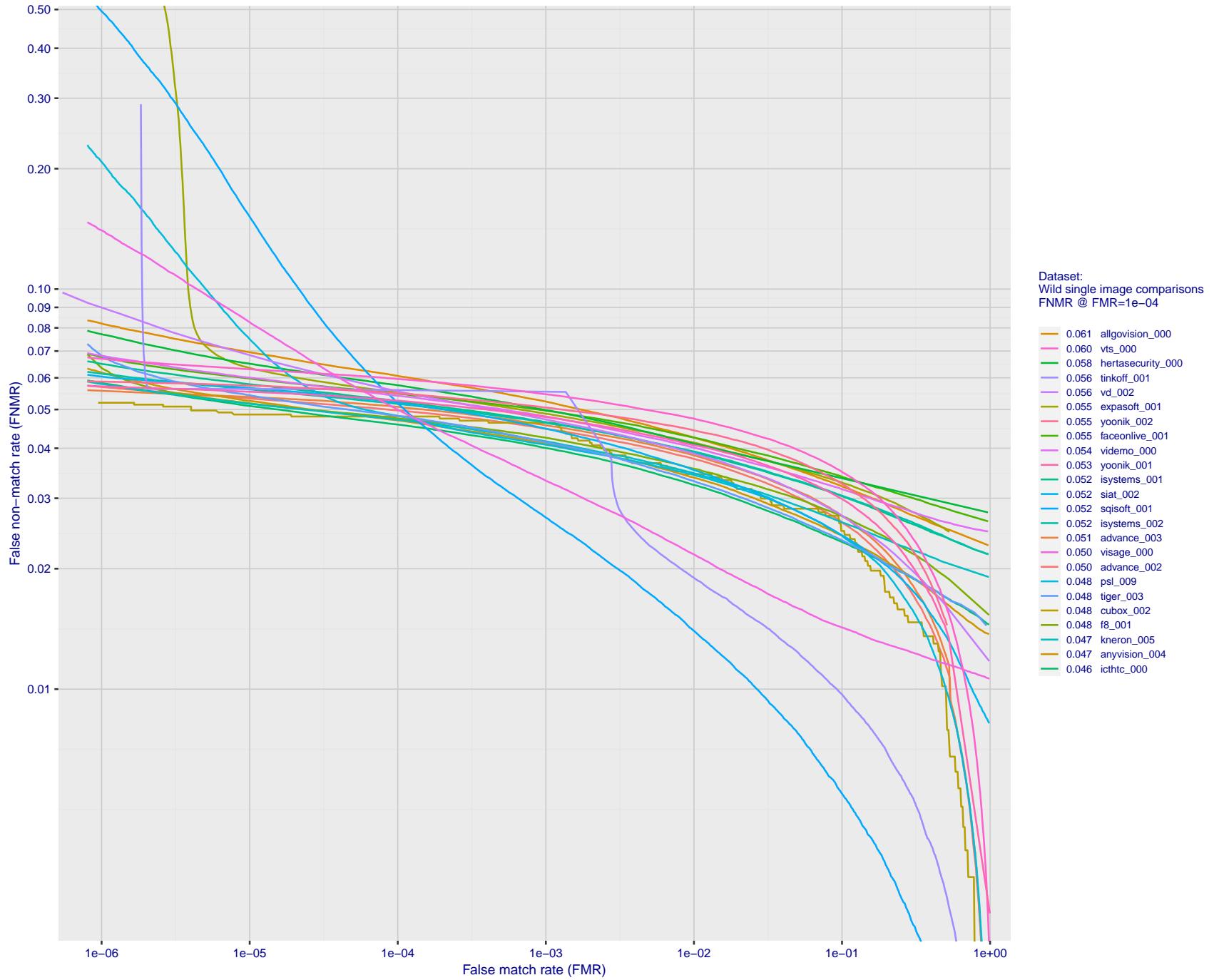


Figure 87: For the 2018 wild image comparisons, detection error tradeoff (DET) characteristics showing false non-match rate vs. false match rate plotted parametrically on threshold, T . The scales are logarithmic in order to show several decades of FMR.

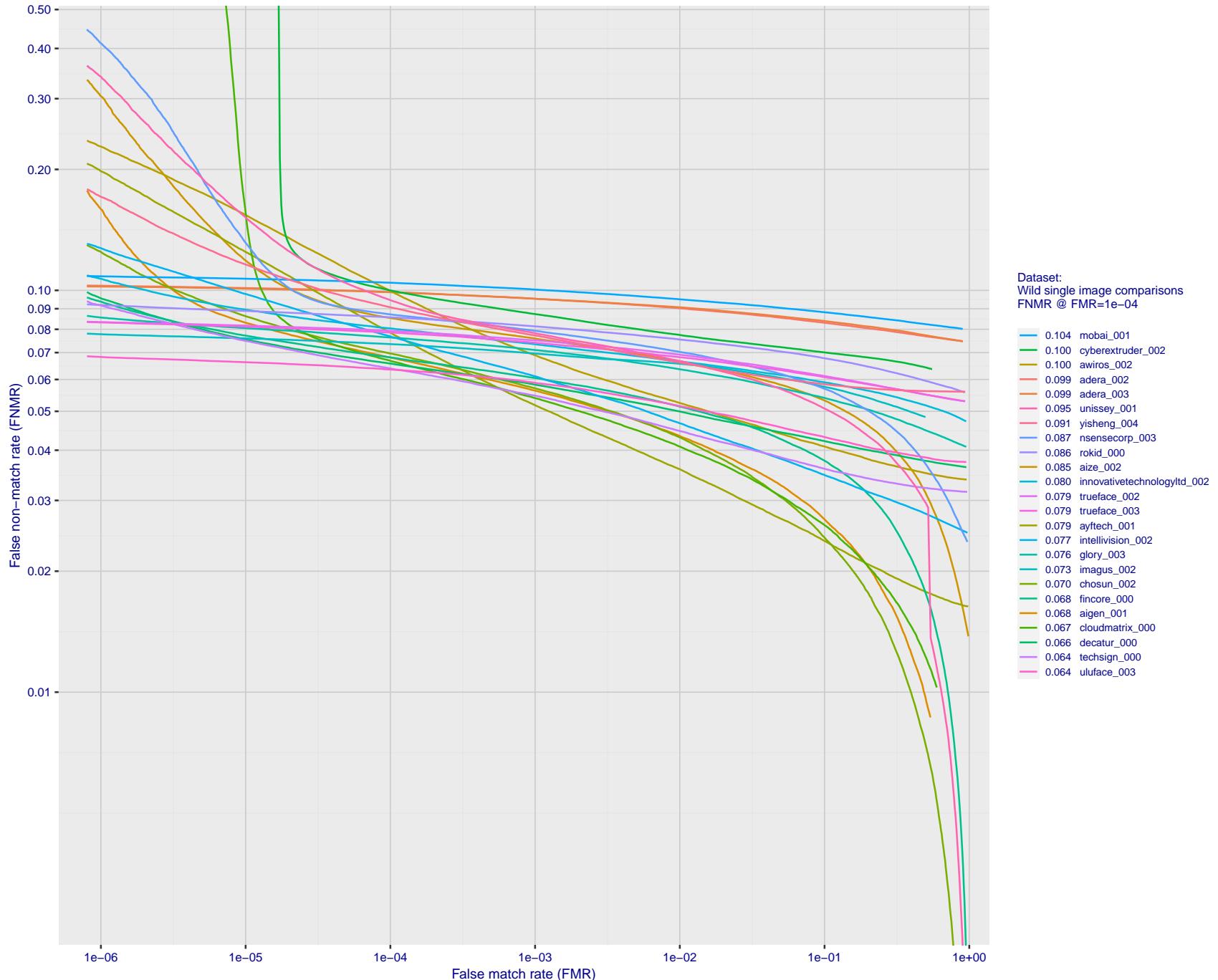
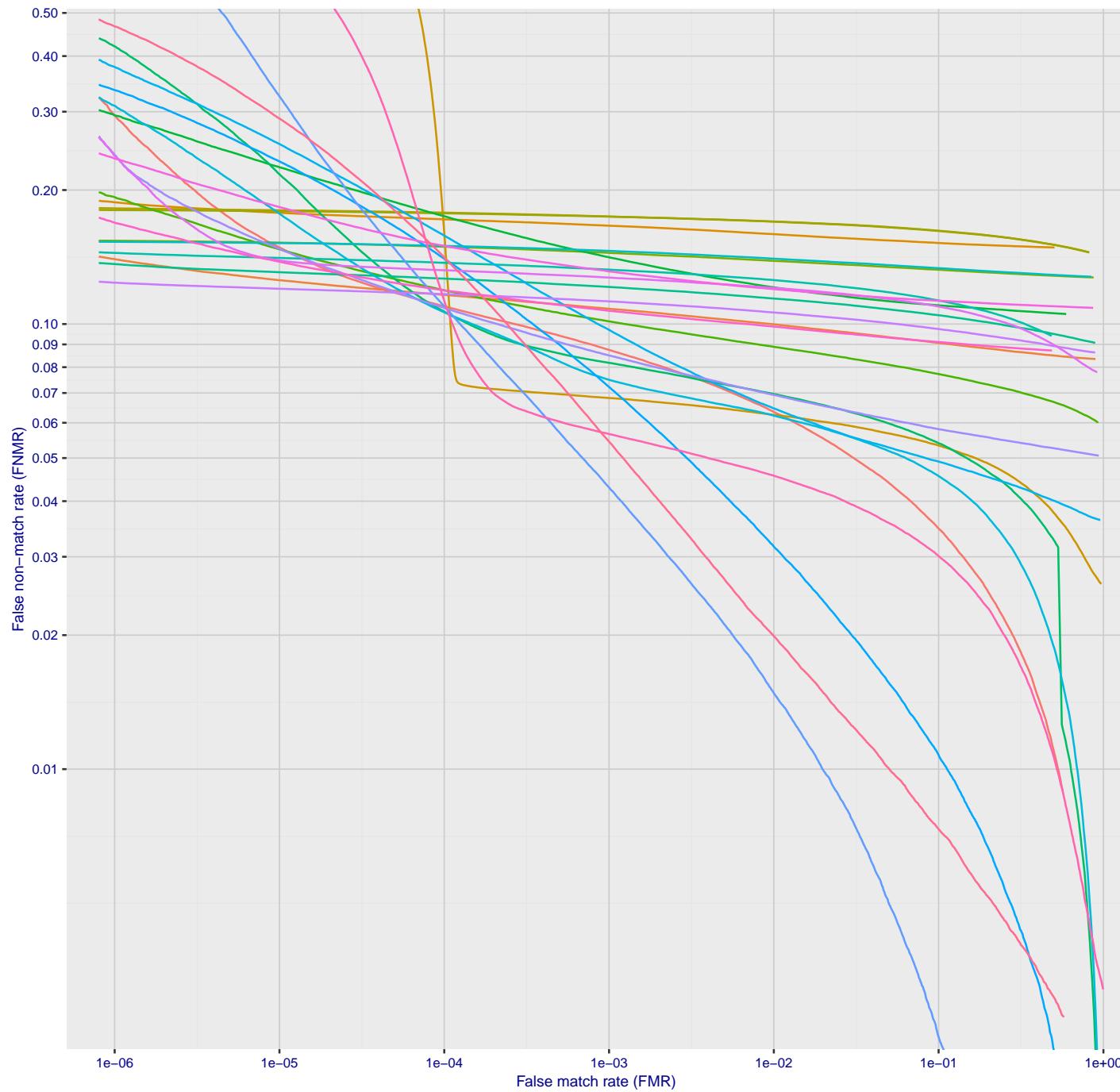


Figure 88: For the 2018 wild image comparisons, detection error tradeoff (DET) characteristics showing false non-match rate vs. false match rate plotted parametrically on threshold, T . The scales are logarithmic in order to show several decades of FMR.

2021/12/16 10:32:53

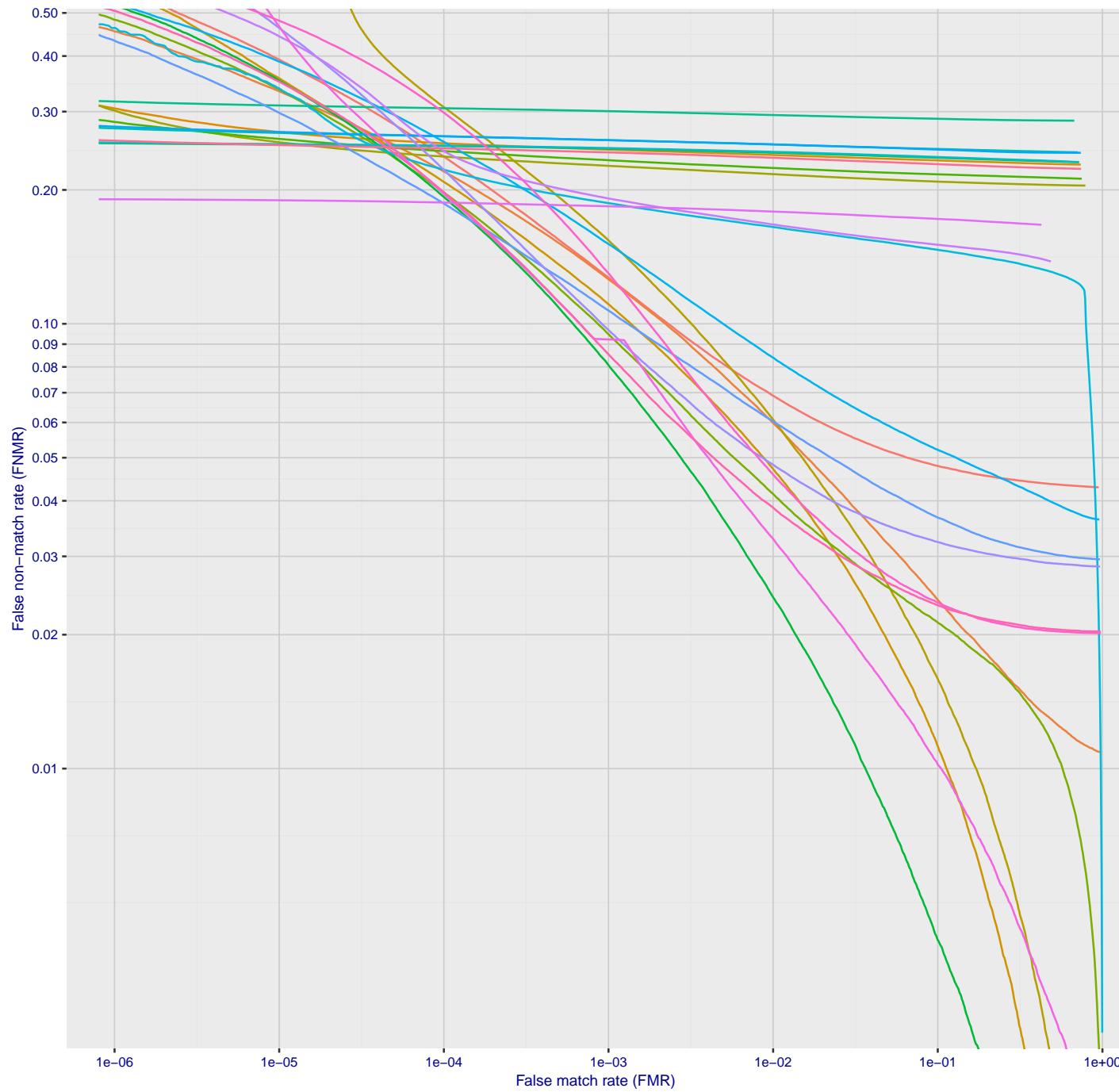


Dataset:
Wild single image comparisons
FNMR @ FMR=1e-04

0.178	csc_002
0.177	csc_003
0.175	cyberextruder_001
0.172	boetech_001
0.163	cloudwalk_hr_004
0.158	microfocus_002
0.150	itmo_008
0.149	cuhkee_001
0.141	visteam_001
0.140	neosystems_003
0.137	it_002
0.132	s1_003
0.127	glory_002
0.119	cybercore_000
0.119	smilart_003
0.117	s1_002
0.116	androvideo_000
0.113	suprema_000
0.110	netbridgeTech_001
0.110	aigen_002
0.109	pxl_001
0.107	dps_000
0.106	meituan_000

Figure 89: For the 2018 wild image comparisons, detection error tradeoff (DET) characteristics showing false non-match rate vs. false match rate plotted parametrically on threshold, T. The scales are logarithmic in order to show several decades of FMR.

2021/12/16 10:32:53

FNMR(T)
"False non-match rate"
"False match rate"Figure 90: For the 2018 wild image comparisons, detection error tradeoff (DET) characteristics showing false non-match rate vs. false match rate plotted parametrically on threshold, T . The scales are logarithmic in order to show several decades of FMR.

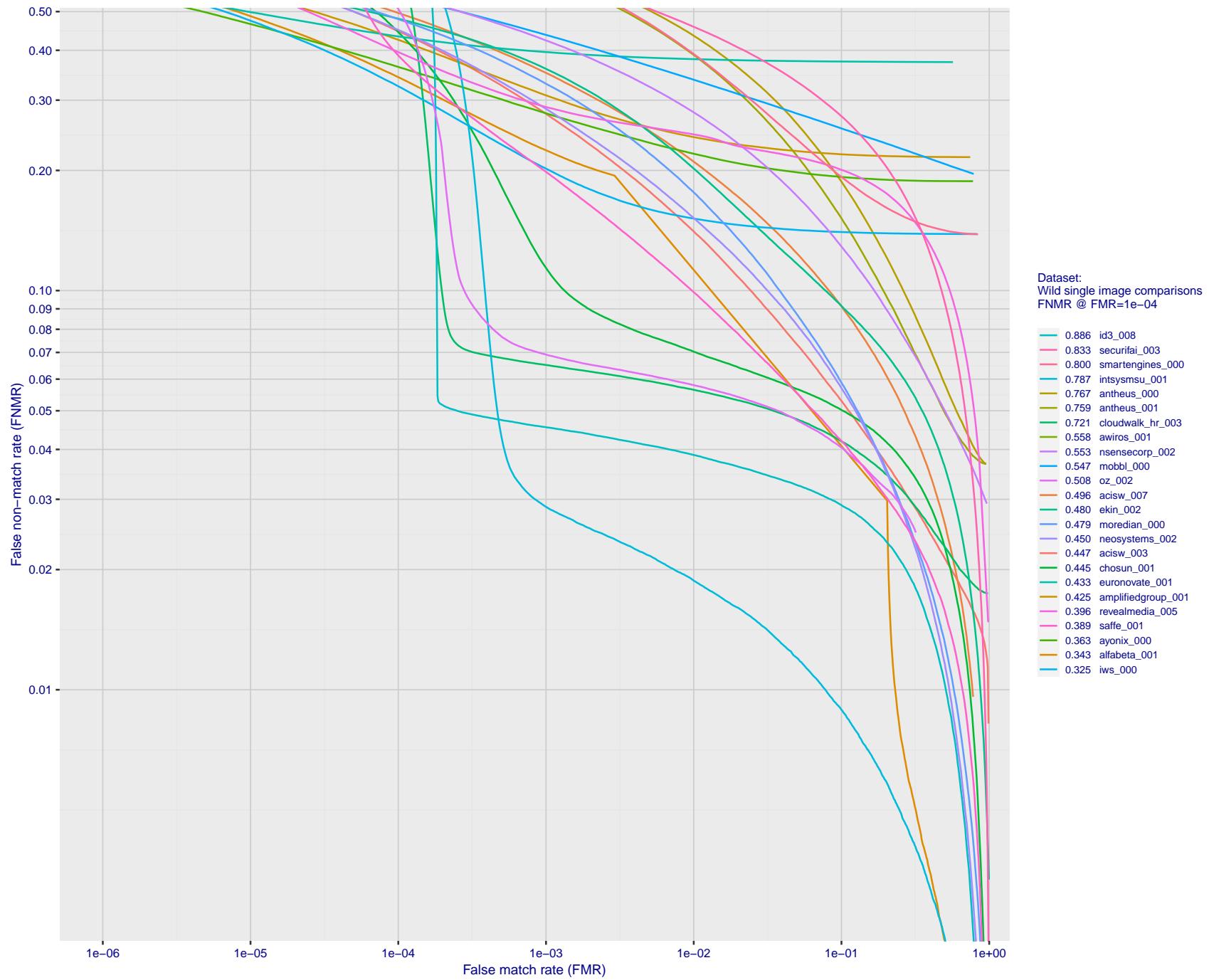


Figure 91: For the 2018 wild image comparisons, detection error tradeoff (DET) characteristics showing false non-match rate vs. false match rate plotted parametrically on threshold, T. The scales are logarithmic in order to show several decades of FMR.

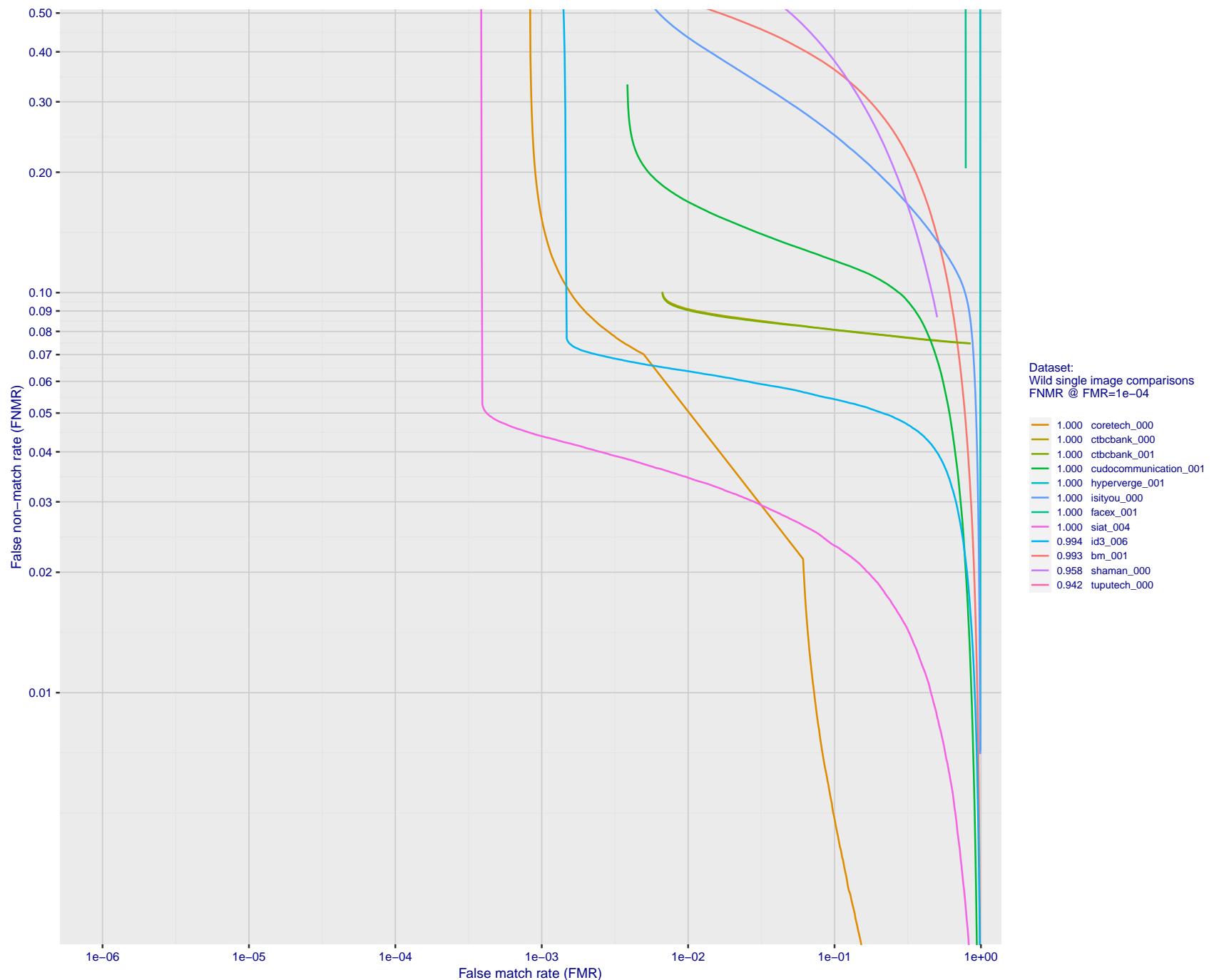


Figure 92: For the 2018 wild image comparisons, detection error tradeoff (DET) characteristics showing false non-match rate vs. false match rate plotted parametrically on threshold, T . The scales are logarithmic in order to show several decades of FMR.

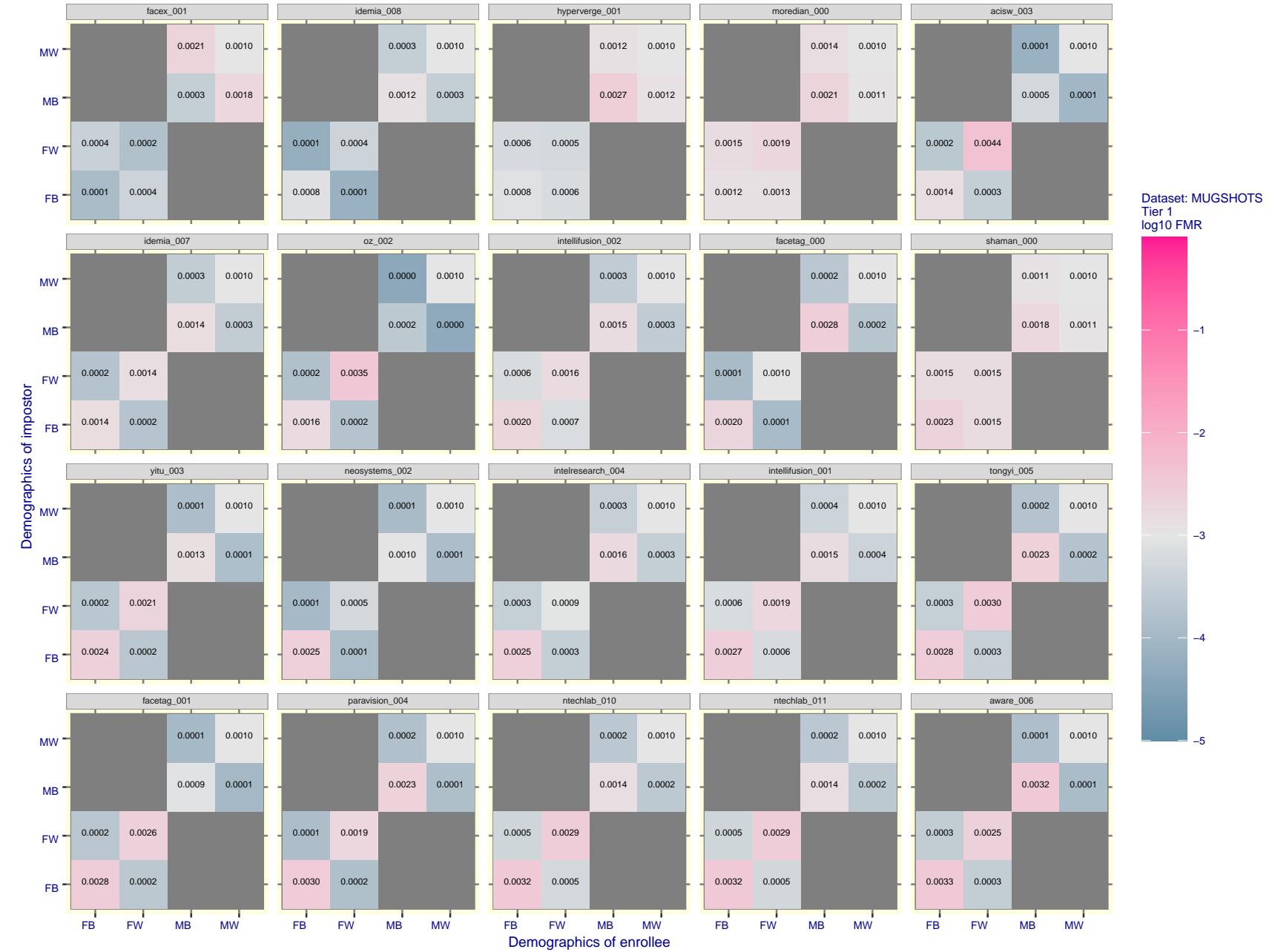


Figure 93: For the mugshot images, FMR for same-sex impostor pairs of images annotated with codes for black female, black male, white female, white male. The threshold is set for each algorithm to give FMR = 0.001 for white males which is the demographic that usually gives the lowest FMR. This means the top right box is the same color in all panels. The panels are sorted over multiple pages in order of FMR on black females, which is the demographic that usually gives the highest FMR.

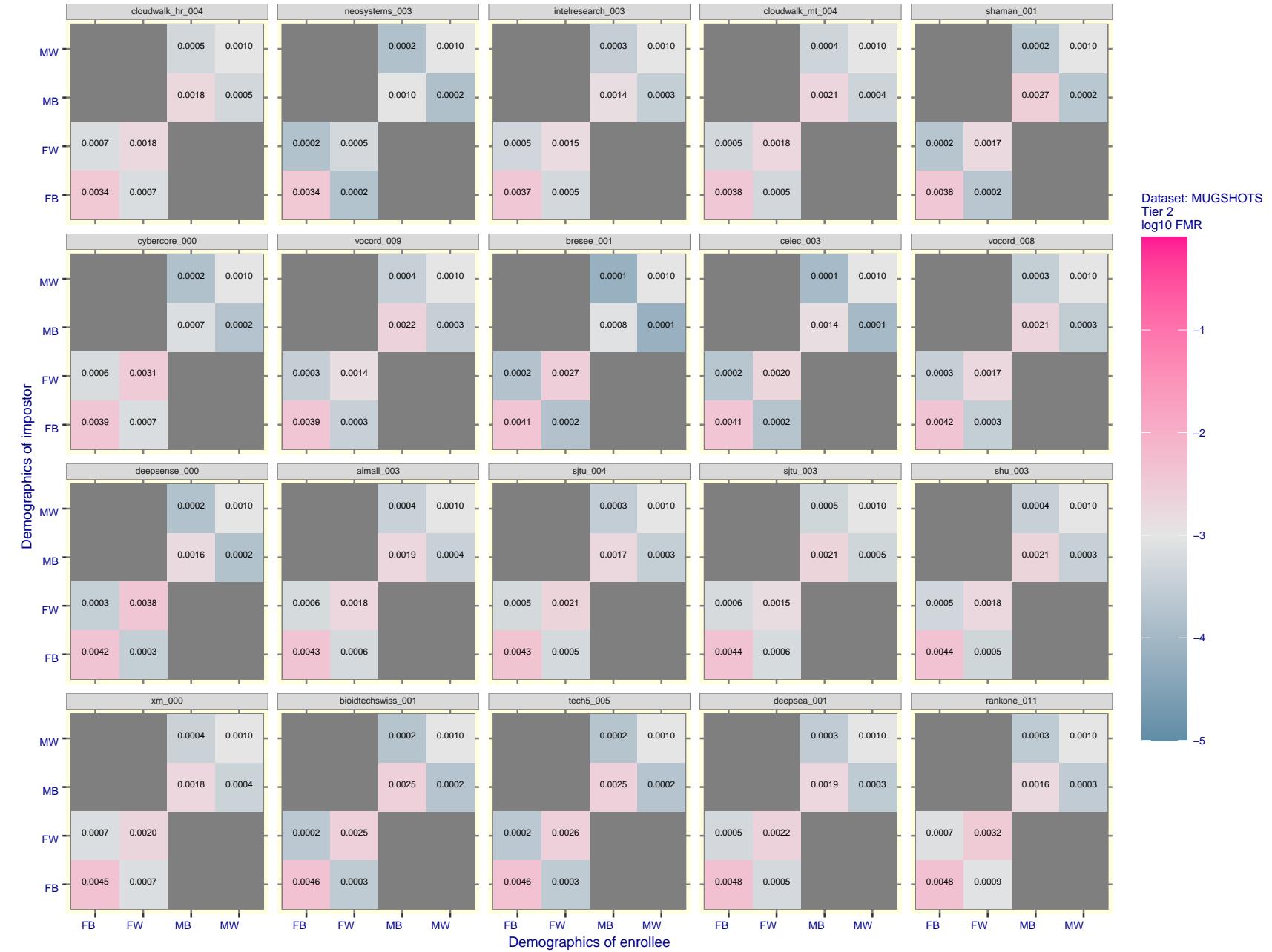


Figure 94: For the mugshot images, FMR for same-sex impostor pairs of images annotated with codes for black female, black male, white female, white male. The threshold is set for each algorithm to give $\text{FMR} = 0.001$ for white males which is the demographic that usually gives the lowest FMR. This means the top right box is the same color in all panels. The panels are sorted over multiple pages in order of FMR on black females, which is the demographic that usually gives the highest FMR.

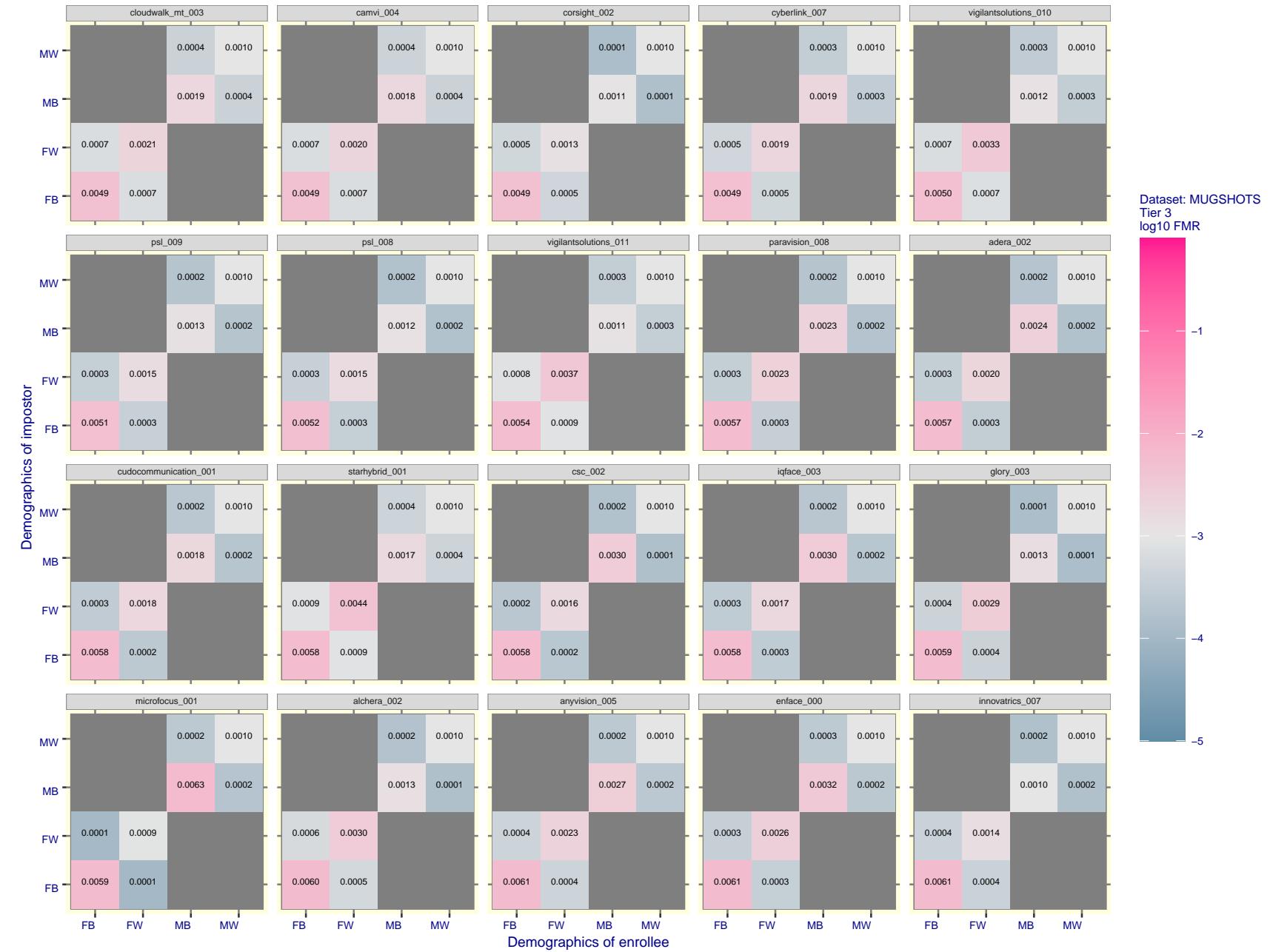


Figure 95: For the mugshot images, FMR for same-sex impostor pairs of images annotated with codes for black female, black male, white female, white male. The threshold is set for each algorithm to give $FMR = 0.001$ for white males which is the demographic that usually gives the lowest FMR. This means the top right box is the same color in all panels. The panels are sorted over multiple pages in order of FMR on black females, which is the demographic that usually gives the highest FMR.

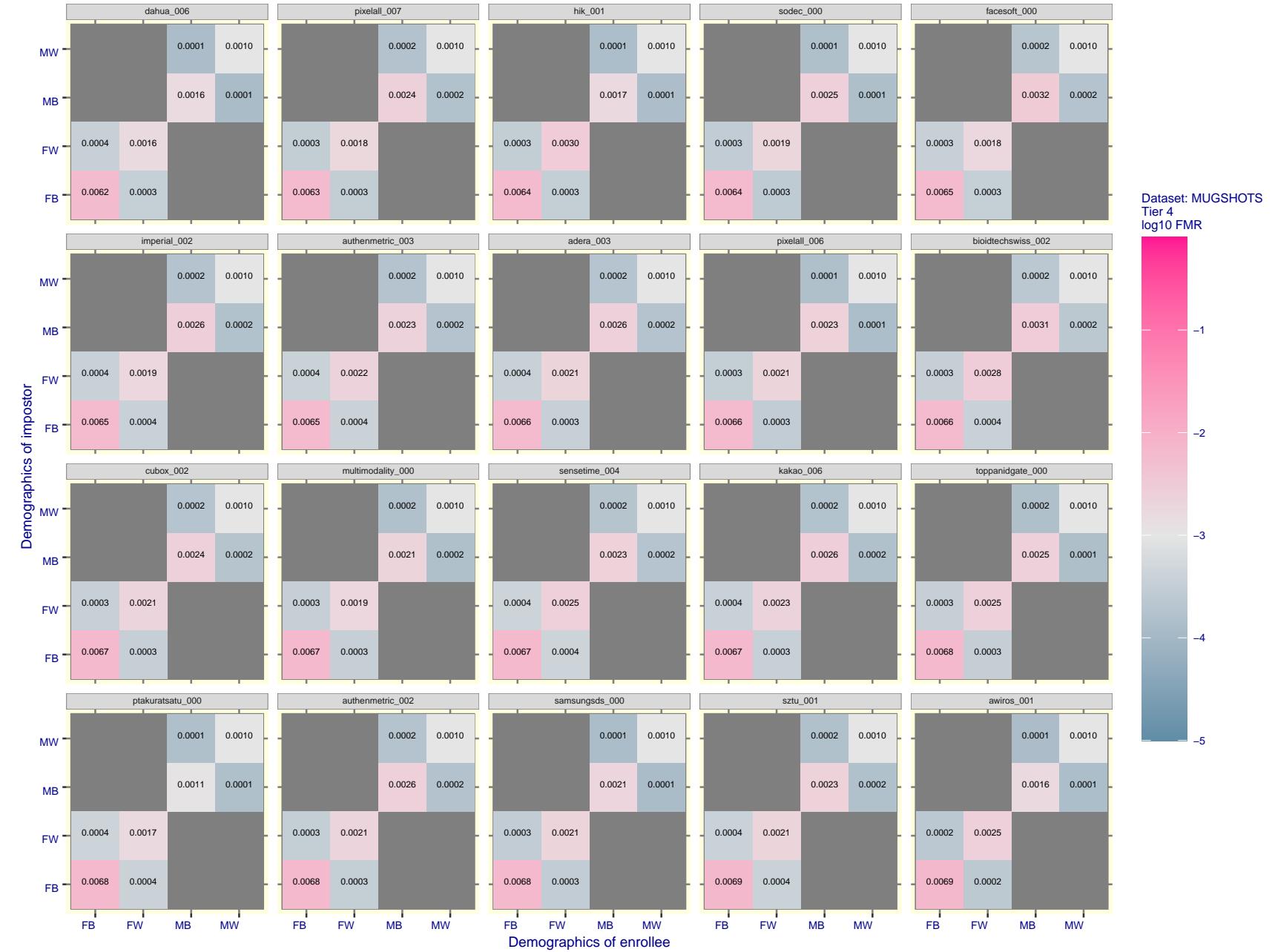


Figure 96: For the mugshot images, FMR for same-sex impostor pairs of images annotated with codes for black female, black male, white female, white male. The threshold is set for each algorithm to give $FMR = 0.001$ for white males which is the demographic that usually gives the lowest FMR. This means the top right box is the same color in all panels. The panels are sorted over multiple pages in order of FMR on black females, which is the demographic that usually gives the highest FMR.

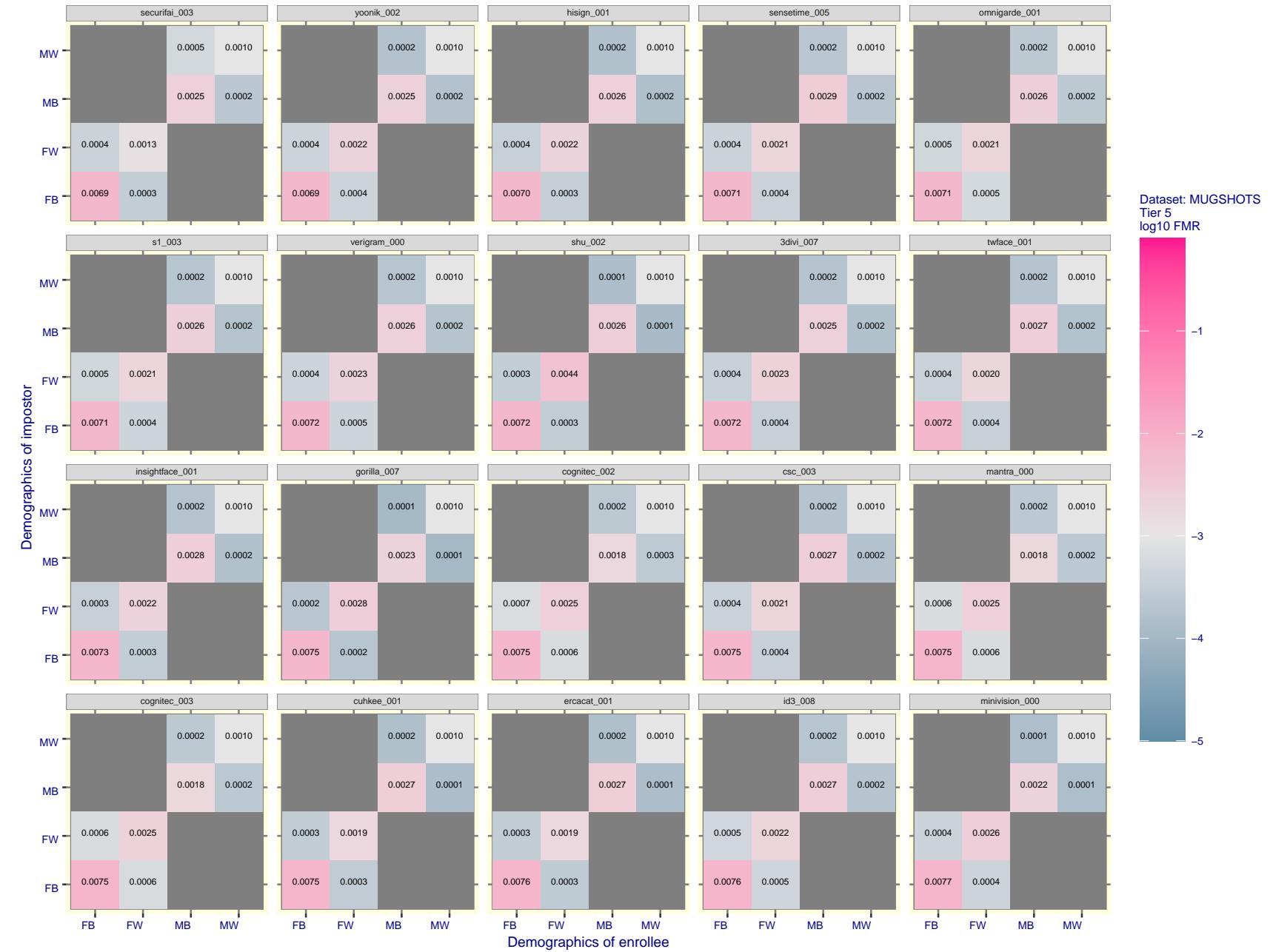


Figure 97: For the mugshot images, FMR for same-sex impostor pairs of images annotated with codes for black female, black male, white female, white male. The threshold is set for each algorithm to give FMR = 0.001 for white males which is the demographic that usually gives the lowest FMR. This means the top right box is the same color in all panels. The panels are sorted over multiple pages in order of FMR on black females, which is the demographic that usually gives the highest FMR.

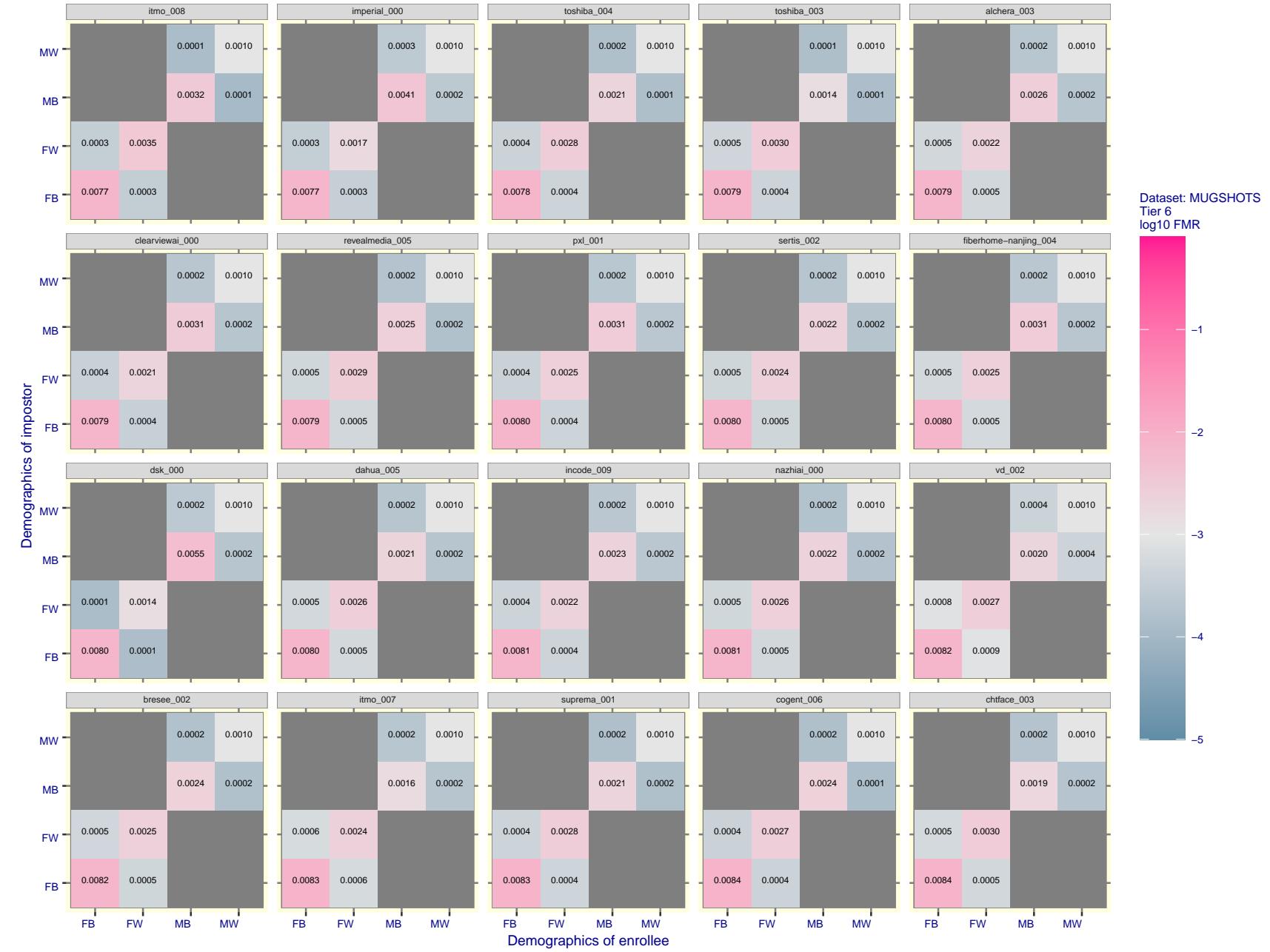


Figure 98: For the mugshot images, FMR for same-sex impostor pairs of images annotated with codes for black female, black male, white female, white male. The threshold is set for each algorithm to give $\text{FMR} = 0.001$ for white males which is the demographic that usually gives the lowest FMR. This means the top right box is the same color in all panels. The panels are sorted over multiple pages in order of FMR on black females, which is the demographic that usually gives the highest FMR.

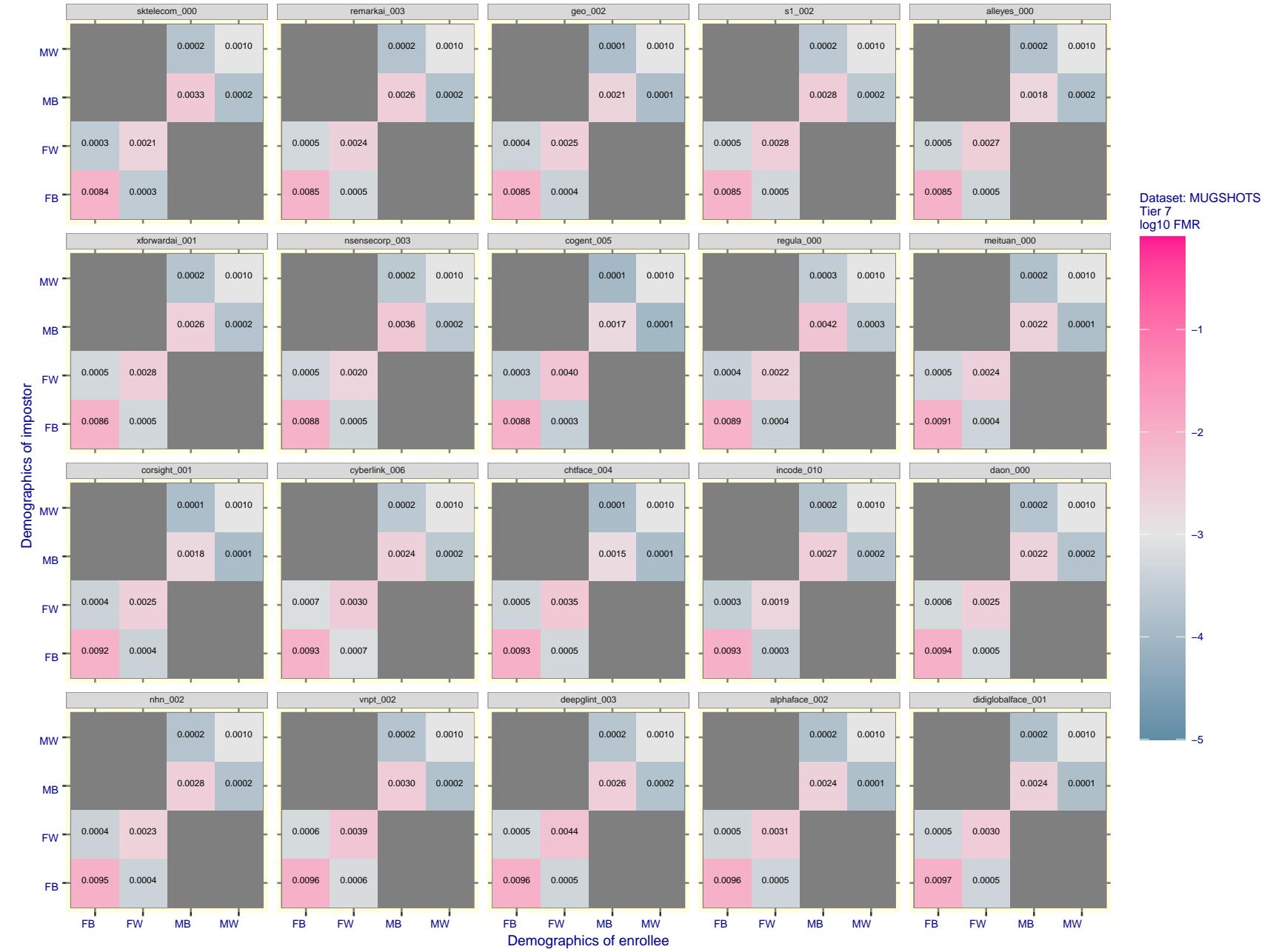


Figure 99: For the mugshot images, FMR for same-sex impostor pairs of images annotated with codes for black female, black male, white female, white male. The threshold is set for each algorithm to give $FMR = 0.001$ for white males which is the demographic that usually gives the lowest FMR. This means the top right box is the same color in all panels. The panels are sorted over multiple pages in order of FMR on black females, which is the demographic that usually gives the highest FMR.

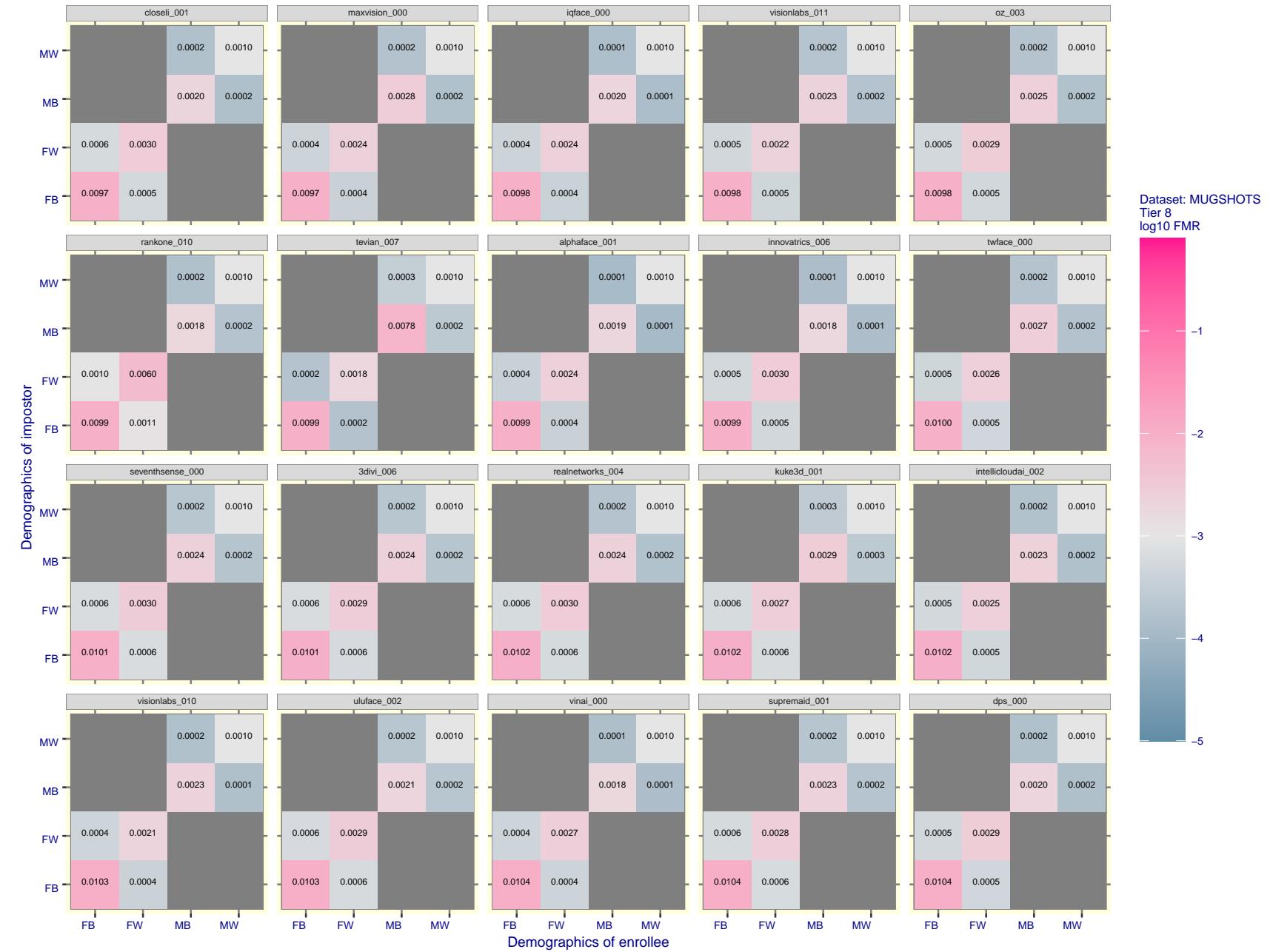


Figure 100: For the mugshot images, FMR for same-sex impostor pairs of images annotated with codes for black female, black male, white female, white male. The threshold is set for each algorithm to give FMR = 0.001 for white males which is the demographic that usually gives the lowest FMR. This means the top right box is the same color in all panels. The panels are sorted over multiple pages in order of FMR on black females, which is the demographic that usually gives the highest FMR.

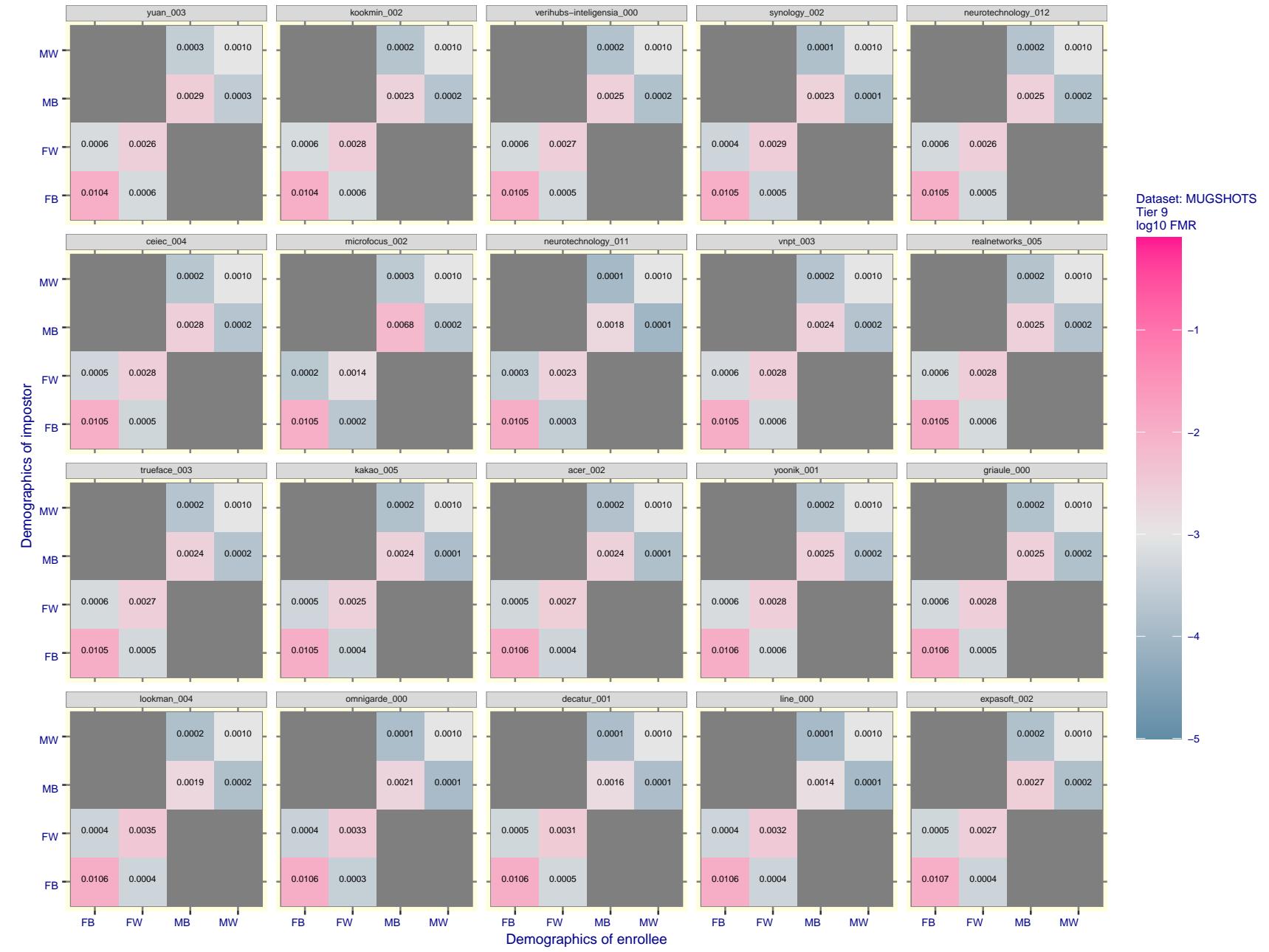


Figure 101: For the mugshot images, FMR for same-sex impostor pairs of images annotated with codes for black female, black male, white female, white male. The threshold is set for each algorithm to give $FMR = 0.001$ for white males which is the demographic that usually gives the lowest FMR. This means the top right box is the same color in all panels. The panels are sorted over multiple pages in order of FMR on black females, which is the demographic that usually gives the highest FMR.

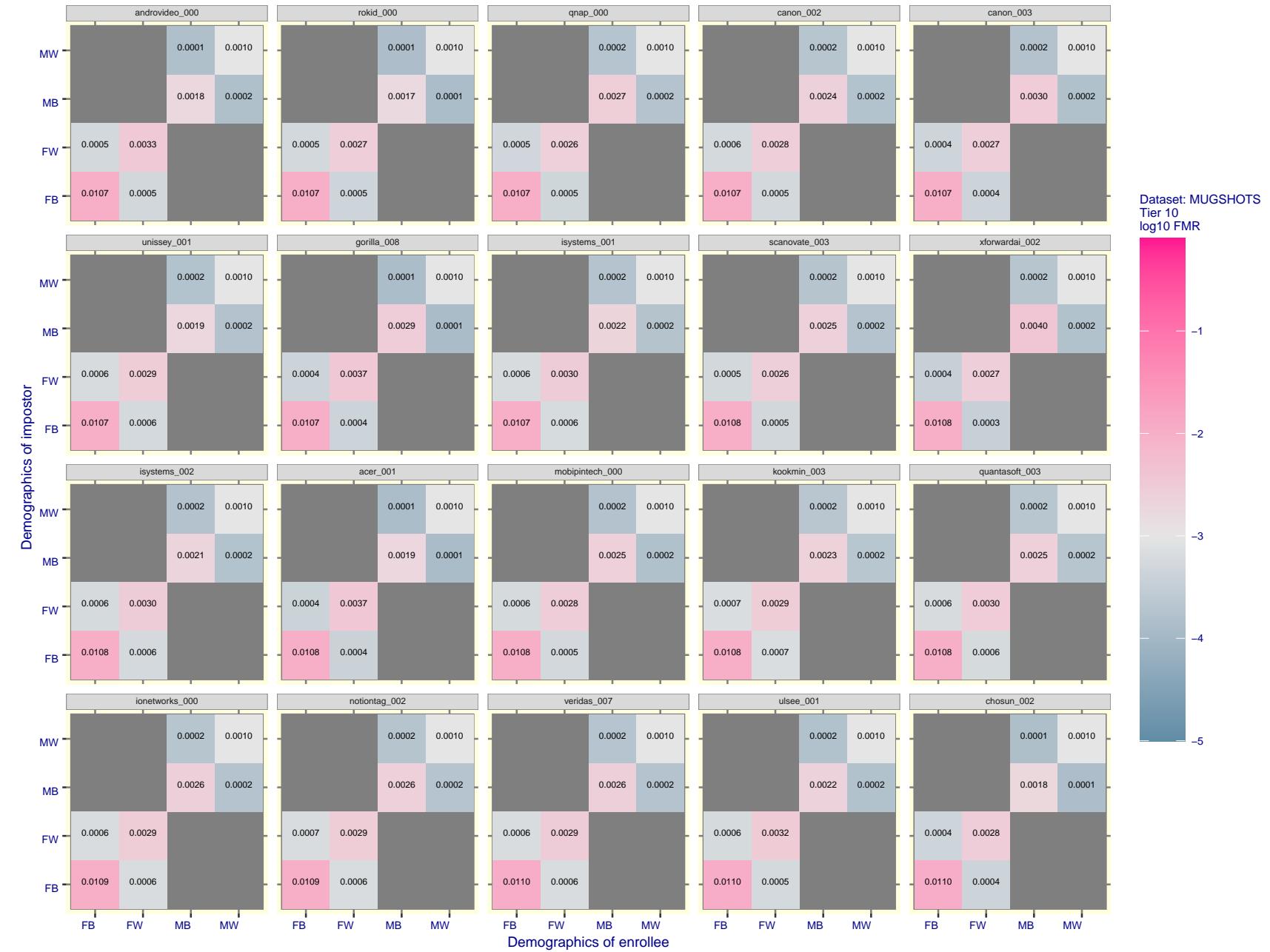


Figure 102: For the mugshot images, FMR for same-sex impostor pairs of images annotated with codes for black female, black male, white female, white male. The threshold is set for each algorithm to give FMR = 0.001 for white males which is the demographic that usually gives the lowest FMR. This means the top right box is the same color in all panels. The panels are sorted over multiple pages in order of FMR on black females, which is the demographic that usually gives the highest FMR.

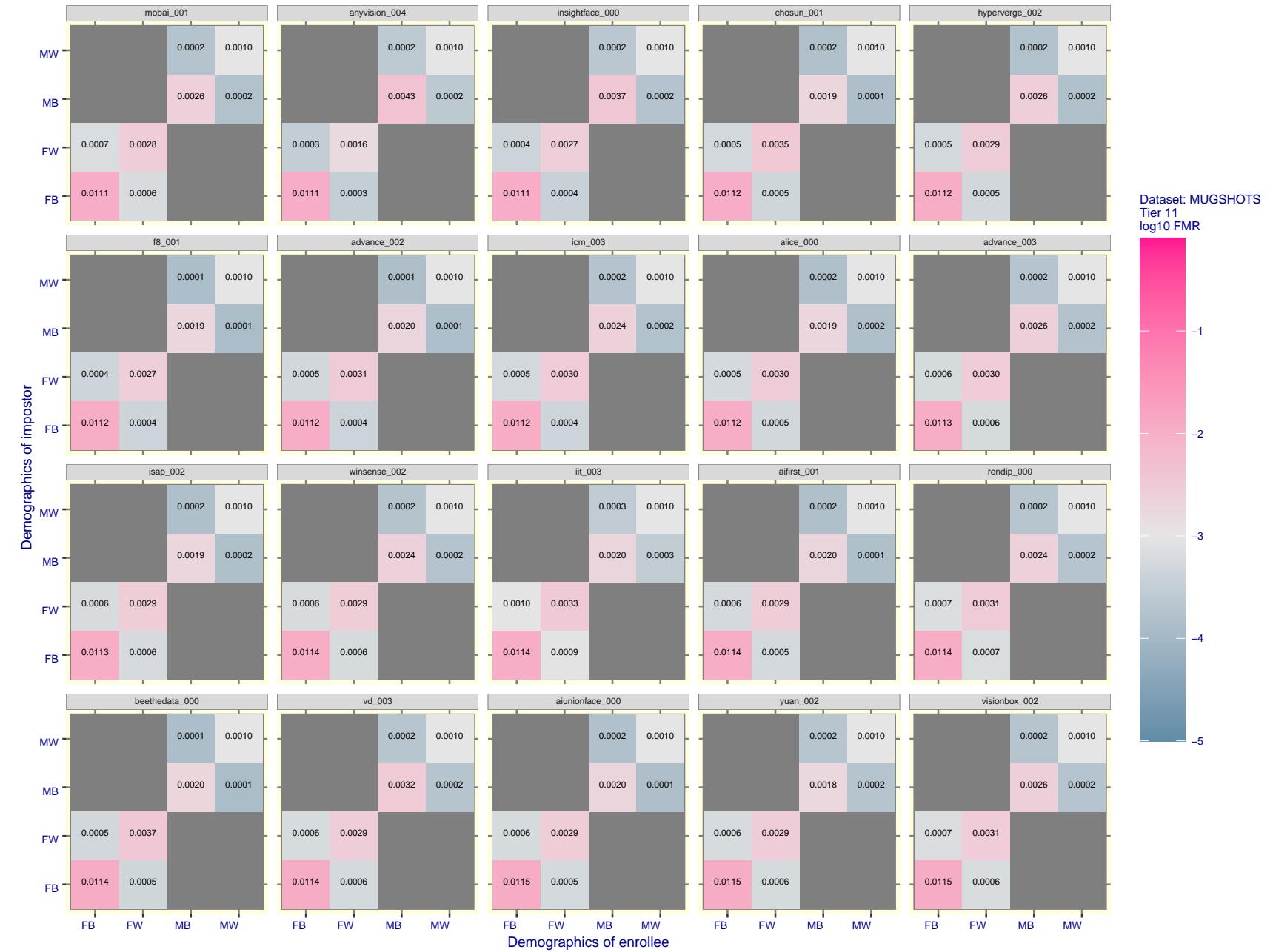


Figure 103: For the mugshot images, FMR for same-sex impostor pairs of images annotated with codes for black female, black male, white female, white male. The threshold is set for each algorithm to give FMR = 0.001 for white males which is the demographic that usually gives the lowest FMR. This means the top right box is the same color in all panels. The panels are sorted over multiple pages in order of FMR on black females, which is the demographic that usually gives the highest FMR.

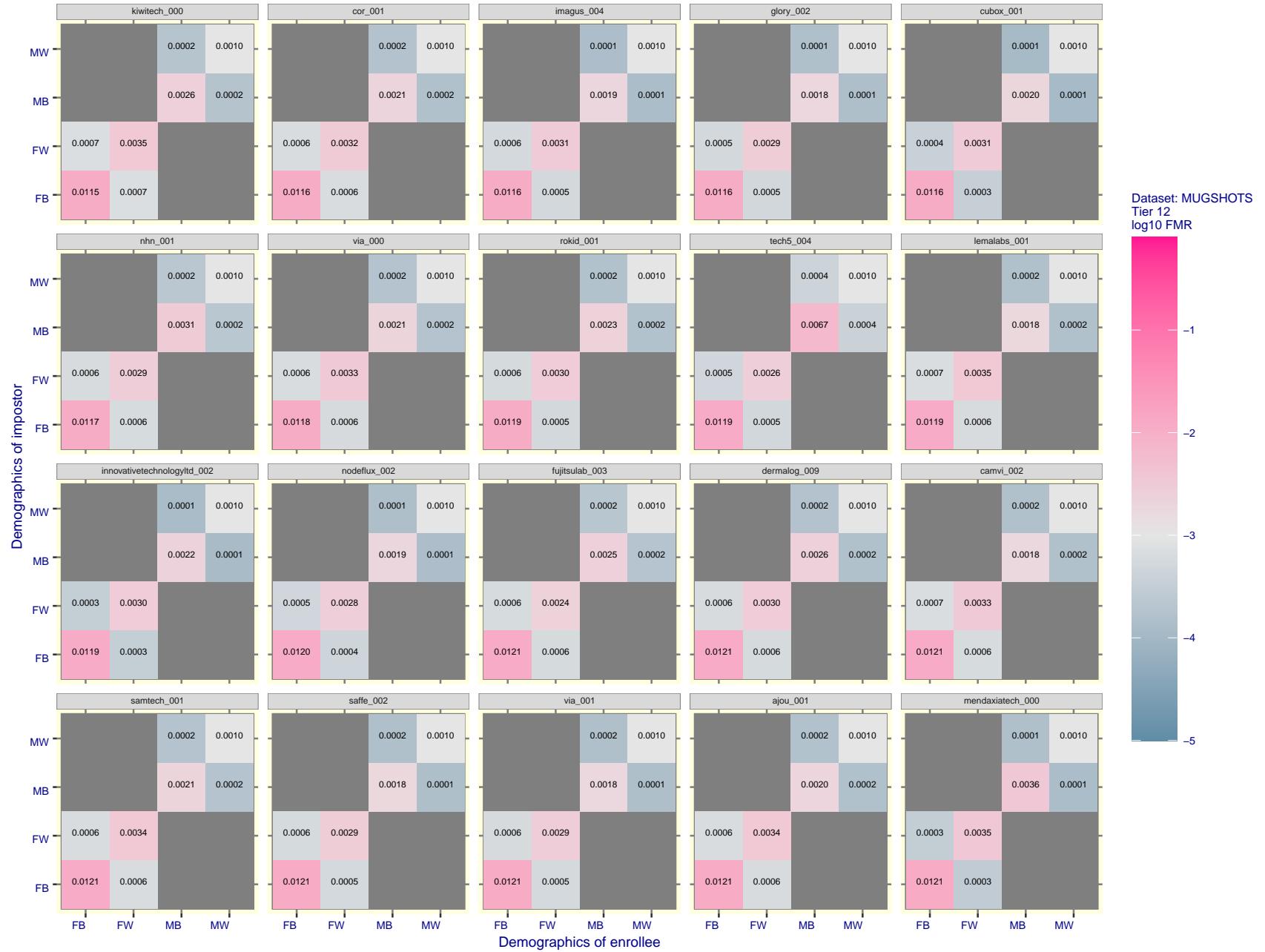


Figure 104: For the mugshot images, FMR for same-sex impostor pairs of images annotated with codes for black female, black male, white female, white male. The threshold is set for each algorithm to give FMR = 0.001 for white males which is the demographic that usually gives the lowest FMR. This means the top right box is the same color in all panels. The panels are sorted over multiple pages in order of FMR on black females, which is the demographic that usually gives the highest FMR.

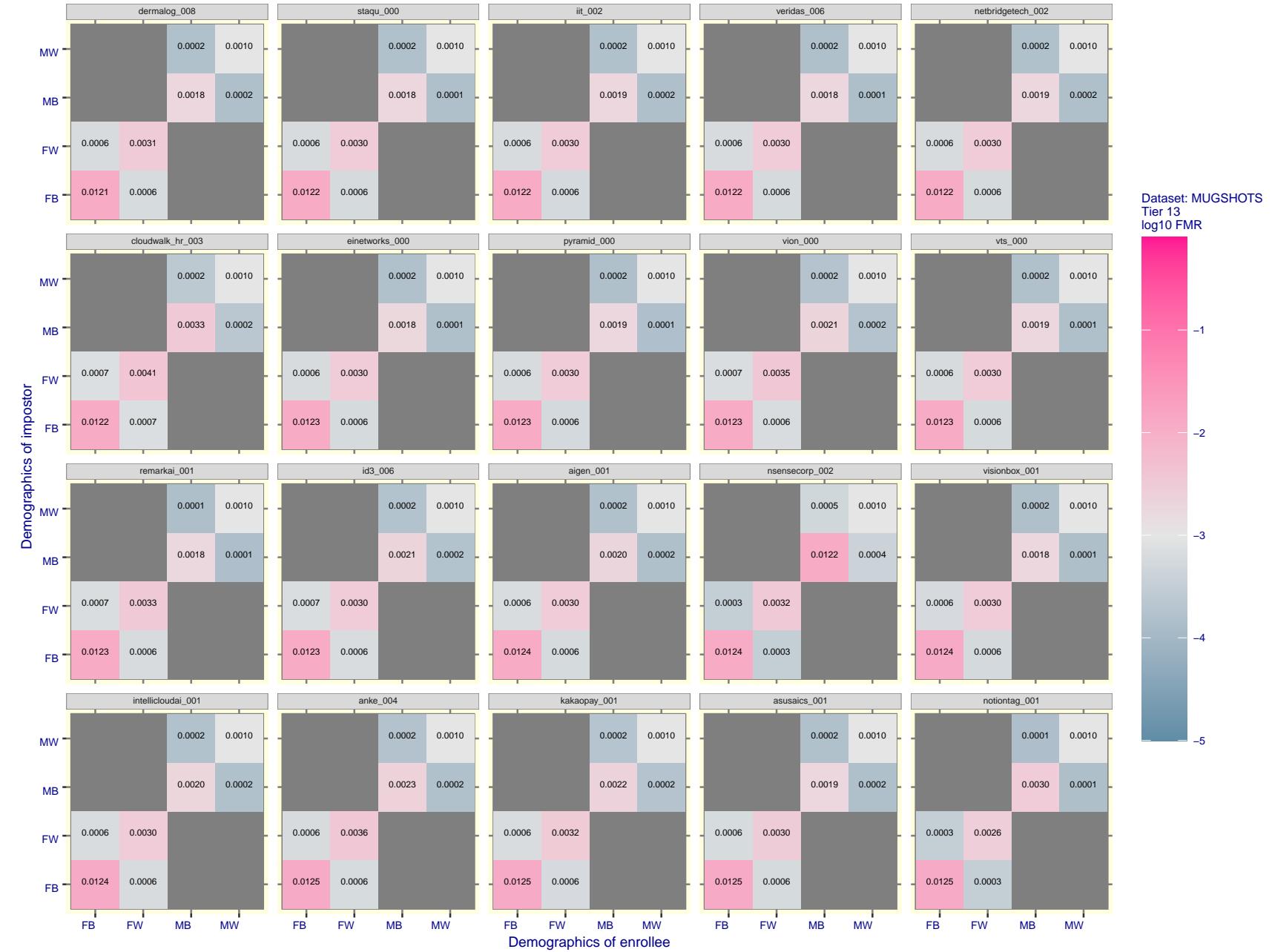


Figure 105: For the mugshot images, FMR for same-sex impostor pairs of images annotated with codes for black female, black male, white female, white male. The threshold is set for each algorithm to give FMR = 0.001 for white males which is the demographic that usually gives the lowest FMR. This means the top right box is the same color in all panels. The panels are sorted over multiple pages in order of FMR on black females, which is the demographic that usually gives the highest FMR.

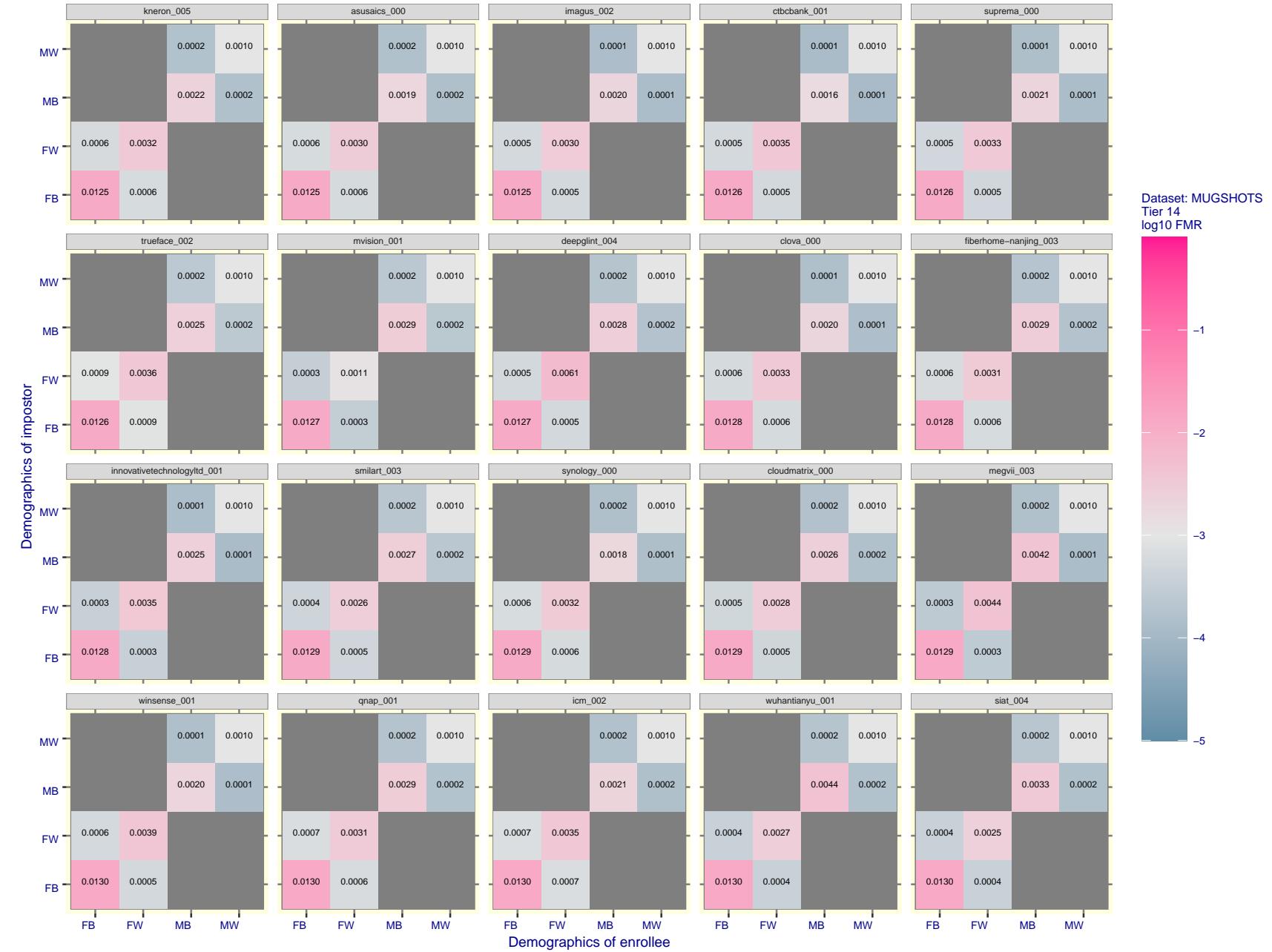


Figure 106: For the mugshot images, FMR for same-sex impostor pairs of images annotated with codes for black female, black male, white female, white male. The threshold is set for each algorithm to give FMR = 0.001 for white males which is the demographic that usually gives the lowest FMR. This means the top right box is the same color in all panels. The panels are sorted over multiple pages in order of FMR on black females, which is the demographic that usually gives the highest FMR.

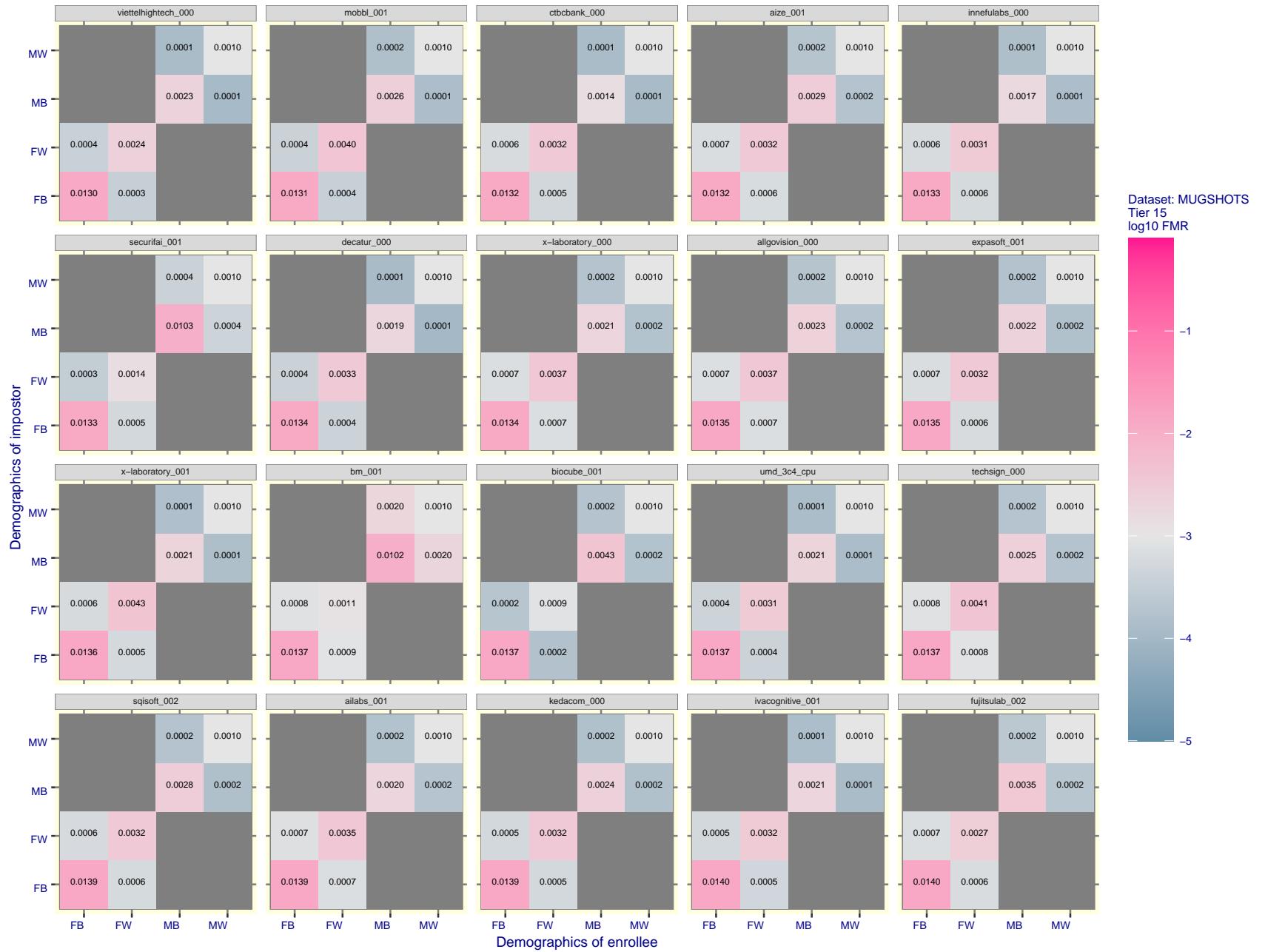


Figure 107: For the mugshot images, FMR for same-sex impostor pairs of images annotated with codes for black female, black male, white female, white male. The threshold is set for each algorithm to give FMR = 0.001 for white males which is the demographic that usually gives the lowest FMR. This means the top right box is the same color in all panels. The panels are sorted over multiple pages in order of FMR on black females, which is the demographic that usually gives the highest FMR.

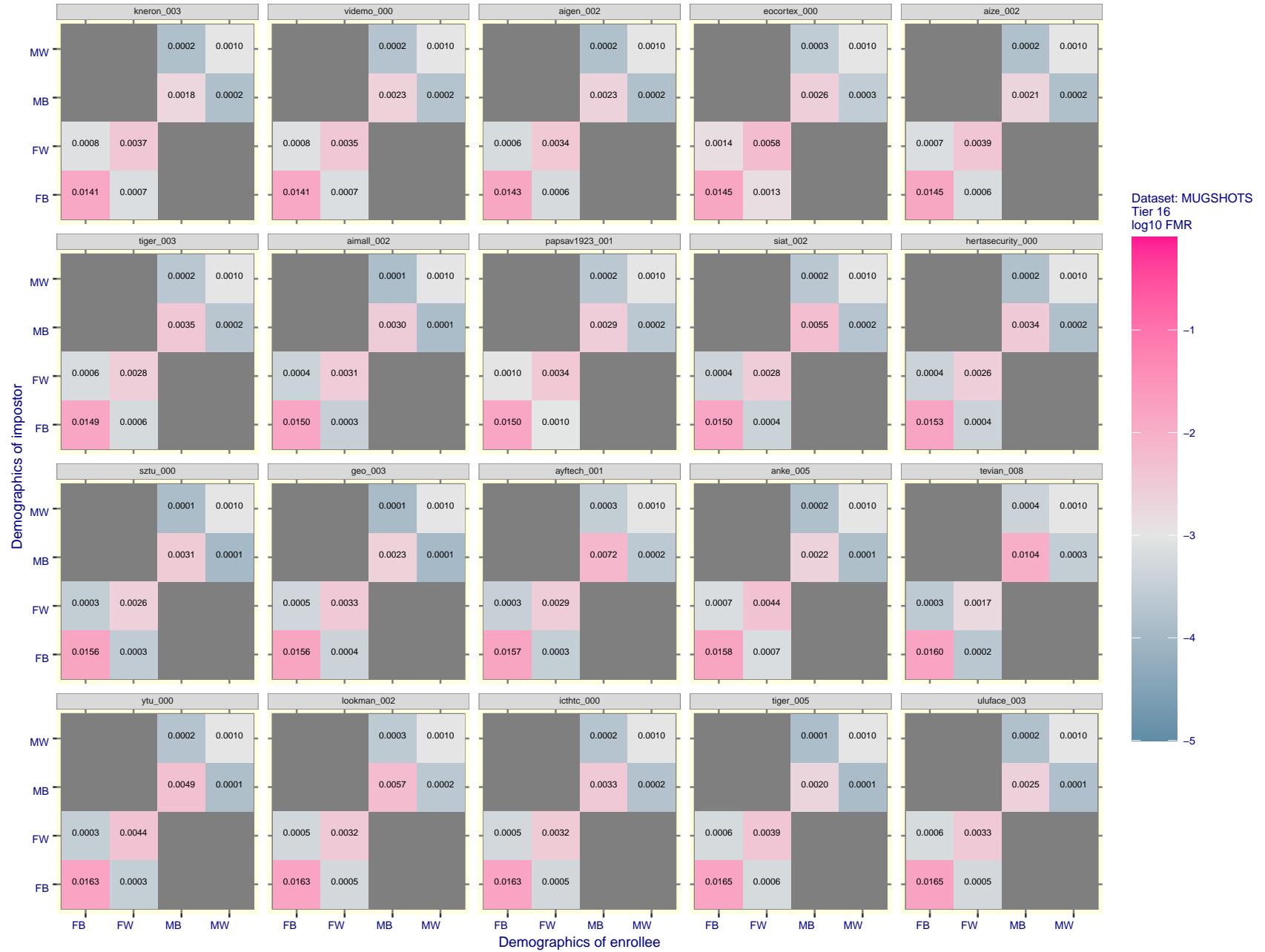


Figure 108: For the mugshot images, FMR for same-sex impostor pairs of images annotated with codes for black female, black male, white female, white male. The threshold is set for each algorithm to give FMR = 0.001 for white males which is the demographic that usually gives the lowest FMR. This means the top right box is the same color in all panels. The panels are sorted over multiple pages in order of FMR on black females, which is the demographic that usually gives the highest FMR.



Figure 109: For the mugshot images, FMR for same-sex impostor pairs of images annotated with codes for black female, black male, white female, white male. The threshold is set for each algorithm to give FMR = 0.001 for white males which is the demographic that usually gives the lowest FMR. This means the top right box is the same color in all panels. The panels are sorted over multiple pages in order of FMR on black females, which is the demographic that usually gives the highest FMR.

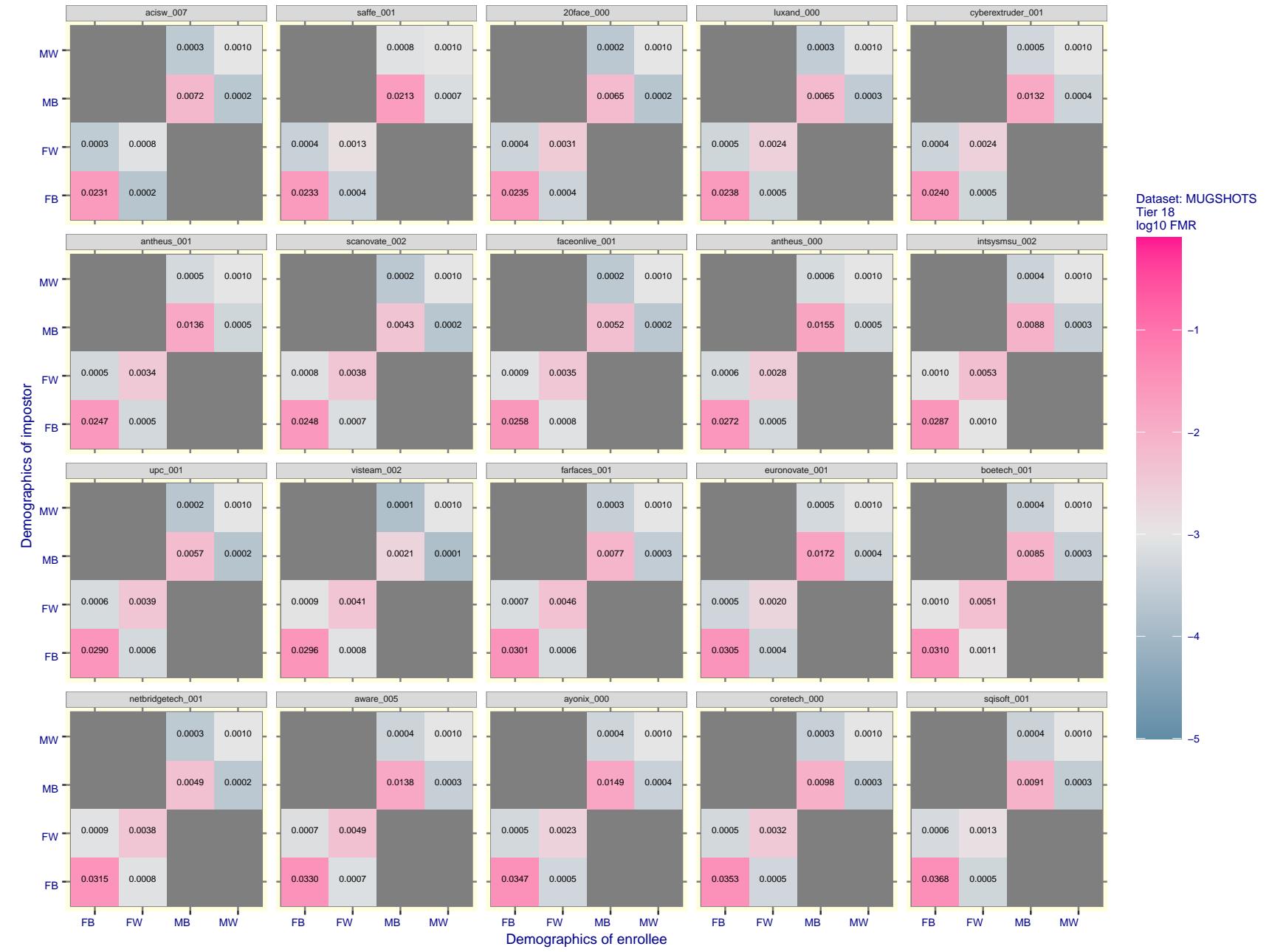


Figure 110: For the mugshot images, FMR for same-sex impostor pairs of images annotated with codes for black female, black male, white female, white male. The threshold is set for each algorithm to give $FMR = 0.001$ for white males which is the demographic that usually gives the lowest FMR. This means the top right box is the same color in all panels. The panels are sorted over multiple pages in order of FMR on black females, which is the demographic that usually gives the highest FMR.



Figure 111: For the mugshot images, FMR for same-sex impostor pairs of images annotated with codes for black female, black male, white female, white male. The threshold is set for each algorithm to give $FMR = 0.001$ for white males which is the demographic that usually gives the lowest FMR. This means the top right box is the same color in all panels. The panels are sorted over multiple pages in order of FMR on black females, which is the demographic that usually gives the highest FMR.

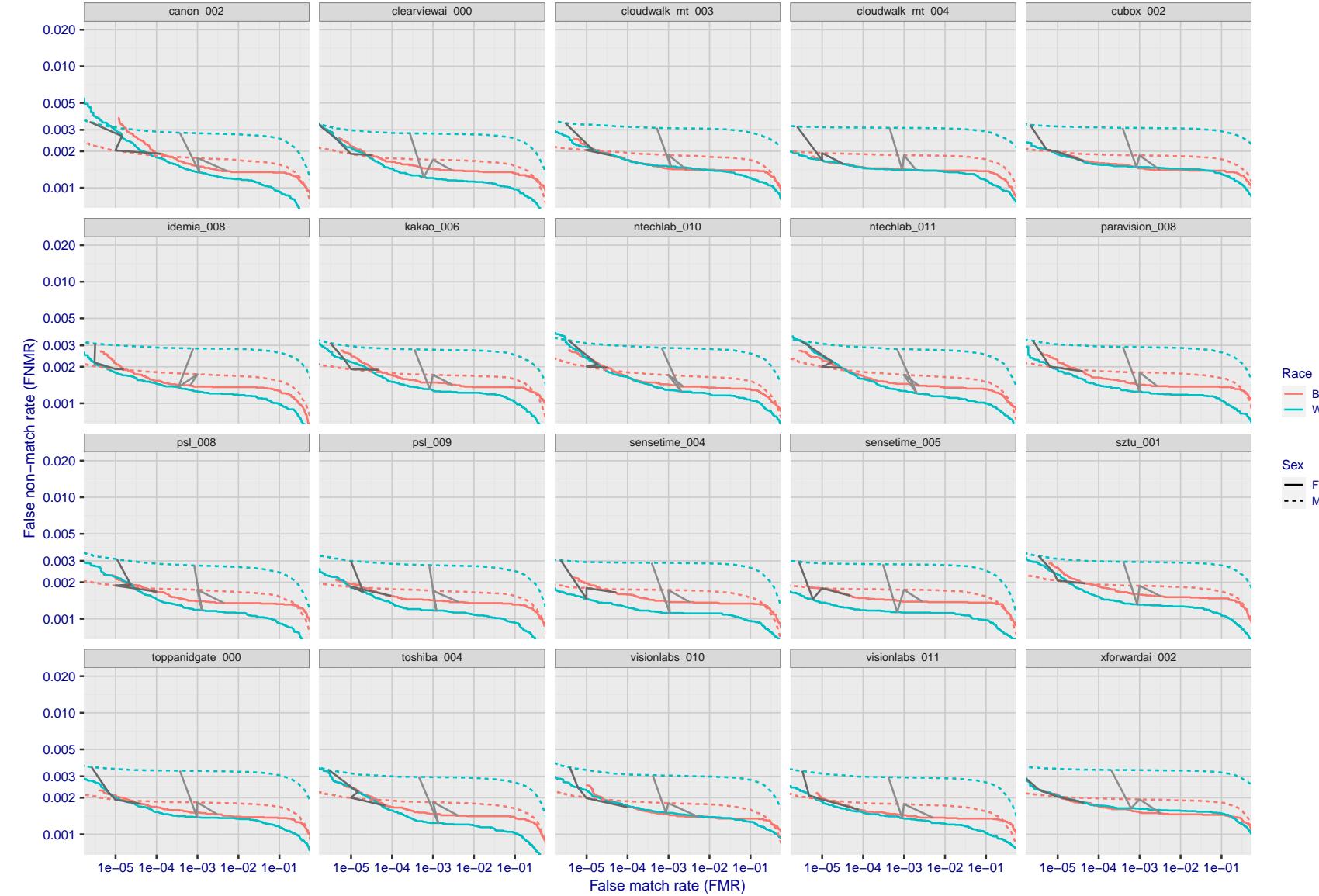


Figure 112: For the mugshot images, error tradeoff characteristics for white females, black females, black males and white males. The Z-shaped grey lines correspond to fixed thresholds, showing both FNMR and FMR vary at one T value. Note: Many of the plots will naively be read as saying women gives worse error rates than men because the solid traces lie above the dotted ones. However, this is misleading and incomplete: The grey lines show the traces reveal horizontal shifts. Thus for the cogent-003 algorithm FNMR for men is higher than for women at a fixed threshold but, at the same time, FMR is higher for women - see Figure 181. As access control systems almost always operate at a fixed threshold, the naive interpretation is incorrect.

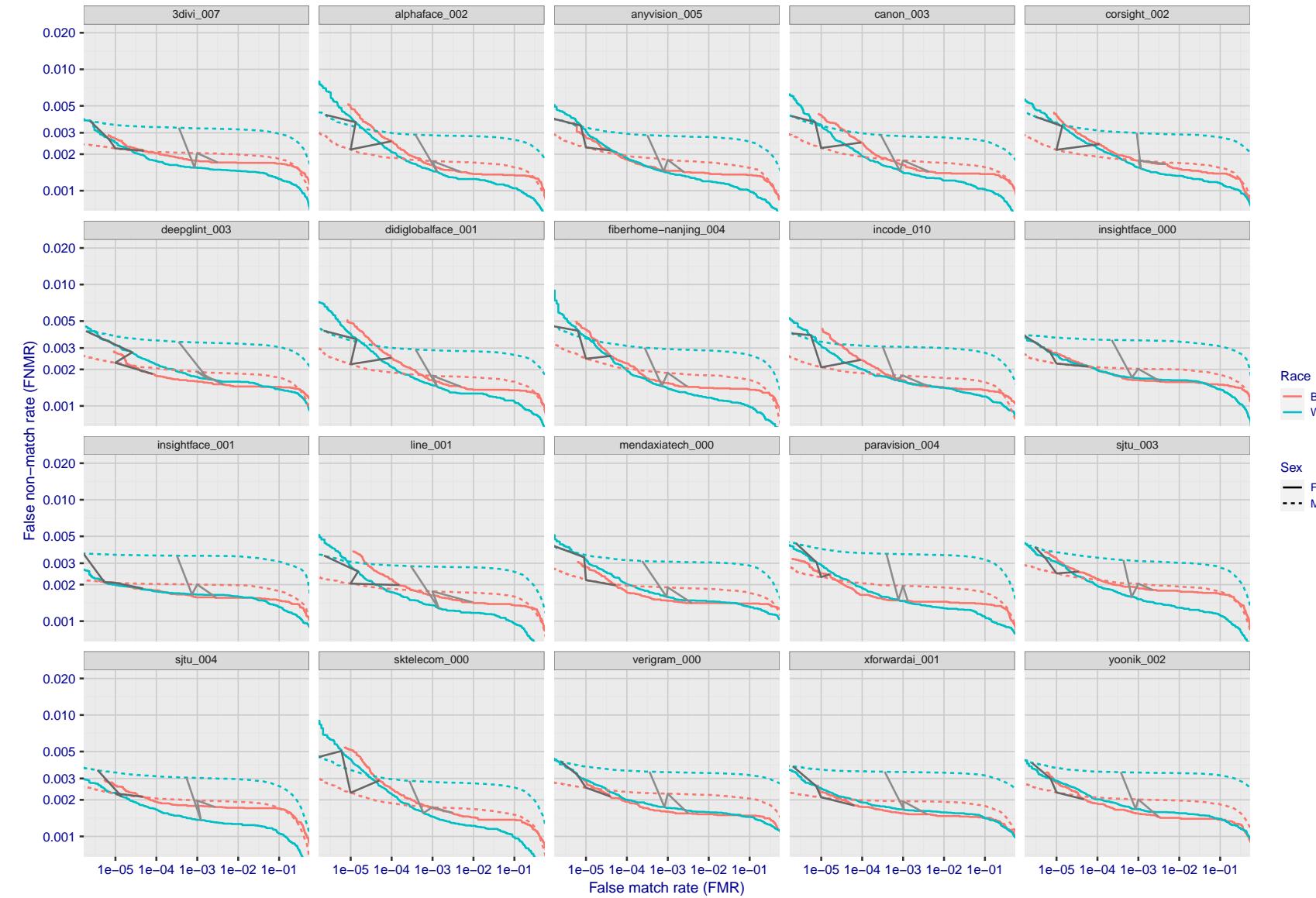


Figure 113: For the mugshot images, error tradeoff characteristics for white females, black females, black males and white males. The Z-shaped grey lines correspond to fixed thresholds, showing both FNMR and FMR vary at one T value. Note: Many of the plots will naively be read as saying women gives worse error rates than men because the solid traces lie above the dotted ones. However, this is misleading and incomplete: The grey lines show the traces reveal horizontal shifts. Thus for the cogent-003 algorithm FNMR for men is higher than for women at a fixed threshold but, at the same time, FMR is higher for women - see Figure 181. As access control systems almost always operate at a fixed threshold, the naive interpretation is incorrect.

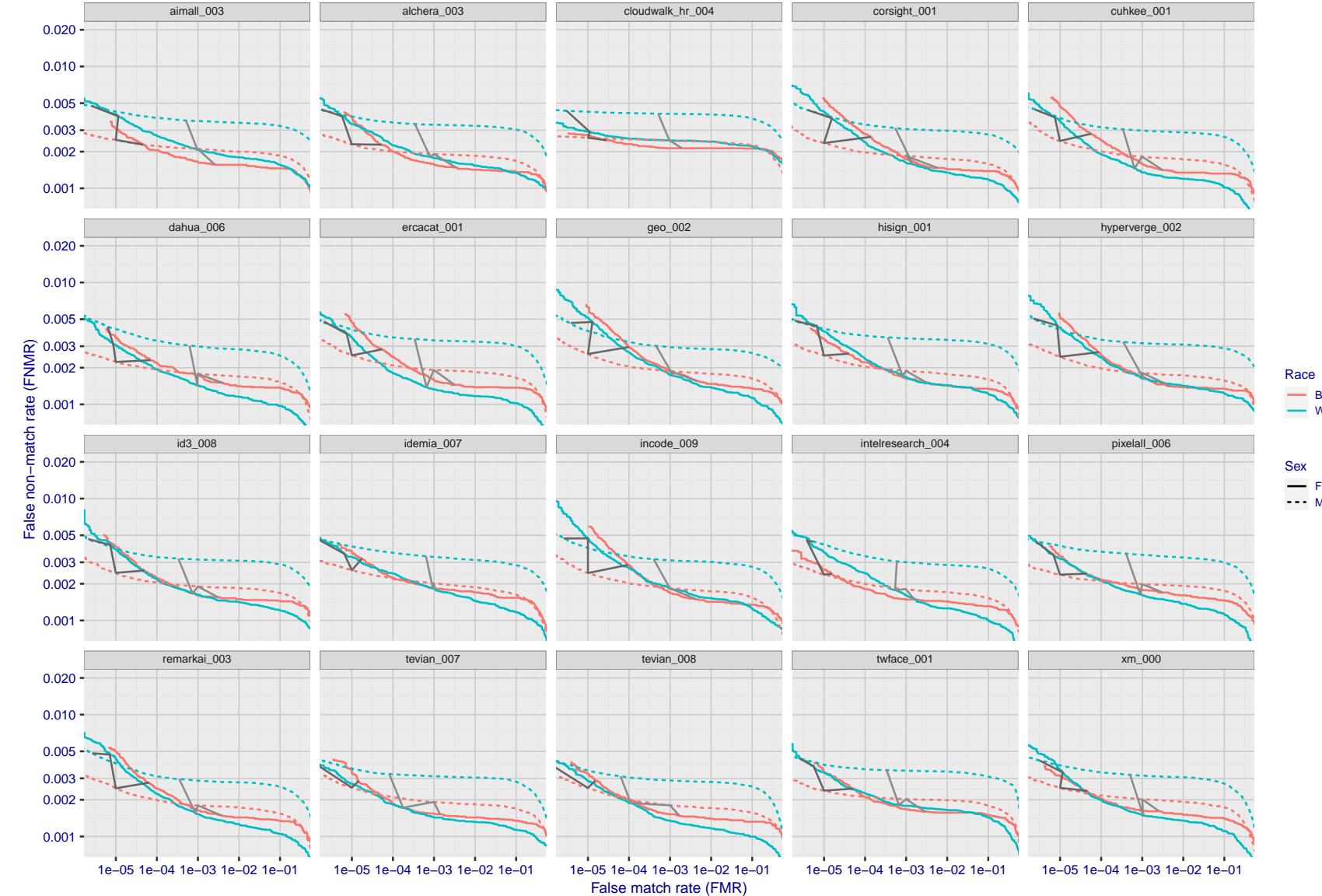


Figure 114: For the mugshot images, error tradeoff characteristics for white females, black females, black males and white males. The Z-shaped grey lines correspond to fixed thresholds, showing both FNMR and FMR vary at one T value. Note: Many of the plots will naively be read as saying women gives worse error rates than men because the solid traces lie above the dotted ones. However, this is misleading and incomplete: The grey lines show the traces reveal horizontal shifts. Thus for the cogent-003 algorithm FNMR for men is higher than for women at a fixed threshold but, at the same time, FMR is higher for women - see Figure 181. As access control systems almost always operate at a fixed threshold, the naive interpretation is incorrect.

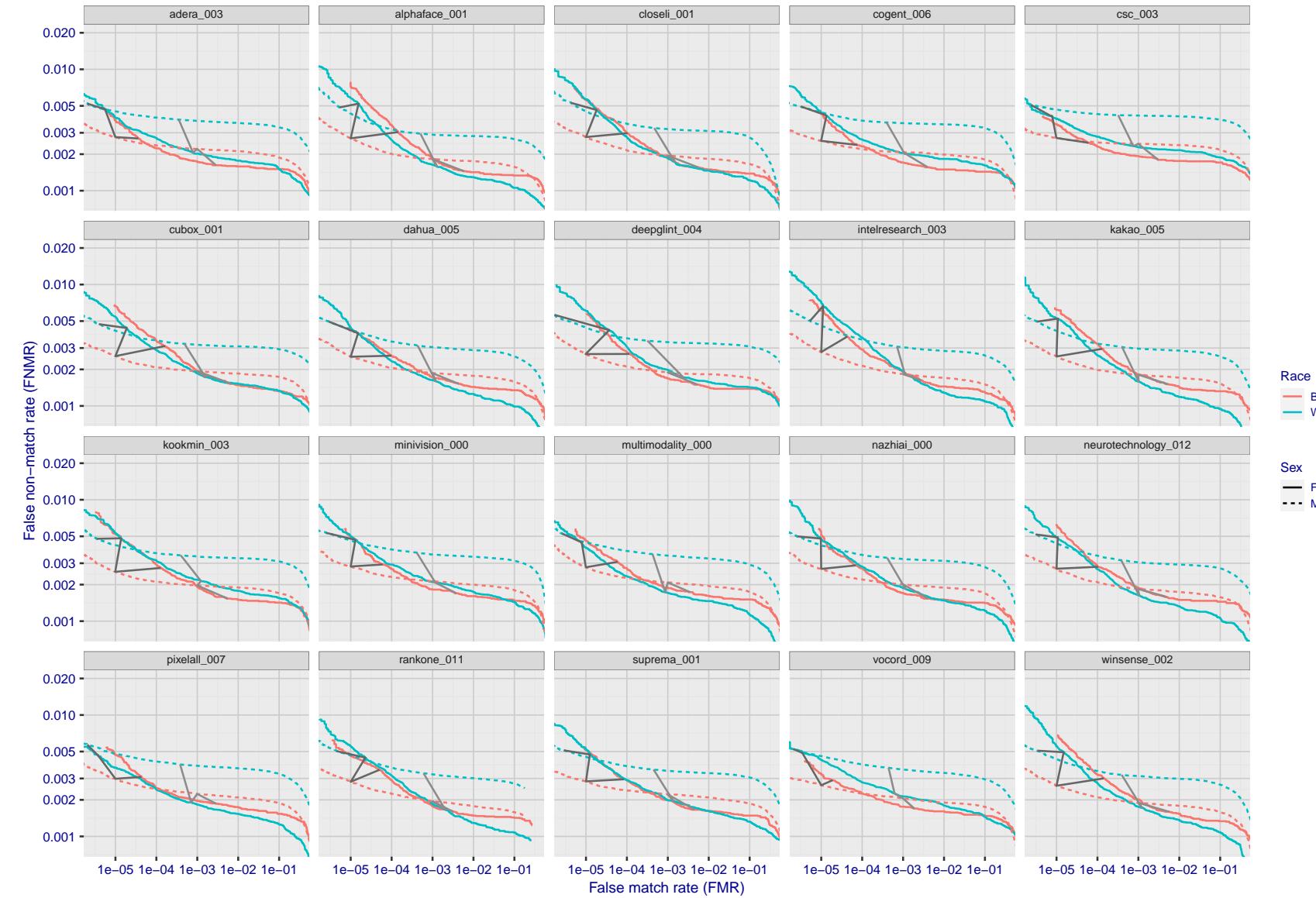


Figure 115: For the mugshot images, error tradeoff characteristics for white females, black females, black males and white males. The Z-shaped grey lines correspond to fixed thresholds, showing both FNMR and FMR vary at one T value. Note: Many of the plots will naively be read as saying women gives worse error rates than men because the solid traces lie above the dotted ones. However, this is misleading and incomplete: The grey lines show the traces reveal horizontal shifts. Thus for the cogent-003 algorithm FNMR for men is higher than for women at a fixed threshold but, at the same time, FMR is higher for women - see Figure 181. As access control systems almost always operate at a fixed threshold, the naive interpretation is incorrect.

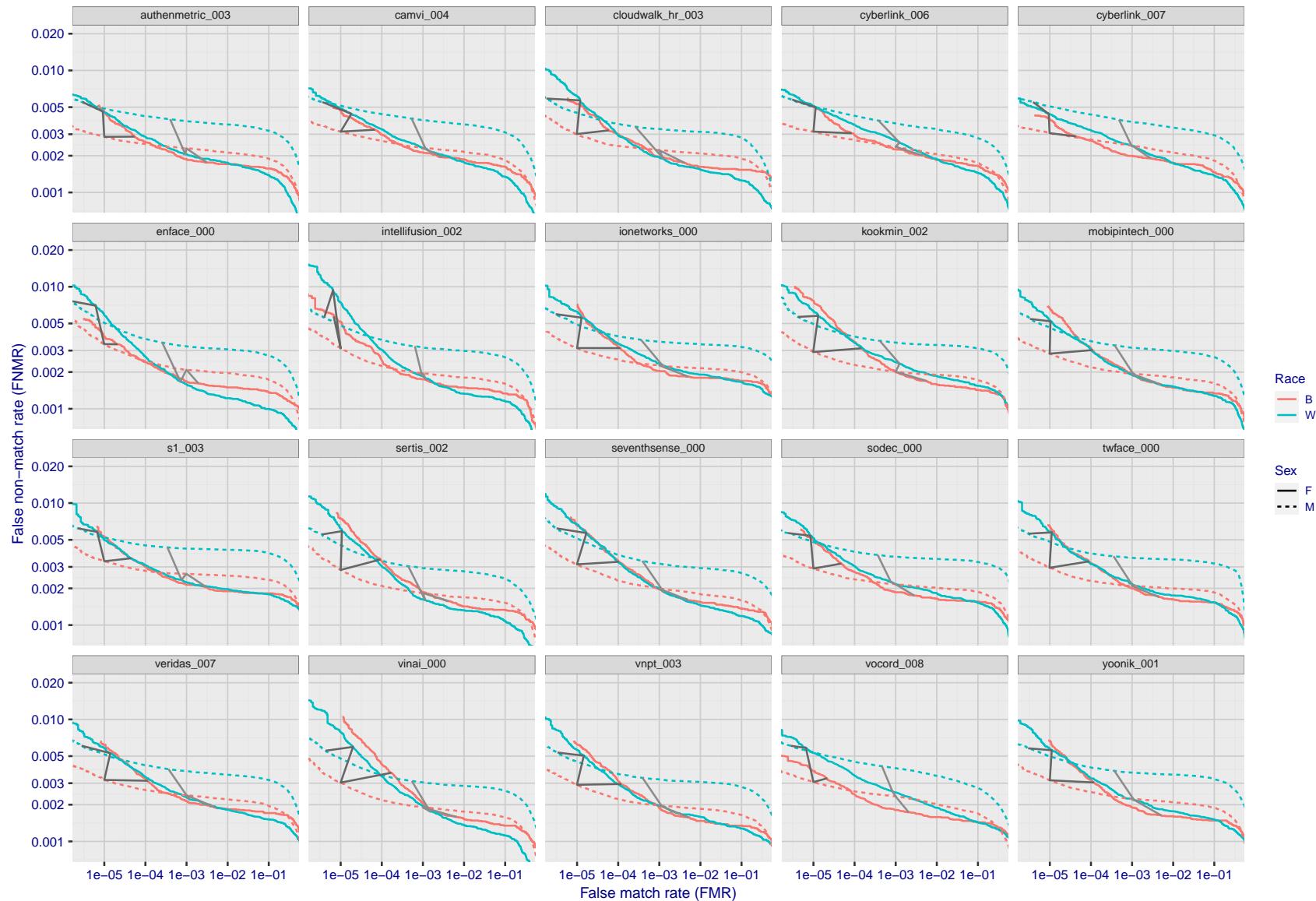


Figure 116: For the mugshot images, error tradeoff characteristics for white females, black females, black males and white males. The Z-shaped grey lines correspond to fixed thresholds, showing both FNMR and FMR vary at one T value. Note: Many of the plots will naively be read as saying women gives worse error rates than men because the solid traces lie above the dotted ones. However, this is misleading and incomplete: The grey lines show the traces reveal horizontal shifts. Thus for the cogent-003 algorithm FNMR for men is higher than for women at a fixed threshold but, at the same time, FMR is higher for women - see Figure 181. As access control systems almost always operate at a fixed threshold, the naive interpretation is incorrect.

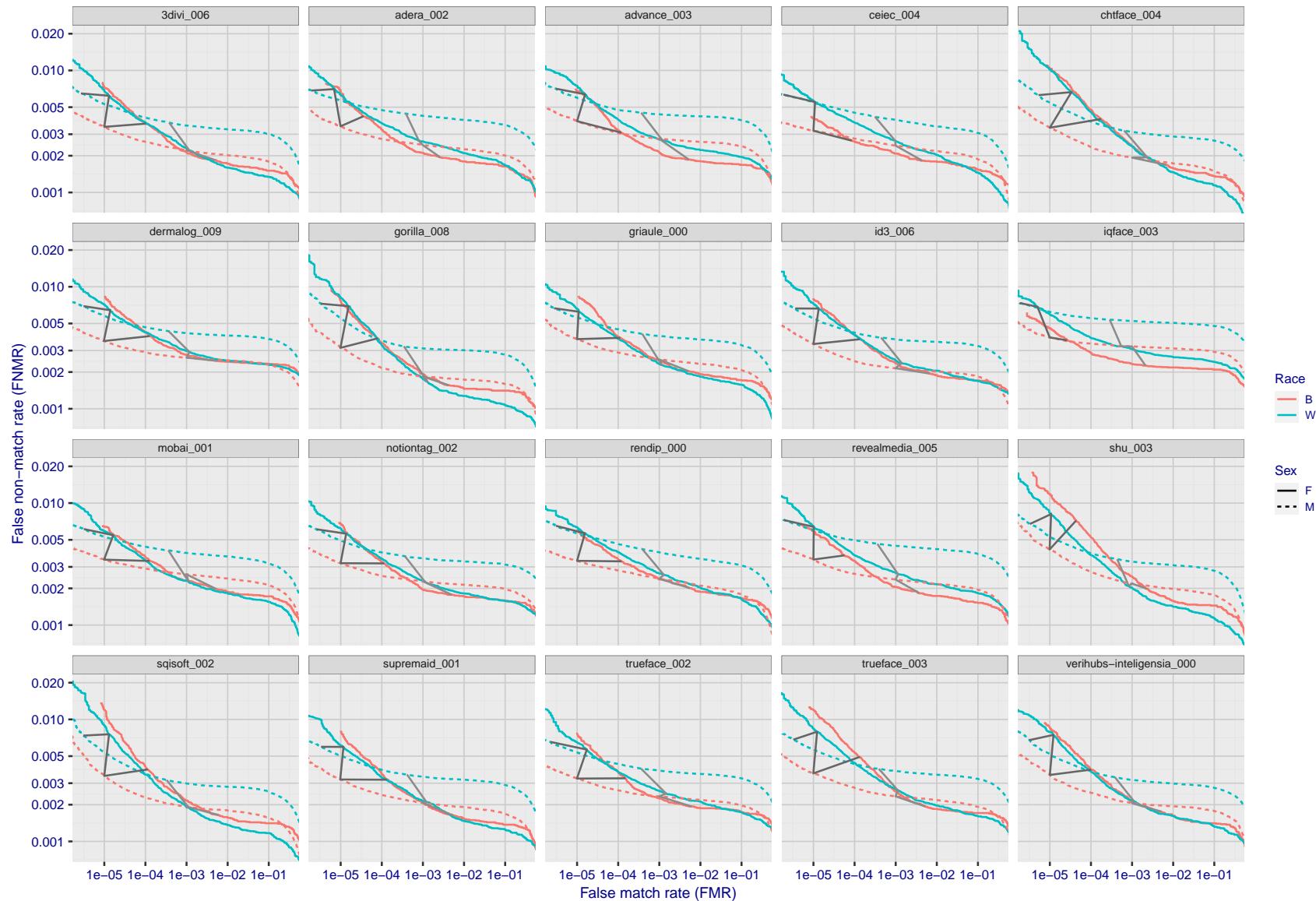


Figure 117: For the mugshot images, error tradeoff characteristics for white females, black females, black males and white males. The Z-shaped grey lines correspond to fixed thresholds, showing both FNMR and FMR vary at one T value. Note: Many of the plots will naively be read as saying women gives worse error rates than men because the solid traces lie above the dotted ones. However, this is misleading and incomplete: The grey lines show the traces reveal horizontal shifts. Thus for the cogent-003 algorithm FNMR for men is higher than for women at a fixed threshold but, at the same time, FMR is higher for women - see Figure 181. As access control systems almost always operate at a fixed threshold, the naive interpretation is incorrect.

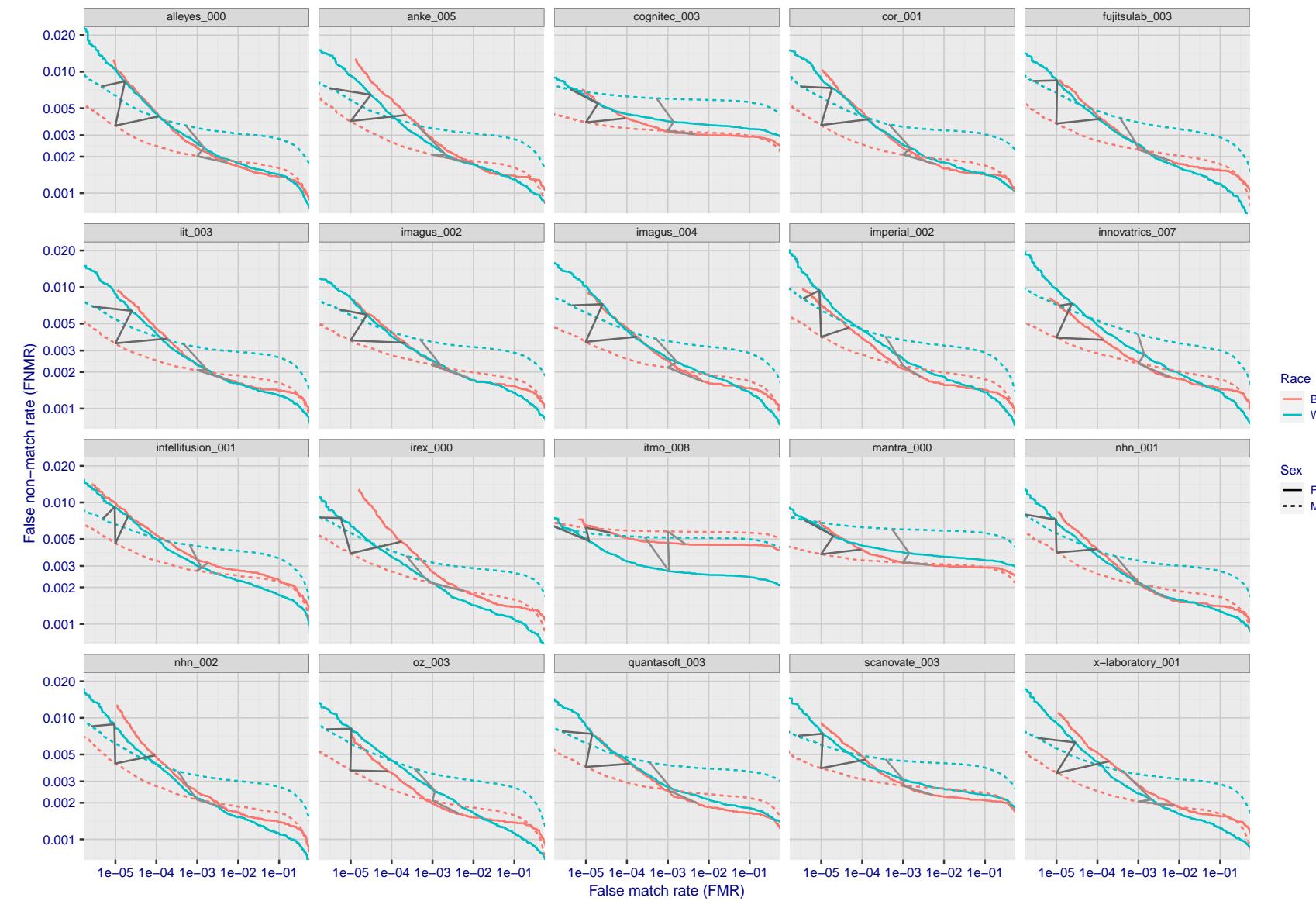


Figure 118: For the mugshot images, error tradeoff characteristics for white females, black females, black males and white males. The Z-shaped grey lines correspond to fixed thresholds, showing both FNMR and FMR vary at one T value. Note: Many of the plots will naively be read as saying women gives worse error rates than men because the solid traces lie above the dotted ones. However, this is misleading and incomplete: The grey lines show the traces reveal horizontal shifts. Thus for the cogent-003 algorithm FNMR for men is higher than for women at a fixed threshold but, at the same time, FMR is higher for women - see Figure 181. As access control systems almost always operate at a fixed threshold, the naive interpretation is incorrect.

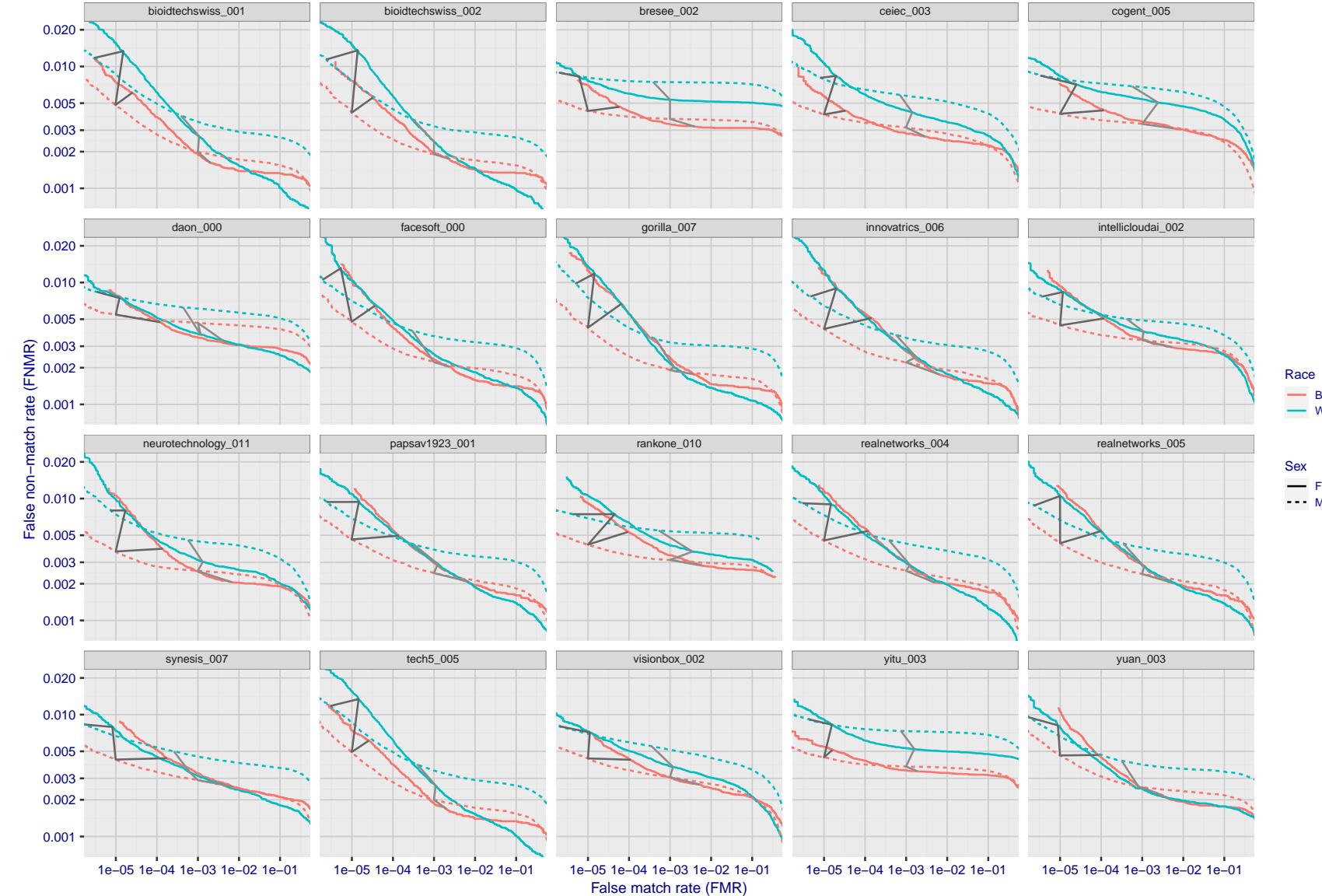


Figure 119: For the mugshot images, error tradeoff characteristics for white females, black females, black males and white males. The Z-shaped grey lines correspond to fixed thresholds, showing both FNMR and FMR vary at one T value. Note: Many of the plots will naively be read as saying women gives worse error rates than men because the solid traces lie above the dotted ones. However, this is misleading and incomplete: The grey lines show the traces reveal horizontal shifts. Thus for the cogent-003 algorithm FNMR for men is higher than for women at a fixed threshold but, at the same time, FMR is higher for women - see Figure 181. As access control systems almost always operate at a fixed threshold, the naive interpretation is incorrect.

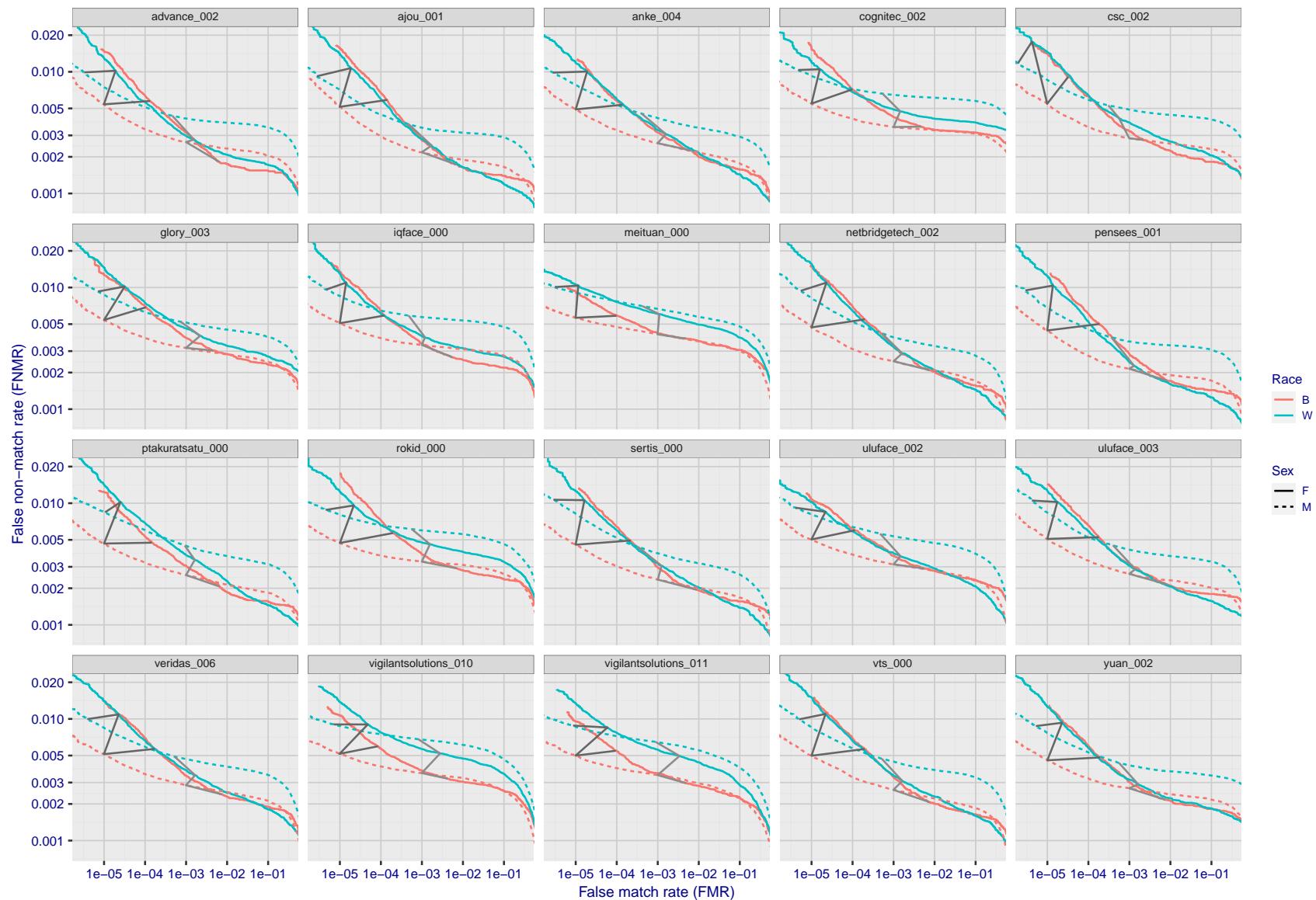


Figure 120: For the mugshot images, error tradeoff characteristics for white females, black females, black males and white males. The Z-shaped grey lines correspond to fixed thresholds, showing both FNMR and FMR vary at one T value. Note: Many of the plots will naively be read as saying women gives worse error rates than men because the solid traces lie above the dotted ones. However, this is misleading and incomplete: The grey lines show the traces reveal horizontal shifts. Thus for the cogent-003 algorithm FNMR for men is higher than for women at a fixed threshold but, at the same time, FMR is higher for women - see Figure 181. As access control systems almost always operate at a fixed threshold, the naive interpretation is incorrect.

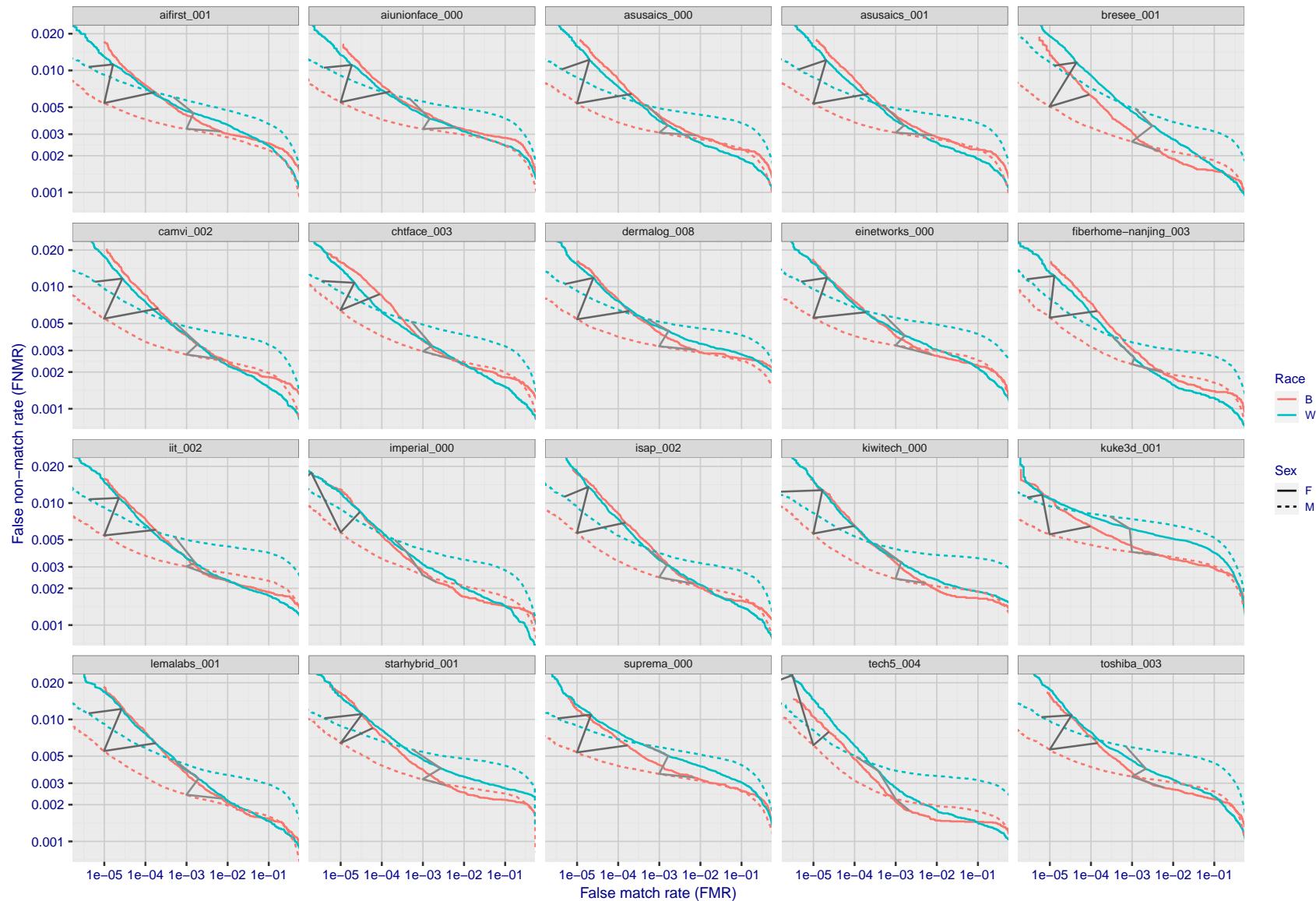


Figure 121: For the mugshot images, error tradeoff characteristics for white females, black females, black males and white males. The Z-shaped grey lines correspond to fixed thresholds, showing both FNMR and FMR vary at one T value. Note: Many of the plots will naively be read as saying women gives worse error rates than men because the solid traces lie above the dotted ones. However, this is misleading and incomplete: The grey lines show the traces reveal horizontal shifts. Thus for the cogent-003 algorithm FNMR for men is higher than for women at a fixed threshold but, at the same time, FMR is higher for women - see Figure 181. As access control systems almost always operate at a fixed threshold, the naive interpretation is incorrect.

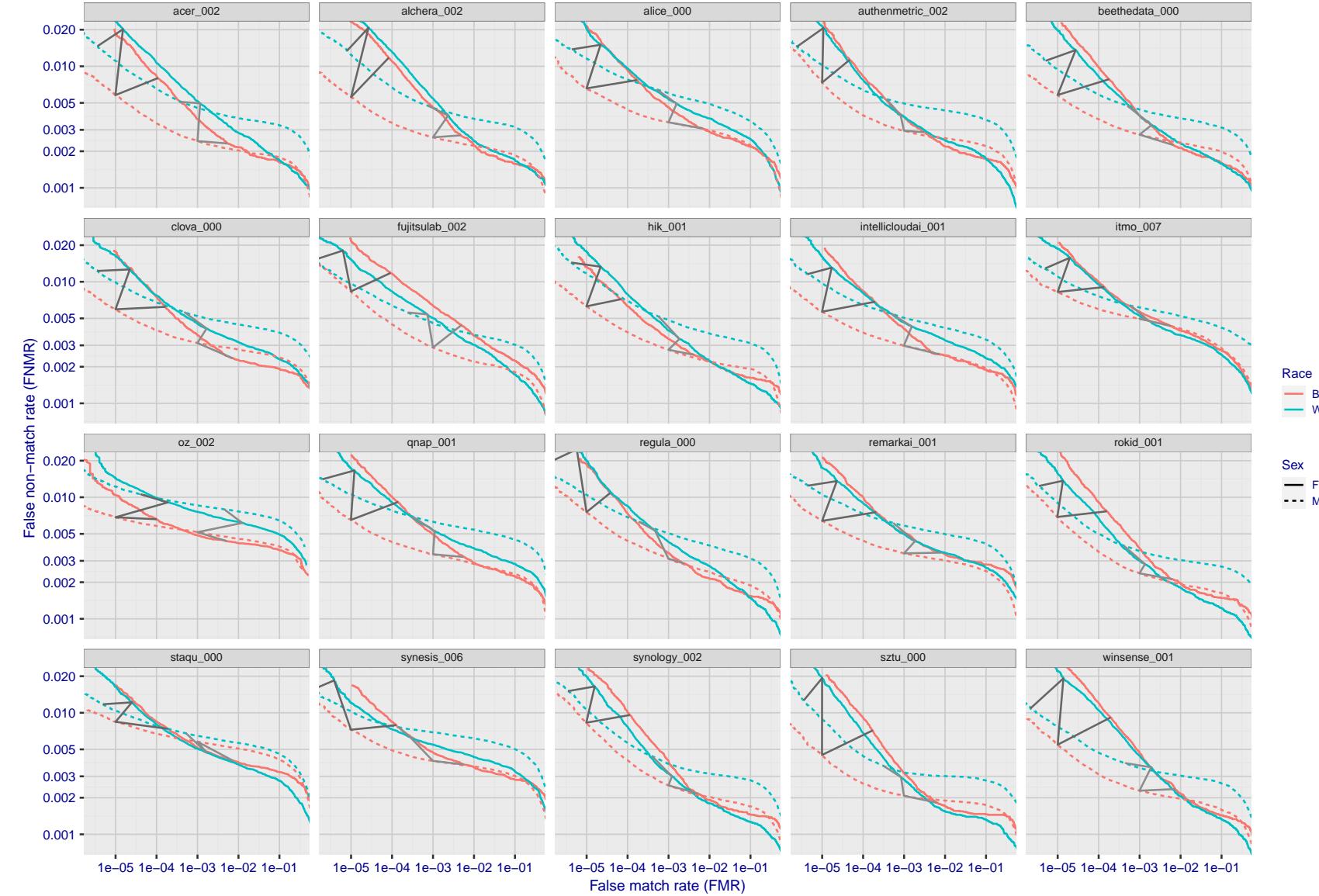


Figure 122: For the mugshot images, error tradeoff characteristics for white females, black females, black males and white males. The Z-shaped grey lines correspond to fixed thresholds, showing both FNMR and FMR vary at one T value. Note: Many of the plots will naively be read as saying women gives worse error rates than men because the solid traces lie above the dotted ones. However, this is misleading and incomplete: The grey lines show the traces reveal horizontal shifts. Thus for the cogent-003 algorithm FNMR for men is higher than for women at a fixed threshold but, at the same time, FMR is higher for women - see Figure 181. As access control systems almost always operate at a fixed threshold, the naive interpretation is incorrect.

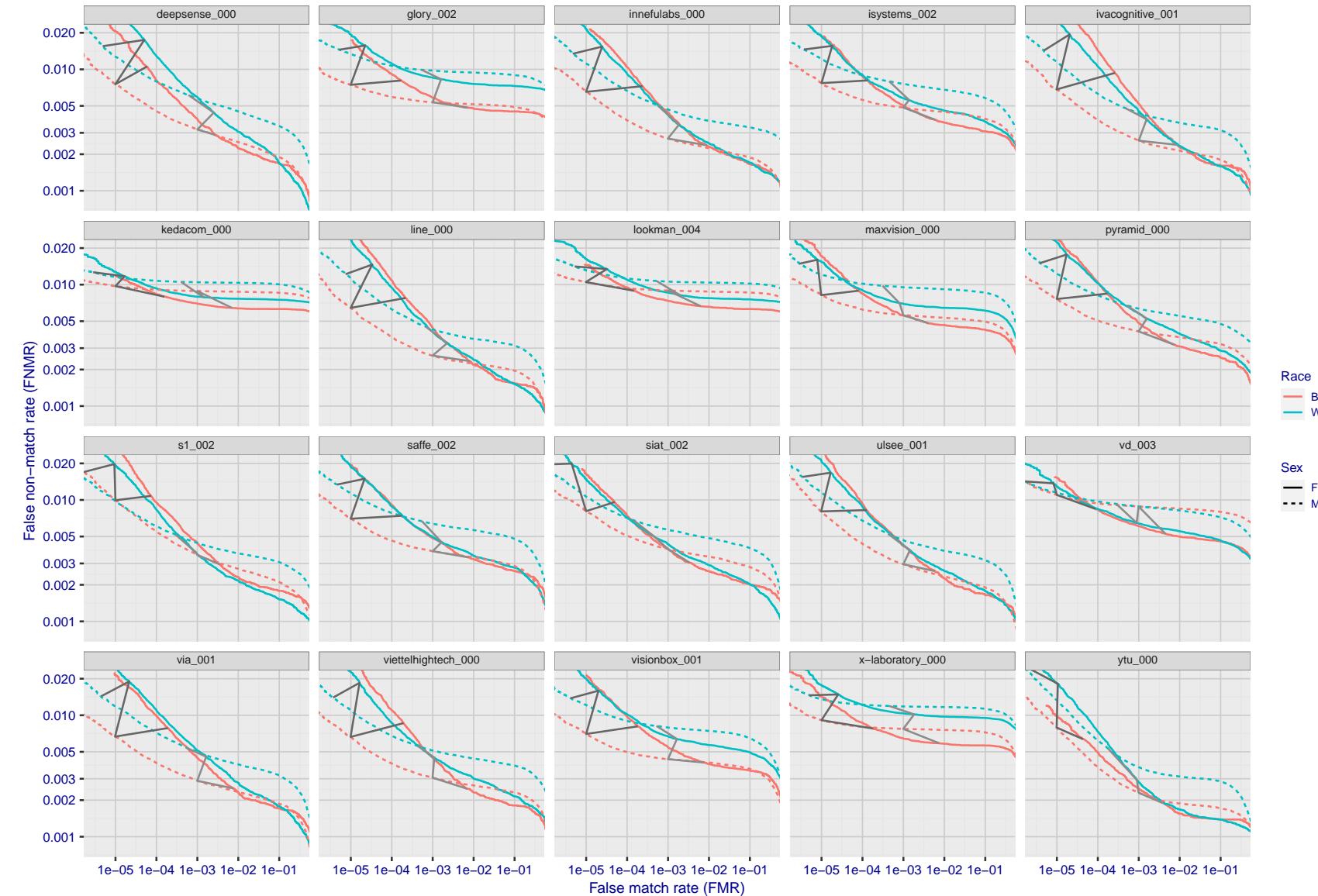


Figure 123: For the mugshot images, error tradeoff characteristics for white females, black females, black males and white males. The Z-shaped grey lines correspond to fixed thresholds, showing both FNMR and FMR vary at one T value. Note: Many of the plots will naively be read as saying women gives worse error rates than men because the solid traces lie above the dotted ones. However, this is misleading and incomplete: The grey lines show the traces reveal horizontal shifts. Thus for the cogent-003 algorithm FNMR for men is higher than for women at a fixed threshold but, at the same time, FMR is higher for women - see Figure 181. As access control systems almost always operate at a fixed threshold, the naive interpretation is incorrect.

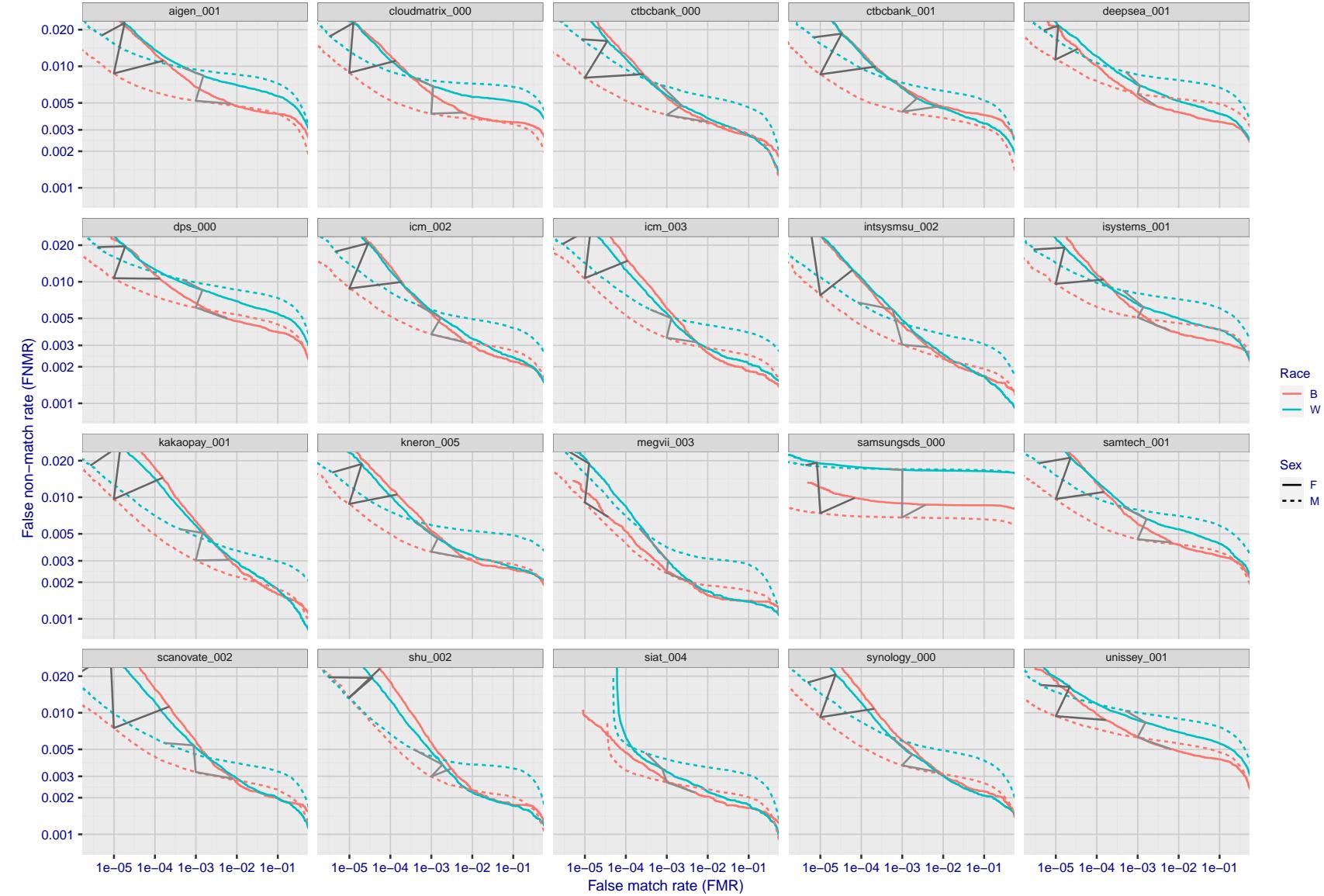


Figure 124: For the mugshot images, error tradeoff characteristics for white females, black females, black males and white males. The Z-shaped grey lines correspond to fixed thresholds, showing both FNMR and FMR vary at one T value. Note: Many of the plots will naively be read as saying women gives worse error rates than men because the solid traces lie above the dotted ones. However, this is misleading and incomplete: The grey lines show the traces reveal horizontal shifts. Thus for the cogent-003 algorithm FNMR for men is higher than for women at a fixed threshold but, at the same time, FMR is higher for women - see Figure 181. As access control systems almost always operate at a fixed threshold, the naive interpretation is incorrect.

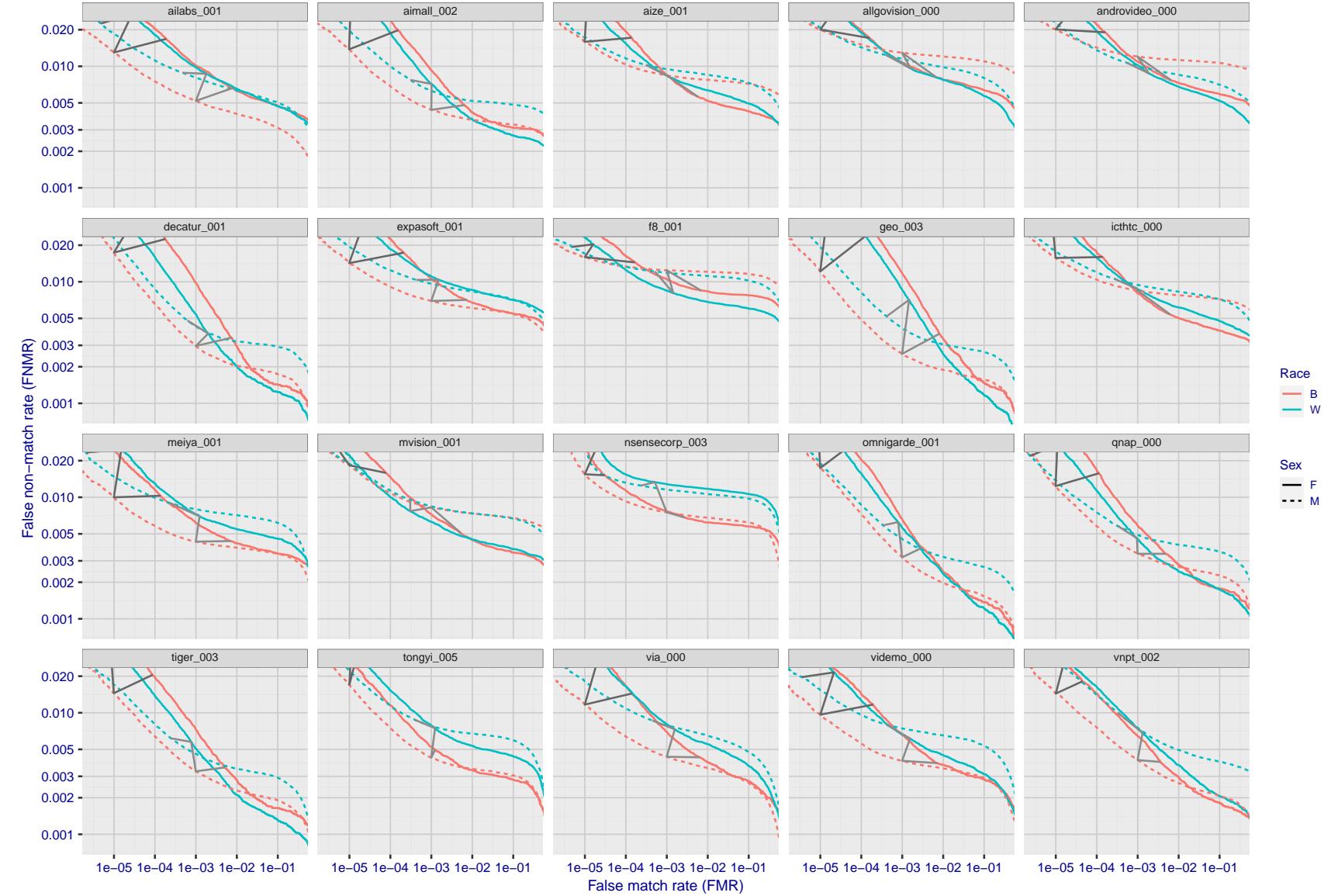


Figure 125: For the mugshot images, error tradeoff characteristics for white females, black females, black males and white males. The Z-shaped grey lines correspond to fixed thresholds, showing both FNMR and FMR vary at one T value. Note: Many of the plots will naively be read as saying women gives worse error rates than men because the solid traces lie above the dotted ones. However, this is misleading and incomplete: The grey lines show the traces reveal horizontal shifts. Thus for the cogent-003 algorithm FNMR for men is higher than for women at a fixed threshold but, at the same time, FMR is higher for women - see Figure 181. As access control systems almost always operate at a fixed threshold, the naive interpretation is incorrect.

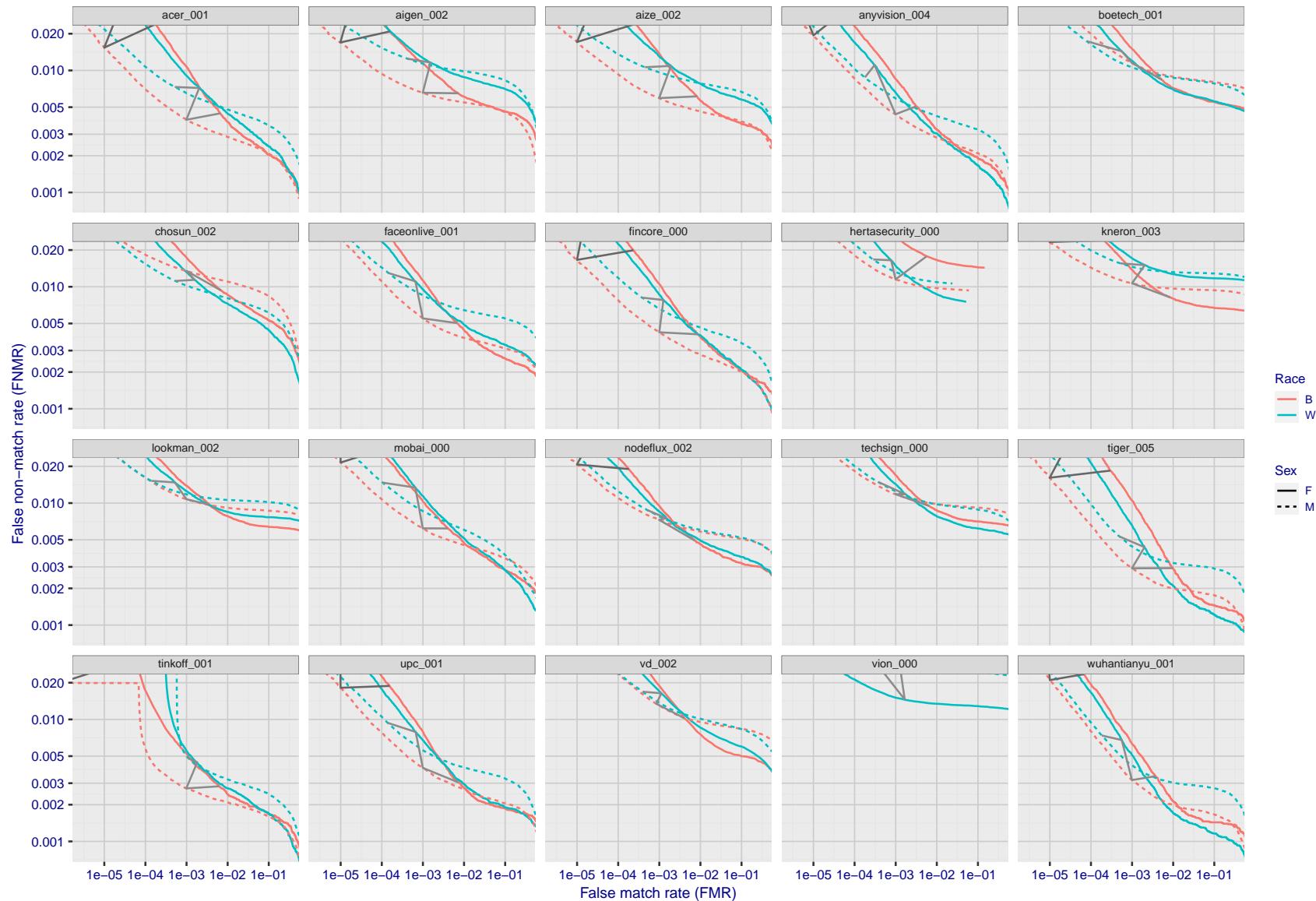


Figure 126: For the mugshot images, error tradeoff characteristics for white females, black females, black males and white males. The Z-shaped grey lines correspond to fixed thresholds, showing both FNMR and FMR vary at one T value. Note: Many of the plots will naively be read as saying women gives worse error rates than men because the solid traces lie above the dotted ones. However, this is misleading and incomplete: The grey lines show the traces reveal horizontal shifts. Thus for the cogent-003 algorithm FNMR for men is higher than for women at a fixed threshold but, at the same time, FMR is higher for women - see Figure 181. As access control systems almost always operate at a fixed threshold, the naive interpretation is incorrect.

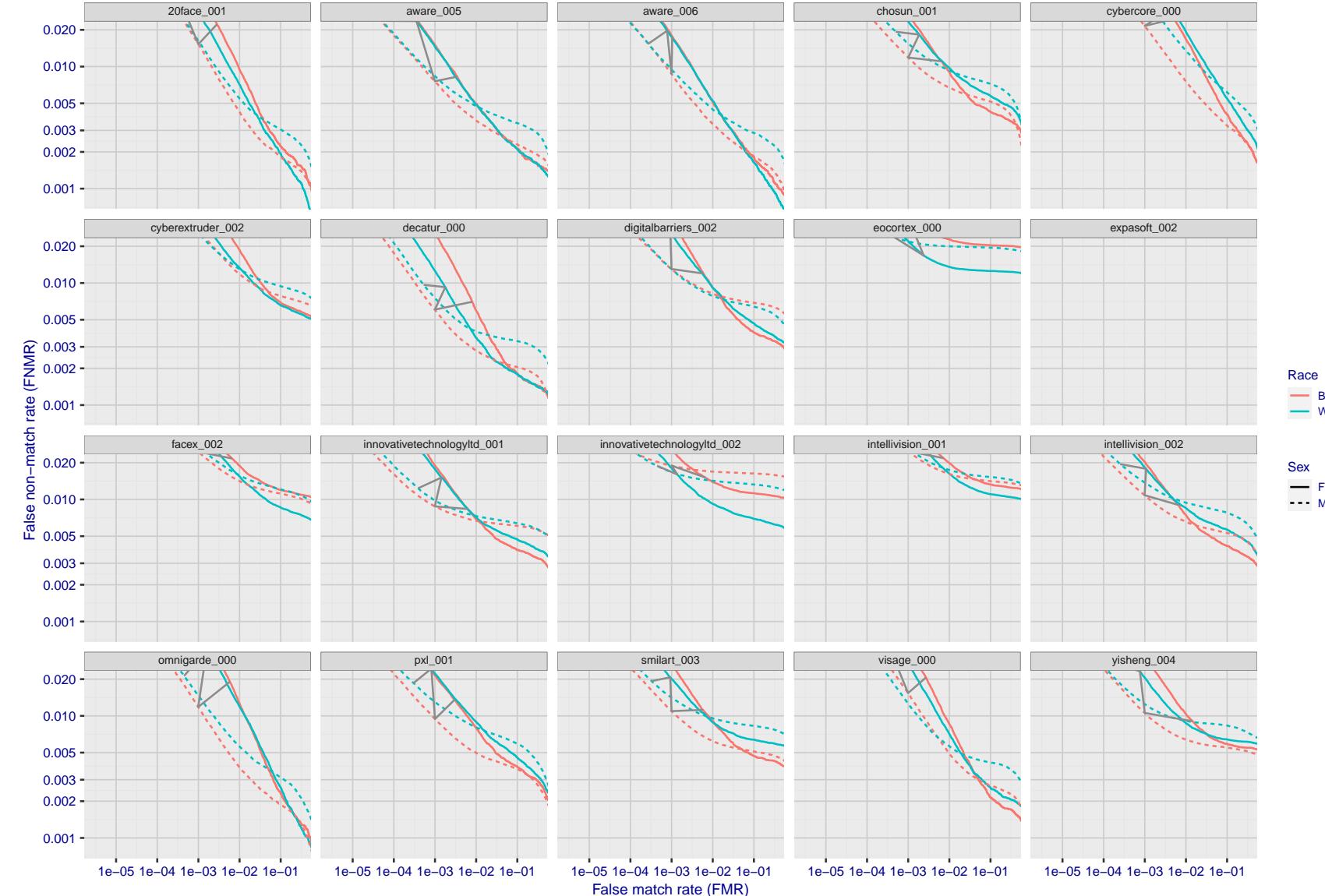


Figure 127: For the mugshot images, error tradeoff characteristics for white females, black females, black males and white males. The Z-shaped grey lines correspond to fixed thresholds, showing both FNMR and FMR vary at one T value. Note: Many of the plots will naively be read as saying women gives worse error rates than men because the solid traces lie above the dotted ones. However, this is misleading and incomplete: The grey lines show the traces reveal horizontal shifts. Thus for the cogent-003 algorithm FNMR for men is higher than for women at a fixed threshold but, at the same time, FMR is higher for women - see Figure 181. As access control systems almost always operate at a fixed threshold, the naive interpretation is incorrect.

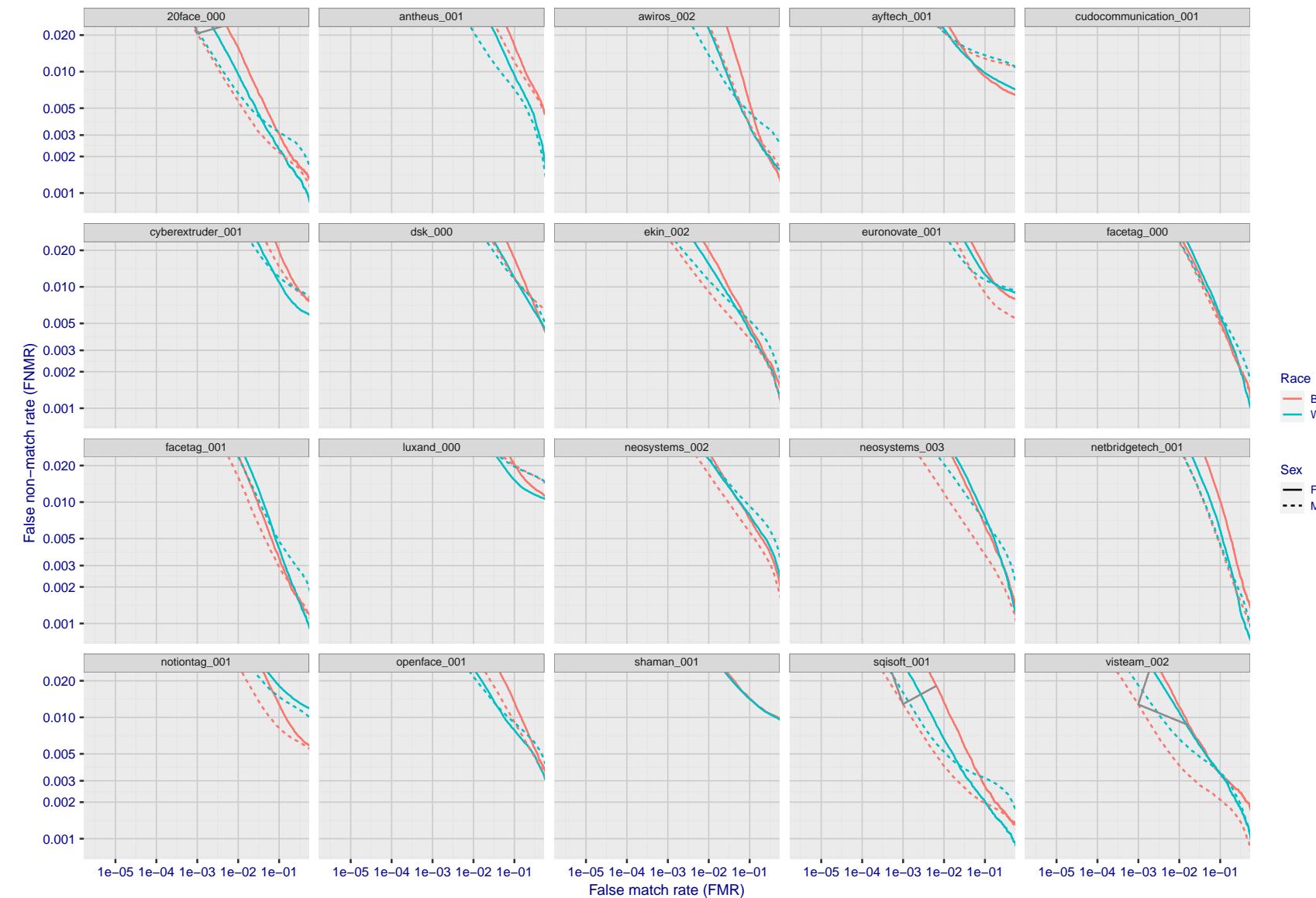


Figure 128: For the mugshot images, error tradeoff characteristics for white females, black females, black males and white males. The Z-shaped grey lines correspond to fixed thresholds, showing both FNMR and FMR vary at one T value. Note: Many of the plots will naively be read as saying women gives worse error rates than men because the solid traces lie above the dotted ones. However, this is misleading and incomplete: The grey lines show the traces reveal horizontal shifts. Thus for the cogent-003 algorithm FNMR for men is higher than for women at a fixed threshold but, at the same time, FMR is higher for women - see Figure 181. As access control systems almost always operate at a fixed threshold, the naive interpretation is incorrect.

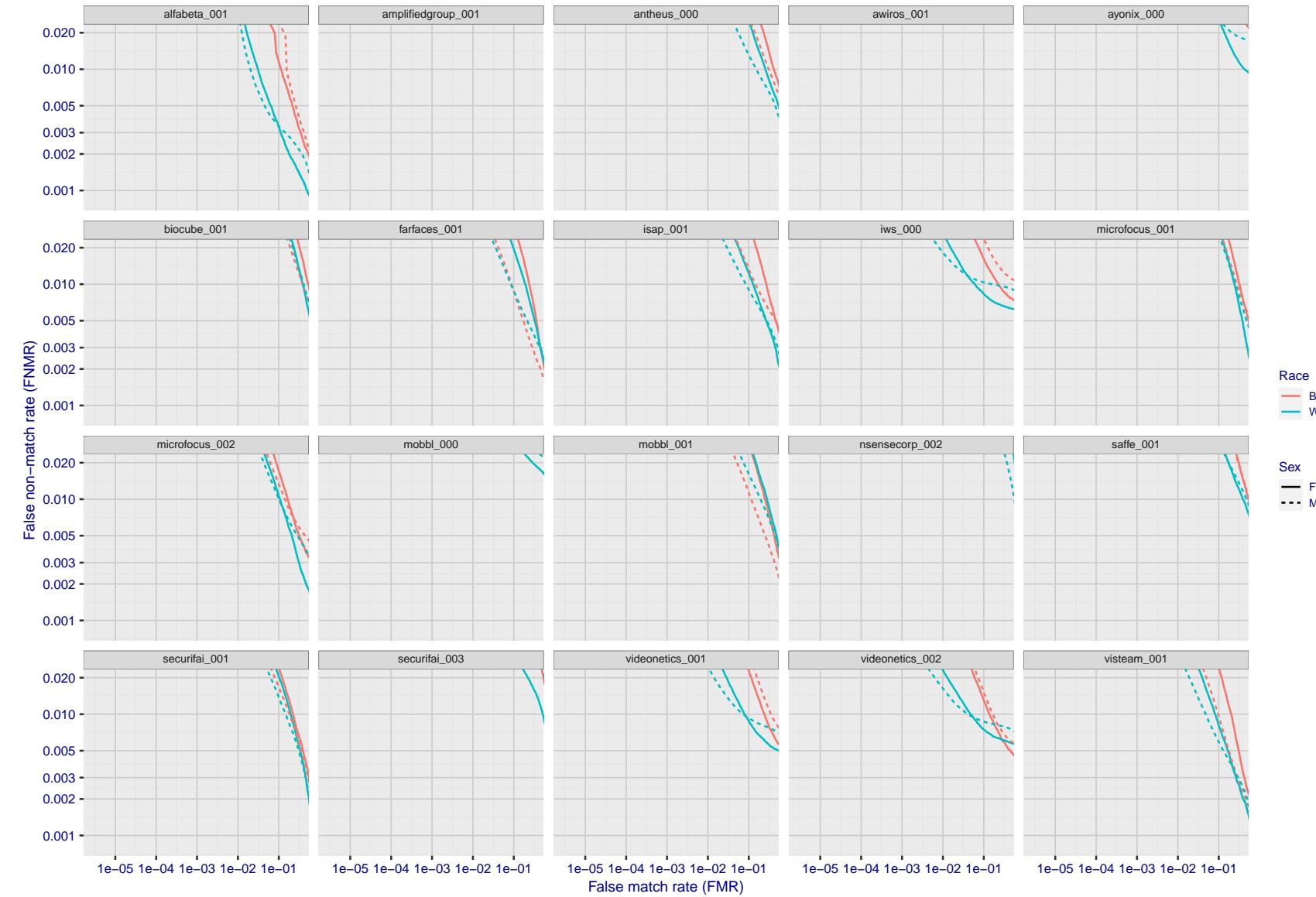


Figure 129: For the mugshot images, error tradeoff characteristics for white females, black females, black males and white males. The Z-shaped grey lines correspond to fixed thresholds, showing both FNMR and FMR vary at one T value. Note: Many of the plots will naively be read as saying women gives worse error rates than men because the solid traces lie above the dotted ones. However, this is misleading and incomplete: The grey lines show the traces reveal horizontal shifts. Thus for the cogent-003 algorithm FNMR for men is higher than for women at a fixed threshold but, at the same time, FMR is higher for women - see Figure 181. As access control systems almost always operate at a fixed threshold, the naive interpretation is incorrect.

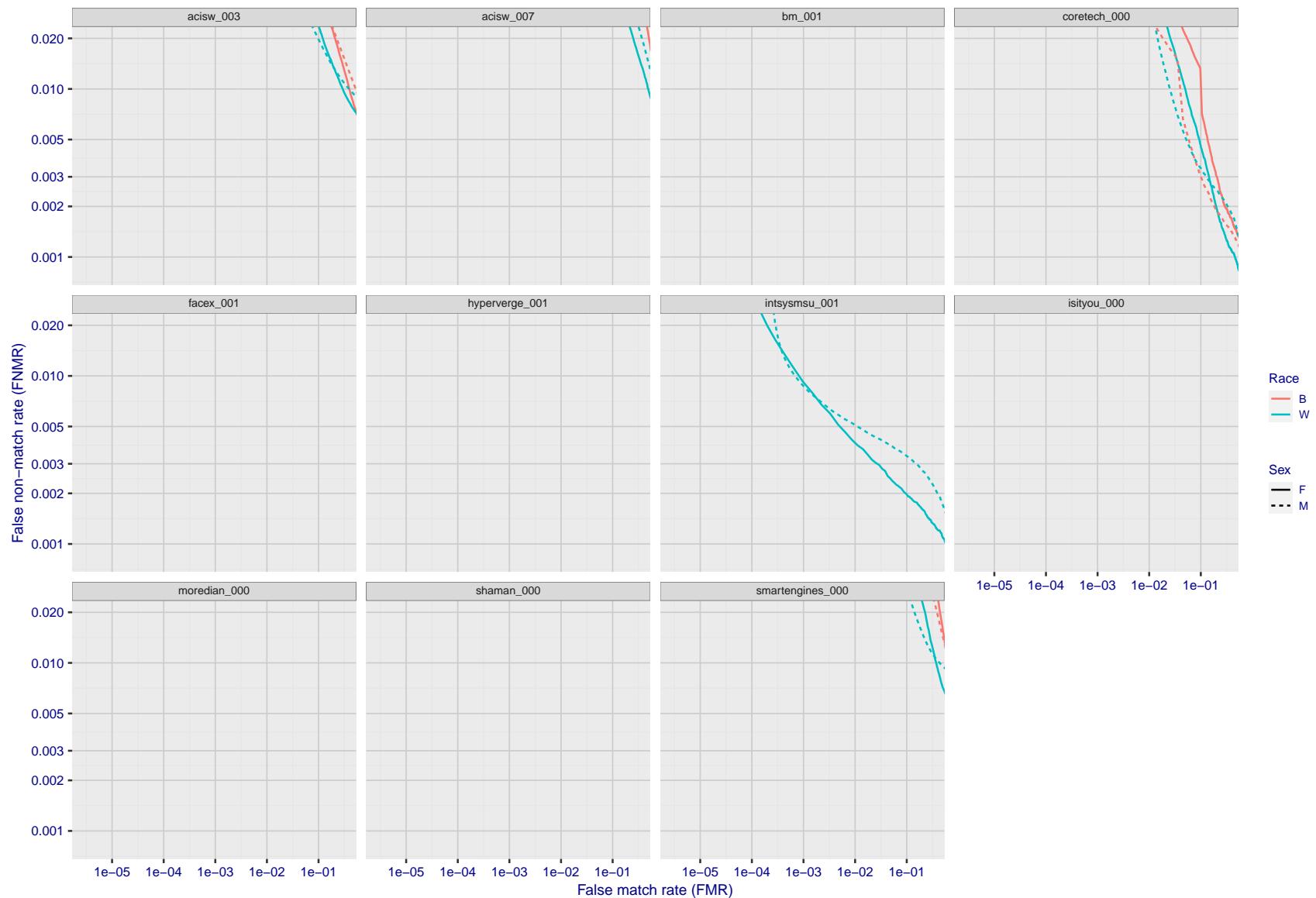


Figure 130: For the mugshot images, error tradeoff characteristics for white females, black females, black males and white males. The Z-shaped grey lines correspond to fixed thresholds, showing both FNMR and FMR vary at one T value. Note: Many of the plots will naively be read as saying women gives worse error rates than men because the solid traces lie above the dotted ones. However, this is misleading and incomplete: The grey lines show the traces reveal horizontal shifts. Thus for the cogent-003 algorithm FNMR for men is higher than for women at a fixed threshold but, at the same time, FMR is higher for women - see Figure 181. As access control systems almost always operate at a fixed threshold, the naive interpretation is incorrect.

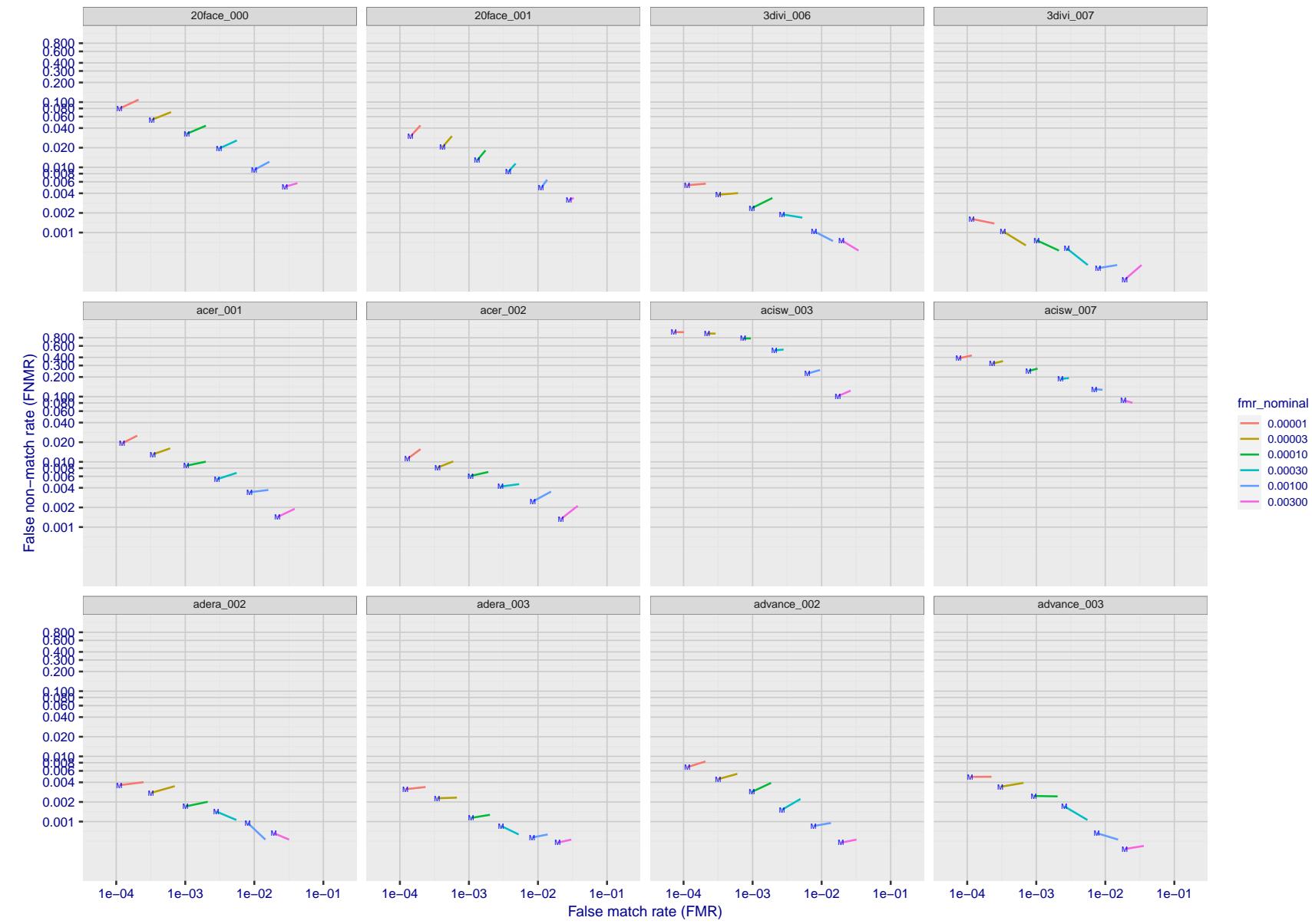


Figure 131: For the visa images, FNMR and FMR at six operating points along the DET characteristic. At each point a line is drawn between $(FMR, FNMR)_{MALE}$ and $(FMR, FNMR)_{FEMALE}$ showing how which sex has lower FMR and/or FNMR. The "M" label denotes male, the other end of the line corresponds to female. The six operating thresholds are selected to give the nominal false match rates given in the legend, and are computed over all impostor pairs regardless of age, sex, and place of birth. The plotted FMR values are broadly an order of magnitude larger than the nominal rates because FMR is computed over demographically-matched impostor pairs i.e individuals of the same sex, from the same geographic region (see section 3.6.1), and the same age group (see section 3.6.2).

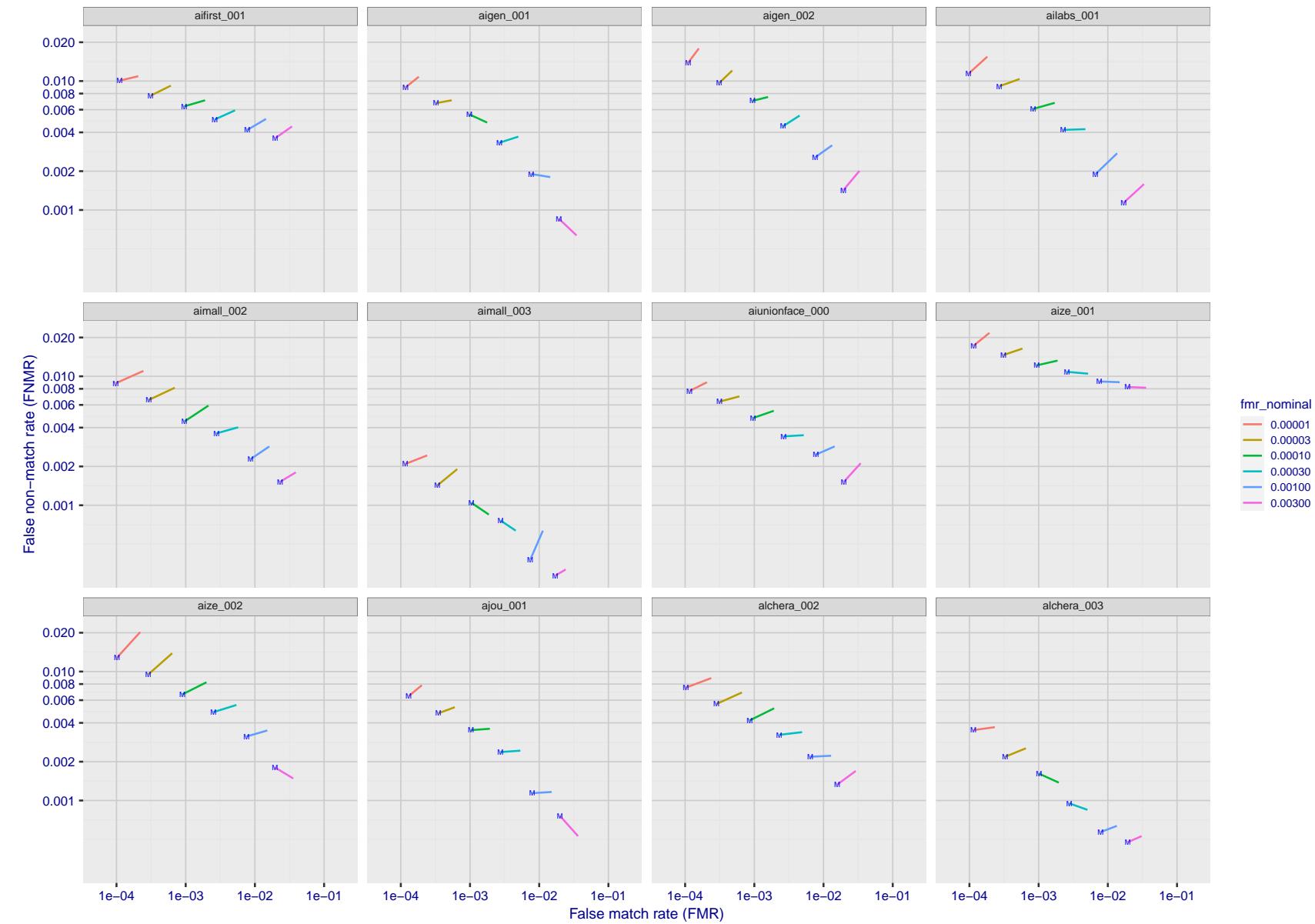


Figure 132: For the visa images, FNMR and FMR at six operating points along the DET characteristic. At each point a line is drawn between $(\text{FMR}, \text{FNMR})_{\text{MALE}}$ and $(\text{FMR}, \text{FNMR})_{\text{FEMALE}}$ showing how which sex has lower FMR and/or FNMR. The "M" label denotes male, the other end of the line corresponds to female. The six operating thresholds are selected to give the nominal false match rates given in the legend, and are computed over all impostor pairs regardless of age, sex, and place of birth. The plotted FMR values are broadly an order of magnitude larger than the nominal rates because FMR is computed over demographically-matched impostor pairs i.e individuals of the same sex, from the same geographic region (see section 3.6.1), and the same age group (see section 3.6.2).

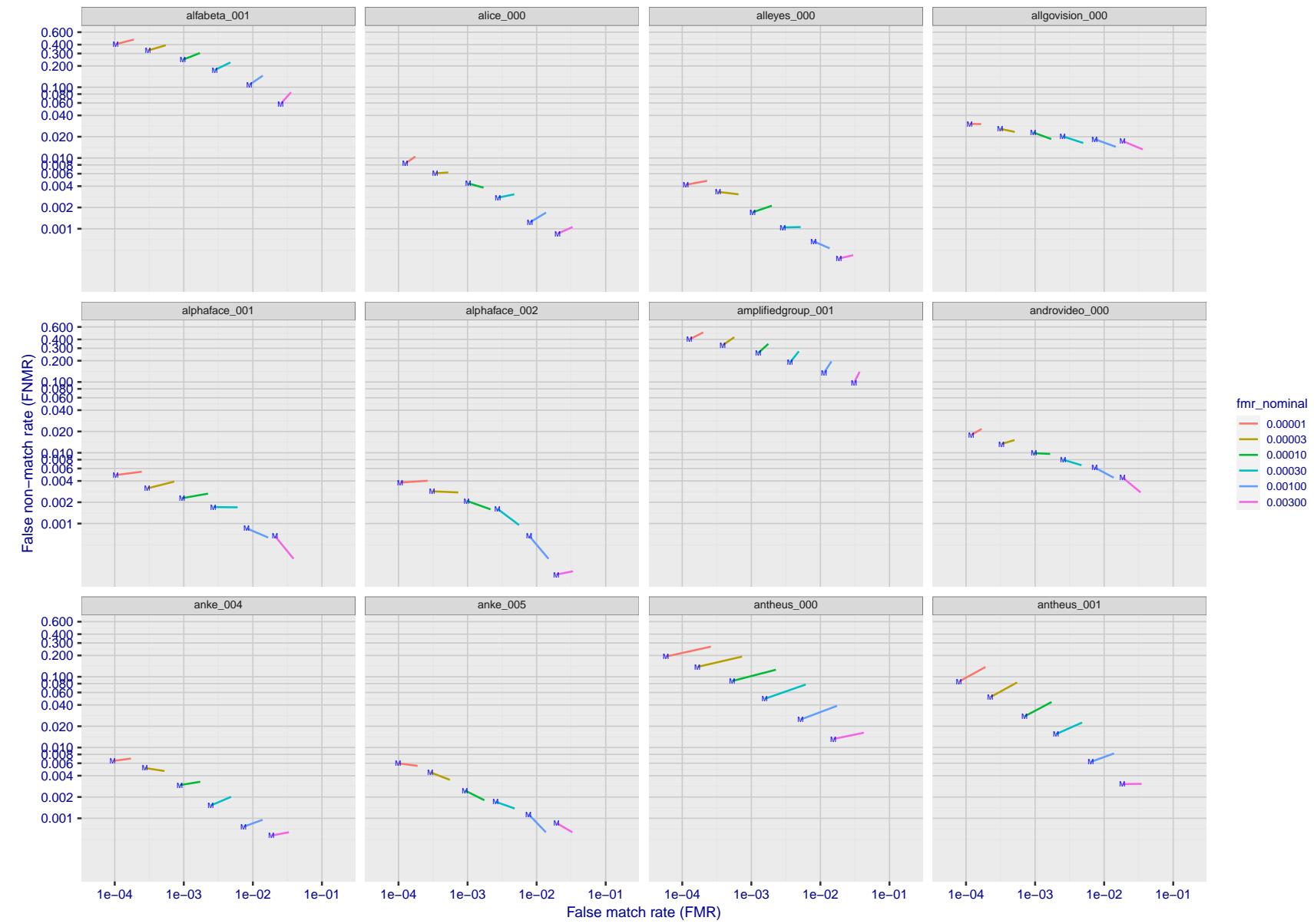


Figure 133: For the visa images, FNMR and FMR at six operating points along the DET characteristic. At each point a line is drawn between $(FMR, FNMR)_{MALE}$ and $(FMR, FNMR)_{FEMALE}$ showing how which sex has lower FMR and/or FNMR. The "M" label denotes male, the other end of the line corresponds to female. The six operating thresholds are selected to give the nominal false match rates given in the legend, and are computed over all impostor pairs regardless of age, sex, and place of birth. The plotted FMR values are broadly an order of magnitude larger than the nominal rates because FMR is computed over demographically-matched impostor pairs i.e individuals of the same sex, from the same geographic region (see section 3.6.1), and the same age group (see section 3.6.2).

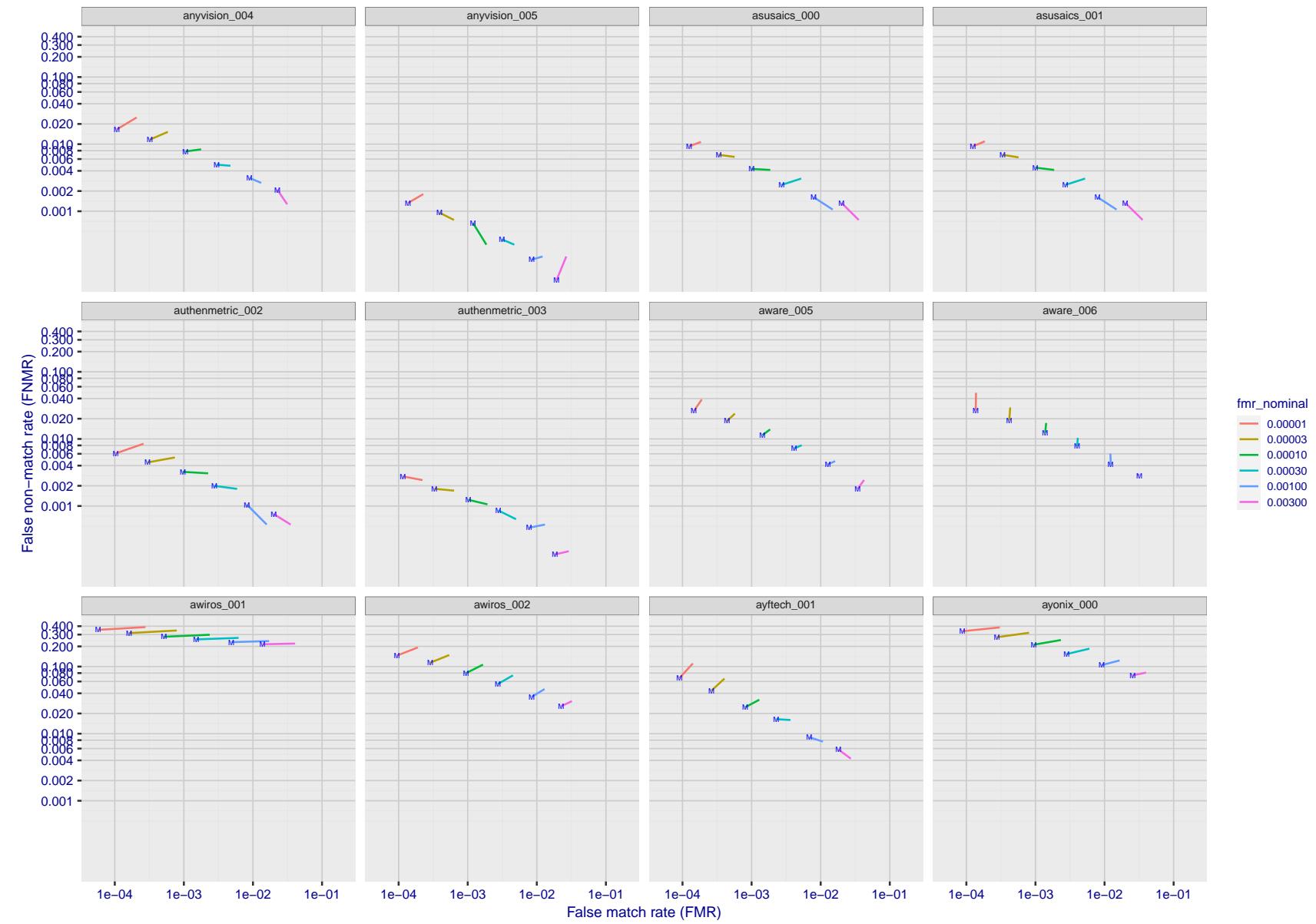


Figure 134: For the visa images, FNMR and FMR at six operating points along the DET characteristic. At each point a line is drawn between $(FMR, FNMR)_{MALE}$ and $(FMR, FNMR)_{FEMALE}$ showing how which sex has lower FMR and/or FNMR. The "M" label denotes male, the other end of the line corresponds to female. The six operating thresholds are selected to give the nominal false match rates given in the legend, and are computed over all impostor pairs regardless of age, sex, and place of birth. The plotted FMR values are broadly an order of magnitude larger than the nominal rates because FMR is computed over demographically-matched impostor pairs i.e individuals of the same sex, from the same geographic region (see section 3.6.1), and the same age group (see section 3.6.2).

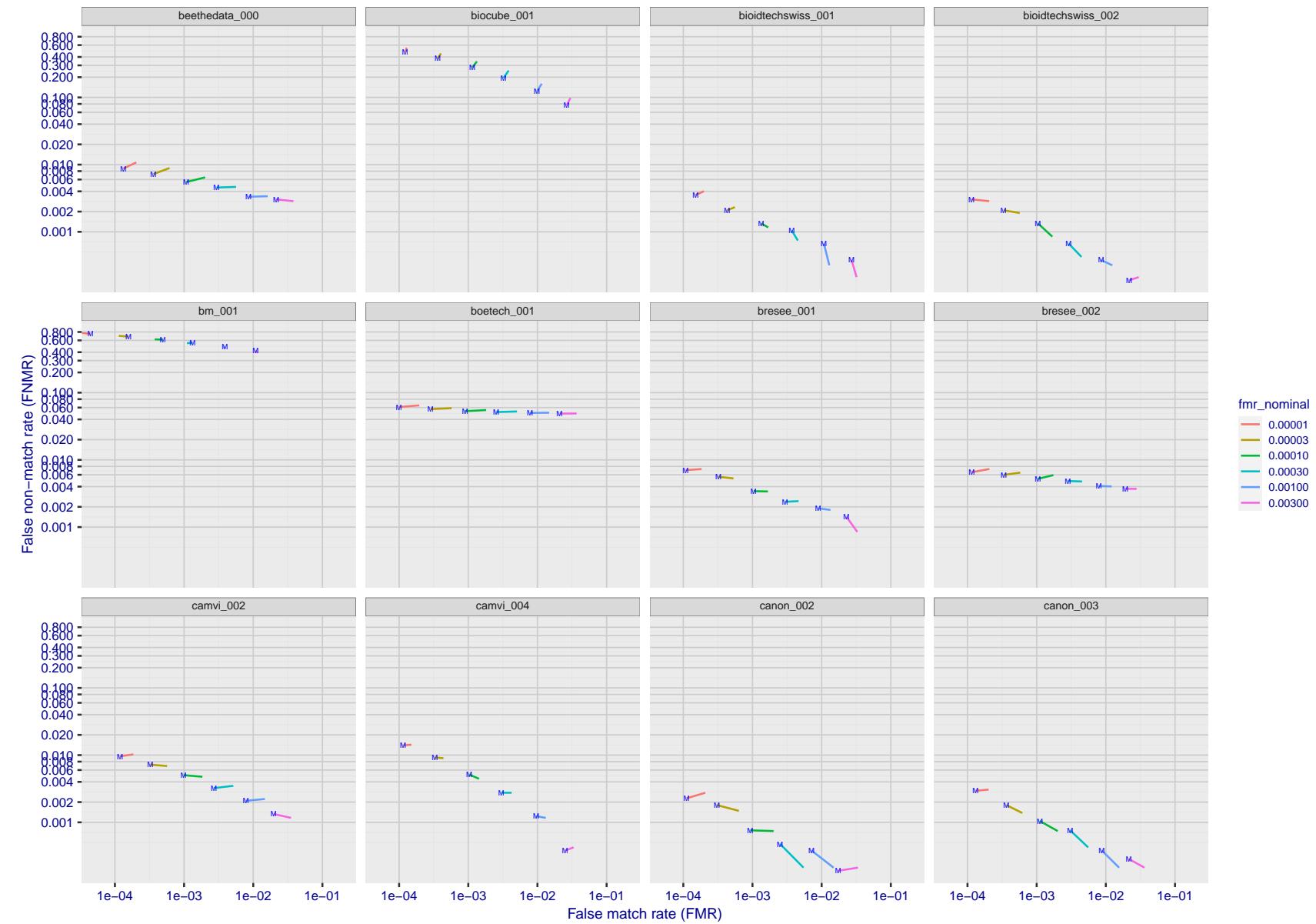


Figure 135: For the visa images, FNMR and FMR at six operating points along the DET characteristic. At each point a line is drawn between $(FMR, FNMR)_{MALE}$ and $(FMR, FNMR)_{FEMALE}$ showing how which sex has lower FMR and/or FNMR. The "M" label denotes male, the other end of the line corresponds to female. The six operating thresholds are selected to give the nominal false match rates given in the legend, and are computed over all impostor pairs regardless of age, sex, and place of birth. The plotted FMR values are broadly an order of magnitude larger than the nominal rates because FMR is computed over demographically-matched impostor pairs i.e individuals of the same sex, from the same geographic region (see section 3.6.1), and the same age group (see section 3.6.2).

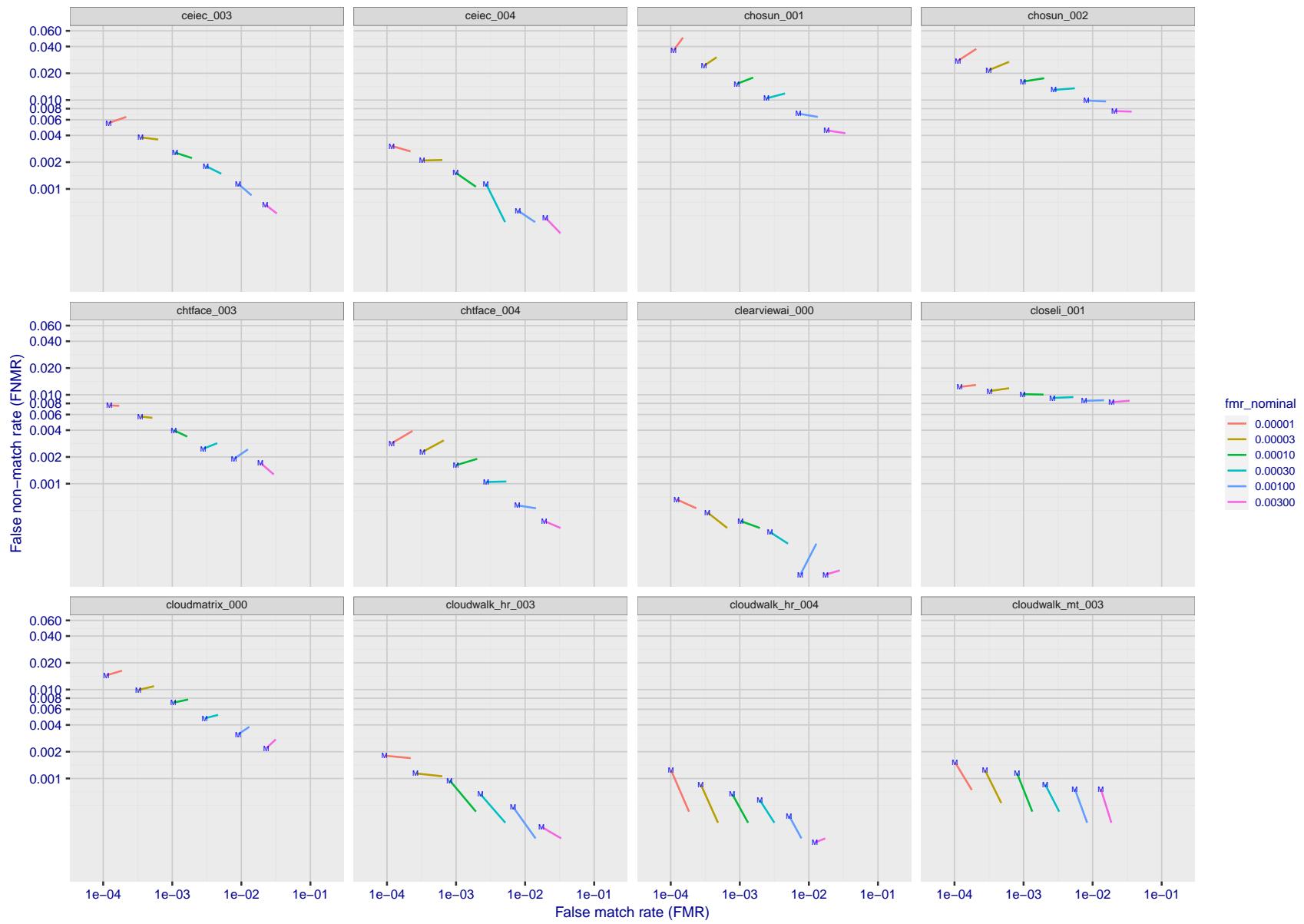


Figure 136: For the visa images, FNMR and FMR at six operating points along the DET characteristic. At each point a line is drawn between $(FMR, FNMR)_{MALE}$ and $(FMR, FNMR)_{FEMALE}$ showing how which sex has lower FMR and/or FNMR. The "M" label denotes male, the other end of the line corresponds to female. The six operating thresholds are selected to give the nominal false match rates given in the legend, and are computed over all impostor pairs regardless of age, sex, and place of birth. The plotted FMR values are broadly an order of magnitude larger than the nominal rates because FMR is computed over demographically-matched impostor pairs i.e individuals of the same sex, from the same geographic region (see section 3.6.1), and the same age group (see section 3.6.2).

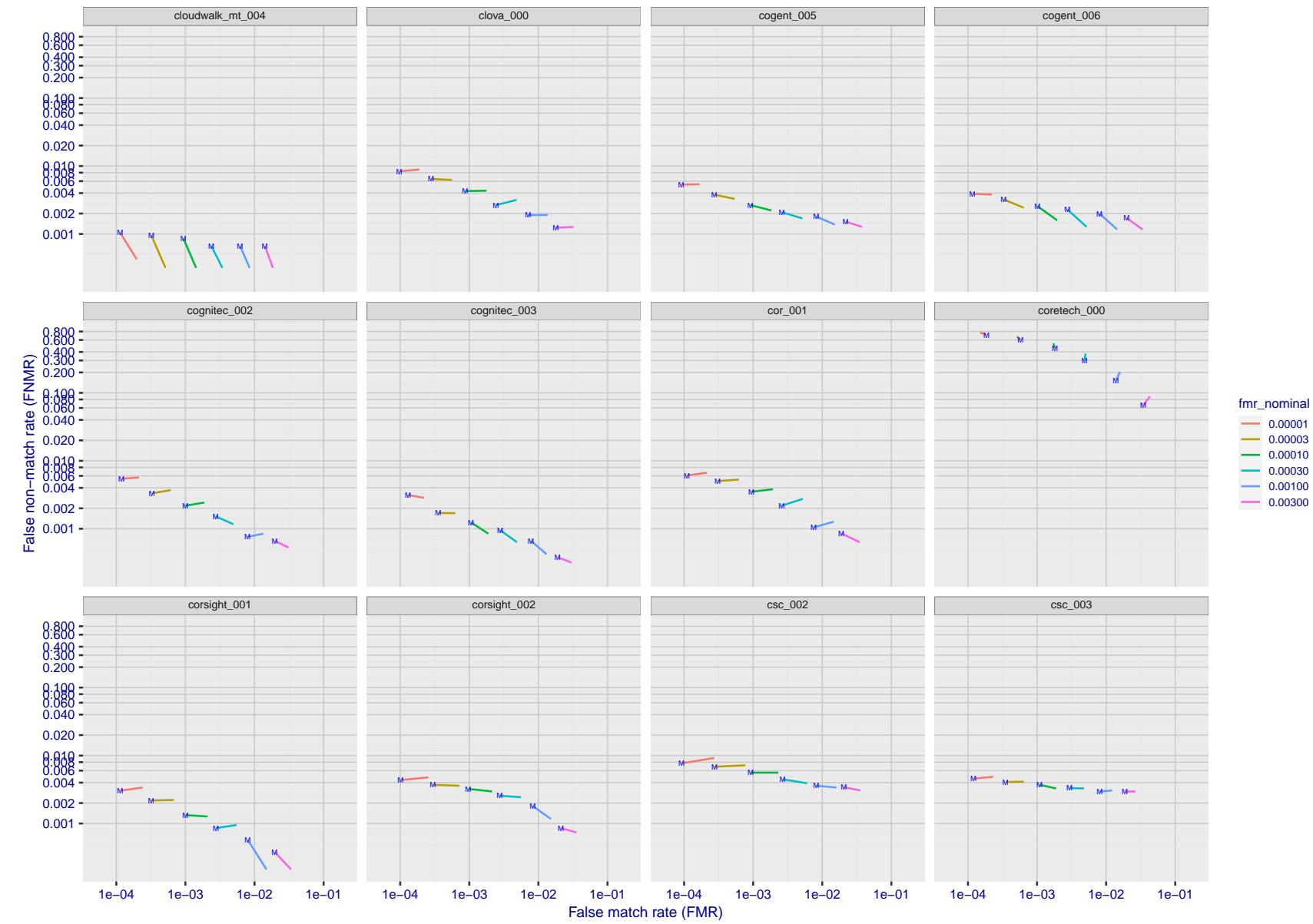


Figure 137: For the visa images, FNMR and FMR at six operating points along the DET characteristic. At each point a line is drawn between $(FMR, FNMR)_{MALE}$ and $(FMR, FNMR)_{FEMALE}$ showing how which sex has lower FMR and/or FNMR. The "M" label denotes male, the other end of the line corresponds to female. The six operating thresholds are selected to give the nominal false match rates given in the legend, and are computed over all impostor pairs regardless of age, sex, and place of birth. The plotted FMR values are broadly an order of magnitude larger than the nominal rates because FMR is computed over demographically-matched impostor pairs i.e individuals of the same sex, from the same geographic region (see section 3.6.1), and the same age group (see section 3.6.2).

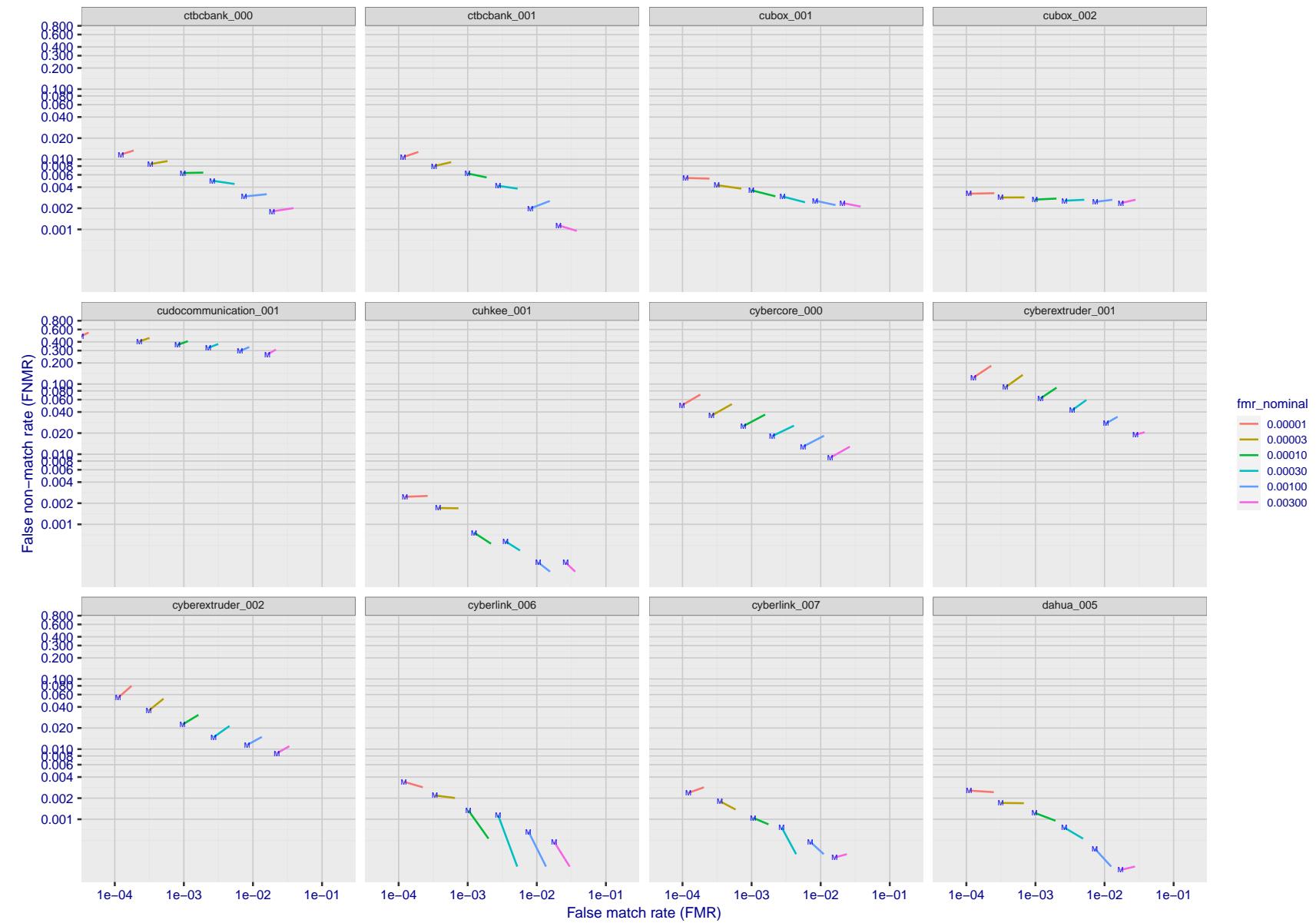


Figure 138: For the visa images, FNMR and FMR at six operating points along the DET characteristic. At each point a line is drawn between $(FMR, FNMR)_{MALE}$ and $(FMR, FNMR)_{FEMALE}$ showing how which sex has lower FMR and/or FNMR. The "M" label denotes male, the other end of the line corresponds to female. The six operating thresholds are selected to give the nominal false match rates given in the legend, and are computed over all impostor pairs regardless of age, sex, and place of birth. The plotted FMR values are broadly an order of magnitude larger than the nominal rates because FMR is computed over demographically-matched impostor pairs i.e individuals of the same sex, from the same geographic region (see section 3.6.1), and the same age group (see section 3.6.2).

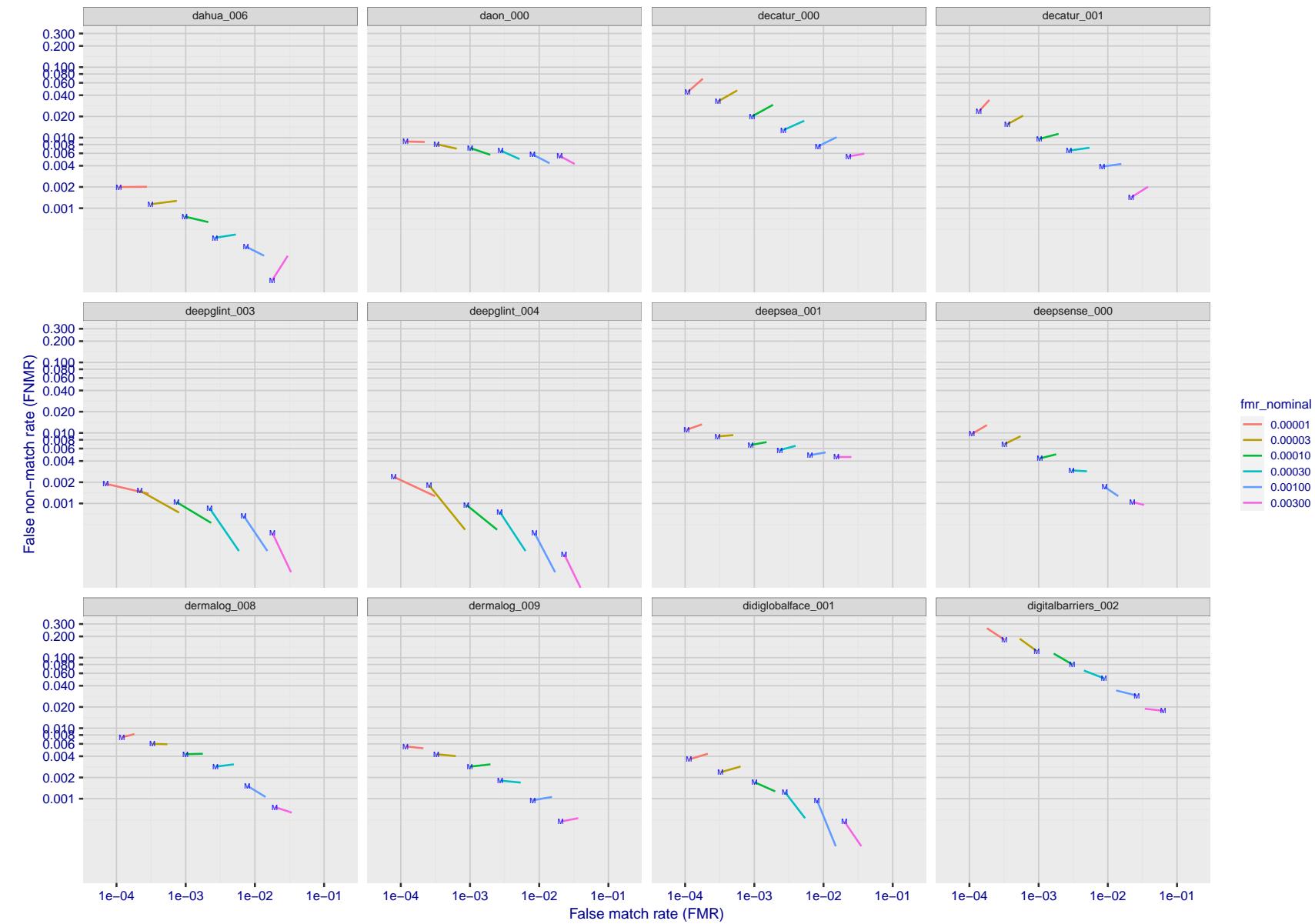


Figure 139: For the visa images, FNMR and FMR at six operating points along the DET characteristic. At each point a line is drawn between $(FMR, FNMR)_{MALE}$ and $(FMR, FNMR)_{FEMALE}$ showing how which sex has lower FMR and/or FNMR. The "M" label denotes male, the other end of the line corresponds to female. The six operating thresholds are selected to give the nominal false match rates given in the legend, and are computed over all impostor pairs regardless of age, sex, and place of birth. The plotted FMR values are broadly an order of magnitude larger than the nominal rates because FMR is computed over demographically-matched impostor pairs i.e individuals of the same sex, from the same geographic region (see section 3.6.1), and the same age group (see section 3.6.2).

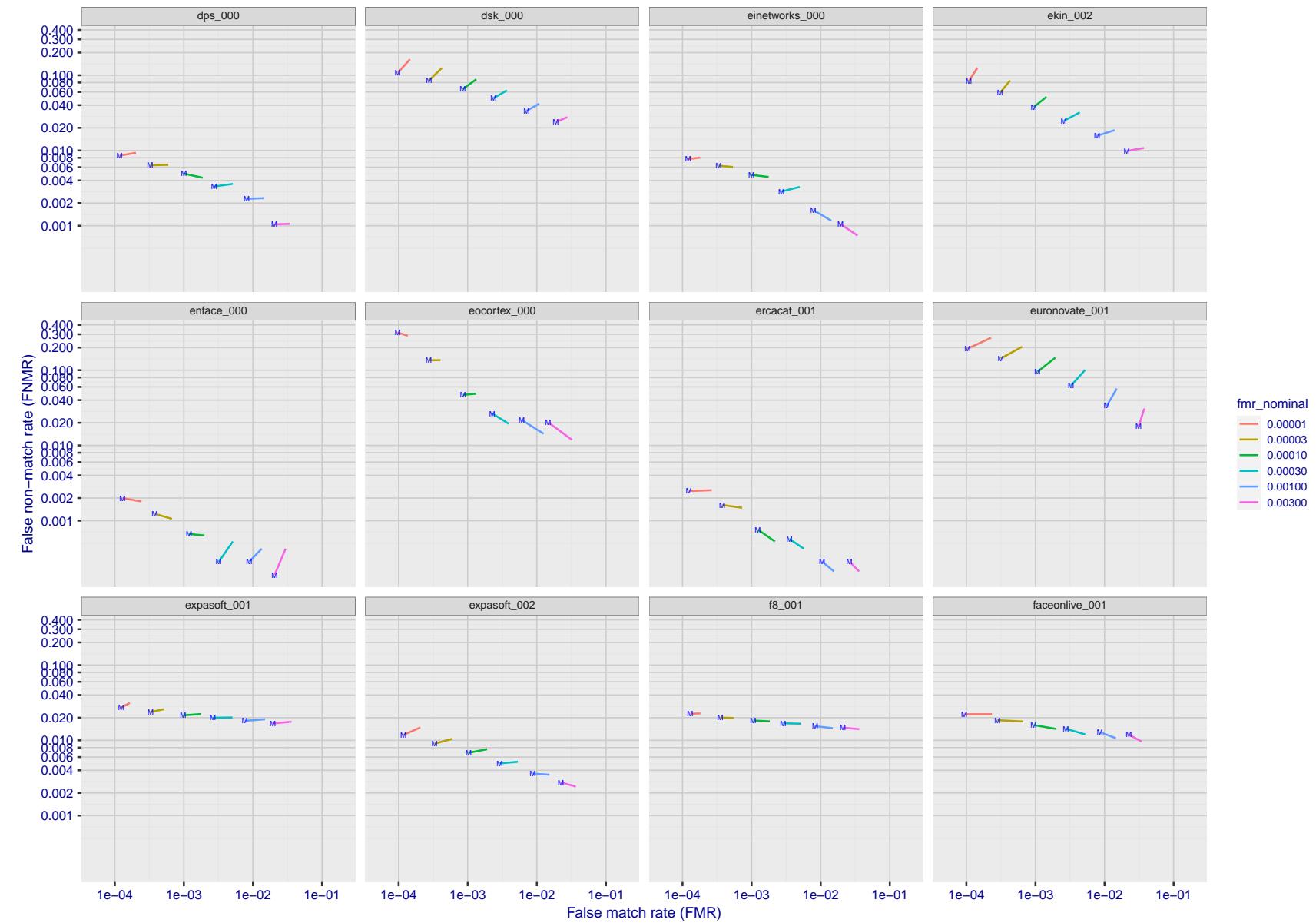


Figure 140: For the visa images, FNMR and FMR at six operating points along the DET characteristic. At each point a line is drawn between $(FMR, FNMR)_{MALE}$ and $(FMR, FNMR)_{FEMALE}$ showing how which sex has lower FMR and/or FNMR. The "M" label denotes male, the other end of the line corresponds to female. The six operating thresholds are selected to give the nominal false match rates given in the legend, and are computed over all impostor pairs regardless of age, sex, and place of birth. The plotted FMR values are broadly an order of magnitude larger than the nominal rates because FMR is computed over demographically-matched impostor pairs i.e individuals of the same sex, from the same geographic region (see section 3.6.1), and the same age group (see section 3.6.2).

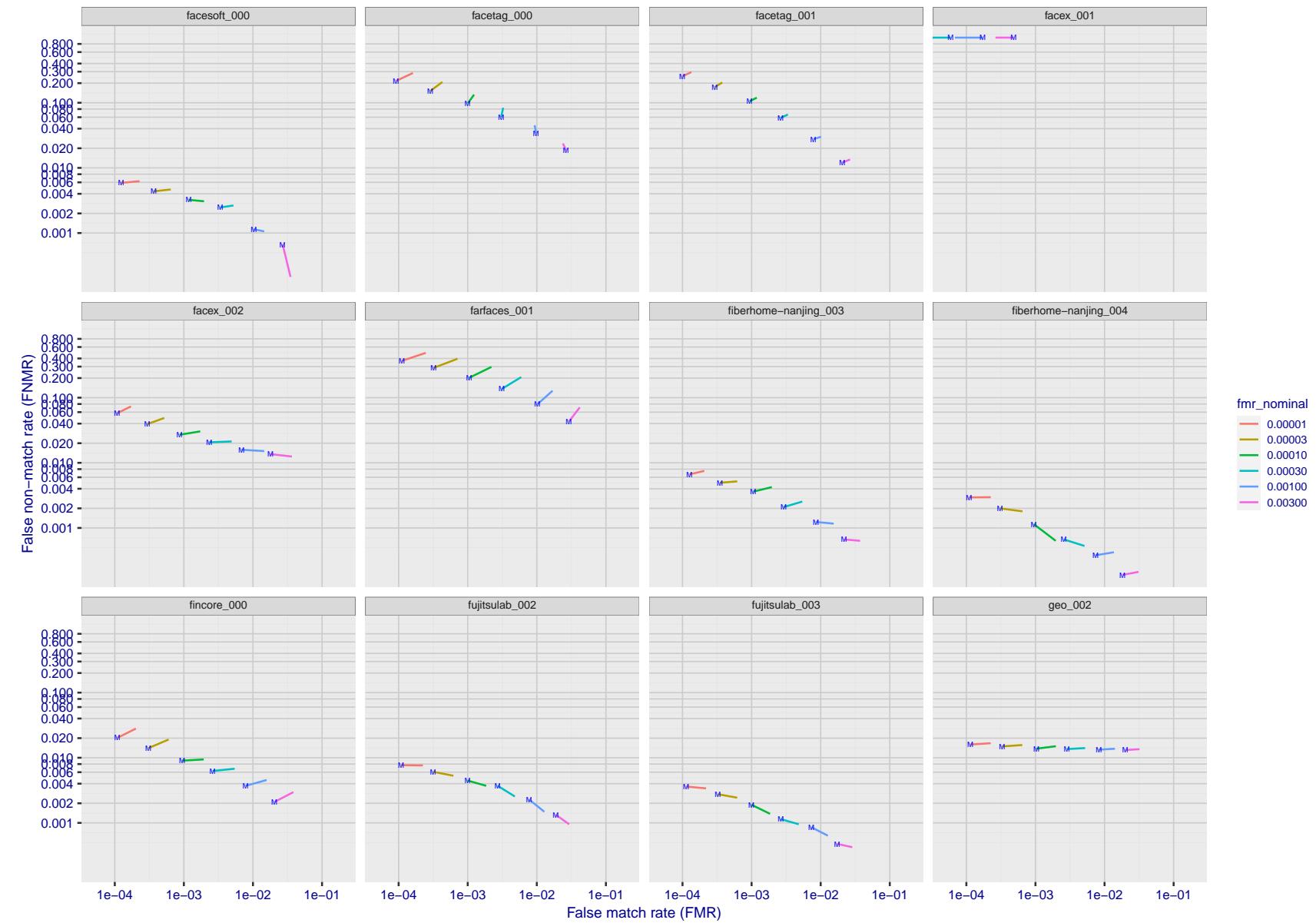


Figure 141: For the visa images, FNMR and FMR at six operating points along the DET characteristic. At each point a line is drawn between $(FMR, FNMR)_{MALE}$ and $(FMR, FNMR)_{FEMALE}$ showing how which sex has lower FMR and/or FNMR. The "M" label denotes male, the other end of the line corresponds to female. The six operating thresholds are selected to give the nominal false match rates given in the legend, and are computed over all impostor pairs regardless of age, sex, and place of birth. The plotted FMR values are broadly an order of magnitude larger than the nominal rates because FMR is computed over demographically-matched impostor pairs i.e individuals of the same sex, from the same geographic region (see section 3.6.1), and the same age group (see section 3.6.2).

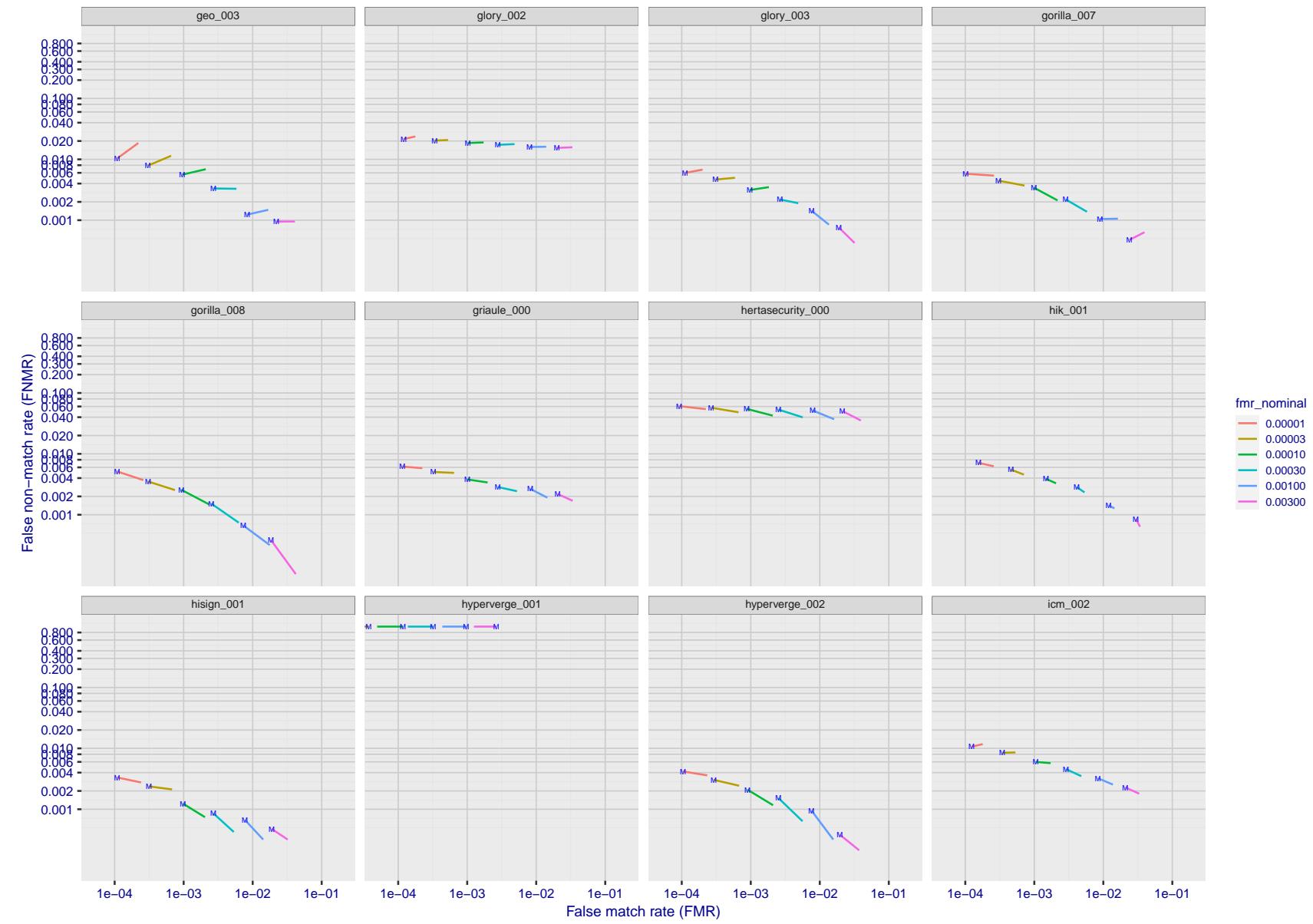


Figure 142: For the visa images, FNMR and FMR at six operating points along the DET characteristic. At each point a line is drawn between $(FMR, FNMR)_{MALE}$ and $(FMR, FNMR)_{FEMALE}$ showing how which sex has lower FMR and/or FNMR. The "M" label denotes male, the other end of the line corresponds to female. The six operating thresholds are selected to give the nominal false match rates given in the legend, and are computed over all impostor pairs regardless of age, sex, and place of birth. The plotted FMR values are broadly an order of magnitude larger than the nominal rates because FMR is computed over demographically-matched impostor pairs i.e individuals of the same sex, from the same geographic region (see section 3.6.1), and the same age group (see section 3.6.2).

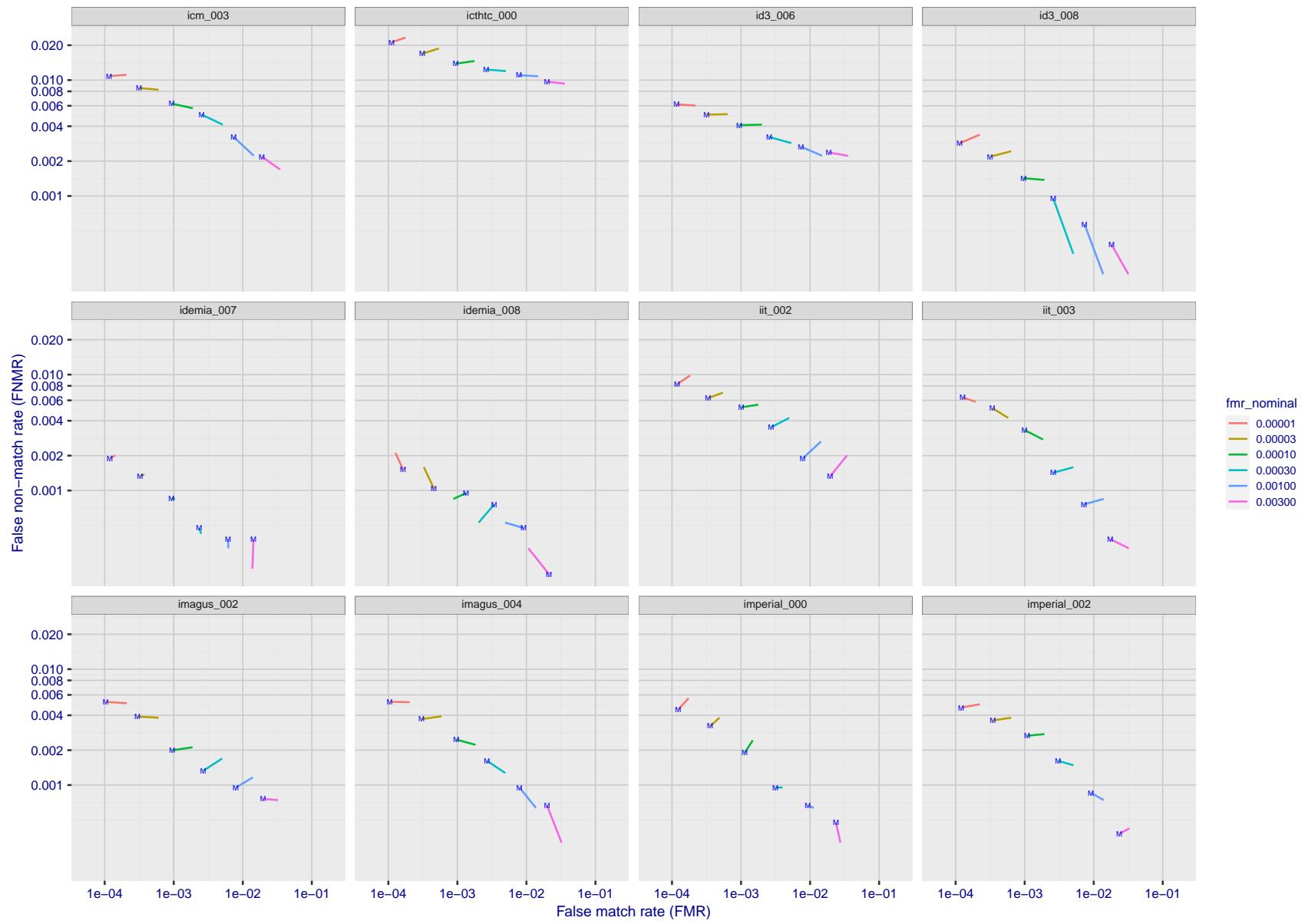


Figure 143: For the visa images, FNMR and FMR at six operating points along the DET characteristic. At each point a line is drawn between $(FMR, FNMR)_{MALE}$ and $(FMR, FNMR)_{FEMALE}$ showing how which sex has lower FMR and/or FNMR. The "M" label denotes male, the other end of the line corresponds to female. The six operating thresholds are selected to give the nominal false match rates given in the legend, and are computed over all impostor pairs regardless of age, sex, and place of birth. The plotted FMR values are broadly an order of magnitude larger than the nominal rates because FMR is computed over demographically-matched impostor pairs i.e individuals of the same sex, from the same geographic region (see section 3.6.1), and the same age group (see section 3.6.2).

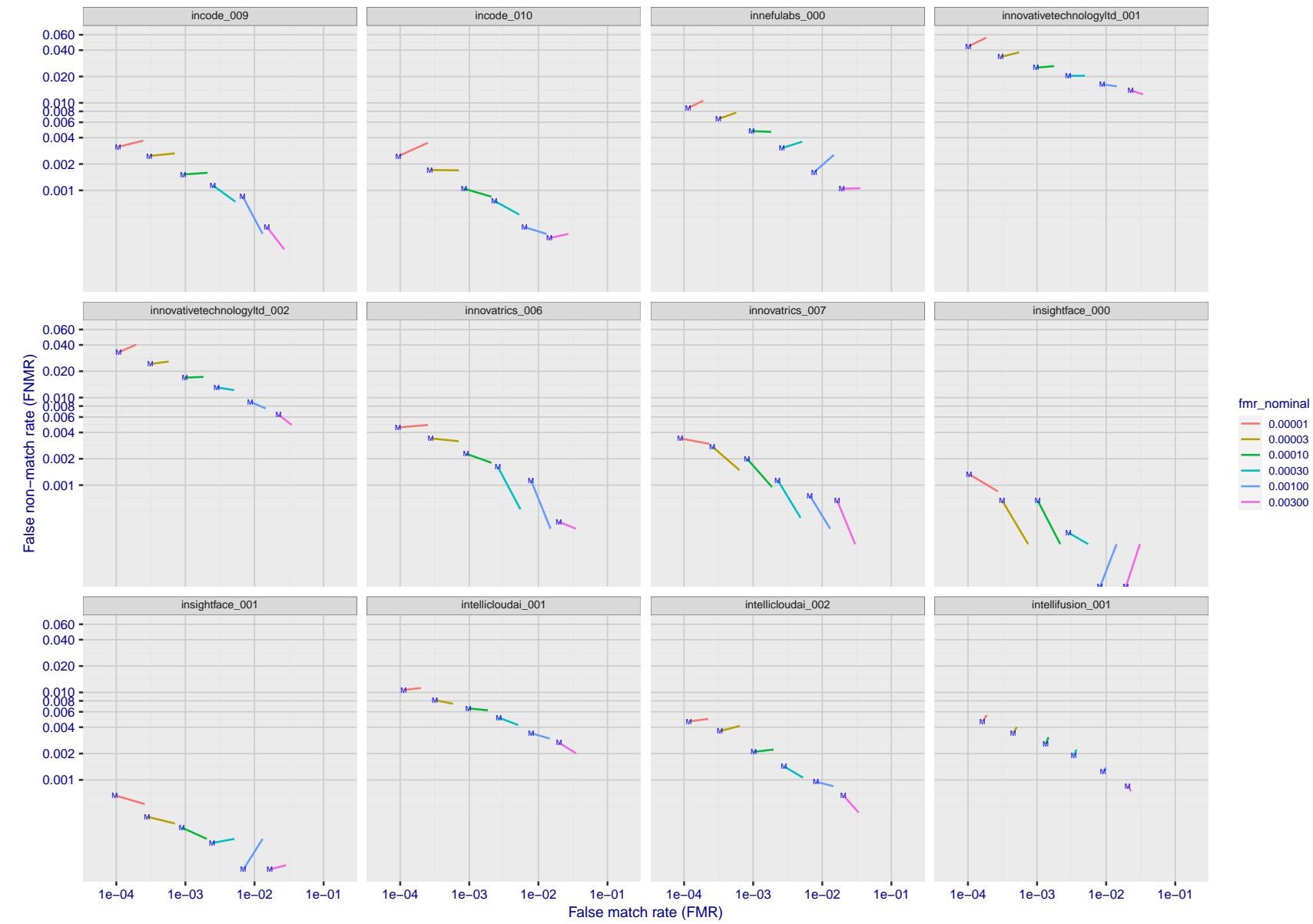


Figure 144: For the visa images, FNMR and FMR at six operating points along the DET characteristic. At each point a line is drawn between $(FMR, FNMR)_{MALE}$ and $(FMR, FNMR)_{FEMALE}$ showing how which sex has lower FMR and/or FNMR. The "M" label denotes male, the other end of the line corresponds to female. The six operating thresholds are selected to give the nominal false match rates given in the legend, and are computed over all impostor pairs regardless of age, sex, and place of birth. The plotted FMR values are broadly an order of magnitude larger than the nominal rates because FMR is computed over demographically-matched impostor pairs i.e individuals of the same sex, from the same geographic region (see section 3.6.1), and the same age group (see section 3.6.2).

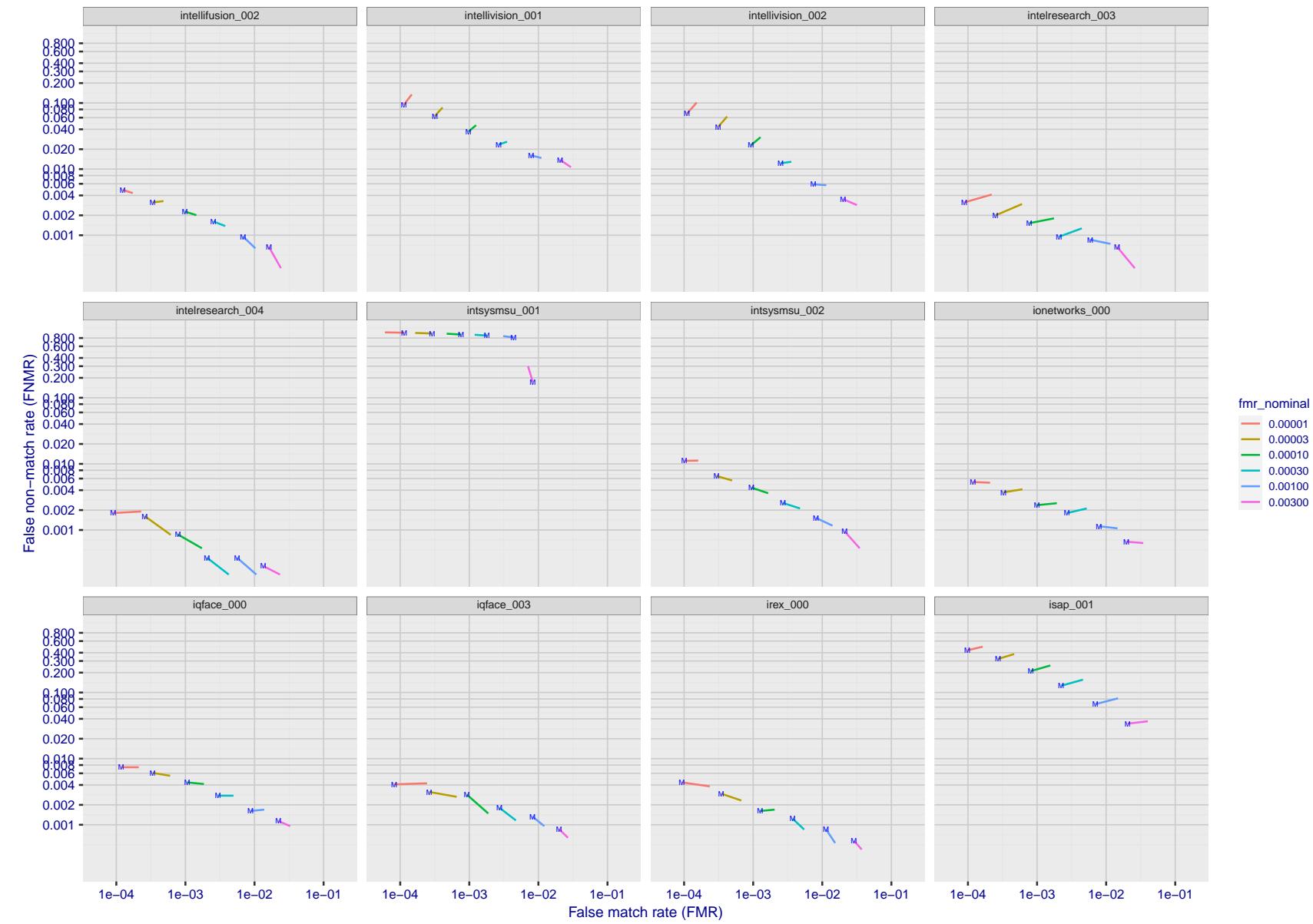


Figure 145: For the visa images, FNMR and FMR at six operating points along the DET characteristic. At each point a line is drawn between $(FMR, FNMR)_{MALE}$ and $(FMR, FNMR)_{FEMALE}$ showing how which sex has lower FMR and/or FNMR. The "M" label denotes male, the other end of the line corresponds to female. The six operating thresholds are selected to give the nominal false match rates given in the legend, and are computed over all impostor pairs regardless of age, sex, and place of birth. The plotted FMR values are broadly an order of magnitude larger than the nominal rates because FMR is computed over demographically-matched impostor pairs i.e individuals of the same sex, from the same geographic region (see section 3.6.1), and the same age group (see section 3.6.2).

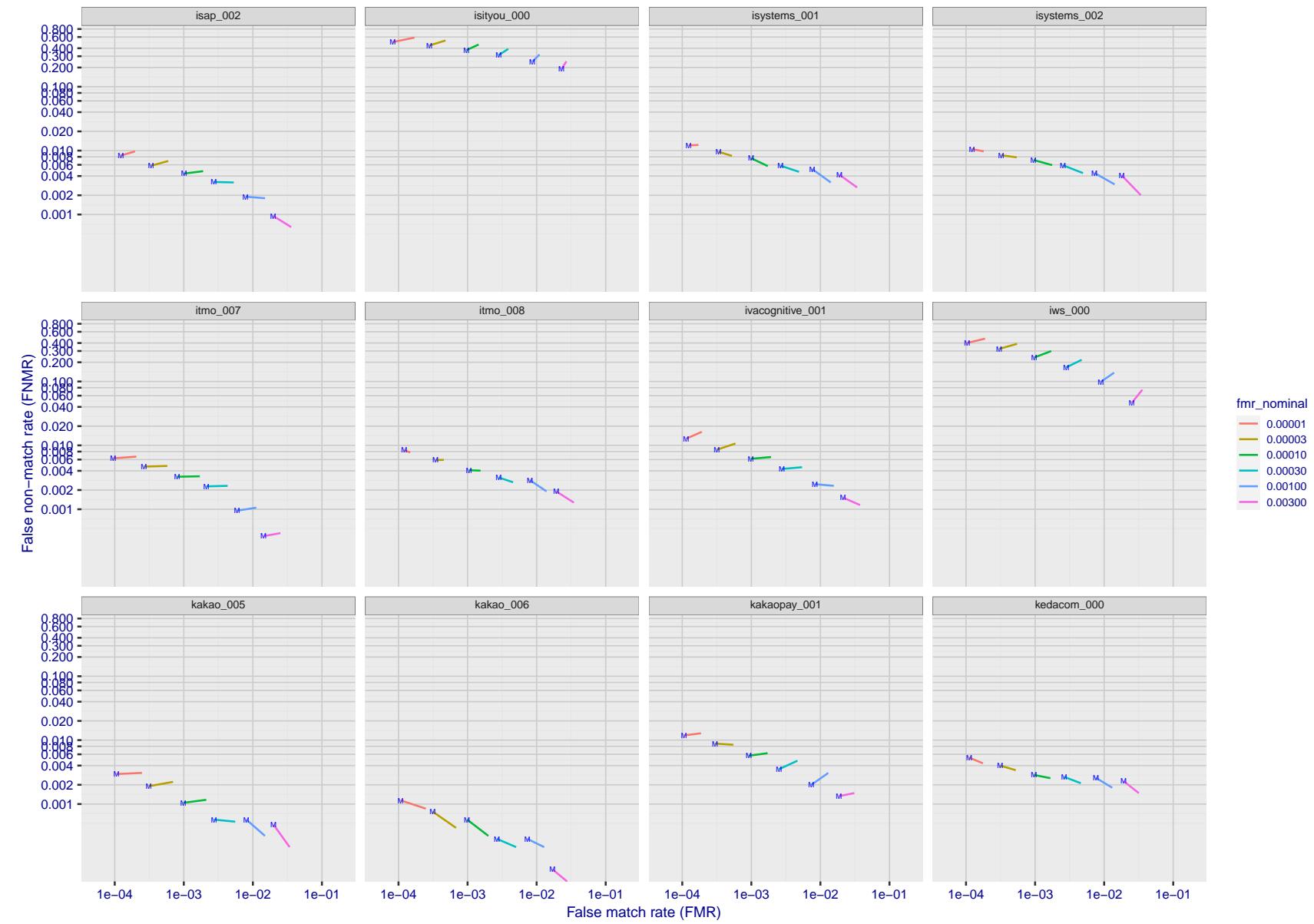


Figure 146: For the visa images, FNMR and FMR at six operating points along the DET characteristic. At each point a line is drawn between $(FMR, FNMR)_{MALE}$ and $(FMR, FNMR)_{FEMALE}$ showing how which sex has lower FMR and/or FNMR. The "M" label denotes male, the other end of the line corresponds to female. The six operating thresholds are selected to give the nominal false match rates given in the legend, and are computed over all impostor pairs regardless of age, sex, and place of birth. The plotted FMR values are broadly an order of magnitude larger than the nominal rates because FMR is computed over demographically-matched impostor pairs i.e individuals of the same sex, from the same geographic region (see section 3.6.1), and the same age group (see section 3.6.2).

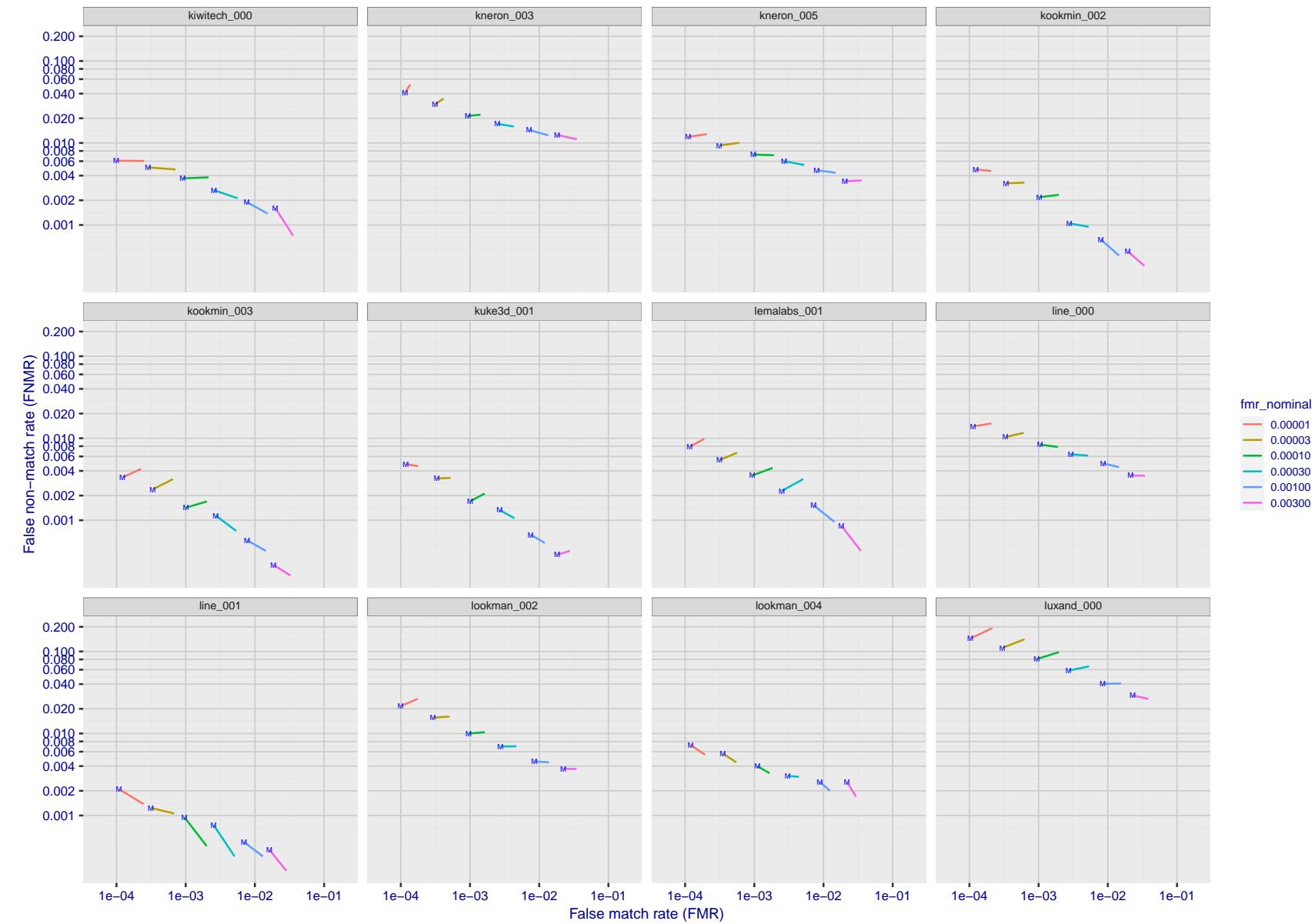


Figure 147: For the visa images, FNMR and FMR at six operating points along the DET characteristic. At each point a line is drawn between $(FMR, FNMR)_{MALE}$ and $(FMR, FNMR)_{FEMALE}$ showing how which sex has lower FMR and/or FNMR. The "M" label denotes male, the other end of the line corresponds to female. The six operating thresholds are selected to give the nominal false match rates given in the legend, and are computed over all impostor pairs regardless of age, sex, and place of birth. The plotted FMR values are broadly an order of magnitude larger than the nominal rates because FMR is computed over demographically-matched impostor pairs i.e individuals of the same sex, from the same geographic region (see section 3.6.1), and the same age group (see section 3.6.2).

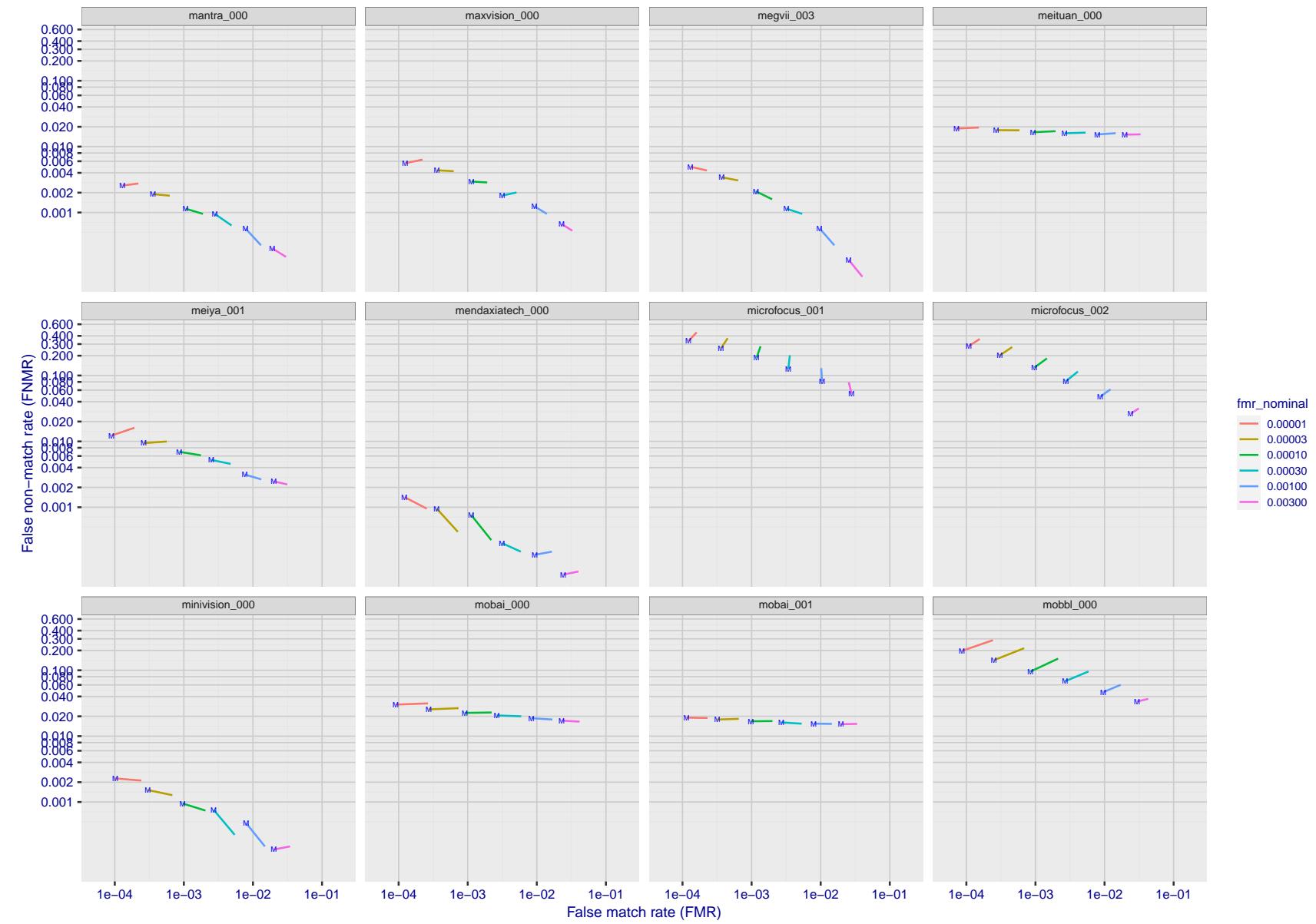


Figure 148: For the visa images, FNMR and FMR at six operating points along the DET characteristic. At each point a line is drawn between $(FMR, FNMR)_{MALE}$ and $(FMR, FNMR)_{FEMALE}$ showing how which sex has lower FMR and/or FNMR. The "M" label denotes male, the other end of the line corresponds to female. The six operating thresholds are selected to give the nominal false match rates given in the legend, and are computed over all impostor pairs regardless of age, sex, and place of birth. The plotted FMR values are broadly an order of magnitude larger than the nominal rates because FMR is computed over demographically-matched impostor pairs i.e individuals of the same sex, from the same geographic region (see section 3.6.1), and the same age group (see section 3.6.2).

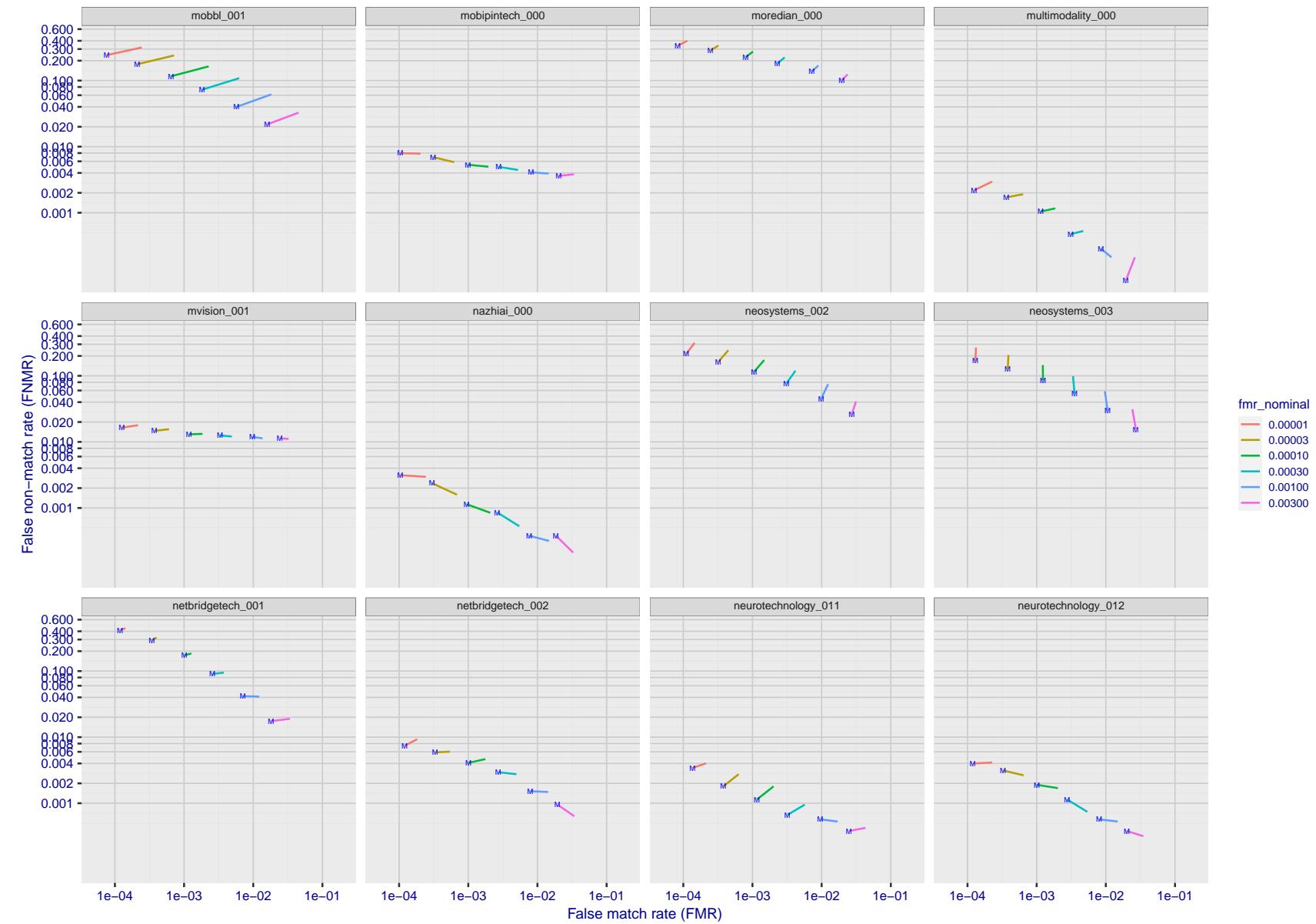


Figure 149: For the visa images, FNMR and FMR at six operating points along the DET characteristic. At each point a line is drawn between $(FMR, FNMR)_{MALE}$ and $(FMR, FNMR)_{FEMALE}$ showing how which sex has lower FMR and/or FNMR. The "M" label denotes male, the other end of the line corresponds to female. The six operating thresholds are selected to give the nominal false match rates given in the legend, and are computed over all impostor pairs regardless of age, sex, and place of birth. The plotted FMR values are broadly an order of magnitude larger than the nominal rates because FMR is computed over demographically-matched impostor pairs i.e individuals of the same sex, from the same geographic region (see section 3.6.1), and the same age group (see section 3.6.2).

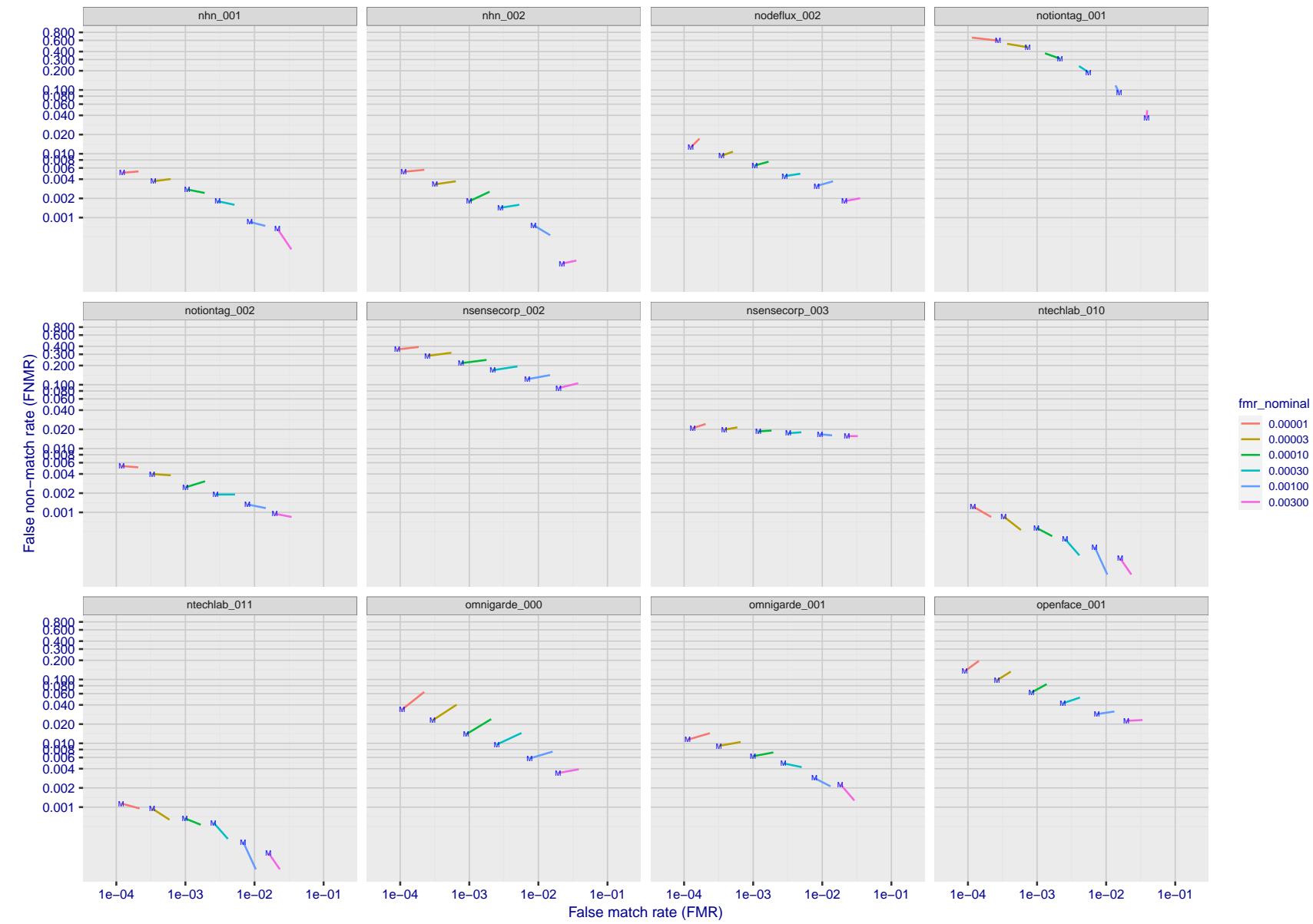


Figure 150: For the visa images, FNMR and FMR at six operating points along the DET characteristic. At each point a line is drawn between $(FMR, FNMR)_{MALE}$ and $(FMR, FNMR)_{FEMALE}$ showing how which sex has lower FMR and/or FNMR. The "M" label denotes male, the other end of the line corresponds to female. The six operating thresholds are selected to give the nominal false match rates given in the legend, and are computed over all impostor pairs regardless of age, sex, and place of birth. The plotted FMR values are broadly an order of magnitude larger than the nominal rates because FMR is computed over demographically-matched impostor pairs i.e individuals of the same sex, from the same geographic region (see section 3.6.1), and the same age group (see section 3.6.2).

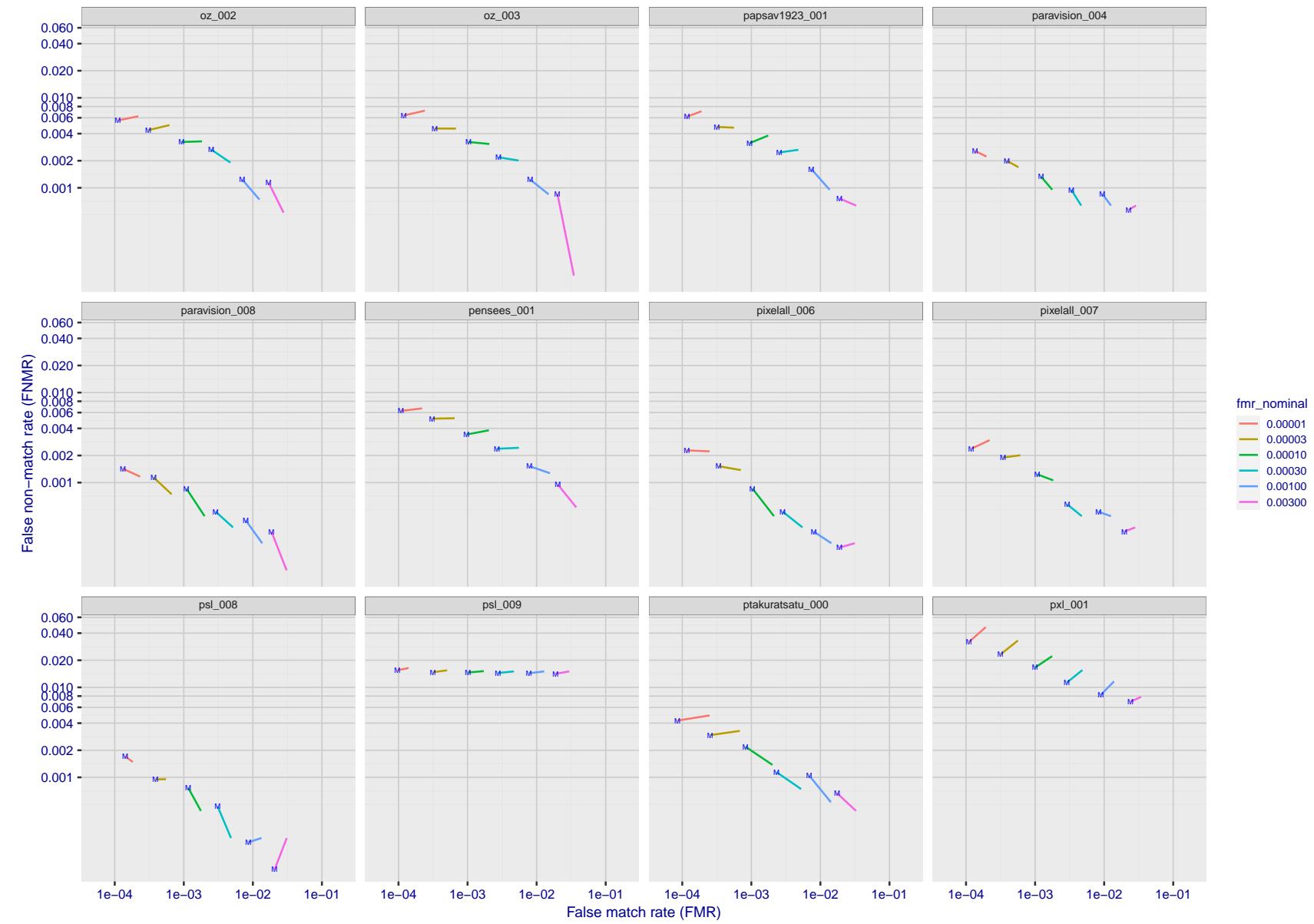


Figure 151: For the visa images, FNMR and FMR at six operating points along the DET characteristic. At each point a line is drawn between $(FMR, FNMR)_{MALE}$ and $(FMR, FNMR)_{FEMALE}$ showing how which sex has lower FMR and/or FNMR. The "M" label denotes male, the other end of the line corresponds to female. The six operating thresholds are selected to give the nominal false match rates given in the legend, and are computed over all impostor pairs regardless of age, sex, and place of birth. The plotted FMR values are broadly an order of magnitude larger than the nominal rates because FMR is computed over demographically-matched impostor pairs i.e individuals of the same sex, from the same geographic region (see section 3.6.1), and the same age group (see section 3.6.2).

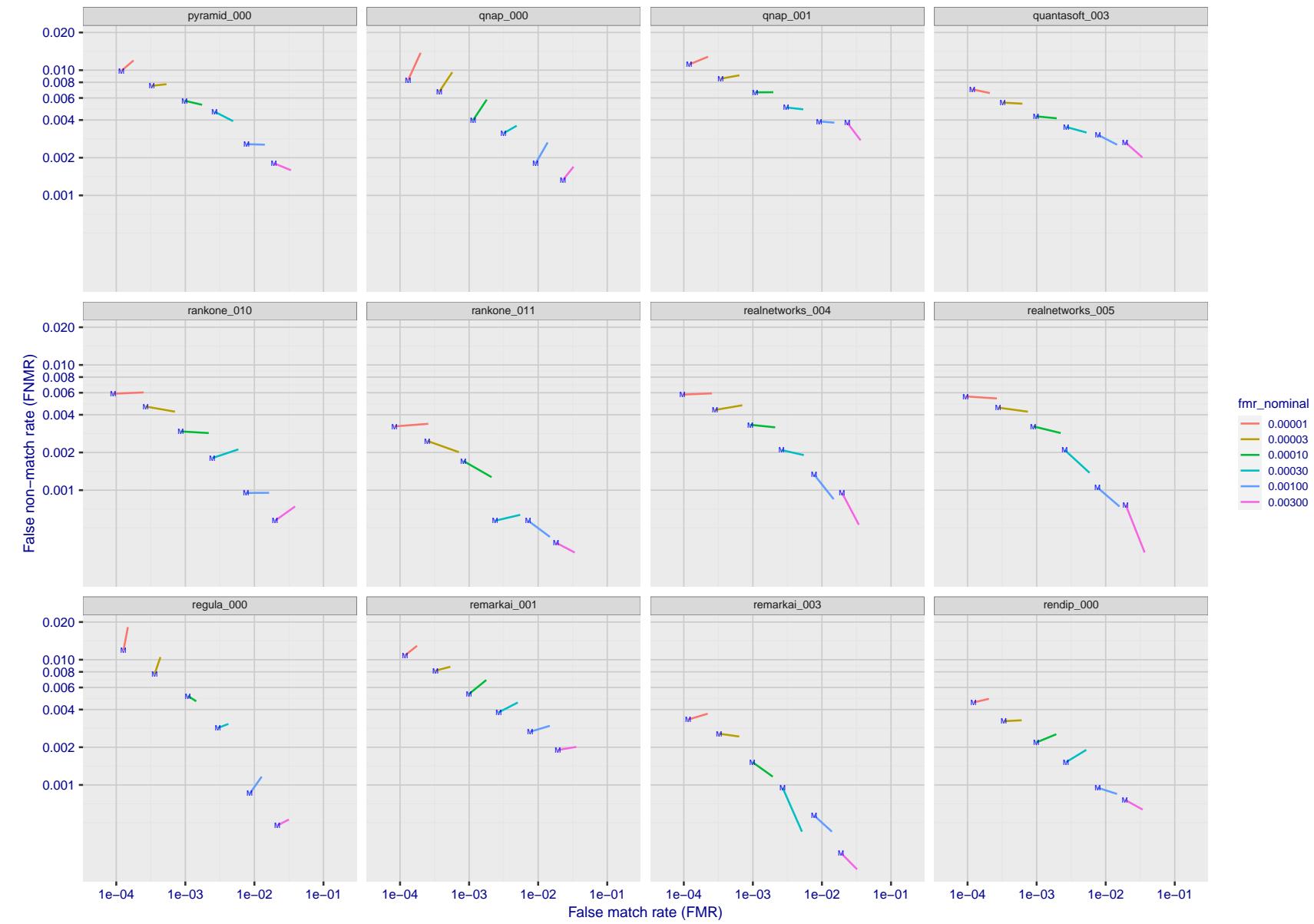


Figure 152: For the visa images, FNMR and FMR at six operating points along the DET characteristic. At each point a line is drawn between $(FMR, FNMR)_{MALE}$ and $(FMR, FNMR)_{FEMALE}$ showing how which sex has lower FMR and/or FNMR. The "M" label denotes male, the other end of the line corresponds to female. The six operating thresholds are selected to give the nominal false match rates given in the legend, and are computed over all impostor pairs regardless of age, sex, and place of birth. The plotted FMR values are broadly an order of magnitude larger than the nominal rates because FMR is computed over demographically-matched impostor pairs i.e individuals of the same sex, from the same geographic region (see section 3.6.1), and the same age group (see section 3.6.2).

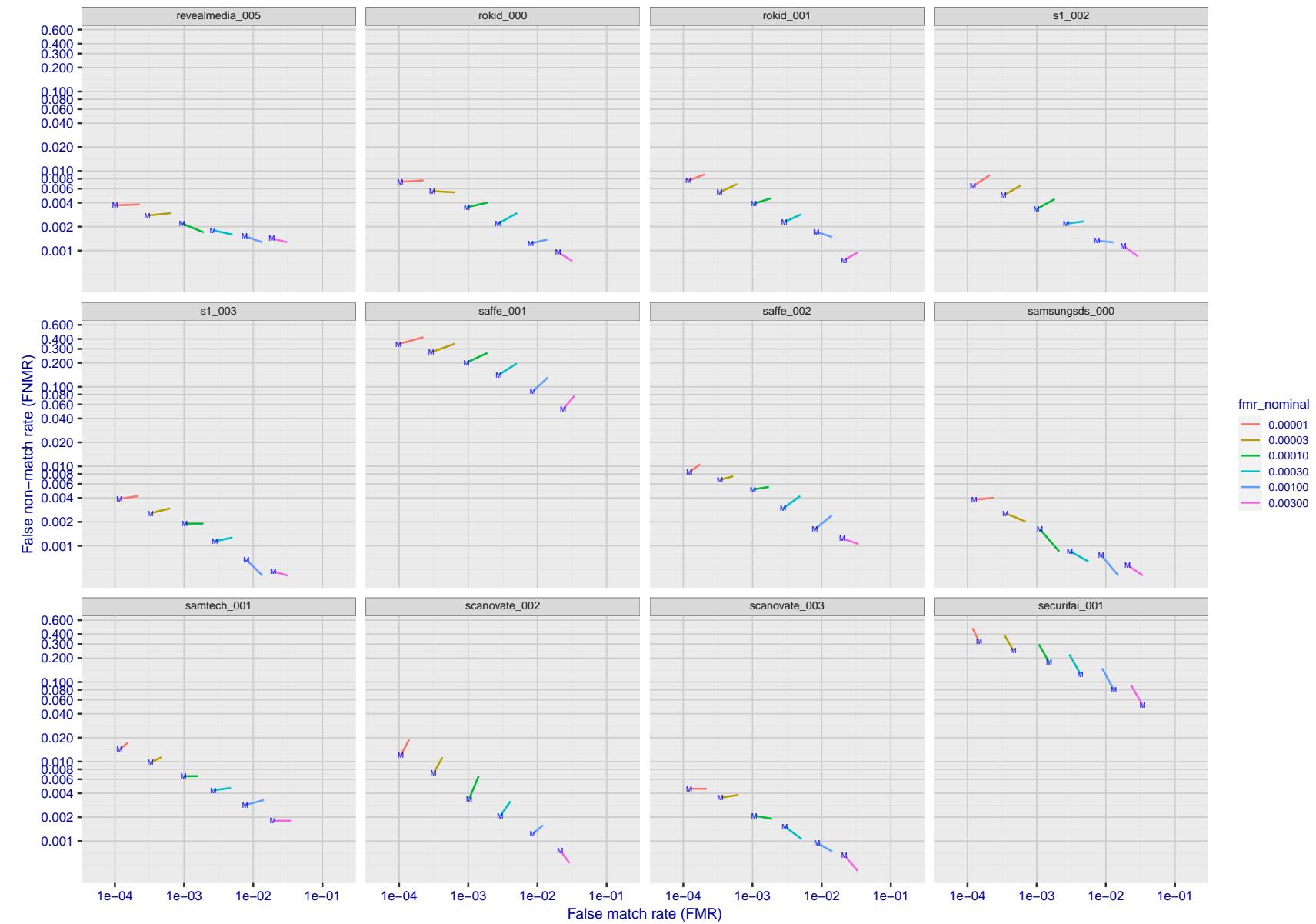


Figure 153: For the visa images, FNMR and FMR at six operating points along the DET characteristic. At each point a line is drawn between $(FMR, FNMR)_{MALE}$ and $(FMR, FNMR)_{FEMALE}$ showing how which sex has lower FMR and/or FNMR. The "M" label denotes male, the other end of the line corresponds to female. The six operating thresholds are selected to give the nominal false match rates given in the legend, and are computed over all impostor pairs regardless of age, sex, and place of birth. The plotted FMR values are broadly an order of magnitude larger than the nominal rates because FMR is computed over demographically-matched impostor pairs i.e individuals of the same sex, from the same geographic region (see section 3.6.1), and the same age group (see section 3.6.2).

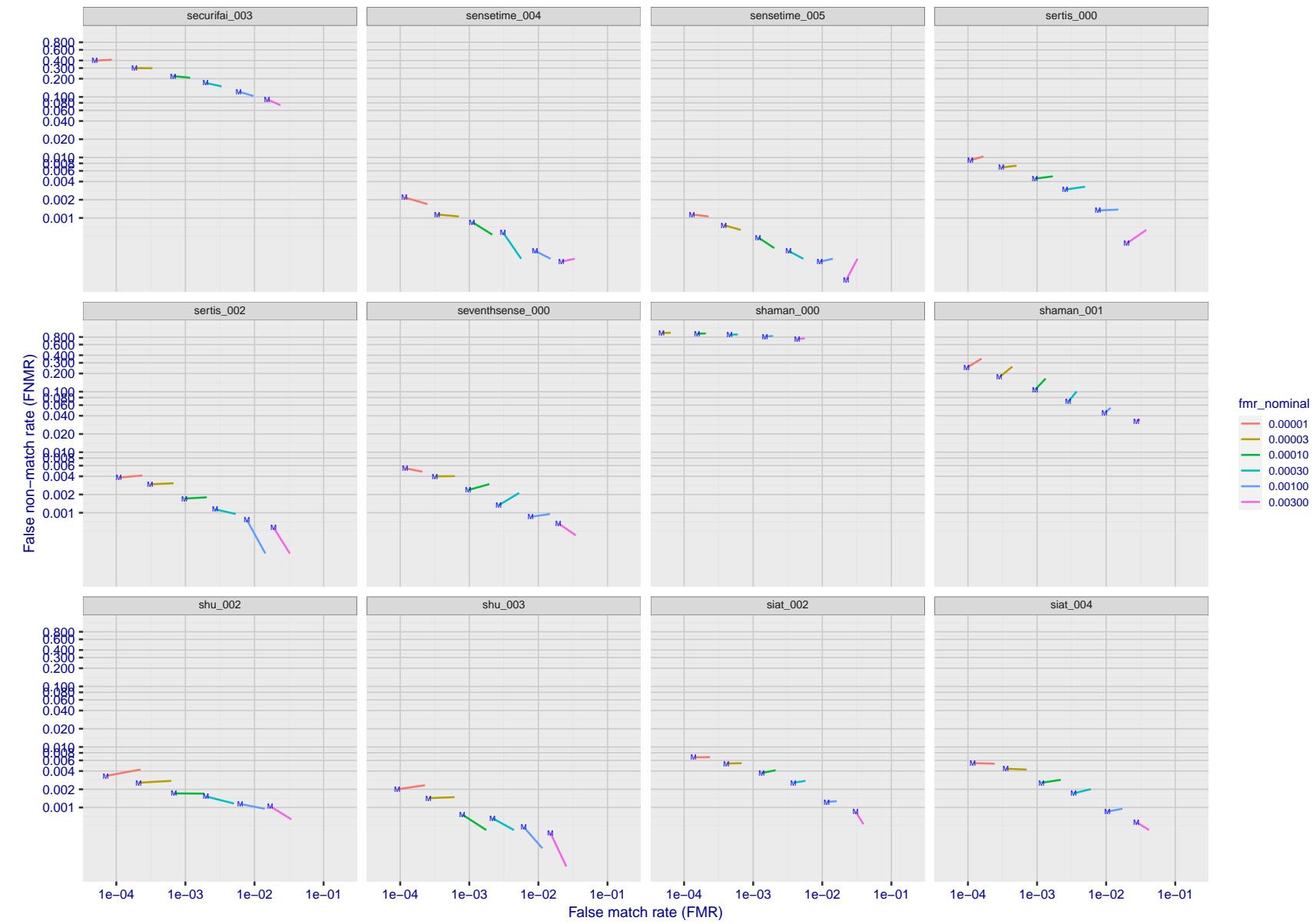


Figure 154: For the visa images, FNMR and FMR at six operating points along the DET characteristic. At each point a line is drawn between $(FMR, FNMR)_{MALE}$ and $(FMR, FNMR)_{FEMALE}$ showing how which sex has lower FMR and/or FNMR. The "M" label denotes male, the other end of the line corresponds to female. The six operating thresholds are selected to give the nominal false match rates given in the legend, and are computed over all impostor pairs regardless of age, sex, and place of birth. The plotted FMR values are broadly an order of magnitude larger than the nominal rates because FMR is computed over demographically-matched impostor pairs i.e individuals of the same sex, from the same geographic region (see section 3.6.1), and the same age group (see section 3.6.2).

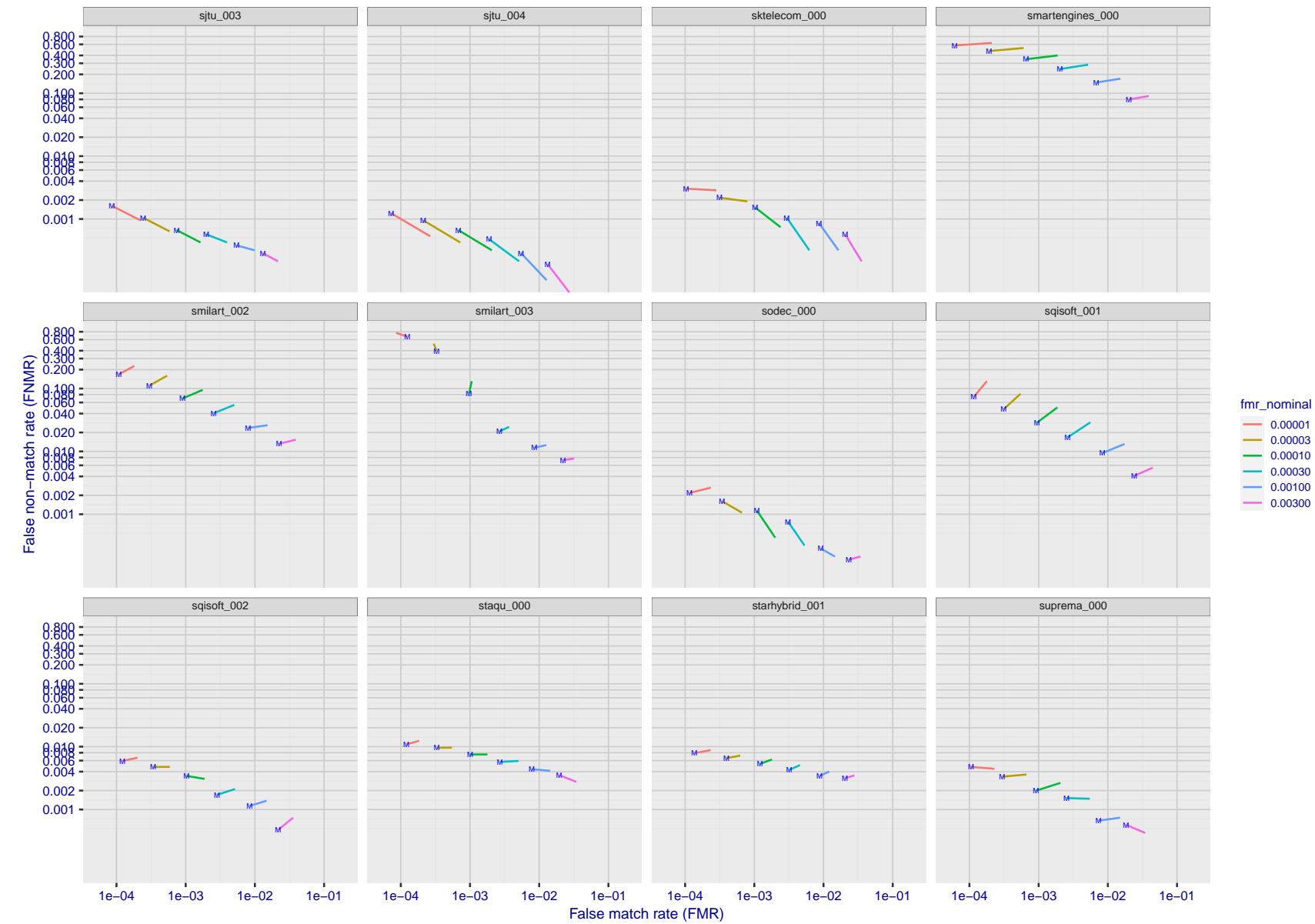


Figure 155: For the visa images, FNMR and FMR at six operating points along the DET characteristic. At each point a line is drawn between $(FMR, FNMR)_{MALE}$ and $(FMR, FNMR)_{FEMALE}$ showing how which sex has lower FMR and/or FNMR. The "M" label denotes male, the other end of the line corresponds to female. The six operating thresholds are selected to give the nominal false match rates given in the legend, and are computed over all impostor pairs regardless of age, sex, and place of birth. The plotted FMR values are broadly an order of magnitude larger than the nominal rates because FMR is computed over demographically-matched impostor pairs i.e individuals of the same sex, from the same geographic region (see section 3.6.1), and the same age group (see section 3.6.2).

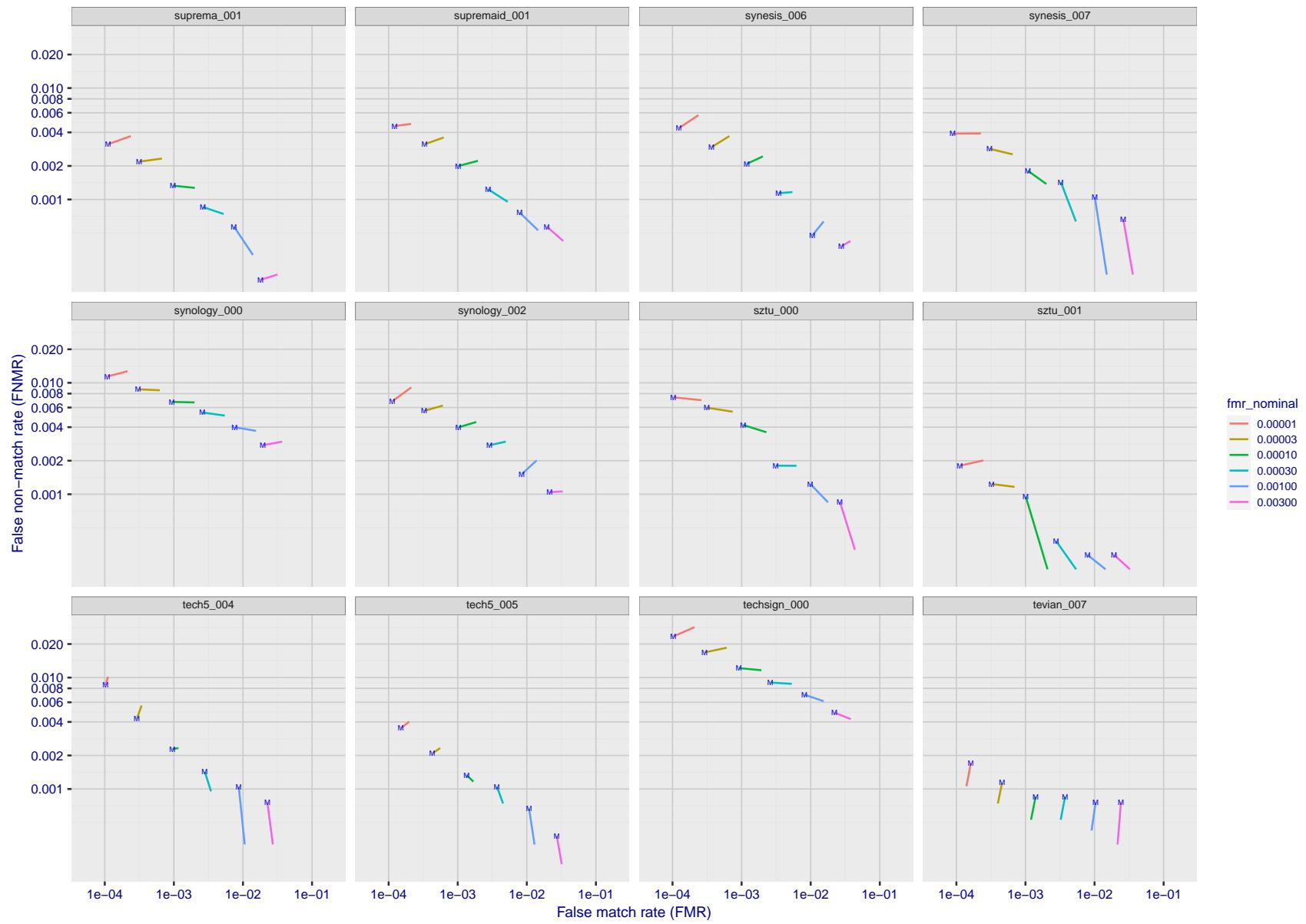


Figure 156: For the visa images, FNMR and FMR at six operating points along the DET characteristic. At each point a line is drawn between $(FMR, FNMR)_{MALE}$ and $(FMR, FNMR)_{FEMALE}$ showing how which sex has lower FMR and/or FNMR. The "M" label denotes male, the other end of the line corresponds to female. The six operating thresholds are selected to give the nominal false match rates given in the legend, and are computed over all impostor pairs regardless of age, sex, and place of birth. The plotted FMR values are broadly an order of magnitude larger than the nominal rates because FMR is computed over demographically-matched impostor pairs i.e individuals of the same sex, from the same geographic region (see section 3.6.1), and the same age group (see section 3.6.2).

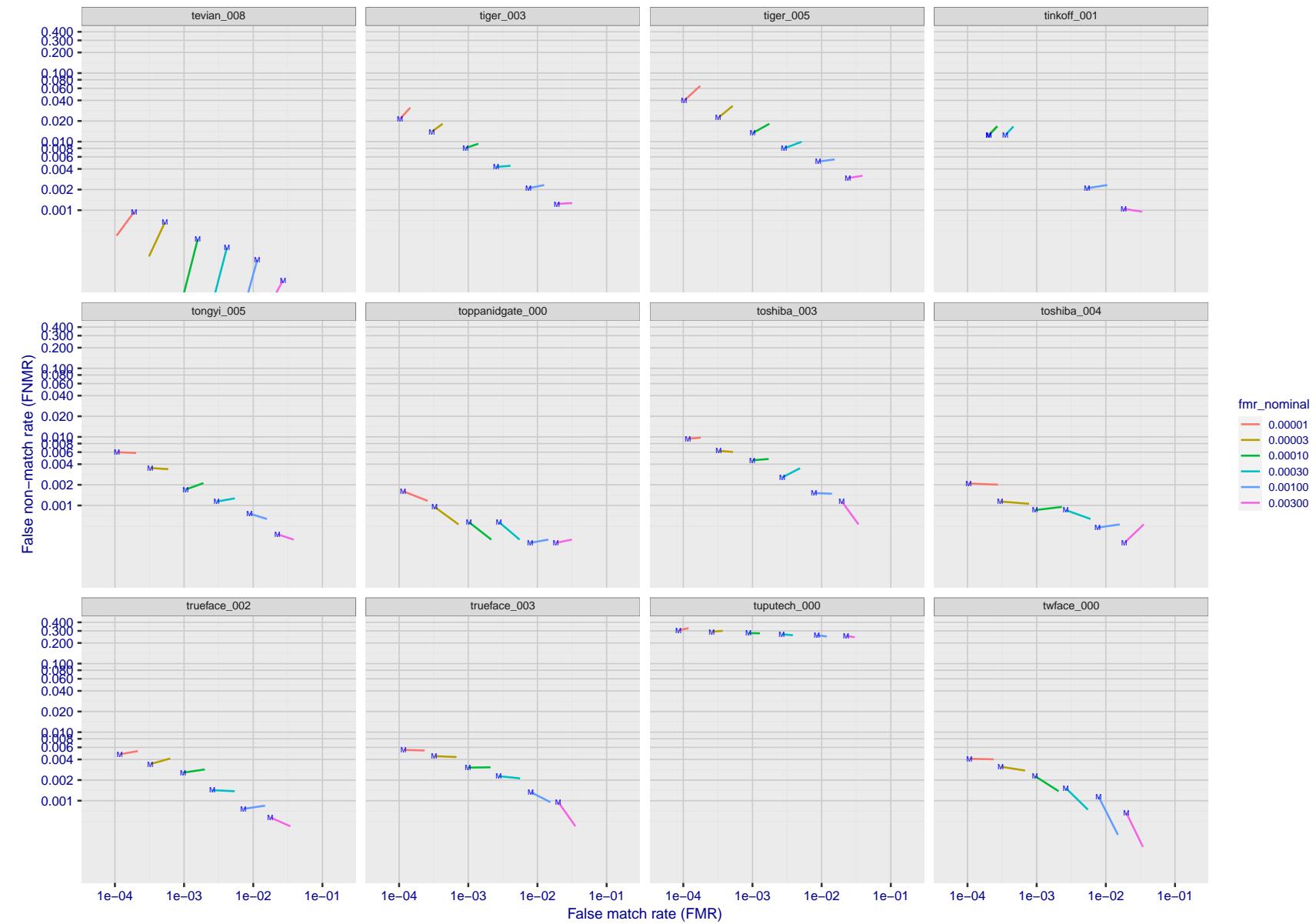


Figure 157: For the visa images, FNMR and FMR at six operating points along the DET characteristic. At each point a line is drawn between $(FMR, FNMR)_{MALE}$ and $(FMR, FNMR)_{FEMALE}$ showing how which sex has lower FMR and/or FNMR. The "M" label denotes male, the other end of the line corresponds to female. The six operating thresholds are selected to give the nominal false match rates given in the legend, and are computed over all impostor pairs regardless of age, sex, and place of birth. The plotted FMR values are broadly an order of magnitude larger than the nominal rates because FMR is computed over demographically-matched impostor pairs i.e individuals of the same sex, from the same geographic region (see section 3.6.1), and the same age group (see section 3.6.2).

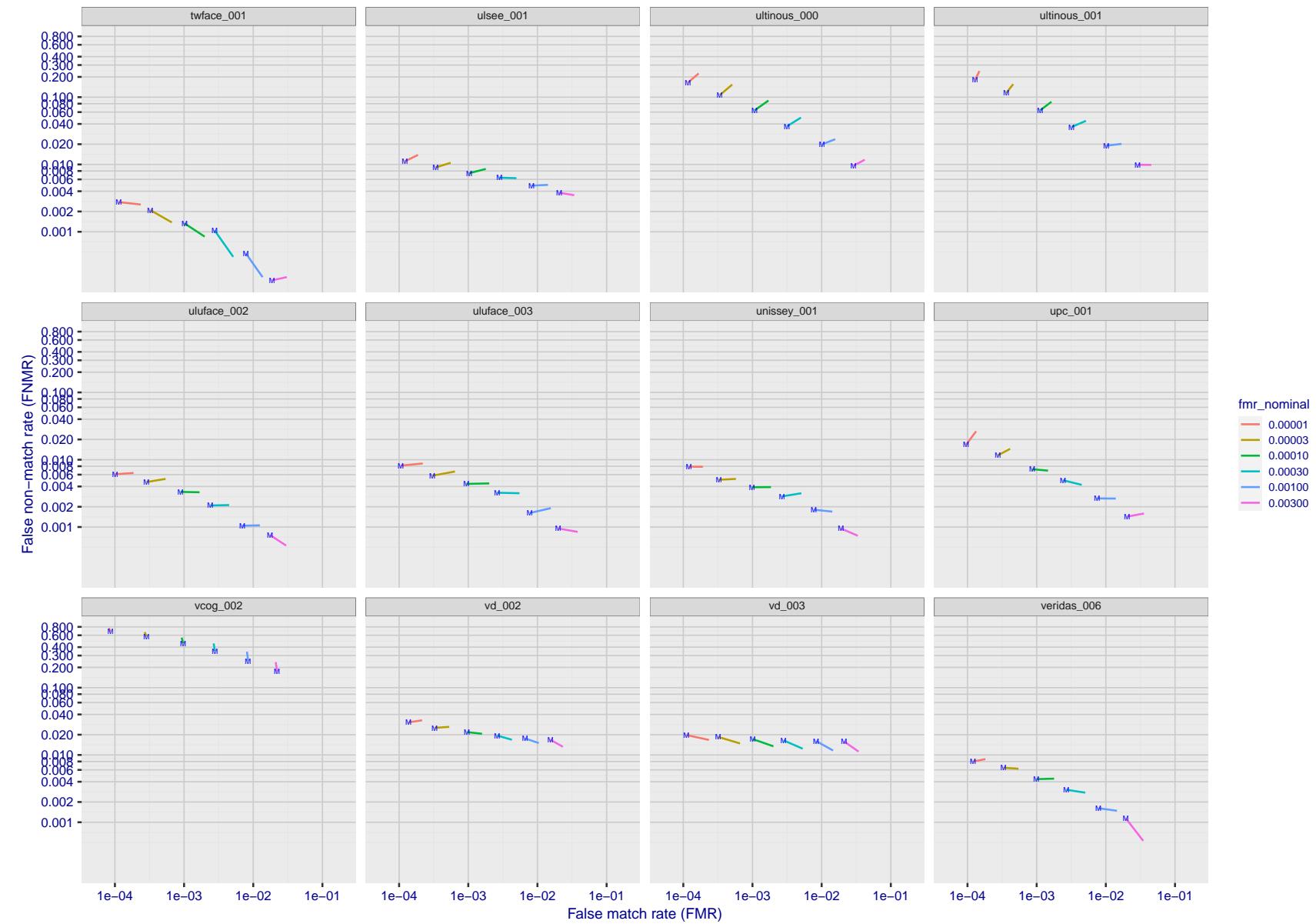


Figure 158: For the visa images, FNMR and FMR at six operating points along the DET characteristic. At each point a line is drawn between $(FMR, FNMR)_{MALE}$ and $(FMR, FNMR)_{FEMALE}$ showing how which sex has lower FMR and/or FNMR. The "M" label denotes male, the other end of the line corresponds to female. The six operating thresholds are selected to give the nominal false match rates given in the legend, and are computed over all impostor pairs regardless of age, sex, and place of birth. The plotted FMR values are broadly an order of magnitude larger than the nominal rates because FMR is computed over demographically-matched impostor pairs i.e individuals of the same sex, from the same geographic region (see section 3.6.1), and the same age group (see section 3.6.2).

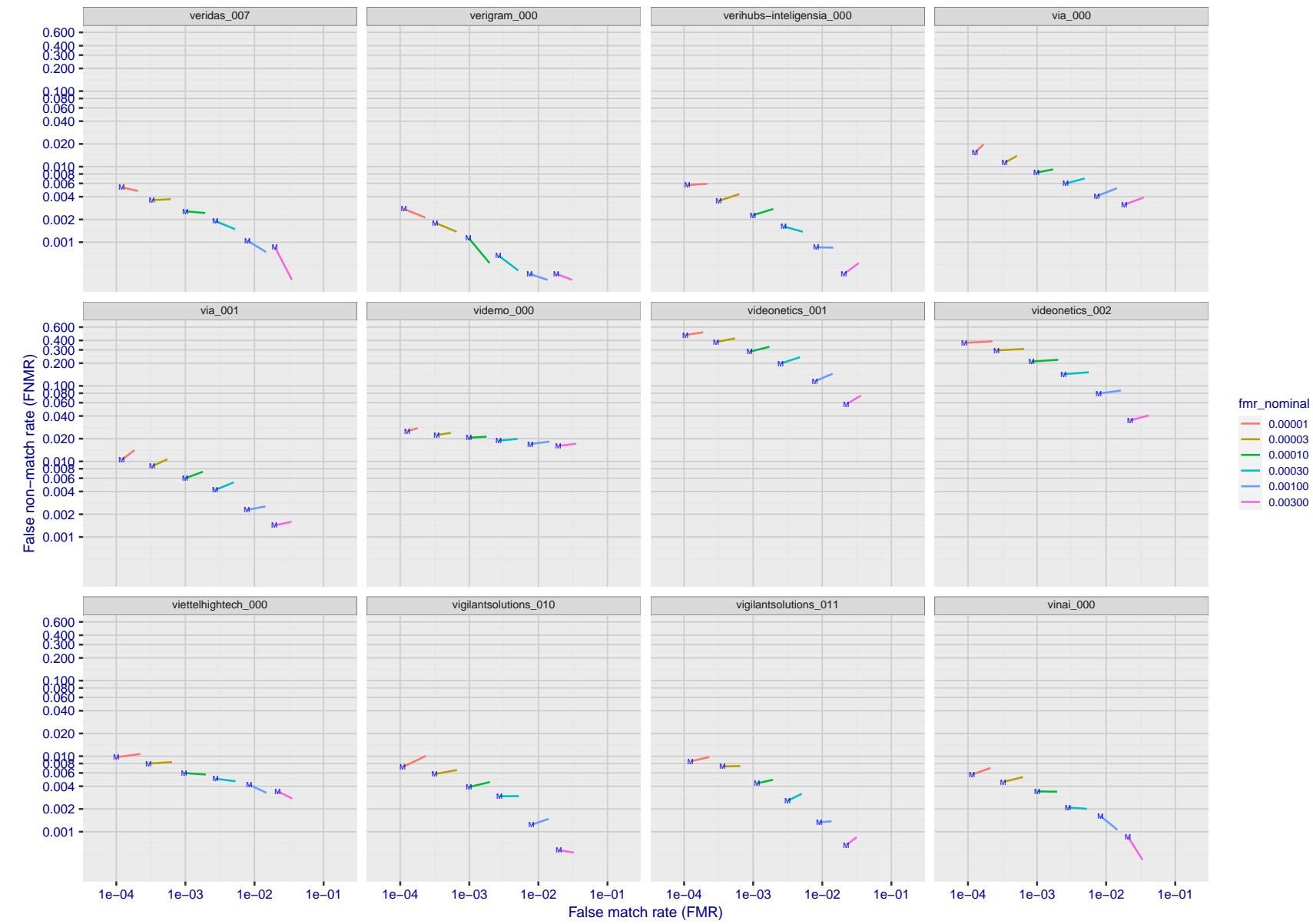


Figure 159: For the visa images, FNMR and FMR at six operating points along the DET characteristic. At each point a line is drawn between $(FMR, FNMR)_{MALE}$ and $(FMR, FNMR)_{FEMALE}$ showing how which sex has lower FMR and/or FNMR. The "M" label denotes male, the other end of the line corresponds to female. The six operating thresholds are selected to give the nominal false match rates given in the legend, and are computed over all impostor pairs regardless of age, sex, and place of birth. The plotted FMR values are broadly an order of magnitude larger than the nominal rates because FMR is computed over demographically-matched impostor pairs i.e individuals of the same sex, from the same geographic region (see section 3.6.1), and the same age group (see section 3.6.2).

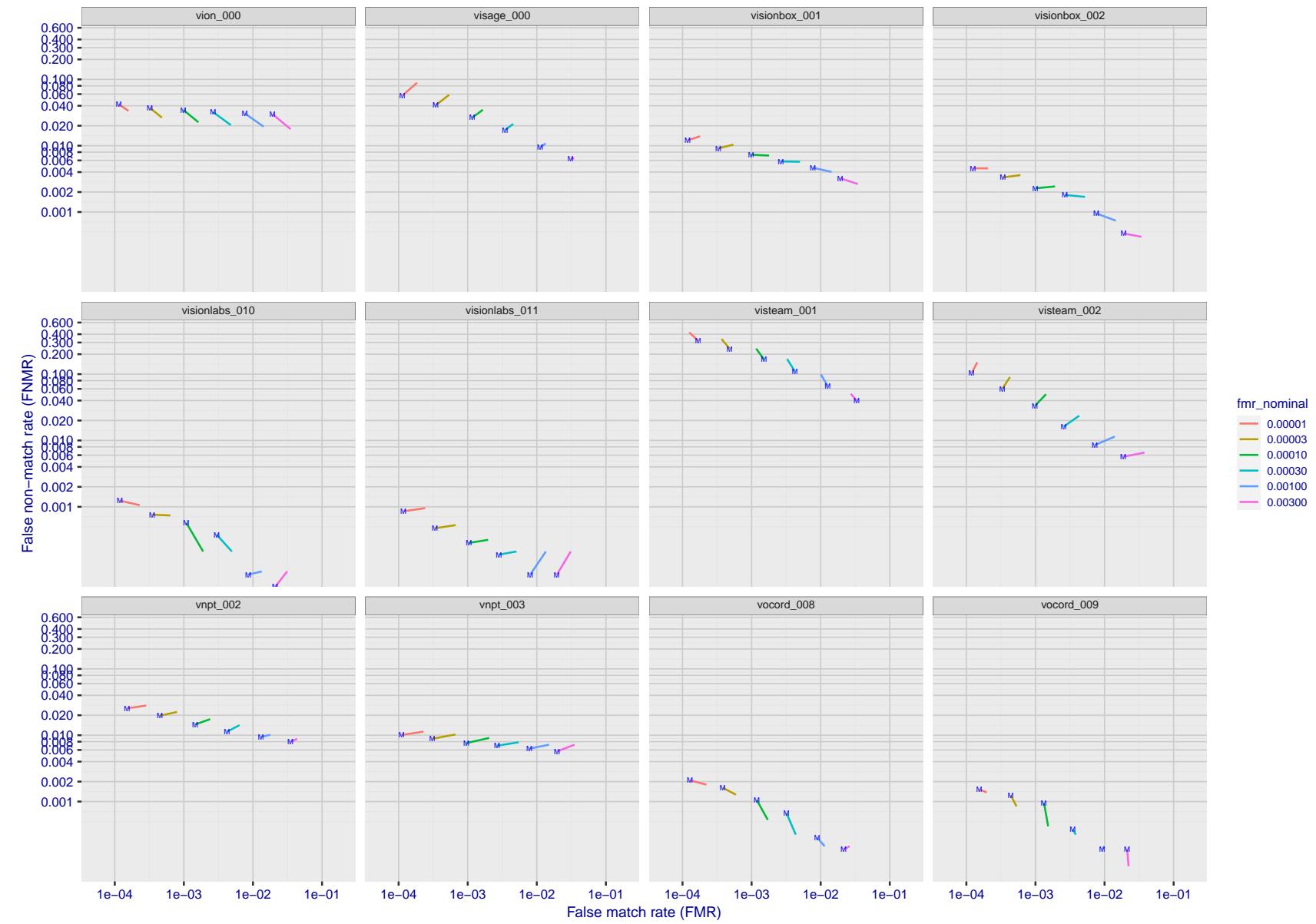


Figure 160: For the visa images, FNMR and FMR at six operating points along the DET characteristic. At each point a line is drawn between $(FMR, FNMR)_{MALE}$ and $(FMR, FNMR)_{FEMALE}$ showing how which sex has lower FMR and/or FNMR. The "M" label denotes male, the other end of the line corresponds to female. The six operating thresholds are selected to give the nominal false match rates given in the legend, and are computed over all impostor pairs regardless of age, sex, and place of birth. The plotted FMR values are broadly an order of magnitude larger than the nominal rates because FMR is computed over demographically-matched impostor pairs i.e individuals of the same sex, from the same geographic region (see section 3.6.1), and the same age group (see section 3.6.2).

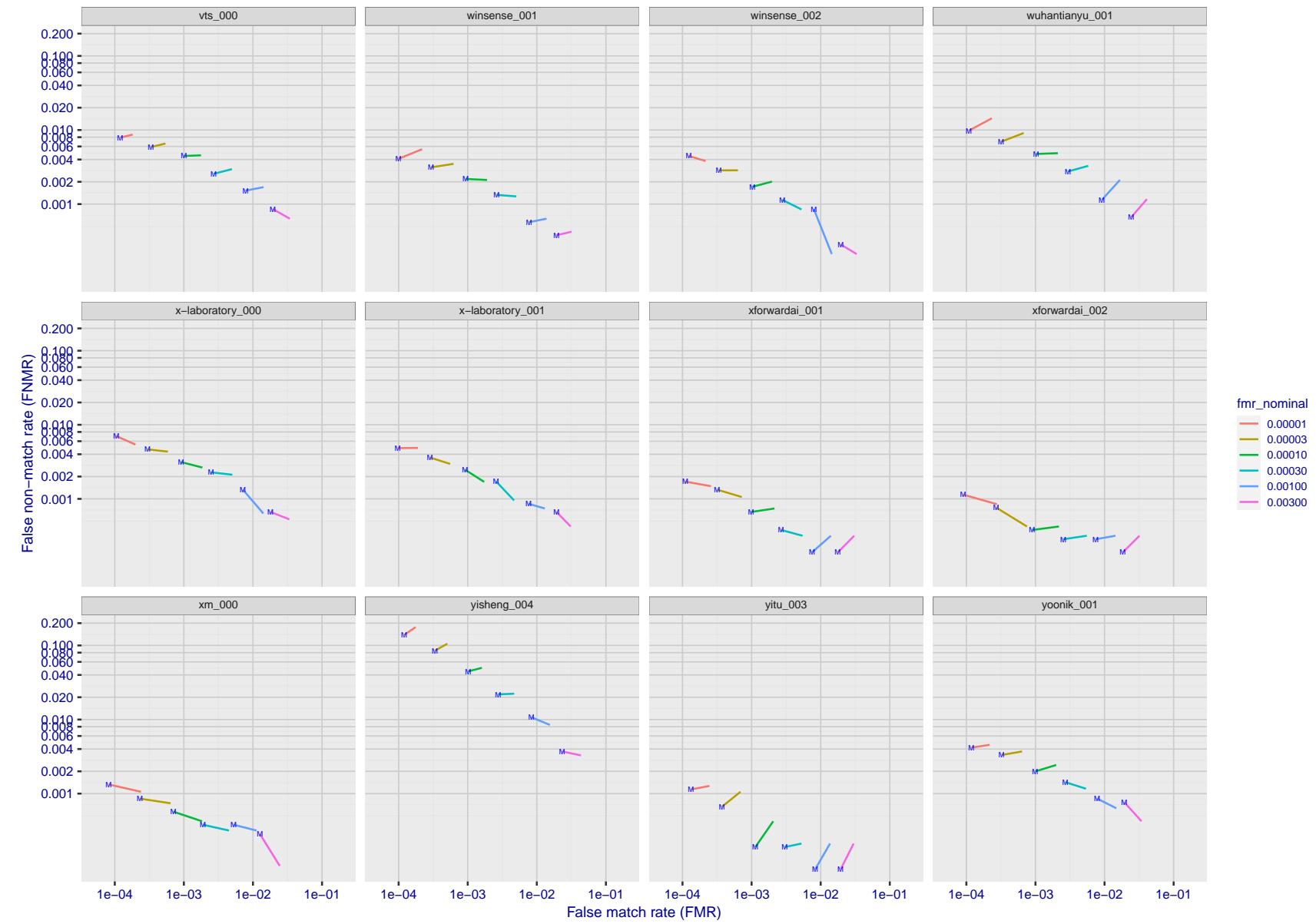


Figure 161: For the visa images, FNMR and FMR at six operating points along the DET characteristic. At each point a line is drawn between $(FMR, FNMR)_{MALE}$ and $(FMR, FNMR)_{FEMALE}$ showing how which sex has lower FMR and/or FNMR. The "M" label denotes male, the other end of the line corresponds to female. The six operating thresholds are selected to give the nominal false match rates given in the legend, and are computed over all impostor pairs regardless of age, sex, and place of birth. The plotted FMR values are broadly an order of magnitude larger than the nominal rates because FMR is computed over demographically-matched impostor pairs i.e individuals of the same sex, from the same geographic region (see section 3.6.1), and the same age group (see section 3.6.2).

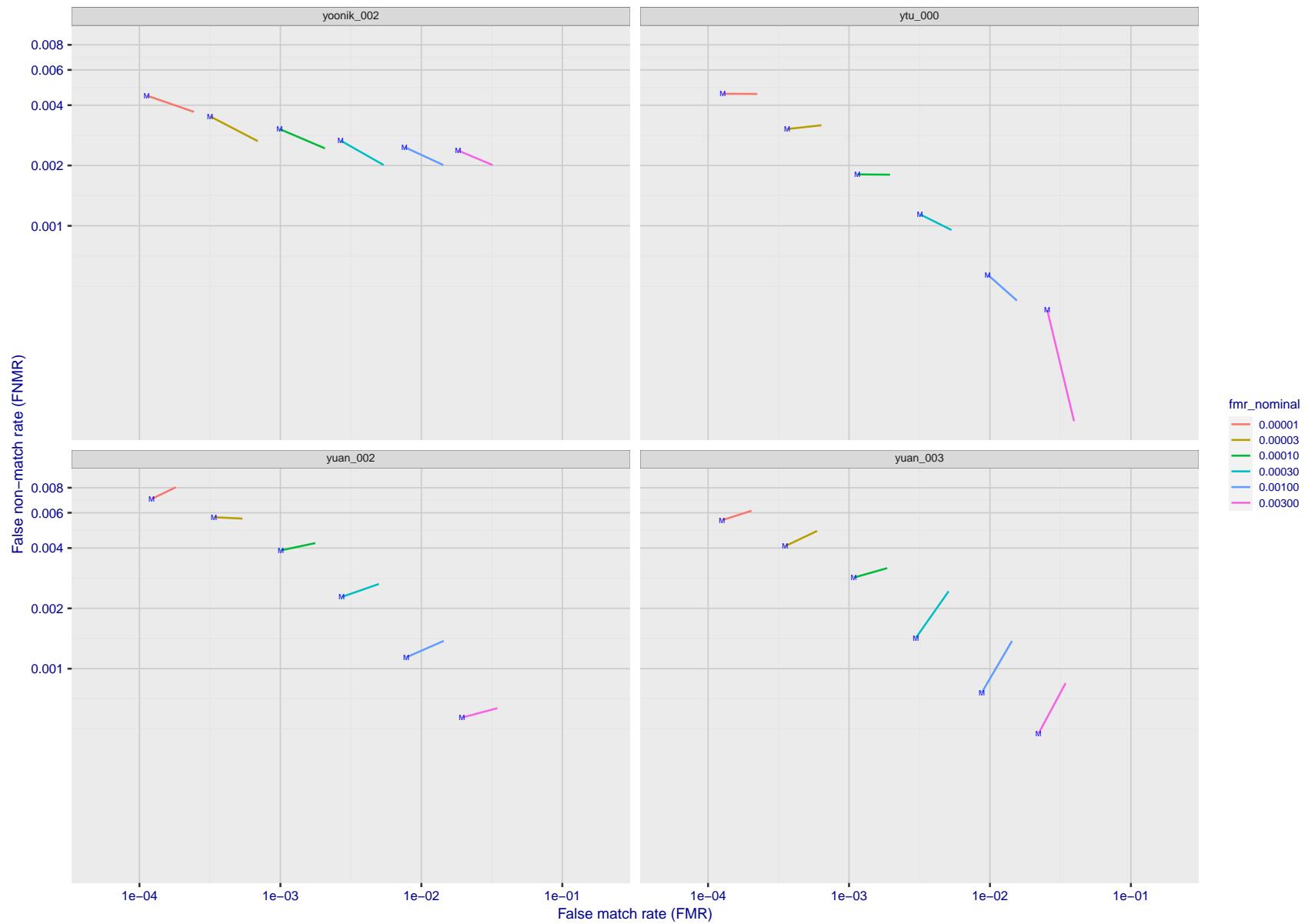


Figure 162: For the visa images, FNMR and FMR at six operating points along the DET characteristic. At each point a line is drawn between $(FMR, FNMR)_{MALE}$ and $(FMR, FNMR)_{FEMALE}$ showing how which sex has lower FMR and/or FNMR. The "M" label denotes male, the other end of the line corresponds to female. The six operating thresholds are selected to give the nominal false match rates given in the legend, and are computed over all impostor pairs regardless of age, sex, and place of birth. The plotted FMR values are broadly an order of magnitude larger than the nominal rates because FMR is computed over demographically-matched impostor pairs i.e individuals of the same sex, from the same geographic region (see section 3.6.1), and the same age group (see section 3.6.2).

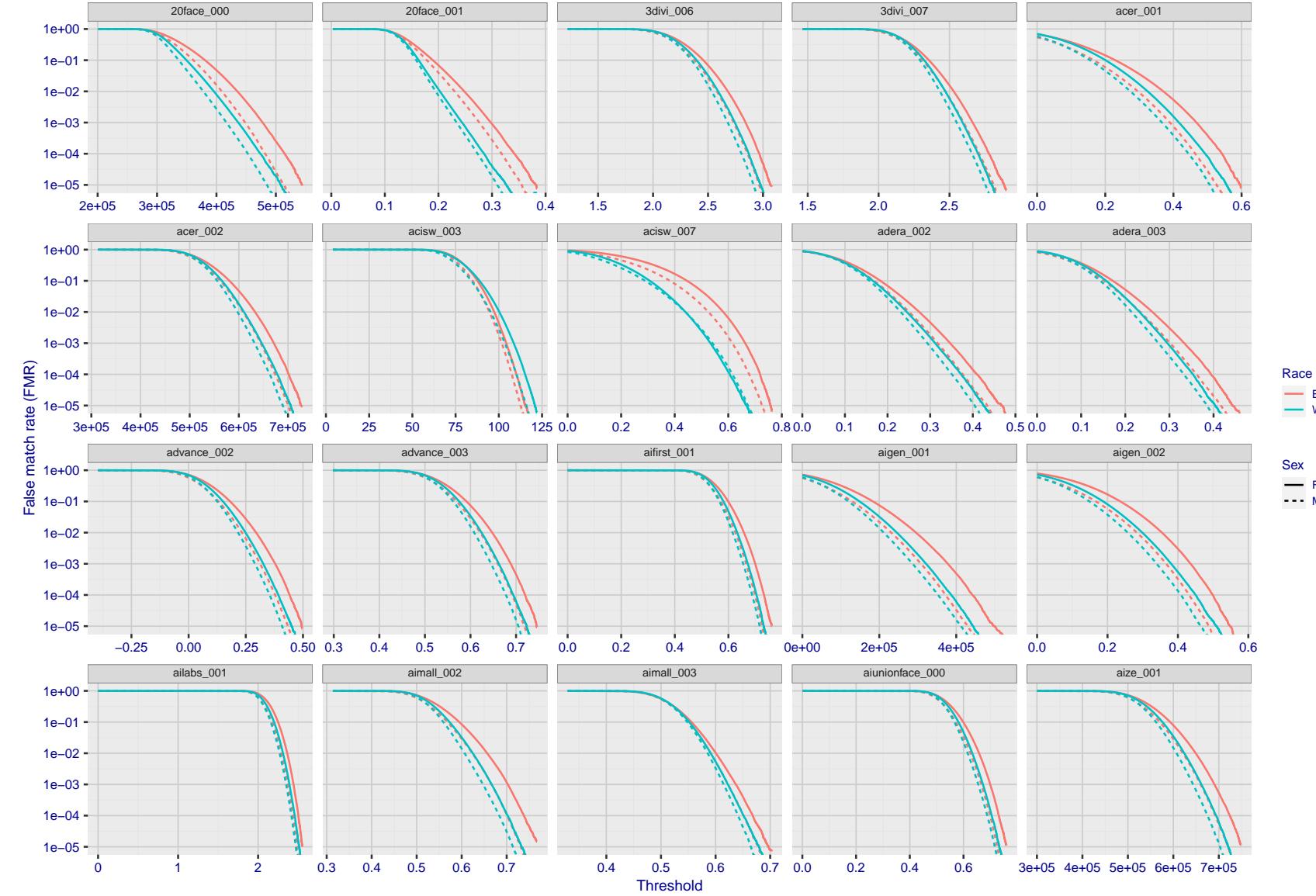


Figure 163: For the mugshot images, the false match calibration curves show false match rate vs. threshold. Separate curves appear for white females, black females, black males and white males.

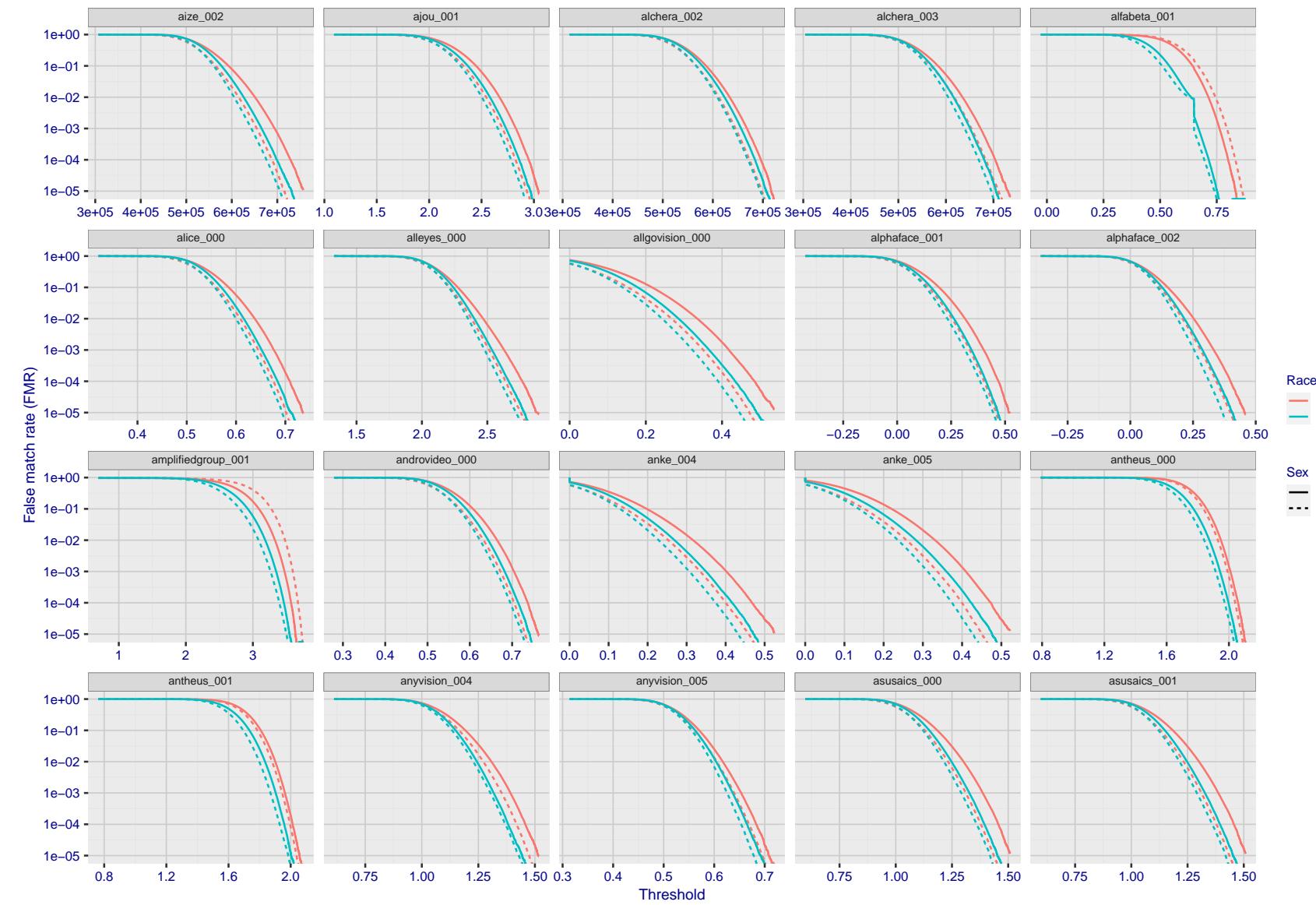
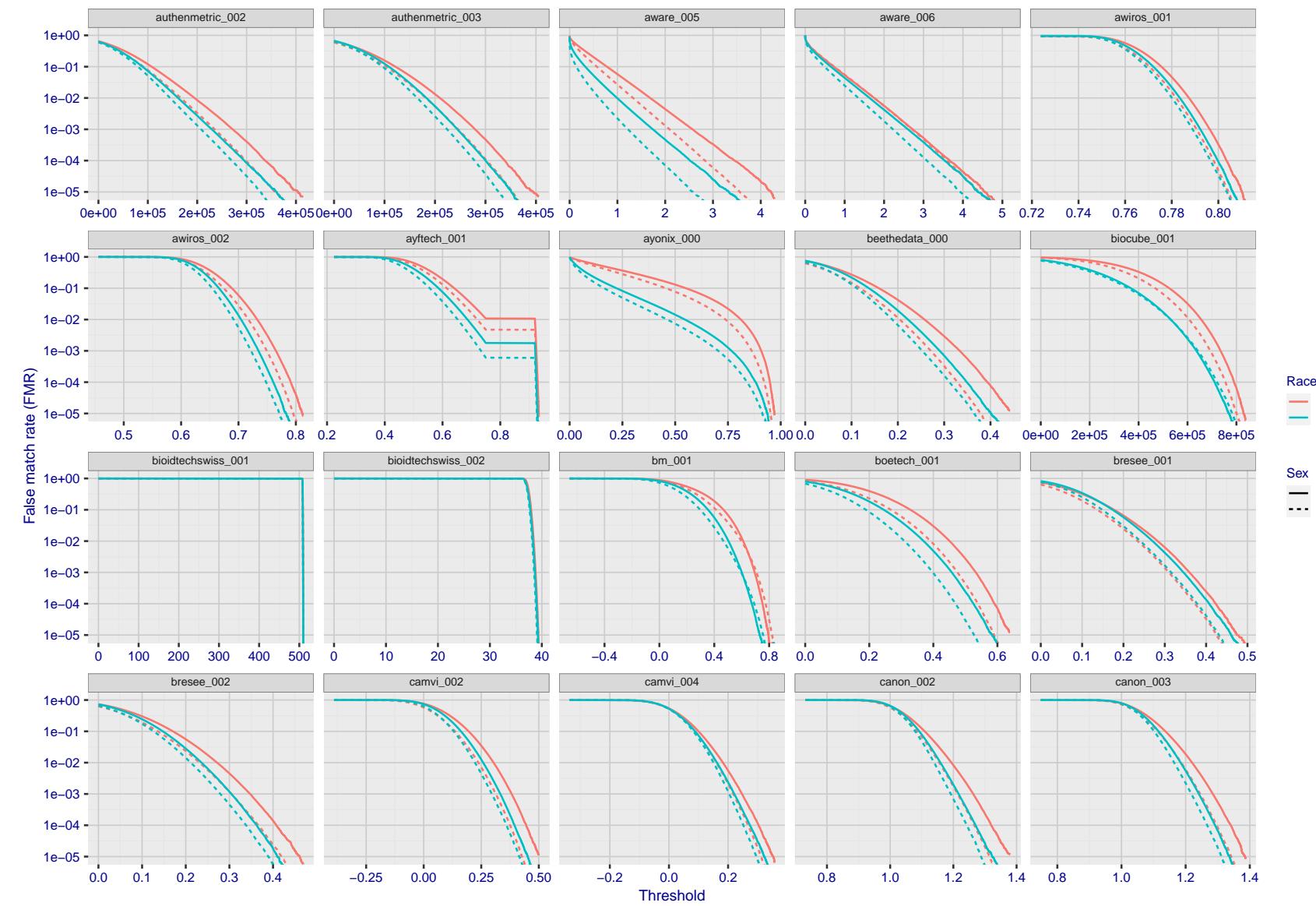


Figure 164: For the mugshot images, the false match calibration curves show false match rate vs. threshold. Separate curves appear for white females, black females, black males and white males.



FNMR(T)

"False non-match rate"

FMR(T)

"False match rate"

Figure 165: For the mugshot images, the false match calibration curves show false match rate vs. threshold. Separate curves appear for white females, black females, black males and white males.

2021/12/16 10:32:53

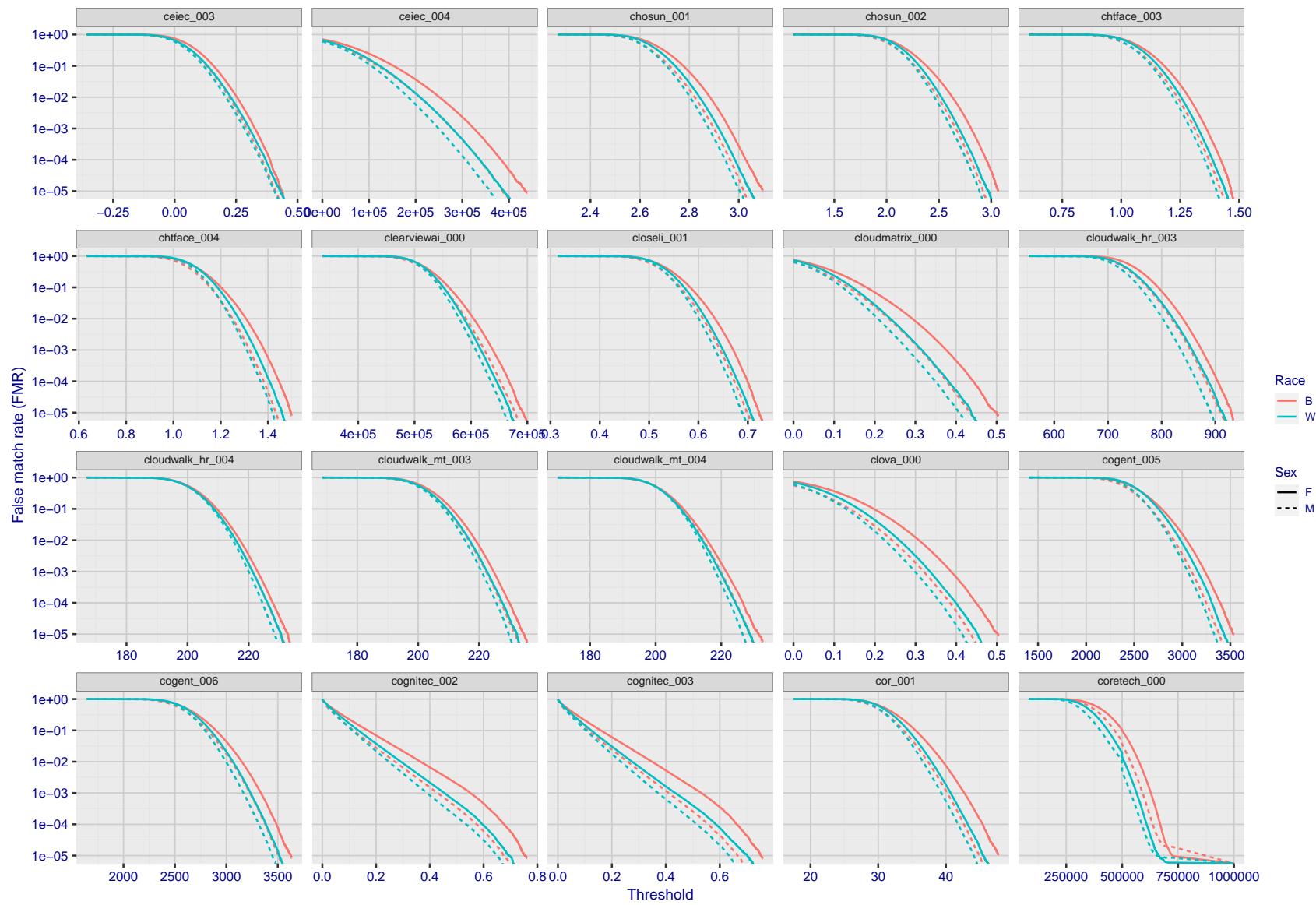


Figure 166: For the mugshot images, the false match calibration curves show false match rate vs. threshold. Separate curves appear for white females, black females, black males and white males.

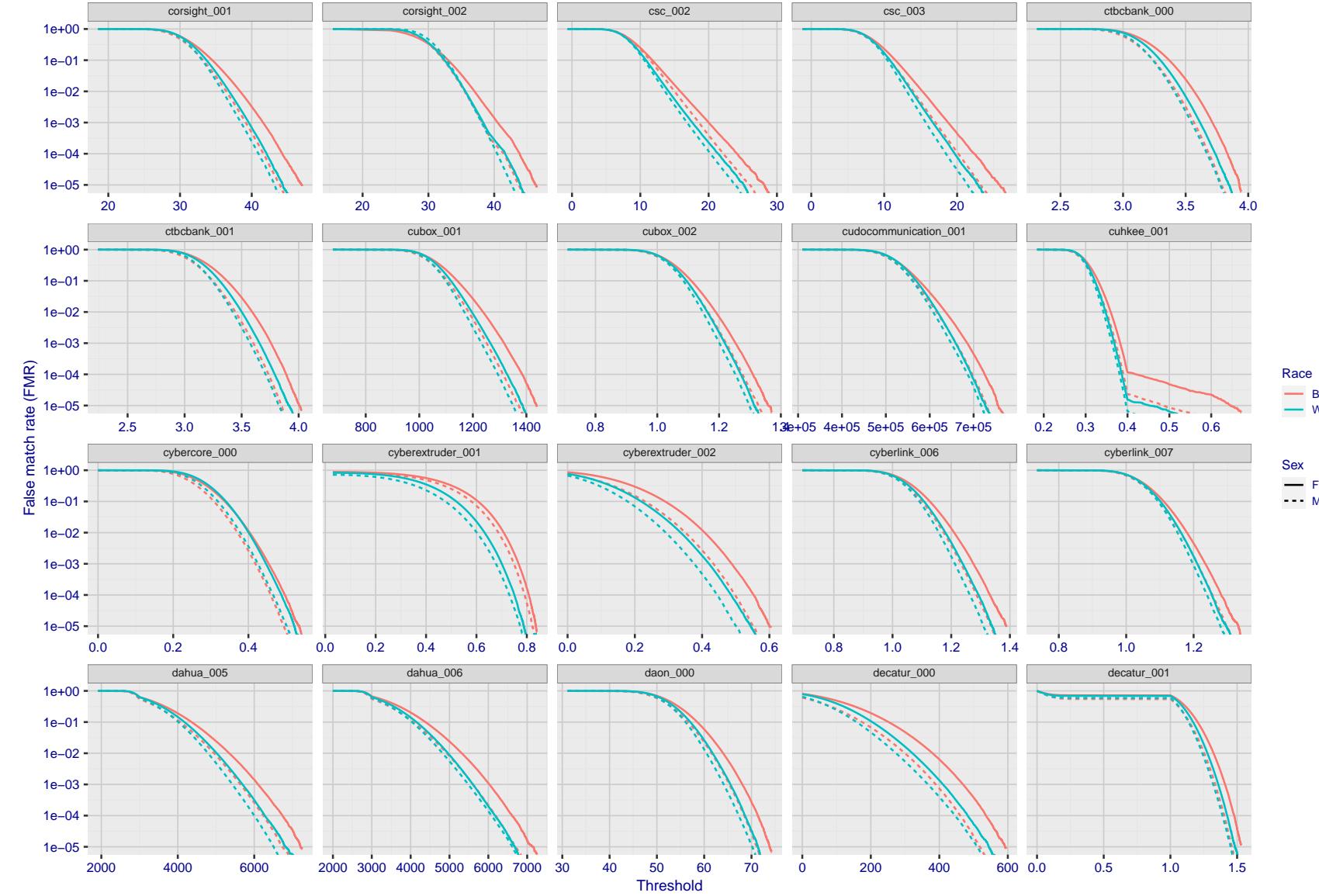


Figure 167: For the mugshot images, the false match calibration curves show false match rate vs. threshold. Separate curves appear for white females, black females, black males and white males.

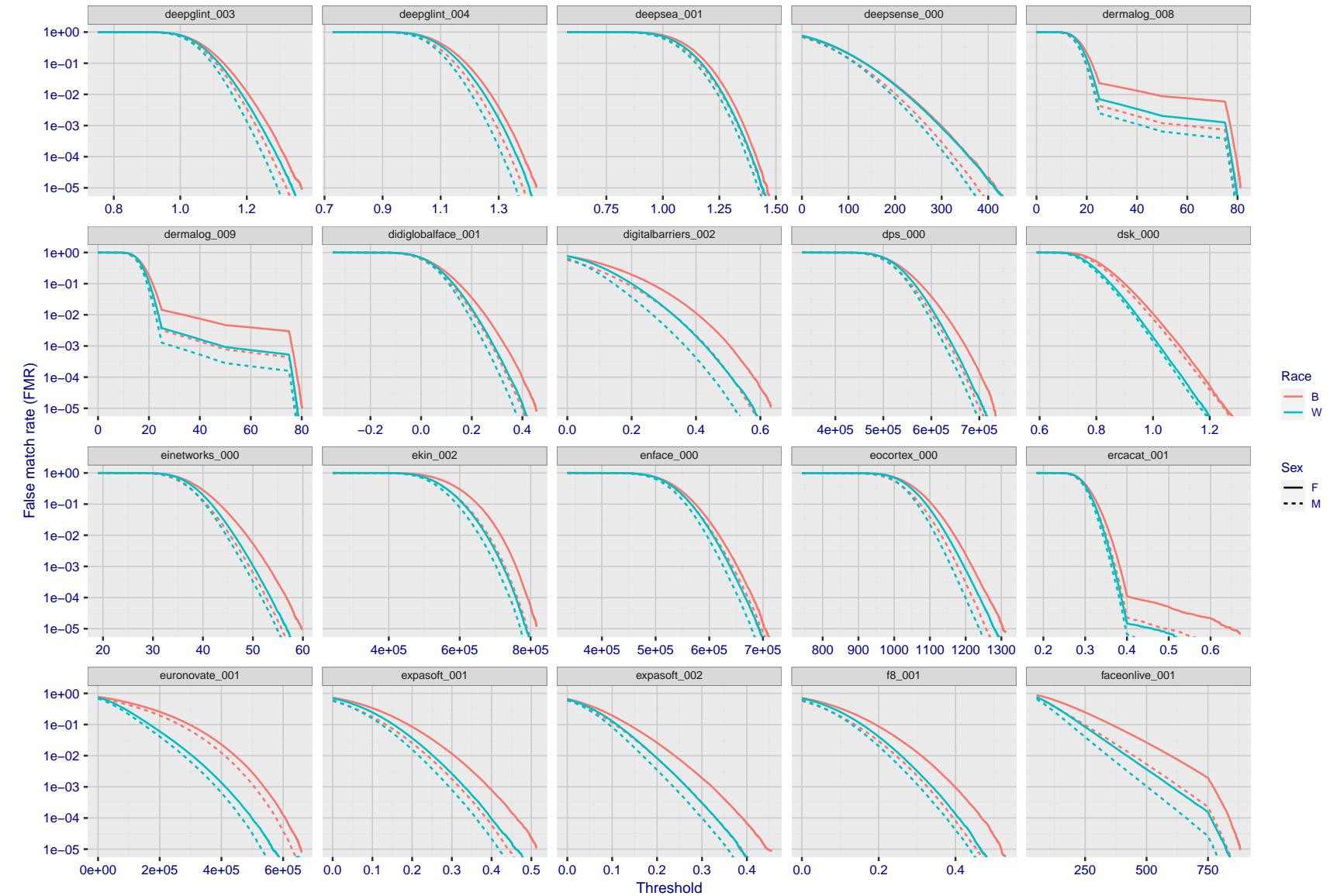


Figure 168: For the mugshot images, the false match calibration curves show false match rate vs. threshold. Separate curves appear for white females, black females, black males and white males.

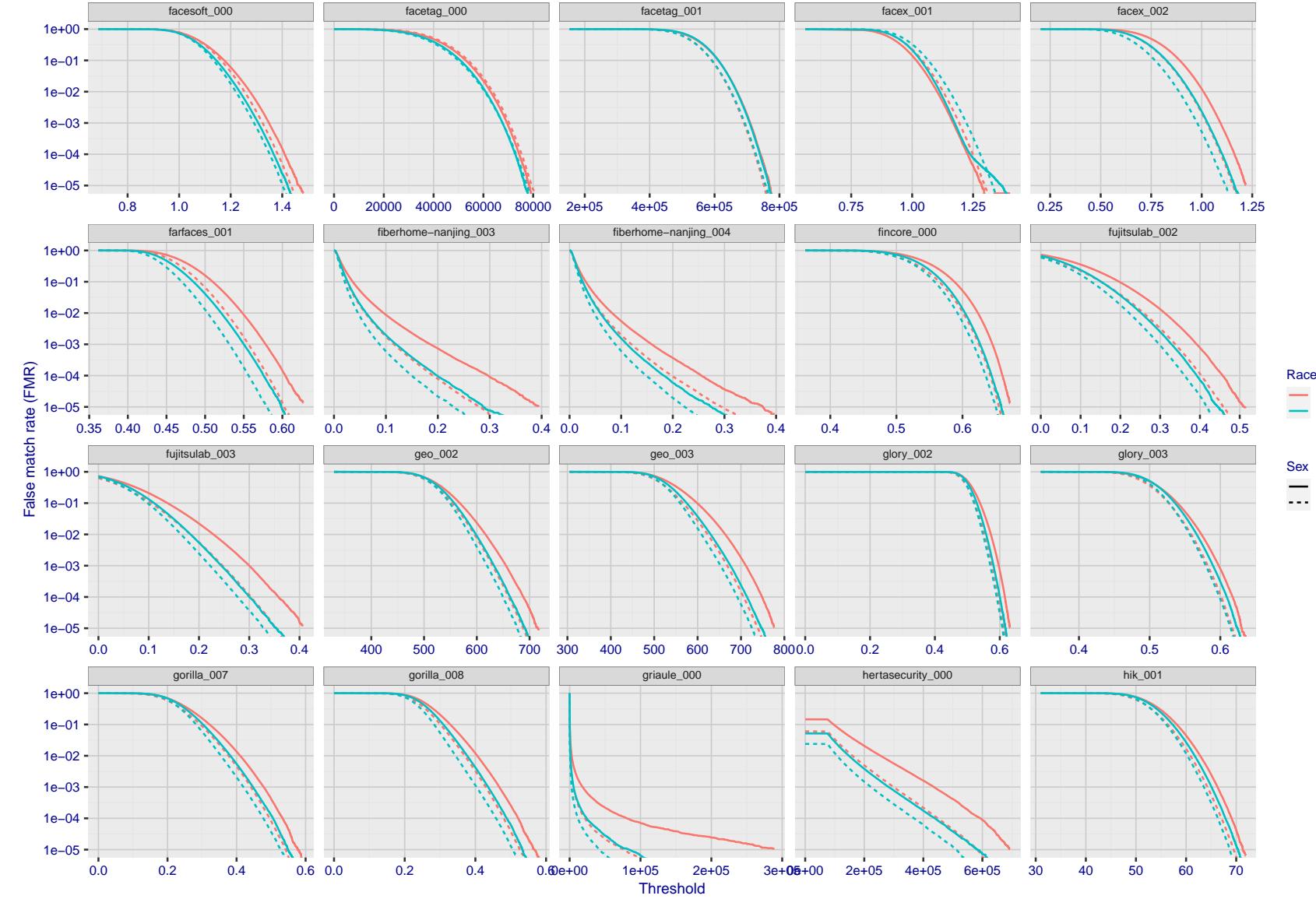


Figure 169: For the mugshot images, the false match calibration curves show false match rate vs. threshold. Separate curves appear for white females, black females, black males and white males.

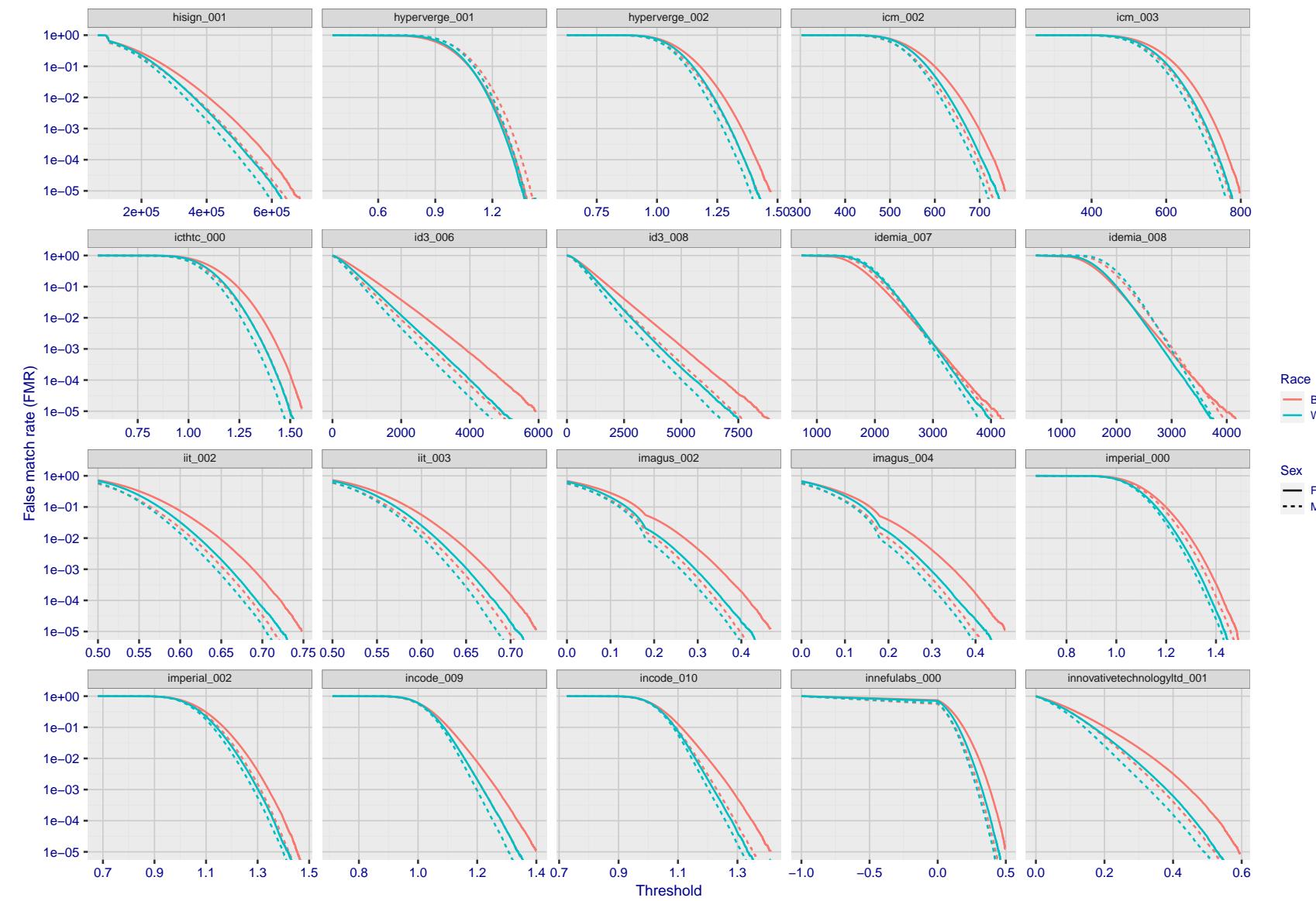


Figure 170: For the mugshot images, the false match calibration curves show false match rate vs. threshold. Separate curves appear for white females, black females, black males and white males.

2021/12/16 10:32:53

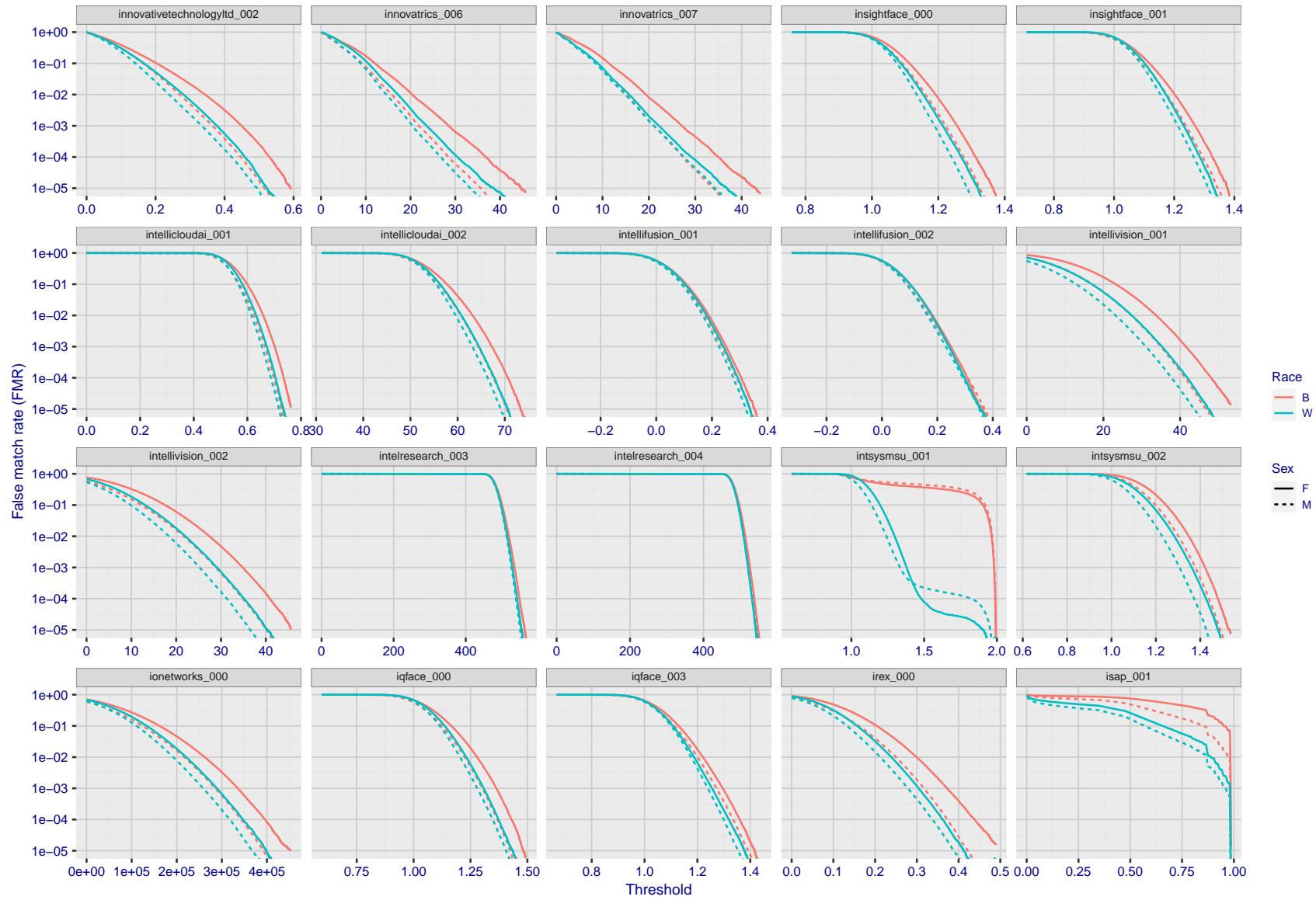


Figure 171: For the mugshot images, the false match calibration curves show false match rate vs. threshold. Separate curves appear for white females, black females, black males and white males.

FNMR(T)
"False non-match rate"
FMR(T)
"False match rate"

2021/12/16 10:32:53

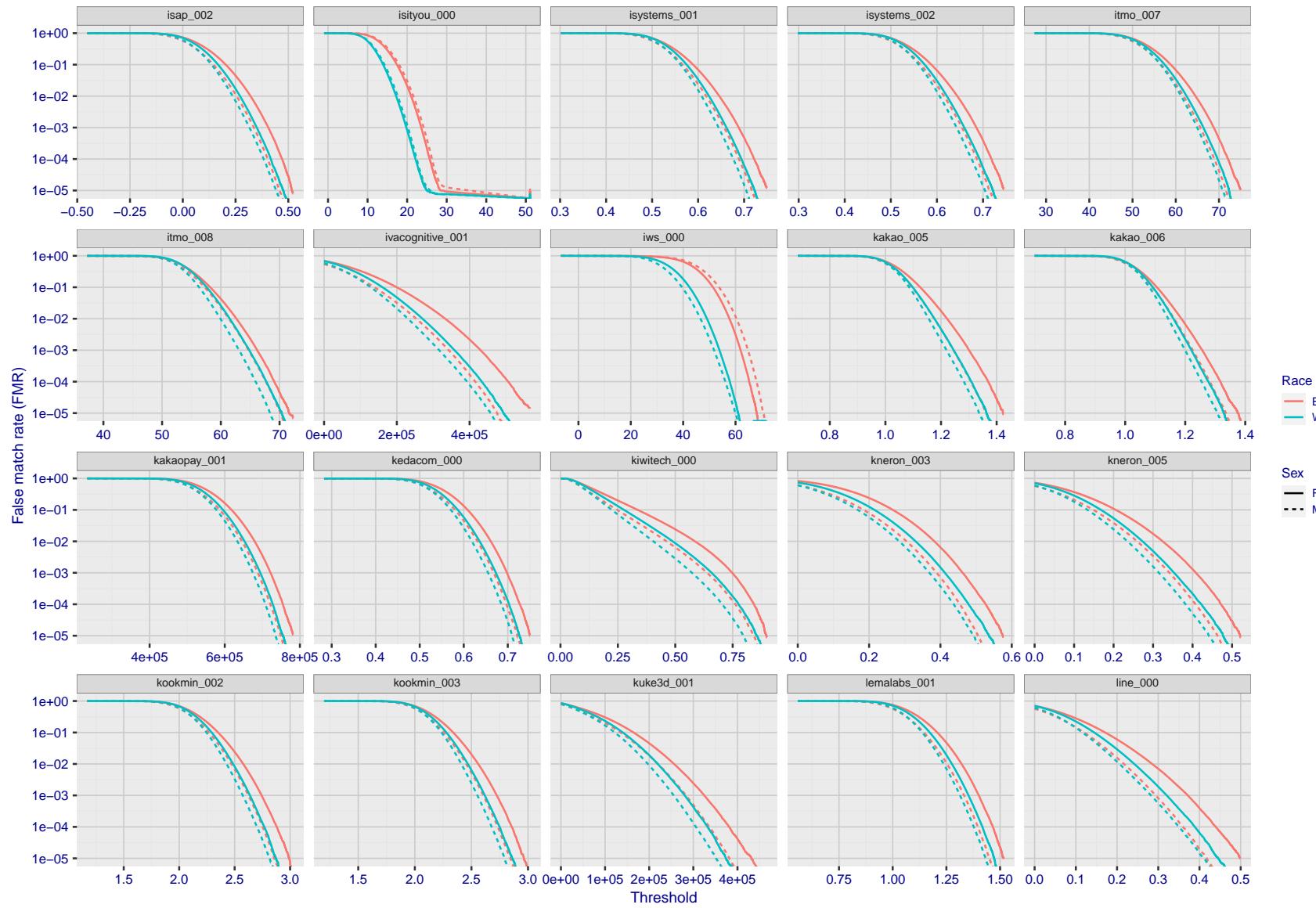


Figure 172: For the mugshot images, the false match calibration curves show false match rate vs. threshold. Separate curves appear for white females, black females, black males and white males.

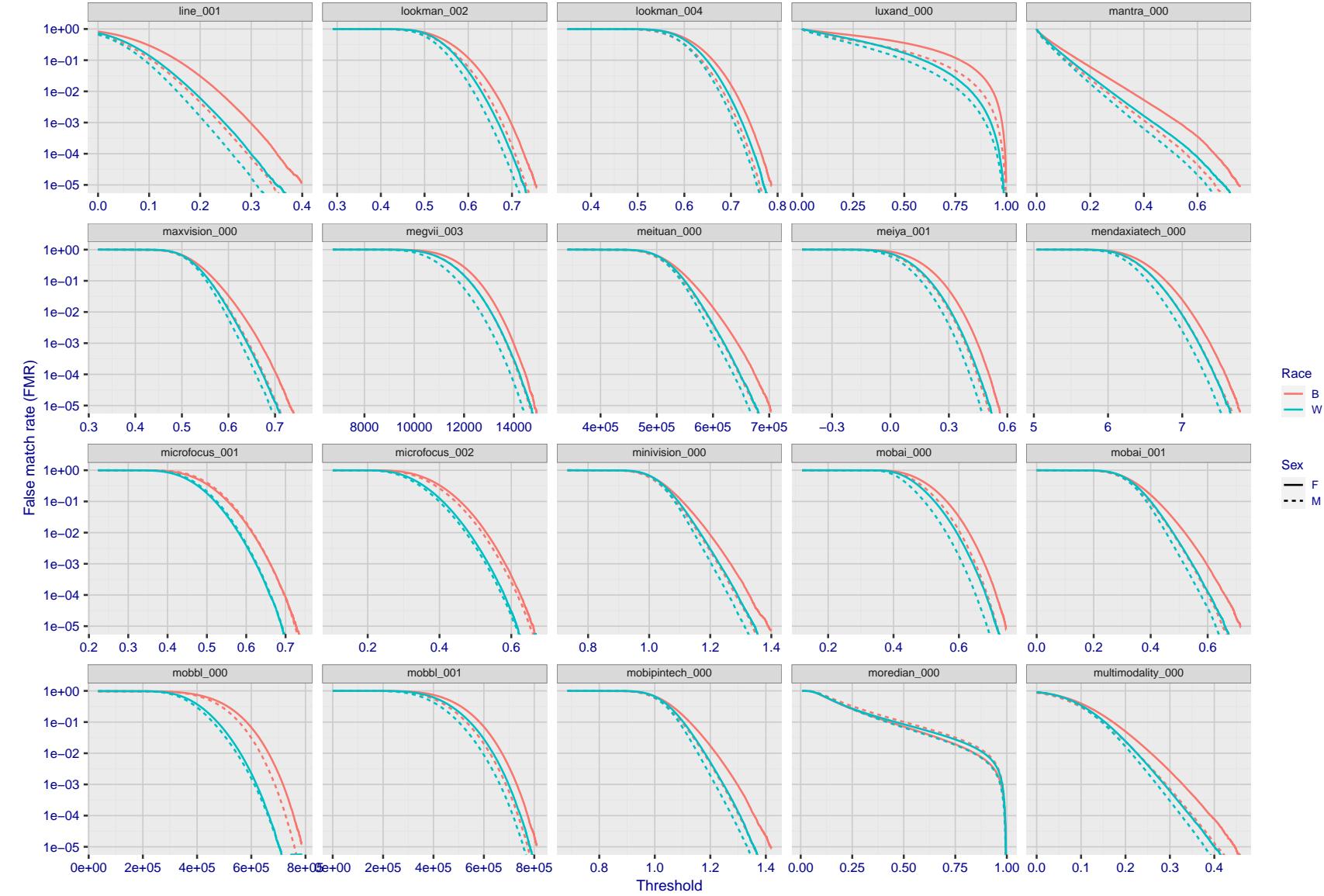


Figure 173: For the mugshot images, the false match calibration curves show false match rate vs. threshold. Separate curves appear for white females, black females, black males and white males.

2021/12/16 10:32:53

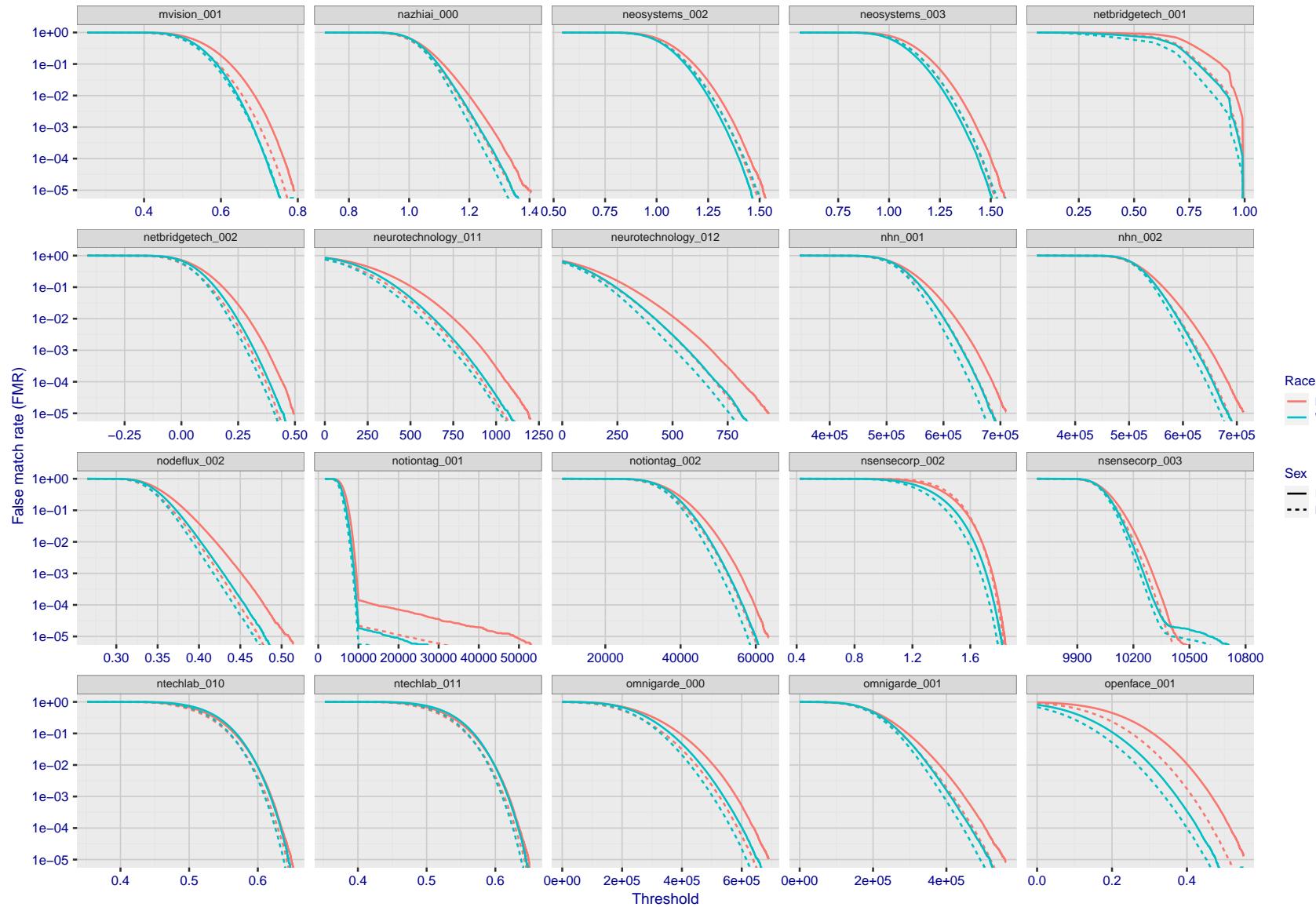


Figure 174: For the mugshot images, the false match calibration curves show false match rate vs. threshold. Separate curves appear for white females, black females, black males and white males.

FNMR(T)

"False non-match rate"

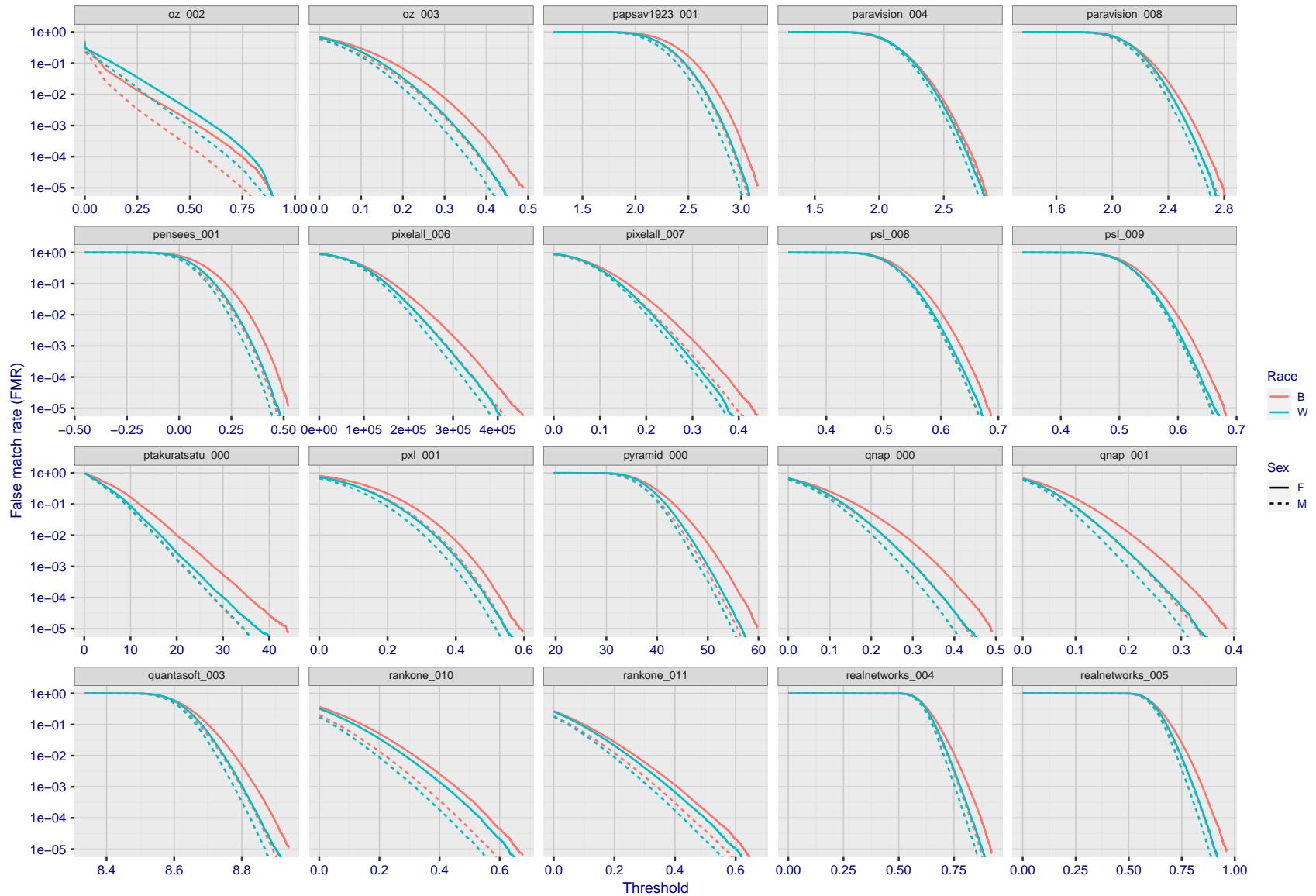


Figure 175: For the mugshot images, the false match calibration curves show false match rate vs. threshold. Separate curves appear for white females, black females, black males and white males.

2021/12/16 10:32:53

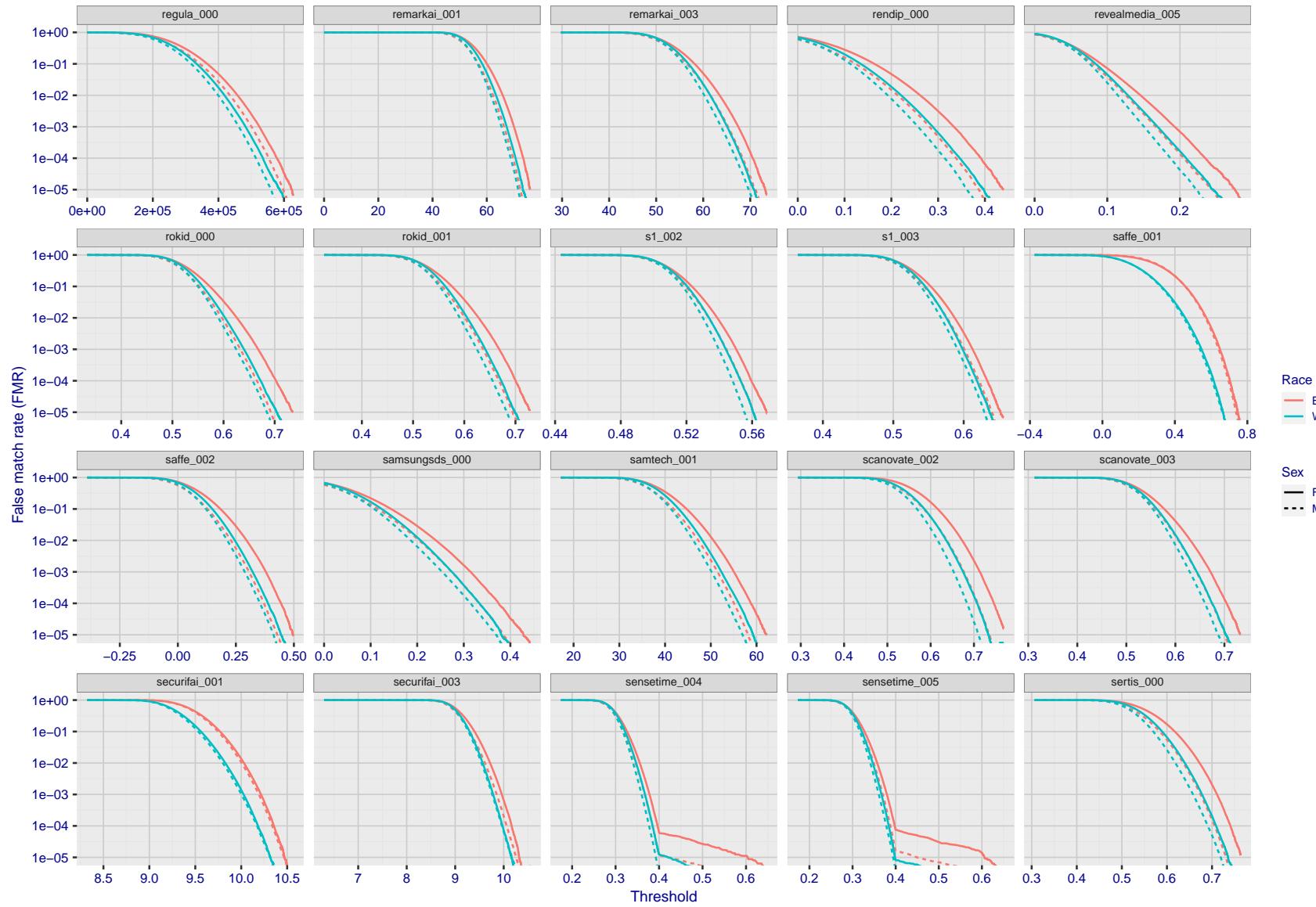


Figure 176: For the mugshot images, the false match calibration curves show false match rate vs. threshold. Separate curves appear for white females, black females, black males and white males.

2021/12/16 10:32:53

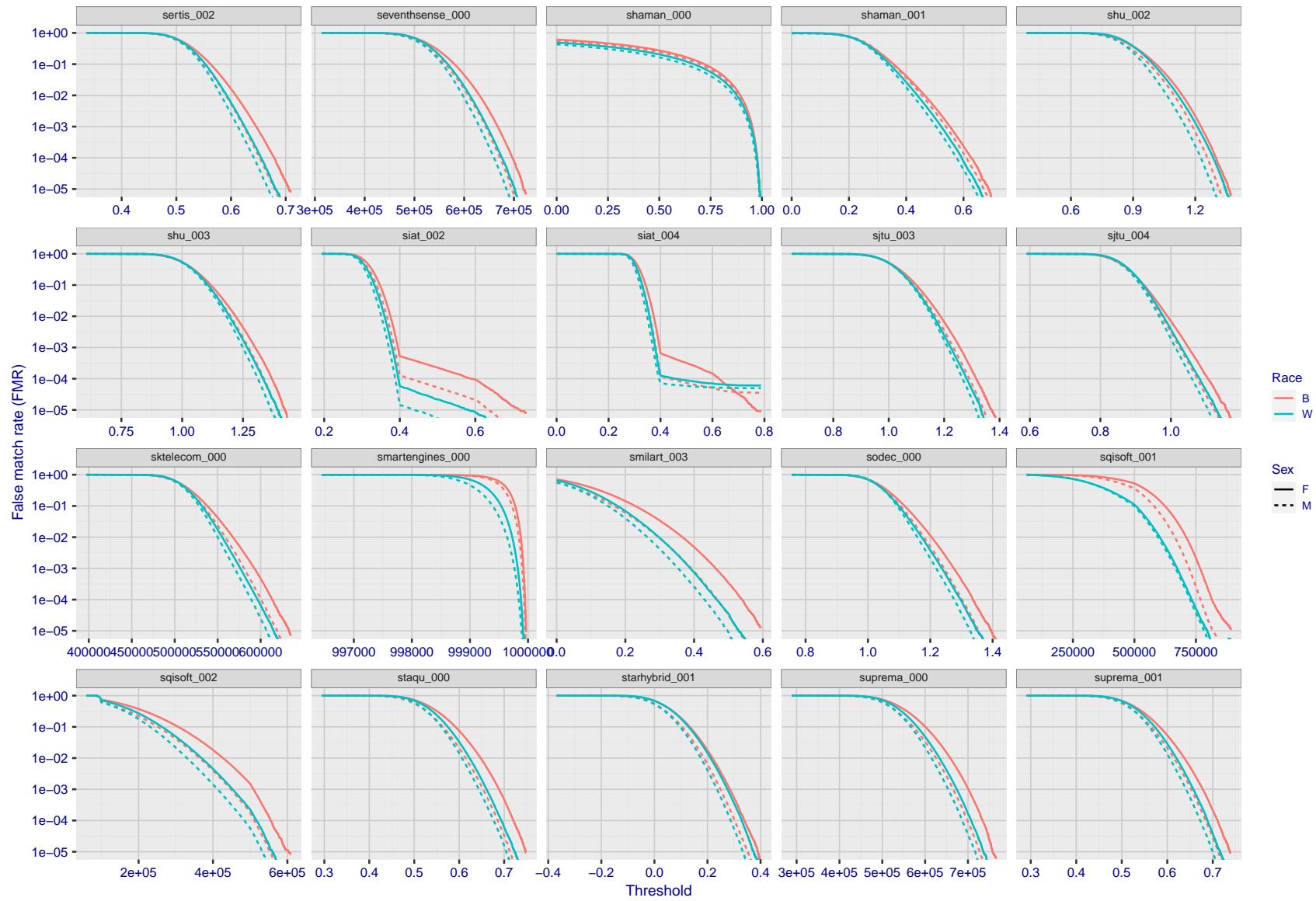


Figure 177: For the mugshot images, the false match calibration curves show false match rate vs. threshold. Separate curves appear for white females, black females, black males and white males.

2021/12/16 10:32:53

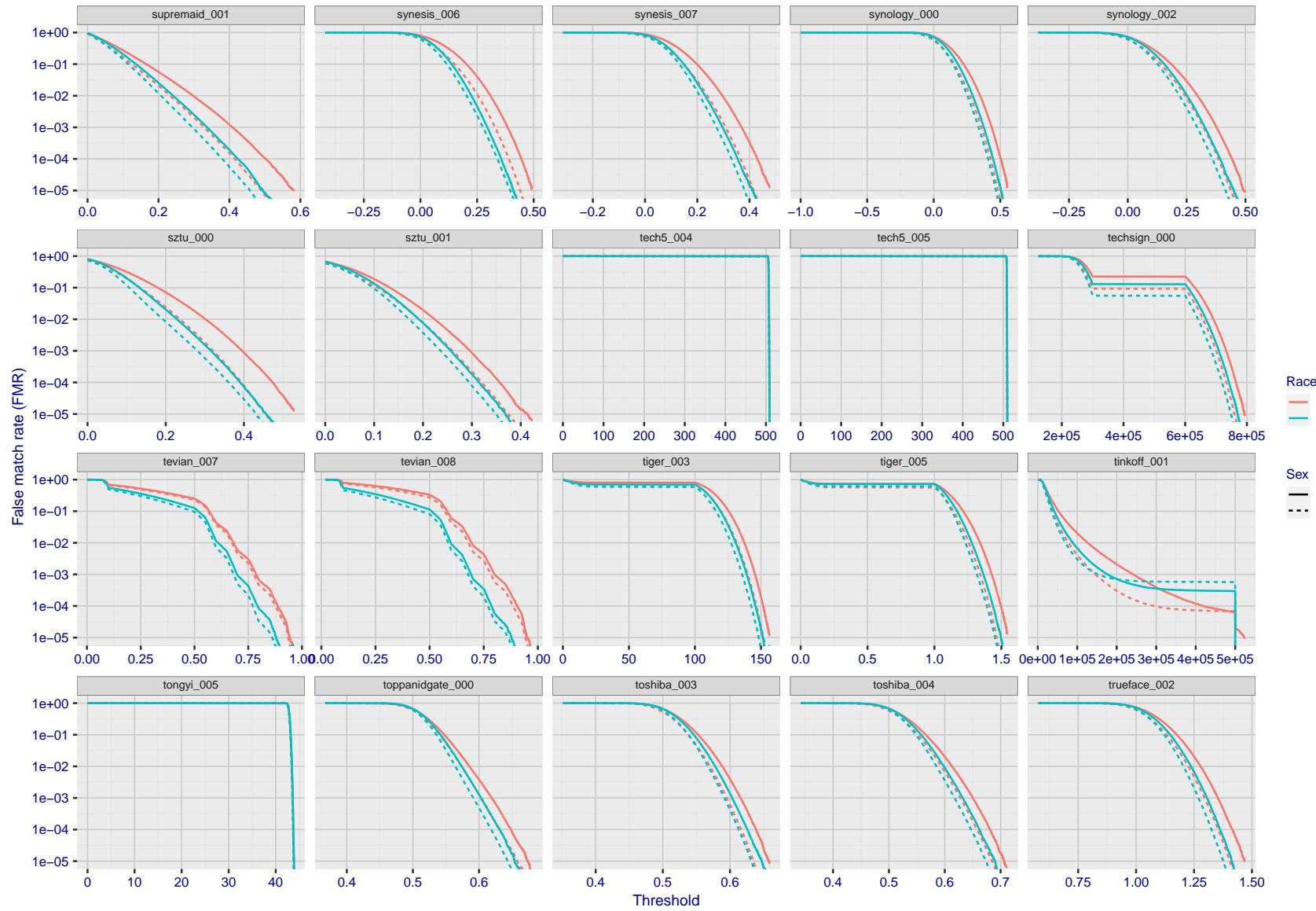


Figure 178: For the mugshot images, the false match calibration curves show false match rate vs. threshold. Separate curves appear for white females, black females, black males and white males.

FNMR(T)
"False non-match rate"
"False match rate"

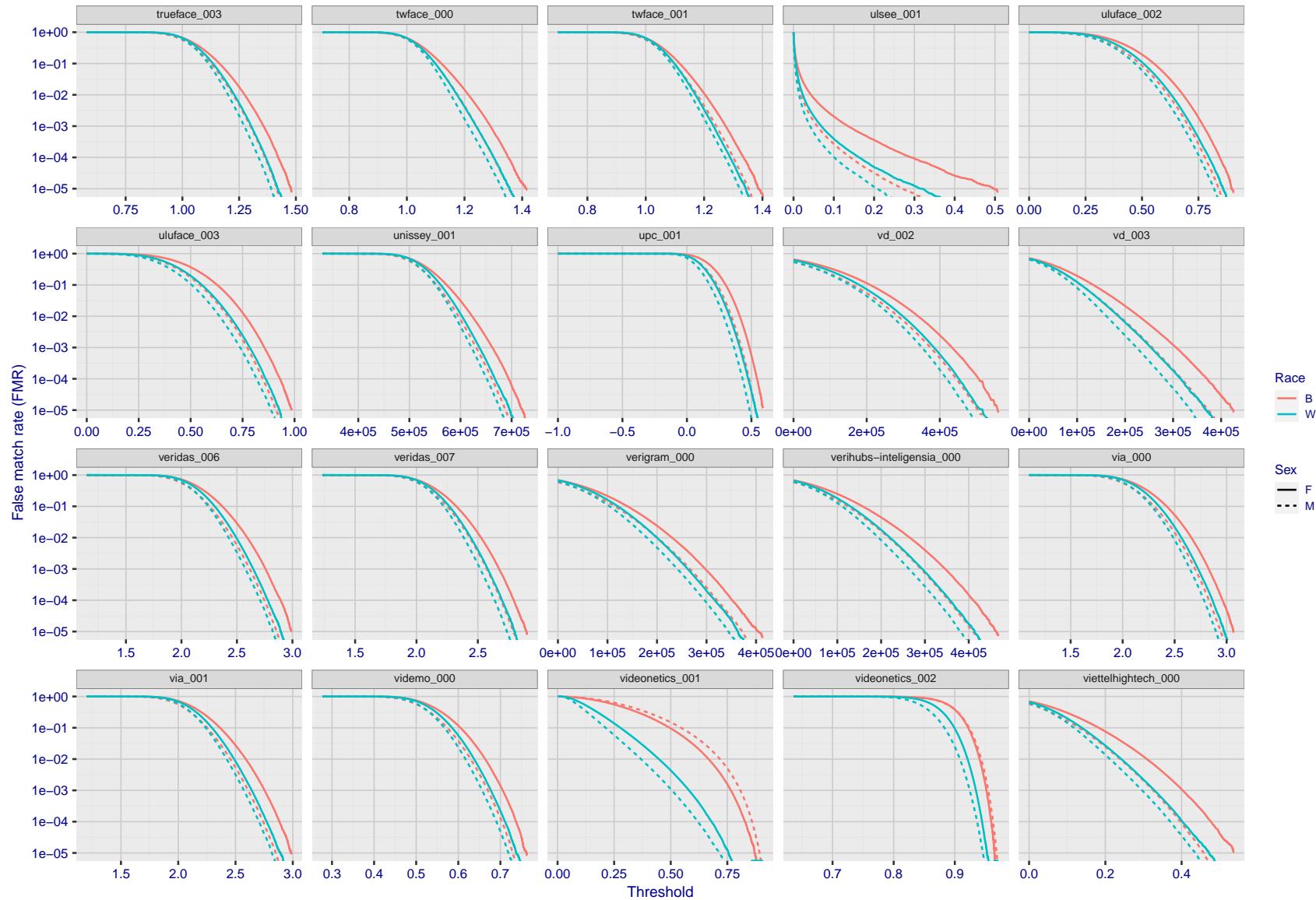


Figure 179: For the mugshot images, the false match calibration curves show false match rate vs. threshold. Separate curves appear for white females, black females, black males and white males.

2021/12/16 10:32:53

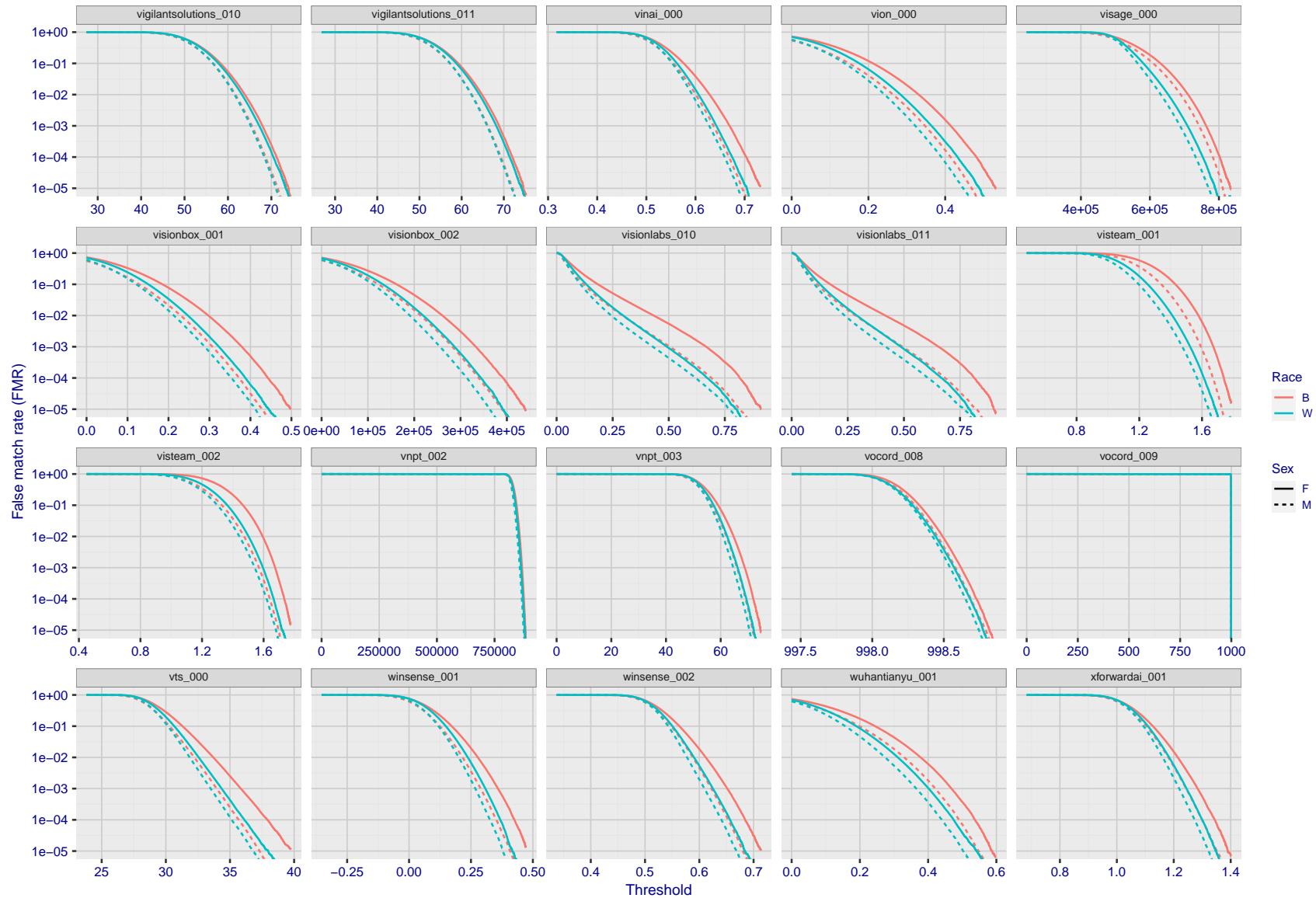


Figure 180: For the mugshot images, the false match calibration curves show false match rate vs. threshold. Separate curves appear for white females, black females, black males and white males.

FNMR(T)

"False non-match rate"

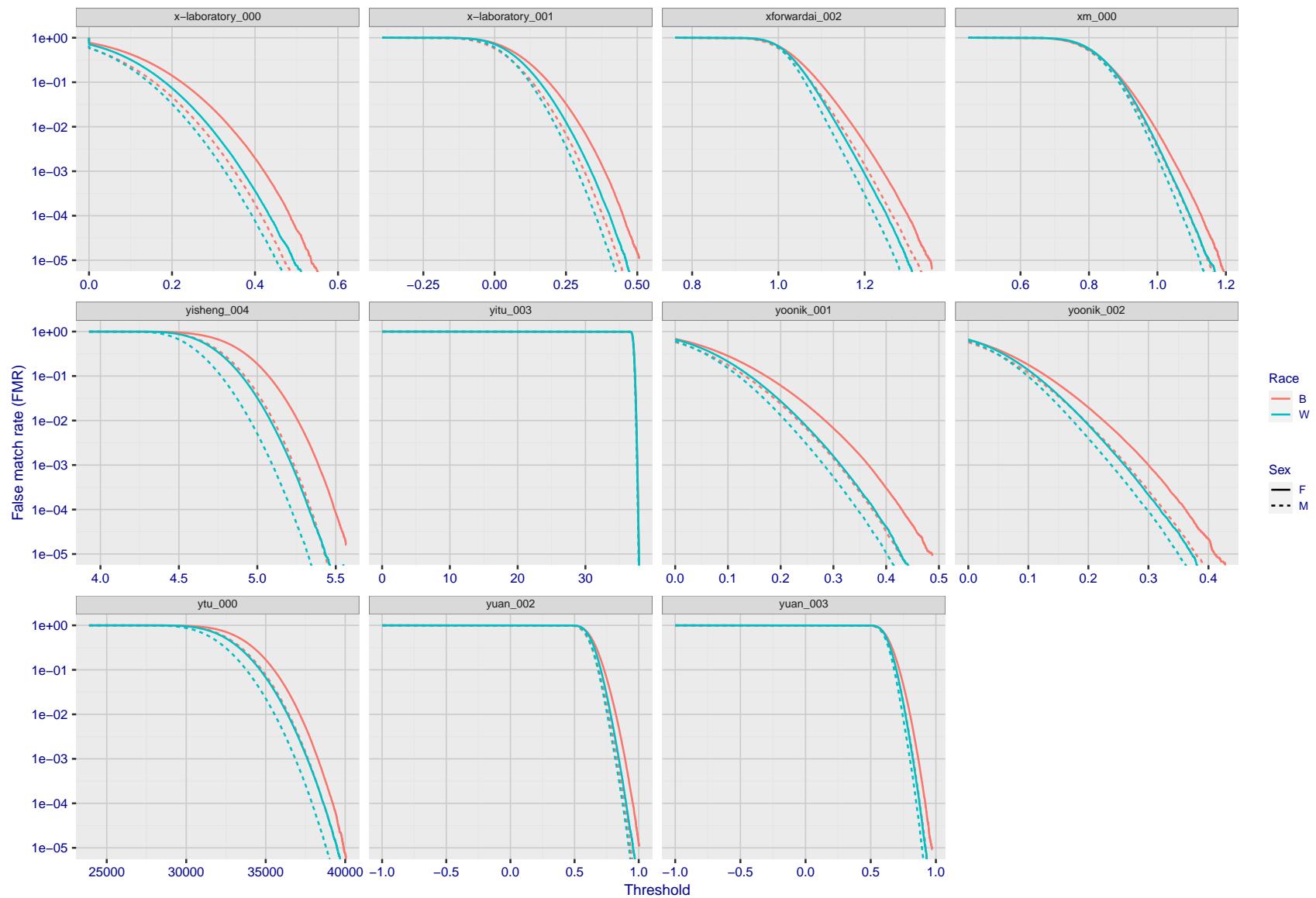


Figure 181: For the mugshot images, the false match calibration curves show false match rate vs. threshold. Separate curves appear for white females, black females, black males and white males.

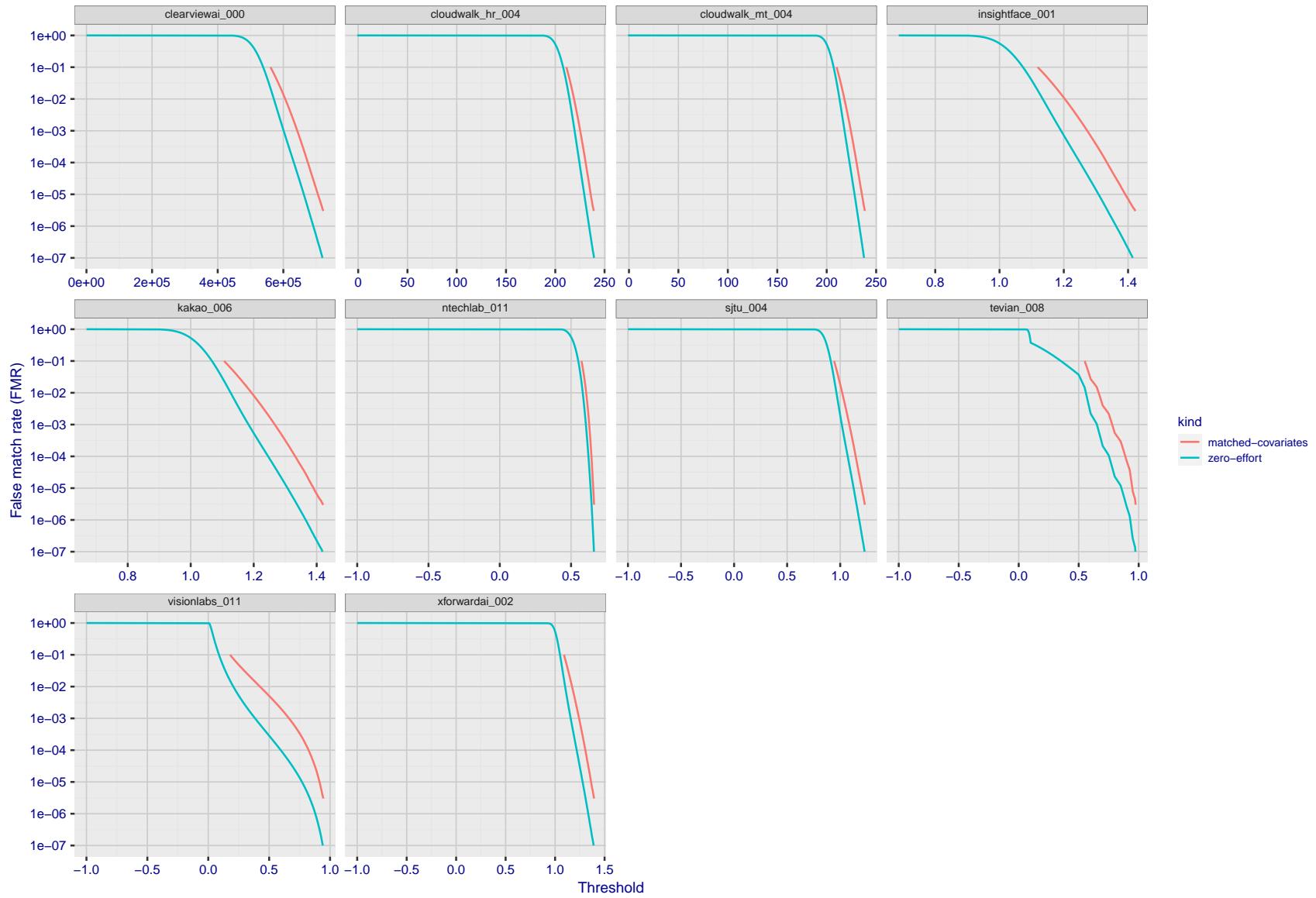


Figure 182: For the visa images, the false match calibration curves show FMR vs. threshold, T . The blue (lower) curves are for zero-effort impostors (i.e. comparing all images against all). The red (upper) curves are for persons of the same-sex, same-age, and same national-origin. This shows that FMR is underestimated (by a factor of 10 or more) by using a zero-effort impostor calculation to calibrate T . As shown later (sec. 3.6), FMR is higher for demographic-matched impostors.

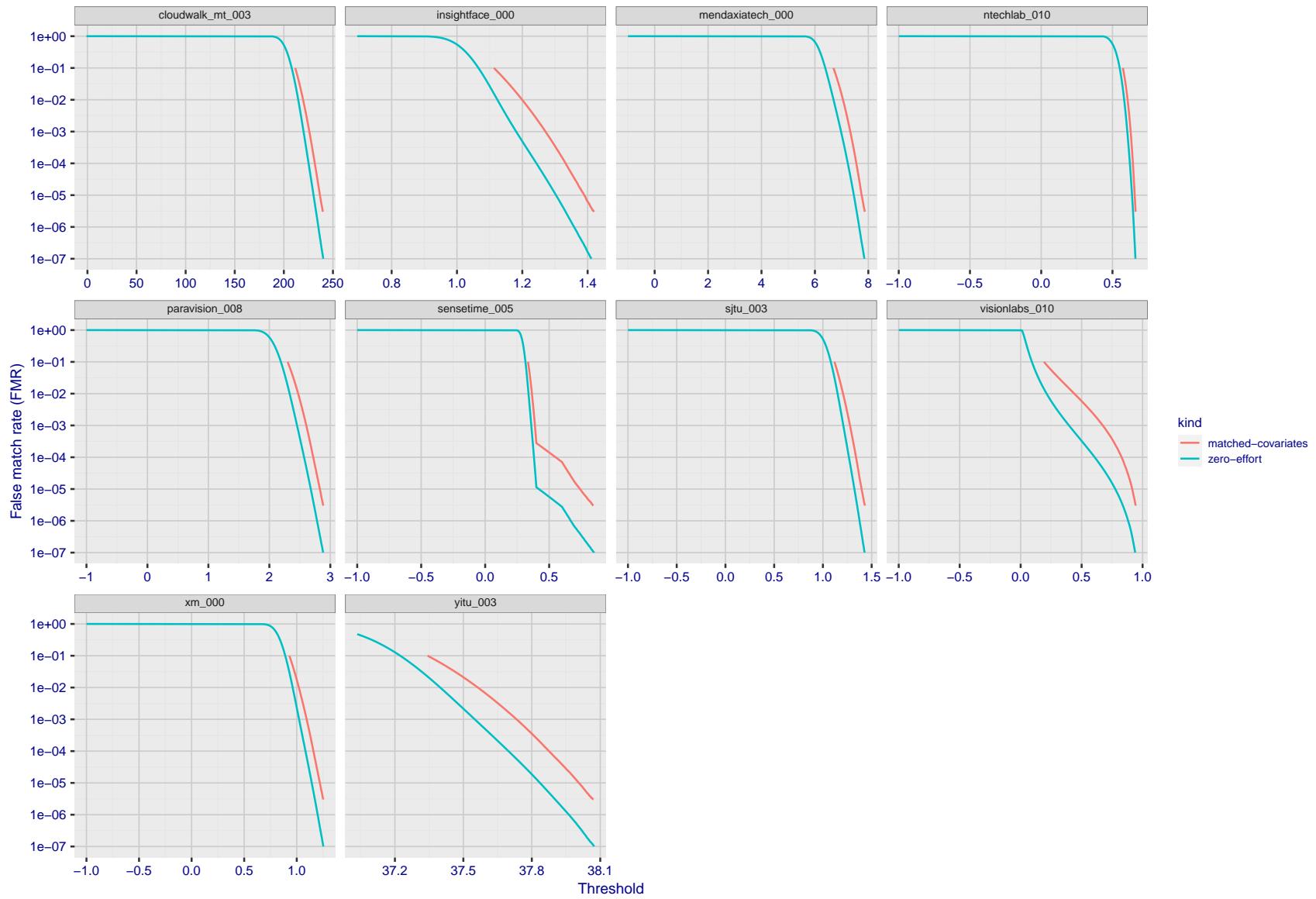


Figure 183: For the visa images, the false match calibration curves show FMR vs. threshold, T . The blue (lower) curves are for zero-effort impostors (i.e. comparing all images against all). The red (upper) curves are for persons of the same-sex, same-age, and same national-origin. This shows that FMR is underestimated (by a factor of 10 or more) by using a zero-effort impostor calculation to calibrate T . As shown later (sec. 3.6), FMR is higher for demographic-matched impostors.

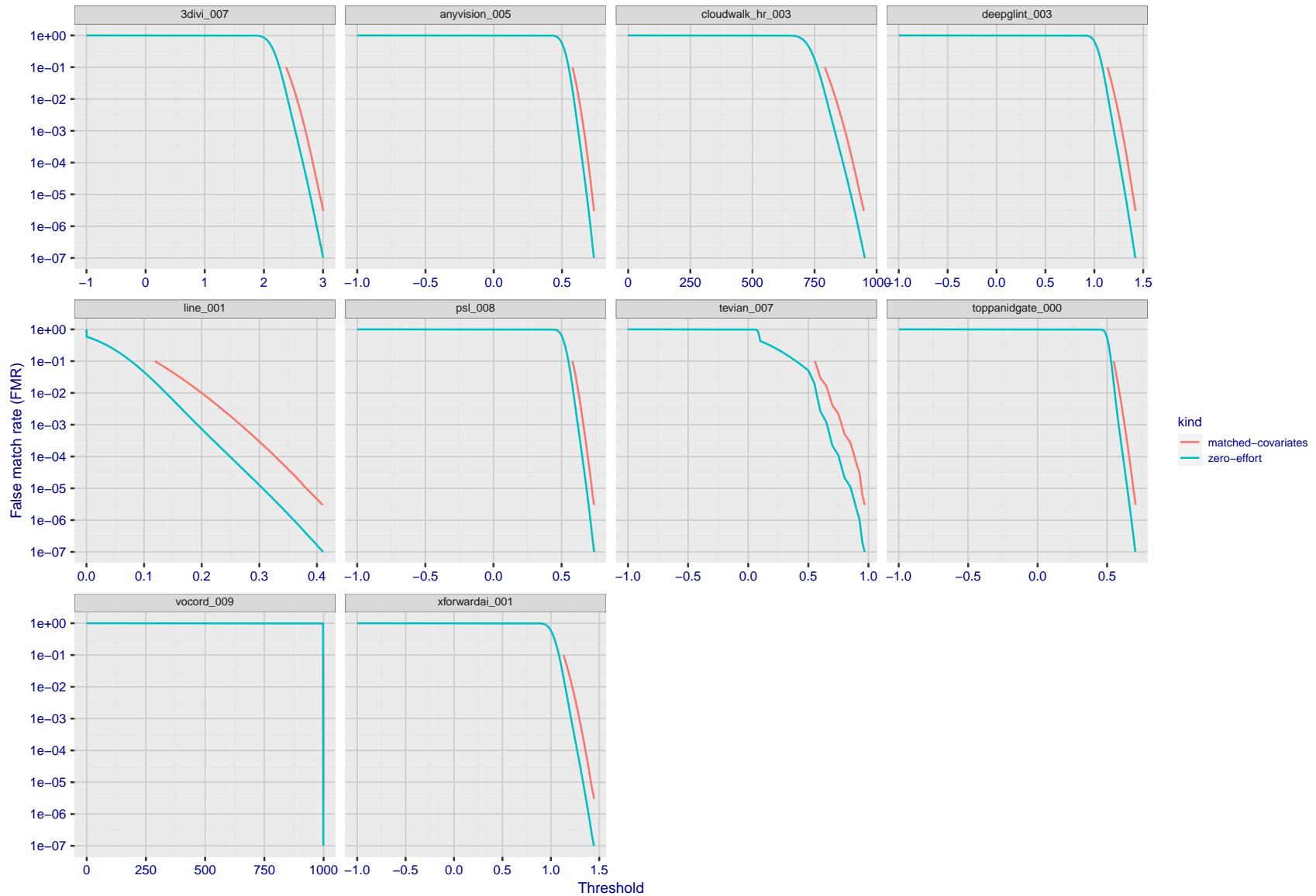


Figure 184: For the visa images, the false match calibration curves show FMR vs. threshold, T . The blue (lower) curves are for zero-effort impostors (i.e. comparing all images against all). The red (upper) curves are for persons of the same-sex, same-age, and same national-origin. This shows that FMR is underestimated (by a factor of 10 or more) by using a zero-effort impostor calculation to calibrate T . As shown later (sec. 3.6), FMR is higher for demographic-matched impostors.

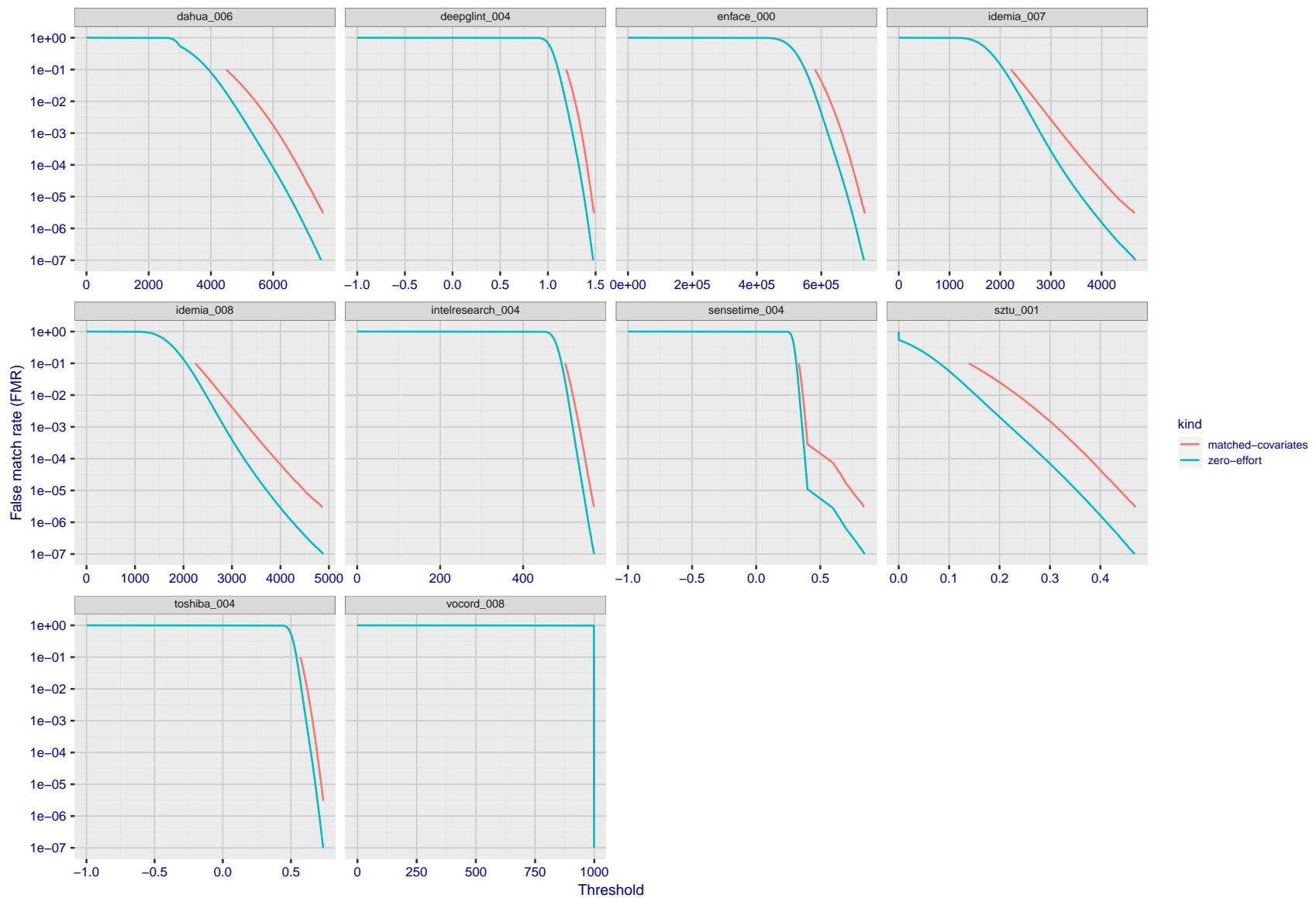


Figure 185: For the visa images, the false match calibration curves show FMR vs. threshold, T . The blue (lower) curves are for zero-effort impostors (i.e. comparing all images against all). The red (upper) curves are for persons of the same-sex, same-age, and same national-origin. This shows that FMR is underestimated (by a factor of 10 or more) by using a zero-effort impostor calculation to calibrate T . As shown later (sec. 3.6), FMR is higher for demographic-matched impostors.

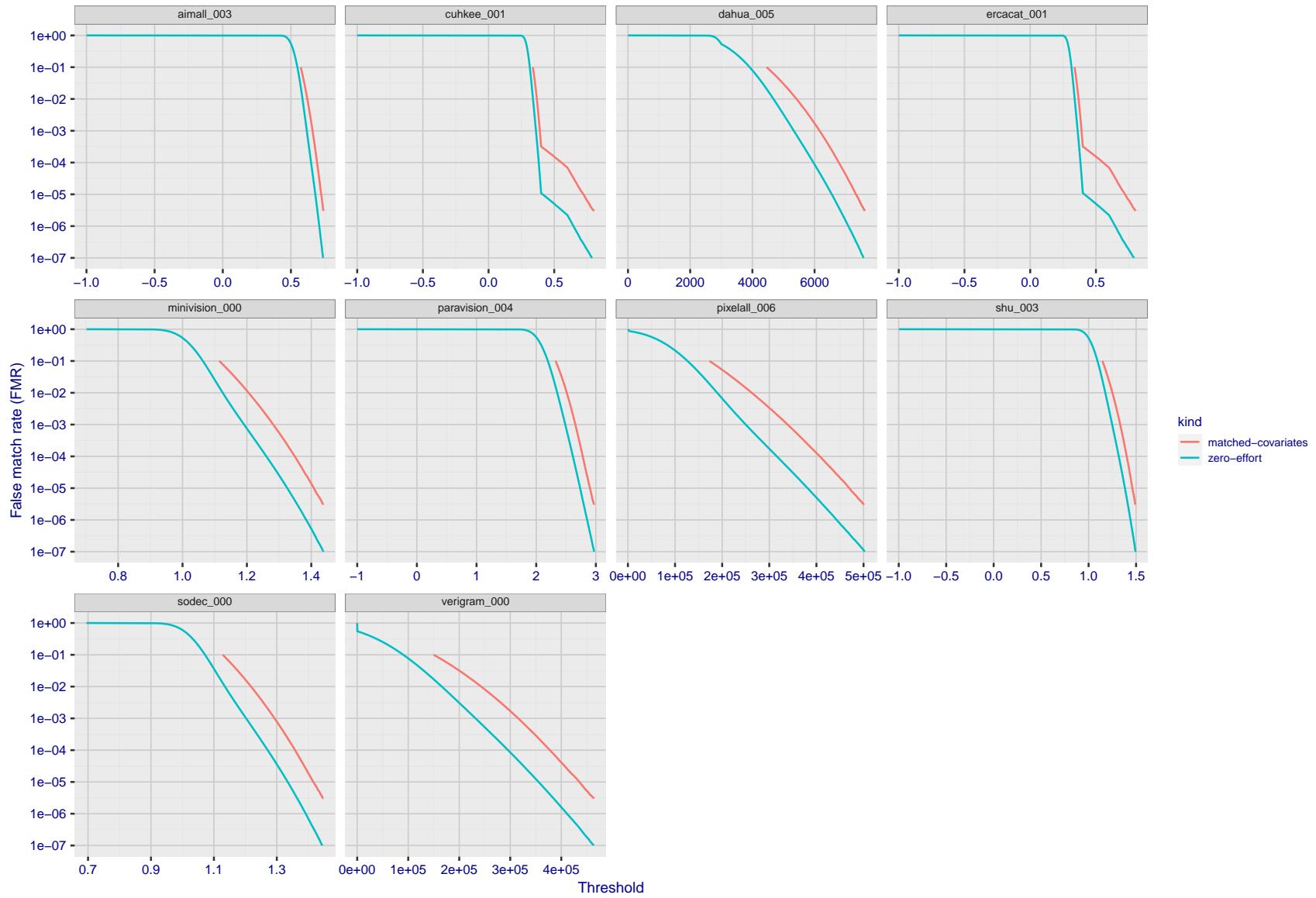


Figure 186: For the visa images, the false match calibration curves show FMR vs. threshold, T . The blue (lower) curves are for zero-effort impostors (i.e. comparing all images against all). The red (upper) curves are for persons of the same-sex, same-age, and same national-origin. This shows that FMR is underestimated (by a factor of 10 or more) by using a zero-effort impostor calculation to calibrate T . As shown later (sec. 3.6), FMR is higher for demographic-matched impostors.

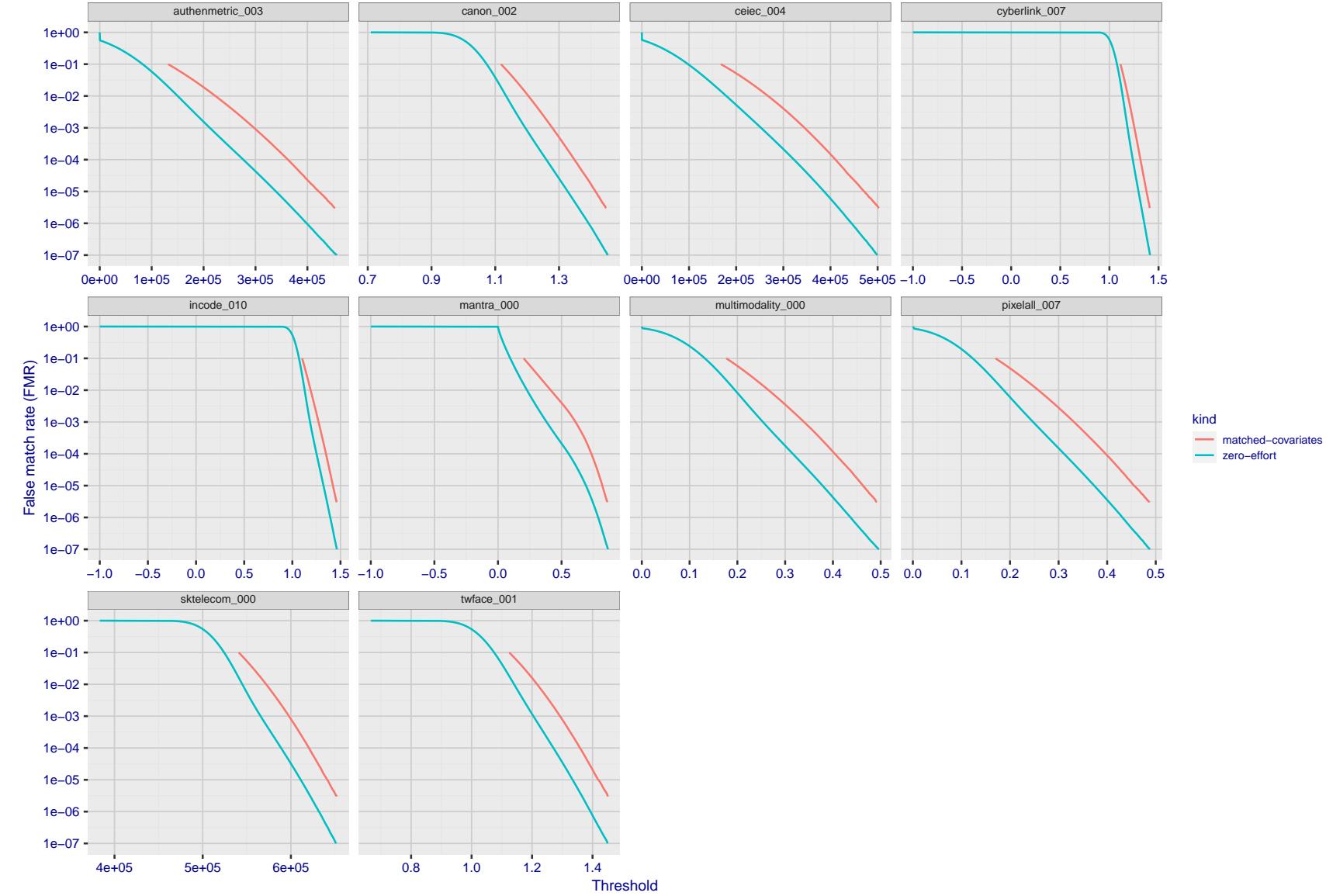


Figure 187: For the visa images, the false match calibration curves show FMR vs. threshold, T . The blue (lower) curves are for zero-effort impostors (i.e. comparing all images against all). The red (upper) curves are for persons of the same-sex, same-age, and same national-origin. This shows that FMR is underestimated (by a factor of 10 or more) by using a zero-effort impostor calculation to calibrate T . As shown later (sec. 3.6), FMR is higher for demographic-matched impostors.

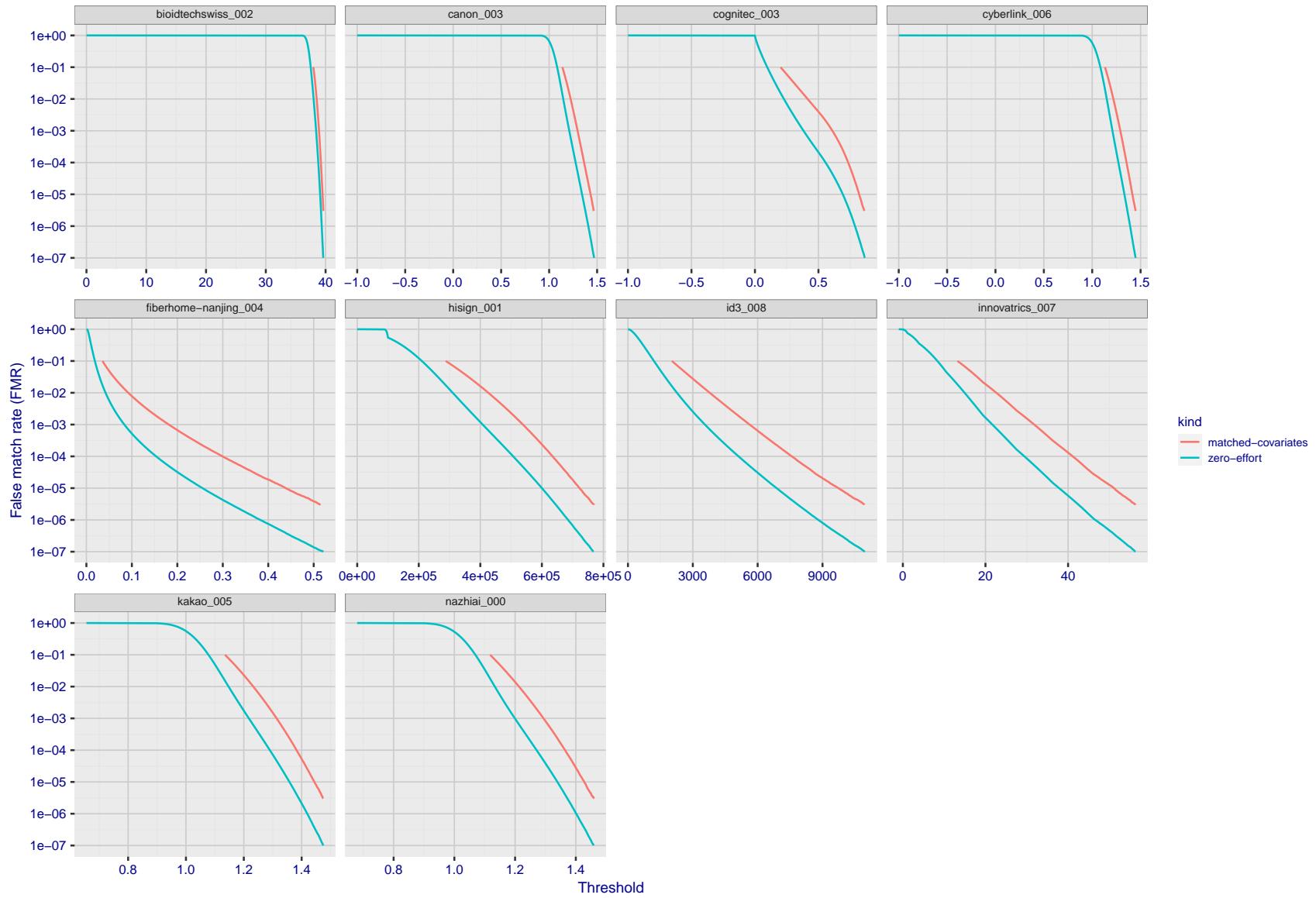


Figure 188: For the visa images, the false match calibration curves show FMR vs. threshold, T . The blue (lower) curves are for zero-effort impostors (i.e. comparing all images against all). The red (upper) curves are for persons of the same-sex, same-age, and same national-origin. This shows that FMR is underestimated (by a factor of 10 or more) by using a zero-effort impostor calculation to calibrate T . As shown later (sec. 3.6), FMR is higher for demographic-matched impostors.

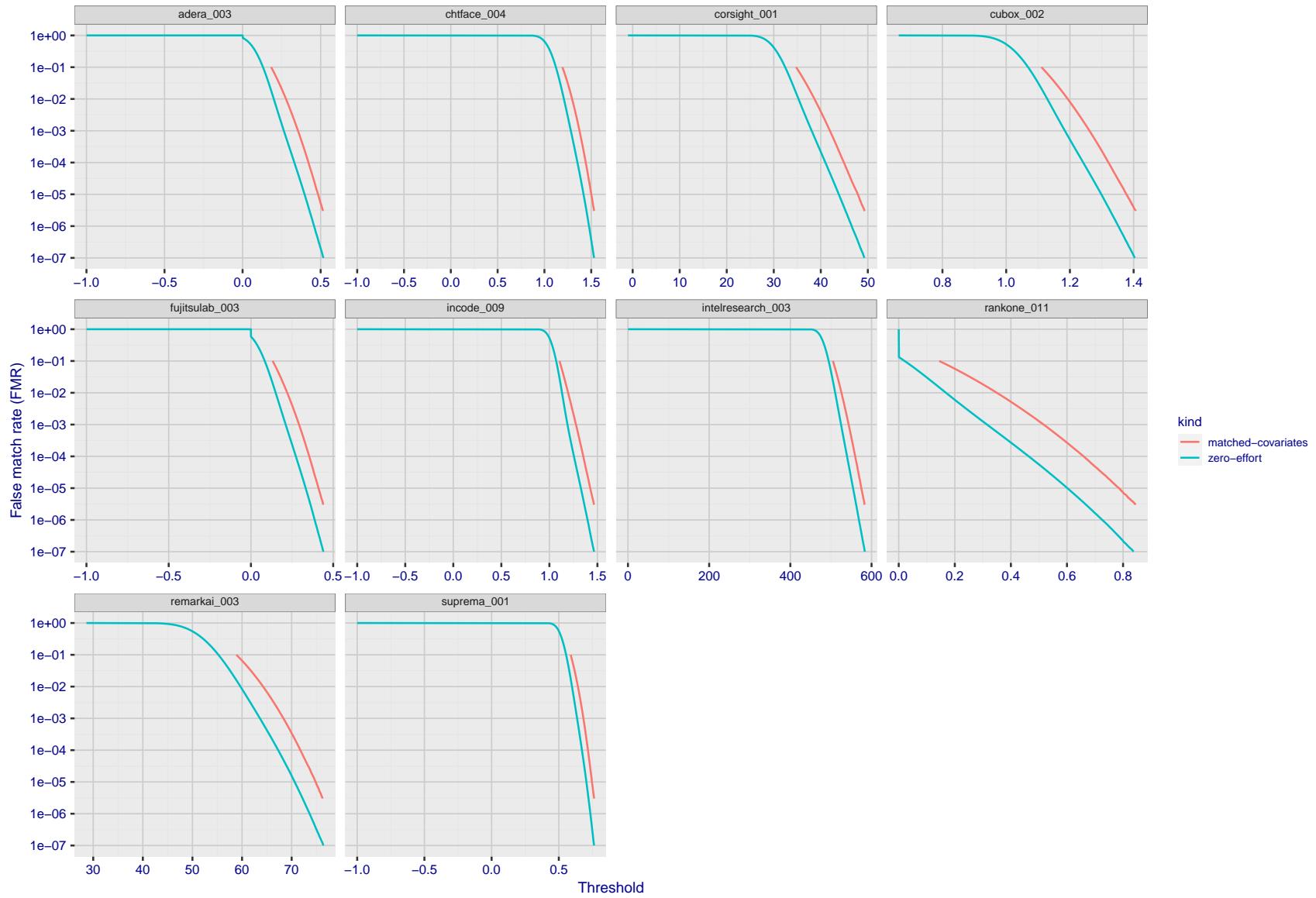


Figure 189: For the visa images, the false match calibration curves show FMR vs. threshold, T . The blue (lower) curves are for zero-effort impostors (i.e. comparing all images against all). The red (upper) curves are for persons of the same-sex, same-age, and same national-origin. This shows that FMR is underestimated (by a factor of 10 or more) by using a zero-effort impostor calculation to calibrate T . As shown later (sec. 3.6), FMR is higher for demographic-matched impostors.

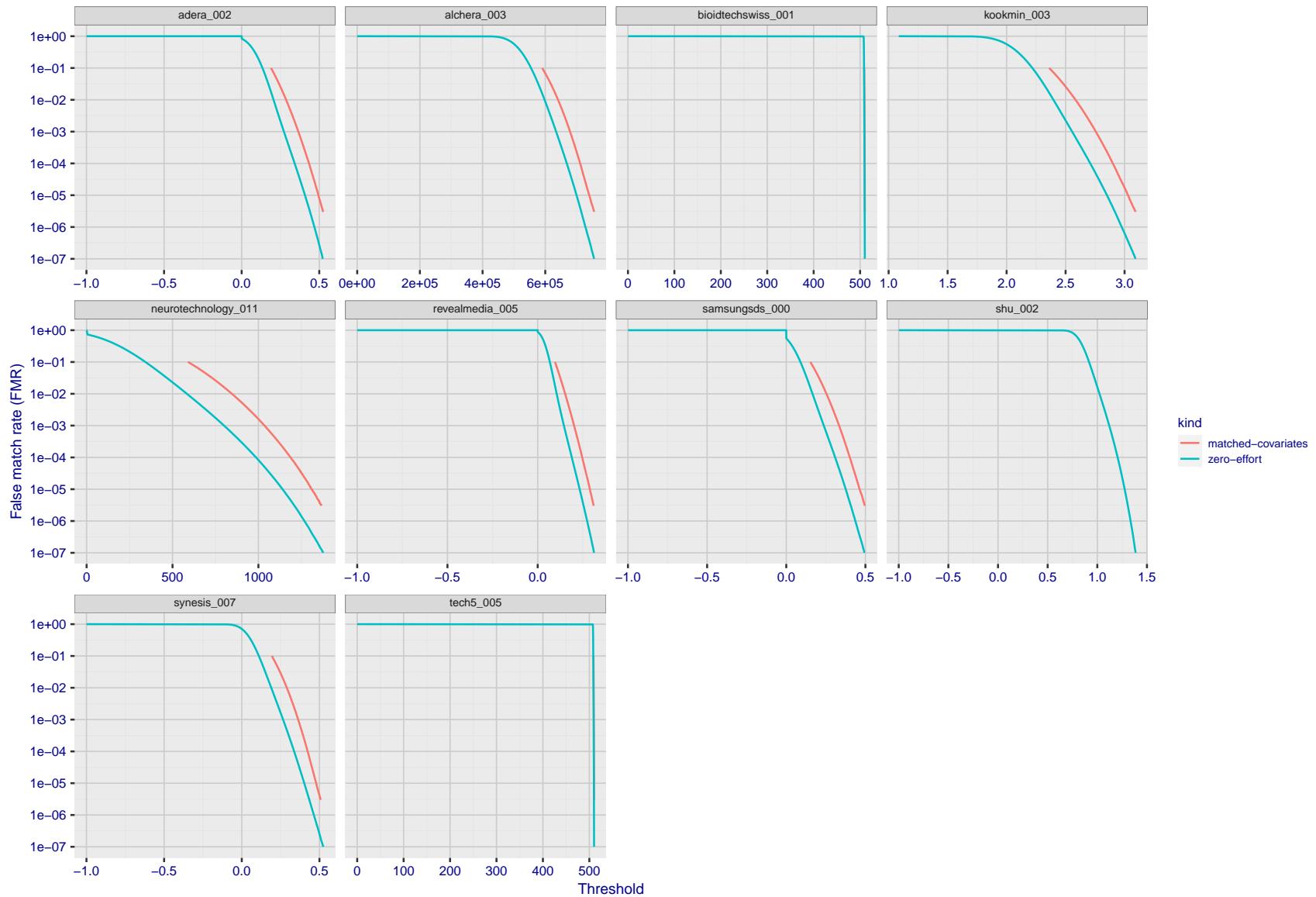


Figure 190: For the visa images, the false match calibration curves show FMR vs. threshold, T . The blue (lower) curves are for zero-effort impostors (i.e. comparing all images against all). The red (upper) curves are for persons of the same-sex, same-age, and same national-origin. This shows that FMR is underestimated (by a factor of 10 or more) by using a zero-effort impostor calculation to calibrate T . As shown later (sec. 3.6), FMR is higher for demographic-matched impostors.

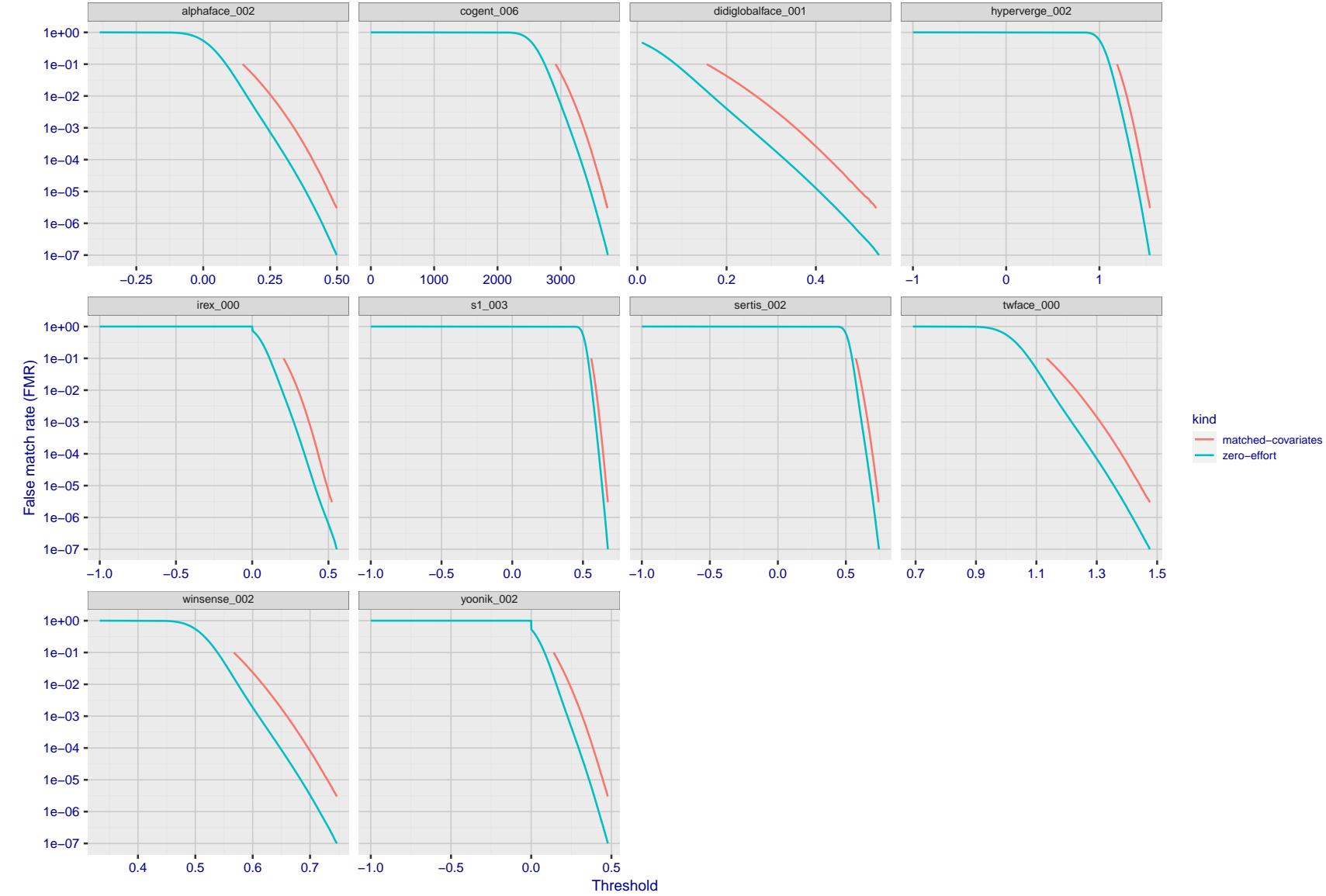


Figure 191: For the visa images, the false match calibration curves show FMR vs. threshold, T . The blue (lower) curves are for zero-effort impostors (i.e. comparing all images against all). The red (upper) curves are for persons of the same-sex, same-age, and same national-origin. This shows that FMR is underestimated (by a factor of 10 or more) by using a zero-effort impostor calculation to calibrate T . As shown later (sec. 3.6), FMR is higher for demographic-matched impostors.

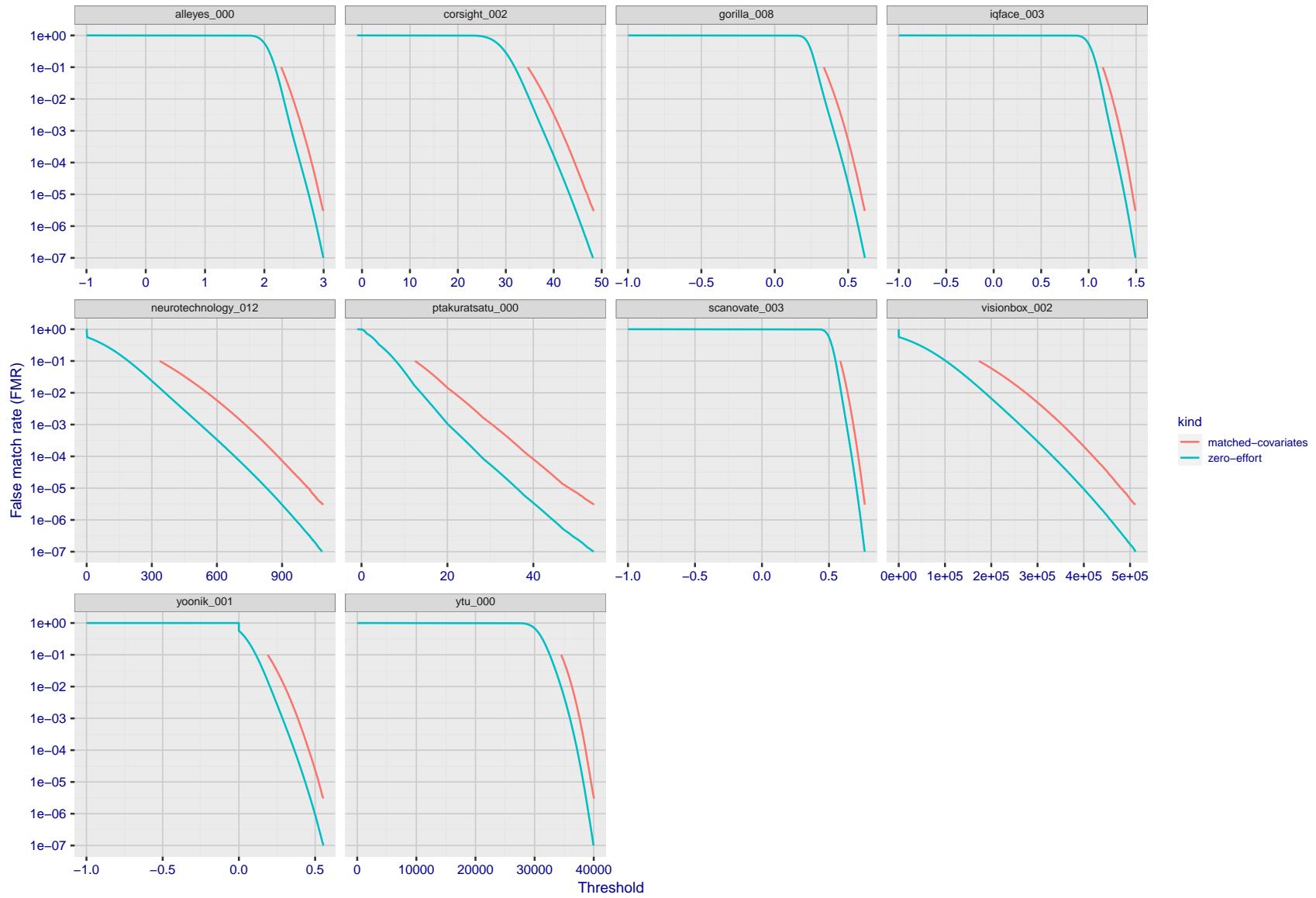


Figure 192: For the visa images, the false match calibration curves show FMR vs. threshold, T . The blue (lower) curves are for zero-effort impostors (i.e. comparing all images against all). The red (upper) curves are for persons of the same-sex, same-age, and same national-origin. This shows that FMR is underestimated (by a factor of 10 or more) by using a zero-effort impostor calculation to calibrate T . As shown later (sec. 3.6), FMR is higher for demographic-matched impostors.

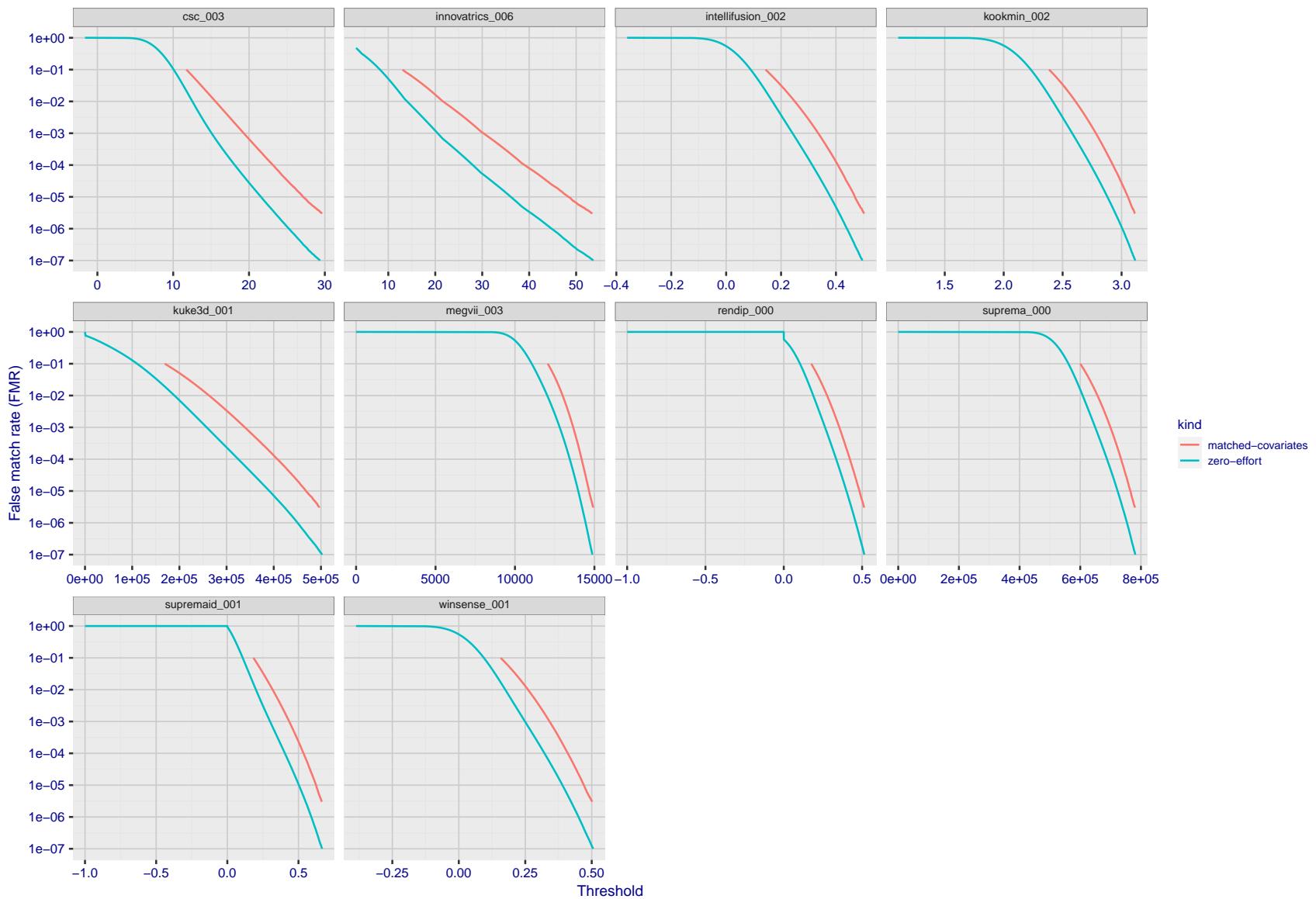


Figure 193: For the visa images, the false match calibration curves show FMR vs. threshold, T . The blue (lower) curves are for zero-effort impostors (i.e. comparing all images against all). The red (upper) curves are for persons of the same-sex, same-age, and same national-origin. This shows that FMR is underestimated (by a factor of 10 or more) by using a zero-effort impostor calculation to calibrate T . As shown later (sec. 3.6), FMR is higher for demographic-matched impostors.

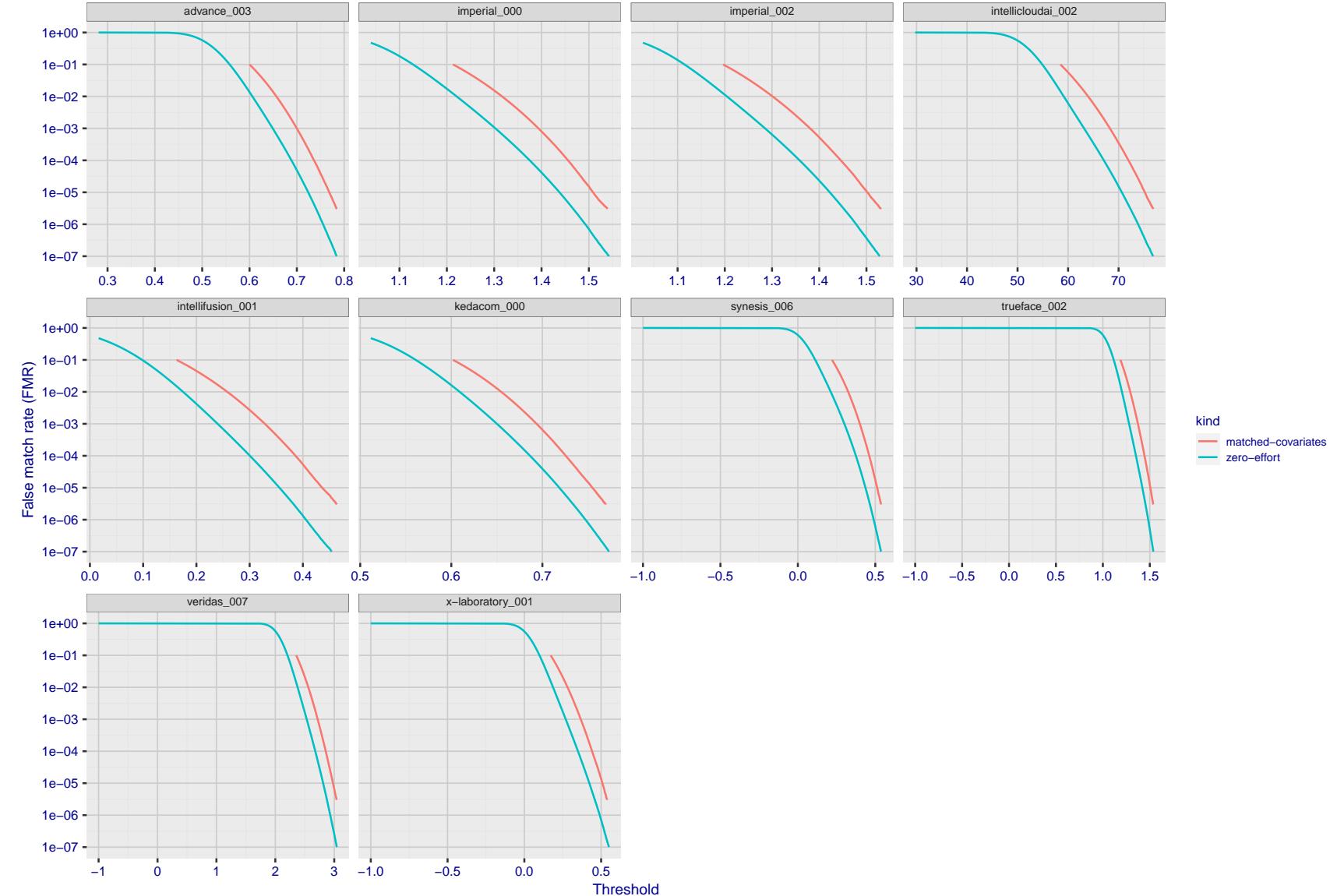


Figure 194: For the visa images, the false match calibration curves show FMR vs. threshold, T . The blue (lower) curves are for zero-effort impostors (i.e. comparing all images against all). The red (upper) curves are for persons of the same-sex, same-age, and same national-origin. This shows that FMR is underestimated (by a factor of 10 or more) by using a zero-effort impostor calculation to calibrate T . As shown later (sec. 3.6), FMR is higher for demographic-matched impostors.

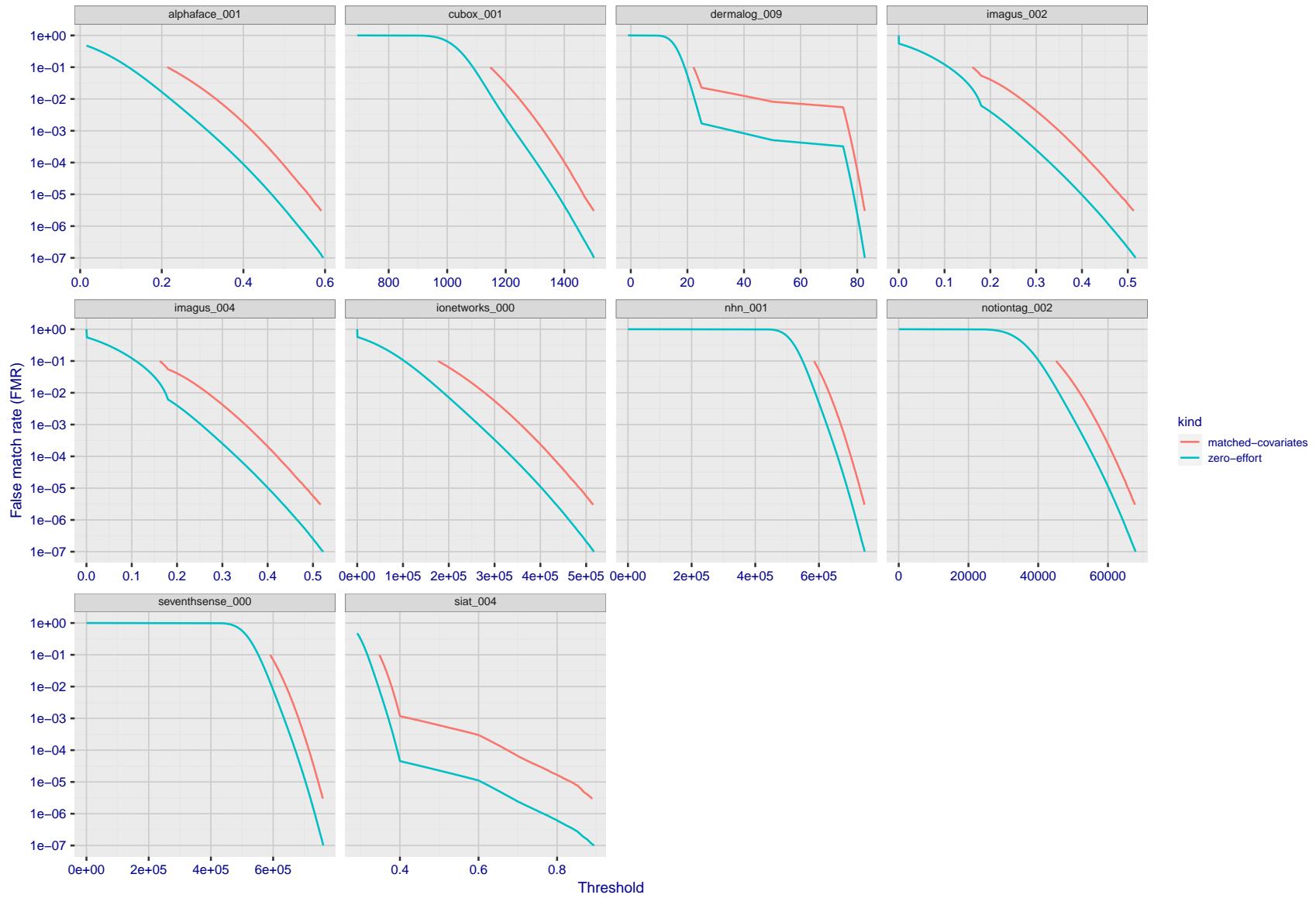


Figure 195: For the visa images, the false match calibration curves show FMR vs. threshold, T . The blue (lower) curves are for zero-effort impostors (i.e. comparing all images against all). The red (upper) curves are for persons of the same-sex, same-age, and same national-origin. This shows that FMR is underestimated (by a factor of 10 or more) by using a zero-effort impostor calculation to calibrate T . As shown later (sec. 3.6), FMR is higher for demographic-matched impostors.

2021/12/16 10:32:53

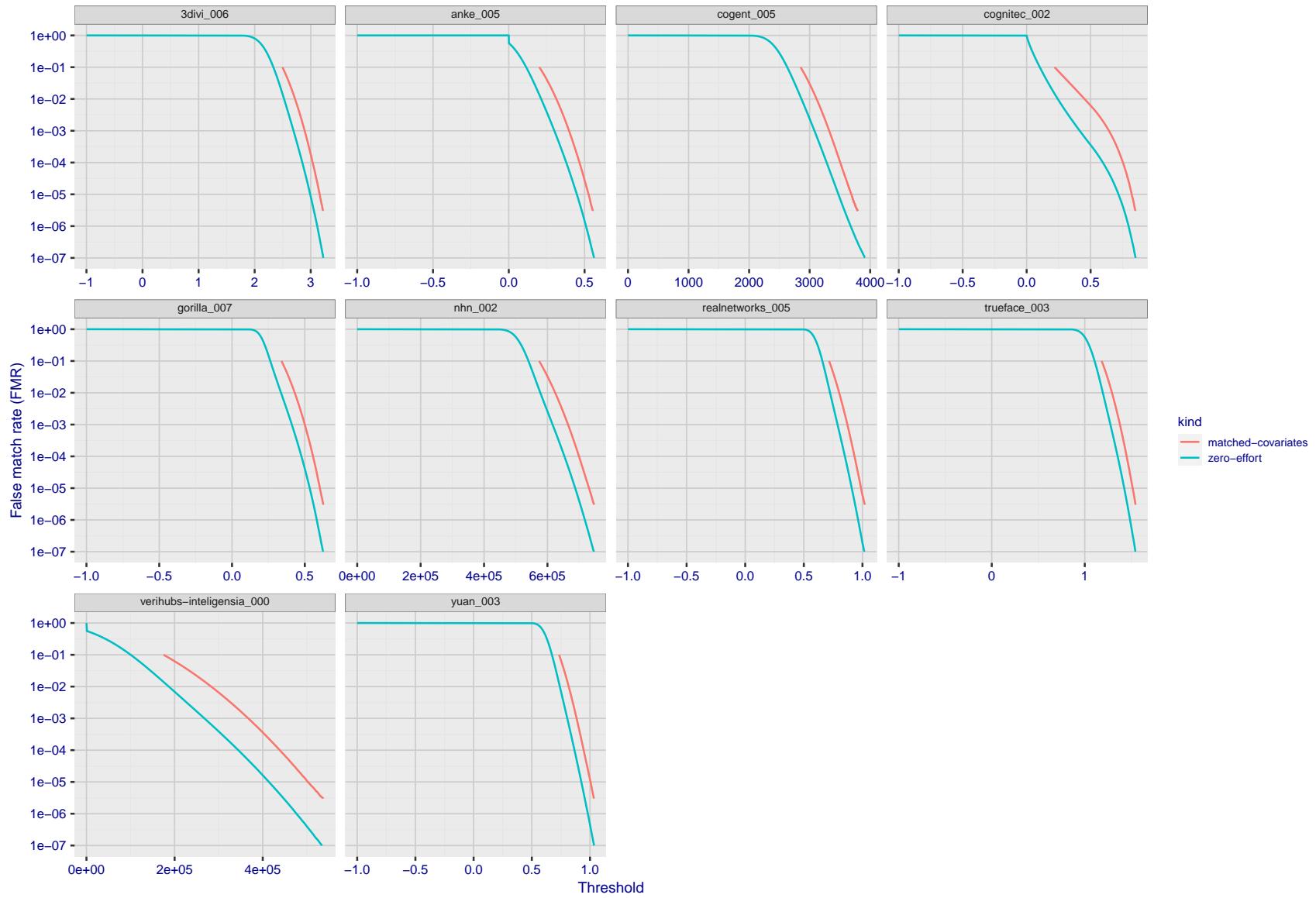


Figure 196: For the visa images, the false match calibration curves show FMR vs. threshold, T . The blue (lower) curves are for zero-effort impostors (i.e. comparing all images against all). The red (upper) curves are for persons of the same-sex, same-age, and same national-origin. This shows that FMR is underestimated (by a factor of 10 or more) by using a zero-effort impostor calculation to calibrate T . As shown later (sec. 3.6), FMR is higher for demographic-matched impostors.

FNMR(T)
"False non-match rate"
"False match rate"

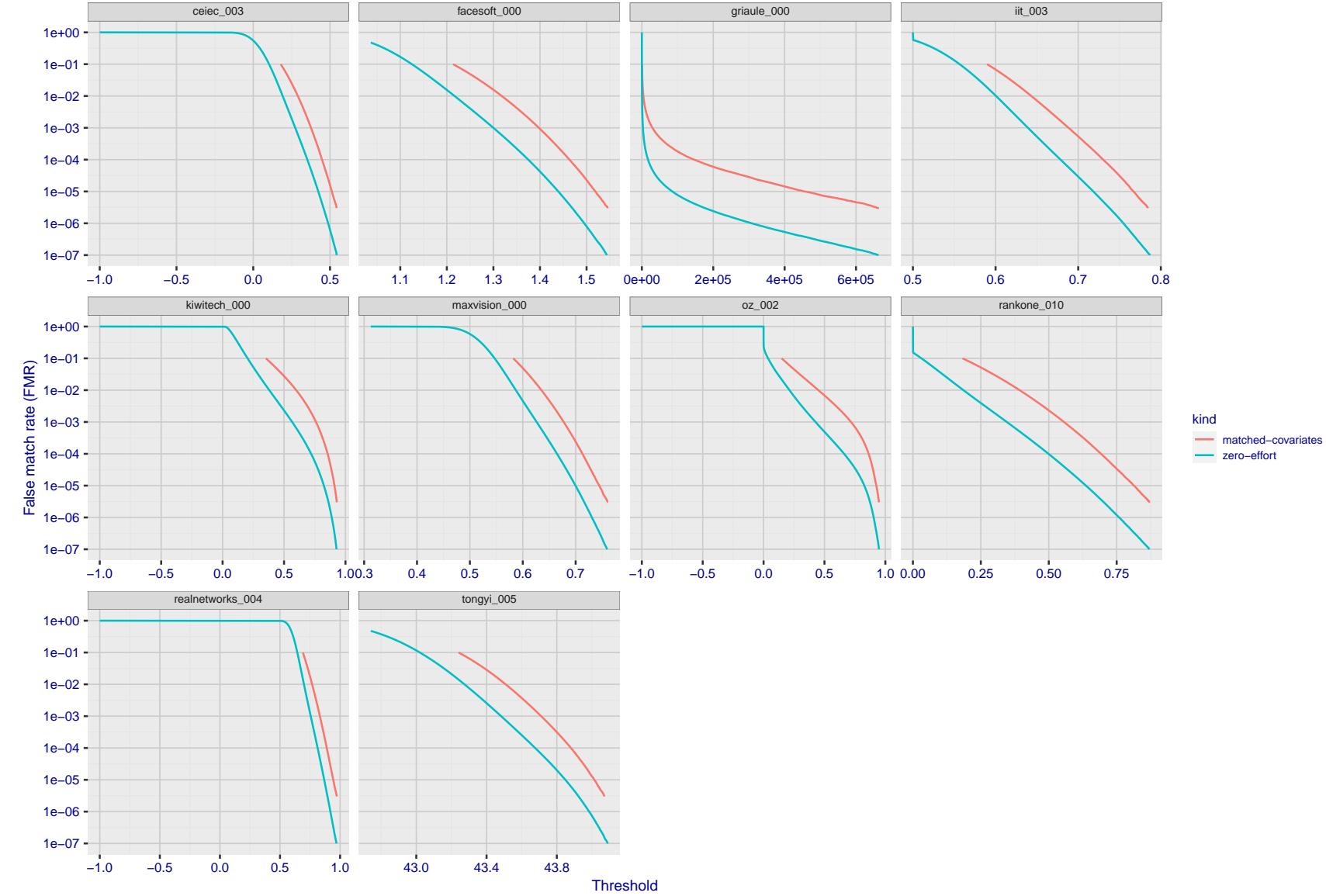


Figure 197: For the visa images, the false match calibration curves show FMR vs. threshold, T . The blue (lower) curves are for zero-effort impostors (i.e. comparing all images against all). The red (upper) curves are for persons of the same-sex, same-age, and same national-origin. This shows that FMR is underestimated (by a factor of 10 or more) by using a zero-effort impostor calculation to calibrate T . As shown later (sec. 3.6), FMR is higher for demographic-matched impostors.

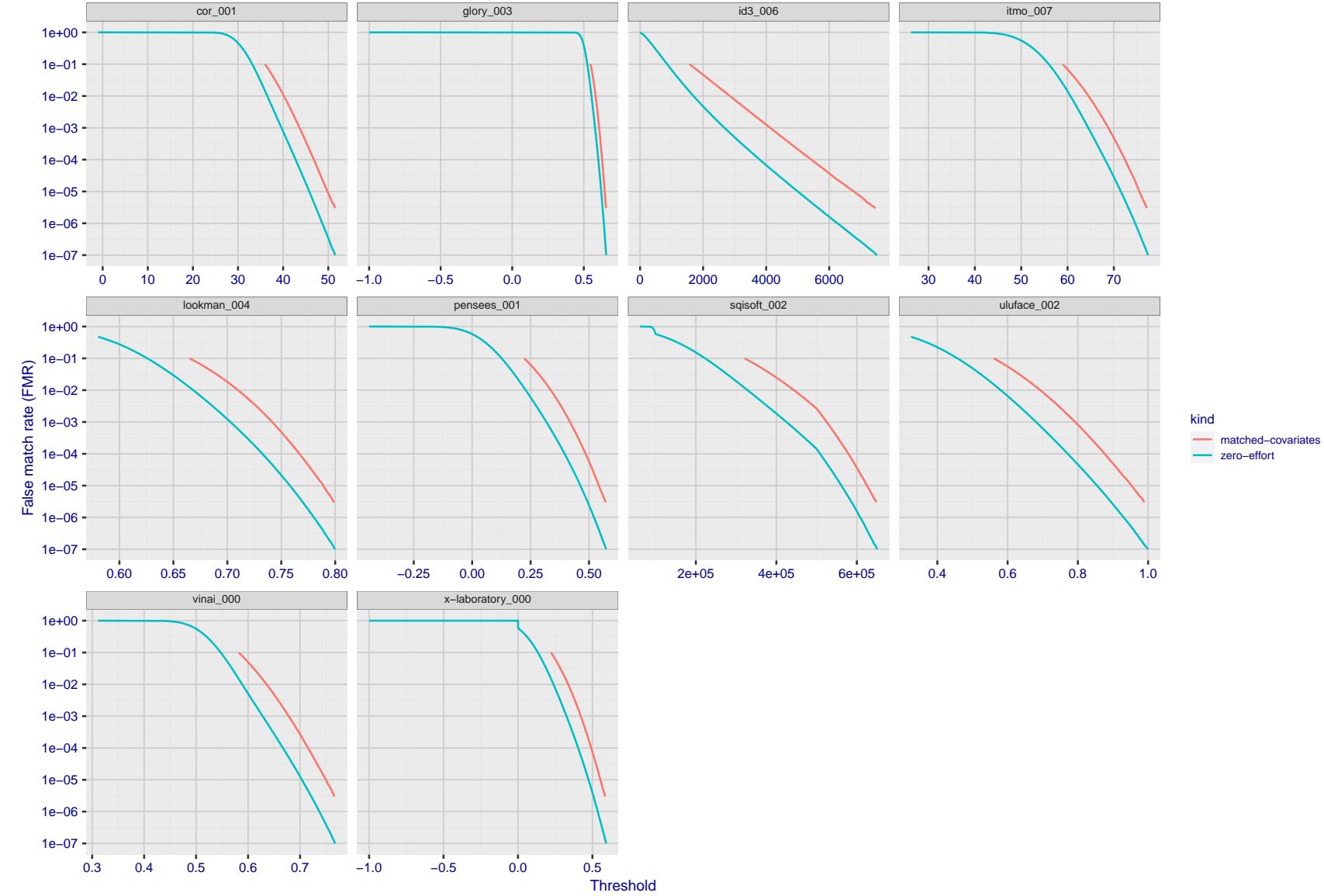


Figure 198: For the visa images, the false match calibration curves show FMR vs. threshold, T . The blue (lower) curves are for zero-effort impostors (i.e. comparing all images against all). The red (upper) curves are for persons of the same-sex, same-age, and same national-origin. This shows that FMR is underestimated (by a factor of 10 or more) by using a zero-effort impostor calculation to calibrate T . As shown later (sec. 3.6), FMR is higher for demographic-matched impostors.

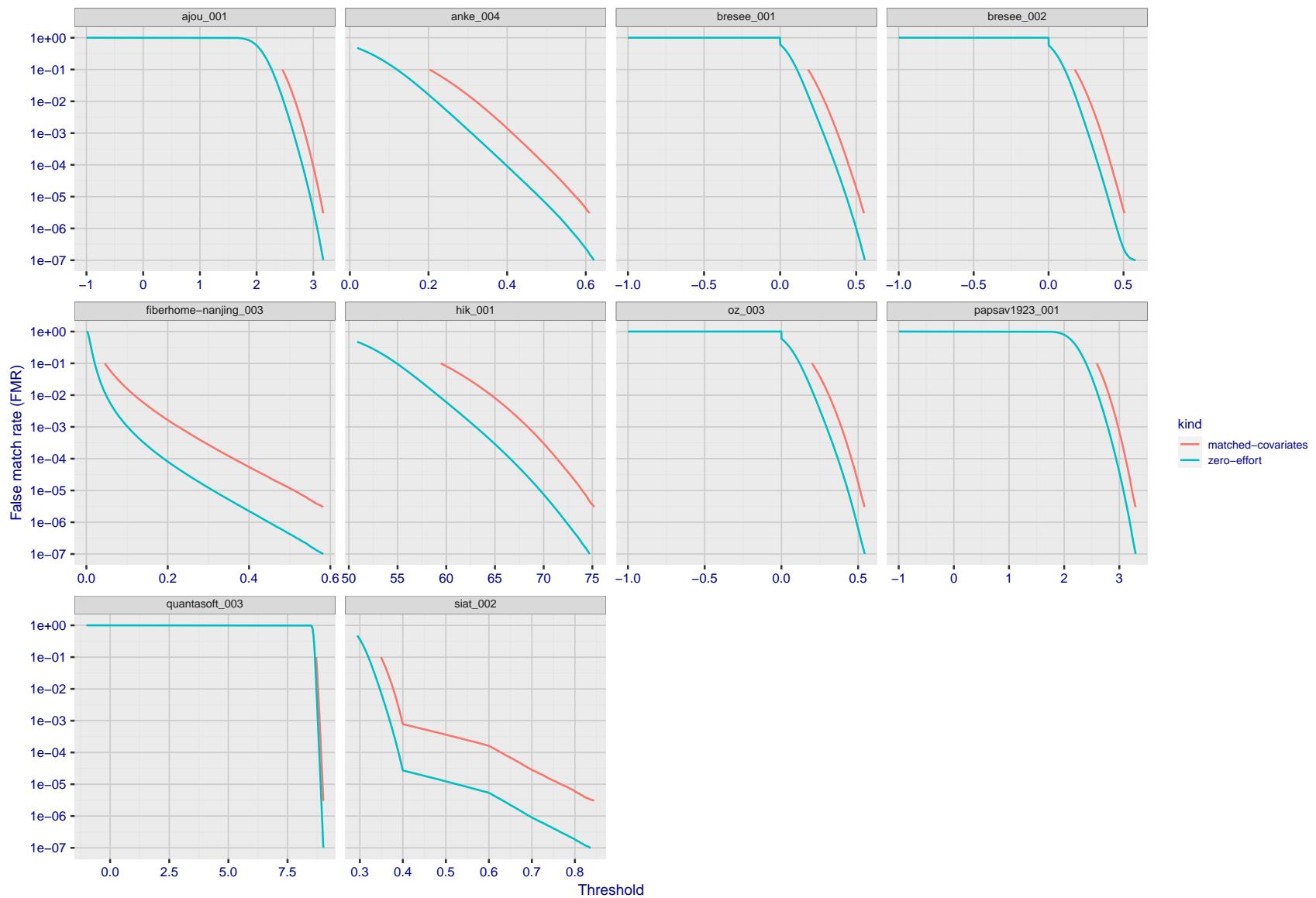


Figure 199: For the visa images, the false match calibration curves show FMR vs. threshold, T . The blue (lower) curves are for zero-effort impostors (i.e. comparing all images against all). The red (upper) curves are for persons of the same-sex, same-age, and same national-origin. This shows that FMR is underestimated (by a factor of 10 or more) by using a zero-effort impostor calculation to calibrate T . As shown later (sec. 3.6), FMR is higher for demographic-matched impostors.

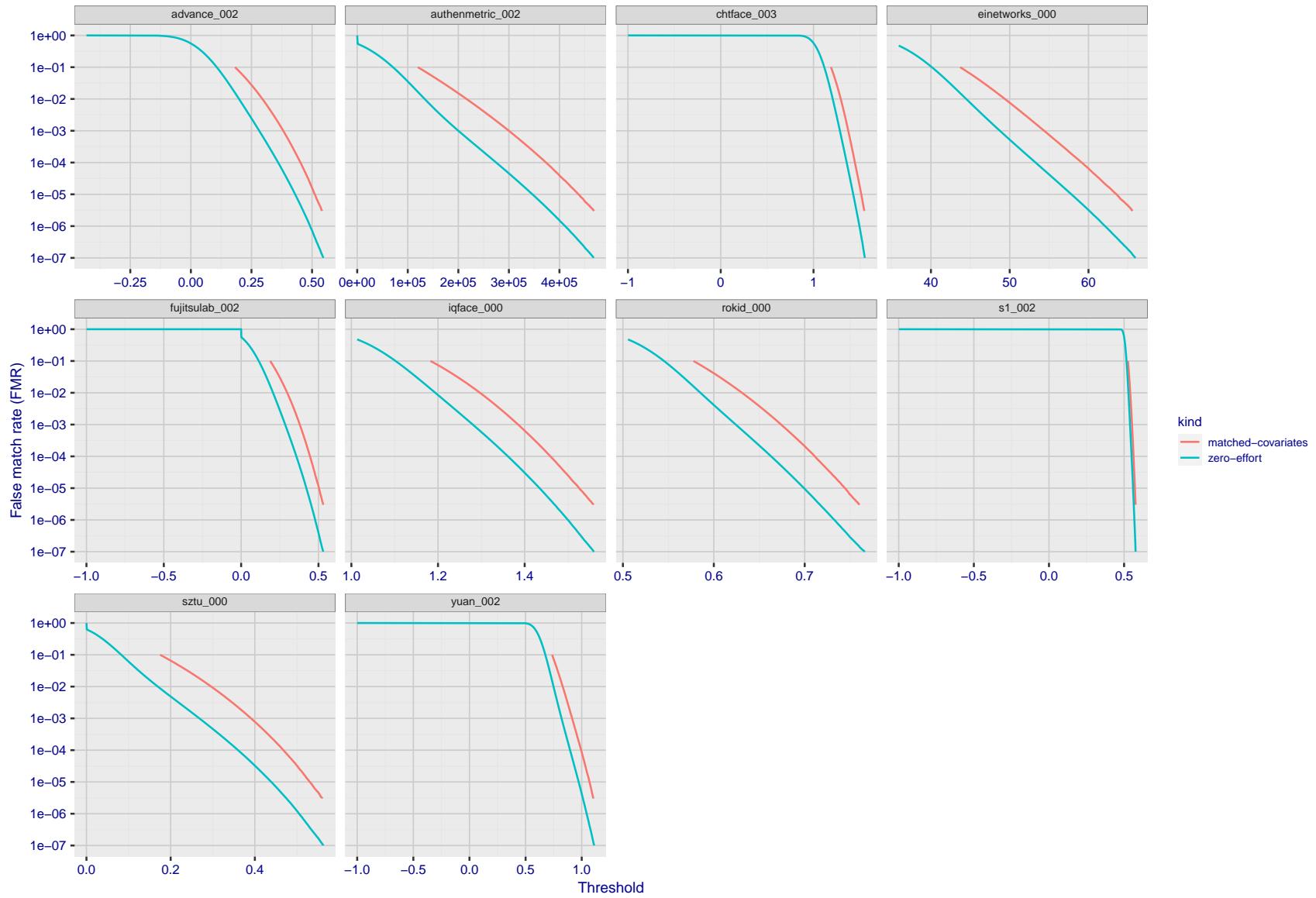


Figure 200: For the visa images, the false match calibration curves show FMR vs. threshold, T . The blue (lower) curves are for zero-effort impostors (i.e. comparing all images against all). The red (upper) curves are for persons of the same-sex, same-age, and same national-origin. This shows that FMR is underestimated (by a factor of 10 or more) by using a zero-effort impostor calculation to calibrate T . As shown later (sec. 3.6), FMR is higher for demographic-matched impostors.

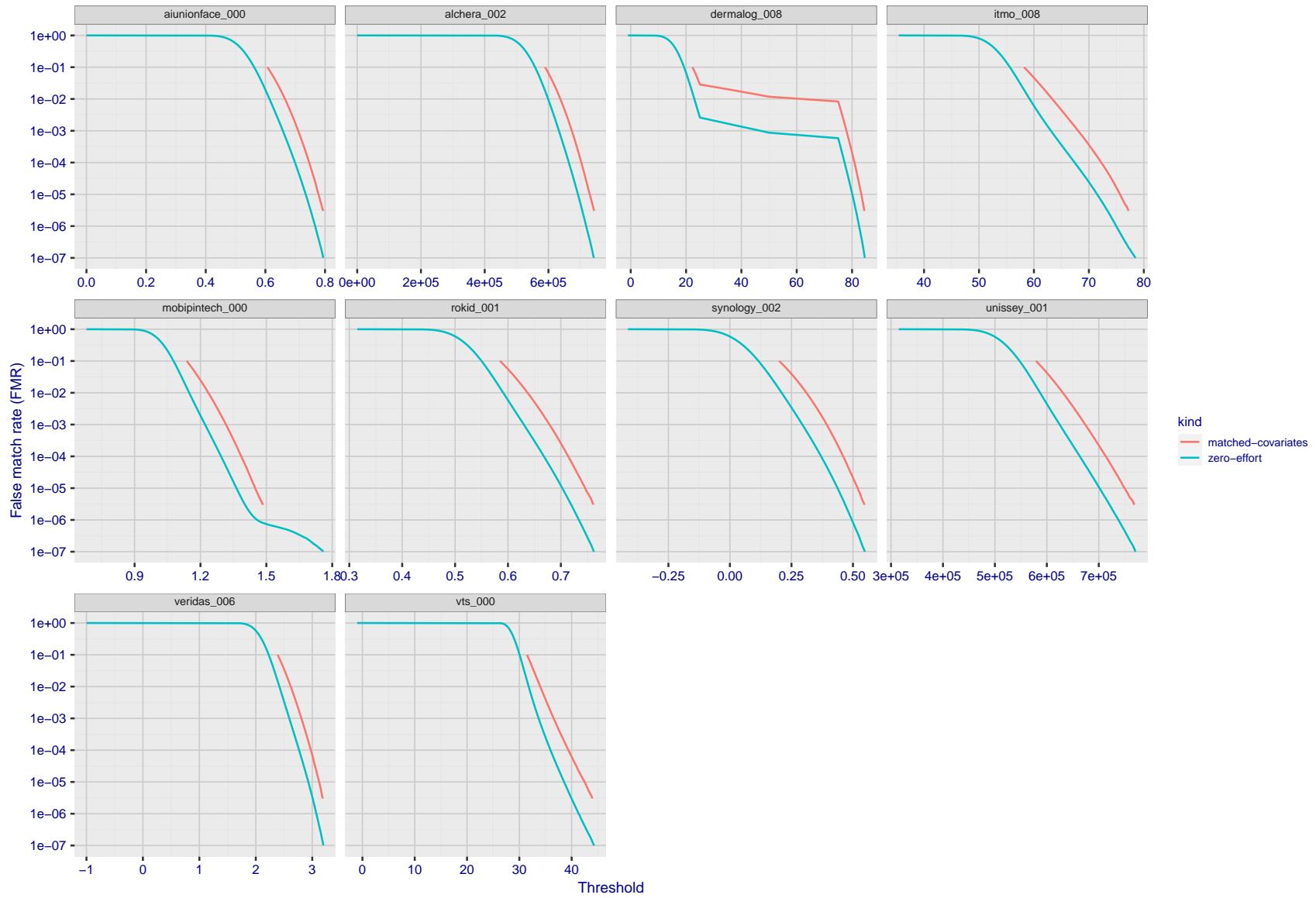


Figure 201: For the visa images, the false match calibration curves show FMR vs. threshold, T . The blue (lower) curves are for zero-effort impostors (i.e. comparing all images against all). The red (upper) curves are for persons of the same-sex, same-age, and same national-origin. This shows that FMR is underestimated (by a factor of 10 or more) by using a zero-effort impostor calculation to calibrate T . As shown later (sec. 3.6), FMR is higher for demographic-matched impostors.

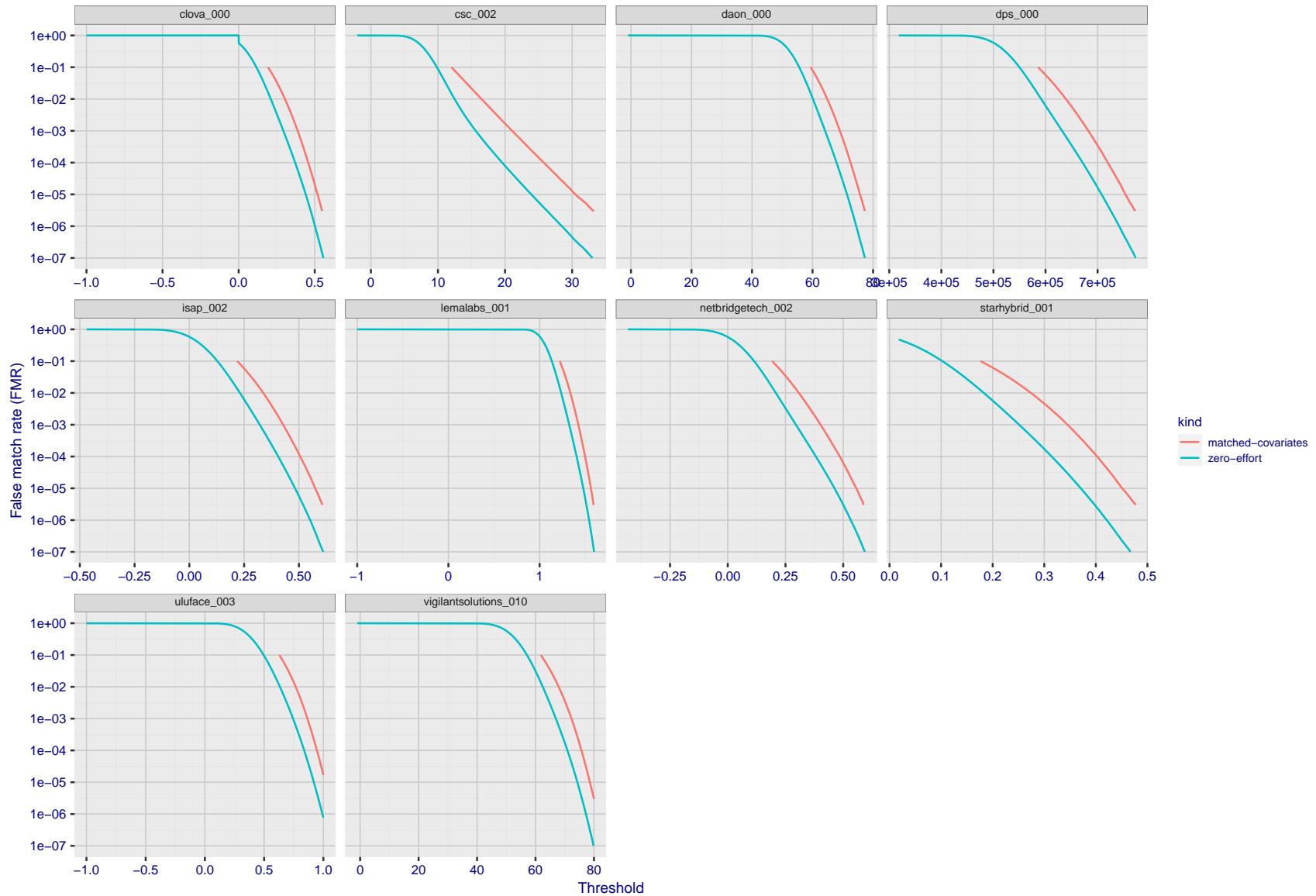


Figure 202: For the visa images, the false match calibration curves show FMR vs. threshold, T . The blue (lower) curves are for zero-effort impostors (i.e. comparing all images against all). The red (upper) curves are for persons of the same-sex, same-age, and same national-origin. This shows that FMR is underestimated (by a factor of 10 or more) by using a zero-effort impostor calculation to calibrate T . As shown later (sec. 3.6), FMR is higher for demographic-matched impostors.

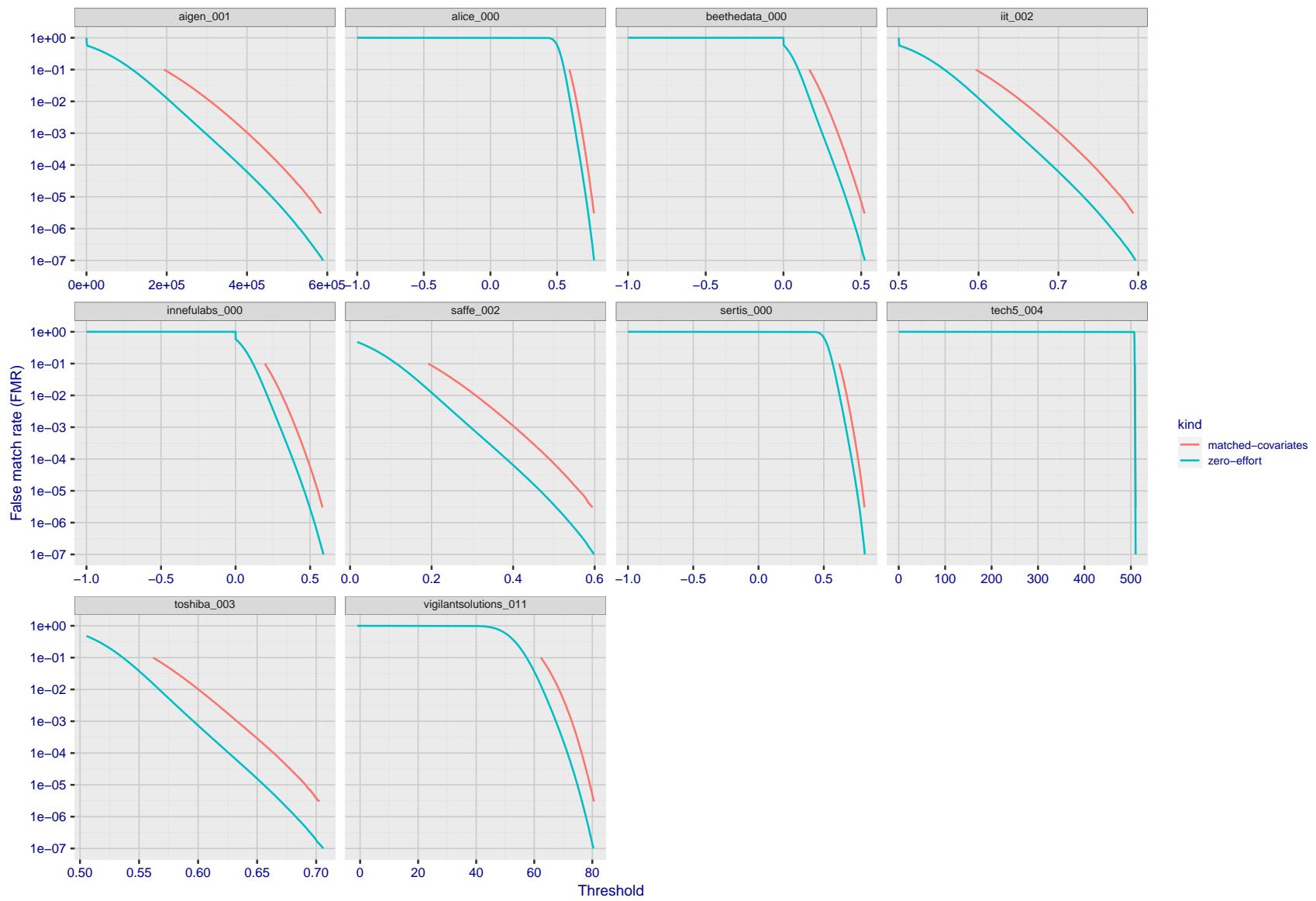


Figure 203: For the visa images, the false match calibration curves show FMR vs. threshold, T . The blue (lower) curves are for zero-effort impostors (i.e. comparing all images against all). The red (upper) curves are for persons of the same-sex, same-age, and same national-origin. This shows that FMR is underestimated (by a factor of 10 or more) by using a zero-effort impostor calculation to calibrate T . As shown later (sec. 3.6), FMR is higher for demographic-matched impostors.

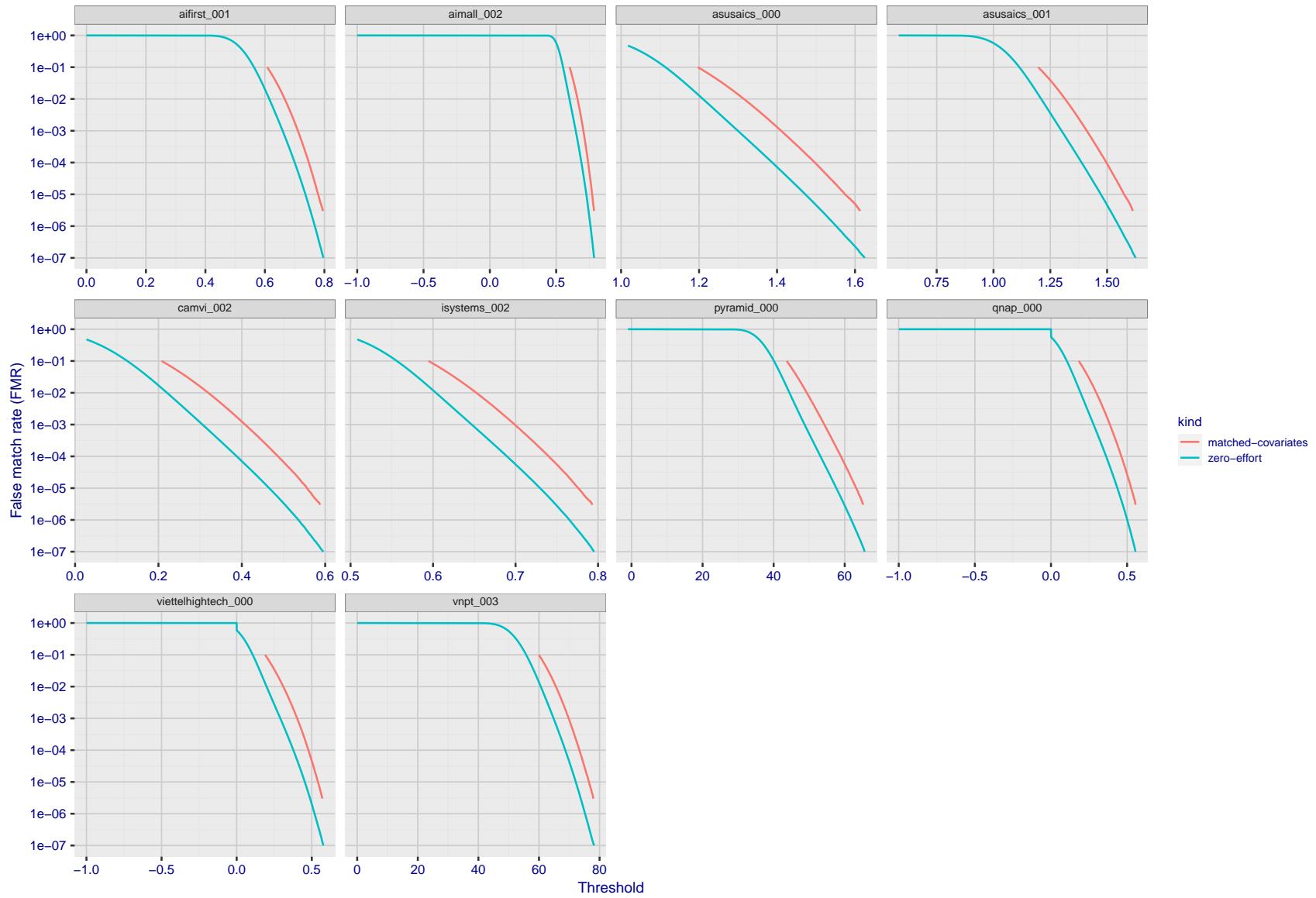


Figure 204: For the visa images, the false match calibration curves show FMR vs. threshold, T . The blue (lower) curves are for zero-effort impostors (i.e. comparing all images against all). The red (upper) curves are for persons of the same-sex, same-age, and same national-origin. This shows that FMR is underestimated (by a factor of 10 or more) by using a zero-effort impostor calculation to calibrate T . As shown later (sec. 3.6), FMR is higher for demographic-matched impostors.

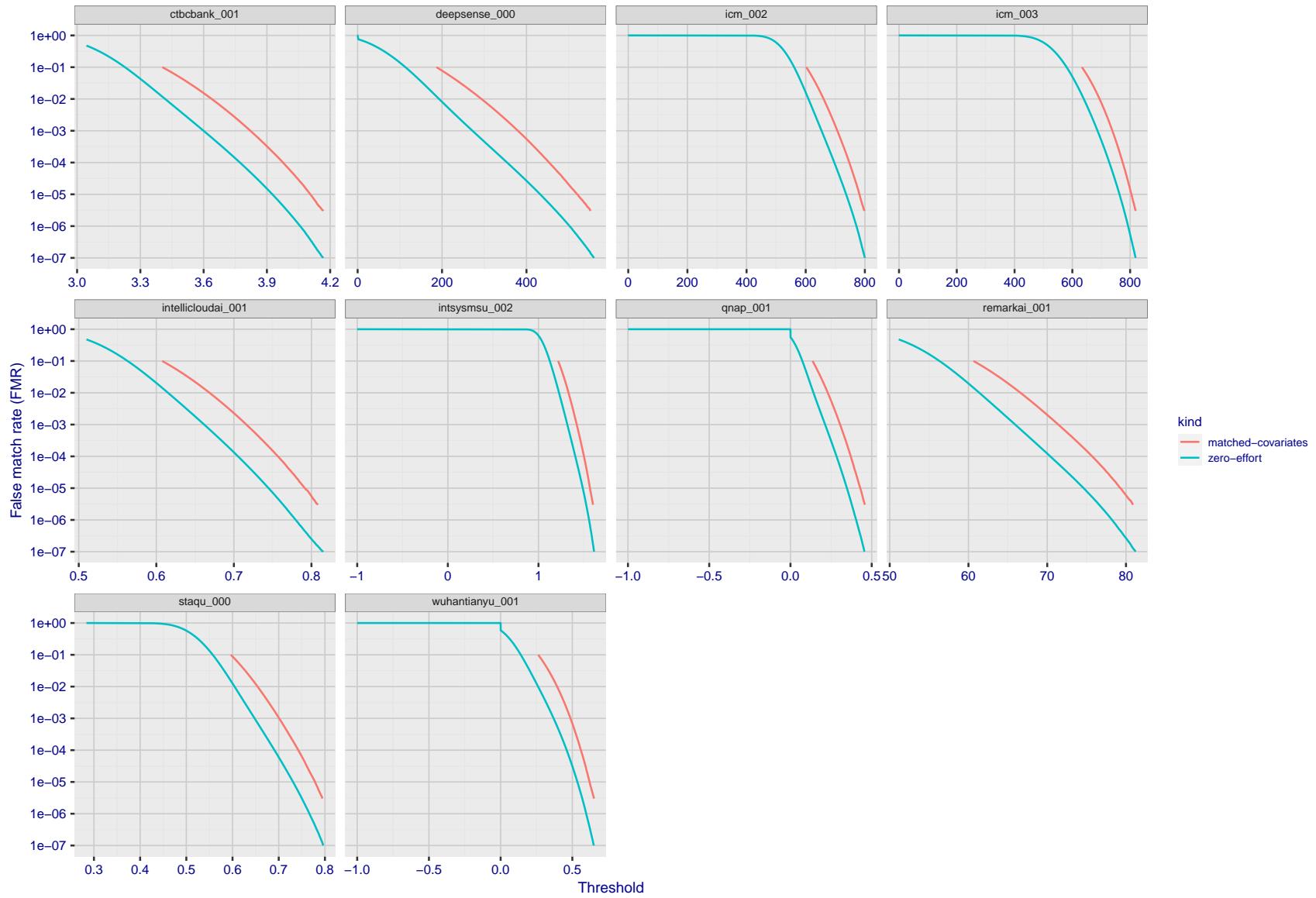


Figure 205: For the visa images, the false match calibration curves show FMR vs. threshold, T . The blue (lower) curves are for zero-effort impostors (i.e. comparing all images against all). The red (upper) curves are for persons of the same-sex, same-age, and same national-origin. This shows that FMR is underestimated (by a factor of 10 or more) by using a zero-effort impostor calculation to calibrate T . As shown later (sec. 3.6), FMR is higher for demographic-matched impostors.

2021/12/16 10:32:53

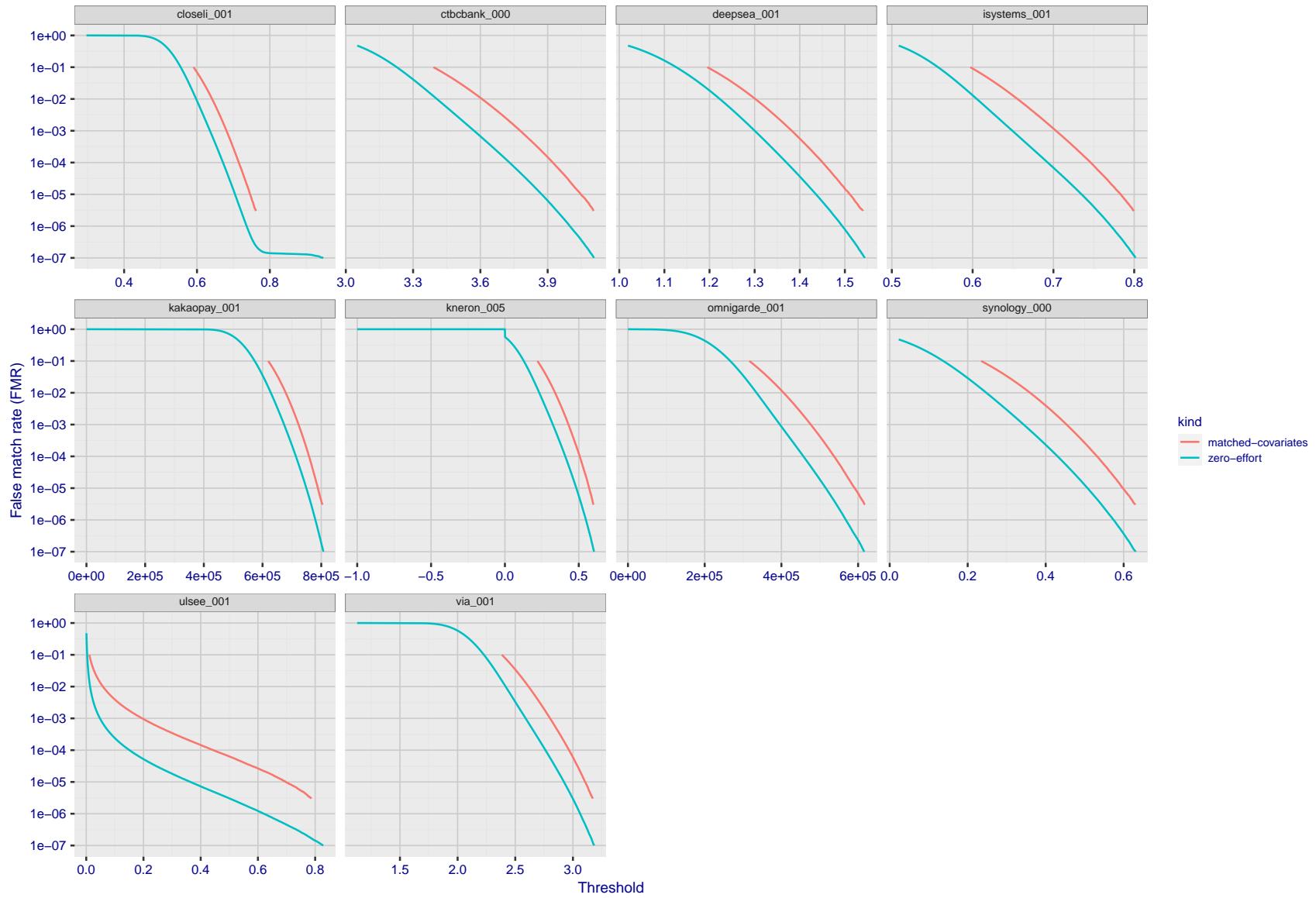


Figure 206: For the visa images, the false match calibration curves show FMR vs. threshold, T . The blue (lower) curves are for zero-effort impostors (i.e. comparing all images against all). The red (upper) curves are for persons of the same-sex, same-age, and same national-origin. This shows that FMR is underestimated (by a factor of 10 or more) by using a zero-effort impostor calculation to calibrate T . As shown later (sec. 3.6), FMR is higher for demographic-matched impostors.

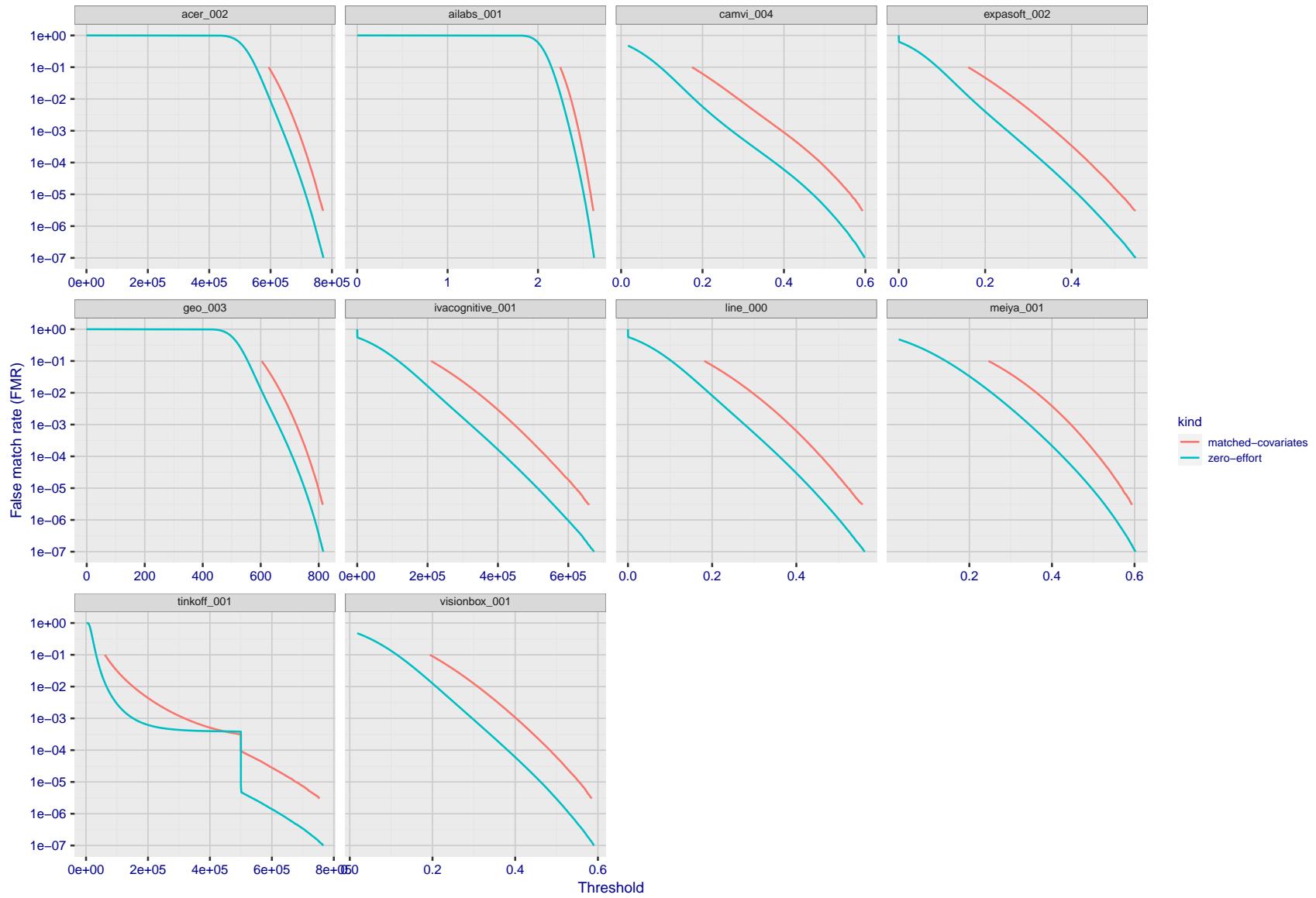


Figure 207: For the visa images, the false match calibration curves show FMR vs. threshold, T . The blue (lower) curves are for zero-effort impostors (i.e. comparing all images against all). The red (upper) curves are for persons of the same-sex, same-age, and same national-origin. This shows that FMR is underestimated (by a factor of 10 or more) by using a zero-effort impostor calculation to calibrate T . As shown later (sec. 3.6), FMR is higher for demographic-matched impostors.

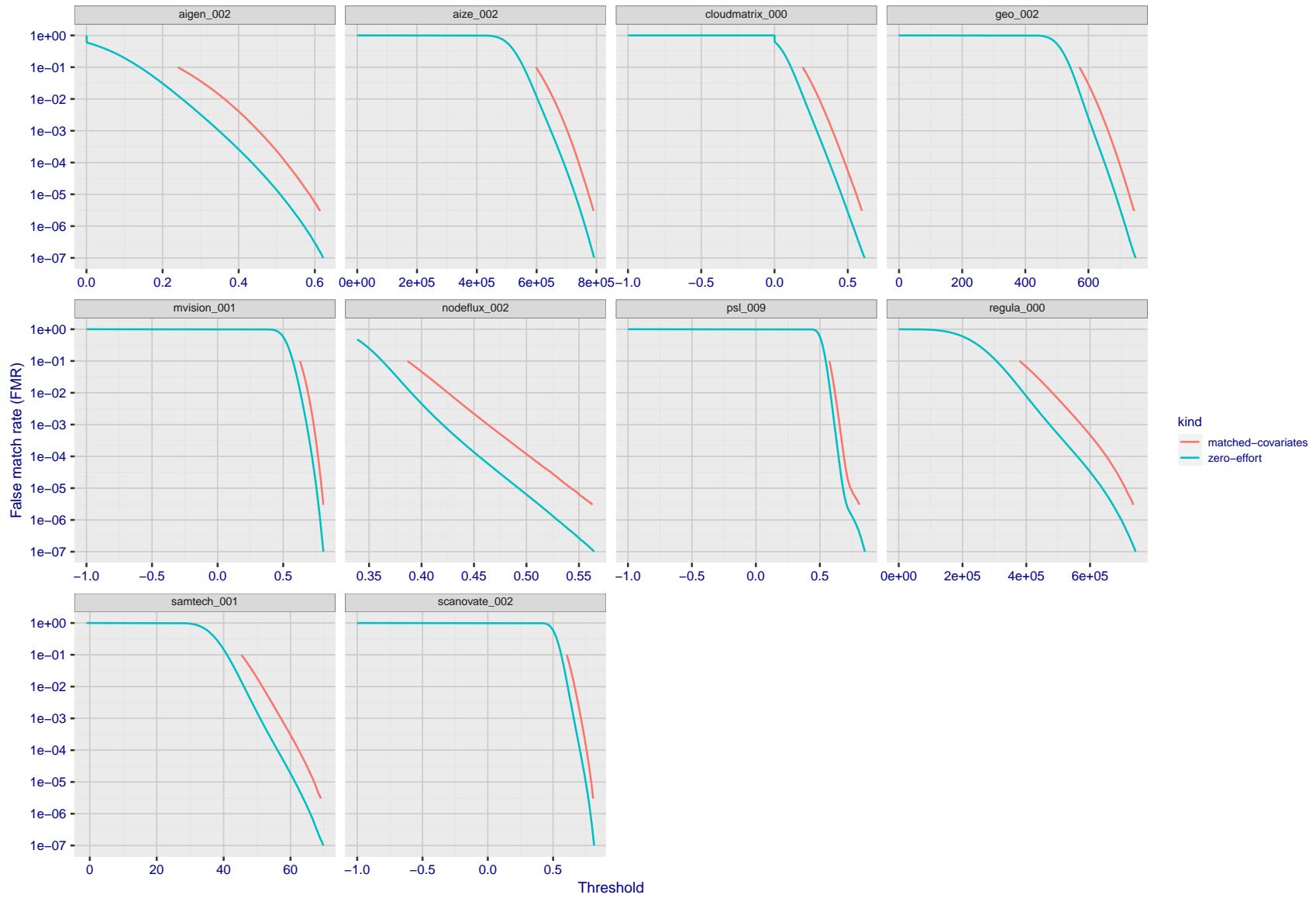


Figure 208: For the visa images, the false match calibration curves show FMR vs. threshold, T . The blue (lower) curves are for zero-effort impostors (i.e. comparing all images against all). The red (upper) curves are for persons of the same-sex, same-age, and same national-origin. This shows that FMR is underestimated (by a factor of 10 or more) by using a zero-effort impostor calculation to calibrate T . As shown later (sec. 3.6), FMR is higher for demographic-matched impostors.

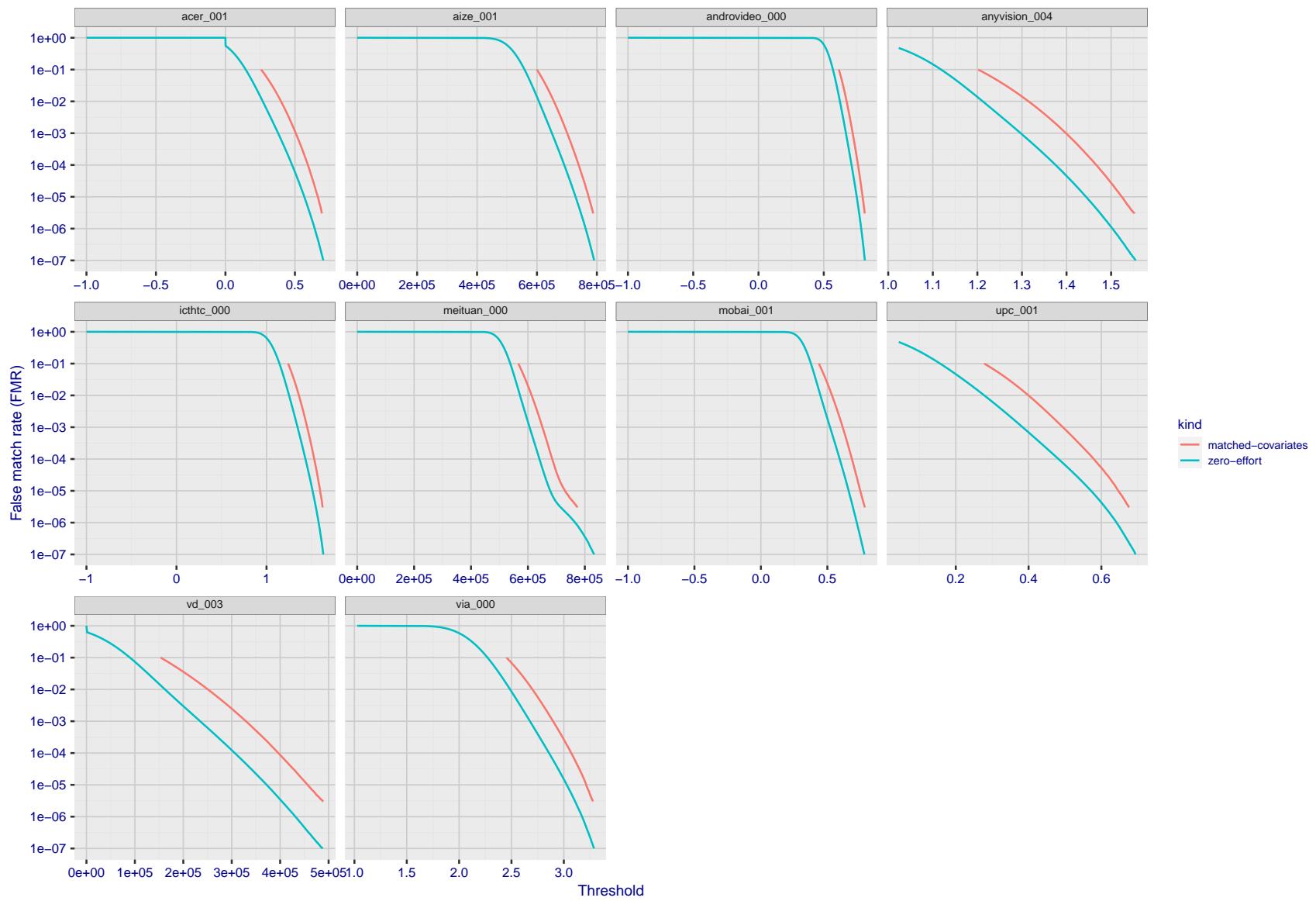


Figure 209: For the visa images, the false match calibration curves show FMR vs. threshold, T . The blue (lower) curves are for zero-effort impostors (i.e. comparing all images against all). The red (upper) curves are for persons of the same-sex, same-age, and same national-origin. This shows that FMR is underestimated (by a factor of 10 or more) by using a zero-effort impostor calculation to calibrate T . As shown later (sec. 3.6), FMR is higher for demographic-matched impostors.

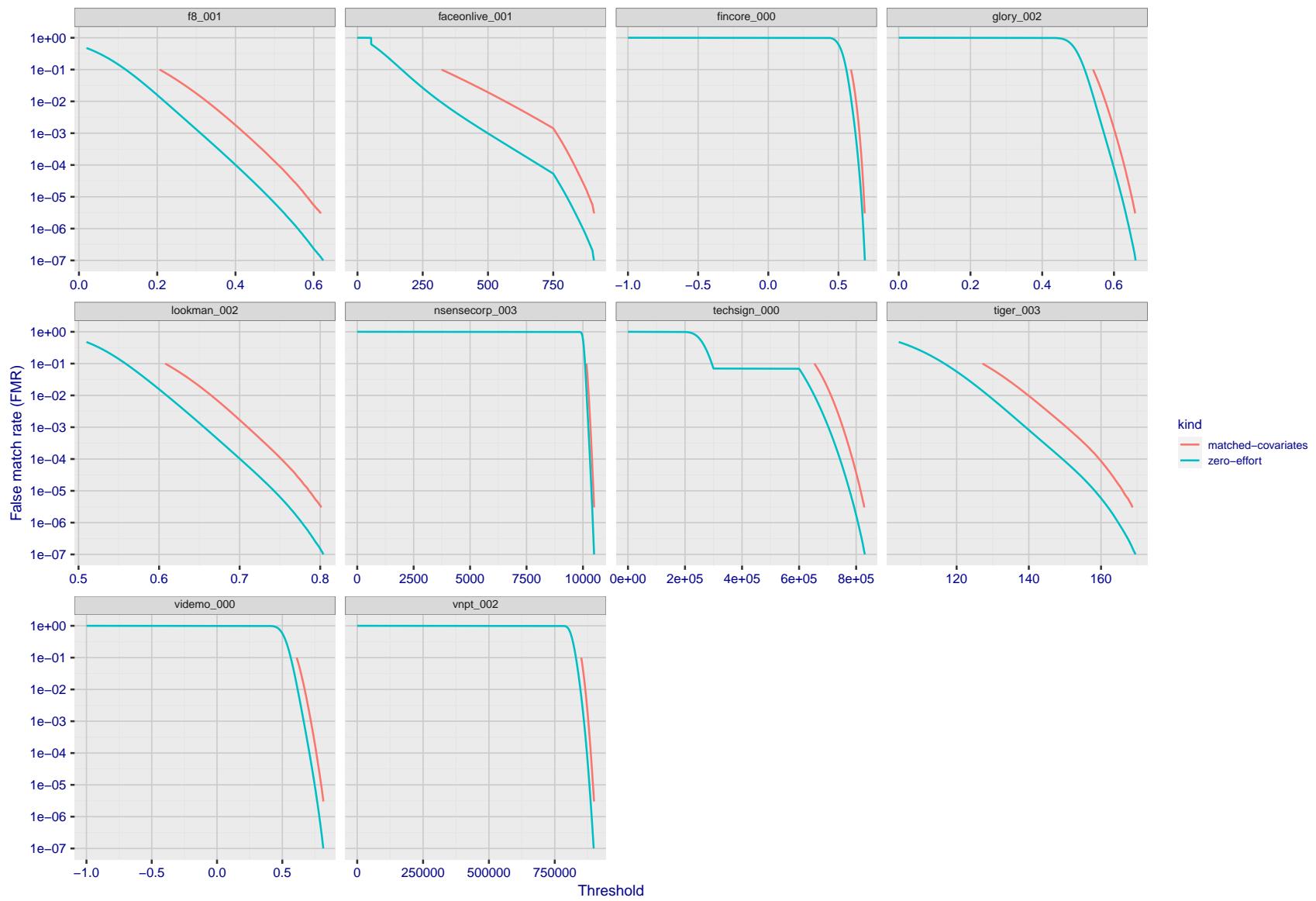


Figure 210: For the visa images, the false match calibration curves show FMR vs. threshold, T . The blue (lower) curves are for zero-effort impostors (i.e. comparing all images against all). The red (upper) curves are for persons of the same-sex, same-age, and same national-origin. This shows that FMR is underestimated (by a factor of 10 or more) by using a zero-effort impostor calculation to calibrate T . As shown later (sec. 3.6), FMR is higher for demographic-matched impostors.

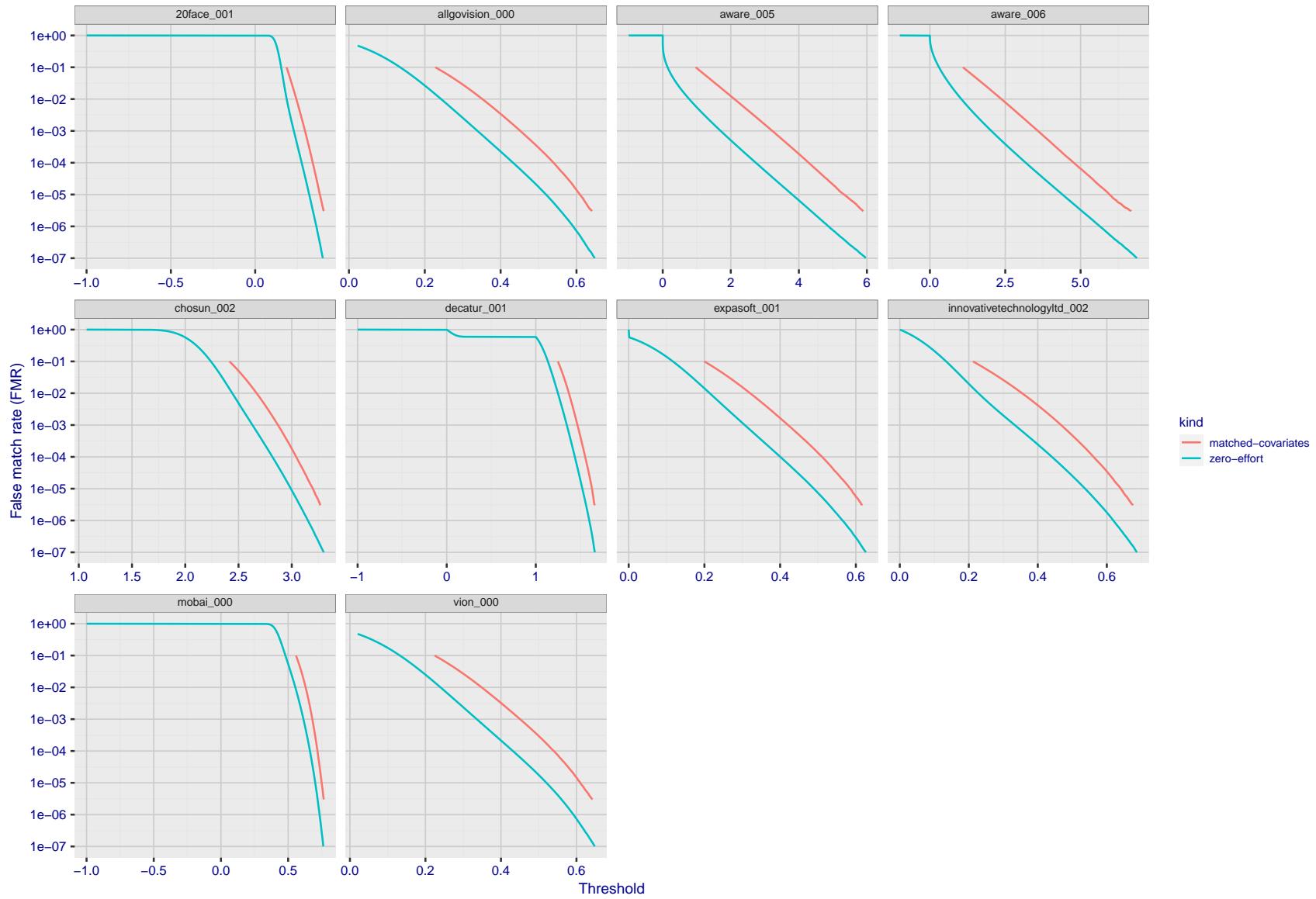


Figure 211: For the visa images, the false match calibration curves show FMR vs. threshold, T . The blue (lower) curves are for zero-effort impostors (i.e. comparing all images against all). The red (upper) curves are for persons of the same-sex, same-age, and same national-origin. This shows that FMR is underestimated (by a factor of 10 or more) by using a zero-effort impostor calculation to calibrate T . As shown later (sec. 3.6), FMR is higher for demographic-matched impostors.

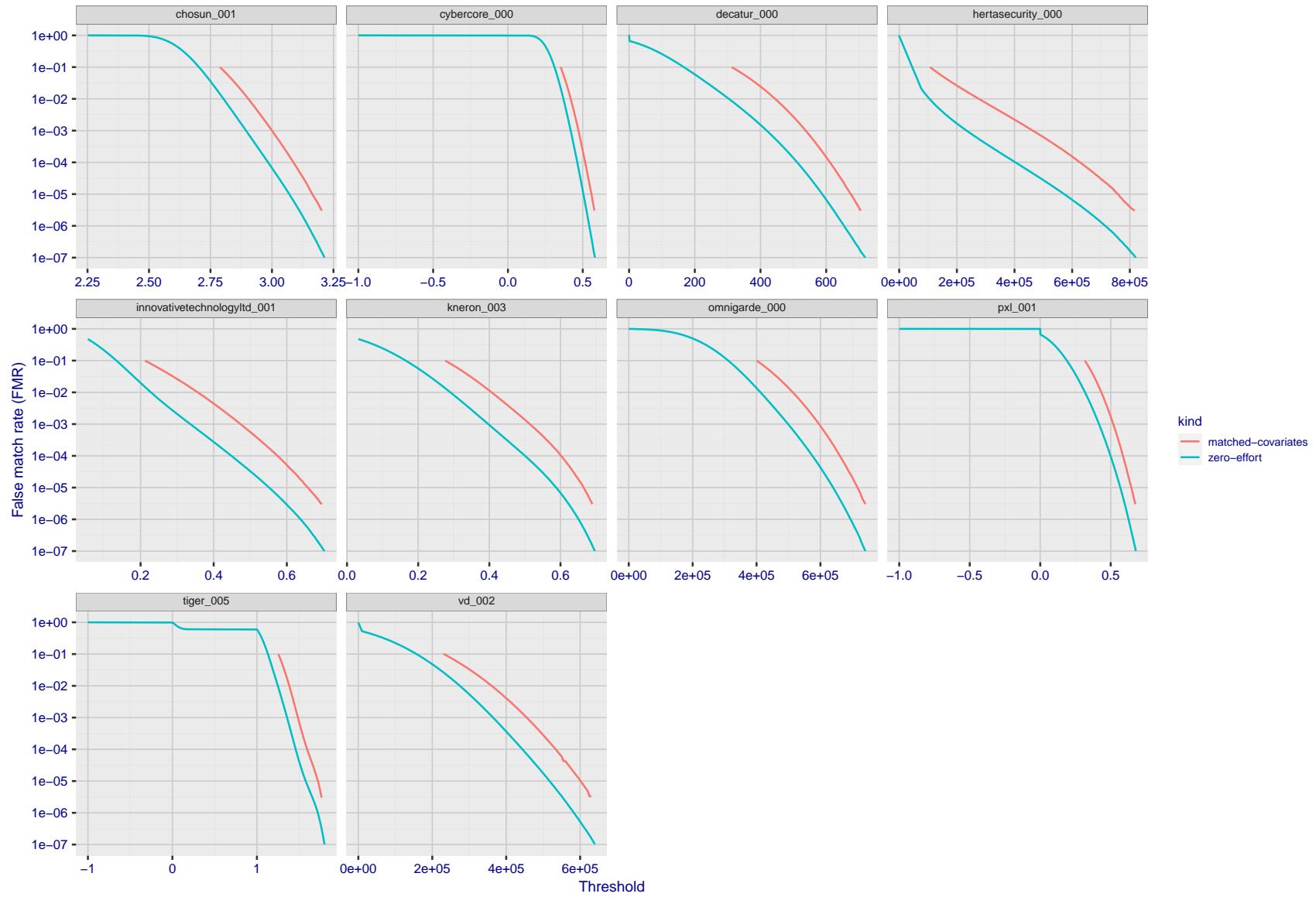


Figure 212: For the visa images, the false match calibration curves show FMR vs. threshold, T . The blue (lower) curves are for zero-effort impostors (i.e. comparing all images against all). The red (upper) curves are for persons of the same-sex, same-age, and same national-origin. This shows that FMR is underestimated (by a factor of 10 or more) by using a zero-effort impostor calculation to calibrate T . As shown later (sec. 3.6), FMR is higher for demographic-matched impostors.

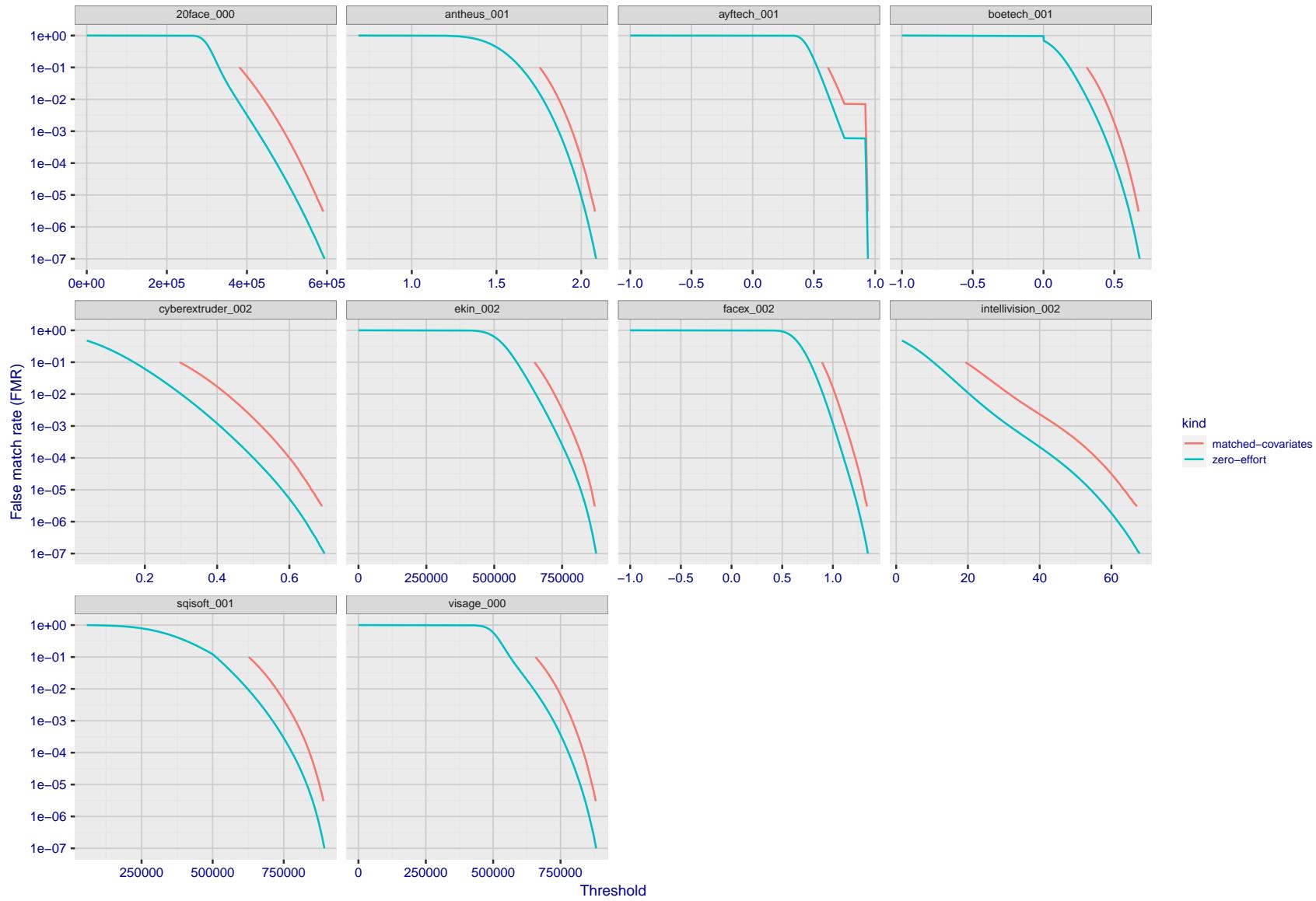


Figure 213: For the visa images, the false match calibration curves show FMR vs. threshold, T . The blue (lower) curves are for zero-effort impostors (i.e. comparing all images against all). The red (upper) curves are for persons of the same-sex, same-age, and same national-origin. This shows that FMR is underestimated (by a factor of 10 or more) by using a zero-effort impostor calculation to calibrate T . As shown later (sec. 3.6), FMR is higher for demographic-matched impostors.

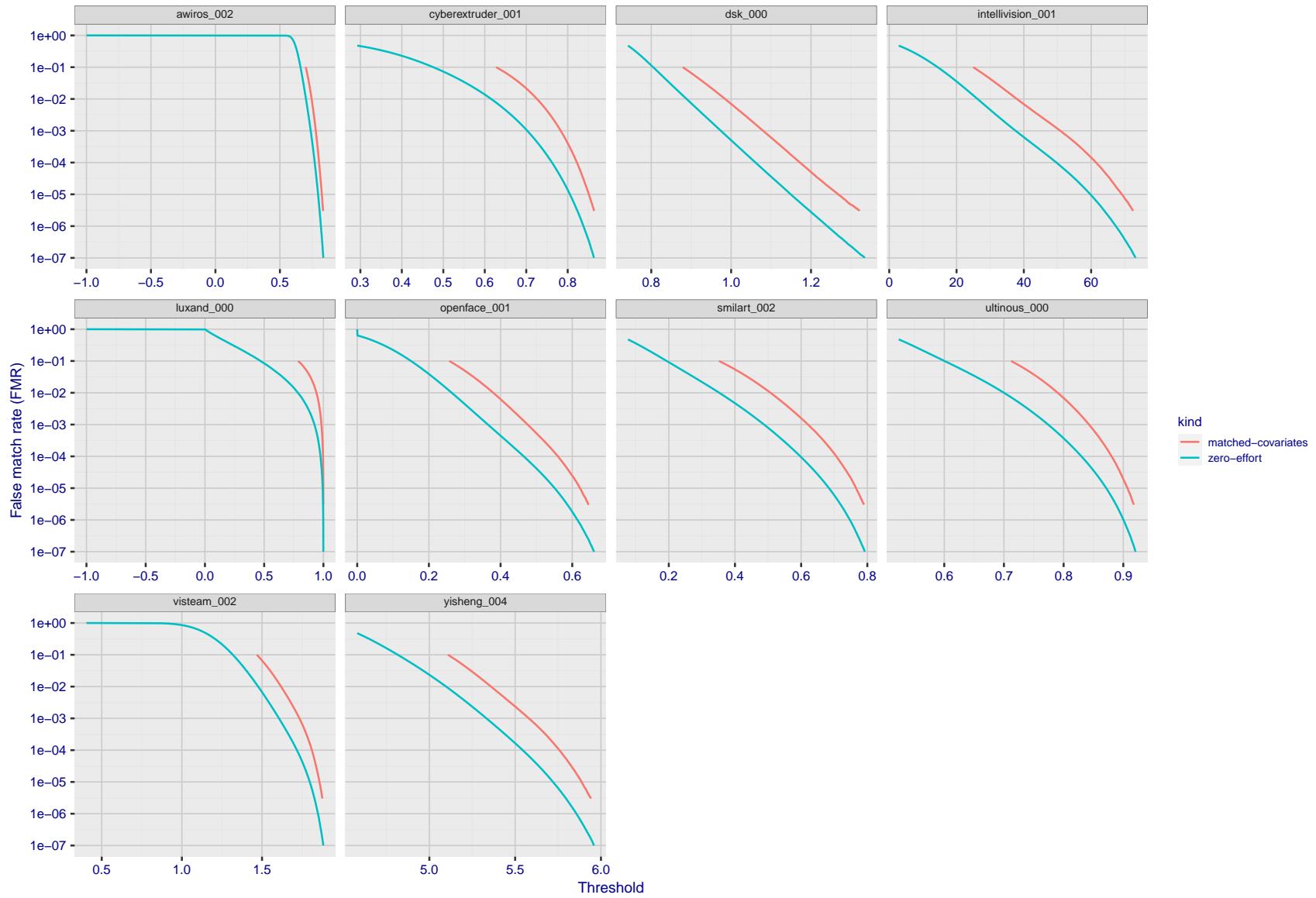


Figure 214: For the visa images, the false match calibration curves show FMR vs. threshold, T . The blue (lower) curves are for zero-effort impostors (i.e. comparing all images against all). The red (upper) curves are for persons of the same-sex, same-age, and same national-origin. This shows that FMR is underestimated (by a factor of 10 or more) by using a zero-effort impostor calculation to calibrate T . As shown later (sec. 3.6), FMR is higher for demographic-matched impostors.

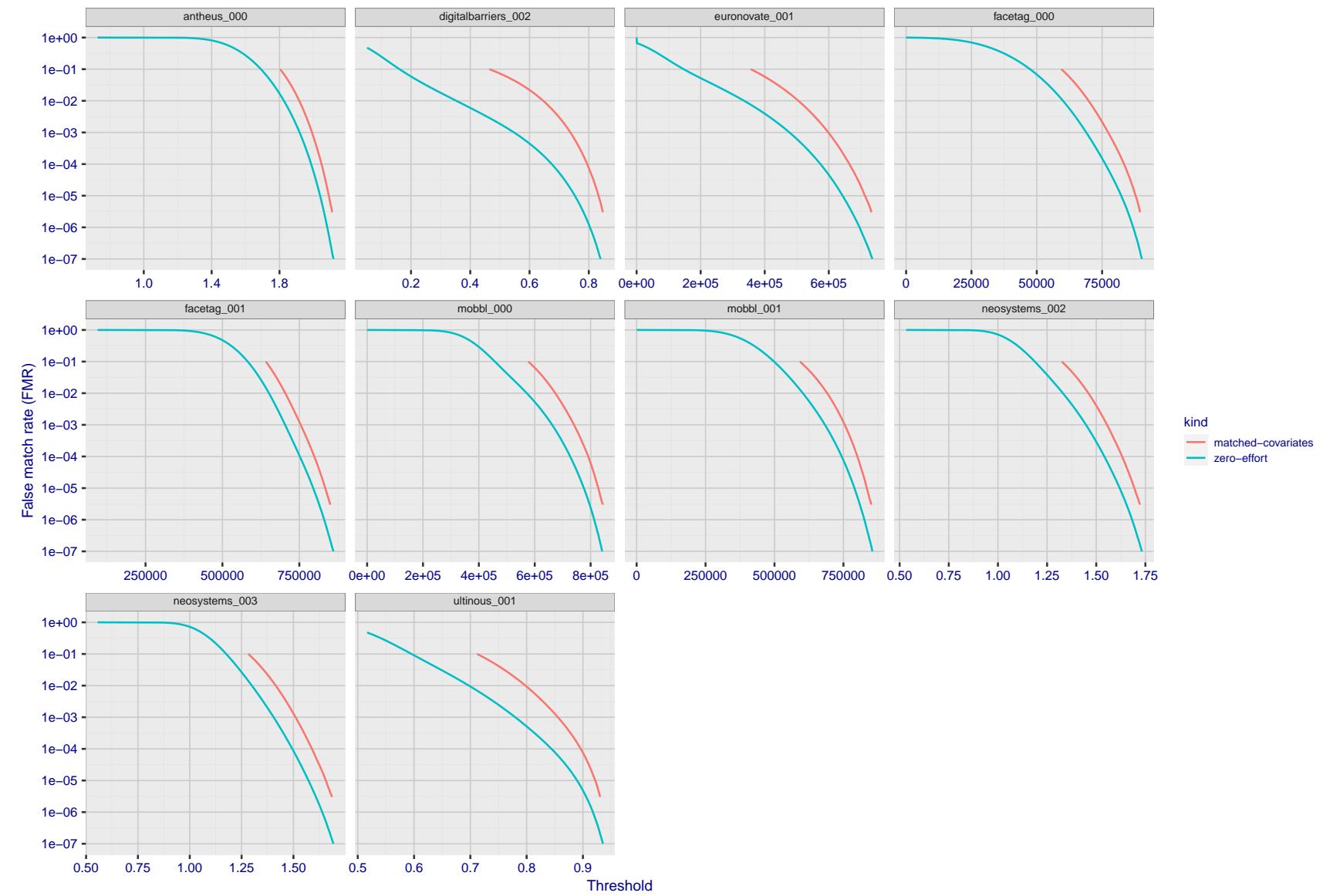


Figure 215: For the visa images, the false match calibration curves show FMR vs. threshold, T . The blue (lower) curves are for zero-effort impostors (i.e. comparing all images against all). The red (upper) curves are for persons of the same-sex, same-age, and same national-origin. This shows that FMR is underestimated (by a factor of 10 or more) by using a zero-effort impostor calculation to calibrate T . As shown later (sec. 3.6), FMR is higher for demographic-matched impostors.

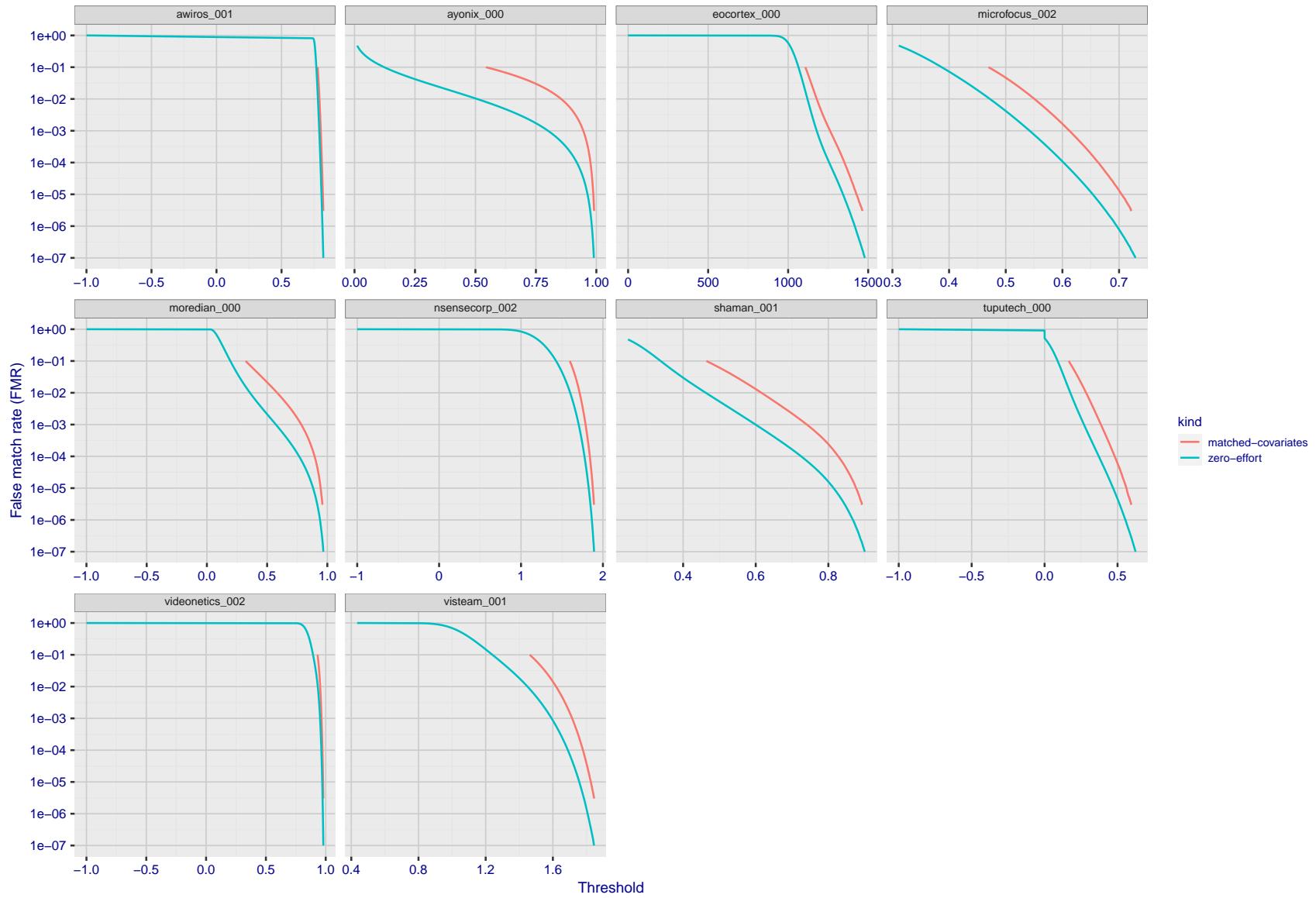


Figure 216: For the visa images, the false match calibration curves show FMR vs. threshold, T . The blue (lower) curves are for zero-effort impostors (i.e. comparing all images against all). The red (upper) curves are for persons of the same-sex, same-age, and same national-origin. This shows that FMR is underestimated (by a factor of 10 or more) by using a zero-effort impostor calculation to calibrate T . As shown later (sec. 3.6), FMR is higher for demographic-matched impostors.

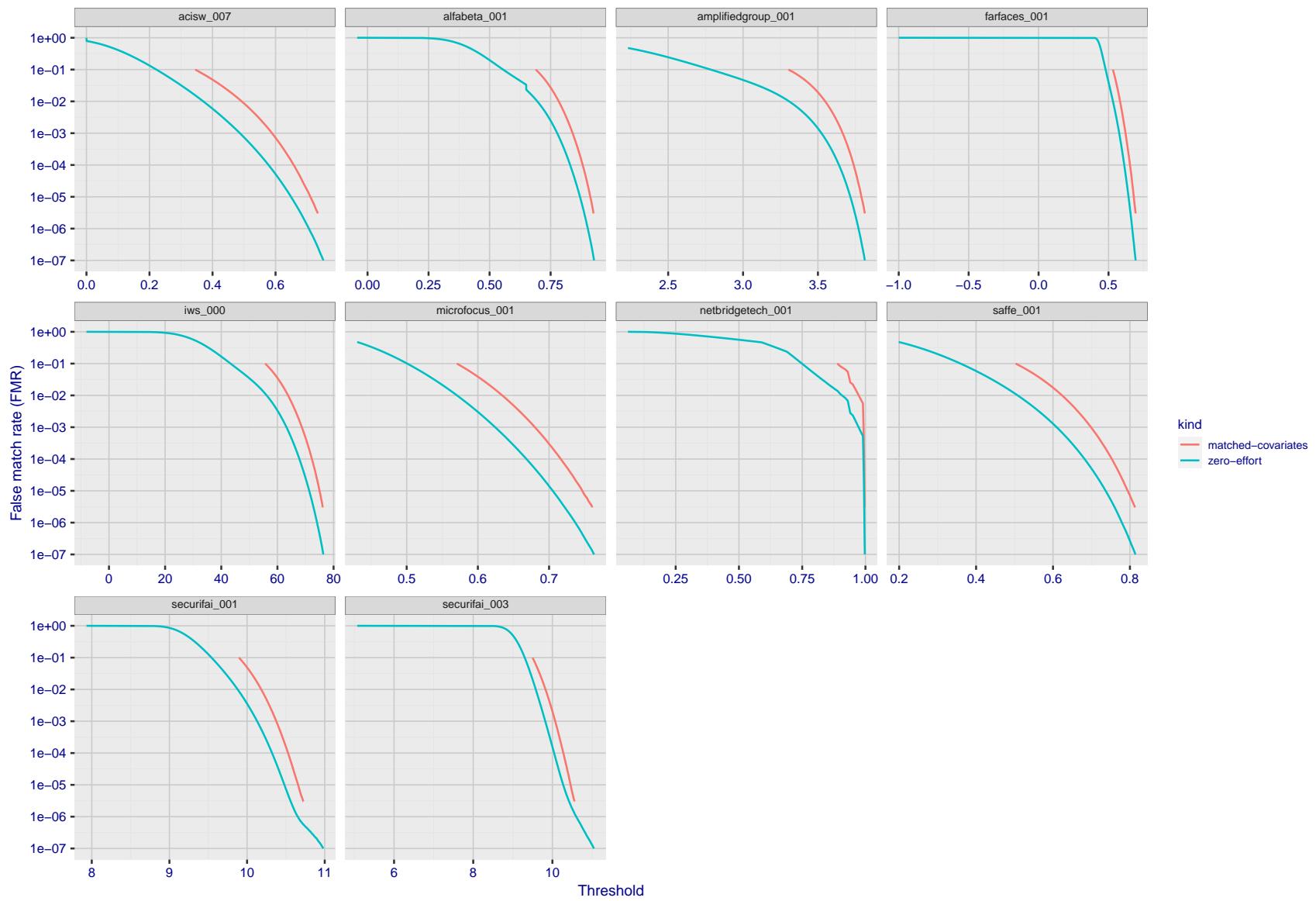


Figure 217: For the visa images, the false match calibration curves show FMR vs. threshold, T . The blue (lower) curves are for zero-effort impostors (i.e. comparing all images against all). The red (upper) curves are for persons of the same-sex, same-age, and same national-origin. This shows that FMR is underestimated (by a factor of 10 or more) by using a zero-effort impostor calculation to calibrate T . As shown later (sec. 3.6), FMR is higher for demographic-matched impostors.

2021/12/16 10:32:53

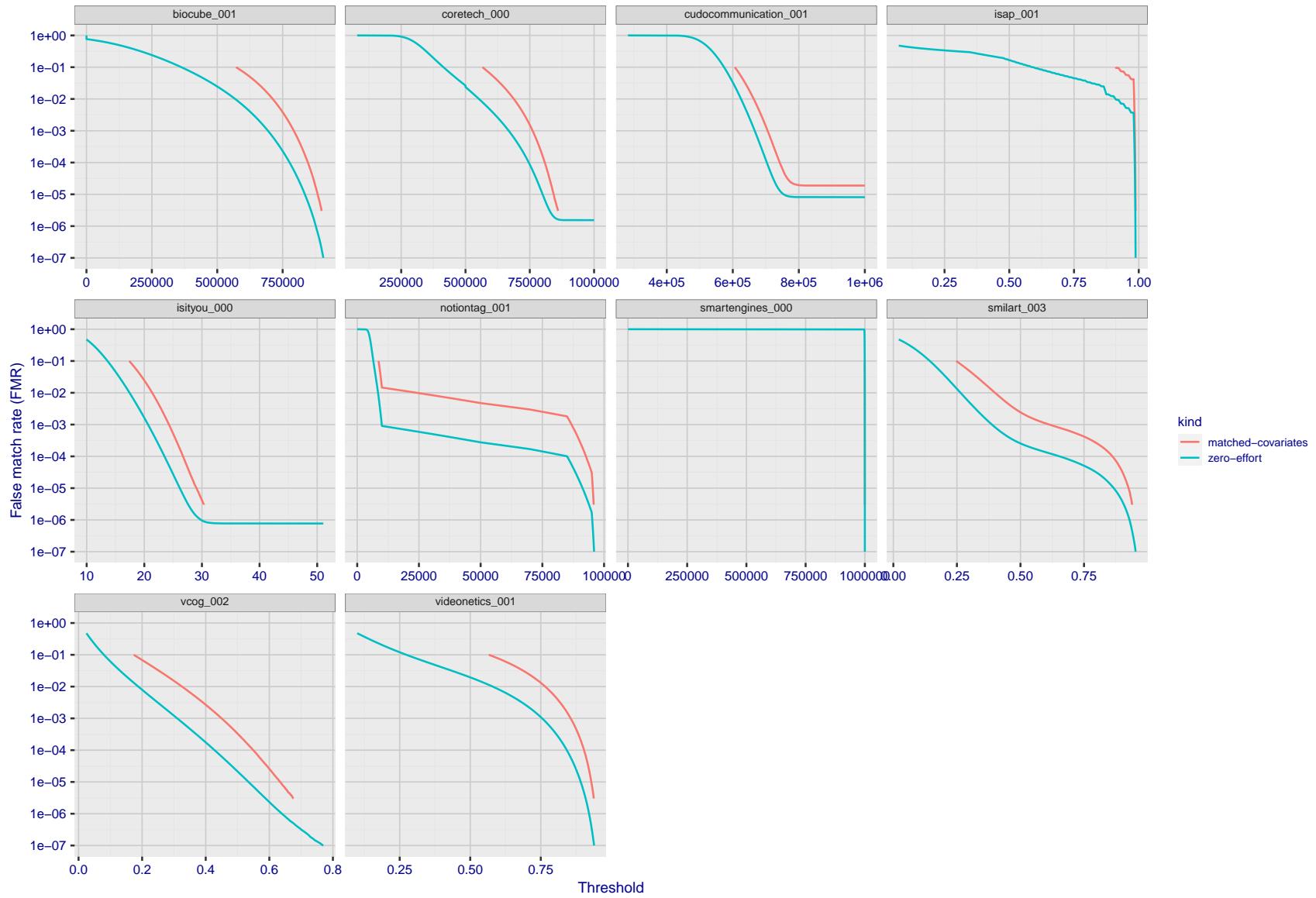


Figure 218: For the visa images, the false match calibration curves show FMR vs. threshold, T . The blue (lower) curves are for zero-effort impostors (i.e. comparing all images against all). The red (upper) curves are for persons of the same-sex, same-age, and same national-origin. This shows that FMR is underestimated (by a factor of 10 or more) by using a zero-effort impostor calculation to calibrate T . As shown later (sec. 3.6), FMR is higher for demographic-matched impostors.

FNMR(T)
FMR(T)
"False non-match rate"
"False match rate"

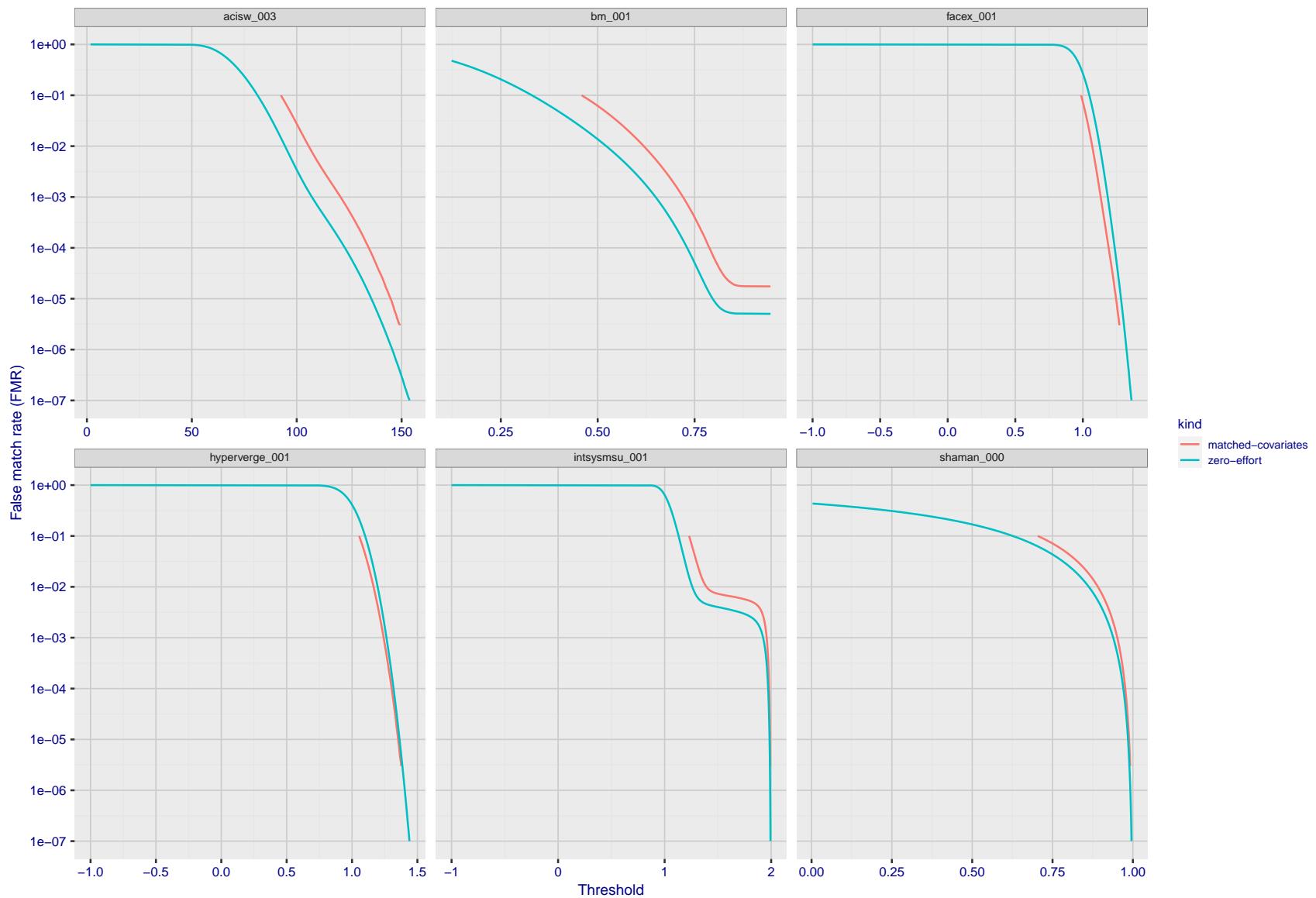


Figure 219: For the visa images, the false match calibration curves show FMR vs. threshold, T . The blue (lower) curves are for zero-effort impostors (i.e. comparing all images against all). The red (upper) curves are for persons of the same-sex, same-age, and same national-origin. This shows that FMR is underestimated (by a factor of 10 or more) by using a zero-effort impostor calculation to calibrate T . As shown later (sec. 3.6), FMR is higher for demographic-matched impostors.

3.5 Genuine distribution stability

3.5.1 Effect of birth place on the genuine distribution

Background: Both skin tone and bone structure vary geographically. Prior studies have reported variations in FNMR and FMR.

Goal: To measure false non-match rate (FNMR) variation with country of birth.

Methods: Thresholds are determined that give $FMR = \{0.001, 0.0001\}$ over the entire impostor set. Then FNMR is measured over 1000 bootstrap replications of the genuine scores. Only those countries with at least 140 individuals are included in the analysis.

Results: Figure 250 shows FNMR by country of birth for the two thresholds.

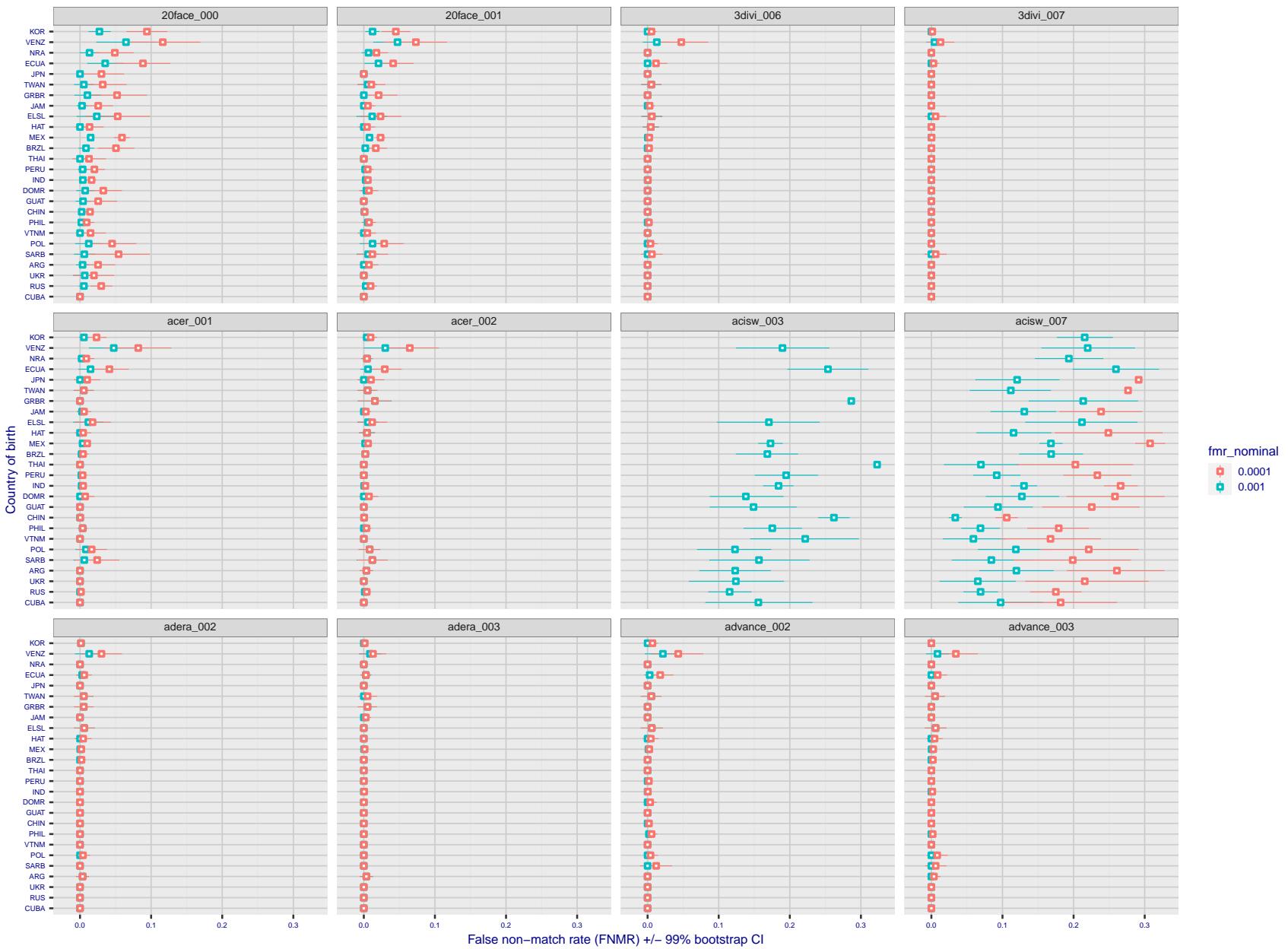


Figure 220: For the visa images, the dots show FNMR by country of birth for two globally set operating thresholds corresponding to $FMR = \{0.001, 0.0001\}$ computed over all on the order of 10^{10} impostor scores. The FMR in each bin will vary also - see subsequent impostor heatmaps in sec. 3.6.1. The figures shows an order of magnitude variation in FNMR across country of birth; these effects are likely due quality variations, then demographics like age and race. The error rates in some cases are zero, and in others the DET is flat so the error rates at the two thresholds are identical. The lines span 1% and 99% of bootstrap replicated FNMR estimates.

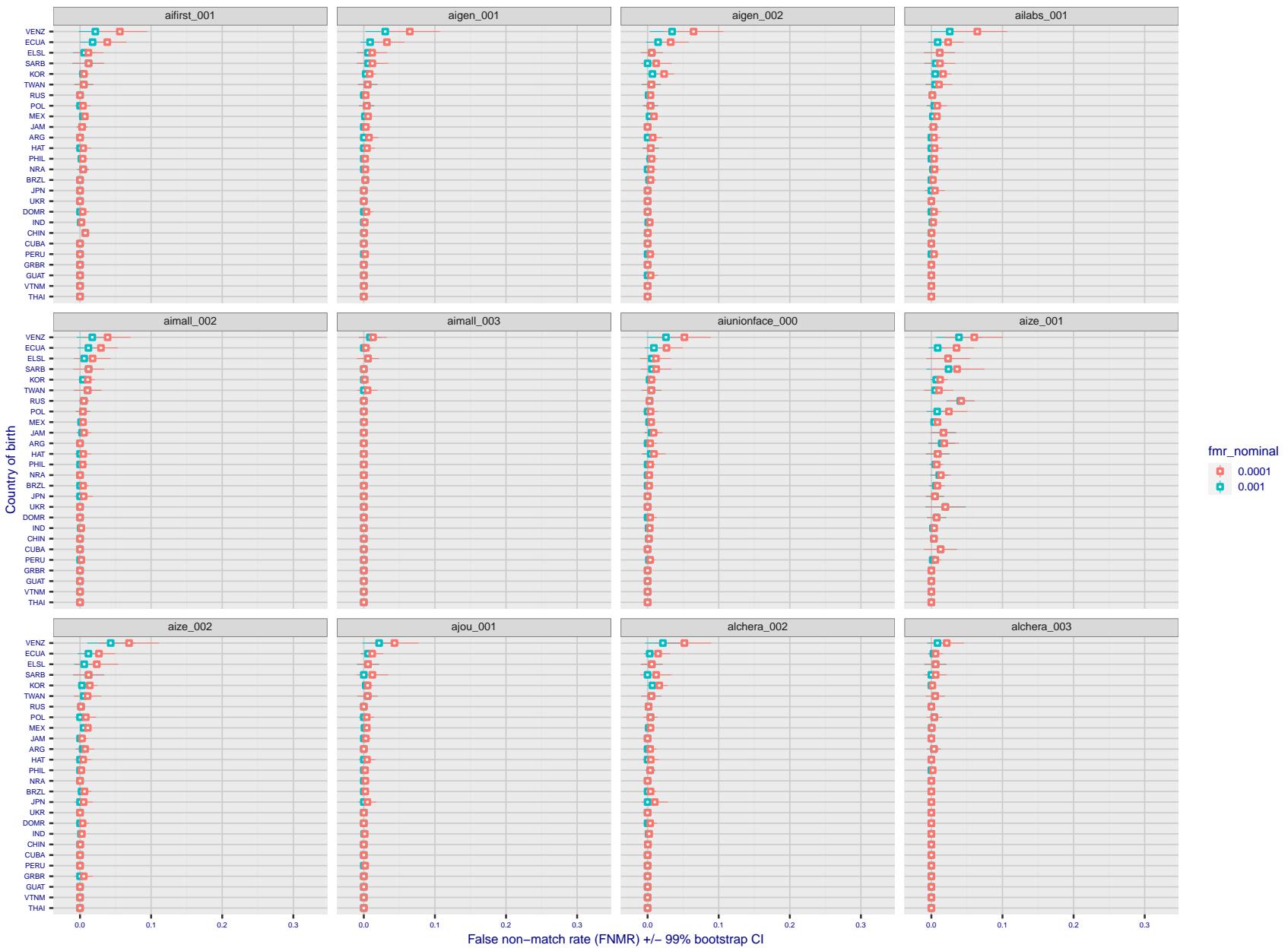


Figure 221: For the visa images, the dots show FNMR by country of birth for two globally set operating thresholds corresponding to $FMR = \{0.001, 0.0001\}$ computed over all on the order of 10^{10} impostor scores. The FMR in each bin will vary also - see subsequent impostor heatmaps in sec. 3.6.1. The figures shows an order of magnitude variation in FNMR across country of birth; these effects are likely due quality variations, then demographics like age and race. The error rates in some cases are zero, and in others the DET is flat so the error rates at the two thresholds are identical. The lines span 1% and 99% of bootstrap replicated FNMR estimates.

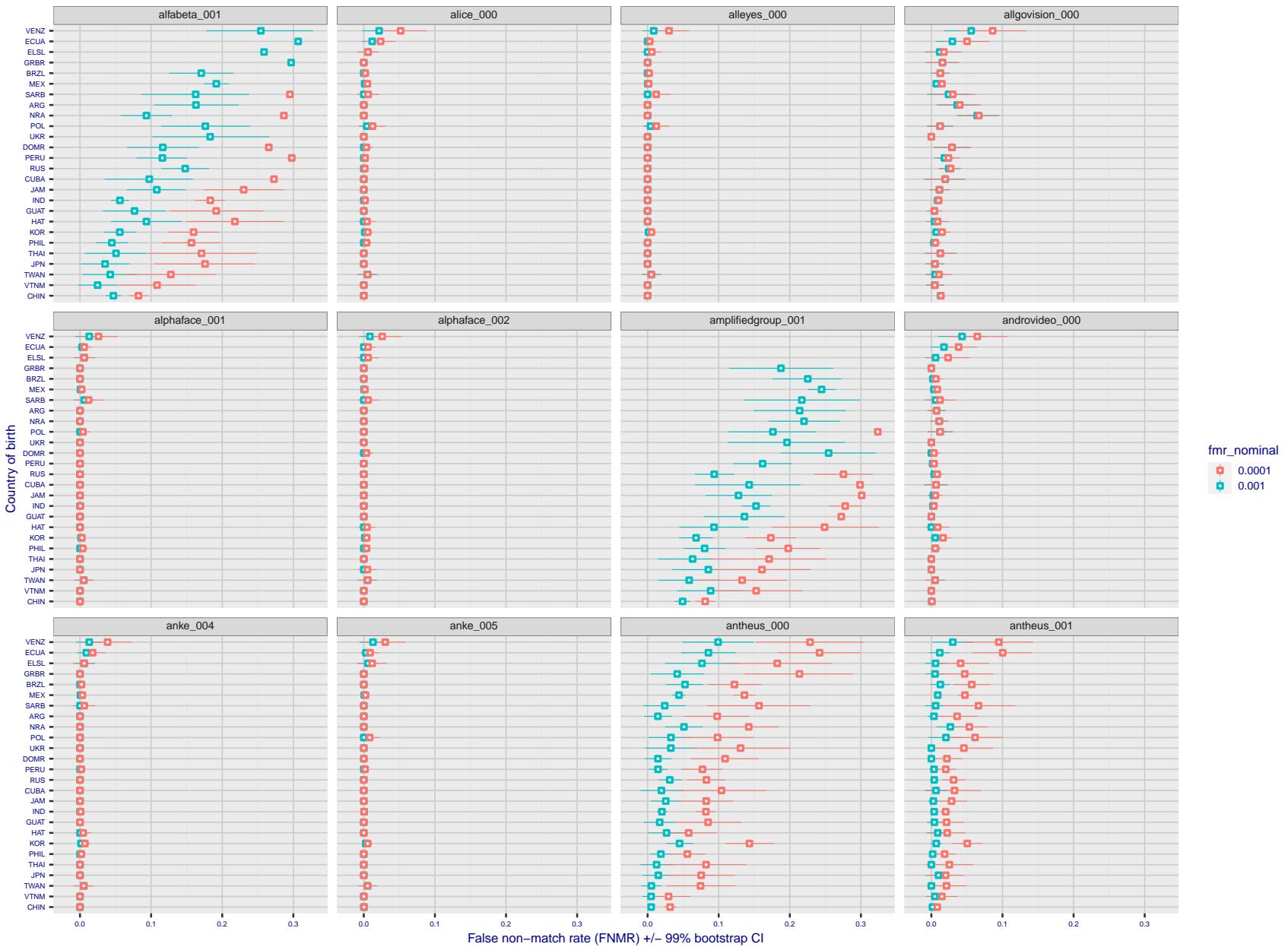


Figure 222: For the visa images, the dots show FNMR by country of birth for two globally set operating thresholds corresponding to $FMR = \{0.001, 0.0001\}$ computed over all on the order of 10^{10} impostor scores. The FMR in each bin will vary also - see subsequent impostor heatmaps in sec. 3.6.1. The figures shows an order of magnitude variation in FNMR across country of birth; these effects are likely due quality variations, then demographics like age and race. The error rates in some cases are zero, and in others the DET is flat so the error rates at the two thresholds are identical. The lines span 1% and 99% of bootstrap replicated FNMR estimates.

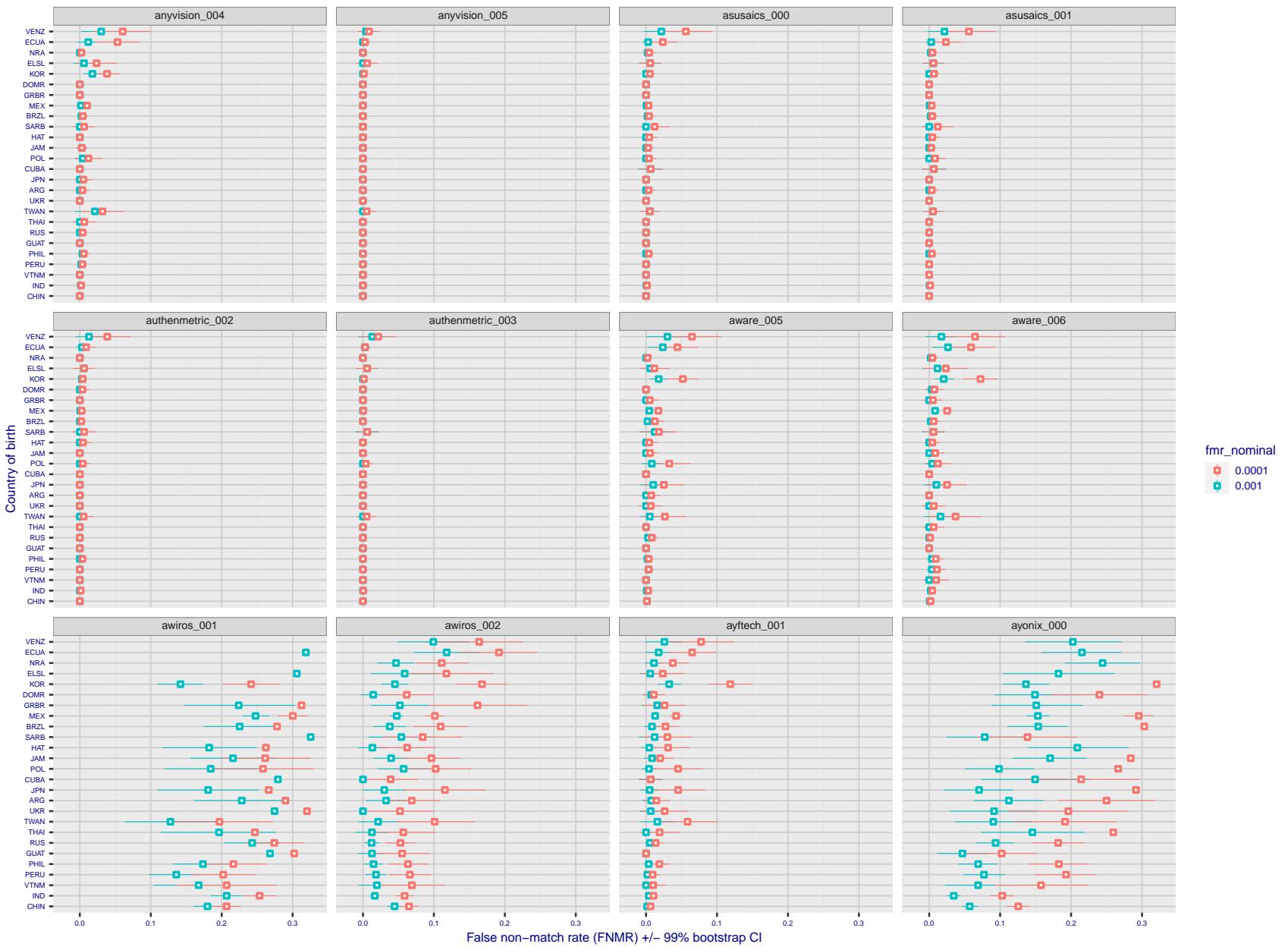


Figure 223: For the visa images, the dots show FNMR by country of birth for two globally set operating thresholds corresponding to $FMR = \{0.001, 0.0001\}$ computed over all on the order of 10^{10} impostor scores. The FMR in each bin will vary also - see subsequent impostor heatmaps in sec. 3.6.1. The figures shows an order of magnitude variation in FNMR across country of birth; these effects are likely due quality variations, then demographics like age and race. The error rates in some cases are zero, and in others the DET is flat so the error rates at the two thresholds are identical. The lines span 1% and 99% of bootstrap replicated FNMR estimates.

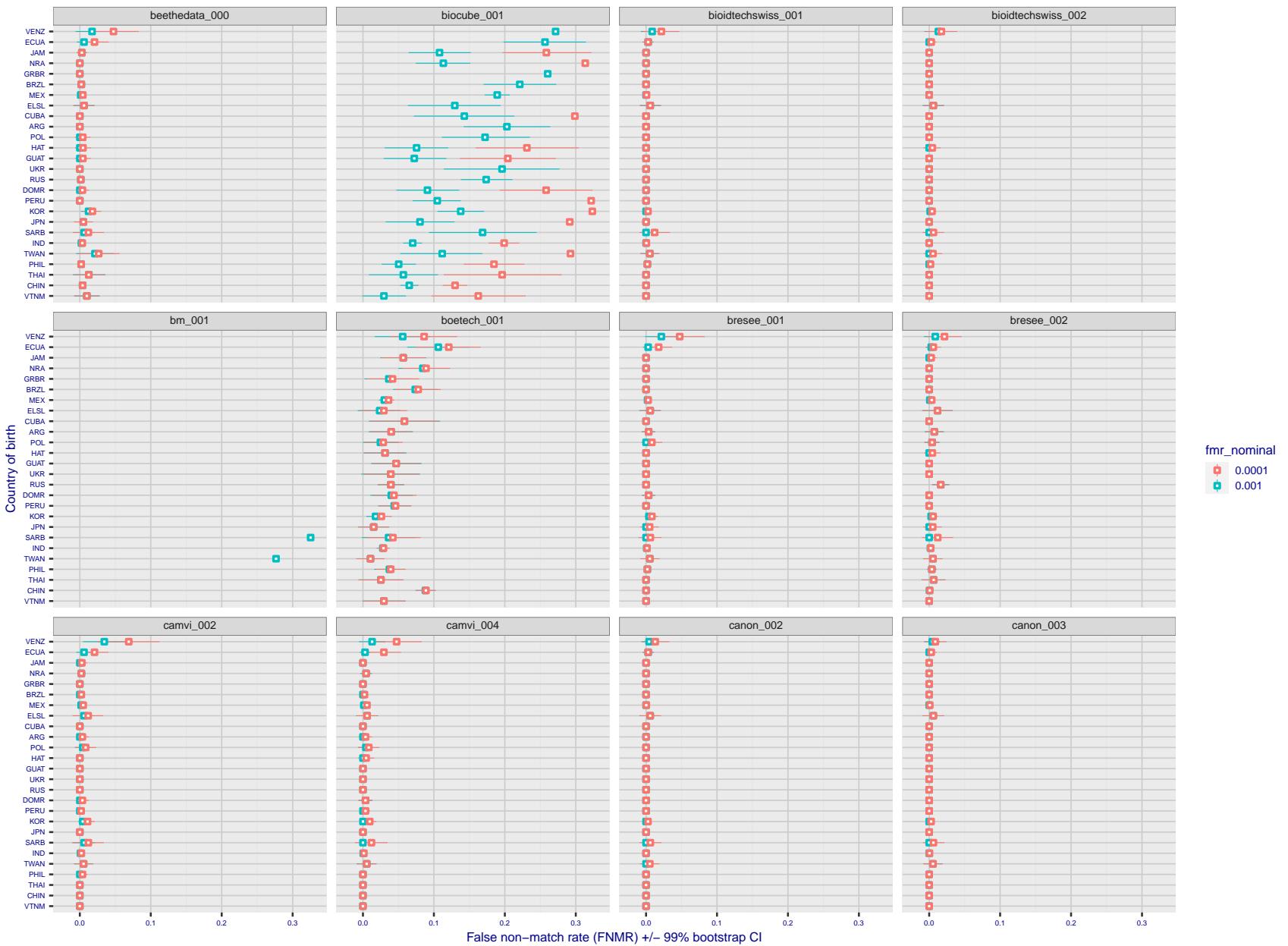


Figure 224: For the visa images, the dots show FNMR by country of birth for two globally set operating thresholds corresponding to $FMR = \{0.001, 0.0001\}$ computed over all on the order of 10^{10} impostor scores. The FMR in each bin will vary also - see subsequent impostor heatmaps in sec. 3.6.1. The figures shows an order of magnitude variation in FNMR across country of birth; these effects are likely due quality variations, then demographics like age and race. The error rates in some cases are zero, and in others the DET is flat so the error rates at the two thresholds are identical. The lines span 1% and 99% of bootstrap replicated FNMR estimates.

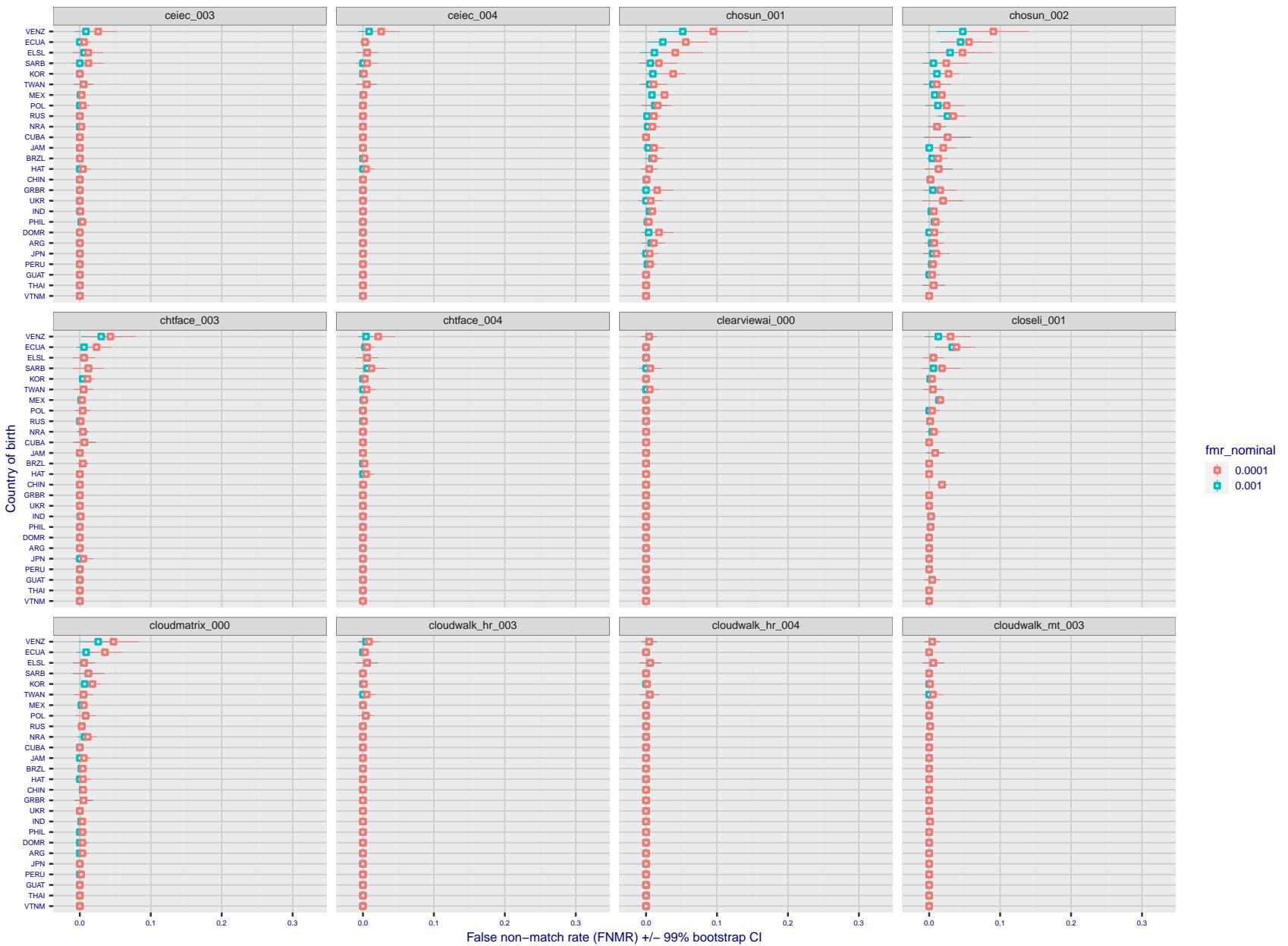


Figure 225: For the visa images, the dots show FNMR by country of birth for two globally set operating thresholds corresponding to $FMR = \{0.001, 0.0001\}$ computed over all on the order of 10^{10} impostor scores. The FMR in each bin will vary also - see subsequent impostor heatmaps in sec. 3.6.1. The figures shows an order of magnitude variation in FNMR across country of birth; these effects are likely due quality variations, then demographics like age and race. The error rates in some cases are zero, and in others the DET is flat so the error rates at the two thresholds are identical. The lines span 1% and 99% of bootstrap replicated FNMR estimates.

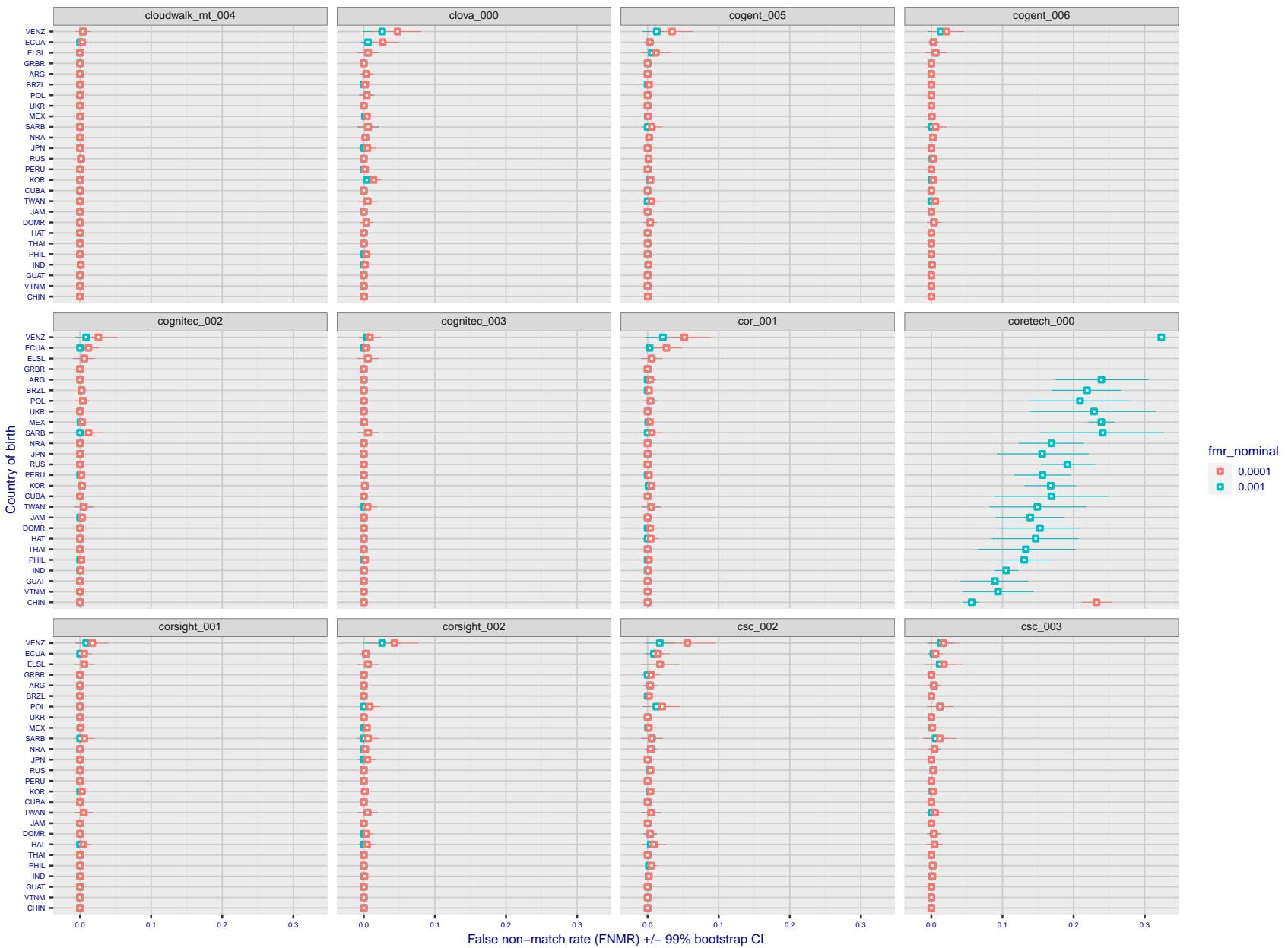


Figure 226: For the visa images, the dots show FNMR by country of birth for two globally set operating thresholds corresponding to $FMR = \{0.001, 0.0001\}$ computed over all on the order of 10^{10} impostor scores. The FMR in each bin will vary also - see subsequent impostor heatmaps in sec. 3.6.1. The figures shows an order of magnitude variation in FNMR across country of birth; these effects are likely due quality variations, then demographics like age and race. The error rates in some cases are zero, and in others the DET is flat so the error rates at the two thresholds are identical. The lines span 1% and 99% of bootstrap replicated FNMR estimates.

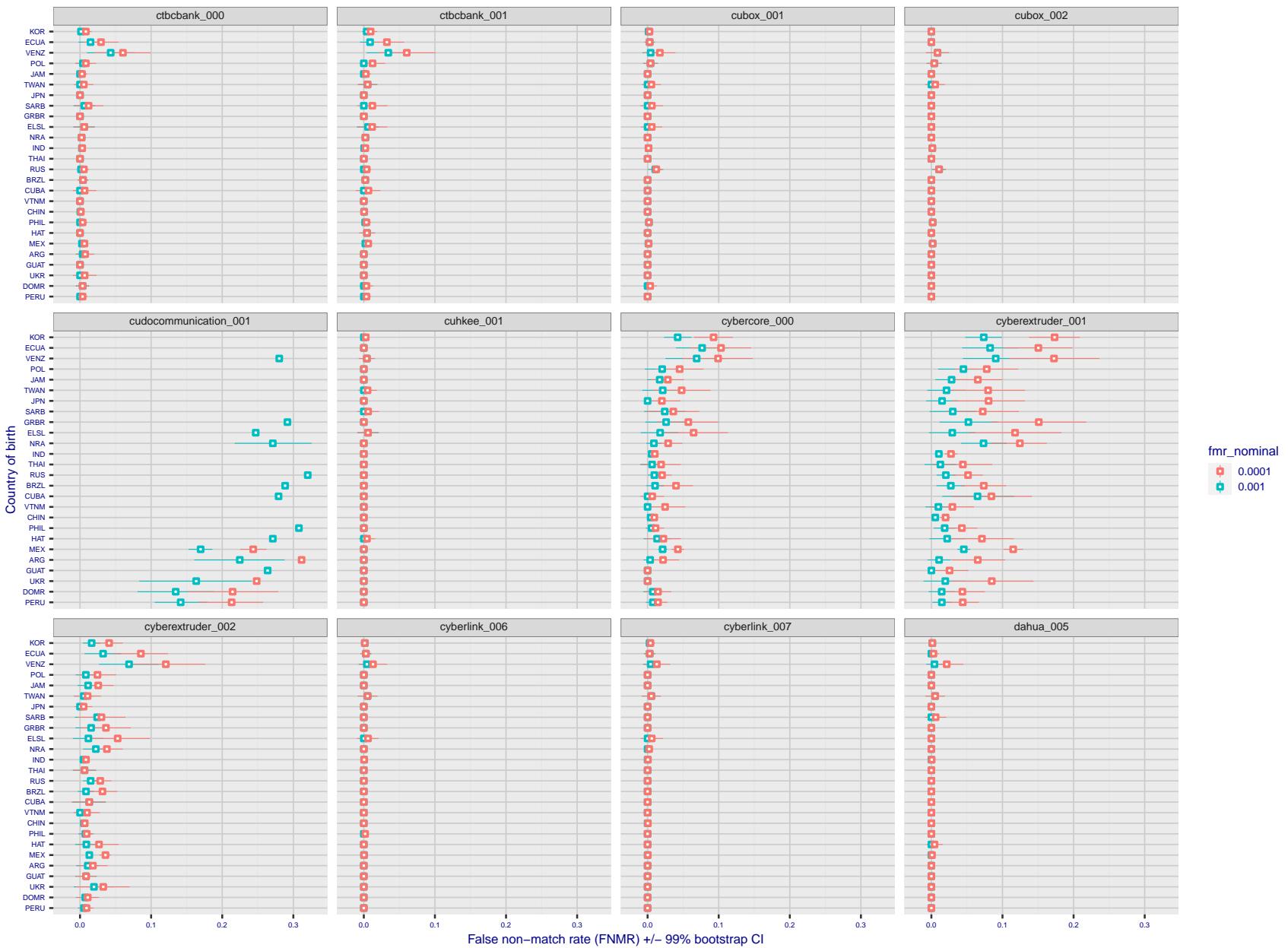


Figure 227: For the visa images, the dots show FNMR by country of birth for two globally set operating thresholds corresponding to $FMR = \{0.001, 0.0001\}$ computed over all on the order of 10^{10} impostor scores. The FMR in each bin will vary also - see subsequent impostor heatmaps in sec. 3.6.1. The figures shows an order of magnitude variation in FNMR across country of birth; these effects are likely due quality variations, then demographics like age and race. The error rates in some cases are zero, and in others the DET is flat so the error rates at the two thresholds are identical. The lines span 1% and 99% of bootstrap replicated FNMR estimates.

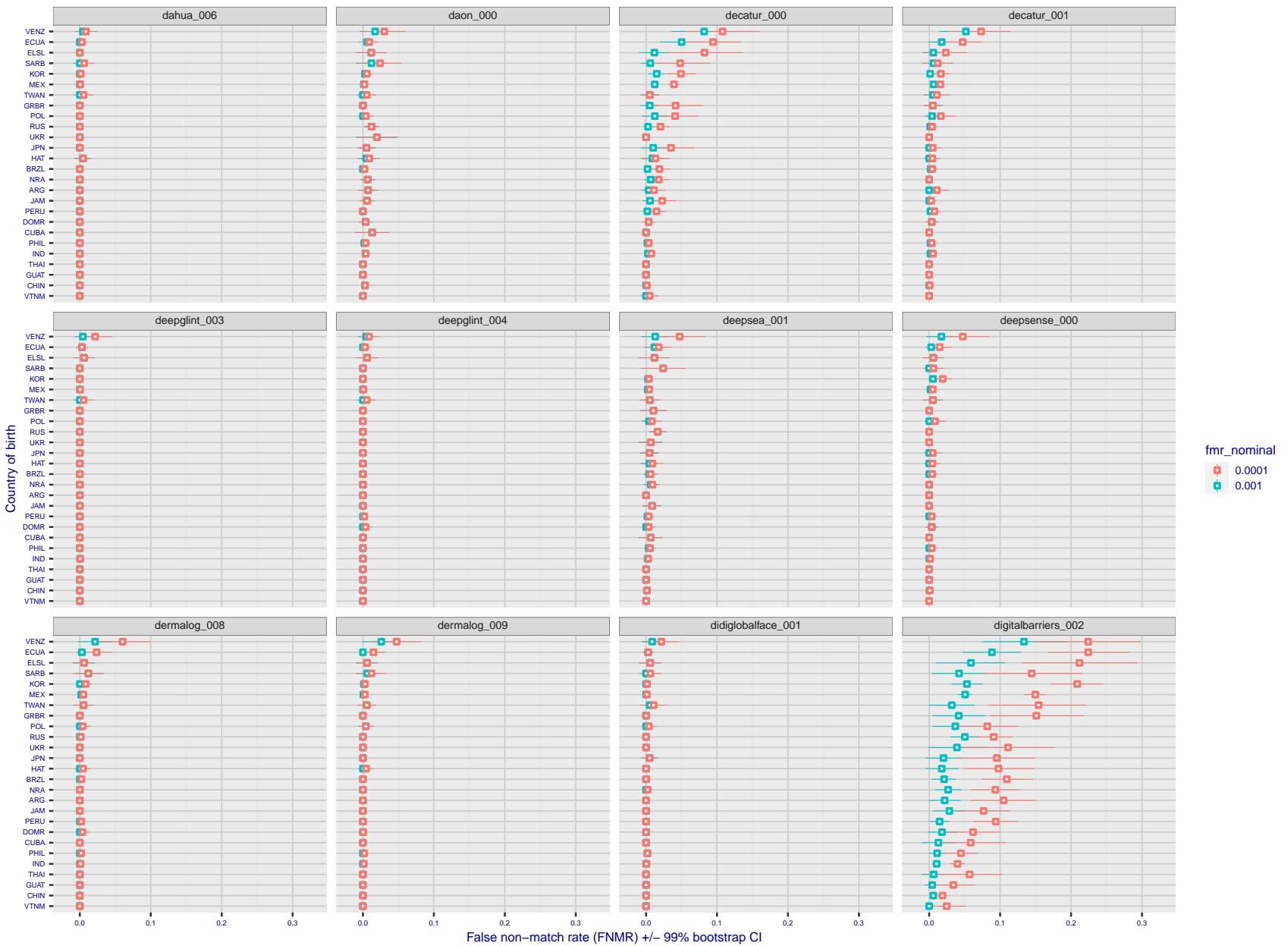


Figure 228: For the visa images, the dots show FNMR by country of birth for two globally set operating thresholds corresponding to $FMR = \{0.001, 0.0001\}$ computed over all on the order of 10^{10} impostor scores. The FMR in each bin will vary also - see subsequent impostor heatmaps in sec. 3.6.1. The figures shows an order of magnitude variation in FNMR across country of birth; these effects are likely due quality variations, then demographics like age and race. The error rates in some cases are zero, and in others the DET is flat so the error rates at the two thresholds are identical. The lines span 1% and 99% of bootstrap replicated FNMR estimates.

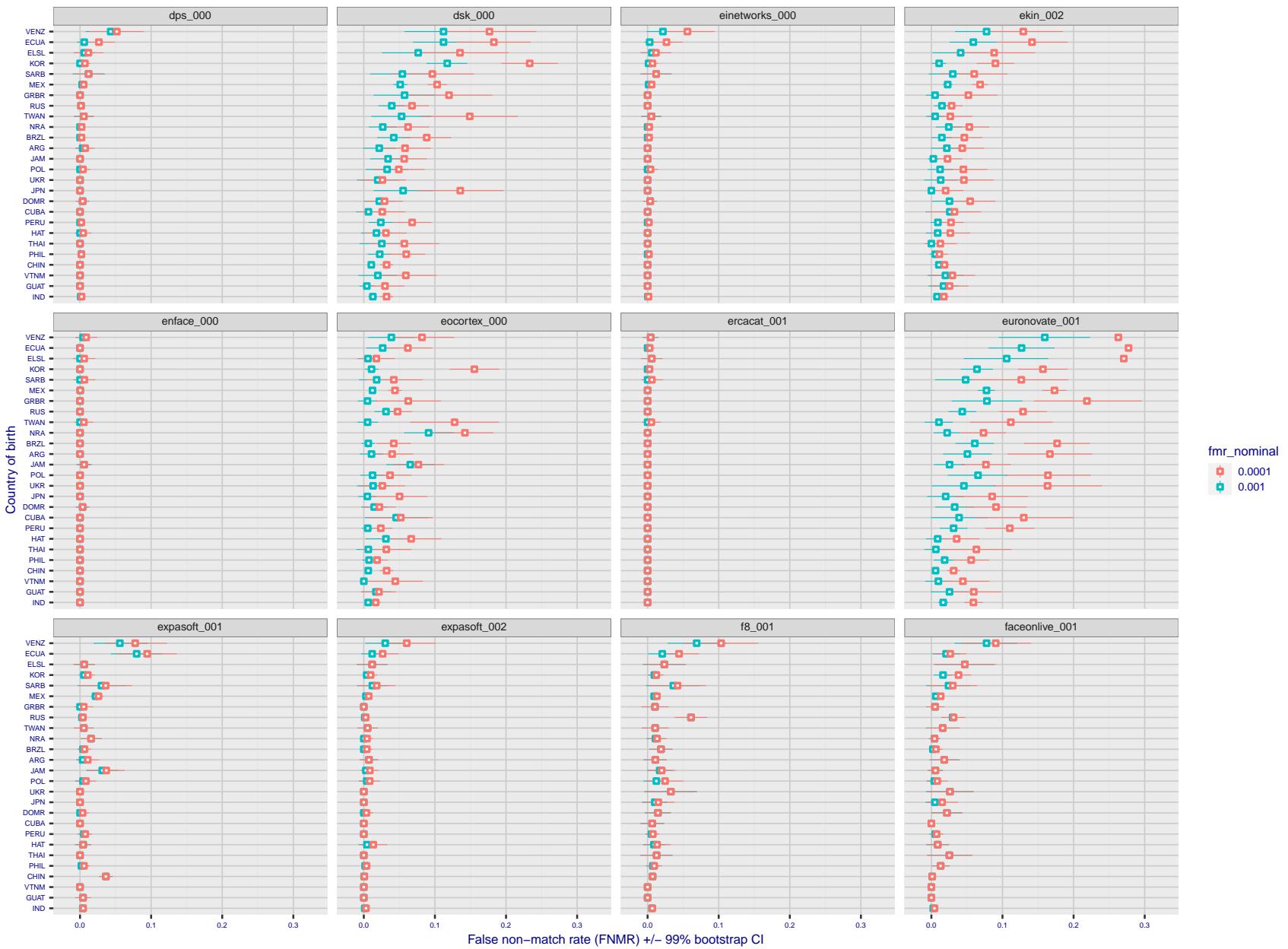


Figure 229: For the visa images, the dots show FNMR by country of birth for two globally set operating thresholds corresponding to $FMR = \{0.001, 0.0001\}$ computed over all on the order of 10^{10} impostor scores. The FMR in each bin will vary also - see subsequent impostor heatmaps in sec. 3.6.1. The figures shows an order of magnitude variation in FNMR across country of birth; these effects are likely due quality variations, then demographics like age and race. The error rates in some cases are zero, and in others the DET is flat so the error rates at the two thresholds are identical. The lines span 1% and 99% of bootstrap replicated FNMR estimates.

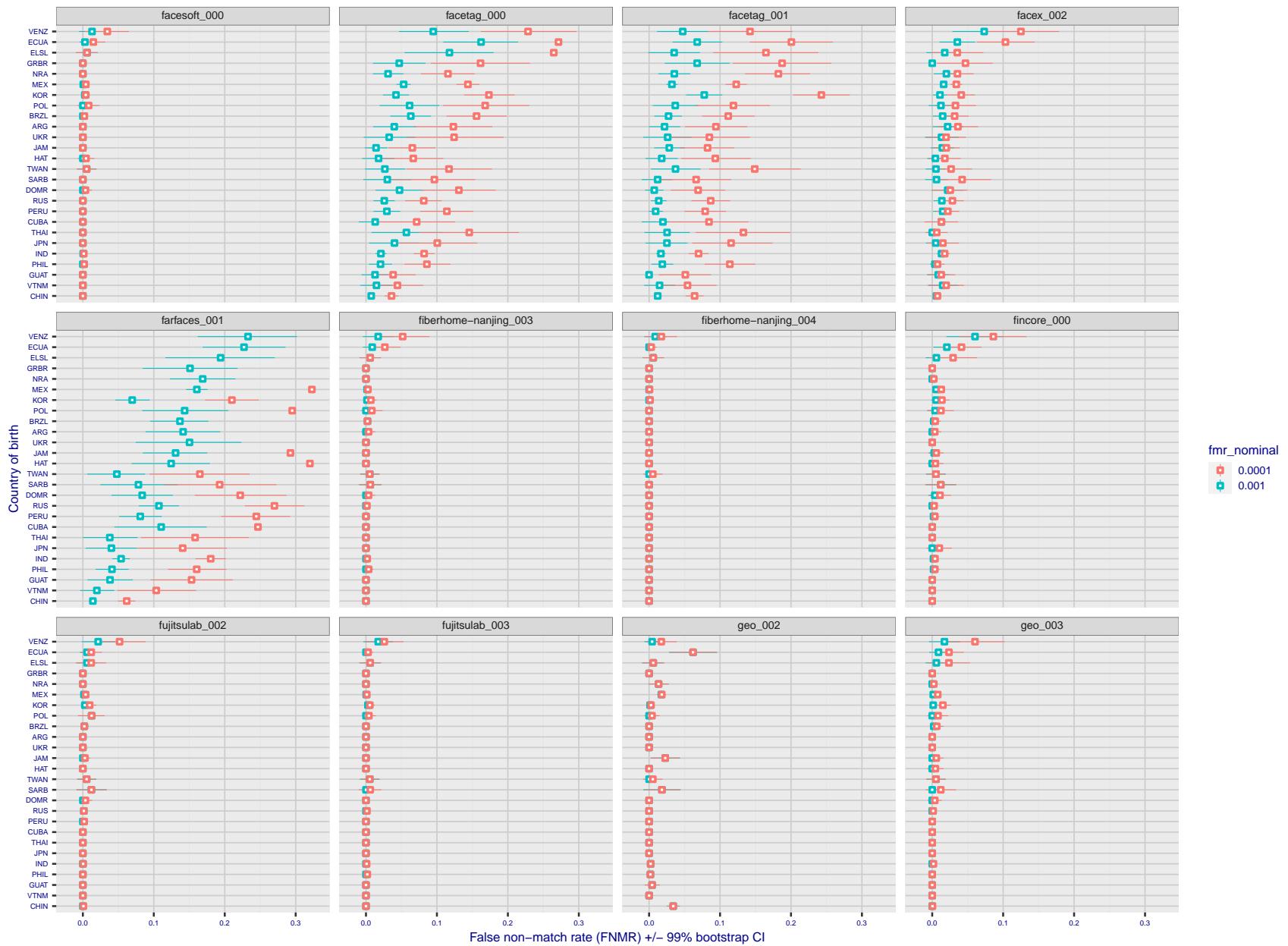


Figure 230: For the visa images, the dots show FNMR by country of birth for two globally set operating thresholds corresponding to $FMR = \{0.001, 0.0001\}$ computed over all on the order of 10^{10} impostor scores. The FMR in each bin will vary also - see subsequent impostor heatmaps in sec. 3.6.1. The figures shows an order of magnitude variation in FNMR across country of birth; these effects are likely due quality variations, then demographics like age and race. The error rates in some cases are zero, and in others the DET is flat so the error rates at the two thresholds are identical. The lines span 1% and 99% of bootstrap replicated FNMR estimates.

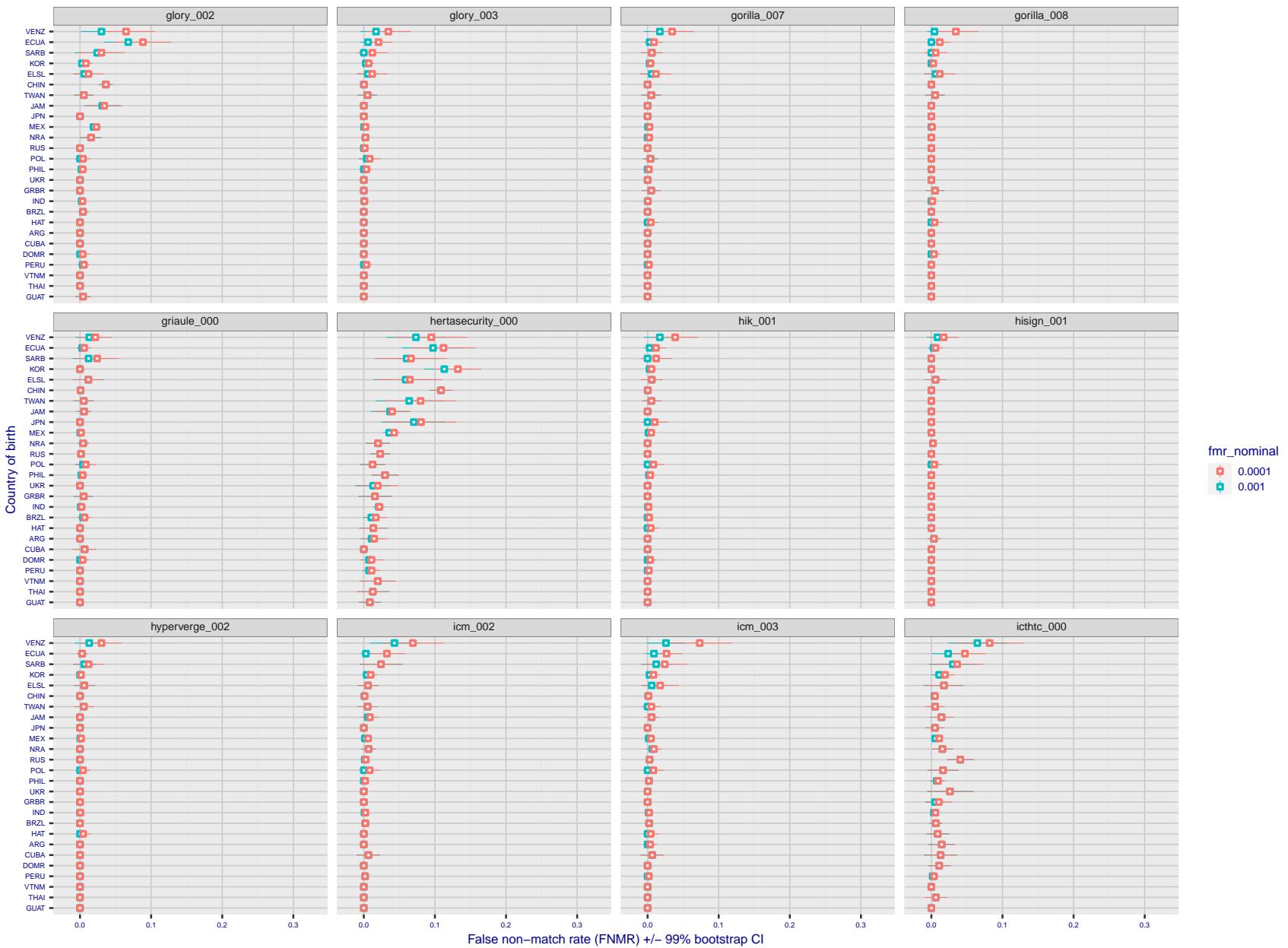


Figure 231: For the visa images, the dots show FNMR by country of birth for two globally set operating thresholds corresponding to $FMR = \{0.001, 0.0001\}$ computed over all on the order of 10^{10} impostor scores. The FMR in each bin will vary also - see subsequent impostor heatmaps in sec. 3.6.1. The figures shows an order of magnitude variation in FNMR across country of birth; these effects are likely due quality variations, then demographics like age and race. The error rates in some cases are zero, and in others the DET is flat so the error rates at the two thresholds are identical. The lines span 1% and 99% of bootstrap replicated FNMR estimates.

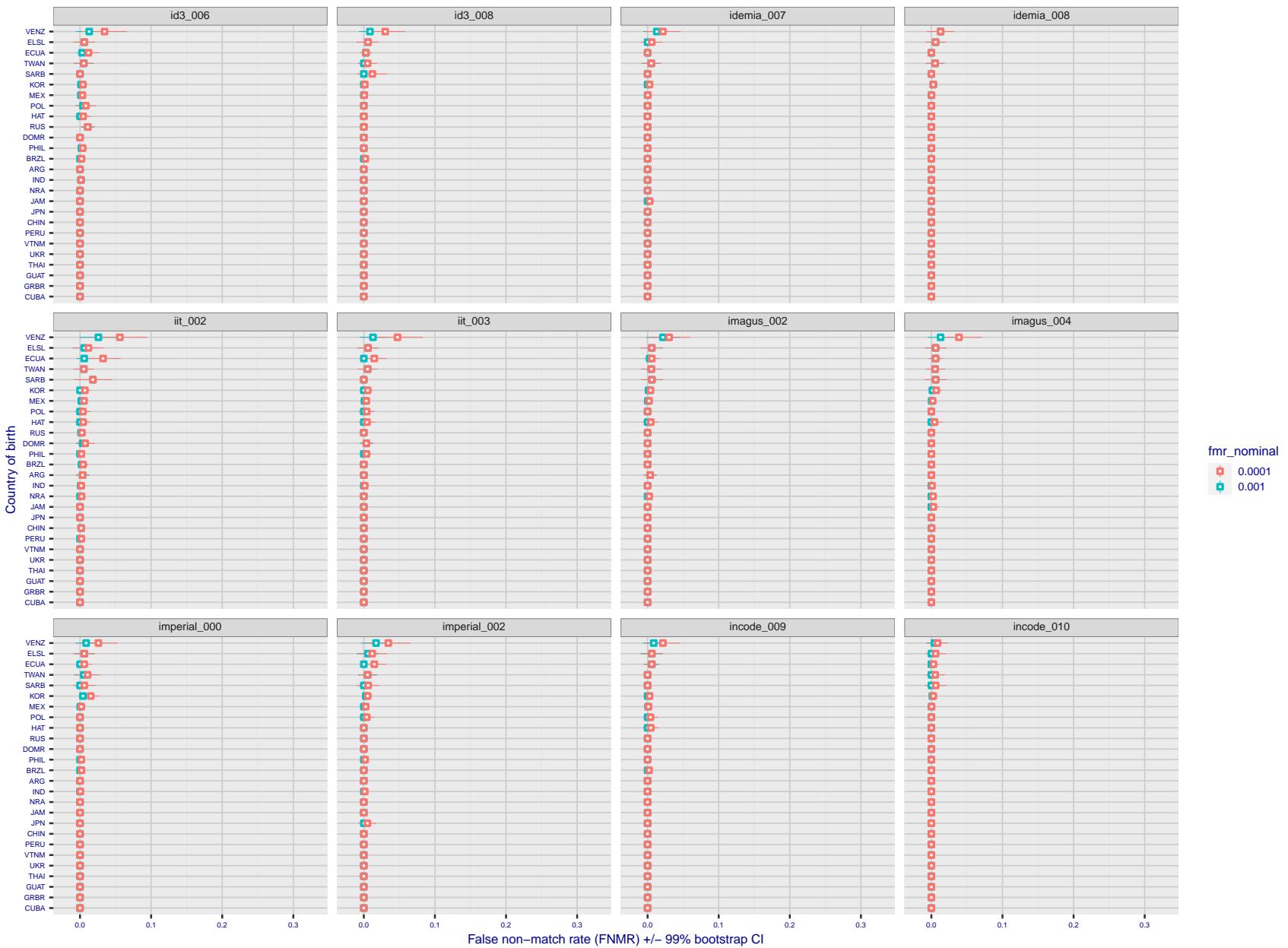


Figure 232: For the visa images, the dots show FNMR by country of birth for two globally set operating thresholds corresponding to $FMR = \{0.001, 0.0001\}$ computed over all on the order of 10^{10} impostor scores. The FMR in each bin will vary also - see subsequent impostor heatmaps in sec. 3.6.1. The figures shows an order of magnitude variation in FNMR across country of birth; these effects are likely due quality variations, then demographics like age and race. The error rates in some cases are zero, and in others the DET is flat so the error rates at the two thresholds are identical. The lines span 1% and 99% of bootstrap replicated FNMR estimates.

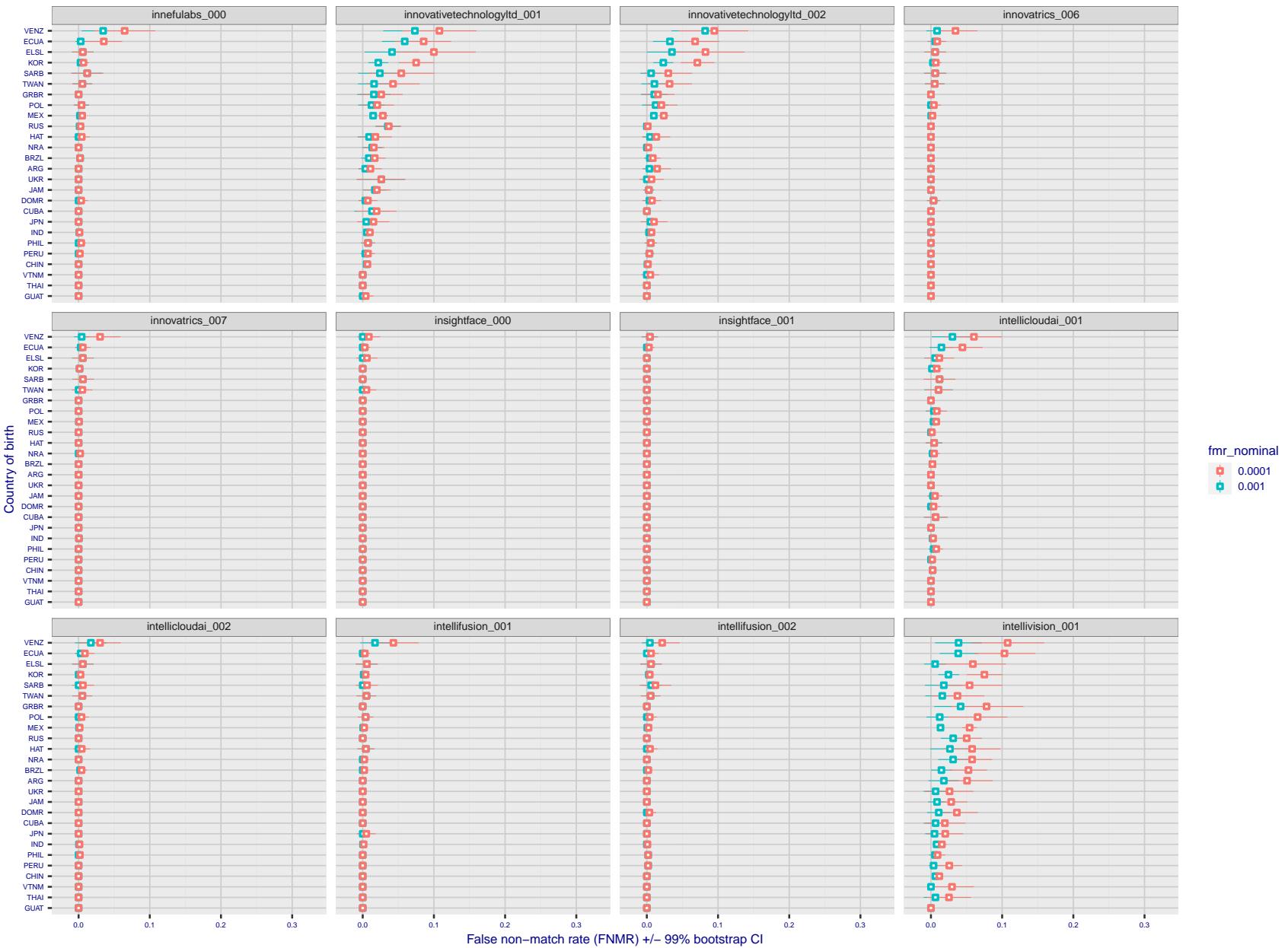


Figure 233: For the visa images, the dots show FNMR by country of birth for two globally set operating thresholds corresponding to $FMR = \{0.001, 0.0001\}$ computed over all on the order of 10^{10} impostor scores. The FMR in each bin will vary also - see subsequent impostor heatmaps in sec. 3.6.1. The figures shows an order of magnitude variation in FNMR across country of birth; these effects are likely due quality variations, then demographics like age and race. The error rates in some cases are zero, and in others the DET is flat so the error rates at the two thresholds are identical. The lines span 1% and 99% of bootstrap replicated FNMR estimates.

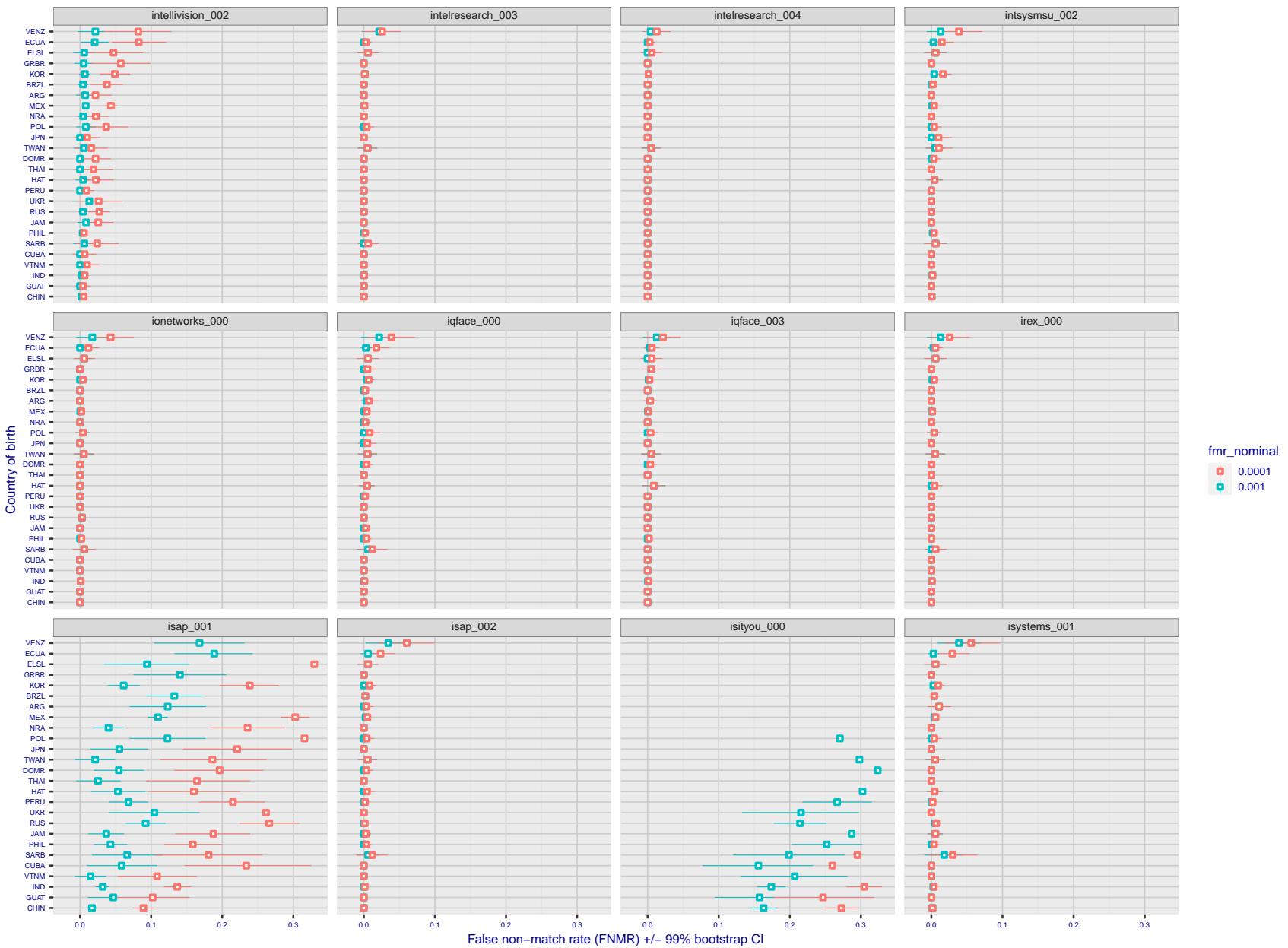


Figure 234: For the visa images, the dots show FNMR by country of birth for two globally set operating thresholds corresponding to $FMR = \{0.001, 0.0001\}$ computed over all on the order of 10^{10} impostor scores. The FMR in each bin will vary also - see subsequent impostor heatmaps in sec. 3.6.1. The figures shows an order of magnitude variation in FNMR across country of birth; these effects are likely due quality variations, then demographics like age and race. The error rates in some cases are zero, and in others the DET is flat so the error rates at the two thresholds are identical. The lines span 1% and 99% of bootstrap replicated FNMR estimates.

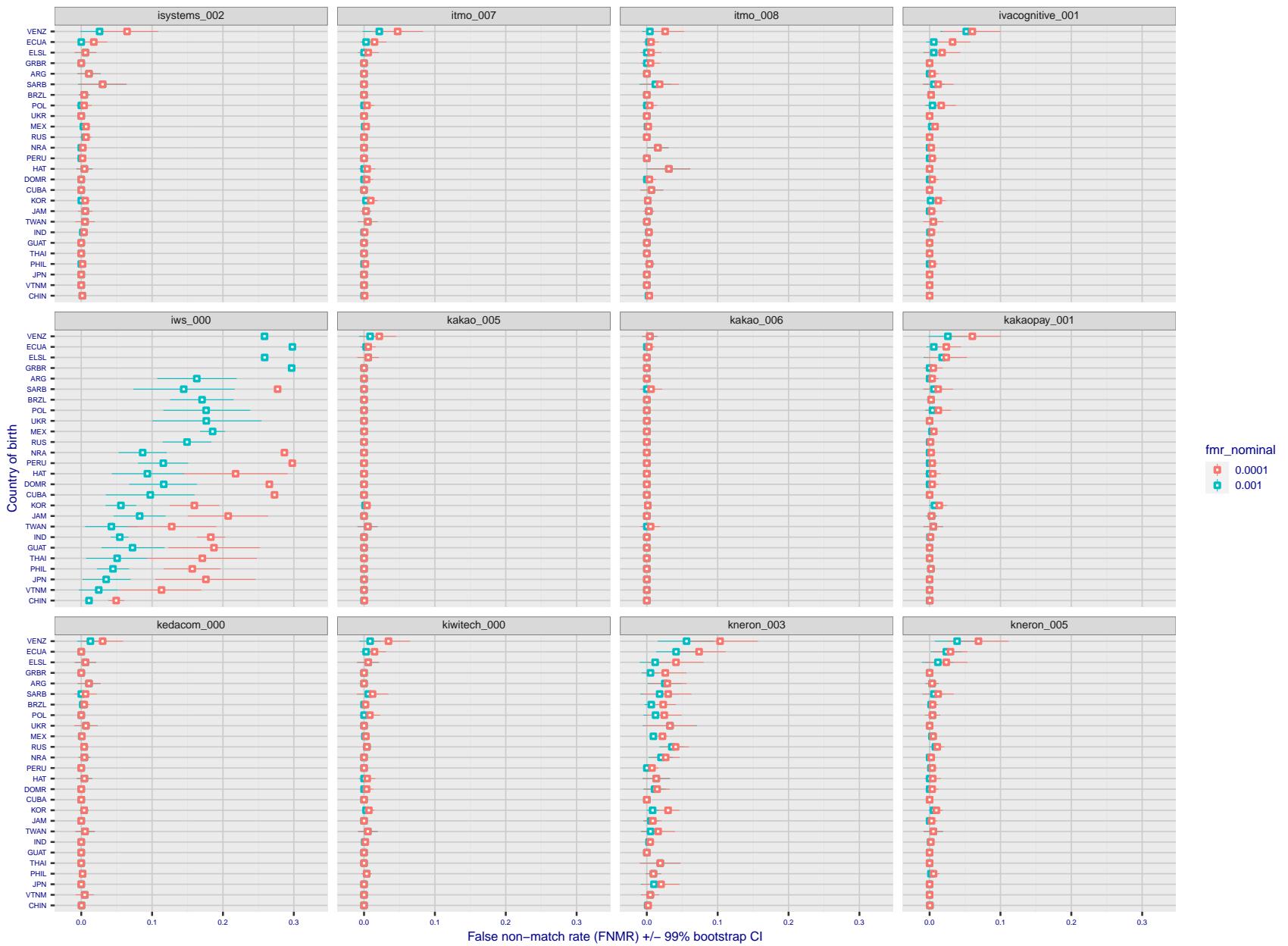


Figure 235: For the visa images, the dots show FNMR by country of birth for two globally set operating thresholds corresponding to $FMR = \{0.001, 0.0001\}$ computed over all on the order of 10^{10} impostor scores. The FMR in each bin will vary also - see subsequent impostor heatmaps in sec. 3.6.1. The figures shows an order of magnitude variation in FNMR across country of birth; these effects are likely due quality variations, then demographics like age and race. The error rates in some cases are zero, and in others the DET is flat so the error rates at the two thresholds are identical. The lines span 1% and 99% of bootstrap replicated FNMR estimates.

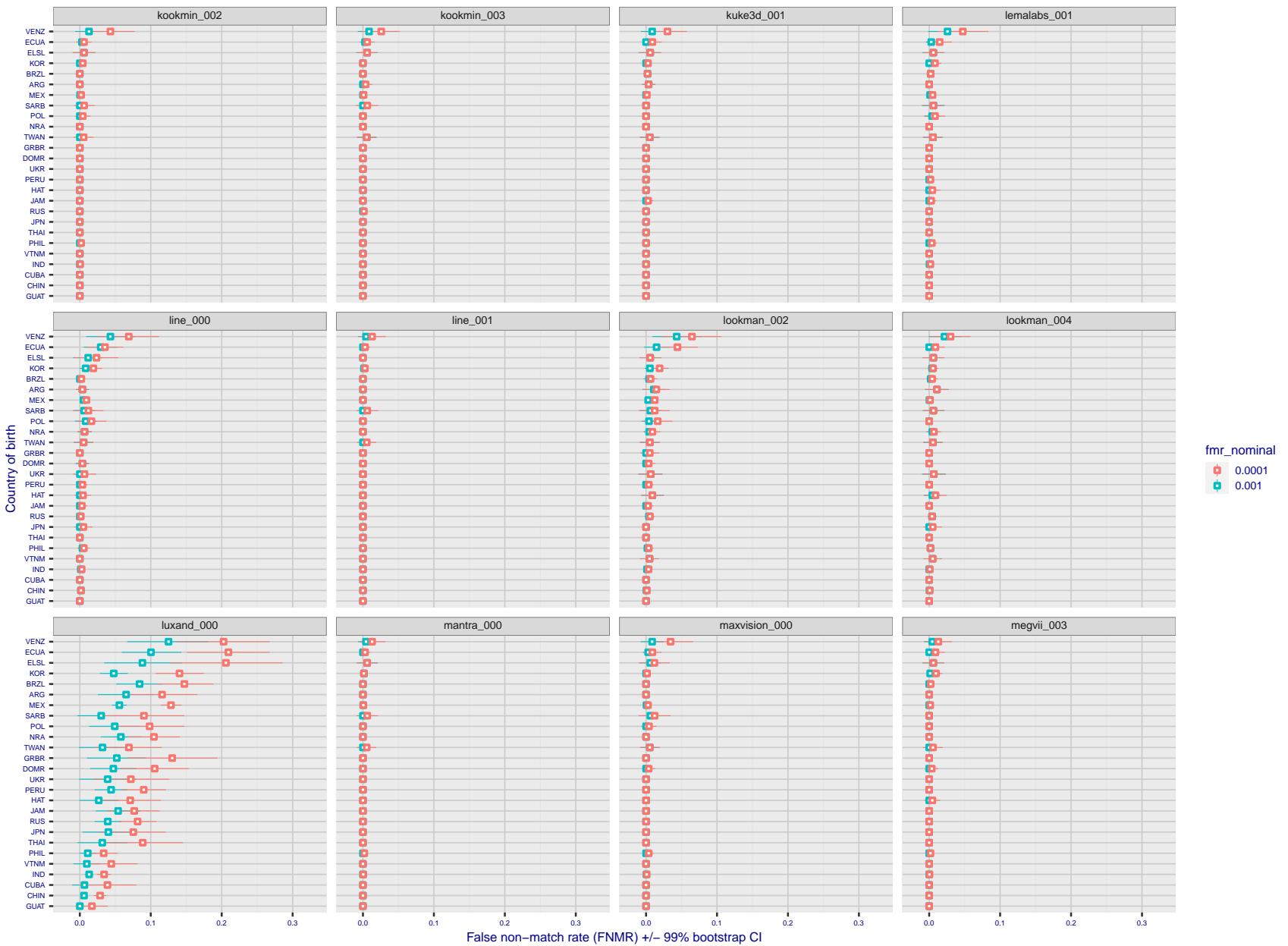


Figure 236: For the visa images, the dots show FNMR by country of birth for two globally set operating thresholds corresponding to $FMR = \{0.001, 0.0001\}$ computed over all on the order of 10^{10} impostor scores. The FMR in each bin will vary also - see subsequent impostor heatmaps in sec. 3.6.1. The figures shows an order of magnitude variation in FNMR across country of birth; these effects are likely due quality variations, then demographics like age and race. The error rates in some cases are zero, and in others the DET is flat so the error rates at the two thresholds are identical. The lines span 1% and 99% of bootstrap replicated FNMR estimates.

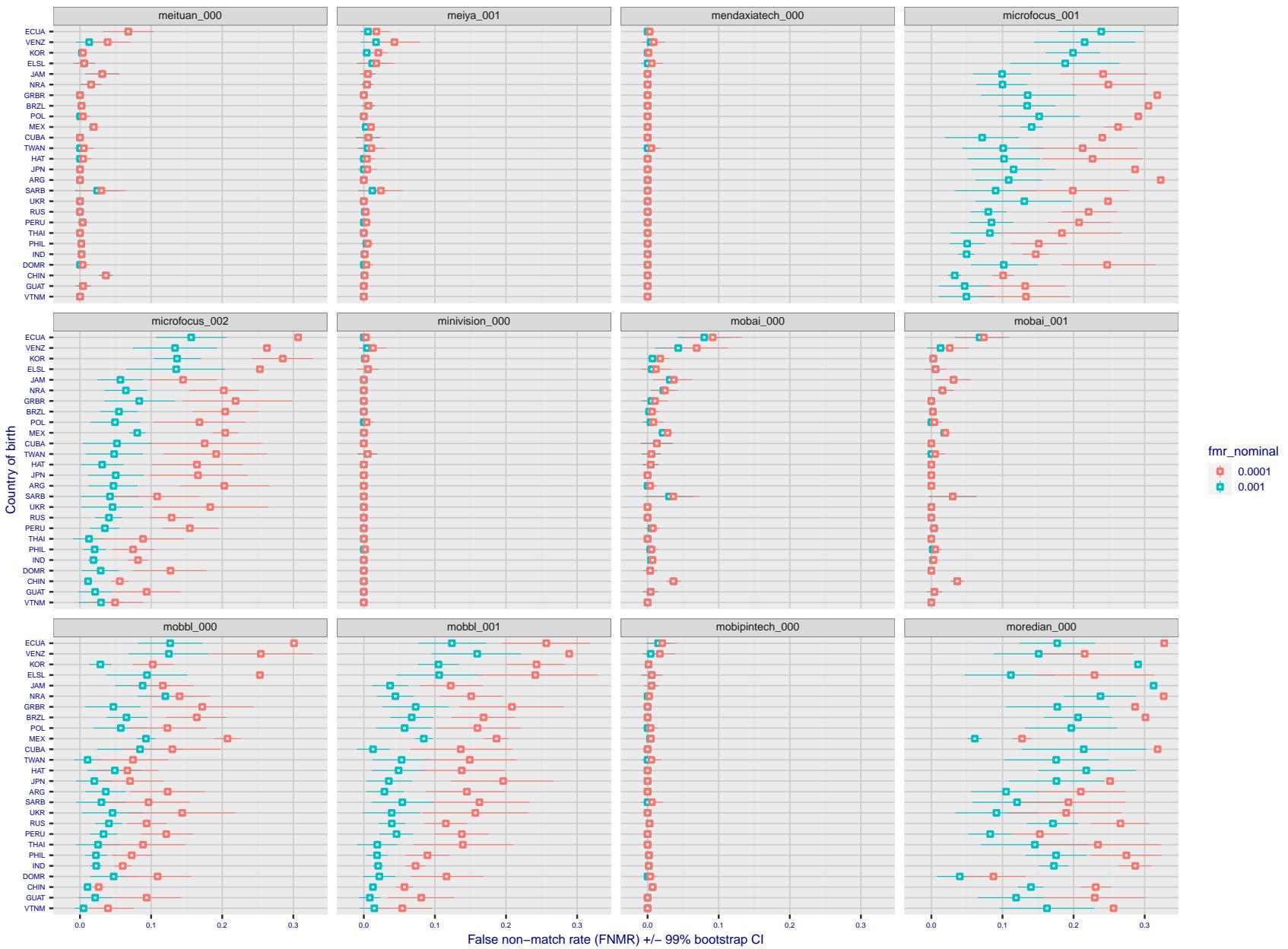


Figure 237: For the visa images, the dots show FNMR by country of birth for two globally set operating thresholds corresponding to $FMR = \{0.001, 0.0001\}$ computed over all on the order of 10^{10} impostor scores. The FMR in each bin will vary also - see subsequent impostor heatmaps in sec. 3.6.1. The figures shows an order of magnitude variation in FNMR across country of birth; these effects are likely due quality variations, then demographics like age and race. The error rates in some cases are zero, and in others the DET is flat so the error rates at the two thresholds are identical. The lines span 1% and 99% of bootstrap replicated FNMR estimates.

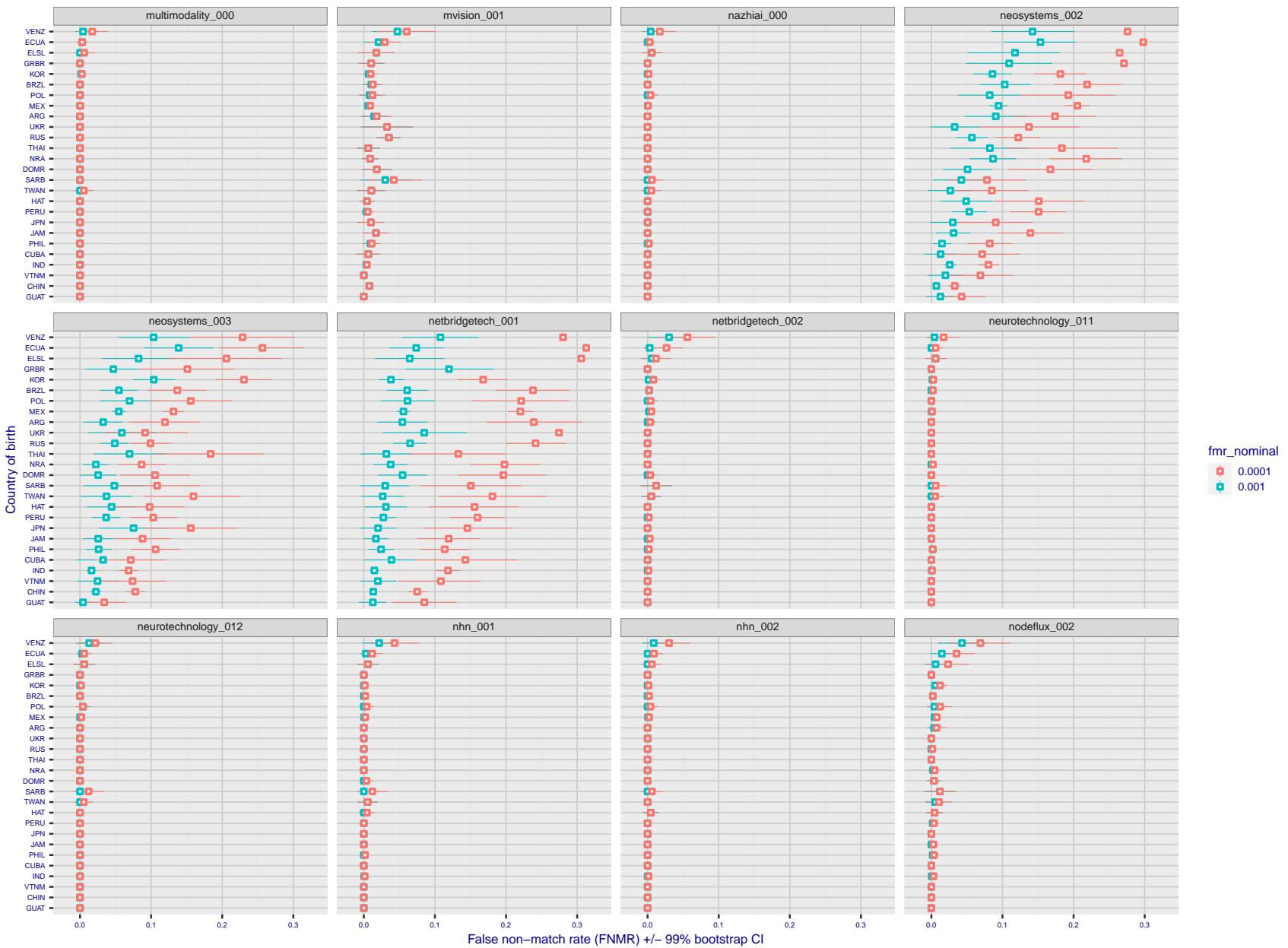


Figure 238: For the visa images, the dots show FNMR by country of birth for two globally set operating thresholds corresponding to $FMR = \{0.001, 0.0001\}$ computed over all on the order of 10^{10} impostor scores. The FMR in each bin will vary also - see subsequent impostor heatmaps in sec. 3.6.1. The figures shows an order of magnitude variation in FNMR across country of birth; these effects are likely due quality variations, then demographics like age and race. The error rates in some cases are zero, and in others the DET is flat so the error rates at the two thresholds are identical. The lines span 1% and 99% of bootstrap replicated FNMR estimates.

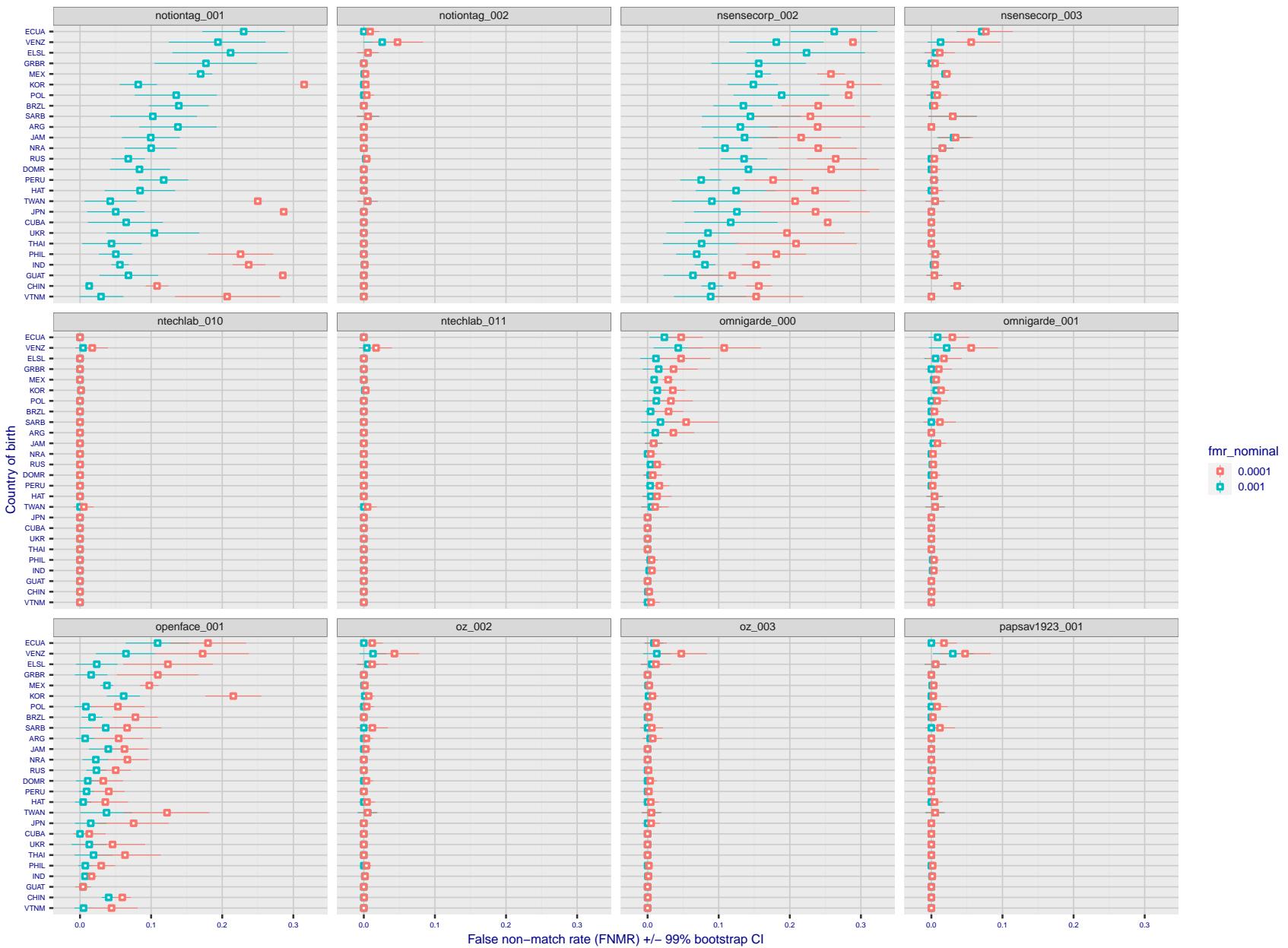


Figure 239: For the visa images, the dots show FNMR by country of birth for two globally set operating thresholds corresponding to $FMR = \{0.001, 0.0001\}$ computed over all on the order of 10^{10} impostor scores. The FMR in each bin will vary also - see subsequent impostor heatmaps in sec. 3.6.1. The figures shows an order of magnitude variation in FNMR across country of birth; these effects are likely due quality variations, then demographics like age and race. The error rates in some cases are zero, and in others the DET is flat so the error rates at the two thresholds are identical. The lines span 1% and 99% of bootstrap replicated FNMR estimates.

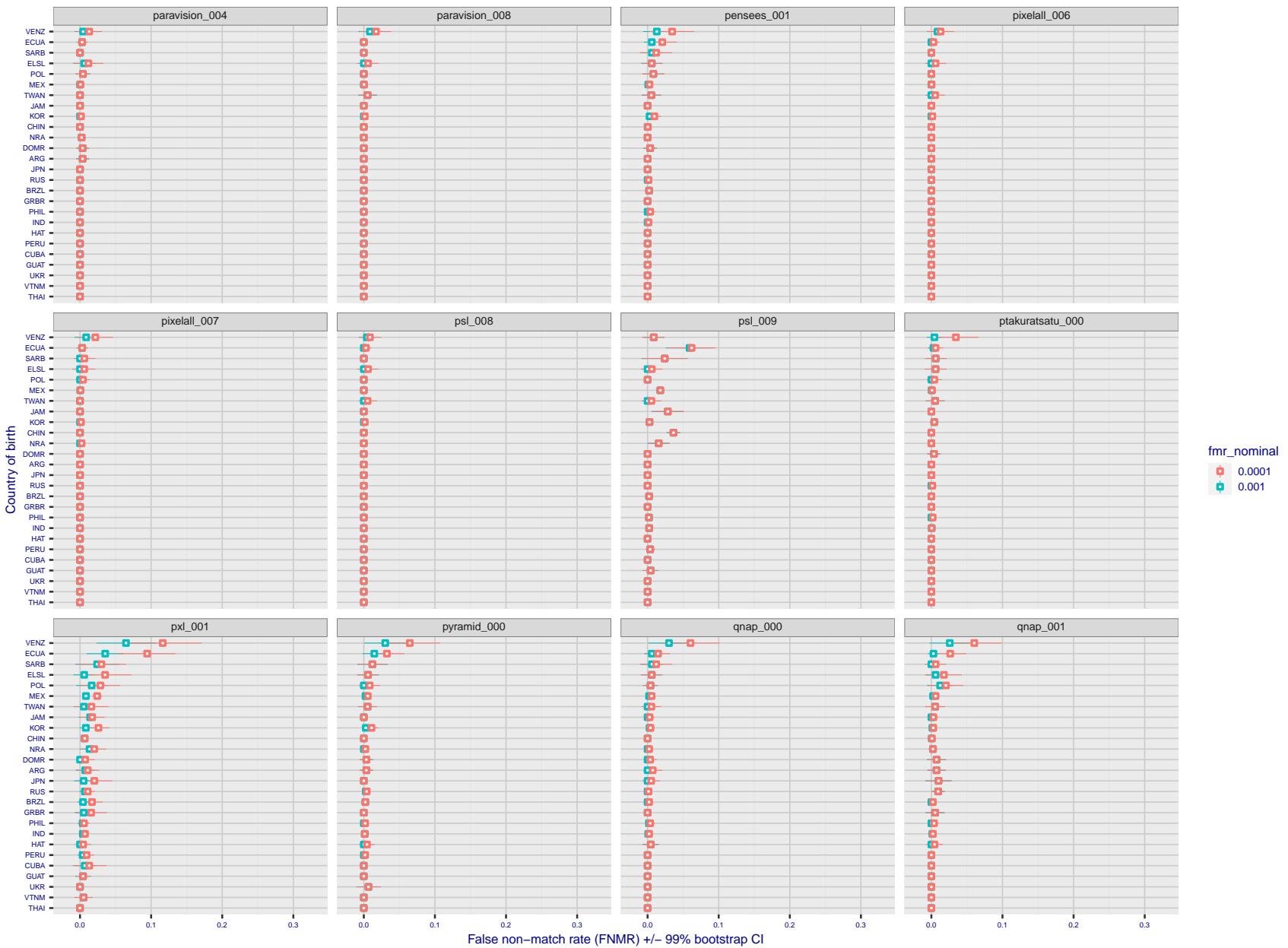


Figure 240: For the visa images, the dots show FNMR by country of birth for two globally set operating thresholds corresponding to $FMR = \{0.001, 0.0001\}$ computed over all on the order of 10^{10} impostor scores. The FMR in each bin will vary also - see subsequent impostor heatmaps in sec. 3.6.1. The figures shows an order of magnitude variation in FNMR across country of birth; these effects are likely due quality variations, then demographics like age and race. The error rates in some cases are zero, and in others the DET is flat so the error rates at the two thresholds are identical. The lines span 1% and 99% of bootstrap replicated FNMR estimates.

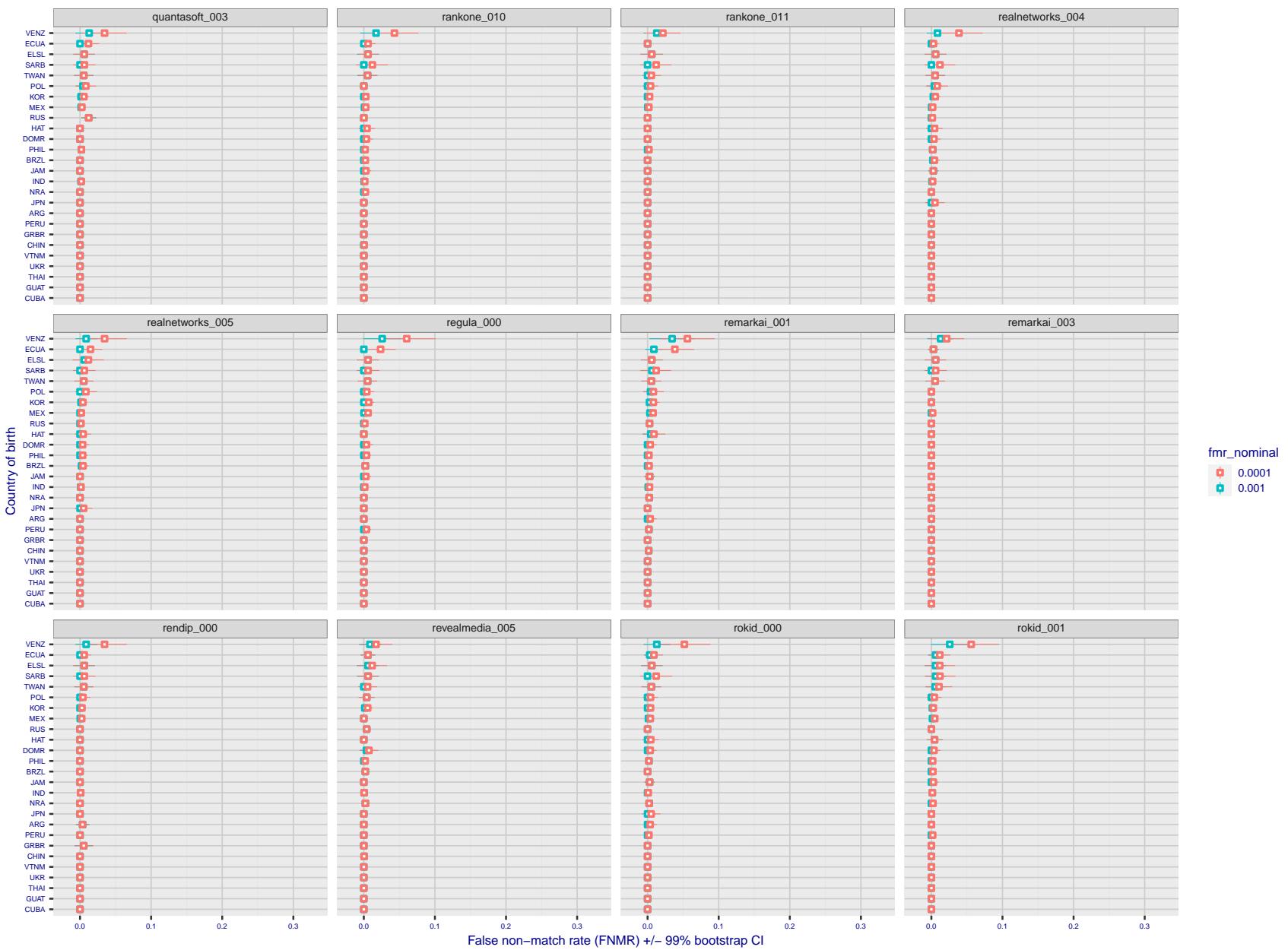


Figure 241: For the visa images, the dots show FNMR by country of birth for two globally set operating thresholds corresponding to $FMR = \{0.001, 0.0001\}$ computed over all on the order of 10^{10} impostor scores. The FMR in each bin will vary also - see subsequent impostor heatmaps in sec. 3.6.1. The figures shows an order of magnitude variation in FNMR across country of birth; these effects are likely due quality variations, then demographics like age and race. The error rates in some cases are zero, and in others the DET is flat so the error rates at the two thresholds are identical. The lines span 1% and 99% of bootstrap replicated FNMR estimates.

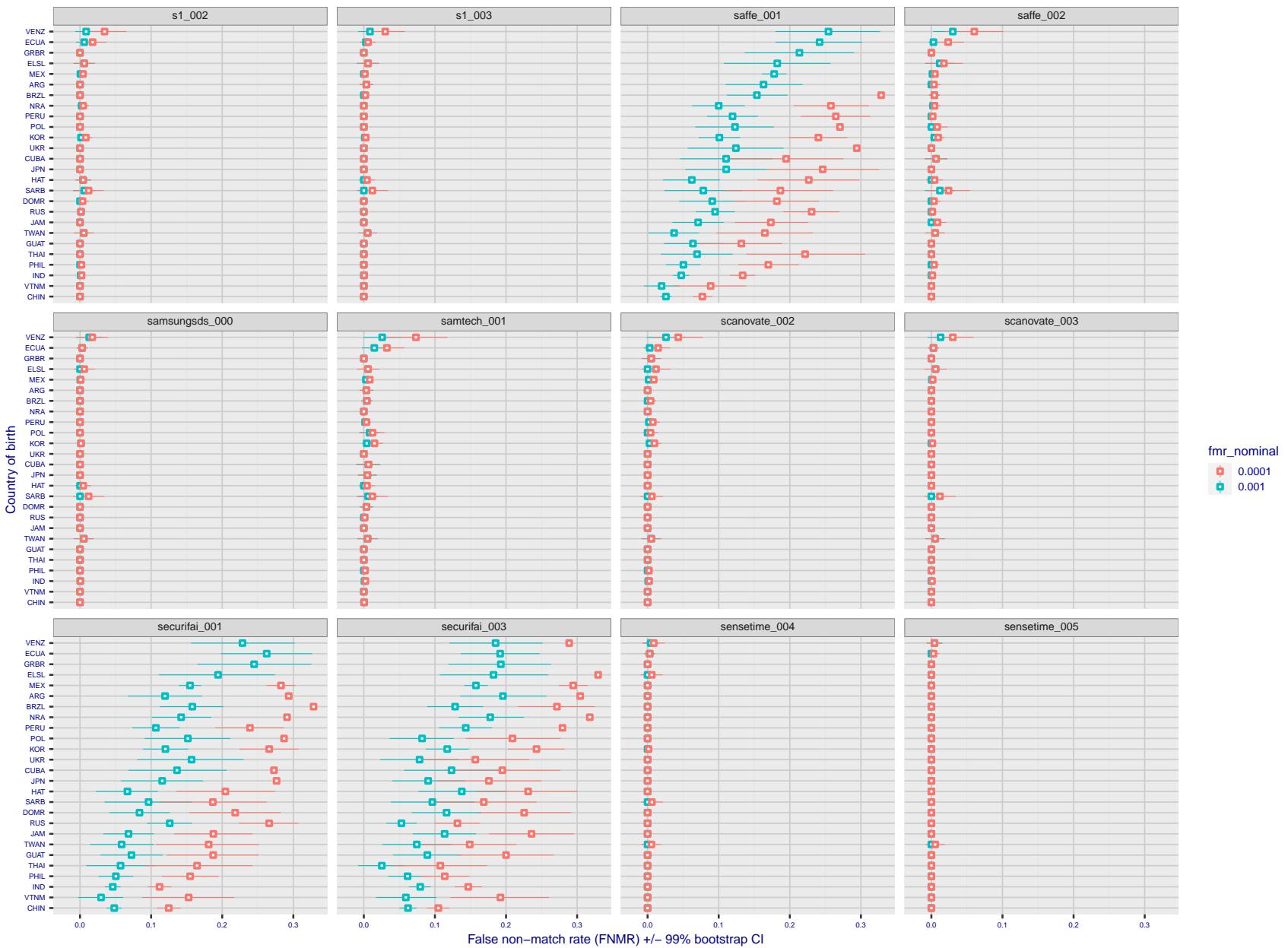


Figure 242: For the visa images, the dots show FNMR by country of birth for two globally set operating thresholds corresponding to $FMR = \{0.001, 0.0001\}$ computed over all on the order of 10^{10} impostor scores. The FMR in each bin will vary also - see subsequent impostor heatmaps in sec. 3.6.1. The figures shows an order of magnitude variation in FNMR across country of birth; these effects are likely due quality variations, then demographics like age and race. The error rates in some cases are zero, and in others the DET is flat so the error rates at the two thresholds are identical. The lines span 1% and 99% of bootstrap replicated FNMR estimates.

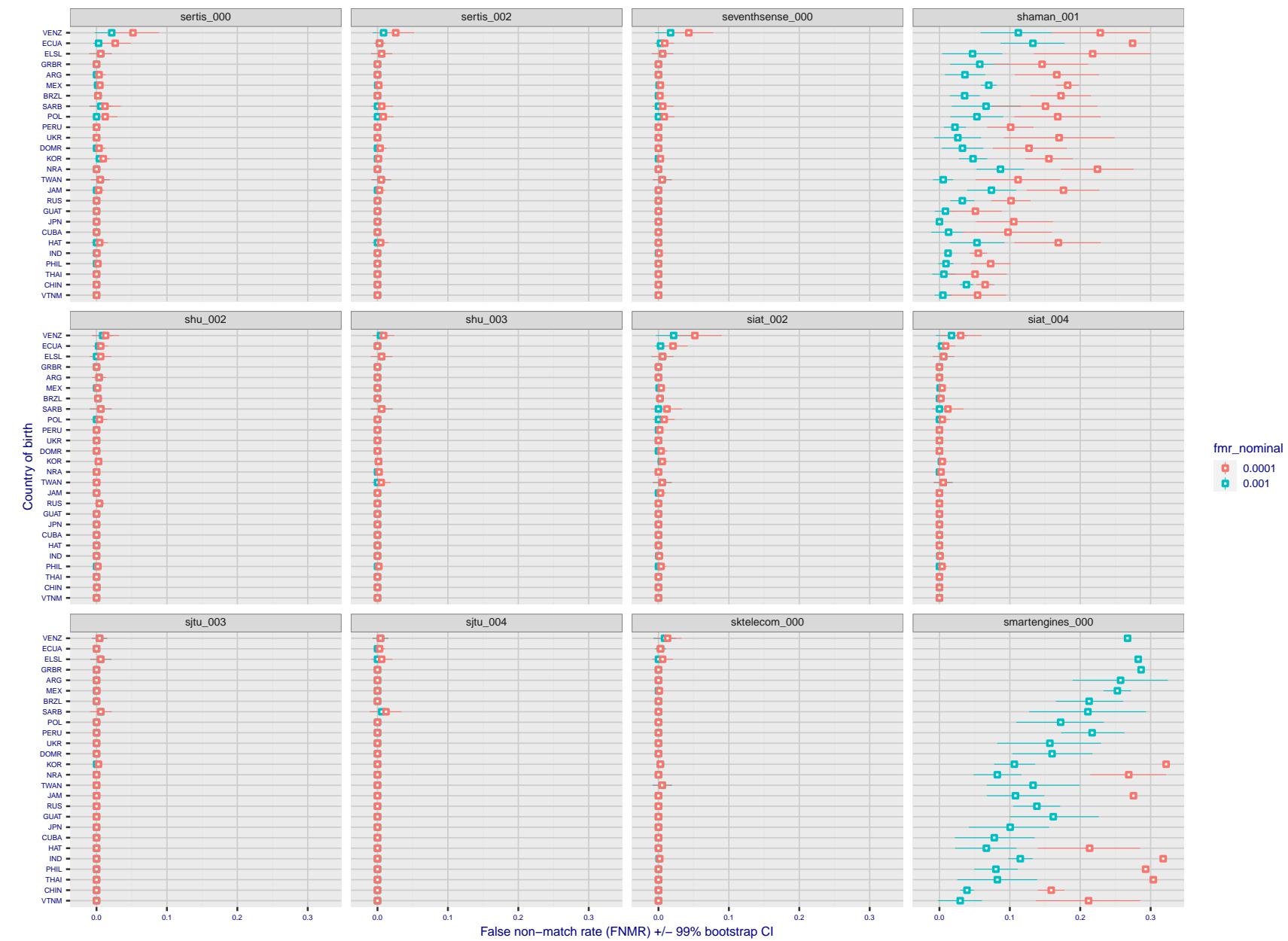


Figure 243: For the visa images, the dots show FNMR by country of birth for two globally set operating thresholds corresponding to $FMR = \{0.001, 0.0001\}$ computed over all on the order of 10^{10} impostor scores. The FMR in each bin will vary also - see subsequent impostor heatmaps in sec. 3.6.1. The figures shows an order of magnitude variation in FNMR across country of birth; these effects are likely due quality variations, then demographics like age and race. The error rates in some cases are zero, and in others the DET is flat so the error rates at the two thresholds are identical. The lines span 1% and 99% of bootstrap replicated FNMR estimates.

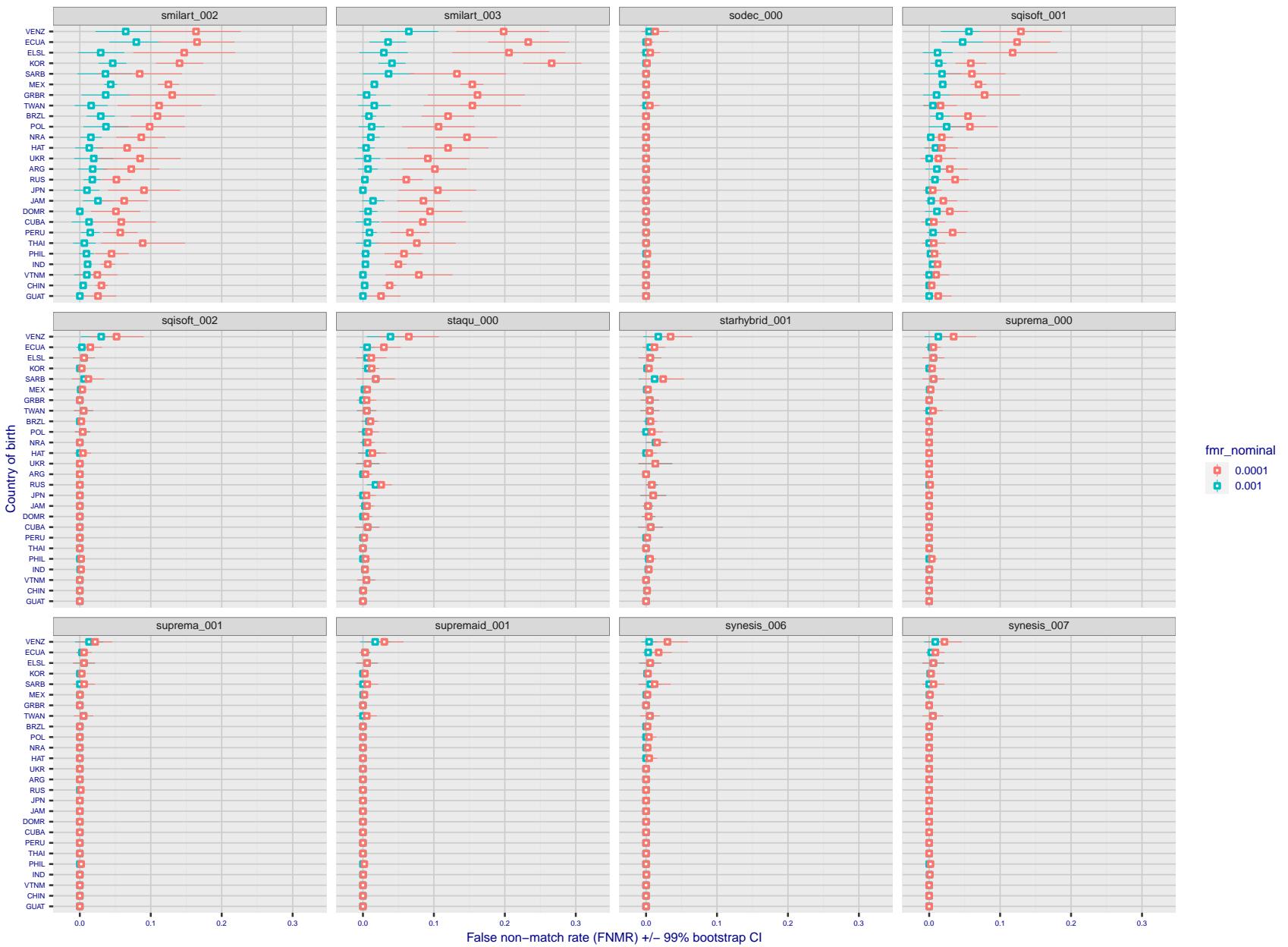


Figure 244: For the visa images, the dots show FNMR by country of birth for two globally set operating thresholds corresponding to $FMR = \{0.001, 0.0001\}$ computed over all on the order of 10^{10} impostor scores. The FMR in each bin will vary also - see subsequent impostor heatmaps in sec. 3.6.1. The figures shows an order of magnitude variation in FNMR across country of birth; these effects are likely due quality variations, then demographics like age and race. The error rates in some cases are zero, and in others the DET is flat so the error rates at the two thresholds are identical. The lines span 1% and 99% of bootstrap replicated FNMR estimates.

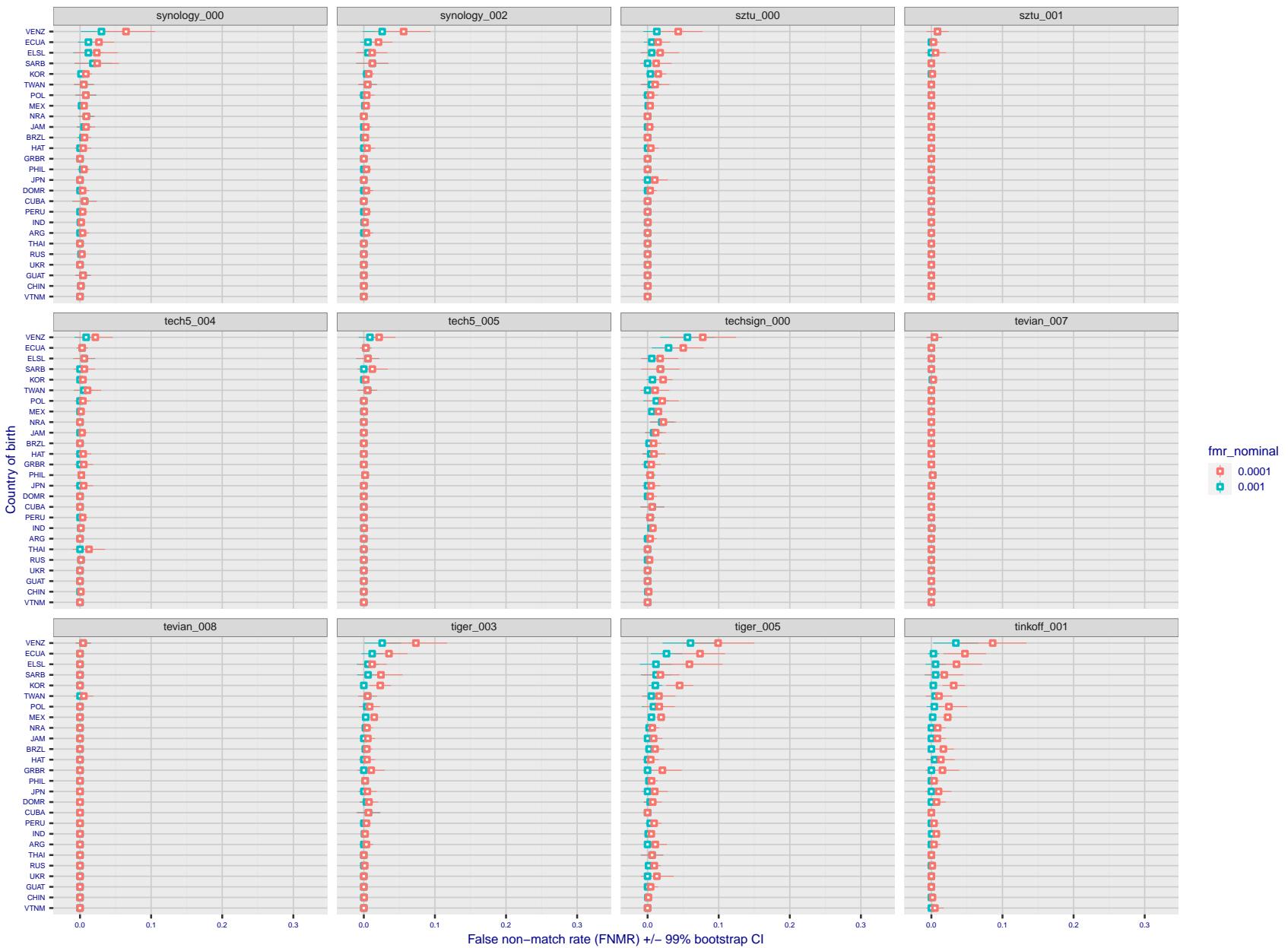


Figure 245: For the visa images, the dots show FNMR by country of birth for two globally set operating thresholds corresponding to $FMR = \{0.001, 0.0001\}$ computed over all on the order of 10^{10} impostor scores. The FMR in each bin will vary also - see subsequent impostor heatmaps in sec. 3.6.1. The figures shows an order of magnitude variation in FNMR across country of birth; these effects are likely due quality variations, then demographics like age and race. The error rates in some cases are zero, and in others the DET is flat so the error rates at the two thresholds are identical. The lines span 1% and 99% of bootstrap replicated FNMR estimates.

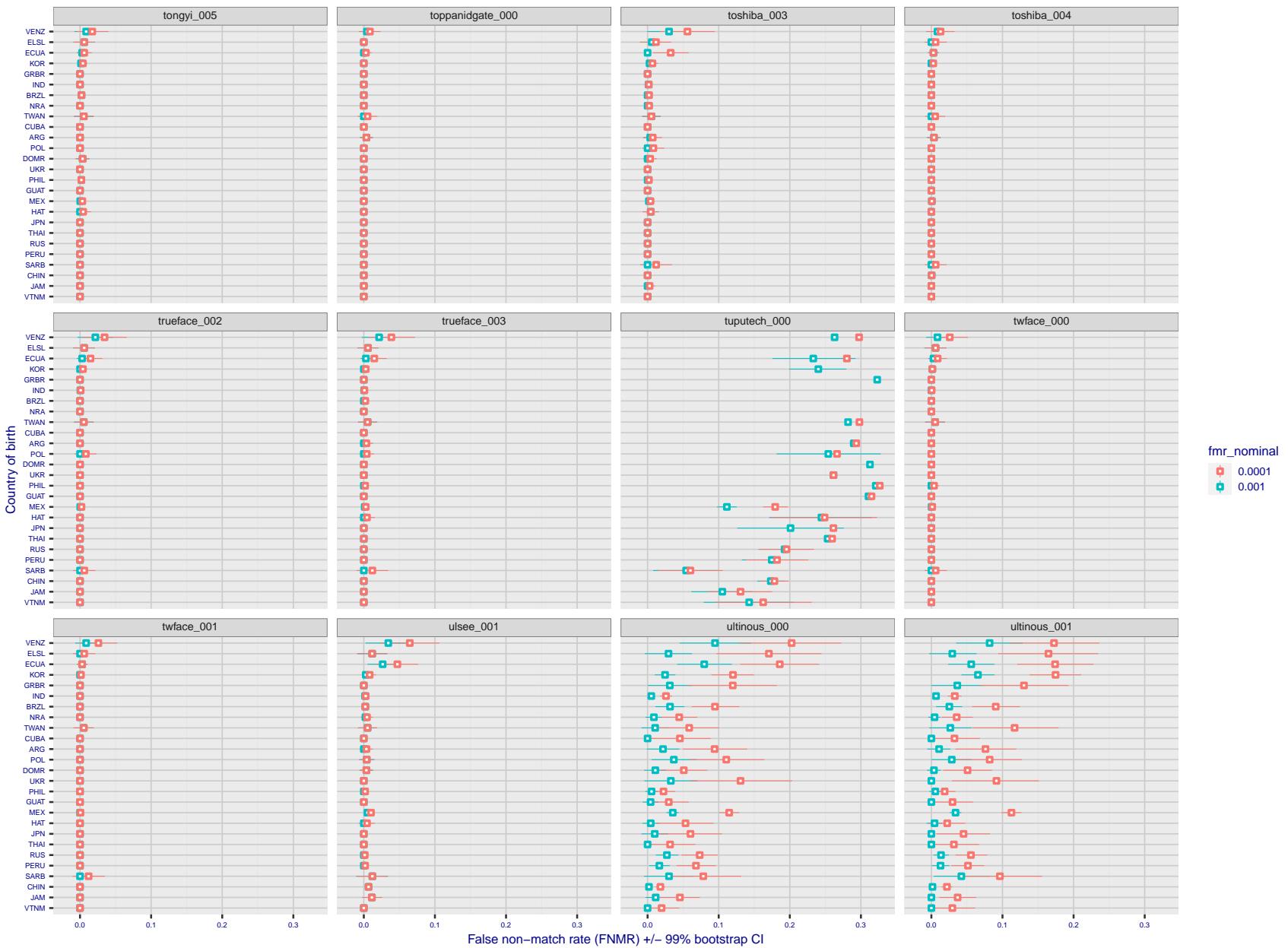


Figure 246: For the visa images, the dots show FNMR by country of birth for two globally set operating thresholds corresponding to $FMR = \{0.001, 0.0001\}$ computed over all on the order of 10^{10} impostor scores. The FMR in each bin will vary also - see subsequent impostor heatmaps in sec. 3.6.1. The figures shows an order of magnitude variation in FNMR across country of birth; these effects are likely due quality variations, then demographics like age and race. The error rates in some cases are zero, and in others the DET is flat so the error rates at the two thresholds are identical. The lines span 1% and 99% of bootstrap replicated FNMR estimates.

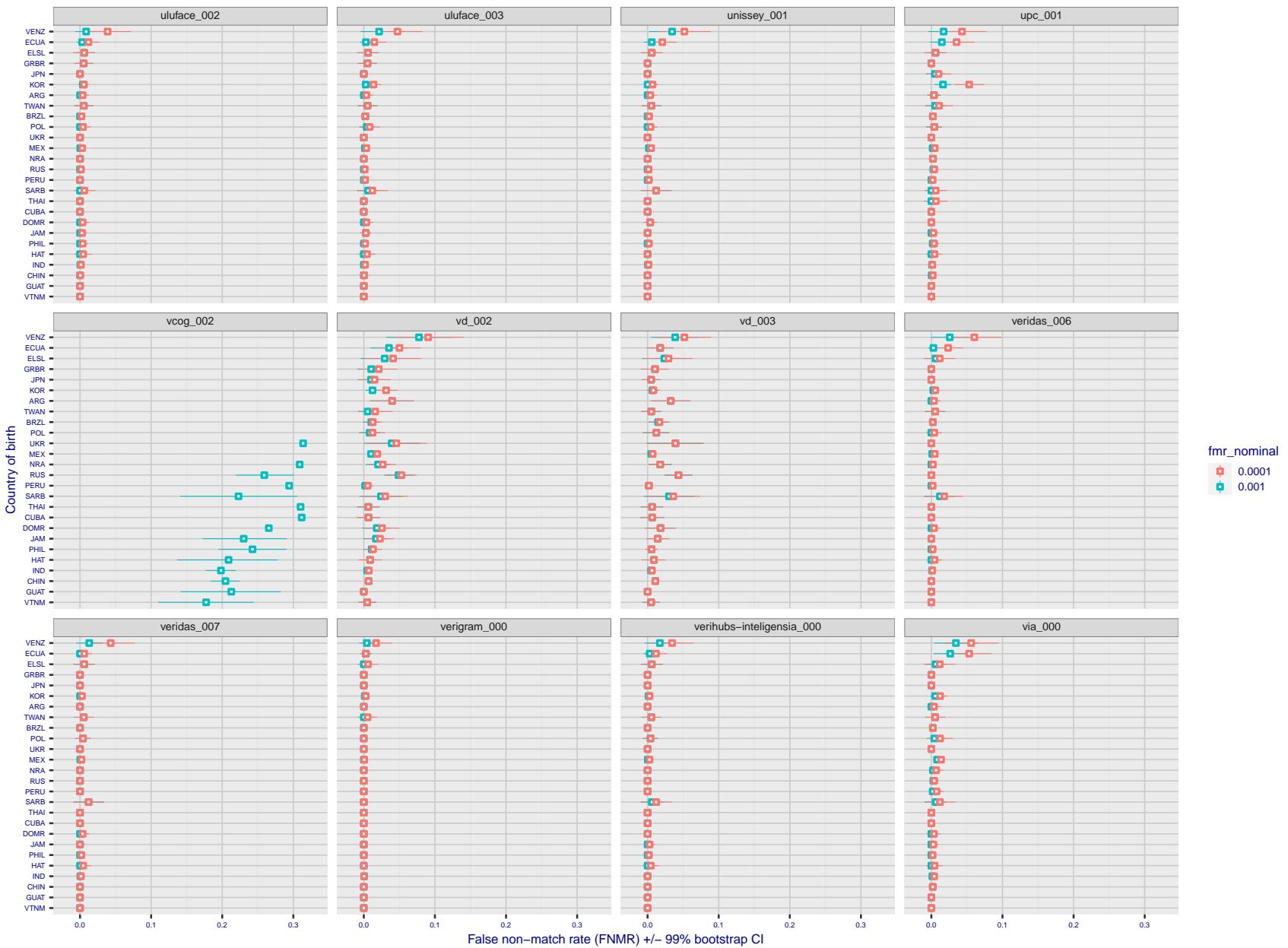


Figure 247: For the visa images, the dots show FNMR by country of birth for two globally set operating thresholds corresponding to $FMR = \{0.001, 0.0001\}$ computed over all on the order of 10^{10} impostor scores. The FMR in each bin will vary also - see subsequent impostor heatmaps in sec. 3.6.1. The figures shows an order of magnitude variation in FNMR across country of birth; these effects are likely due quality variations, then demographics like age and race. The error rates in some cases are zero, and in others the DET is flat so the error rates at the two thresholds are identical. The lines span 1% and 99% of bootstrap replicated FNMR estimates.

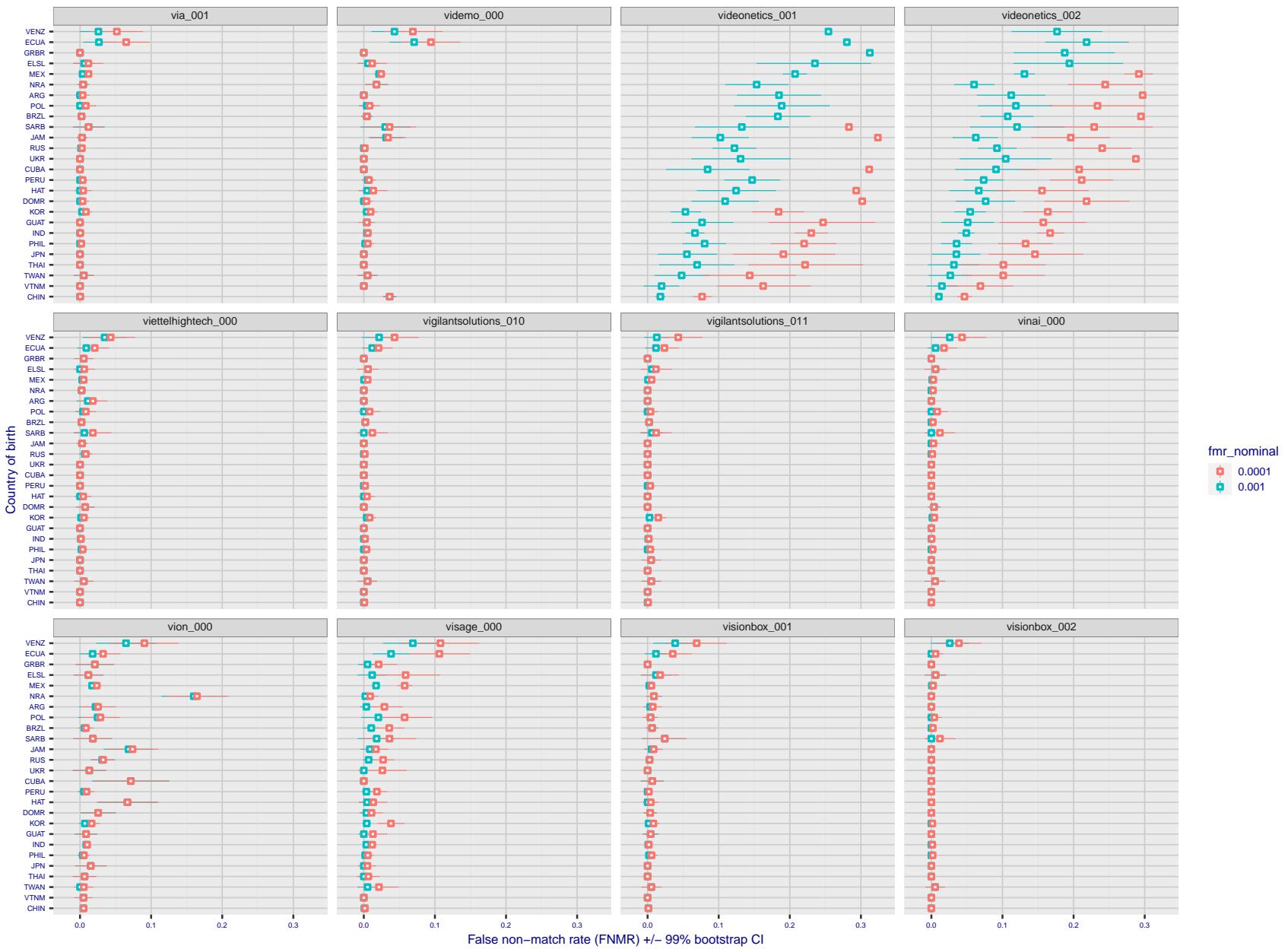


Figure 248: For the visa images, the dots show FNMR by country of birth for two globally set operating thresholds corresponding to $FMR = \{0.001, 0.0001\}$ computed over all on the order of 10^{10} impostor scores. The FMR in each bin will vary also - see subsequent impostor heatmaps in sec. 3.6.1. The figures shows an order of magnitude variation in FNMR across country of birth; these effects are likely due quality variations, then demographics like age and race. The error rates in some cases are zero, and in others the DET is flat so the error rates at the two thresholds are identical. The lines span 1% and 99% of bootstrap replicated FNMR estimates.

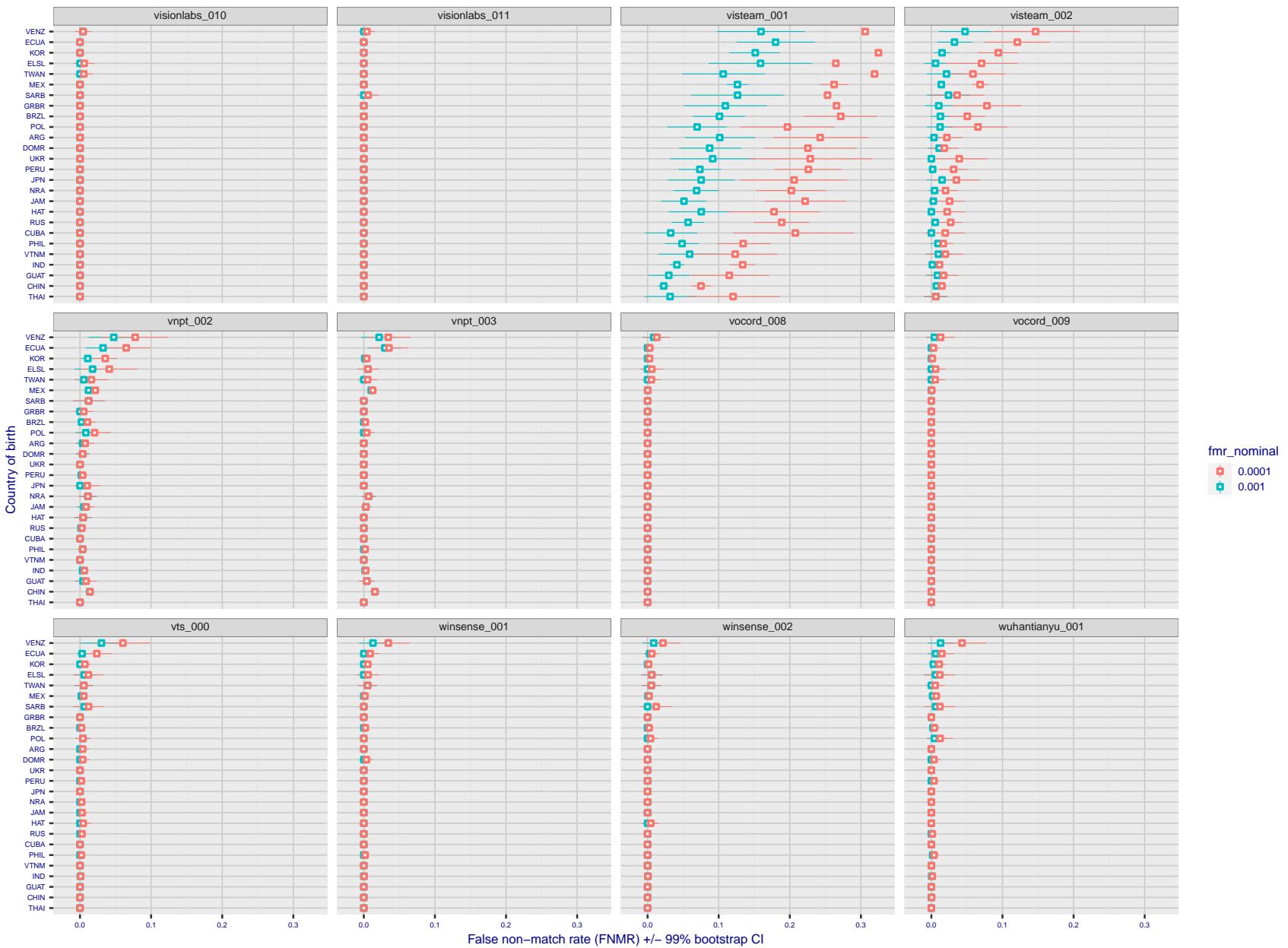


Figure 249: For the visa images, the dots show FNMR by country of birth for two globally set operating thresholds corresponding to $FMR = \{0.001, 0.0001\}$ computed over all on the order of 10^{10} impostor scores. The FMR in each bin will vary also - see subsequent impostor heatmaps in sec. 3.6.1. The figures shows an order of magnitude variation in FNMR across country of birth; these effects are likely due quality variations, then demographics like age and race. The error rates in some cases are zero, and in others the DET is flat so the error rates at the two thresholds are identical. The lines span 1% and 99% of bootstrap replicated FNMR estimates.

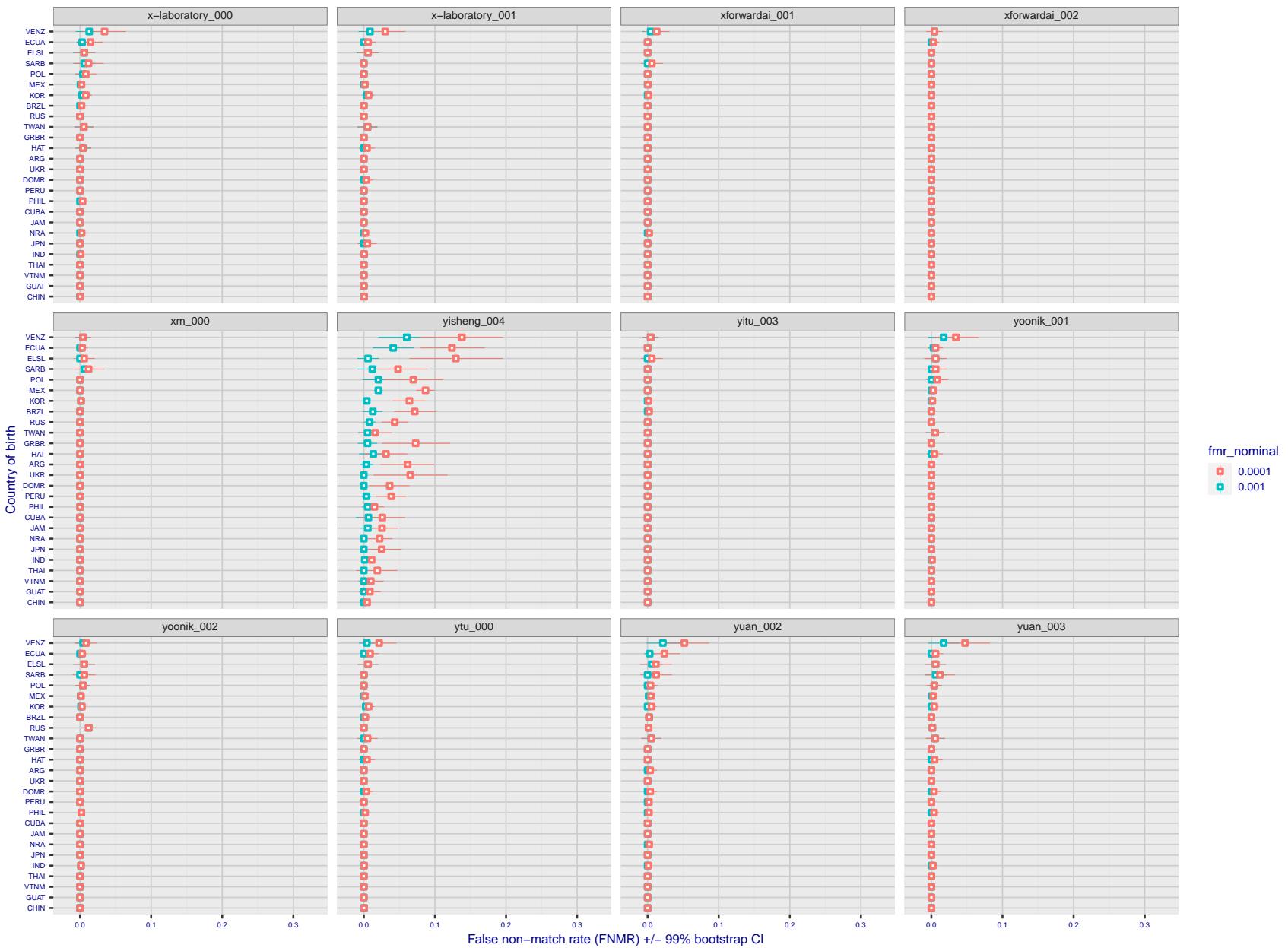


Figure 250: For the visa images, the dots show FNMR by country of birth for two globally set operating thresholds corresponding to $FMR = \{0.001, 0.0001\}$ computed over all on the order of 10^{10} impostor scores. The FMR in each bin will vary also - see subsequent impostor heatmaps in sec. 3.6.1. The figures shows an order of magnitude variation in FNMR across country of birth; these effects are likely due quality variations, then demographics like age and race. The error rates in some cases are zero, and in others the DET is flat so the error rates at the two thresholds are identical. The lines span 1% and 99% of bootstrap replicated FNMR estimates.

Caveats: The results may not relate to subject-specific properties. Instead they could reflect image-specific quality differences, which could occur due to collection protocol or software processing variations.

3.5.2 Effect of ageing

Background: Faces change appearance throughout life. This change gradually reduces similarity of a new image to an earlier image. Face recognition algorithms give reduced similarity scores and more frequent false rejections.

Goal: To quantify false non-match rates (FNMR) as a function of elapsed time in an adult population.

Methods: Using the mugshot images, a threshold is set to give FMR = 0.00001 over the entire impostor set. Then FNMR is measured over 1000 bootstrap replications of the genuine scores.

Results: For the visa images, Figure 273 shows how false non-match rates for genuine users, as a function of age group.

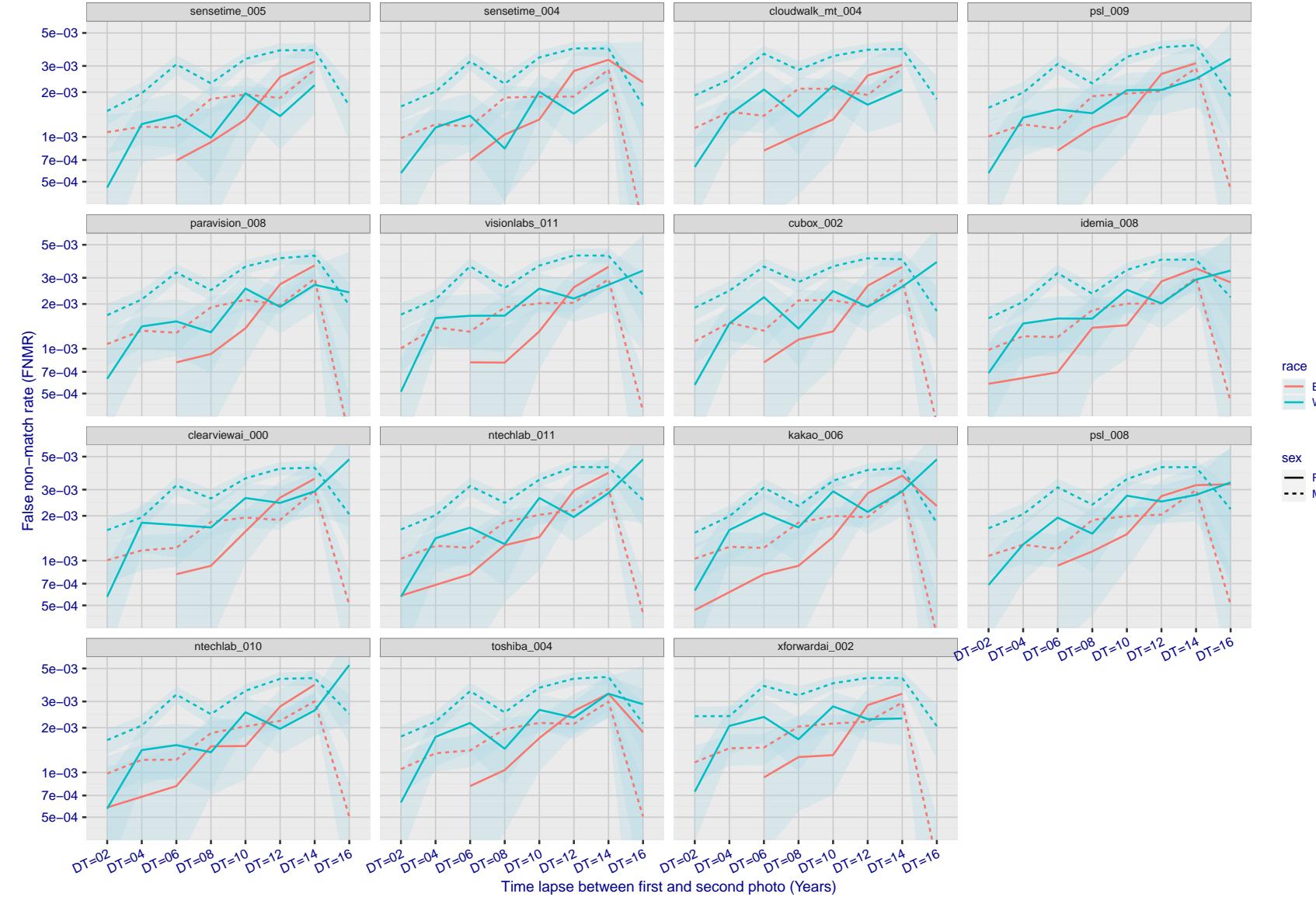


Figure 251: For the mugshot images, FNMR as a function of elapsed time between initial enrollment and second verification images. The panels appear most accurate first, and vertical scale changes on each page. The four traces correspond to images annotated with codes for black female, black male, white female, white male. The threshold is fixed for each algorithm to give FMR = 0.00001 over all (10^8) impostor comparisons. For short time-lapses, the most accurate algorithms give very few errors (FNMR < 0.001) so that the uncertainty estimates are high.

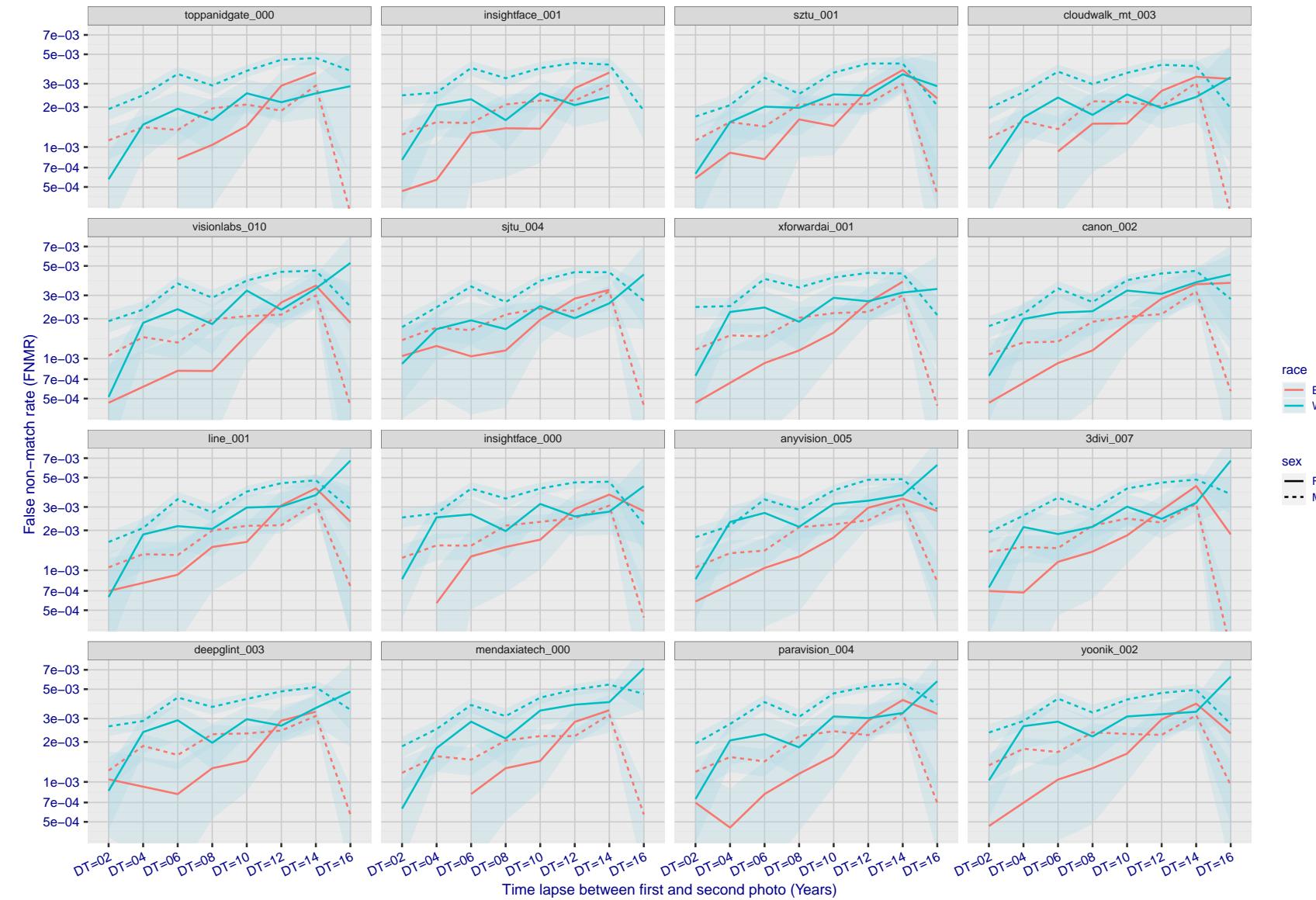


Figure 252: For the mugshot images, FNMR as a function of elapsed time between initial enrollment and second verification images. The panels appear most accurate first, and vertical scale changes on each page. The four traces correspond to images annotated with codes for black female, black male, white female, white male. The threshold is fixed for each algorithm to give $FMR = 0.00001$ over all (10^8) impostor comparisons. For short time-lapses, the most accurate algorithms give very few errors ($FNMR < 0.001$) so that the uncertainty estimates are high.

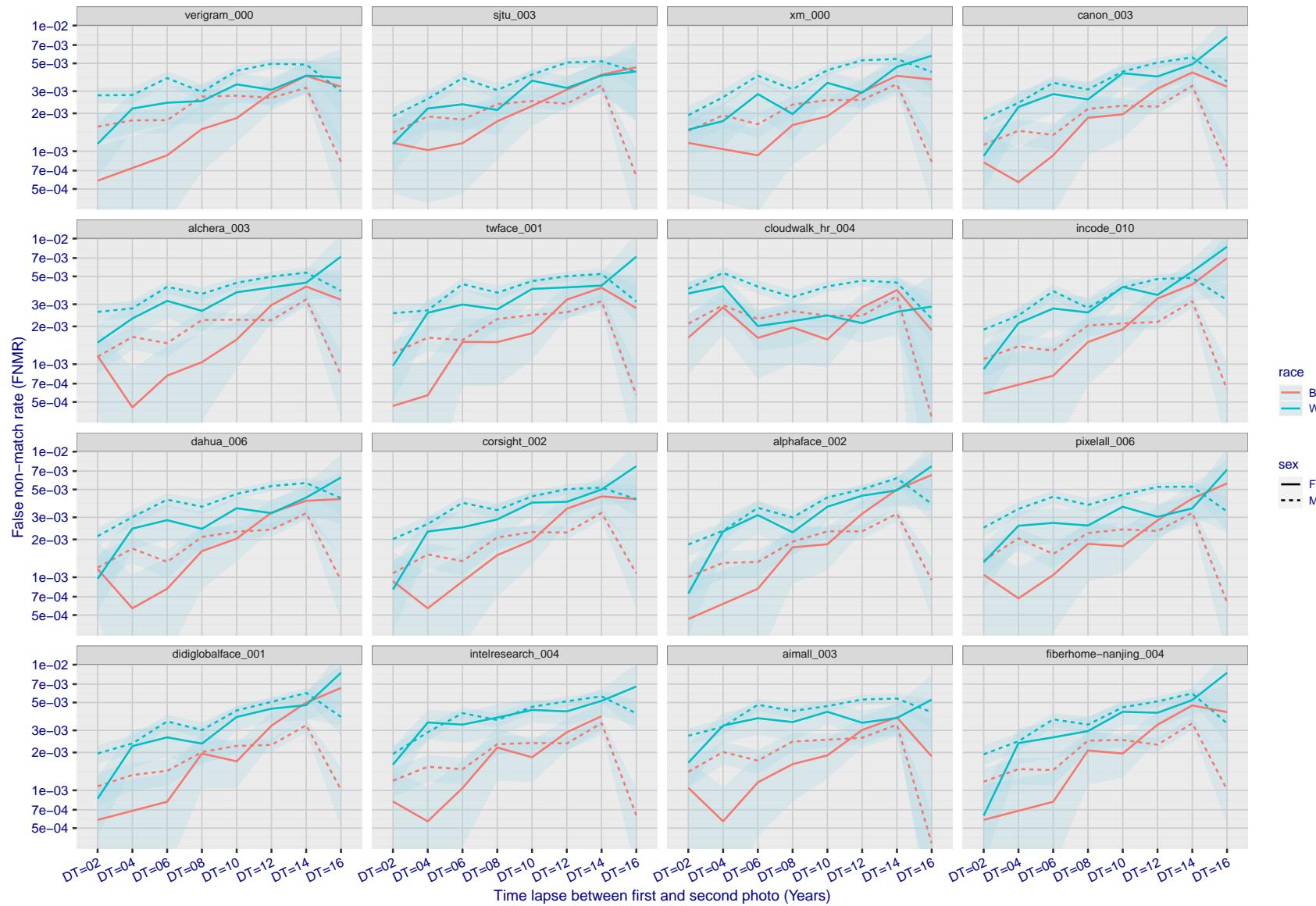


Figure 253: For the mugshot images, FNMR as a function of elapsed time between initial enrollment and second verification images. The panels appear most accurate first, and vertical scale changes on each page. The four traces correspond to images annotated with codes for black female, black male, white female, white male. The threshold is fixed for each algorithm to give $FMR = 0.00001$ over all (10^8) impostor comparisons. For short time-lapses, the most accurate algorithms give very few errors ($FNMR < 0.001$) so that the uncertainty estimates are high.

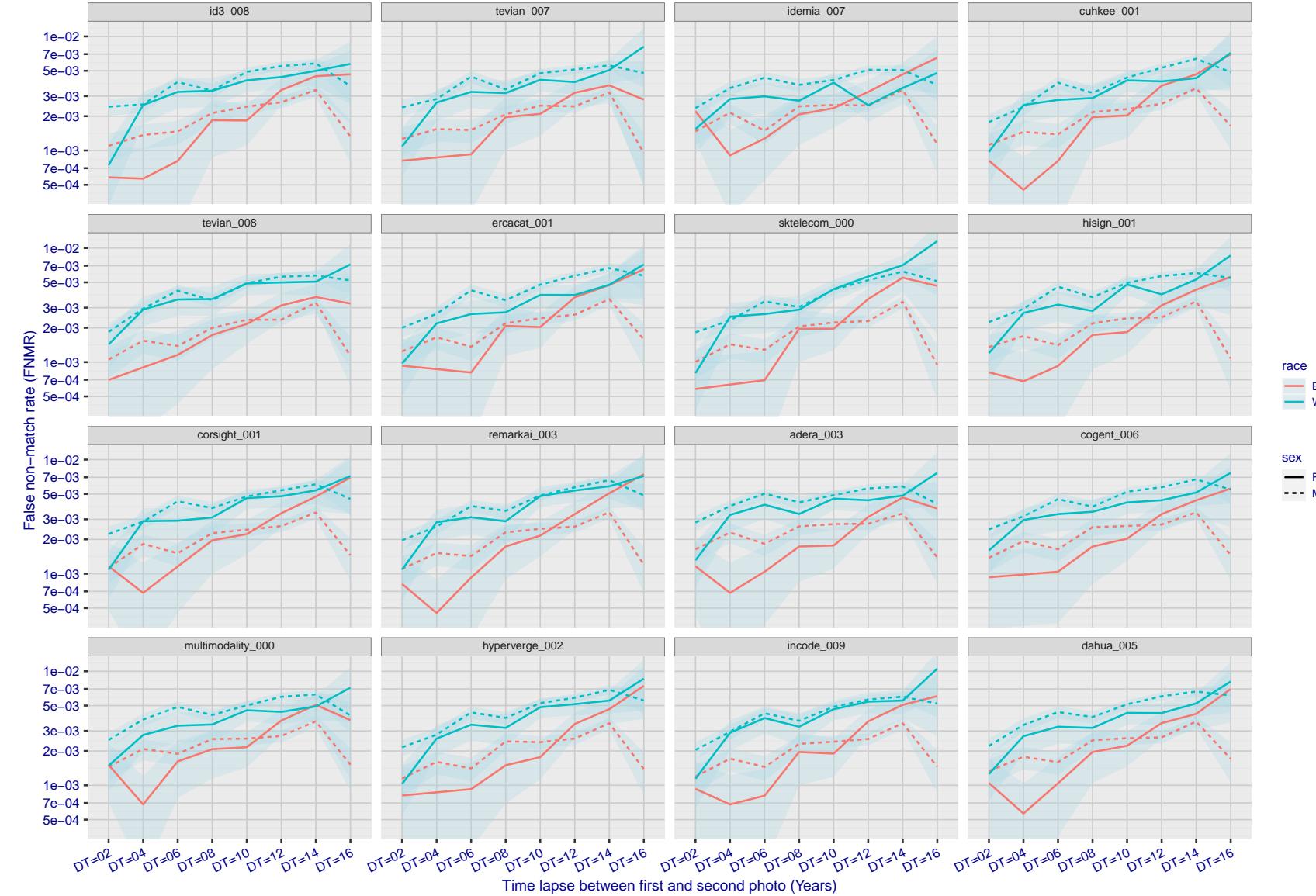


Figure 254: For the mugshot images, FNMR as a function of elapsed time between initial enrollment and second verification images. The panels appear most accurate first, and vertical scale changes on each page. The four traces correspond to images annotated with codes for black female, black male, white female, white male. The threshold is fixed for each algorithm to give $FMR = 0.00001$ over all (10^8) impostor comparisons. For short time-lapses, the most accurate algorithms give very few errors ($FNMR < 0.001$) so that the uncertainty estimates are high.

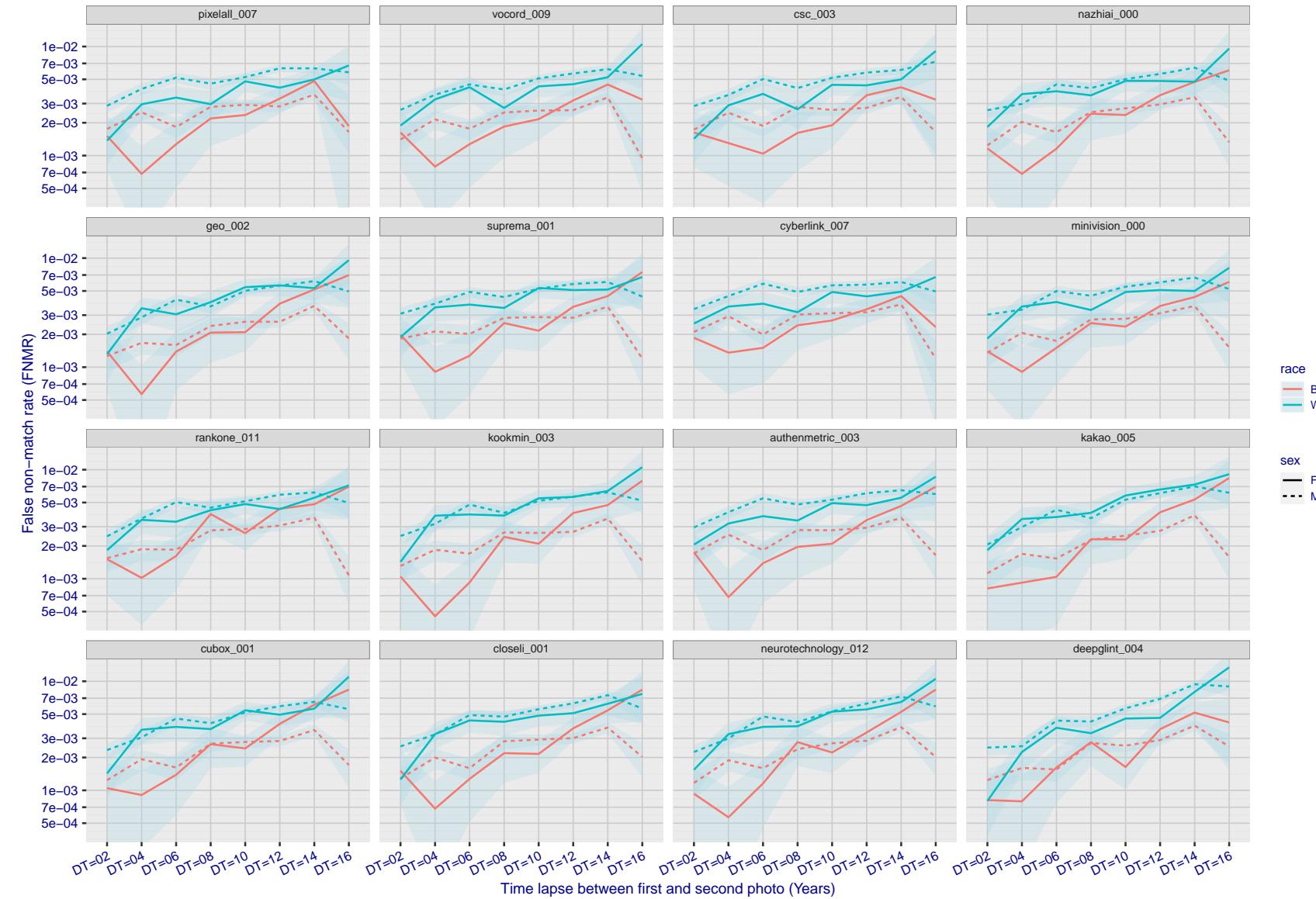


Figure 255: For the mugshot images, FNMR as a function of elapsed time between initial enrollment and second verification images. The panels appear most accurate first, and vertical scale changes on each page. The four traces correspond to images annotated with codes for black female, black male, white female, white male. The threshold is fixed for each algorithm to give $FMR = 0.00001$ over all (10^8) impostor comparisons. For short time-lapses, the most accurate algorithms give very few errors ($FNMR < 0.001$) so that the uncertainty estimates are high.

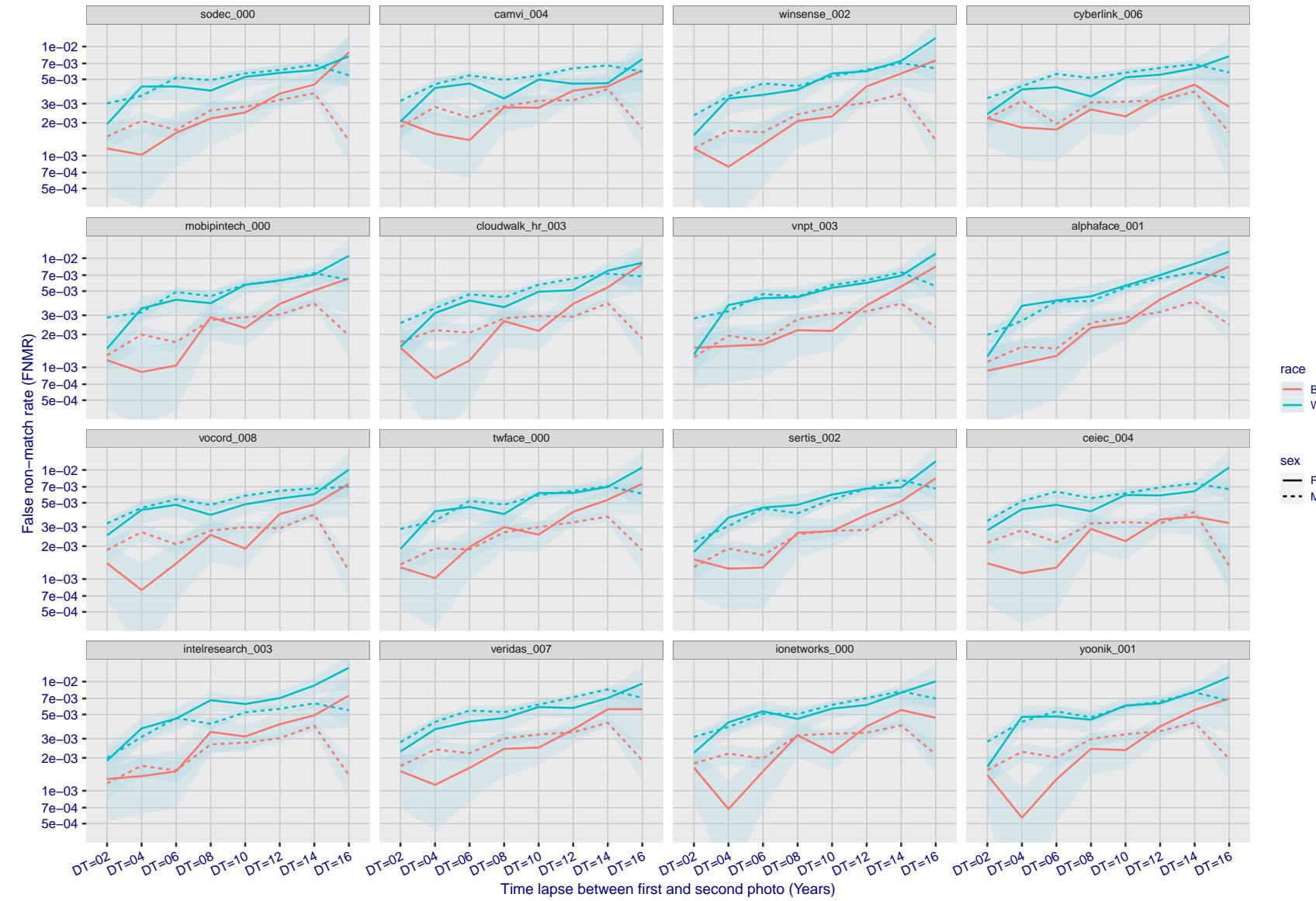


Figure 256: For the mugshot images, FNMR as a function of elapsed time between initial enrollment and second verification images. The panels appear most accurate first, and vertical scale changes on each page. The four traces correspond to images annotated with codes for black female, black male, white female, white male. The threshold is fixed for each algorithm to give $FMR = 0.00001$ over all (10^8) impostor comparisons. For short time-lapses, the most accurate algorithms give very few errors ($FNMR < 0.001$) so that the uncertainty estimates are high.

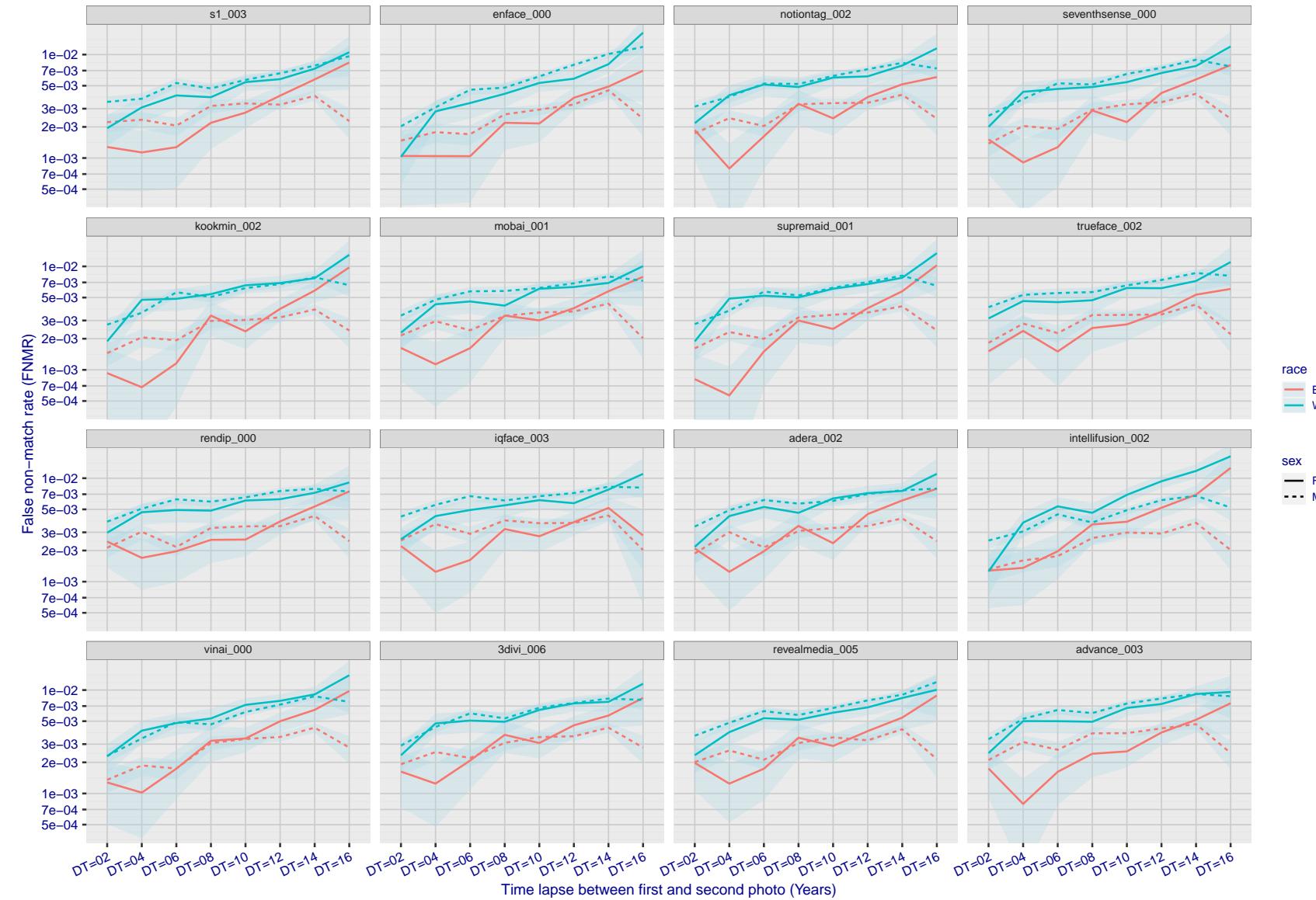


Figure 257: For the mugshot images, FNMR as a function of elapsed time between initial enrollment and second verification images. The panels appear most accurate first, and vertical scale changes on each page. The four traces correspond to images annotated with codes for black female, black male, white female, white male. The threshold is fixed for each algorithm to give FMR = 0.00001 over all (10^8) impostor comparisons. For short time-lapses, the most accurate algorithms give very few errors (FNMR < 0.001) so that the uncertainty estimates are high.

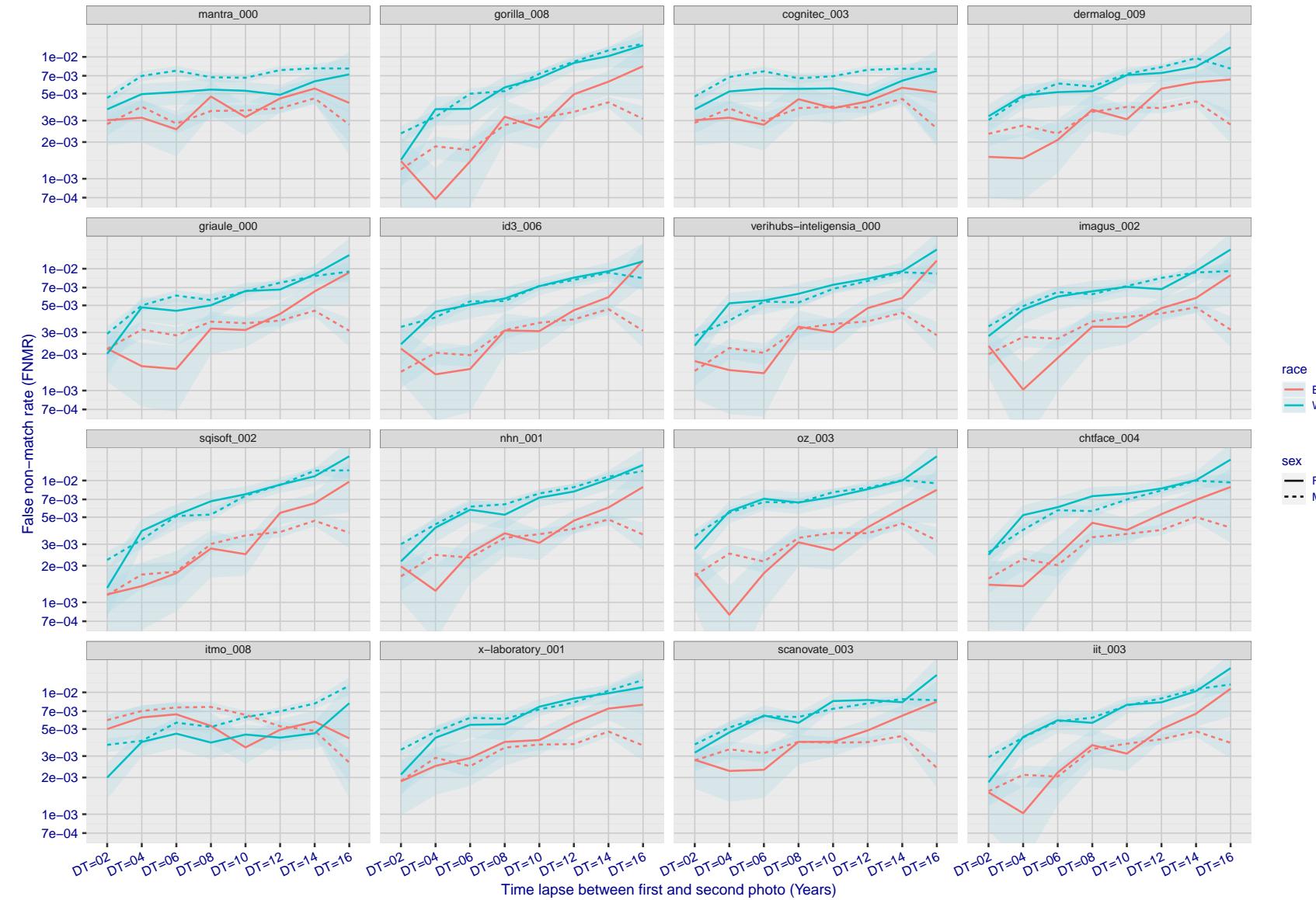


Figure 258: For the mugshot images, FNMR as a function of elapsed time between initial enrollment and second verification images. The panels appear most accurate first, and vertical scale changes on each page. The four traces correspond to images annotated with codes for black female, black male, white female, white male. The threshold is fixed for each algorithm to give $FMR = 0.00001$ over all (10^8) impostor comparisons. For short time-lapses, the most accurate algorithms give very few errors ($FNMR < 0.001$) so that the uncertainty estimates are high.

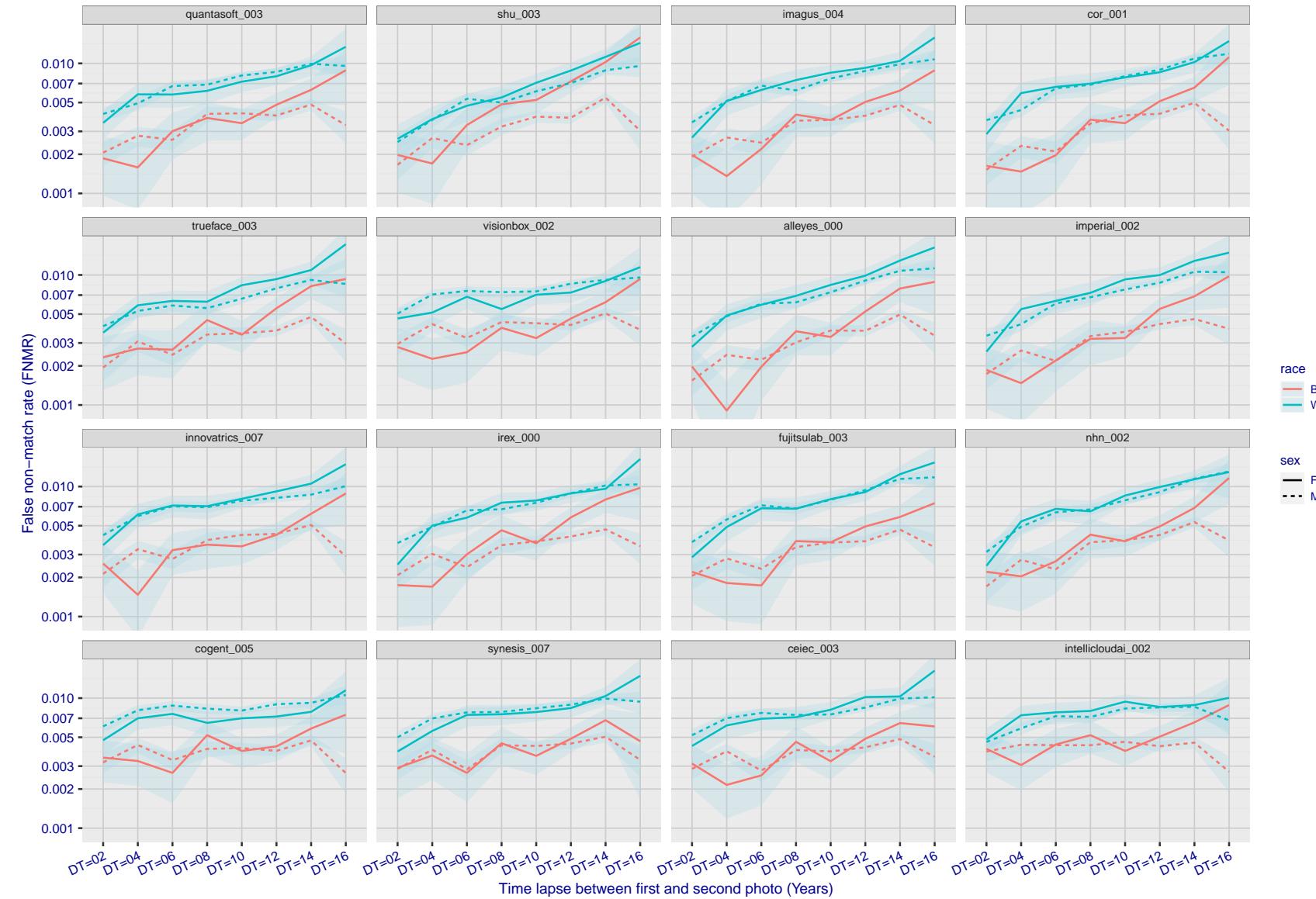


Figure 259: For the mugshot images, FNMR as a function of elapsed time between initial enrollment and second verification images. The panels appear most accurate first, and vertical scale changes on each page. The four traces correspond to images annotated with codes for black female, black male, white female, white male. The threshold is fixed for each algorithm to give FMR = 0.00001 over all (10^8) impostor comparisons. For short time-lapses, the most accurate algorithms give very few errors (FNMR < 0.001) so that the uncertainty estimates are high.

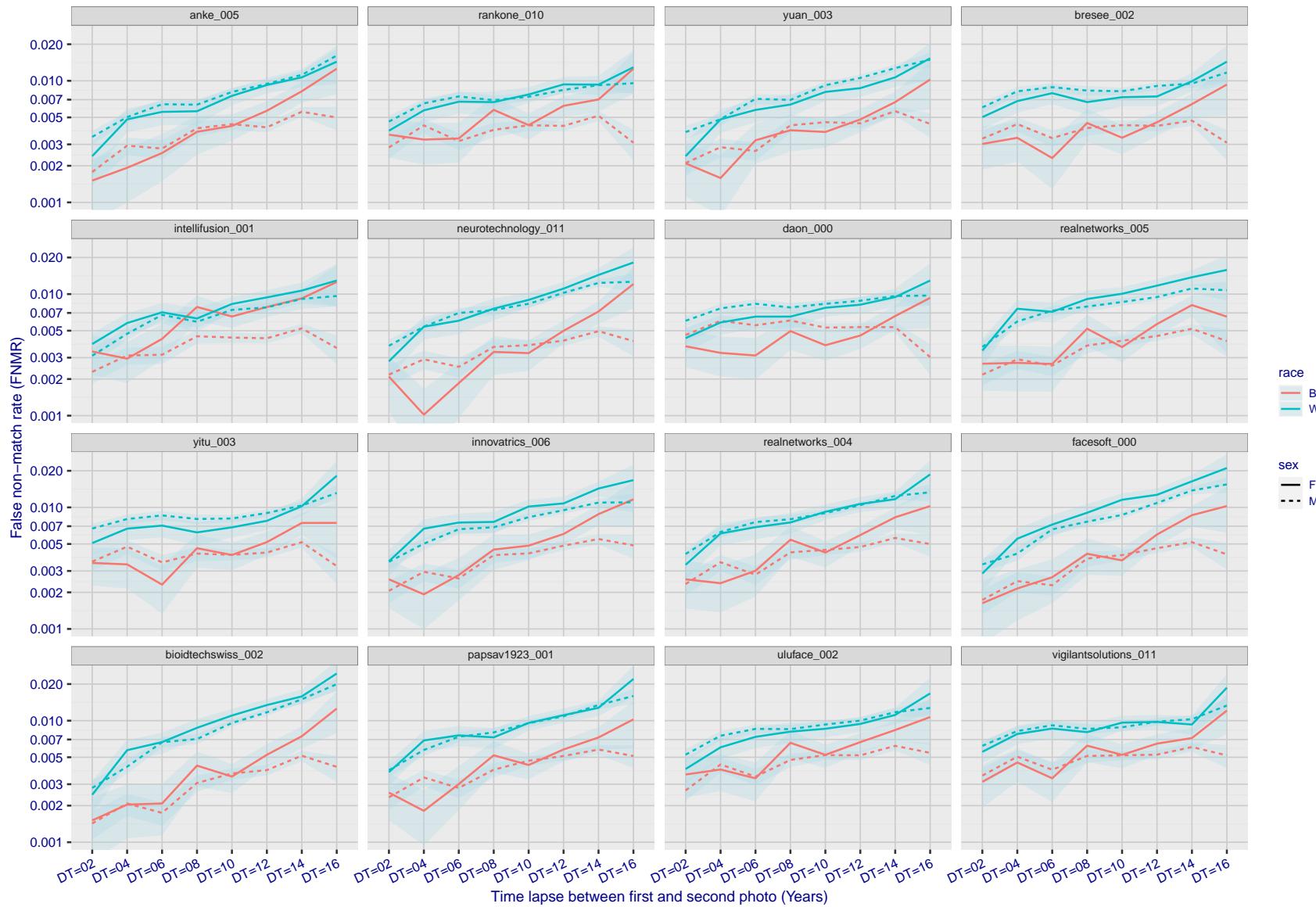


Figure 260: For the mugshot images, FNMR as a function of elapsed time between initial enrollment and second verification images. The panels appear most accurate first, and vertical scale changes on each page. The four traces correspond to images annotated with codes for black female, black male, white female, white male. The threshold is fixed for each algorithm to give FMR = 0.00001 over all (10^8) impostor comparisons. For short time-lapses, the most accurate algorithms give very few errors (FNMR < 0.001) so that the uncertainty estimates are high.

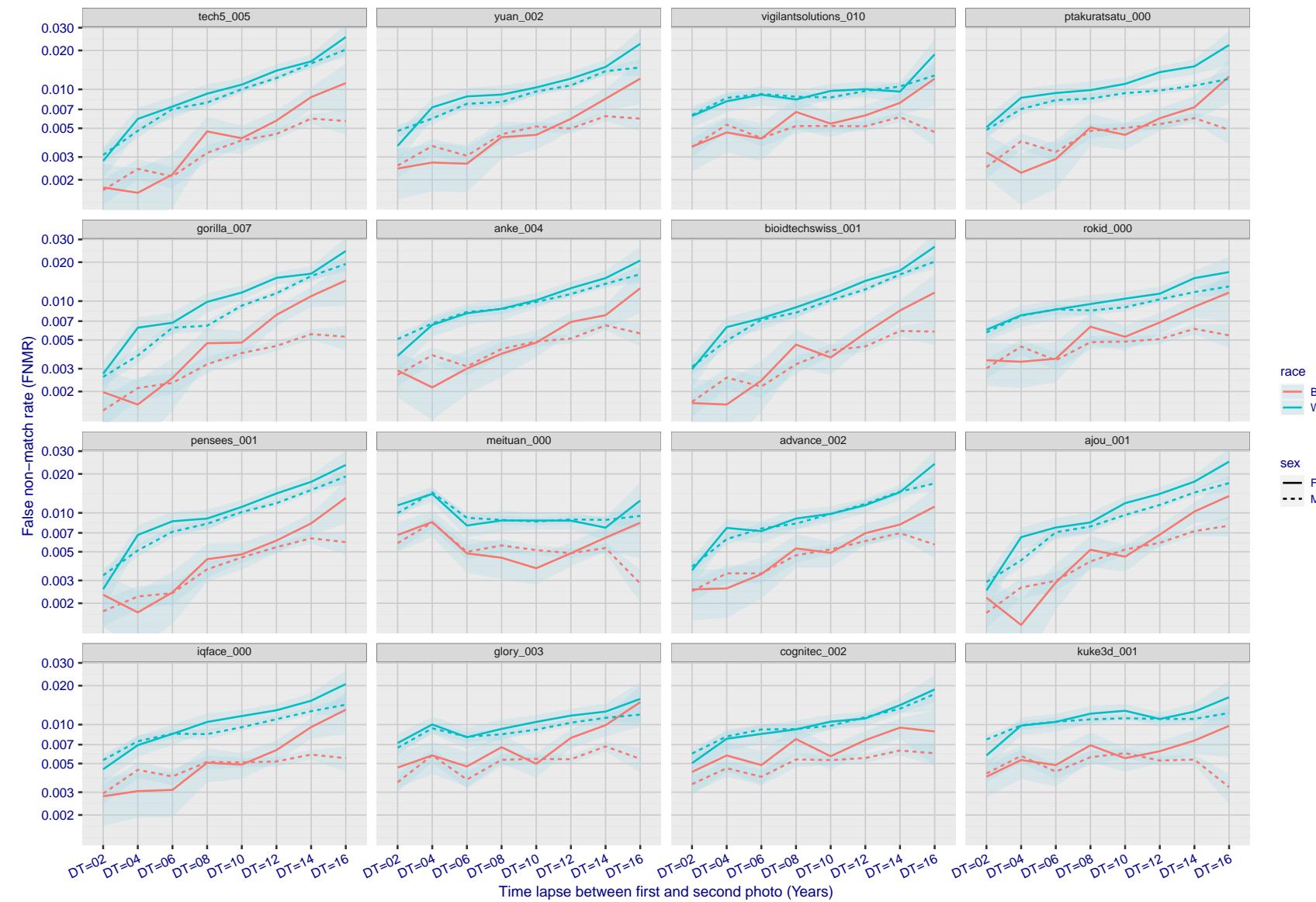


Figure 261: For the mugshot images, FNMR as a function of elapsed time between initial enrollment and second verification images. The panels appear most accurate first, and vertical scale changes on each page. The four traces correspond to images annotated with codes for black female, black male, white female, white male. The threshold is fixed for each algorithm to give FMR = 0.00001 over all (10^8) impostor comparisons. For short time-lapses, the most accurate algorithms give very few errors (FNMR < 0.001) so that the uncertainty estimates are high.

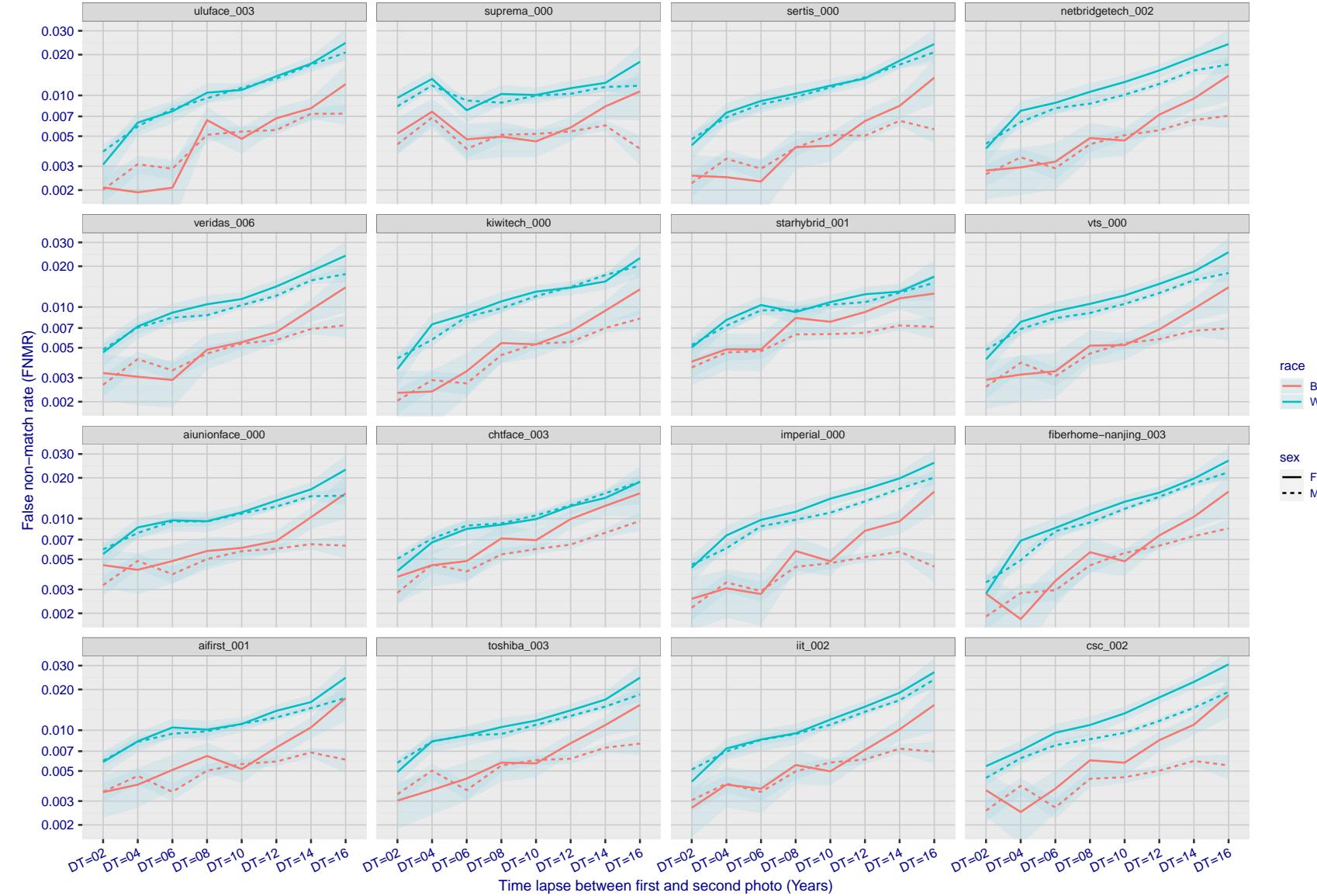


Figure 262: For the mugshot images, FNMR as a function of elapsed time between initial enrollment and second verification images. The panels appear most accurate first, and vertical scale changes on each page. The four traces correspond to images annotated with codes for black female, black male, white female, white male. The threshold is fixed for each algorithm to give FMR = 0.00001 over all (10^8) impostor comparisons. For short time-lapses, the most accurate algorithms give very few errors (FNMR < 0.001) so that the uncertainty estimates are high.

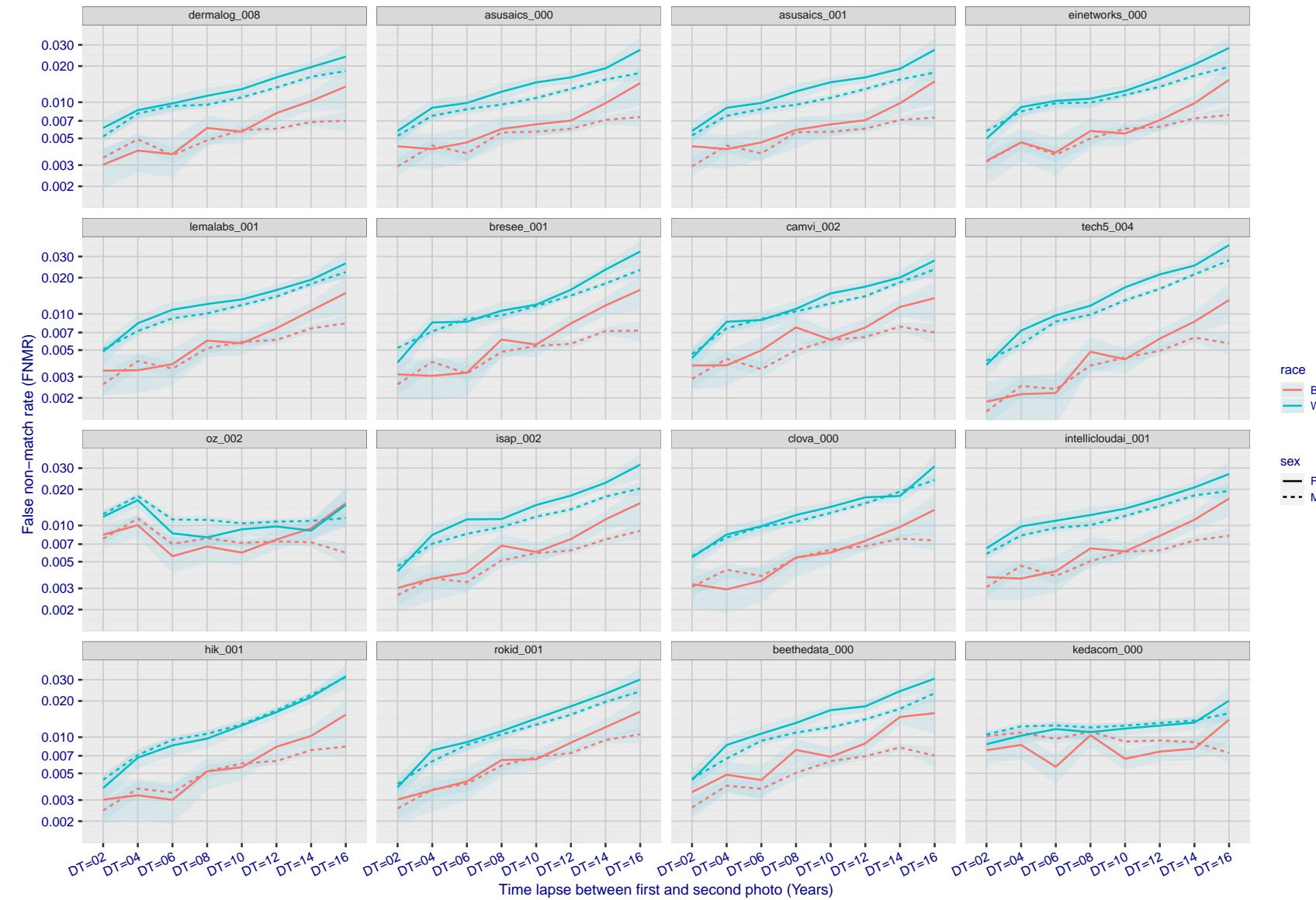


Figure 263: For the mugshot images, FNMR as a function of elapsed time between initial enrollment and second verification images. The panels appear most accurate first, and vertical scale changes on each page. The four traces correspond to images annotated with codes for black female, black male, white female, white male. The threshold is fixed for each algorithm to give FMR = 0.00001 over all (10^8) impostor comparisons. For short time-lapses, the most accurate algorithms give very few errors (FNMR < 0.001) so that the uncertainty estimates are high.

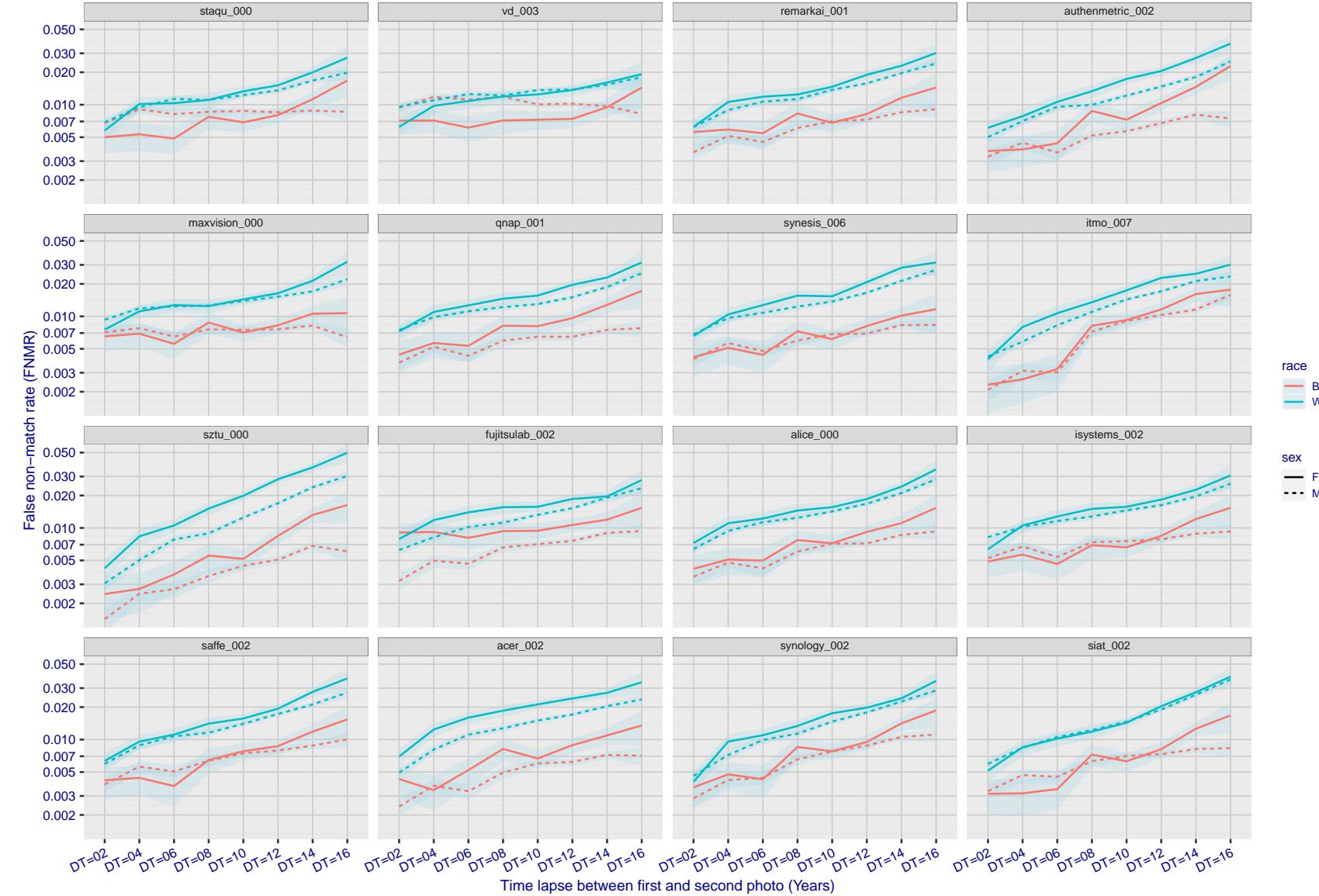
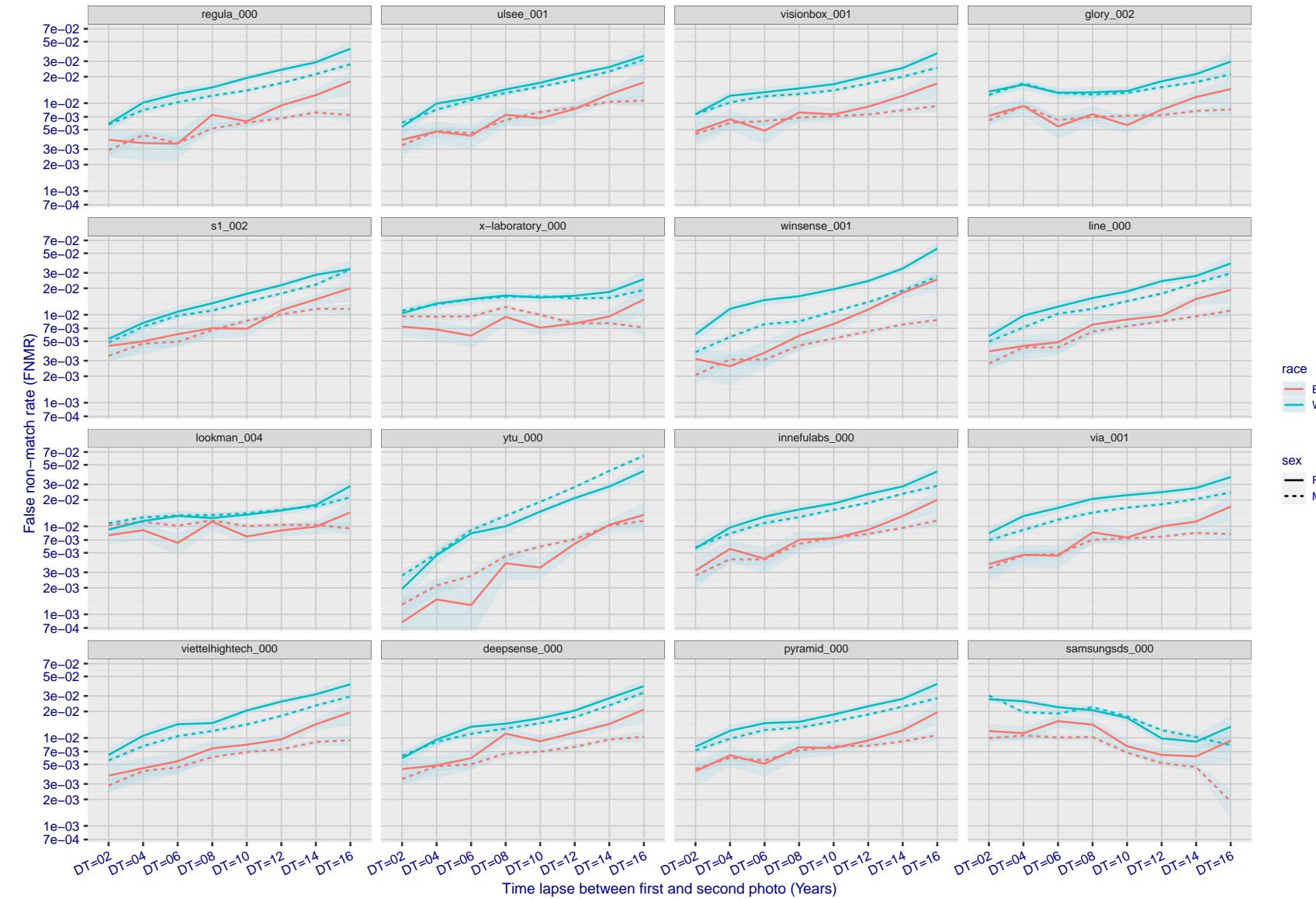


Figure 264: For the mugshot images, FNMR as a function of elapsed time between initial enrollment and second verification images. The panels appear most accurate first, and vertical scale changes on each page. The four traces correspond to images annotated with codes for black female, black male, white female, white male. The threshold is fixed for each algorithm to give FMR = 0.00001 over all (10^8) impostor comparisons. For short time-lapses, the most accurate algorithms give very few errors (FNMR < 0.001) so that the uncertainty estimates are high.



race
B
W
sex
F
M

Figure 265: For the mugshot images, FNMR as a function of elapsed time between initial enrollment and second verification images. The panels appear most accurate first, and vertical scale changes on each page. The four traces correspond to images annotated with codes for black female, black male, white female, white male. The threshold is fixed for each algorithm to give $FMR = 0.00001$ over all (10^8) impostor comparisons. For short time-lapses, the most accurate algorithms give very few errors ($FNMR < 0.001$) so that the uncertainty estimates are high.

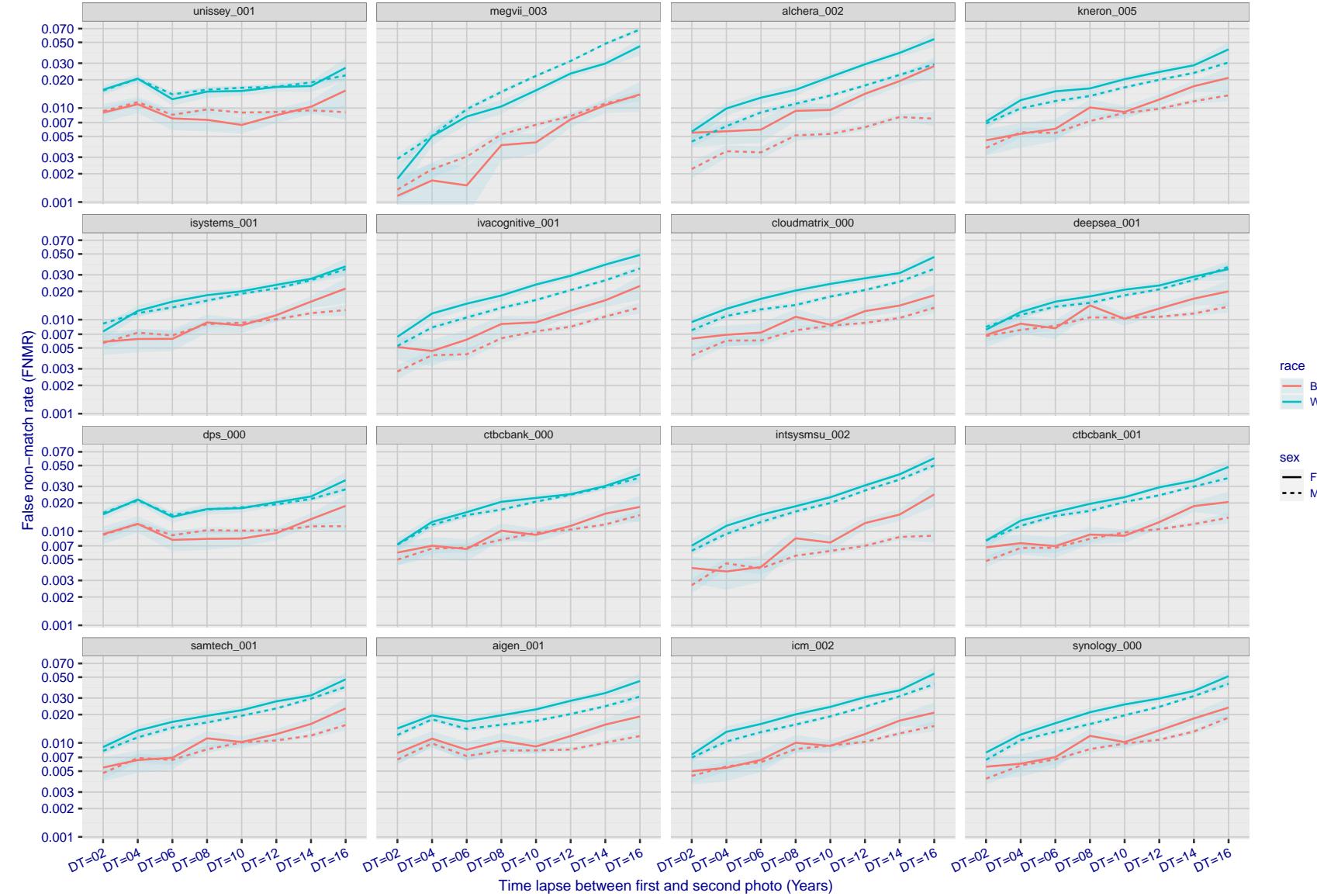


Figure 266: For the mugshot images, FNMR as a function of elapsed time between initial enrollment and second verification images. The panels appear most accurate first, and vertical scale changes on each page. The four traces correspond to images annotated with codes for black female, black male, white female, white male. The threshold is fixed for each algorithm to give FMR = 0.00001 over all (10^8) impostor comparisons. For short time-lapses, the most accurate algorithms give very few errors (FNMR < 0.001) so that the uncertainty estimates are high.

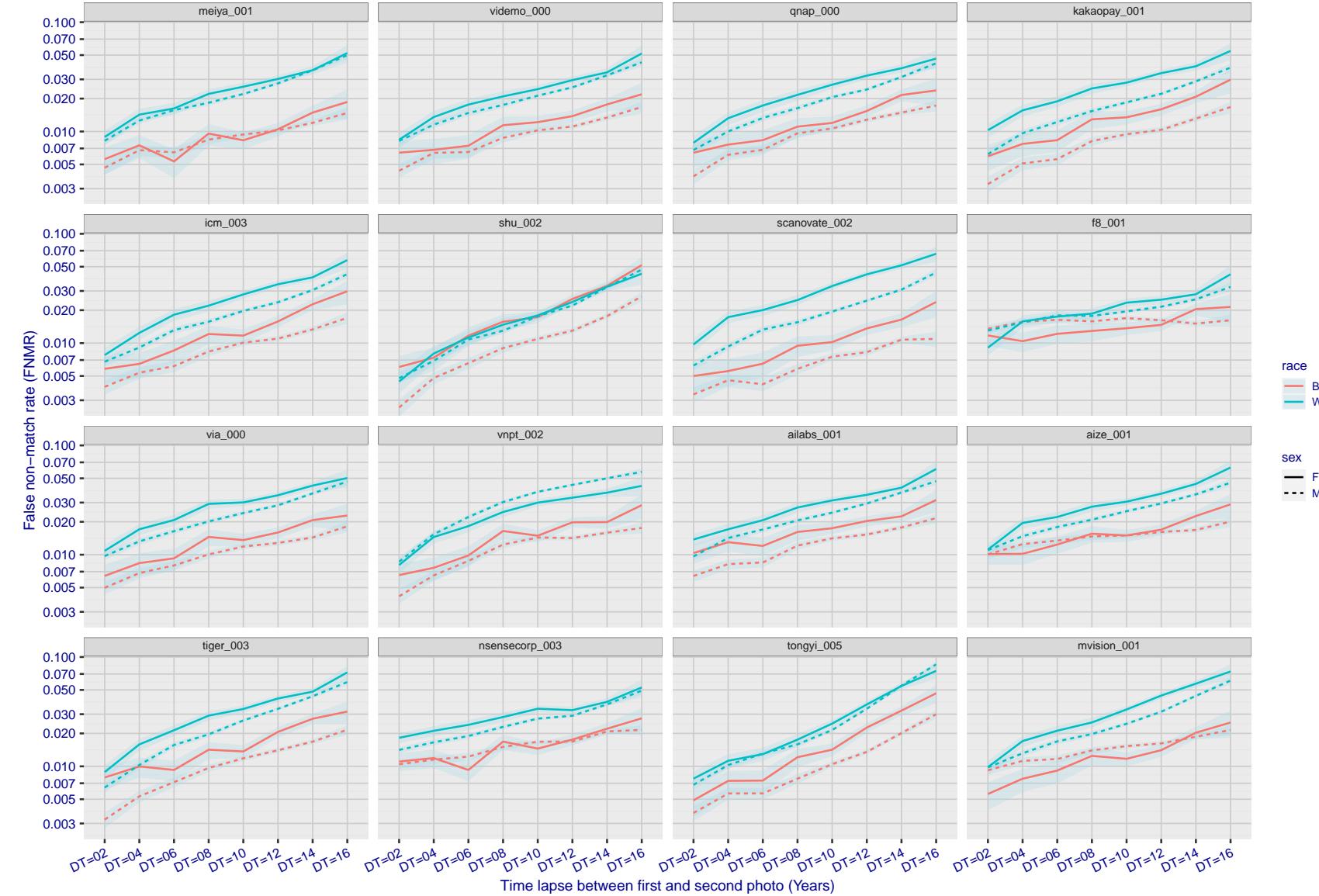


Figure 267: For the mugshot images, FNMR as a function of elapsed time between initial enrollment and second verification images. The panels appear most accurate first, and vertical scale changes on each page. The four traces correspond to images annotated with codes for black female, black male, white female, white male. The threshold is fixed for each algorithm to give FMR = 0.00001 over all (10^8) impostor comparisons. For short time-lapses, the most accurate algorithms give very few errors (FNMR < 0.001) so that the uncertainty estimates are high.

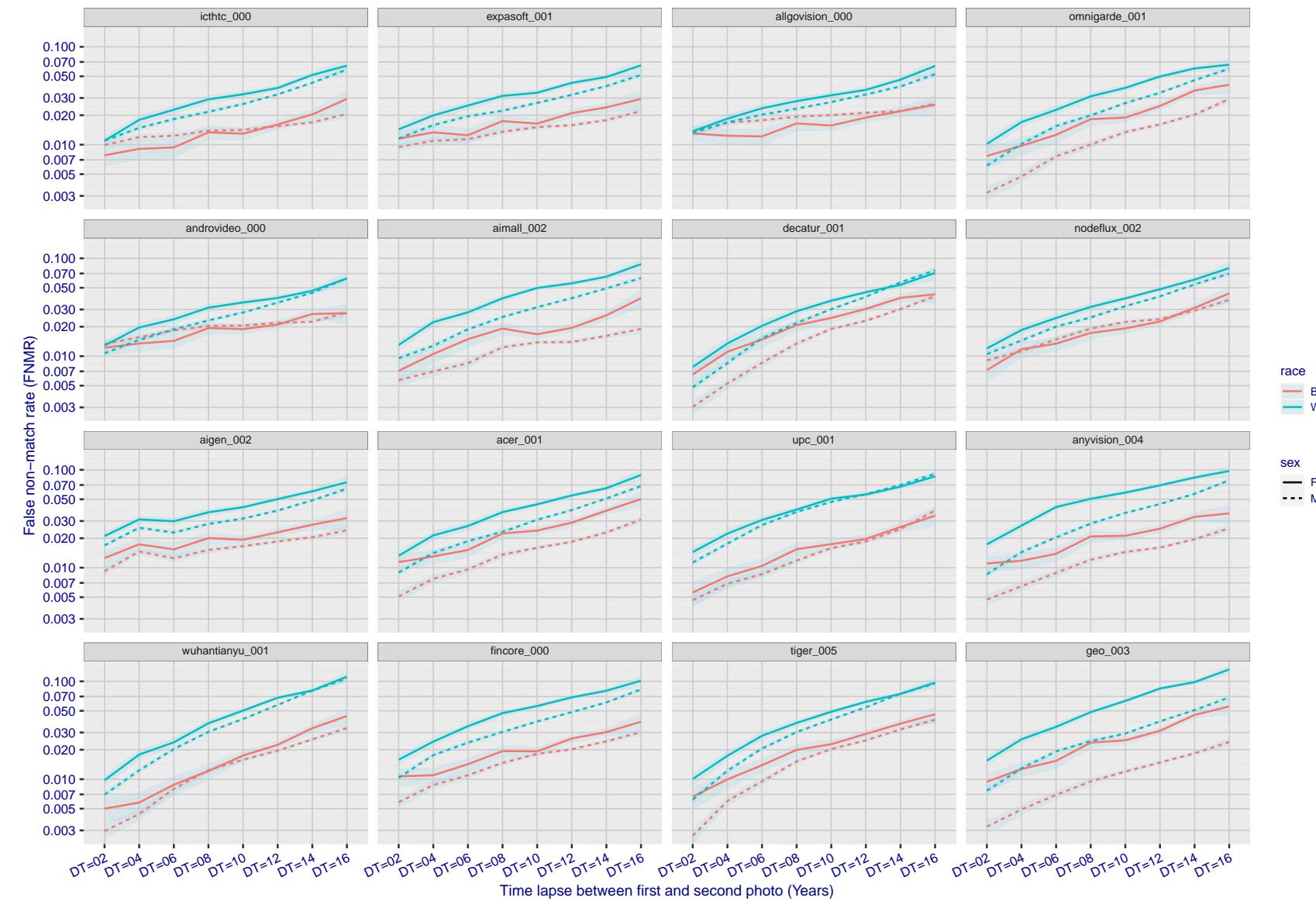


Figure 268: For the mugshot images, FNMR as a function of elapsed time between initial enrollment and second verification images. The panels appear most accurate first, and vertical scale changes on each page. The four traces correspond to images annotated with codes for black female, black male, white female, white male. The threshold is fixed for each algorithm to give FMR = 0.00001 over all (10^8) impostor comparisons. For short time-lapses, the most accurate algorithms give very few errors (FNMR < 0.001) so that the uncertainty estimates are high.

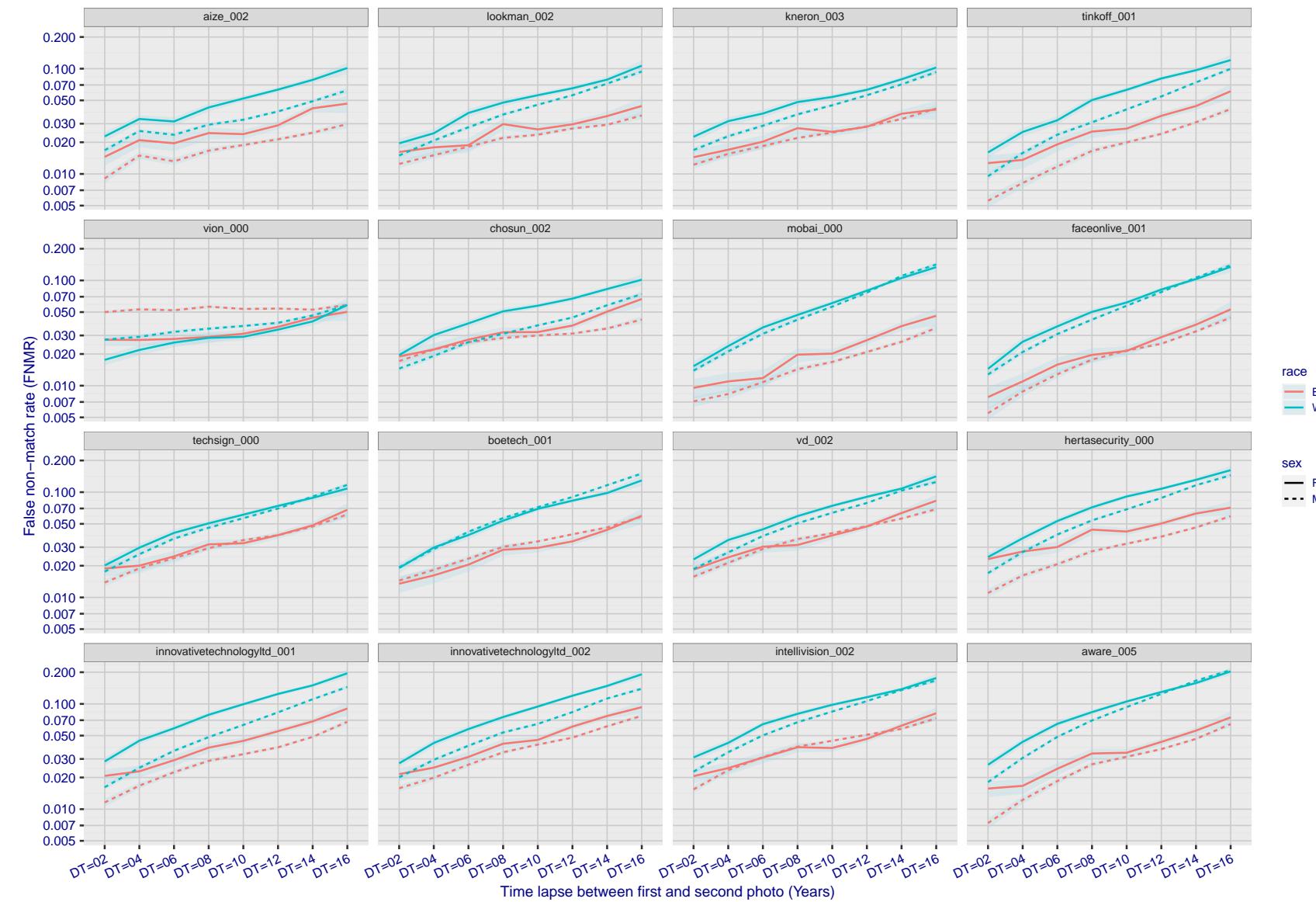


Figure 269: For the mugshot images, FNMR as a function of elapsed time between initial enrollment and second verification images. The panels appear most accurate first, and vertical scale changes on each page. The four traces correspond to images annotated with codes for black female, black male, white female, white male. The threshold is fixed for each algorithm to give $FMR = 0.00001$ over all (10^8) impostor comparisons. For short time-lapses, the most accurate algorithms give very few errors ($FNMR < 0.001$) so that the uncertainty estimates are high.

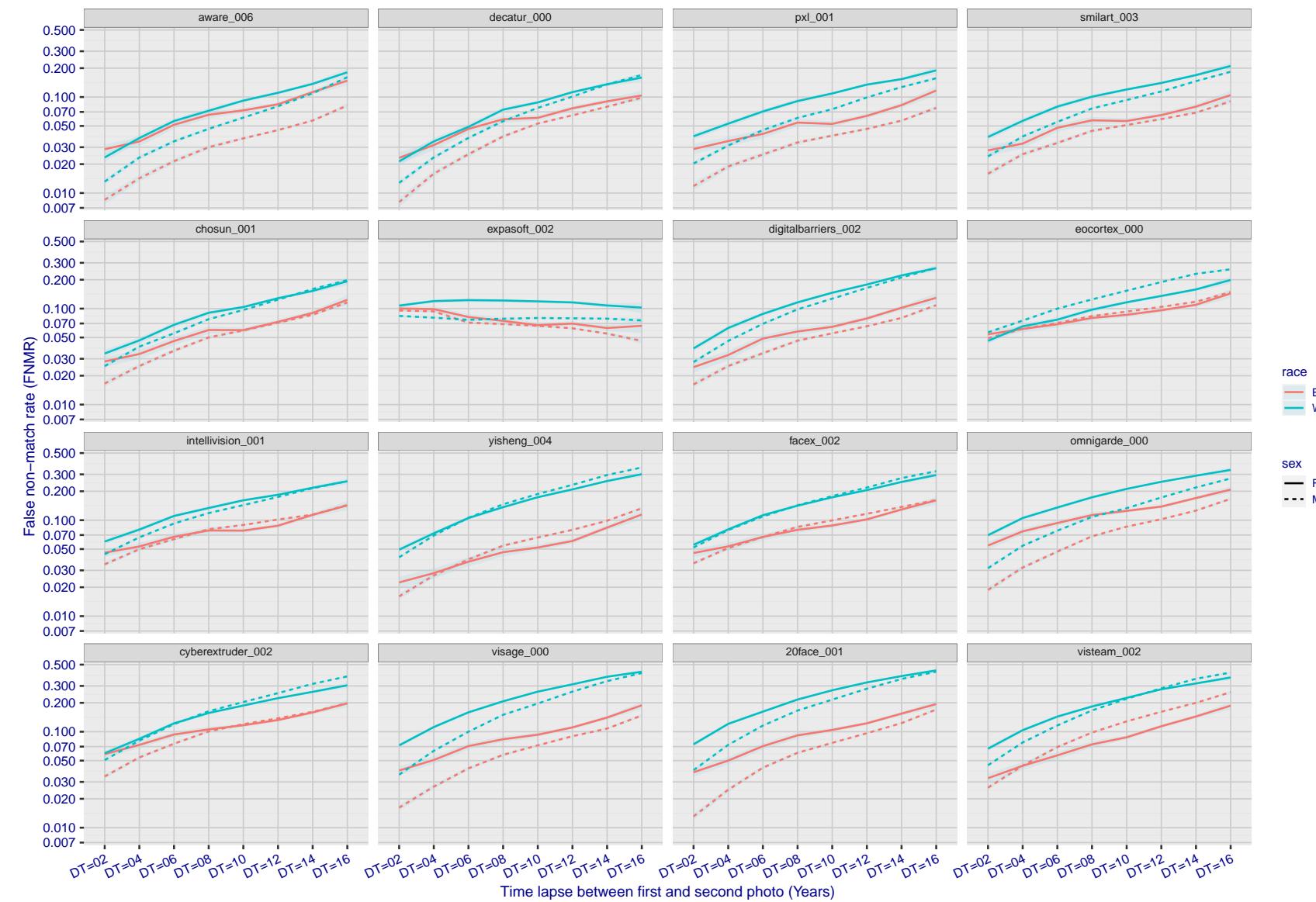


Figure 270: For the mugshot images, FNMR as a function of elapsed time between initial enrollment and second verification images. The panels appear most accurate first, and vertical scale changes on each page. The four traces correspond to images annotated with codes for black female, black male, white female, white male. The threshold is fixed for each algorithm to give FMR = 0.00001 over all (10^8) impostor comparisons. For short time-lapses, the most accurate algorithms give very few errors (FNMR < 0.001) so that the uncertainty estimates are high.

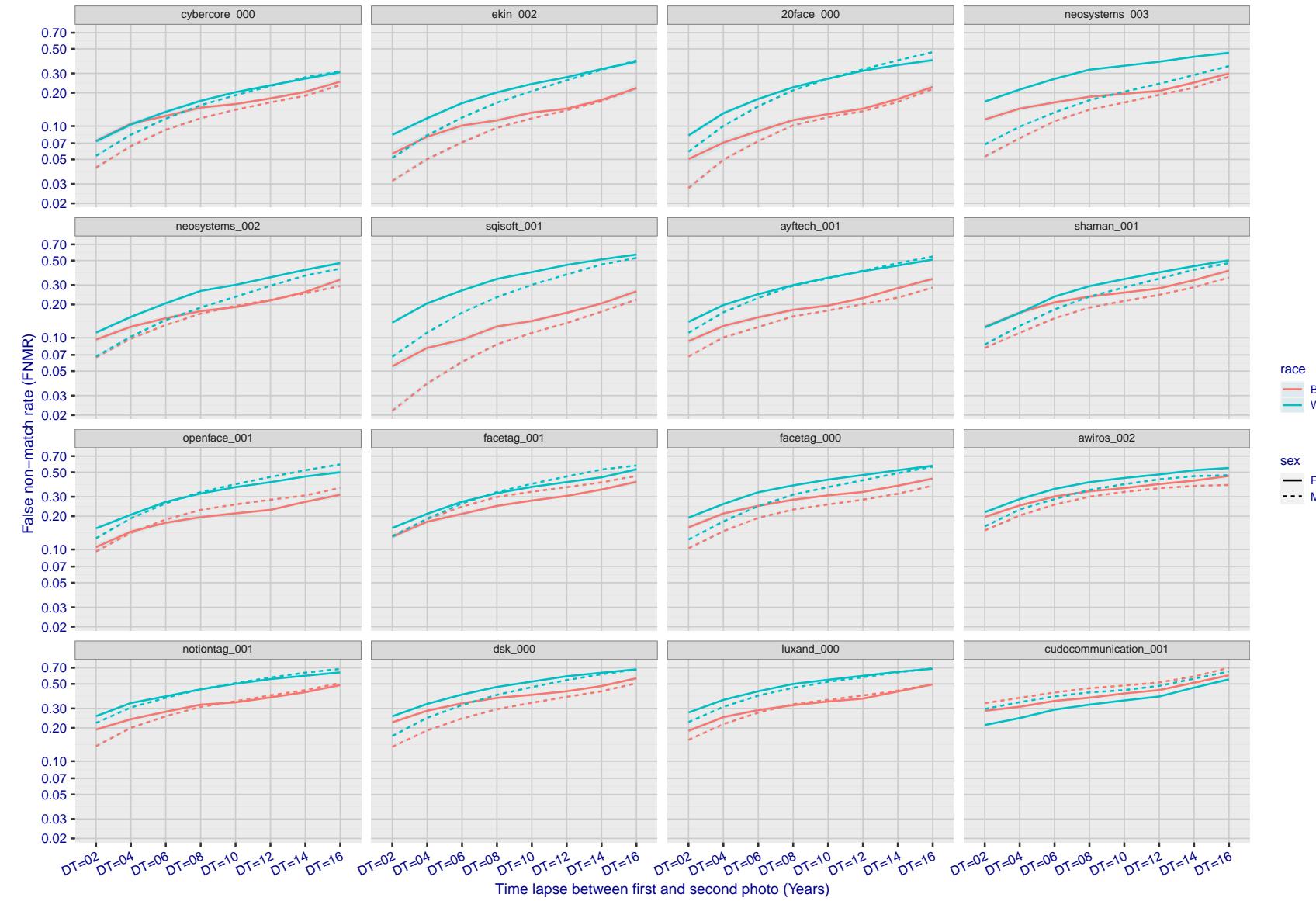


Figure 271: For the mugshot images, FNMR as a function of elapsed time between initial enrollment and second verification images. The panels appear most accurate first, and vertical scale changes on each page. The four traces correspond to images annotated with codes for black female, black male, white female, white male. The threshold is fixed for each algorithm to give $FMR = 0.00001$ over all (10^8) impostor comparisons. For short time-lapses, the most accurate algorithms give very few errors ($FNMR < 0.001$) so that the uncertainty estimates are high.

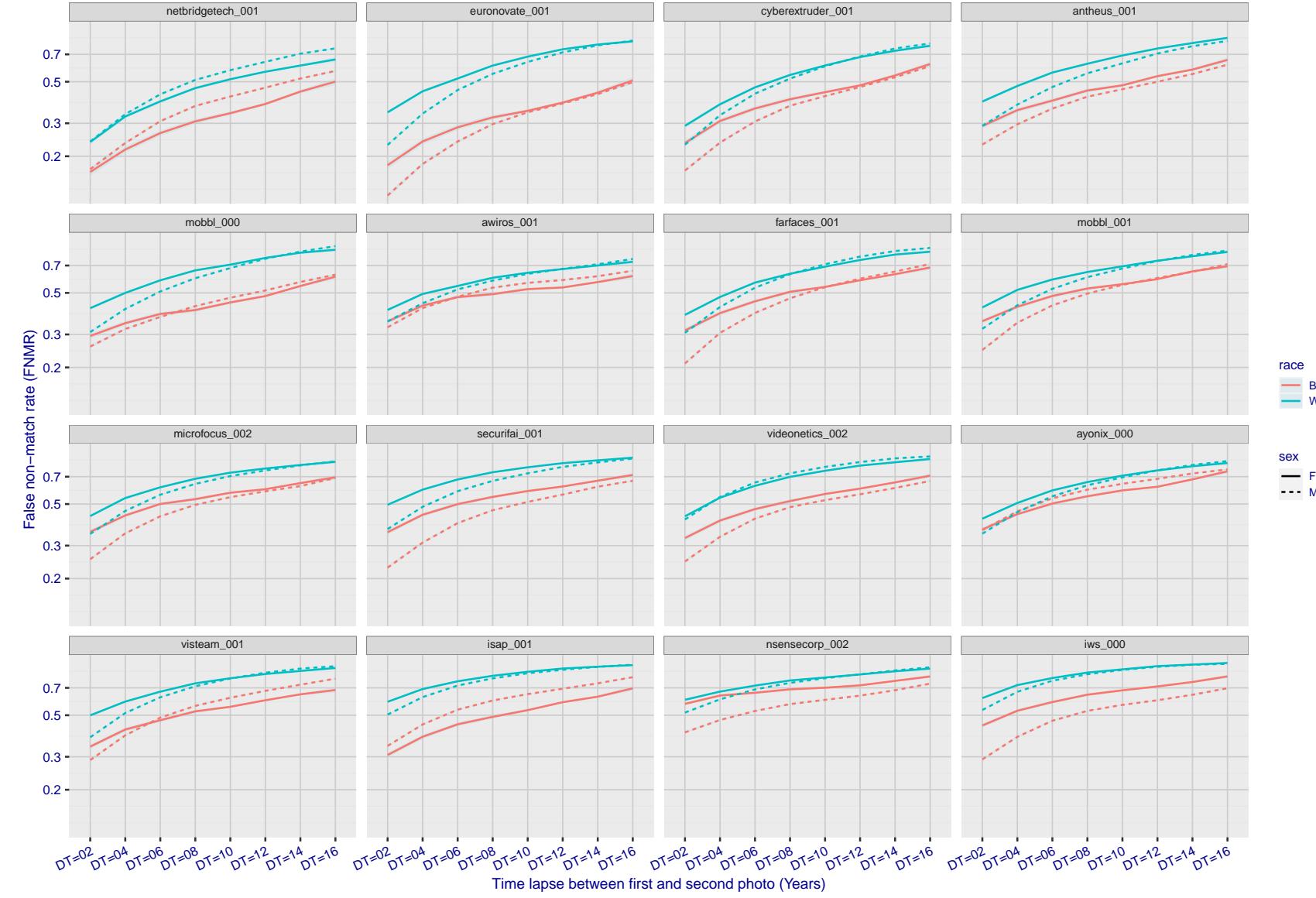


Figure 272: For the mugshot images, FNMR as a function of elapsed time between initial enrollment and second verification images. The panels appear most accurate first, and vertical scale changes on each page. The four traces correspond to images annotated with codes for black female, black male, white female, white male. The threshold is fixed for each algorithm to give $FMR = 0.00001$ over all (10^8) impostor comparisons. For short time-lapses, the most accurate algorithms give very few errors ($FNMR < 0.001$) so that the uncertainty estimates are high.

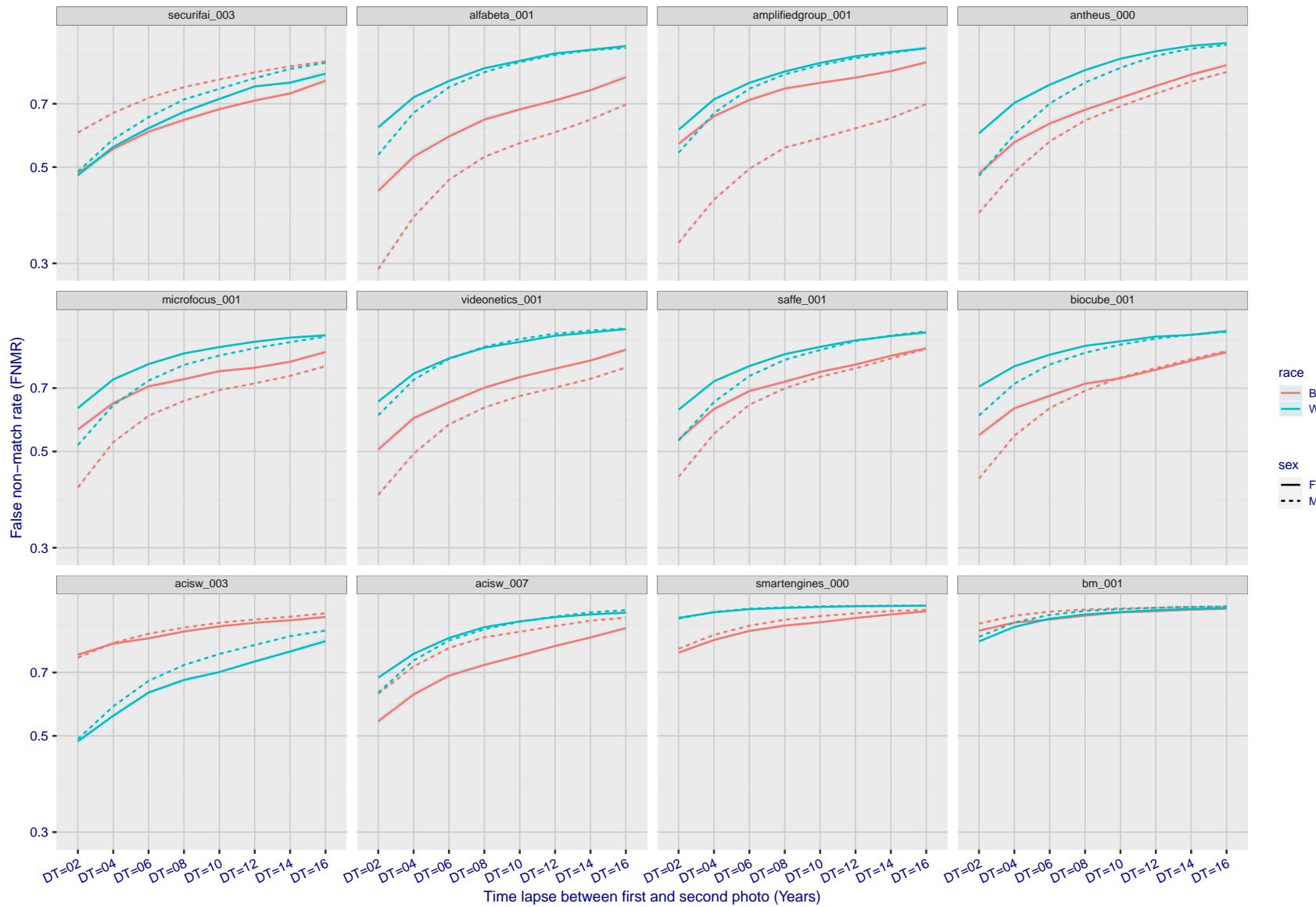


Figure 273: For the mugshot images, FNMR as a function of elapsed time between initial enrollment and second verification images. The panels appear most accurate first, and vertical scale changes on each page. The four traces correspond to images annotated with codes for black female, black male, white female, white male. The threshold is fixed for each algorithm to give FMR = 0.00001 over all (10^8) impostor comparisons. For short time-lapses, the most accurate algorithms give very few errors (FNMR < 0.001) so that the uncertainty estimates are high.

3.5.3 Effect of age on genuine subjects

Background: Faces change appearance throughout life. Face recognition algorithms have previously been reported to give better accuracy on older individuals (See NIST IR 8009).

Goal: To quantify false non-match rates (FNMR) as a function of age, without an ageing component.

Methods: Using the visa images, which span fewer than five years, thresholds are determined that give FMR = 0.001 and 0.0001 over the entire impostor set. Then FNMR is measured over 1000 bootstrap replications of the genuine scores.

Results: For the visa images, Figure 305 shows how false non-match rates for genuine users, as a function of age group.

The notable aspects are:

- ▷ Younger subjects give considerably higher FNMR. This is likely due to rapid growth and change in facial appearance.
- ▷ FNMR trends down throughout life. The last bin, AGE > 72, contains fewer than 140 mated pairs, and may be affected by small sample size.

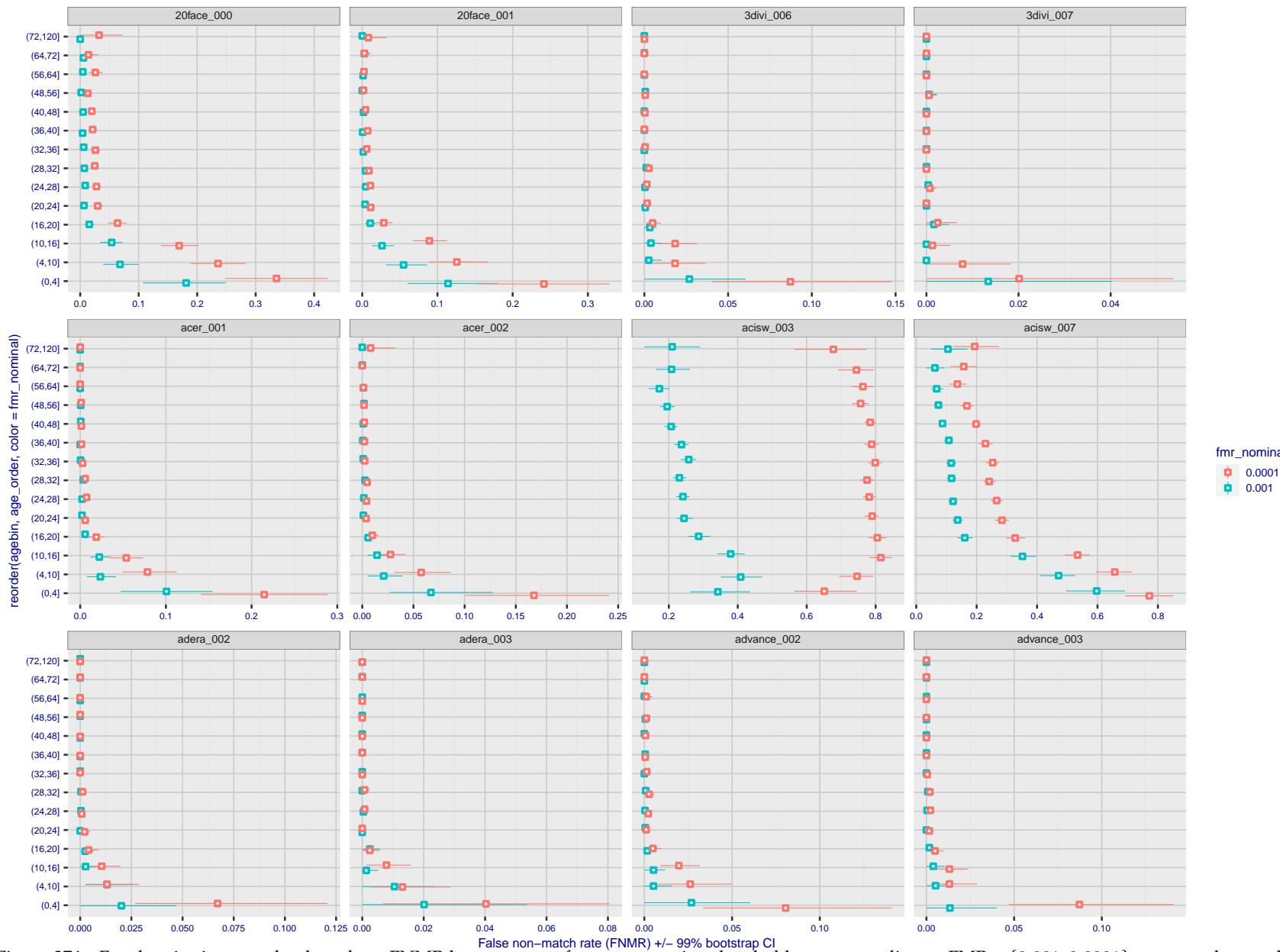


Figure 274: For the visa images, the dots show FNMR by age group for two operating thresholds corresponding to $FMR = \{0.001, 0.0001\}$ computed over all on the order of 10^{10} impostor scores. The FMR in each bin will vary also - see subsequent impostor heatmaps in sec. 3.6.2. Given a pair of face images taken at different times, we assign the comparison to the bin that is the arithmetic average of the subject's ages. This plot shows only the effect of age, not ageing. The number of comparisons in each bin is generally in the thousands, however the first and last bins are computed over 149 and 124 respectively. The error rates in some (adult) cases are zero, and in others the DET is flat so the error rates at the two thresholds are identical. The lines span 1% and 99% of bootstrap replicated FNMR estimates.



FNMR(T)
FMR(T)
"False non-match rate"
"False match rate"

Figure 275: For the visa images, the dots show FNMR by age group for two operating thresholds corresponding to $FMR = \{0.001, 0.0001\}$ computed over all on the order of 10^{10} impostor scores. The FMR in each bin will vary also - see subsequent impostor heatmaps in sec. 3.6.2. Given a pair of face images taken at different times, we assign the comparison to the bin that is the arithmetic average of the subject's ages. This plot shows only the effect of age, not ageing. The number of comparisons in each bin is generally in the thousands, however the first and last bins are computed over 149 and 124 respectively. The error rates in some (adult) cases are zero, and in others the DET is flat so the error rates at the two thresholds are identical. The lines span 1% and 99% of bootstrap replicated FNMR estimates.

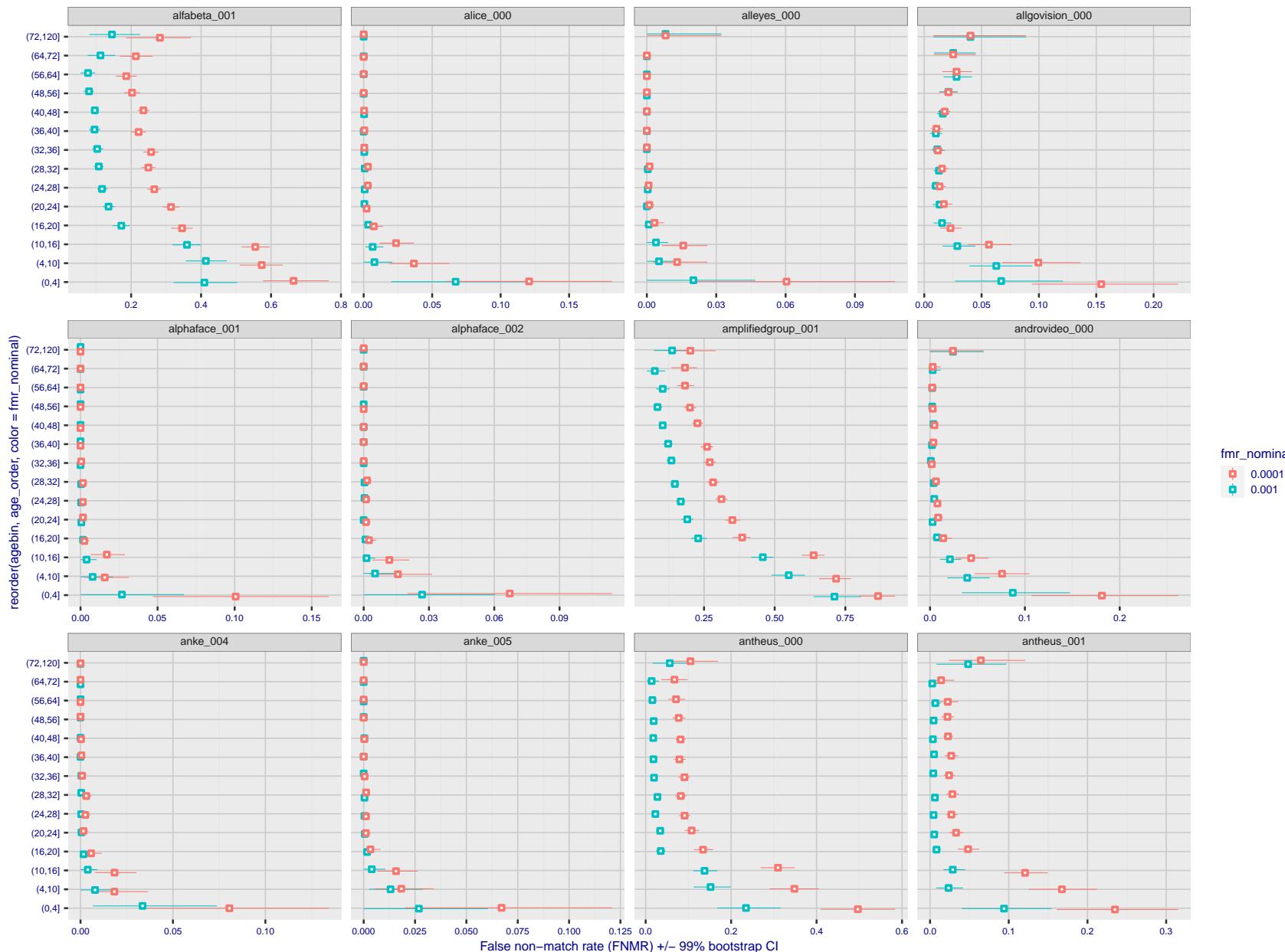


Figure 276: For the visa images, the dots show FNMR by age group for two operating thresholds corresponding to $FMR = \{0.001, 0.0001\}$ computed over all on the order of 10^{10} impostor scores. The FMR in each bin will vary also - see subsequent impostor heatmaps in sec. 3.6.2. Given a pair of face images taken at different times, we assign the comparison to the bin that is the arithmetic average of the subject's ages. This plot shows only the effect of age, not ageing. The number of comparisons in each bin is generally in the thousands, however the first and last bins are computed over 149 and 124 respectively. The error rates in some (adult) cases are zero, and in others the DET is flat so the error rates at the two thresholds are identical. The lines span 1% and 99% of bootstrap replicated FNMR estimates.



Figure 277: For the visa images, the dots show FNMR by age group for two operating thresholds corresponding to $FMR = \{0.001, 0.0001\}$ computed over all on the order of 10^{10} impostor scores. The FMR in each bin will vary also - see subsequent impostor heatmaps in sec. 3.6.2. Given a pair of face images taken at different times, we assign the comparison to the bin that is the arithmetic average of the subject's ages. This plot shows only the effect of age, not ageing. The number of comparisons in each bin is generally in the thousands, however the first and last bins are computed over 149 and 124 respectively. The error rates in some (adult) cases are zero, and in others the DET is flat so the error rates at the two thresholds are identical. The lines span 1% and 99% of bootstrap replicated FNMR estimates.

2021/12/16 10:32:53



Figure 278: For the visa images, the dots show FNMR by age group for two operating thresholds corresponding to $FMR = \{0.001, 0.0001\}$ computed over all on the order of 10^{10} impostor scores. The FMR in each bin will vary also - see subsequent impostor heatmaps in sec. 3.6.2. Given a pair of face images taken at different times, we assign the comparison to the bin that is the arithmetic average of the subject's ages. This plot shows only the effect of age, not ageing. The number of comparisons in each bin is generally in the thousands, however the first and last bins are computed over 149 and 124 respectively. The error rates in some (adult) cases are zero, and in others the DET is flat so the error rates at the two thresholds are identical. The lines span 1% and 99% of bootstrap replicated FNMR estimates.



Figure 279: For the visa images, the dots show FNMR by age group for two operating thresholds corresponding to $FMR = \{0.001, 0.0001\}$ computed over all on the order of 10^{10} impostor scores. The FMR in each bin will vary also - see subsequent impostor heatmaps in sec. 3.6.2. Given a pair of face images taken at different times, we assign the comparison to the bin that is the arithmetic average of the subject's ages. This plot shows only the effect of age, not ageing. The number of comparisons in each bin is generally in the thousands, however the first and last bins are computed over 149 and 124 respectively. The error rates in some (adult) cases are zero, and in others the DET is flat so the error rates at the two thresholds are identical. The lines span 1% and 99% of bootstrap replicated FNMR estimates.

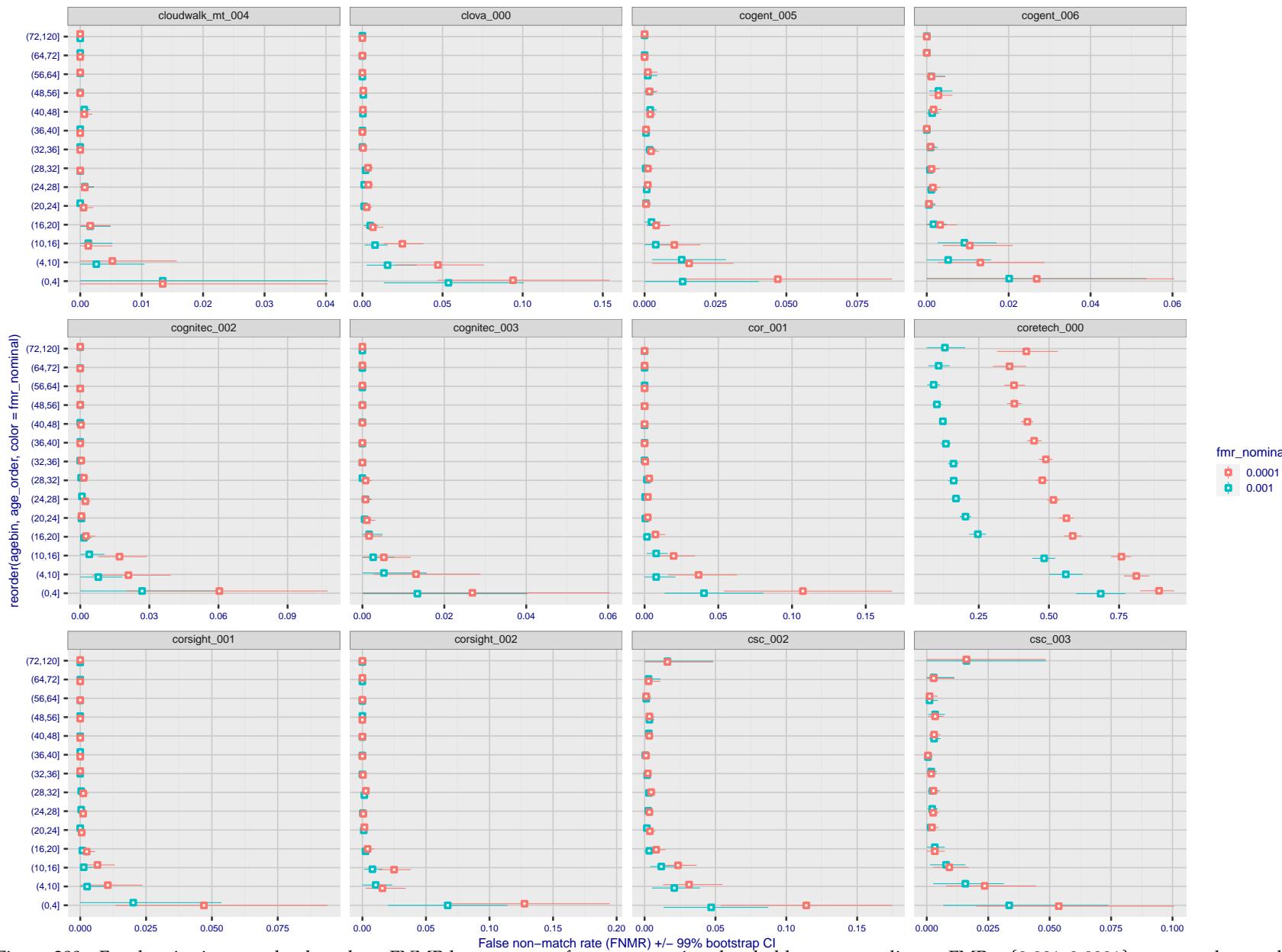


Figure 280: For the visa images, the dots show FNMR by age group for two operating thresholds corresponding to $FMR = \{0.001, 0.0001\}$ computed over all on the order of 10^{10} impostor scores. The FMR in each bin will vary also - see subsequent impostor heatmaps in sec. 3.6.2. Given a pair of face images taken at different times, we assign the comparison to the bin that is the arithmetic average of the subject's ages. This plot shows only the effect of age, not ageing. The number of comparisons in each bin is generally in the thousands, however the first and last bins are computed over 149 and 124 respectively. The error rates in some (adult) cases are zero, and in others the DET is flat so the error rates at the two thresholds are identical. The lines span 1% and 99% of bootstrap replicated FNMR estimates.

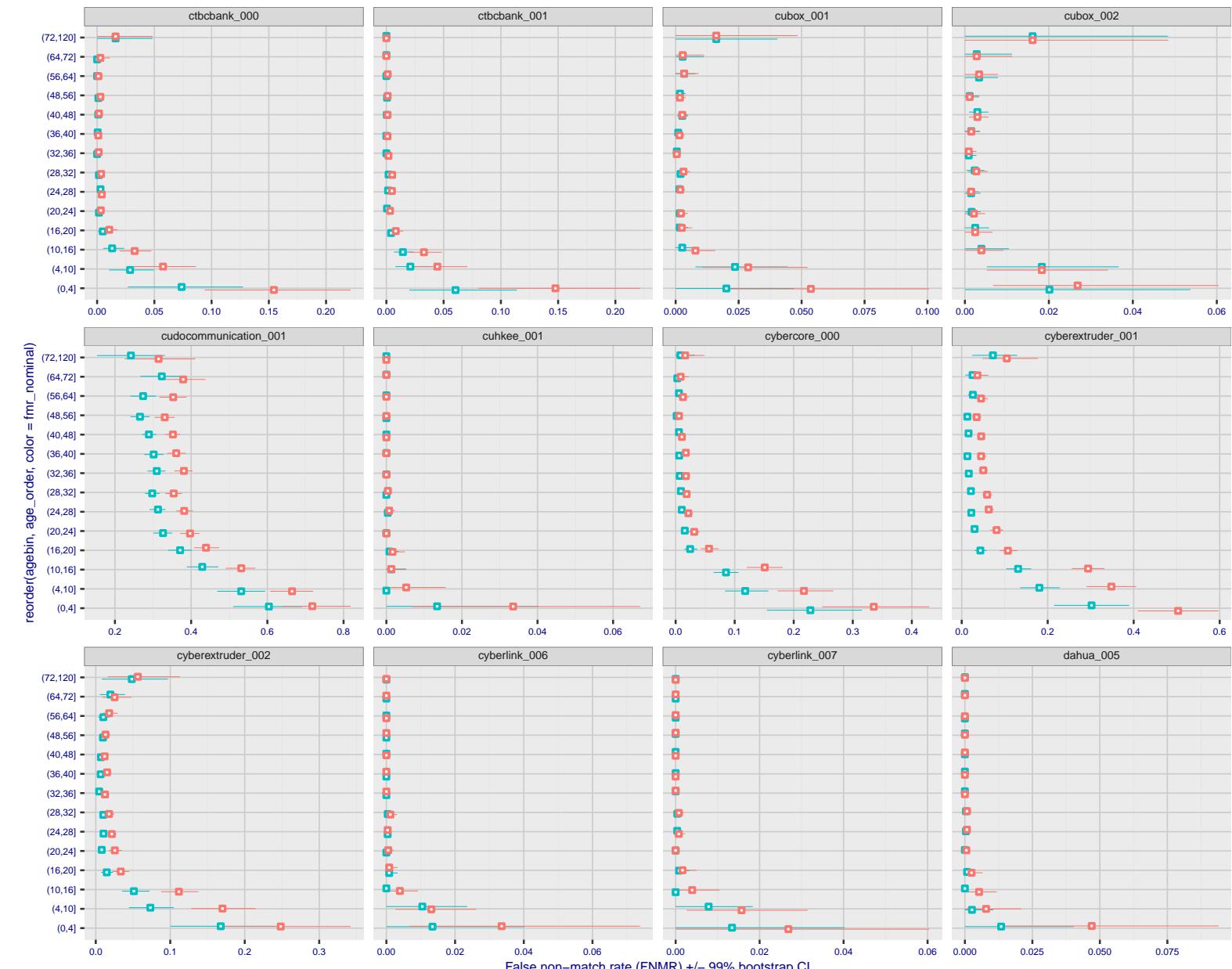
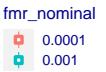


Figure 281: For the visa images, the dots show FNMR by age group for two operating thresholds corresponding to $FMR = \{0.001, 0.0001\}$ computed over all on the order of 10^{10} impostor scores. The FMR in each bin will vary also - see subsequent impostor heatmaps in sec. 3.6.2. Given a pair of face images taken at different times, we assign the comparison to the bin that is the arithmetic average of the subject's ages. This plot shows only the effect of age, not ageing. The number of comparisons in each bin is generally in the thousands, however the first and last bins are computed over 149 and 124 respectively. The error rates in some (adult) cases are zero, and in others the DET is flat so the error rates at the two thresholds are identical. The lines span 1% and 99% of bootstrap replicated FNMR estimates.



Figure 282: For the visa images, the dots show FNMR by age group for two operating thresholds corresponding to $FMR = \{0.001, 0.0001\}$ computed over all on the order of 10^{10} impostor scores. The FMR in each bin will vary also - see subsequent impostor heatmaps in sec. 3.6.2. Given a pair of face images taken at different times, we assign the comparison to the bin that is the arithmetic average of the subject's ages. This plot shows only the effect of age, not ageing. The number of comparisons in each bin is generally in the thousands, however the first and last bins are computed over 149 and 124 respectively. The error rates in some (adult) cases are zero, and in others the DET is flat so the error rates at the two thresholds are identical. The lines span 1% and 99% of bootstrap replicated FNMR estimates.

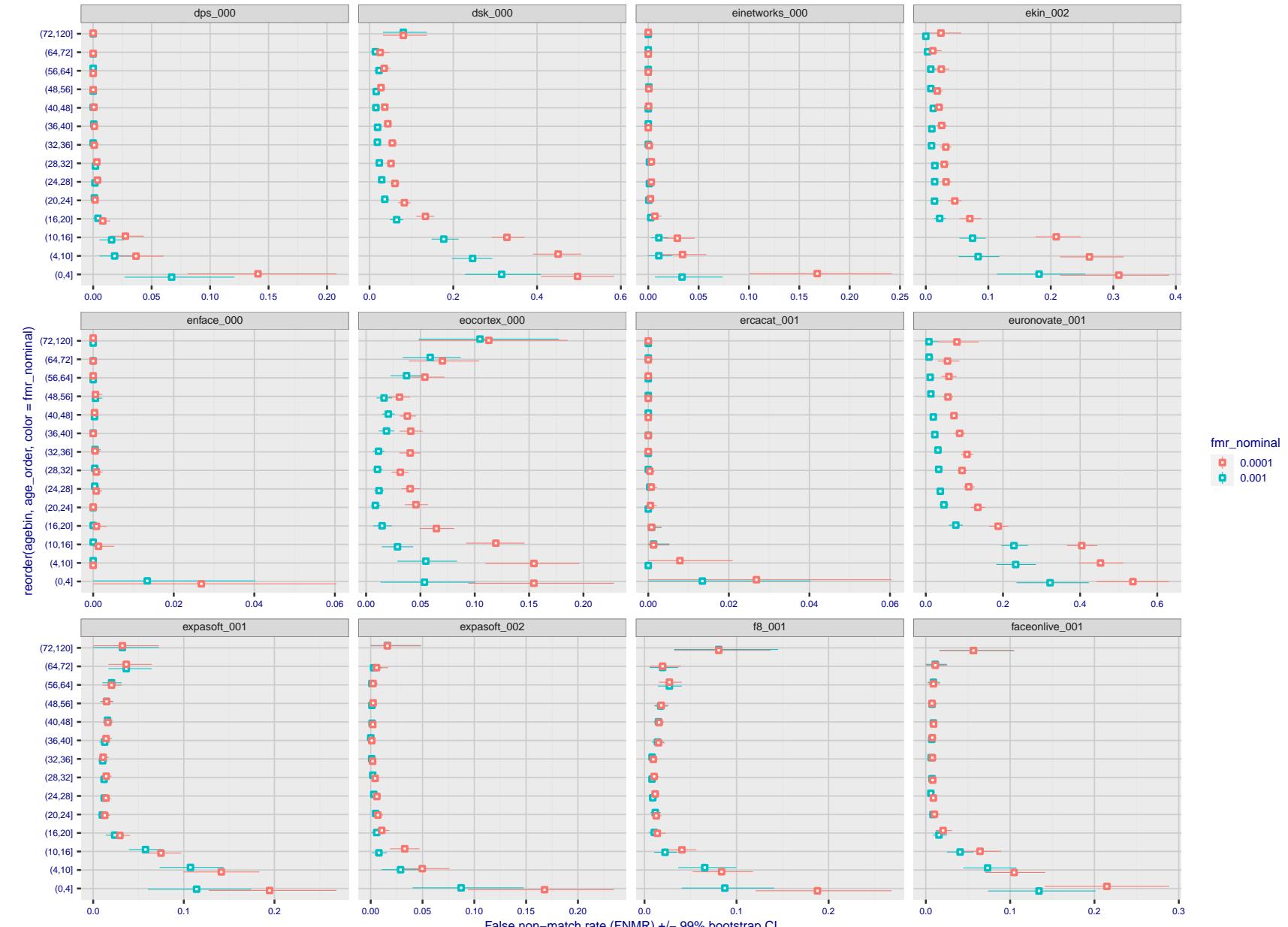


Figure 283: For the visa images, the dots show FNMR by age group for two operating thresholds corresponding to $FMR = \{0.001, 0.0001\}$ computed over all on the order of 10^{10} impostor scores. The FMR in each bin will vary also - see subsequent impostor heatmaps in sec. 3.6.2. Given a pair of face images taken at different times, we assign the comparison to the bin that is the arithmetic average of the subject's ages. This plot shows only the effect of age, not ageing. The number of comparisons in each bin is generally in the thousands, however the first and last bins are computed over 149 and 124 respectively. The error rates in some (adult) cases are zero, and in others the DET is flat so the error rates at the two thresholds are identical. The lines span 1% and 99% of bootstrap replicated FNMR estimates.

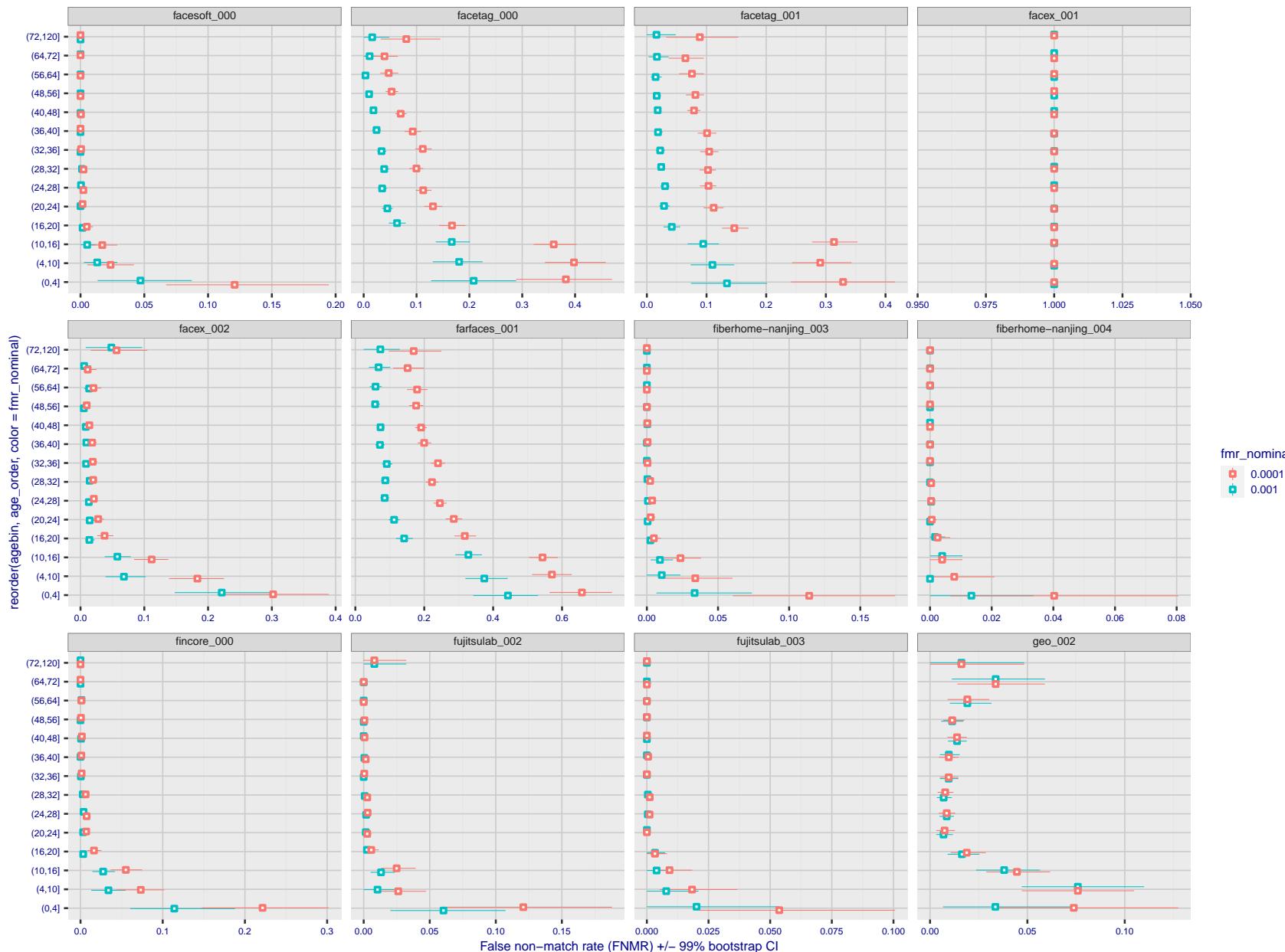


Figure 284: For the visa images, the dots show FNMR by age group for two operating thresholds corresponding to $FMR = \{0.001, 0.0001\}$ computed over all on the order of 10^{10} impostor scores. The FMR in each bin will vary also - see subsequent impostor heatmaps in sec. 3.6.2. Given a pair of face images taken at different times, we assign the comparison to the bin that is the arithmetic average of the subject's ages. This plot shows only the effect of age, not ageing. The number of comparisons in each bin is generally in the thousands, however the first and last bins are computed over 149 and 124 respectively. The error rates in some (adult) cases are zero, and in others the DET is flat so the error rates at the two thresholds are identical. The lines span 1% and 99% of bootstrap replicated FNMR estimates.



Figure 285: For the visa images, the dots show FNMR by age group for two operating thresholds corresponding to $FMR = \{0.001, 0.0001\}$ computed over all on the order of 10^{10} impostor scores. The FMR in each bin will vary also - see subsequent impostor heatmaps in sec. 3.6.2. Given a pair of face images taken at different times, we assign the comparison to the bin that is the arithmetic average of the subject's ages. This plot shows only the effect of age, not ageing. The number of comparisons in each bin is generally in the thousands, however the first and last bins are computed over 149 and 124 respectively. The error rates in some (adult) cases are zero, and in others the DET is flat so the error rates at the two thresholds are identical. The lines span 1% and 99% of bootstrap replicated FNMR estimates.



Figure 286: For the visa images, the dots show FNMR by age group for two operating thresholds corresponding to $FMR = \{0.001, 0.0001\}$ computed over all on the order of 10^{10} impostor scores. The FMR in each bin will vary also - see subsequent impostor heatmaps in sec. 3.6.2. Given a pair of face images taken at different times, we assign the comparison to the bin that is the arithmetic average of the subject's ages. This plot shows only the effect of age, not ageing. The number of comparisons in each bin is generally in the thousands, however the first and last bins are computed over 149 and 124 respectively. The error rates in some (adult) cases are zero, and in others the DET is flat so the error rates at the two thresholds are identical. The lines span 1% and 99% of bootstrap replicated FNMR estimates.



Figure 287: For the visa images, the dots show FNMR by age group for two operating thresholds corresponding to $FMR = \{0.001, 0.0001\}$ computed over all on the order of 10^{10} impostor scores. The FMR in each bin will vary also - see subsequent impostor heatmaps in sec. 3.6.2. Given a pair of face images taken at different times, we assign the comparison to the bin that is the arithmetic average of the subject's ages. This plot shows only the effect of age, not ageing. The number of comparisons in each bin is generally in the thousands, however the first and last bins are computed over 149 and 124 respectively. The error rates in some (adult) cases are zero, and in others the DET is flat so the error rates at the two thresholds are identical. The lines span 1% and 99% of bootstrap replicated FNMR estimates.

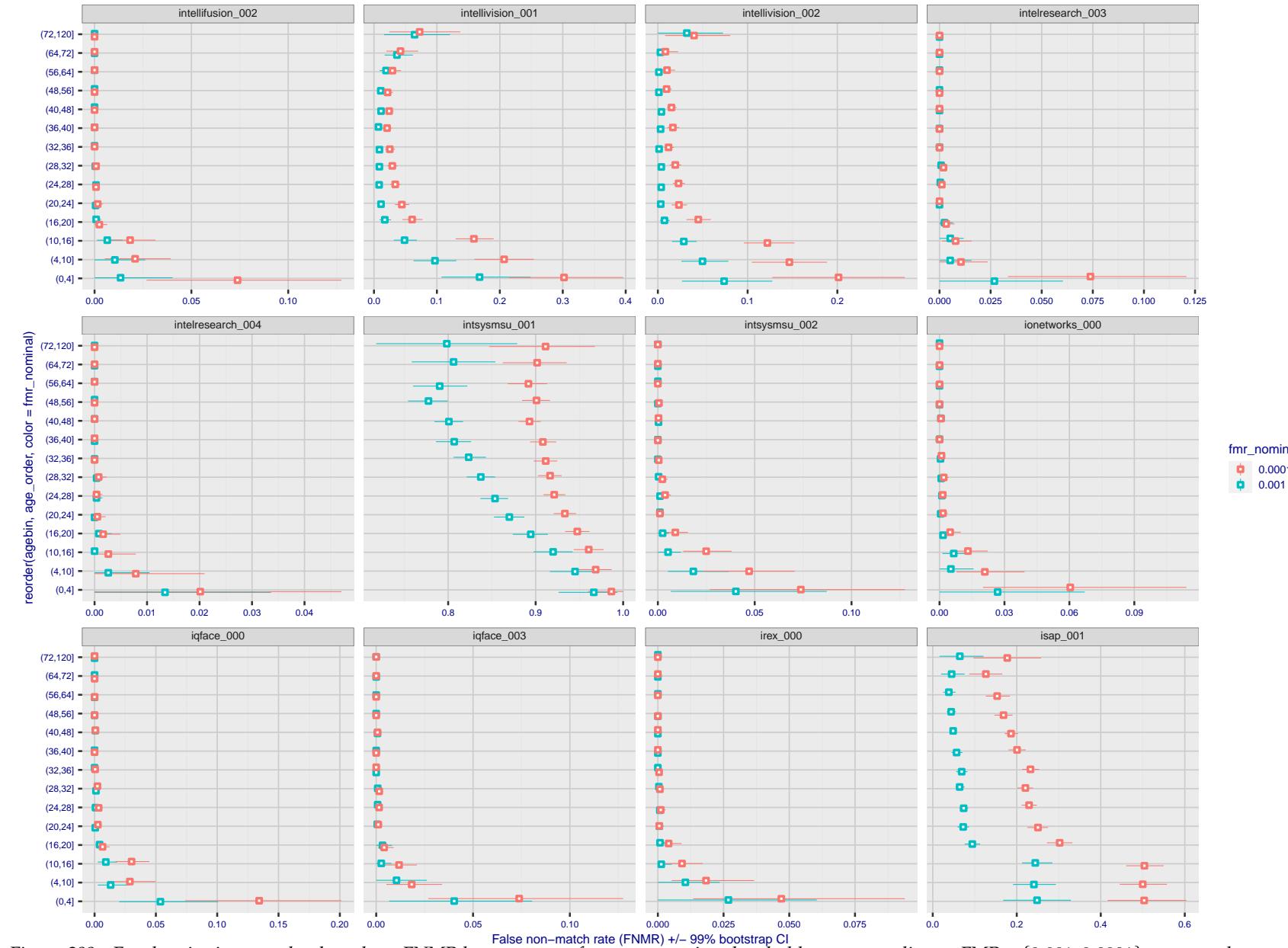


Figure 288: For the visa images, the dots show FNMR by age group for two operating thresholds corresponding to $FMR = \{0.001, 0.0001\}$ computed over all on the order of 10^{10} impostor scores. The FMR in each bin will vary also - see subsequent impostor heatmaps in sec. 3.6.2. Given a pair of face images taken at different times, we assign the comparison to the bin that is the arithmetic average of the subject's ages. This plot shows only the effect of age, not ageing. The number of comparisons in each bin is generally in the thousands, however the first and last bins are computed over 149 and 124 respectively. The error rates in some (adult) cases are zero, and in others the DET is flat so the error rates at the two thresholds are identical. The lines span 1% and 99% of bootstrap replicated FNMR estimates.

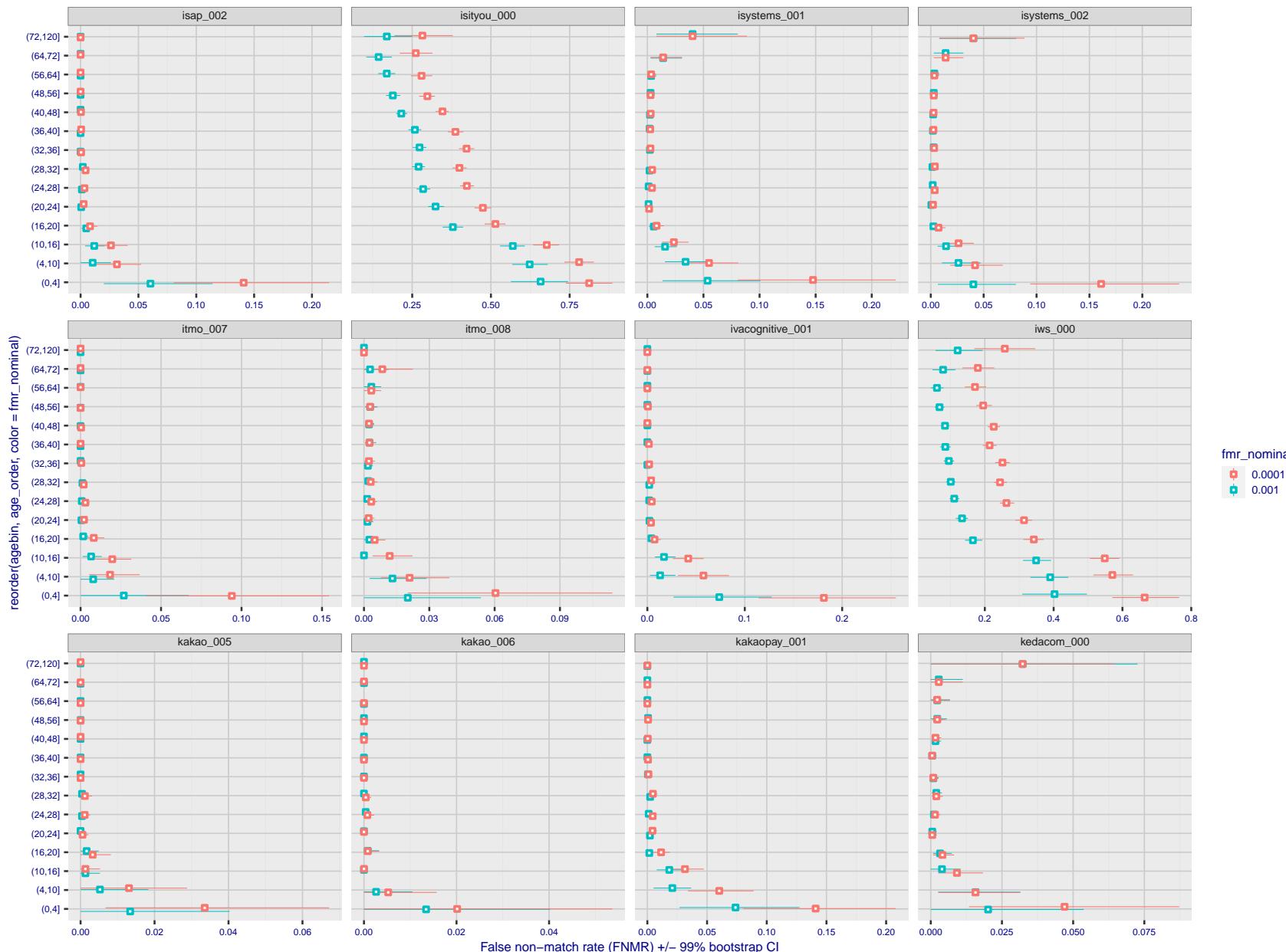


Figure 289: For the visa images, the dots show FNMR by age group for two operating thresholds corresponding to $FMR = \{0.001, 0.0001\}$ computed over all on the order of 10^{10} impostor scores. The FMR in each bin will vary also - see subsequent impostor heatmaps in sec. 3.6.2. Given a pair of face images taken at different times, we assign the comparison to the bin that is the arithmetic average of the subject's ages. This plot shows only the effect of age, not ageing. The number of comparisons in each bin is generally in the thousands, however the first and last bins are computed over 149 and 124 respectively. The error rates in some (adult) cases are zero, and in others the DET is flat so the error rates at the two thresholds are identical. The lines span 1% and 99% of bootstrap replicated FNMR estimates.



Figure 290: For the visa images, the dots show FNMR by age group for two operating thresholds corresponding to $FMR = \{0.001, 0.0001\}$ computed over all on the order of 10^{10} impostor scores. The FMR in each bin will vary also - see subsequent impostor heatmaps in sec. 3.6.2. Given a pair of face images taken at different times, we assign the comparison to the bin that is the arithmetic average of the subject's ages. This plot shows only the effect of age, not ageing. The number of comparisons in each bin is generally in the thousands, however the first and last bins are computed over 149 and 124 respectively. The error rates in some (adult) cases are zero, and in others the DET is flat so the error rates at the two thresholds are identical. The lines span 1% and 99% of bootstrap replicated FNMR estimates.

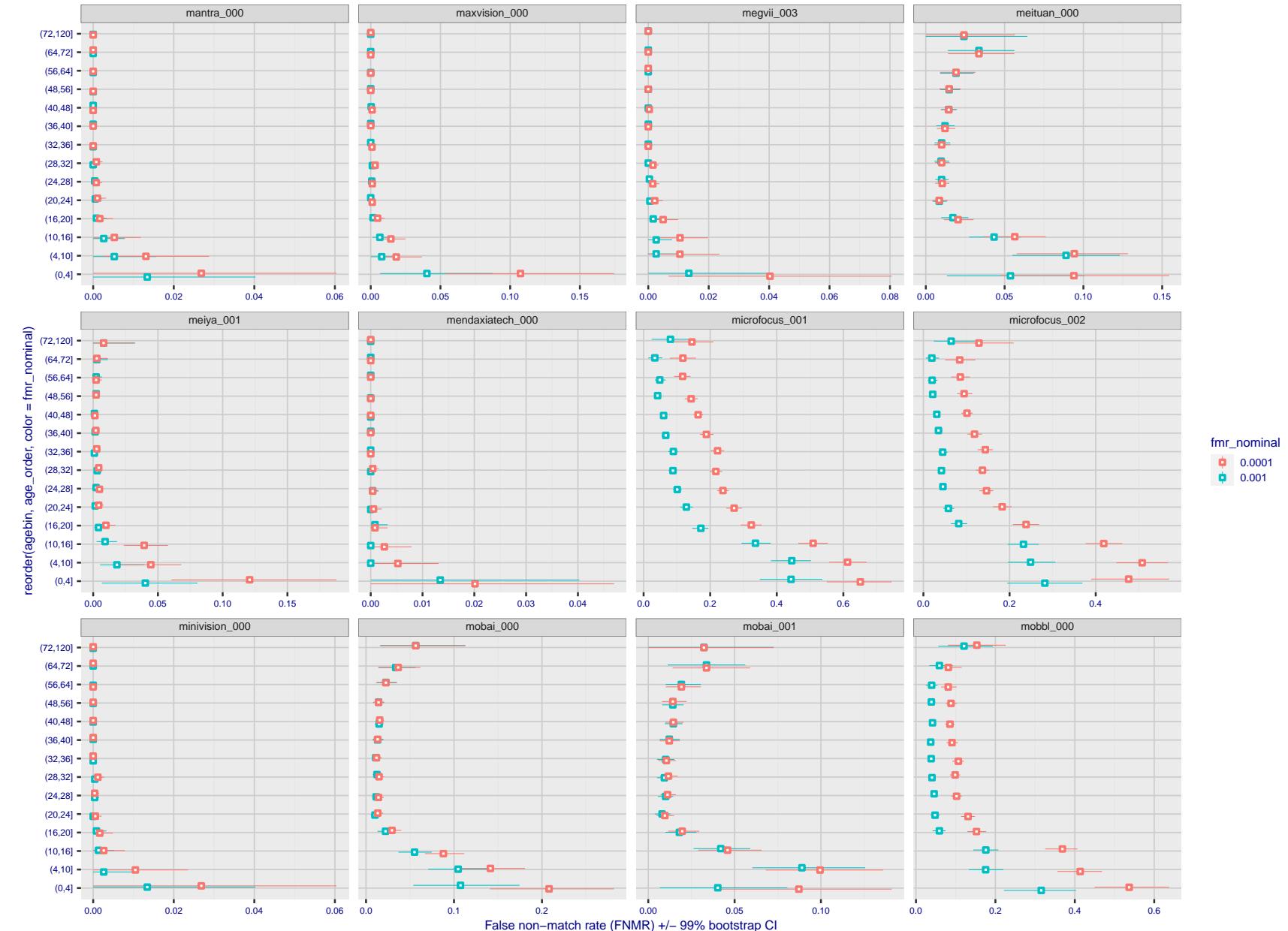
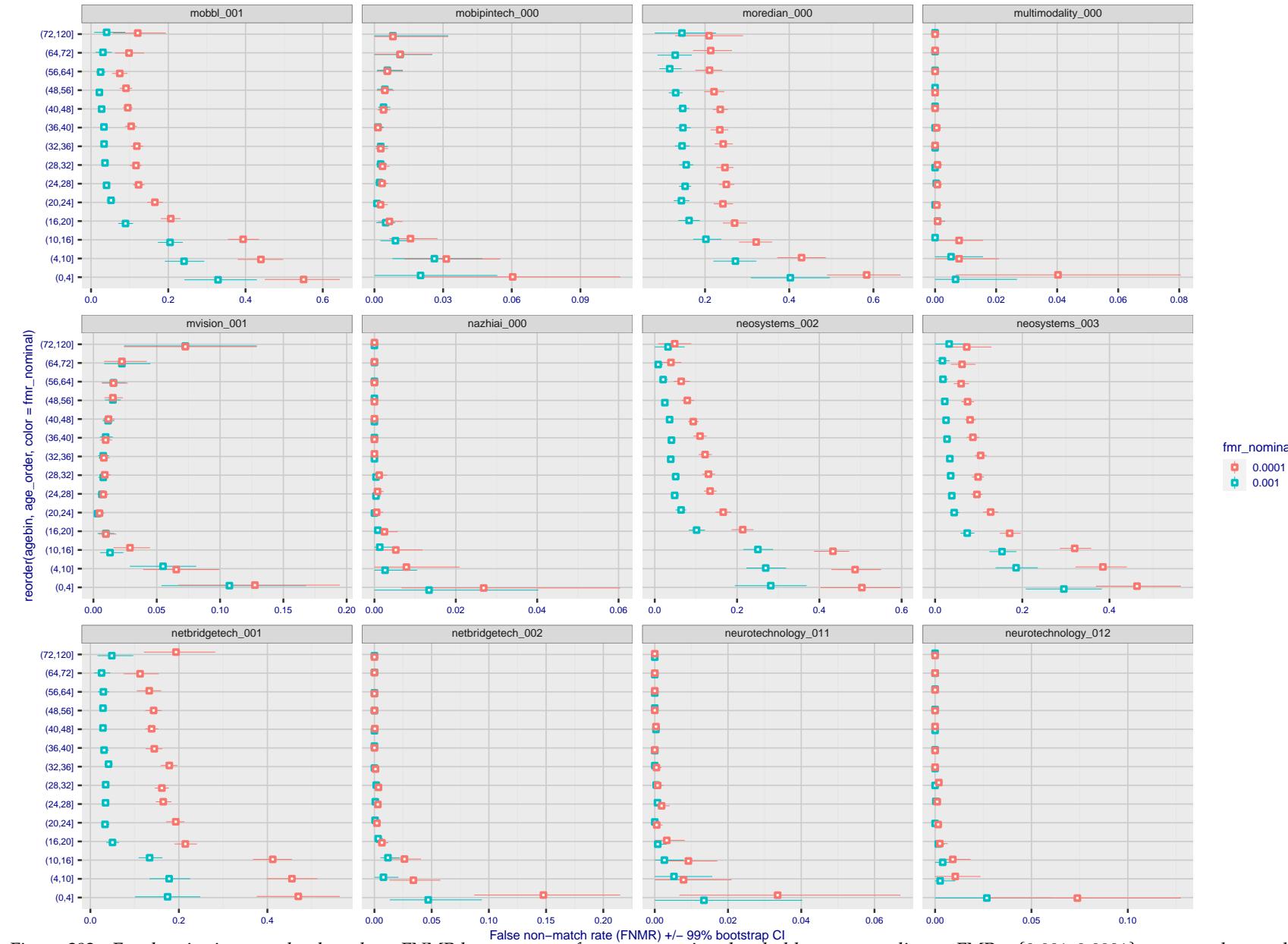


Figure 291: For the visa images, the dots show FNMR by age group for two operating thresholds corresponding to $FMR = \{0.001, 0.0001\}$ computed over all on the order of 10^{10} impostor scores. The FMR in each bin will vary also - see subsequent impostor heatmaps in sec. 3.6.2. Given a pair of face images taken at different times, we assign the comparison to the bin that is the arithmetic average of the subject's ages. This plot shows only the effect of age, not ageing. The number of comparisons in each bin is generally in the thousands, however the first and last bins are computed over 149 and 124 respectively. The error rates in some (adult) cases are zero, and in others the DET is flat so the error rates at the two thresholds are identical. The lines span 1% and 99% of bootstrap replicated FNMR estimates.



fmr_nominal
◻ 0.0001
◻ 0.001

Figure 292: For the visa images, the dots show FNMR by age group for two operating thresholds corresponding to $FMR = \{0.001, 0.0001\}$ computed over all on the order of 10^{10} impostor scores. The FMR in each bin will vary also - see subsequent impostor heatmaps in sec. 3.6.2. Given a pair of face images taken at different times, we assign the comparison to the bin that is the arithmetic average of the subject's ages. This plot shows only the effect of age, not ageing. The number of comparisons in each bin is generally in the thousands, however the first and last bins are computed over 149 and 124 respectively. The error rates in some (adult) cases are zero, and in others the DET is flat so the error rates at the two thresholds are identical. The lines span 1% and 99% of bootstrap replicated FNMR estimates.

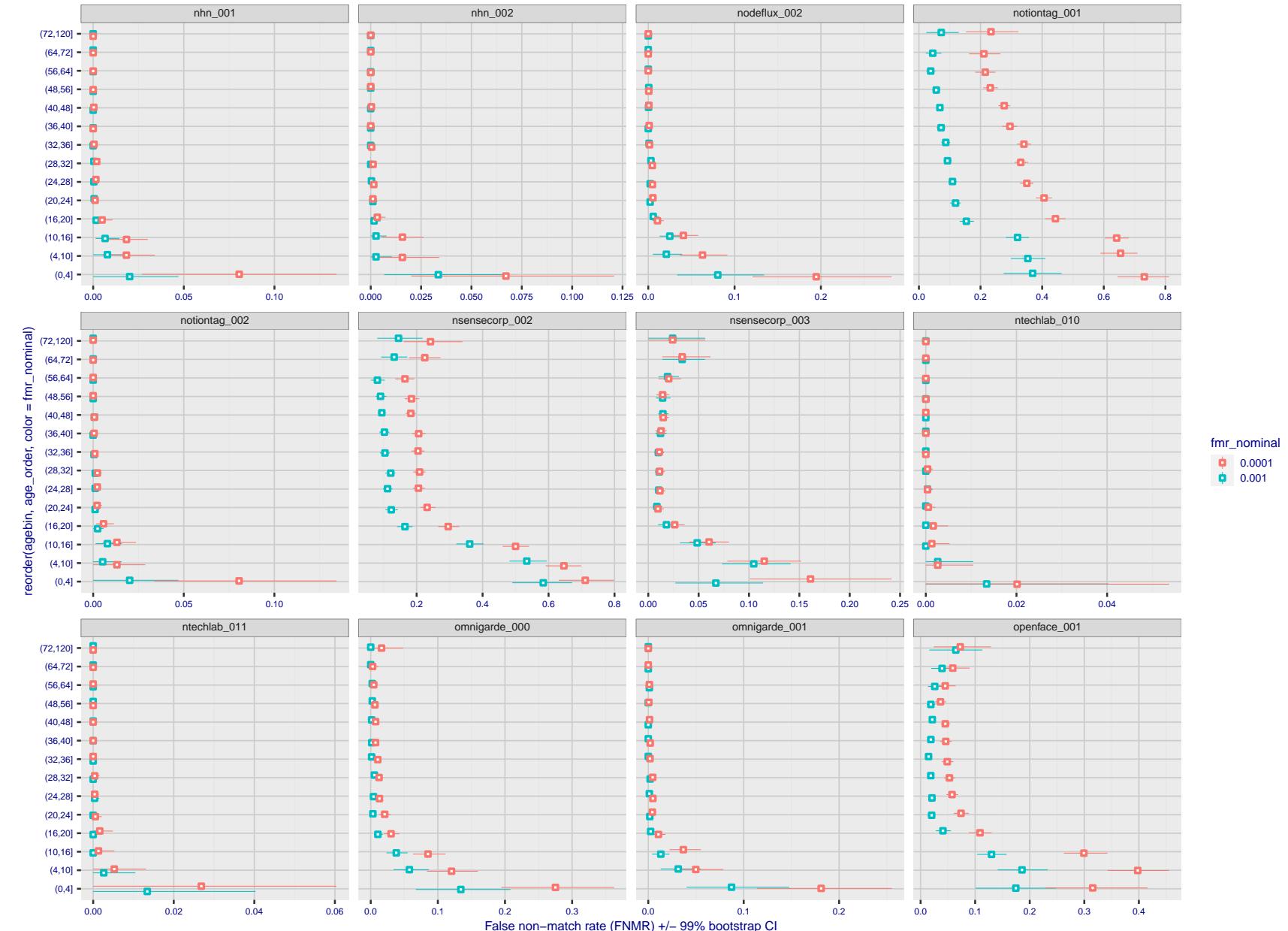


Figure 293: For the visa images, the dots show FNMR by age group for two operating thresholds corresponding to $FMR = \{0.001, 0.0001\}$ computed over all on the order of 10^{10} impostor scores. The FMR in each bin will vary also - see subsequent impostor heatmaps in sec. 3.6.2. Given a pair of face images taken at different times, we assign the comparison to the bin that is the arithmetic average of the subject's ages. This plot shows only the effect of age, not ageing. The number of comparisons in each bin is generally in the thousands, however the first and last bins are computed over 149 and 124 respectively. The error rates in some (adult) cases are zero, and in others the DET is flat so the error rates at the two thresholds are identical. The lines span 1% and 99% of bootstrap replicated FNMR estimates.



Figure 294: For the visa images, the dots show FNMR by age group for two operating thresholds corresponding to $FMR = \{0.001, 0.0001\}$ computed over all on the order of 10^{10} impostor scores. The FMR in each bin will vary also - see subsequent impostor heatmaps in sec. 3.6.2. Given a pair of face images taken at different times, we assign the comparison to the bin that is the arithmetic average of the subject's ages. This plot shows only the effect of age, not ageing. The number of comparisons in each bin is generally in the thousands, however the first and last bins are computed over 149 and 124 respectively. The error rates in some (adult) cases are zero, and in others the DET is flat so the error rates at the two thresholds are identical. The lines span 1% and 99% of bootstrap replicated FNMR estimates.



Figure 295: For the visa images, the dots show FNMR by age group for two operating thresholds corresponding to $FMR = \{0.001, 0.0001\}$ computed over all on the order of 10^{10} impostor scores. The FMR in each bin will vary also - see subsequent impostor heatmaps in sec. 3.6.2. Given a pair of face images taken at different times, we assign the comparison to the bin that is the arithmetic average of the subject's ages. This plot shows only the effect of age, not ageing. The number of comparisons in each bin is generally in the thousands, however the first and last bins are computed over 149 and 124 respectively. The error rates in some (adult) cases are zero, and in others the DET is flat so the error rates at the two thresholds are identical. The lines span 1% and 99% of bootstrap replicated FNMR estimates.

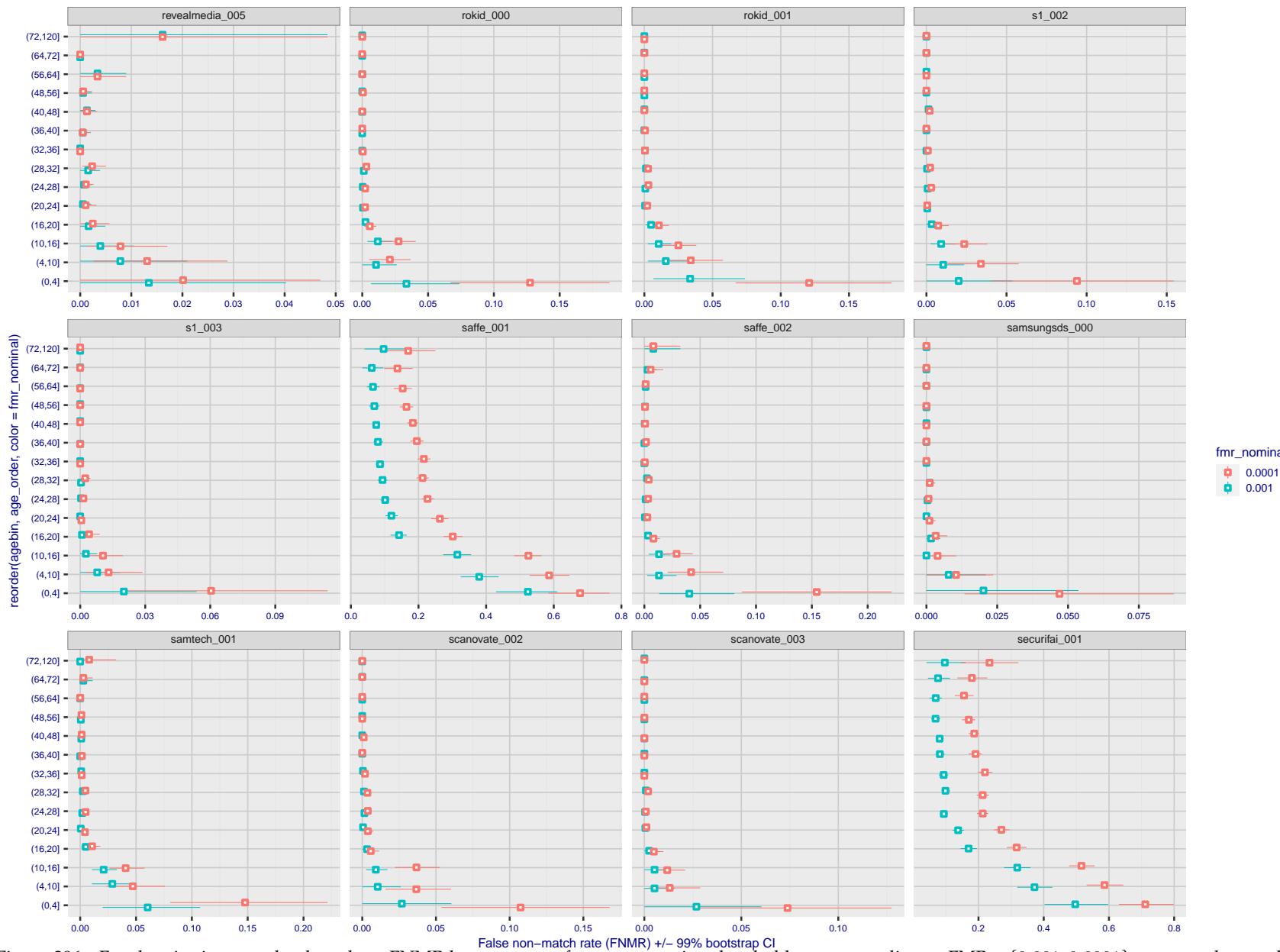


Figure 296: For the visa images, the dots show FNMR by age group for two operating thresholds corresponding to $FMR = \{0.001, 0.0001\}$ computed over all on the order of 10^{10} impostor scores. The FMR in each bin will vary also - see subsequent impostor heatmaps in sec. 3.6.2. Given a pair of face images taken at different times, we assign the comparison to the bin that is the arithmetic average of the subject's ages. This plot shows only the effect of age, not ageing. The number of comparisons in each bin is generally in the thousands, however the first and last bins are computed over 149 and 124 respectively. The error rates in some (adult) cases are zero, and in others the DET is flat so the error rates at the two thresholds are identical. The lines span 1% and 99% of bootstrap replicated FNMR estimates.

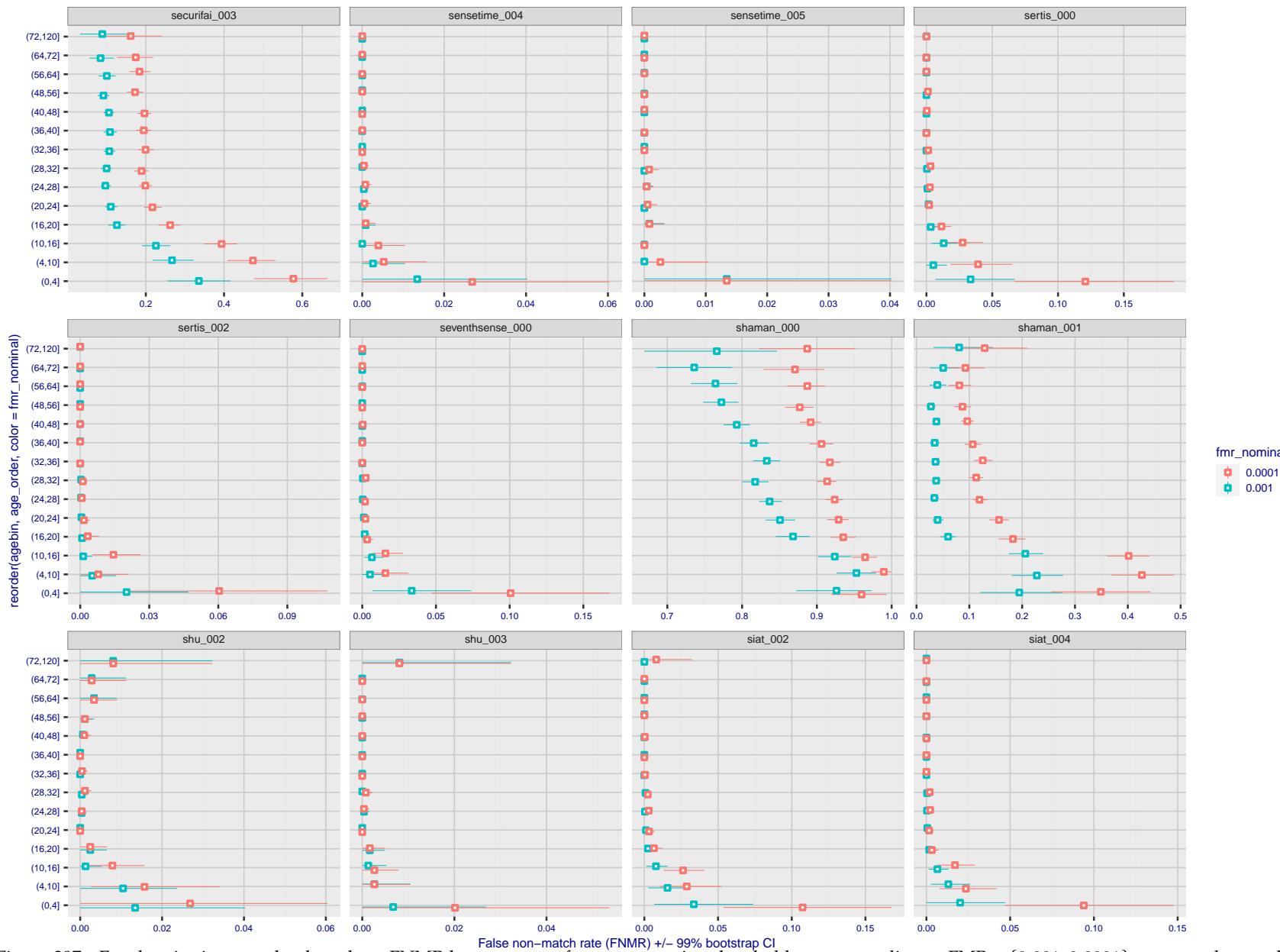


Figure 297: For the visa images, the dots show FNMR by age group for two operating thresholds corresponding to $FMR = \{0.001, 0.0001\}$ computed over all on the order of 10^{10} impostor scores. The FMR in each bin will vary also - see subsequent impostor heatmaps in sec. 3.6.2. Given a pair of face images taken at different times, we assign the comparison to the bin that is the arithmetic average of the subject's ages. This plot shows only the effect of age, not ageing. The number of comparisons in each bin is generally in the thousands, however the first and last bins are computed over 149 and 124 respectively. The error rates in some (adult) cases are zero, and in others the DET is flat so the error rates at the two thresholds are identical. The lines span 1% and 99% of bootstrap replicated FNMR estimates.

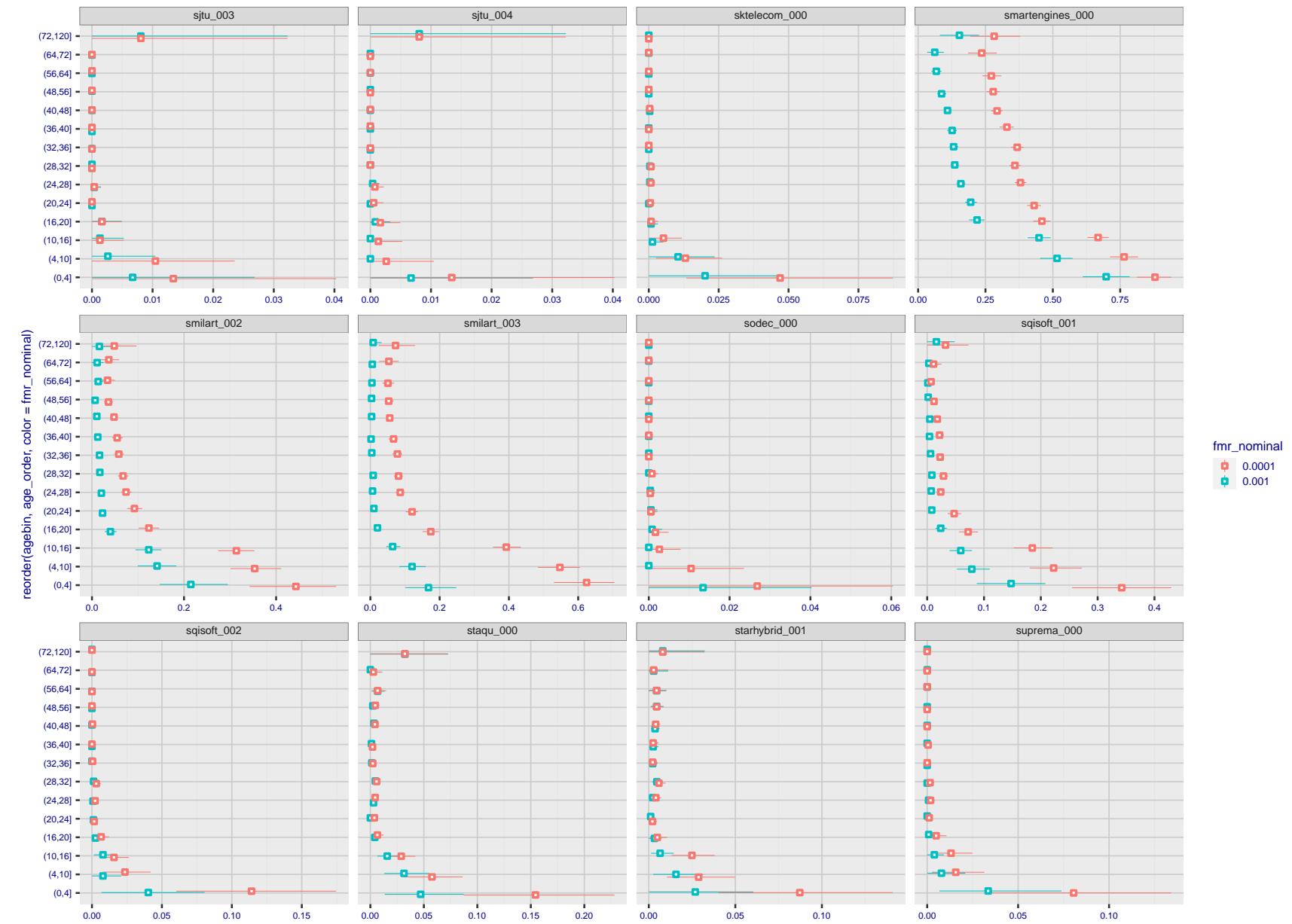


Figure 298: For the visa images, the dots show FNMR by age group for two operating thresholds corresponding to $FMR = \{0.001, 0.0001\}$ computed over all on the order of 10^{10} impostor scores. The FMR in each bin will vary also - see subsequent impostor heatmaps in sec. 3.6.2. Given a pair of face images taken at different times, we assign the comparison to the bin that is the arithmetic average of the subject's ages. This plot shows only the effect of age, not ageing. The number of comparisons in each bin is generally in the thousands, however the first and last bins are computed over 149 and 124 respectively. The error rates in some (adult) cases are zero, and in others the DET is flat so the error rates at the two thresholds are identical. The lines span 1% and 99% of bootstrap replicated FNMR estimates.

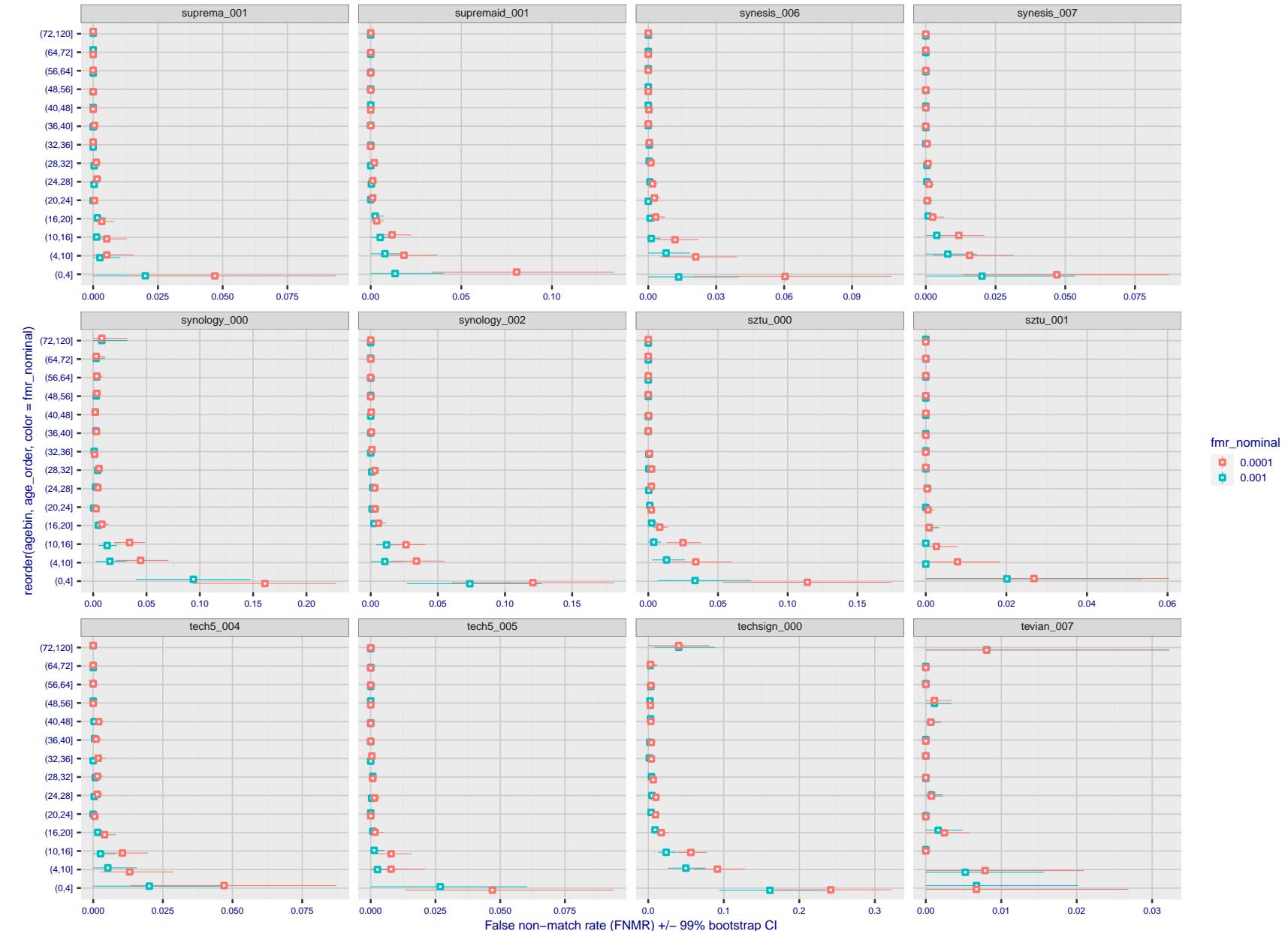


Figure 299: For the visa images, the dots show FNMR by age group for two operating thresholds corresponding to $FMR = \{0.001, 0.0001\}$ computed over all on the order of 10^{10} impostor scores. The FMR in each bin will vary also - see subsequent impostor heatmaps in sec. 3.6.2. Given a pair of face images taken at different times, we assign the comparison to the bin that is the arithmetic average of the subject's ages. This plot shows only the effect of age, not ageing. The number of comparisons in each bin is generally in the thousands, however the first and last bins are computed over 149 and 124 respectively. The error rates in some (adult) cases are zero, and in others the DET is flat so the error rates at the two thresholds are identical. The lines span 1% and 99% of bootstrap replicated FNMR estimates.

2021/12/16 10:32:53



Figure 300: For the visa images, the dots show FNMR by age group for two operating thresholds corresponding to $FMR = \{0.001, 0.0001\}$ computed over all on the order of 10^{10} impostor scores. The FMR in each bin will vary also - see subsequent impostor heatmaps in sec. 3.6.2. Given a pair of face images taken at different times, we assign the comparison to the bin that is the arithmetic average of the subject's ages. This plot shows only the effect of age, not ageing. The number of comparisons in each bin is generally in the thousands, however the first and last bins are computed over 149 and 124 respectively. The error rates in some (adult) cases are zero, and in others the DET is flat so the error rates at the two thresholds are identical. The lines span 1% and 99% of bootstrap replicated FNMR estimates.



Figure 301: For the visa images, the dots show FNMR by age group for two operating thresholds corresponding to $FMR = \{0.001, 0.0001\}$ computed over all on the order of 10^{10} impostor scores. The FMR in each bin will vary also - see subsequent impostor heatmaps in sec. 3.6.2. Given a pair of face images taken at different times, we assign the comparison to the bin that is the arithmetic average of the subject's ages. This plot shows only the effect of age, not ageing. The number of comparisons in each bin is generally in the thousands, however the first and last bins are computed over 149 and 124 respectively. The error rates in some (adult) cases are zero, and in others the DET is flat so the error rates at the two thresholds are identical. The lines span 1% and 99% of bootstrap replicated FNMR estimates.

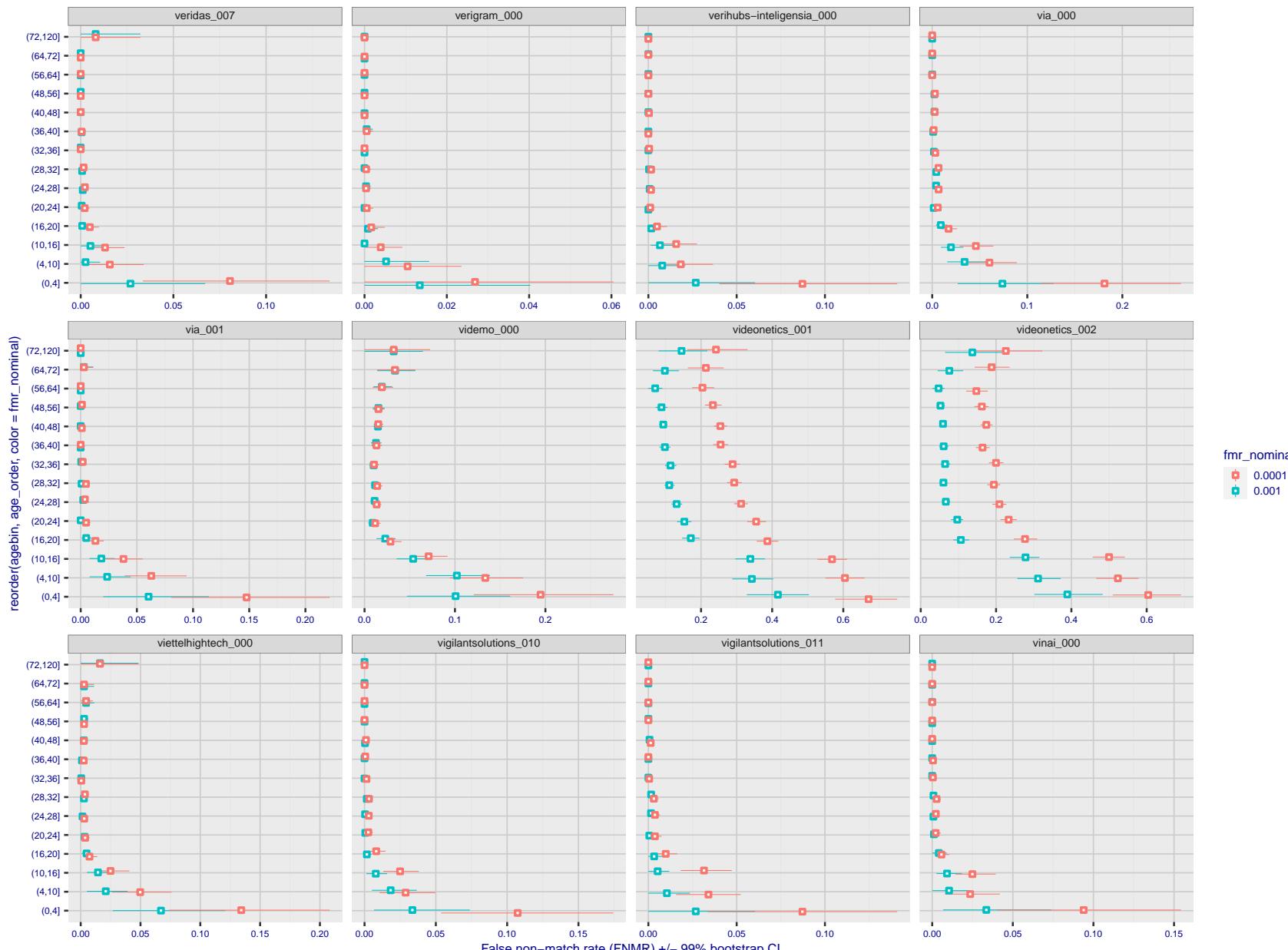


Figure 302: For the visa images, the dots show FNMR by age group for two operating thresholds corresponding to $FMR = \{0.001, 0.0001\}$ computed over all on the order of 10^{10} impostor scores. The FMR in each bin will vary also - see subsequent impostor heatmaps in sec. 3.6.2. Given a pair of face images taken at different times, we assign the comparison to the bin that is the arithmetic average of the subject's ages. This plot shows only the effect of age, not ageing. The number of comparisons in each bin is generally in the thousands, however the first and last bins are computed over 149 and 124 respectively. The error rates in some (adult) cases are zero, and in others the DET is flat so the error rates at the two thresholds are identical. The lines span 1% and 99% of bootstrap replicated FNMR estimates.

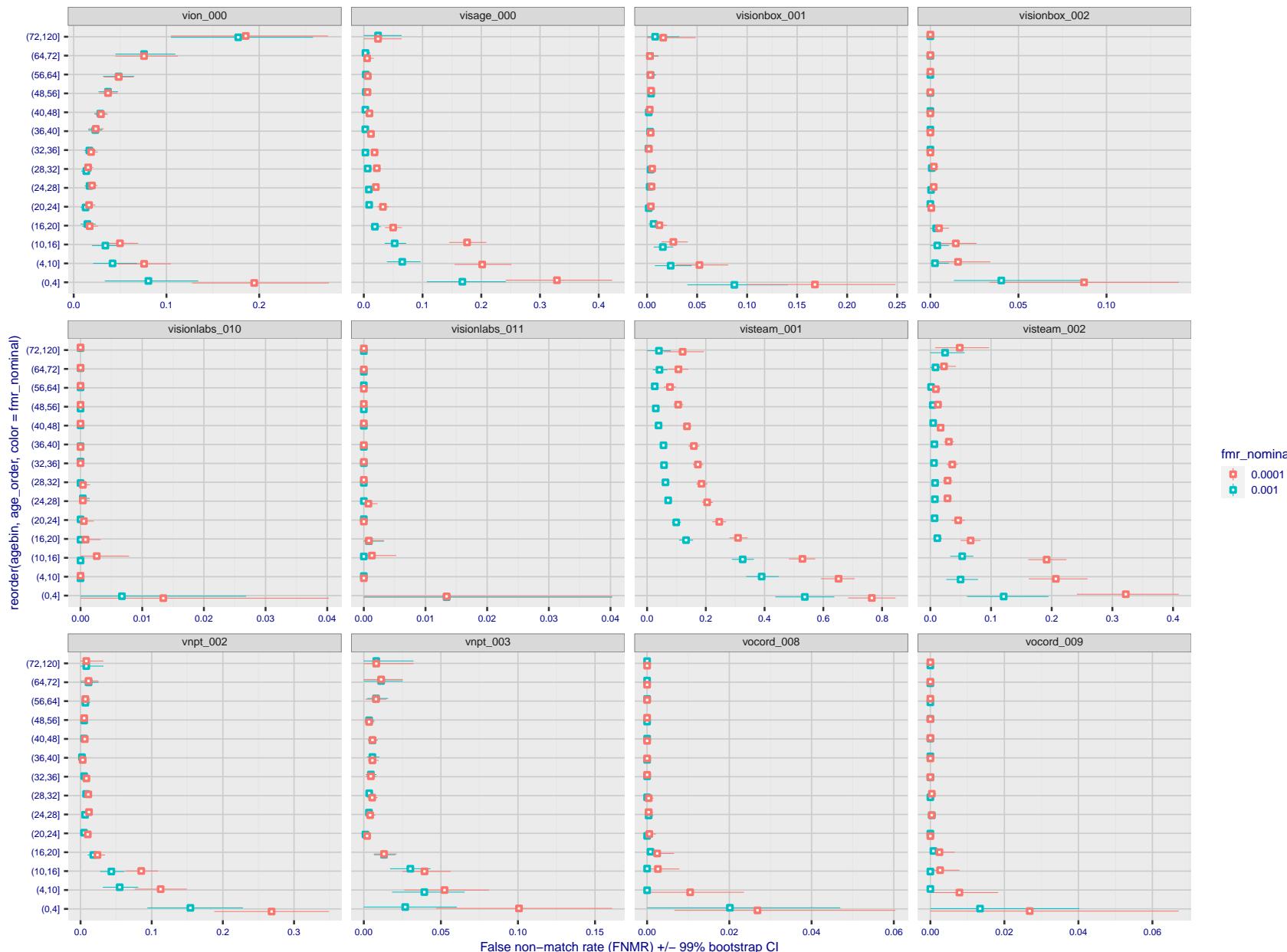


Figure 303: For the visa images, the dots show FNMR by age group for two operating thresholds corresponding to $FMR = \{0.001, 0.0001\}$ computed over all on the order of 10^{10} impostor scores. The FMR in each bin will vary also - see subsequent impostor heatmaps in sec. 3.6.2. Given a pair of face images taken at different times, we assign the comparison to the bin that is the arithmetic average of the subject's ages. This plot shows only the effect of age, not ageing. The number of comparisons in each bin is generally in the thousands, however the first and last bins are computed over 149 and 124 respectively. The error rates in some (adult) cases are zero, and in others the DET is flat so the error rates at the two thresholds are identical. The lines span 1% and 99% of bootstrap replicated FNMR estimates.

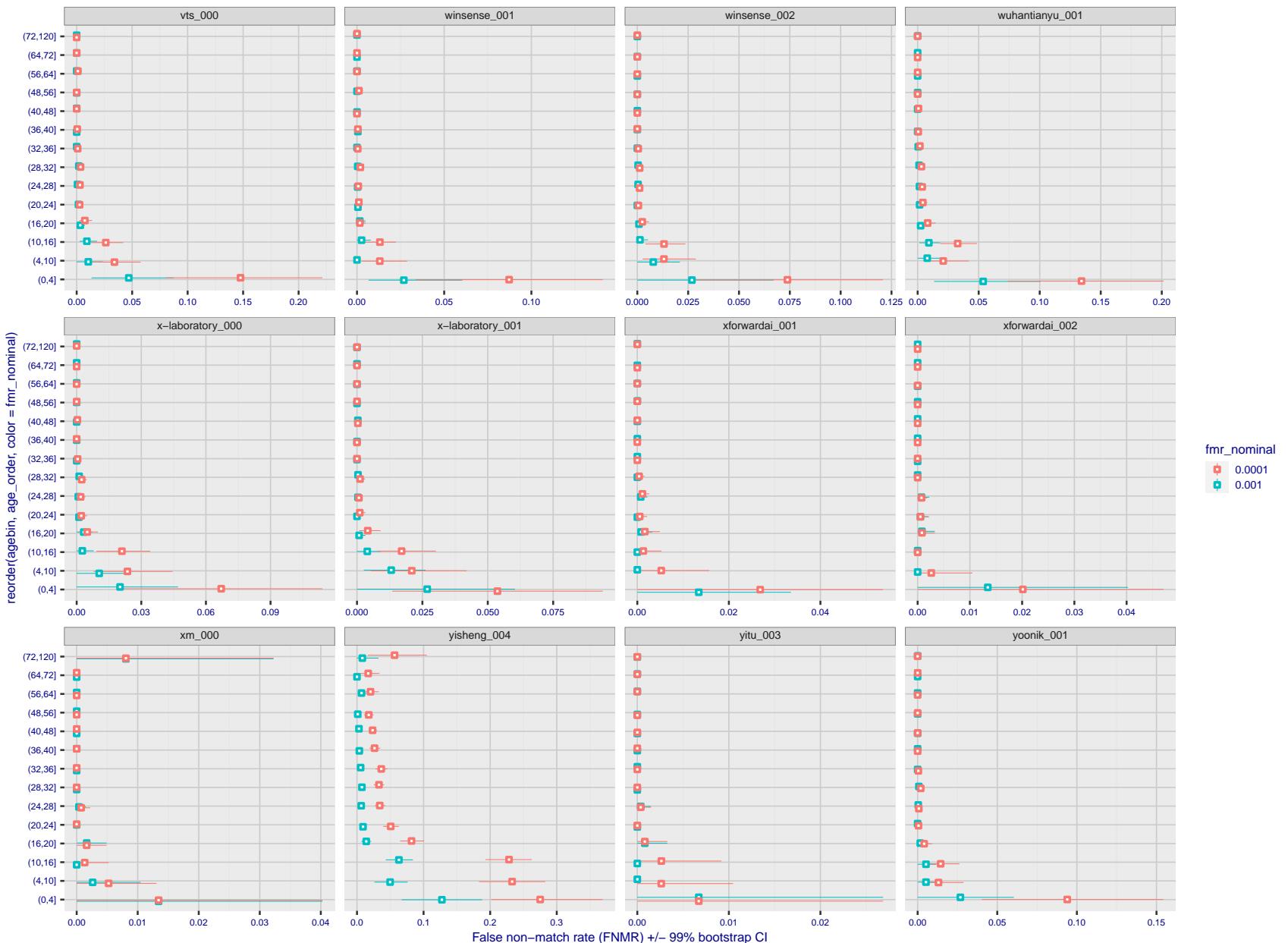


Figure 304: For the visa images, the dots show FNMR by age group for two operating thresholds corresponding to $FMR = \{0.001, 0.0001\}$ computed over all on the order of 10^{10} impostor scores. The FMR in each bin will vary also - see subsequent impostor heatmaps in sec. 3.6.2. Given a pair of face images taken at different times, we assign the comparison to the bin that is the arithmetic average of the subject's ages. This plot shows only the effect of age, not ageing. The number of comparisons in each bin is generally in the thousands, however the first and last bins are computed over 149 and 124 respectively. The error rates in some (adult) cases are zero, and in others the DET is flat so the error rates at the two thresholds are identical. The lines span 1% and 99% of bootstrap replicated FNMR estimates.

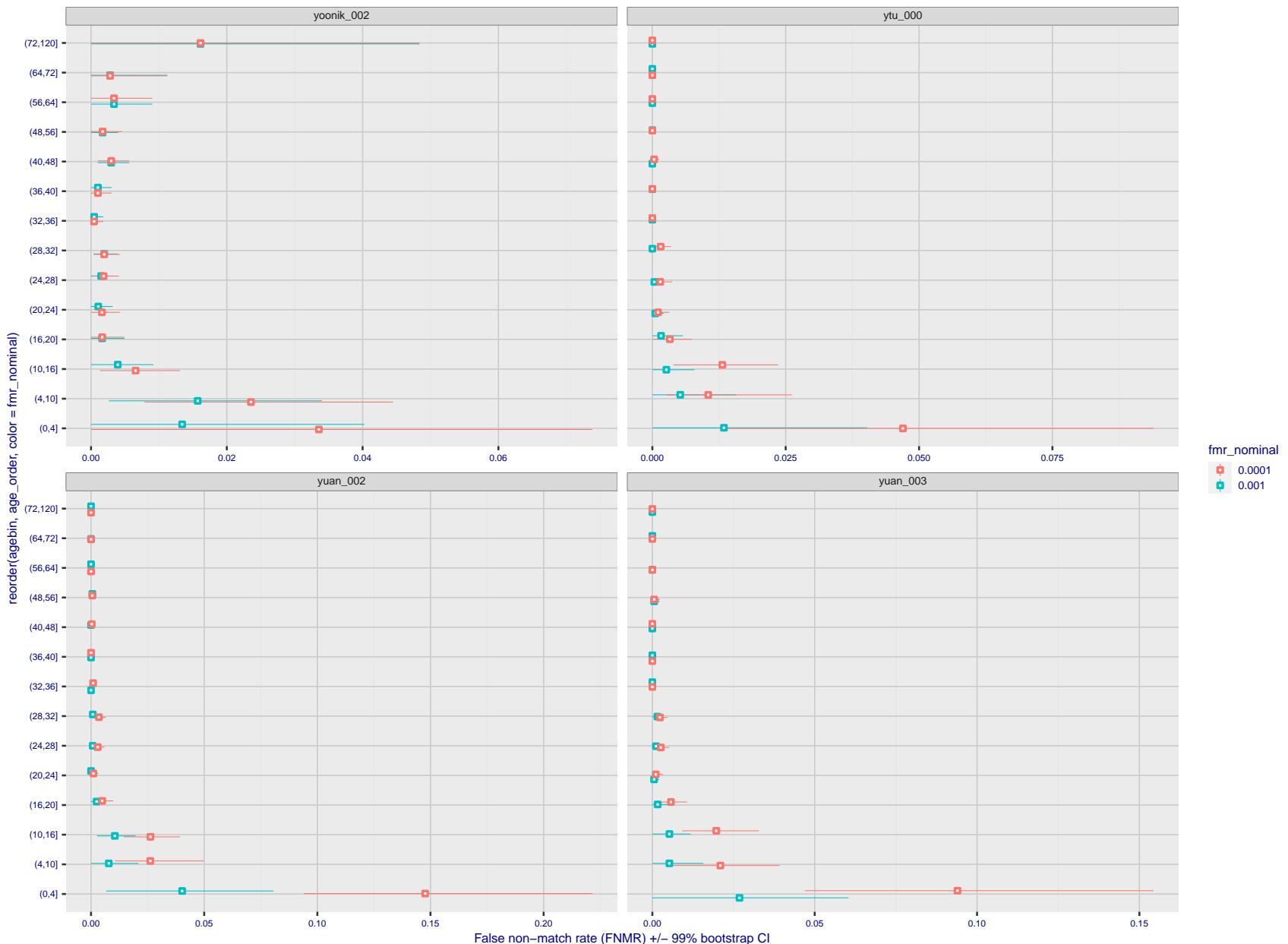


Figure 305: For the visa images, the dots show FNMR by age group for two operating thresholds corresponding to $FMR = \{0.001, 0.0001\}$ computed over all on the order of 10^{10} impostor scores. The FMR in each bin will vary also - see subsequent impostor heatmaps in sec. 3.6.2. Given a pair of face images taken at different times, we assign the comparison to the bin that is the arithmetic average of the subject's ages. This plot shows only the effect of age, not ageing. The number of comparisons in each bin is generally in the thousands, however the first and last bins are computed over 149 and 124 respectively. The error rates in some (adult) cases are zero, and in others the DET is flat so the error rates at the two thresholds are identical. The lines span 1% and 99% of bootstrap replicated FNMR estimates.

Caveats: None.

3.6 Impostor distribution stability

3.6.1 Effect of birth place on the impostor distribution

Background: Facial appearance varies geographically, both in terms of skin tone, cranio-facial structure and size. This section addresses whether false match rates vary intra- and inter-regionally.

Goals:

- ▷ To show the effect of birth region of the impostor and enrollee on false match rates.
- ▷ To determine whether some algorithms give better impostor distribution stability.

Methods:

- ▷ For the visa images, NIST defined 10 regions: Sub-Saharan Africa, South Asia, Polynesia, North Africa, Middle East, Europe, East Asia, Central and South America, Central Asia, and the Caribbean.
- ▷ For the visa images, NIST mapped each country of birth to a region. There is some arbitrariness to this. For example, Egypt could reasonably be assigned to the Middle East instead of North Africa. An alternative methodology could, for example, assign the Philippines to *both* Polynesia and East Asia.
- ▷ FMR is computed for cases where all face images of impostors born in region r_2 are compared with enrolled face images of persons born in region r_1 .

$$\text{FMR}(r_1, r_2, T) = \frac{\sum_{i=1}^{N_{r_1, r_2}} H(s_i - T)}{N_{r_1, r_2}} \quad (5)$$

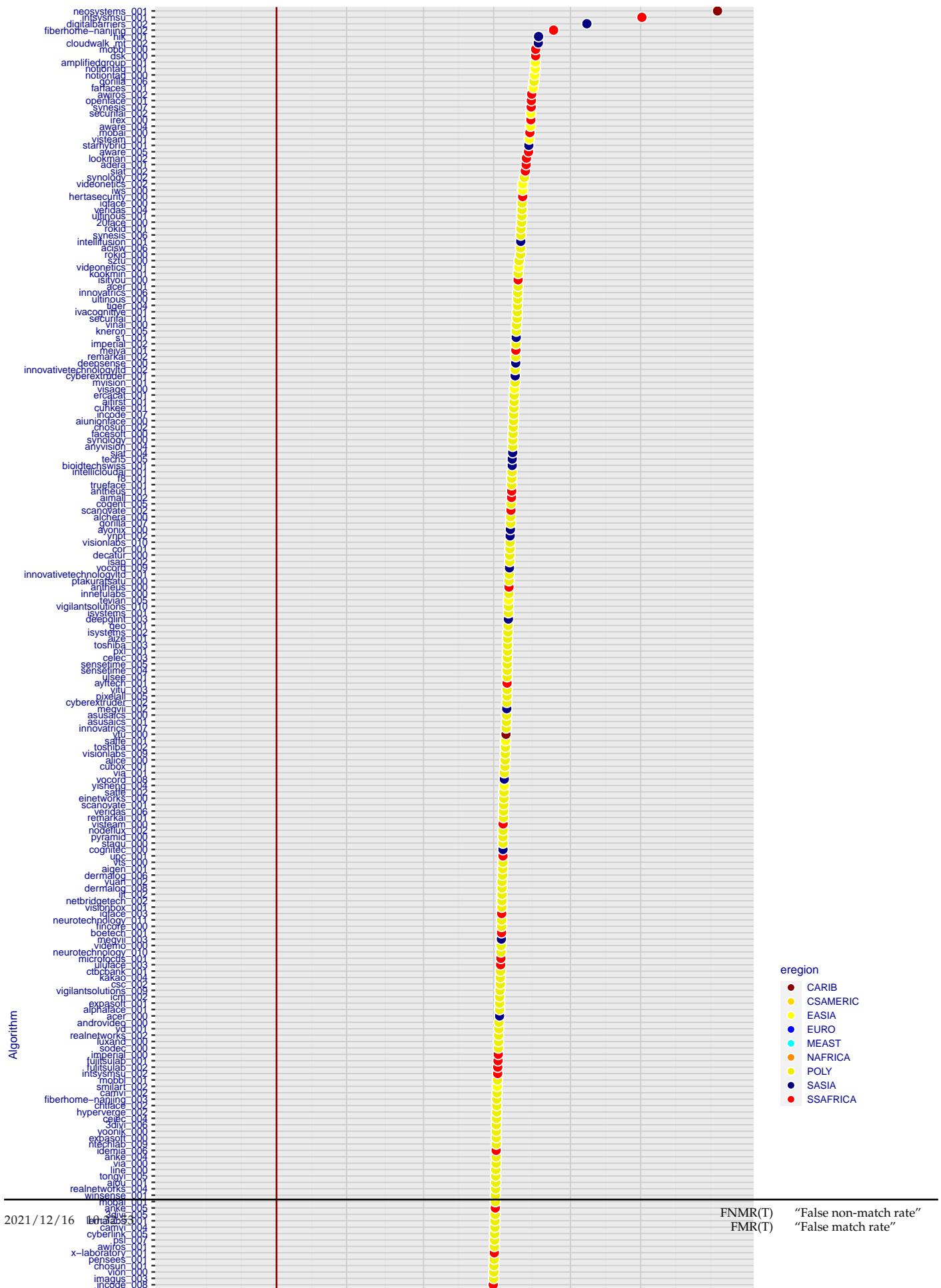
where the same threshold, T , is used in all cells, and H is the unit step function. The threshold is set to give $\text{FMR}(T) = 0.001$ over the entire set of visa image impostor comparisons.

- ▷ This analysis is then repeated by country-pair, but only for those country pairs where both have at least 1000 images available. The countries¹ appear in the axes of graphs that follow.
- ▷ The mean number of impostor scores in any cross-region bin is 33 million. The smallest number of impostor scores in any bin is 135000, for Central Asia - North Africa. While these counts are large enough to support reasonable significance, the number of individual faces is much smaller, on the order of $N^{0.5}$.
- ▷ The numbers of impostor scores in any cross-country bin is shown in Figure ??.

Results: Subsequent figures show heatmaps that use color to represent the base-10 logarithm of the false match rate. Red colors indicate high (bad) false match rates. Dark colors indicate benign false match rates. There are two series of graphs corresponding to aggregated geographical regions, and to countries. The notable observations are:

- ▷ The on-diagonal elements correspond to within-region impostors. FMR is generally above the nominal value of $\text{FMR} = 0.001$. Particularly there is usually higher FMR in, Sub-Saharan Africa, South Asia, and the Caribbean. Europe and Central Asia, on the other hand, usually give FMR closer to the nominal value.
- ▷ The off-diagonal elements correspond to across-region impostors. The highest FMR is produced between the Caribbean and Sub-Saharan Africa.
- ▷ Algorithms vary.

¹These are Argentina, Australia, Brazil, Chile, China, Costa Rica, Cuba, Czech Republic, Dominican Republic, Ecuador, Egypt, El Salvador, Germany, Ghana, Great Britain, Greece, Guatemala, Haiti, Hong Kong, Honduras, Indonesia, India, Israel, Jamaica, Japan, Kenya, Korea, Lebanon, Mexico, Malaysia, Nepal, Nigeria, Peru, Philippines, Pakistan, Poland, Romania, Russia, South Africa, Saudi Arabia, Thailand, Trinidad, Turkey, Taiwan, Ukraine, Venezuela, and Vietnam.



- ▷ We computed the same quantities for a global FMR = 0.0001. The effects are similar.

Caveats:

- ▷ The effects of variable impostor rates on one-to-many identification systems may well differ from what's implied by these one-to-one verification results. Two reasons for this are a) the enrollment galleries are usually imbalanced across countries of birth, age and sex; b) one-to-many identification algorithms often implement techniques aimed at stabilizing the impostor distribution. Further research is necessary.
- ▷ In principle, the effects seen in this subsection could be due to differences in the image capture process. We consider this unlikely since the effects are maintained across geography - e.g. Caribbean vs. Africa, or Japan vs. China.

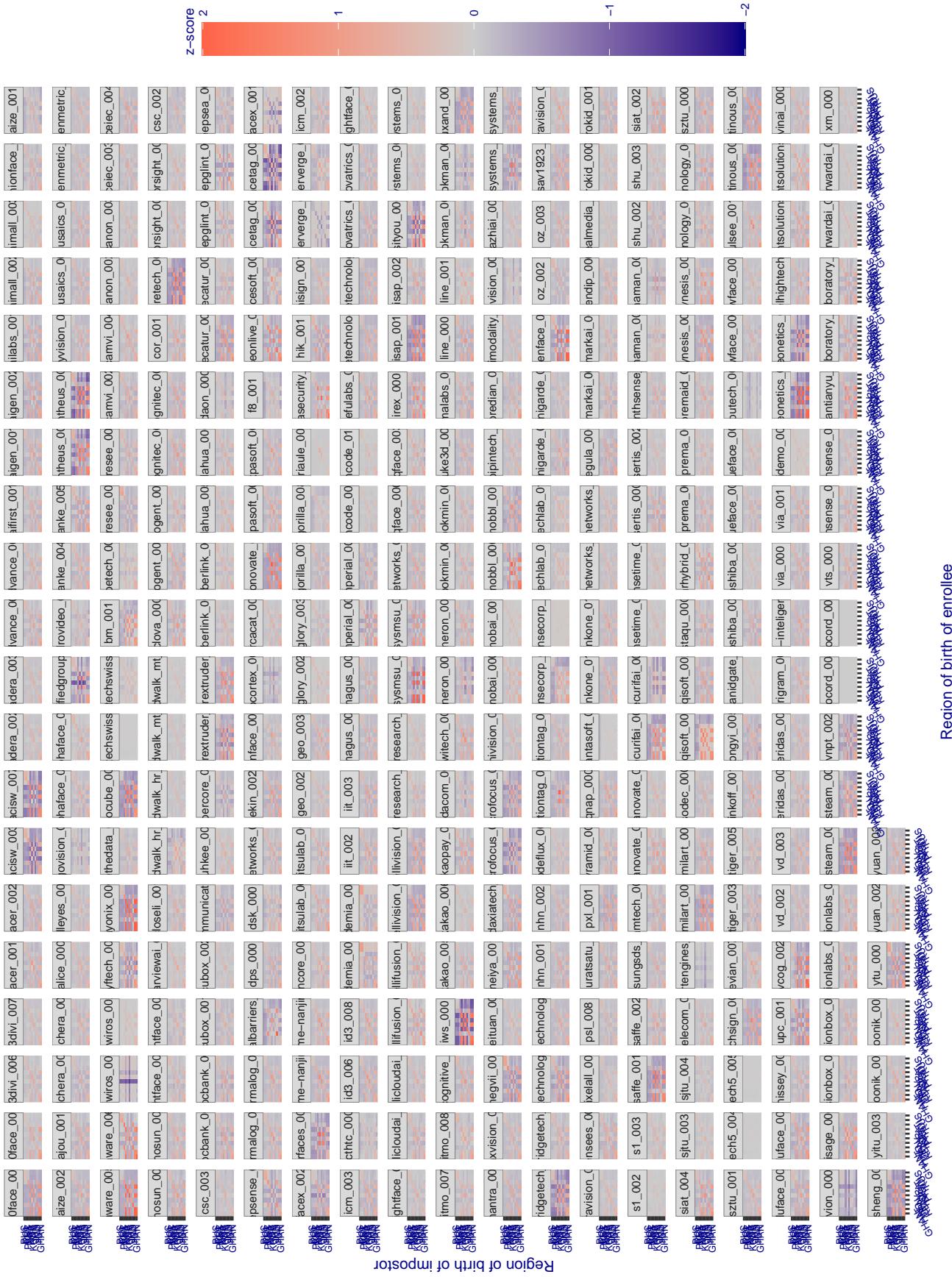


Figure 307: For visa images, the heatmap shows how the mean of the impostor distribution for the country pair (a,b) is shifted relative to the mean of the global impostor distribution, expressed as a number of standard deviations of the global impostor distribution. This statistic is designed to show shifts in the entire impostor distribution, not just tail effects that manifest as the anomalously high (or low) false match rates that appear in the subsequent figures. The countries are chosen to show that skin tone alone does not explain impostor distribution shifts. The reduced shift in Asian populations with the Yitu and Tong YiTrans algorithms, is accompanied by positive shifts in the European populations. This reversal relative to most other algorithms, may derive from use of nationally weighted training sets. The figure is computed from same-sex and same-age impostor pairs.

3.6.2 Effect of age on impostors

Background: This section shows the effect of age on the impostor distribution. The ideal behaviour is that the age of the enrollee and the impostor would not affect impostor scores. This would support FMR stability over sub-populations.

Goals:

- ▷ To show the effect of relative ages of the impostor and enrollee on false match rates.
- ▷ To determine whether some algorithms have better impostor distribution stability.

Methods:

- ▷ Define 14 age group bins, spanning 0 to over 100 years old.
- ▷ Compute FMR over all impostor comparisons for which the subjects in the enrollee and impostor images have ages in two bins.
- ▷ Compute FMR over all impostor comparisons for which the subjects are additionally of the same sex, and born in the same geographic region.

Results:

The notable aspects are:

- ▷ Diagonal dominance: Impostors are more likely to be matched against their same age group.
- ▷ Same sex and same region impostors are more successful. On the diagonal, an impostor is more likely to succeed by posing as someone of the same sex. If $\Delta \log_{10} \text{FMR} = 0.2$, then same-sex same-region FMR exceeds the all-pairs FMR by factor of $10^{0.2} = 1.6$.
- ▷ Young children impostors give elevated FMR against young children. Older adult impostor give elevated FMR against older adults. These effects are quite large, for example if $\Delta \log_{10} \text{FMR} = 1.0$ larger than a 32 year old, then these groups have higher FMR by a factor of $10^1 = 10$. This would imply an FMR above 0.01 for a nominal (global) FMR = 0.001.
- ▷ Algorithms vary.
- ▷ We computed the same quantities for a global FMR = 0.0001. The effects are similar.

Note the calculations in this section include impostors paired across all countries of birth.

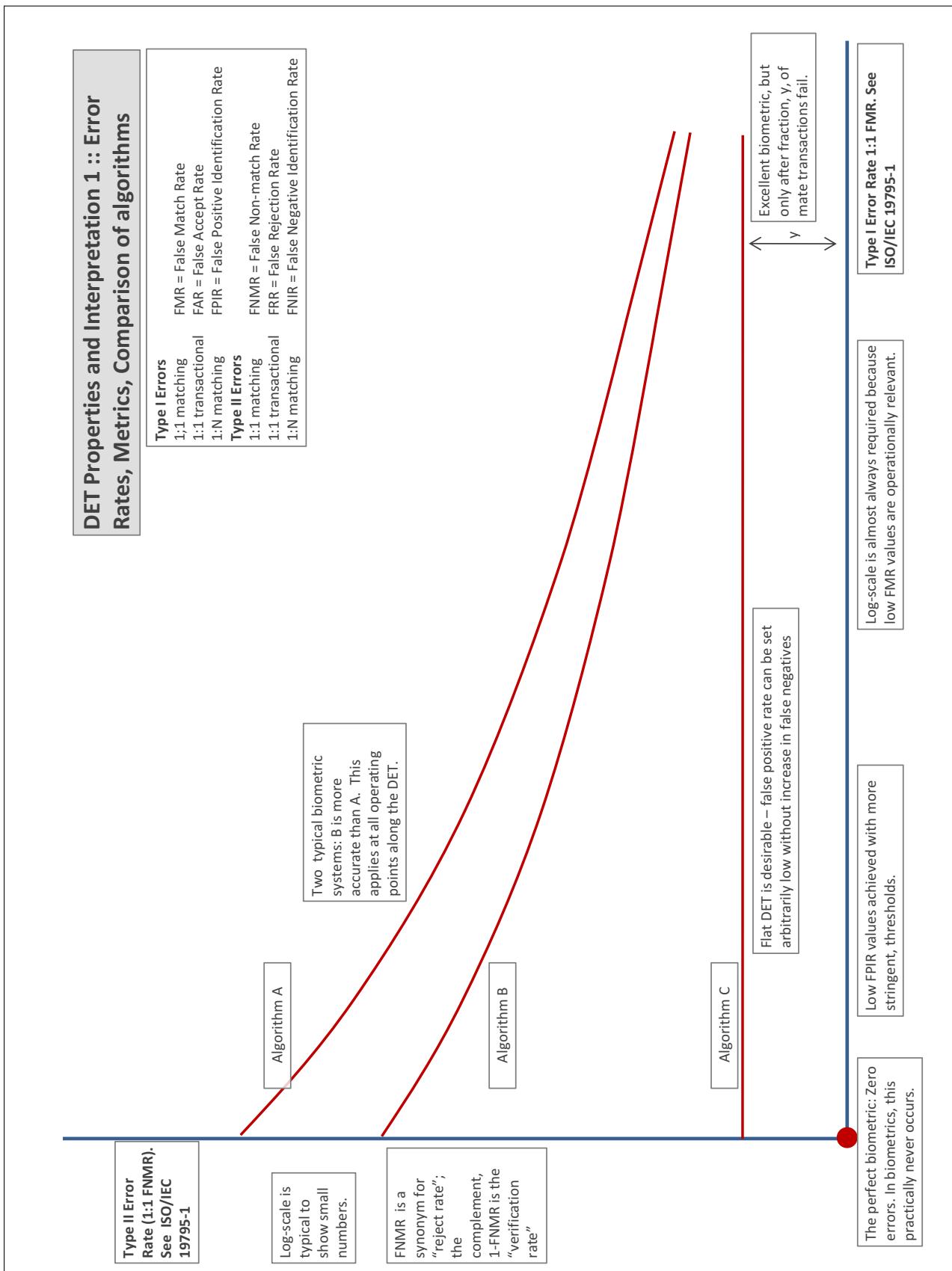
Accuracy Terms + Definitions

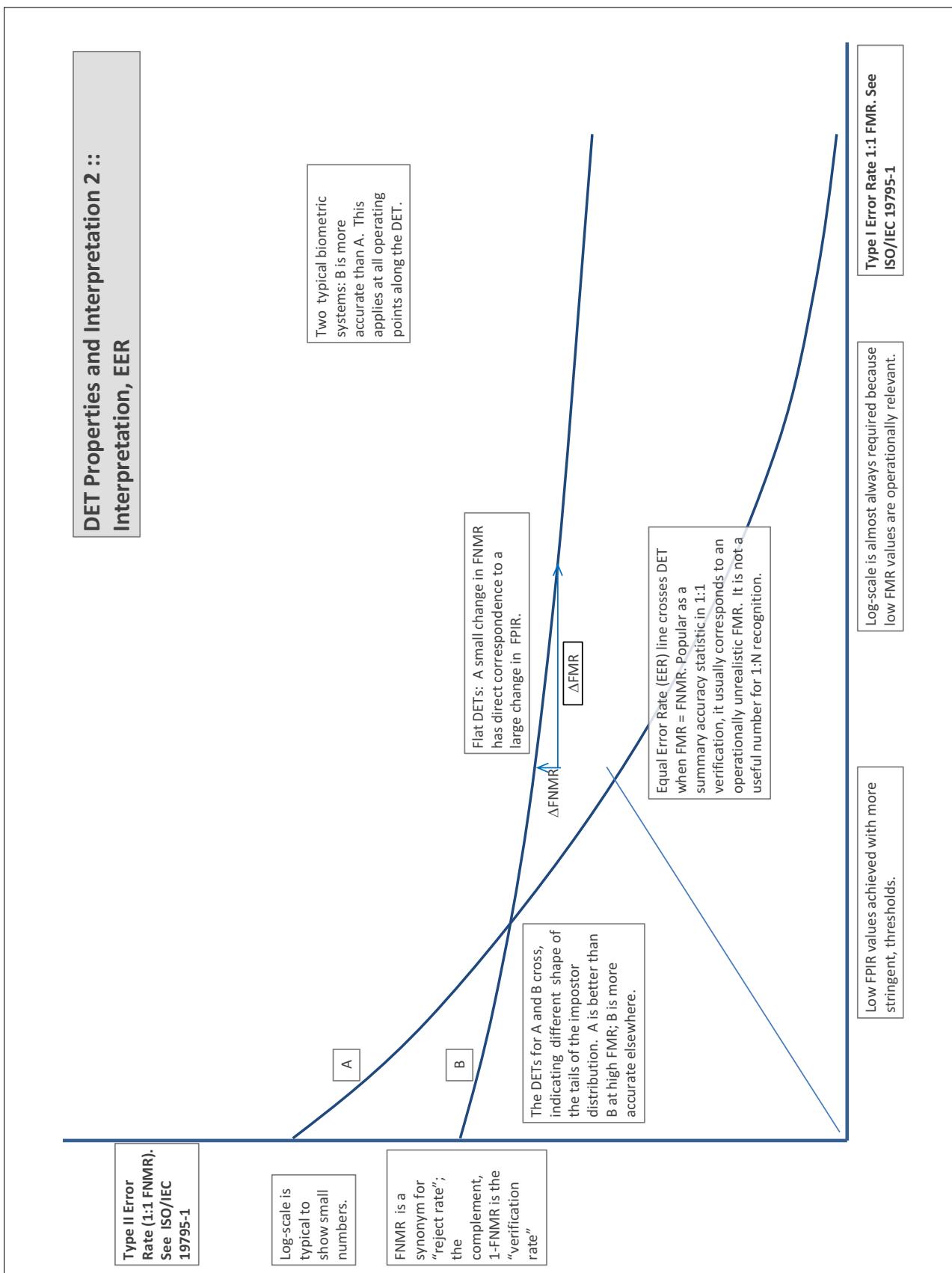
In biometrics, Type II errors occur when two samples of one person do not match – this is called a **false negative**. Correspondingly, Type I errors occur when samples from two persons do match – this is called a **false positive**. Matches are declared by a biometric system when the native comparison score from the recognition algorithm meets some **threshold**. Comparison scores can be either **similarity scores**, in which case higher values indicate that the samples are more likely to come from the same person, or **dissimilarity scores**, in which case higher values indicate different people. Similarity scores are traditionally computed by **fingerprint** and **face** recognition algorithms, while dissimilarities are used in **iris recognition**. In some cases, the dissimilarity score is a distance; this applies only when **metric** properties are obeyed. In any case, scores can be either **mate** scores, coming from a comparison of one person's samples, or **nonmate** scores, coming from comparison of different persons' samples. The words **genuine** or **authentic** are synonyms for mate, and the word **impostor** is used as a synonym for nonmatch. The words mate and nonmatch are traditionally used in identification applications (such as law enforcement search, or background checks) while genuine and impostor are used in verification applications (such as access control).

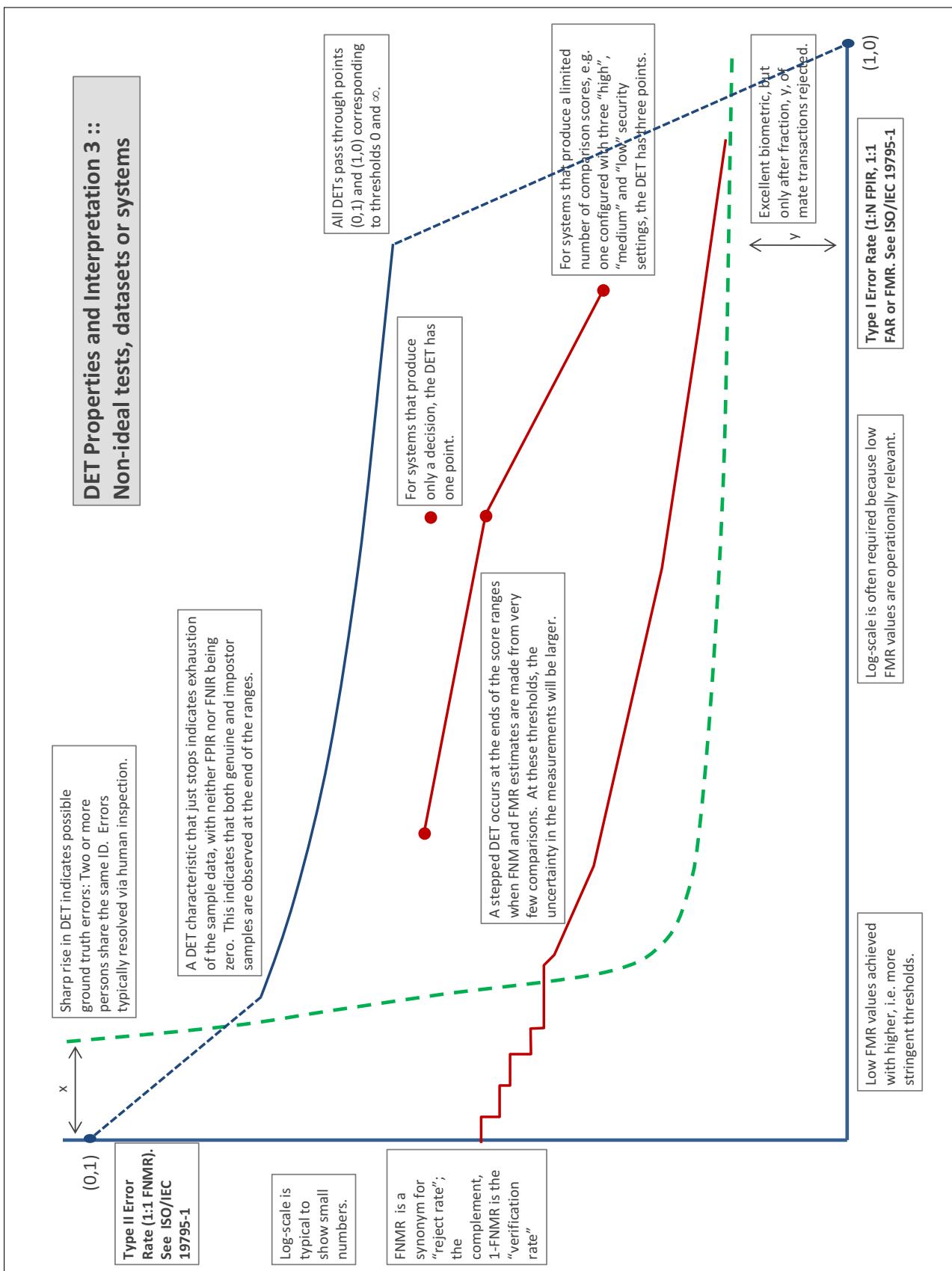
A **error tradeoff** characteristic represents the tradeoff between Type II and Type I classification errors. For verification this plots false non-match rate (FNMR) vs. false match rate (FMR) parametrically with T.

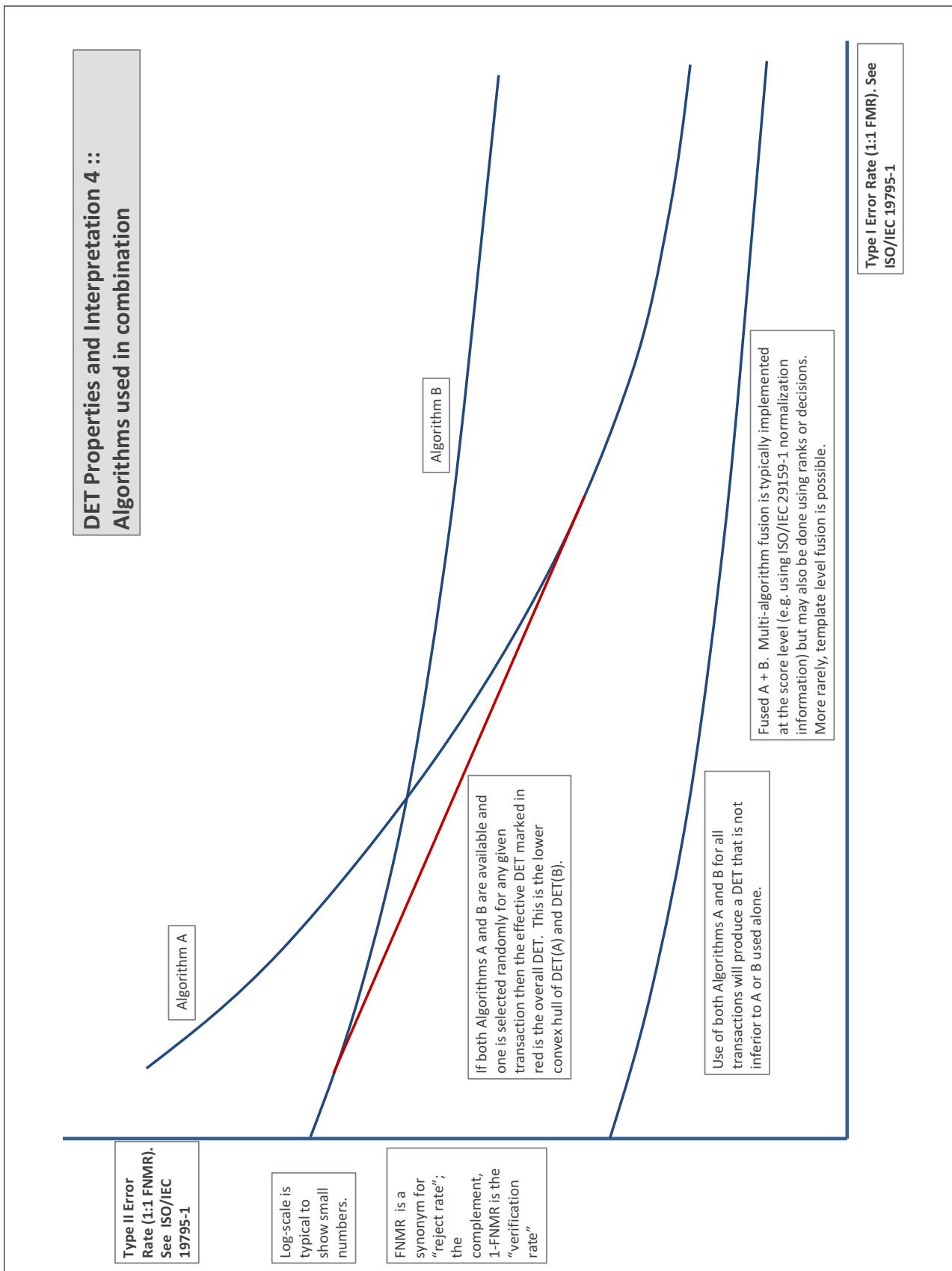
The error tradeoff plots are often called **detection error tradeoff (DET)** characteristics or **receiver operating characteristic (ROC)**. These serve the same function but differ, for example, in plotting the complement of an error rate (e.g., $TMR = 1 - FNMR$) and in transforming the axes most commonly using logarithms, to show multiple decades of FMR. More rarely, the function might be the inverse Gaussian function.

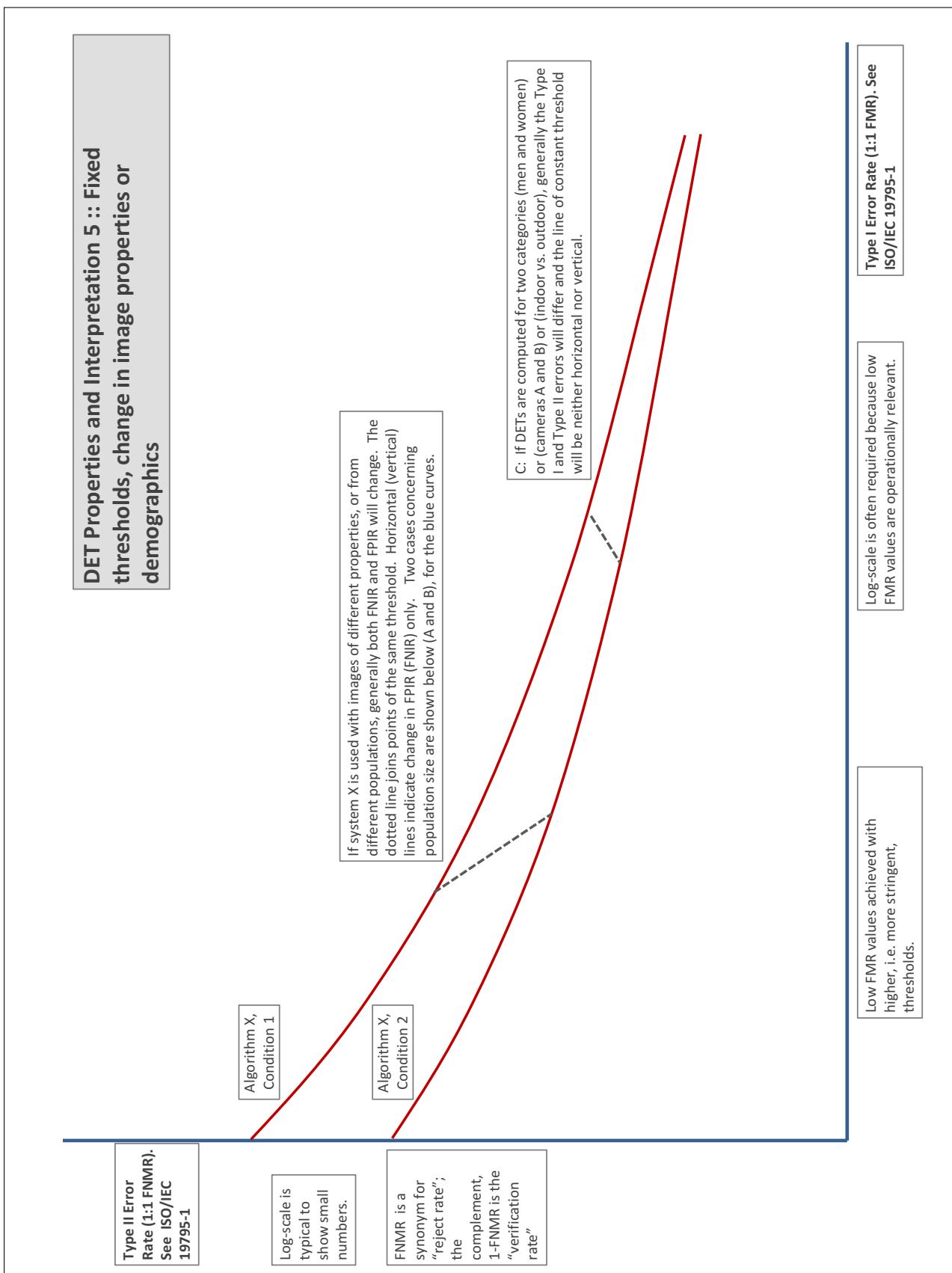
More detail and generality is provided in formal biometrics testing standards, see the various parts of [ISO/IEC 19795 Biometrics Testing and Reporting](#). More terms, including and beyond those to do with accuracy, see [ISO/IEC 2382-37 Information technology -- Vocabulary -- Part 37: Harmonized biometric vocabulary](#)











References

- [1] P. Jonathon Phillips, Amy N. Yates, Ying Hu, Carina A. Hahn, Eilidh Noyes, Kelsey Jackson, Jacqueline G. Cavazos, Géraldine Jeckeln, Rajeev Ranjan, Swami Sankaranarayanan, Jun-Cheng Chen, Carlos D. Castillo, Rama Chellappa, David White, and Alice J. O'Toole. Face recognition accuracy of forensic examiners, superrecognizers, and face recognition algorithms. *Proceedings of the National Academy of Sciences*, 115(24):6171–6176, 2018.